

ABSTRACT

Title of Dissertation: New molecules to combat the bacterial antibiotic resistance problem

Jingxin Wang, Doctor of Philosophy, 2011

Dissertation directed by: Professor Herman O. Sintim

Department of Chemistry and Biochemistry

Platensimycin/platencin are recently discovered natural products that inhibit membrane formation in bacteria and cyclic diguanylic acid (c-di-GMP) is a master regulator of bacterial biofilm formation. The rise of bacterial antibiotic resistance and the dwindling pipeline of new antibiotics make these molecules of interest to the scientific community. This dissertation reports the design, synthesis and biological evaluation of analogs of platensimycin/platencin and c-di-GMP.

Platensimycin and platencin have garnered interest from synthetic chemists due to the complexity of their molecular architecture, coupled with their exciting biological profile (inhibition of bacterial fatty acid synthases). We have developed a concise synthetic approach towards the platensimycin/platencin class of antibiotics. The highlight of our synthesis is the use of dynamic ring-closing metathesis to prepare a bicyclo intermediate and a tandem nucleophilic addition of organolithium to a ketone moiety,

followed by a subsequent ring opening of a nearby epoxide to generate complex tricyclic framework.

The synthesis of platensimycin or closely related analogs requires multi-steps (average of 17 overall steps). Using a function-oriented synthetic approach, we developed short syntheses of *N,N*-dialkyl benzoic acid derivatives of platensimycin, and we demonstrate that these readily prepared molecules have comparable antibiotic properties to the difficult-to-synthesize platensimycin/platencin.

C-di-GMP has been dubbed the master regulator of bacterial “lifestyle” due to the key role that this molecule plays in bacterial biofilm formation and virulence formation. In order to study c-di-GMP signaling in bacteria, with the ultimate goal of using key insights gained from such studies to develop anti-biofilm or anti-virulence agents, we prepared analogs of c-di-GMP and studied their biophysical and biological profiles. Interestingly, we reveal that conservative modifications to c-di-GMP affect both the biophysical and biochemical properties of this molecule. We also demonstrate a concept called “conformational steering” as a powerful principle to selectively target different classes of receptor proteins that bind to c-di-GMP.

NEW MOLECULES TO COMBAT THE BACTERIAL ANTIBIOTIC RESISTANCE

PROBLEM

by

Jingxin Wang

Dissertation submitted to the Faculty of the Graduate School of the
University of Maryland, College Park in partial fulfillment
of the requirements for the degree of
Doctor of Philosophy
2011

Advisory Committee:

Assistant Professor Herman O. Sintim, Chair

Professor Michael P. Doyle

Professor Lyle Isaacs

Associate Professor Andrei N. Vedernikov

Professor Sergei I. Sukharev

DEDICATION

To mom, dad and Jinxi

ACKNOWLEDGEMENTS

Firstly, I would like to thank my dissertation advisor, Dr. Herman Sintim, for his numerous helpful directions and advices in the past four and a half years.

I also thank my dissertation committee member Dr. Andrei N. Vedernikov and my friend Dr. Yuanyuan Wang for help with the use of the Gaussian software to perform calculations shown in Chapters 2 and 4.

I thank Dr. Vincent Lee and his student, Mr. Gregory Donaldson, for help with the determination of minimum inhibitory concentrations of platensimycin analogs (Dr. Lee) and binding assays of c-di-GMP and endo-S-c-di-GMP and adaptor/metabolism proteins (Greg Donaldson) in Chapter 2 and Chapter 4, respectively.

I thank my colleague, Dr. Shizuka Nakayama, for measuring the CD spectra in Chapter 4 and training me to operate the DNA/RNA synthesizer, to perform HPLC purifications and bacterial MIC assays.

I thank my colleague, Mr. Andrew Shurer, for synthesizing the sulfonylethyl-ODMT modified CPG beads.

I thank my colleagues, Ms. Jie Zhou, Dr. Lei Yan and Dr. Nirmal Pahadi, for helping me with the preparation and HPLC purifications of c-di-GMP analogs (Chapter 4).

I also thank Drs. Yiu-fai Lam, Yinde Wang and Yue Li for the helpful discussions on NMR and mass spectrometry.

Last but not least, I appreciate the National Science Foundation (CHE0746446) and Bailey Summer Research Scholarship for the generous financial support.

TABLE OF CONTENTS

LIST OF TABLES.....	vii
LIST OF FIGURES	viii
LIST OF SCHEMES.....	xii
LIST OF ABBREVIATIONS.....	xv
 Chapter 1. Introduction.....	 1
1.1 Bacterial antibiotic resistance problem.....	1
1.2 Fatty acid biosynthesis –untapped opportunities to develop novel antibiotics.....	10
1.2.1 Introduction of fatty acid biosynthesis and its inhibition.....	10
1.2.2 Modes of action of type II fatty acid biosyntheses.....	14
1.2.3 Type II FAS inhibitors.....	22
1.2.4 Other considerations when developing new antibiotics.....	35
1.3 Biofilm formation – another important antibiotic target.....	35
1.3.1 Introduction of c-di-GMP signaling.....	35
1.3.2 Polymorphism of c-di-GMP.....	41
 Chapter 2. The synthesis and antibiotic activities of oxazinidinyl platensimycin	 43
2.1 Syntheses of novel FAS inhibitors, platensimycin and platencin.....	43
2.1.1 KAS inhibition by platensimycin and platencin: mechanism of action.....	45
2.1.2 Previous total syntheses of platensimycin and platencin.....	49
2.2 Design, syntheses and antibiotic activities of first generation platensimycin analog – oxazinidinyl platensimycin.....	51
2.2.1 The design of oxazinidinyl platensimycin	52
2.2.2 Synthesis of oxazinidinyl platensimycin	55
2.2.3 Biological evaluation.....	64
 Chapter 3. Syntheses and antibiotic activities of <i>N,N</i> -dialkylamino benzoic acids – second generation design of the platensimycin analogs.....	 66
3.1 The design of dialkylamino benzoic acid analogs	66
3.2 Synthesis and biological evaluation	67

Chapter 4. C-di-GMP mediated biofilm formation in bacteria and efforts towards anti-biofilm agents.....	72
4.1 Endo-S-c-di-GMP, a conservative change to the phosphate moiety of c-di-GMP... ..	72
4.1.1 Introduction.....	72
4.1.2 Synthesis of endo-S-c-di-GMP.....	75
4.1.3 Polymorphism of c-di-GMP and endo-S-c-di-GMP.....	77
4.1.4 C-di-GMP and endo-S-c-di-GMP binding to metabolism and “adaptor” proteins.....	84
4.1.5 Conclusion.....	90
4.2 Design and syntheses of c-di-GMP analogs.....	91
4.2.1 The design of the c-di-GMP analogs.....	91
4.2.2 Previous syntheses of c-di-GMP.....	93
4.2.3 The synthesis of the designed c-di-GMP analogs.....	98
Chapter 5. Conclusions and future directions.....	101
5.1 FAS inhibitors.....	101
5.2 Development of dynamic ring-closing metathesis.....	102
5.3 Biofilm formation in bacteria.....	103
Chapter 6. Experimental details.....	104
6.1 General Experimental.....	104
6.1.1 General reaction conditions.....	104
6.1.2 Preparation of the solvents.....	104
6.1.3 Reagents.....	105
6.1.4 Instruments.....	106
6.2 Synthetic protocols for compounds in Chapter 2.....	108
6.3 Synthetic protocols for compounds in Chapter 3.....	130
6.3.1 Synthetic strategies.....	130
6.3.2 Physical data of the analogs.....	133
6.4 Synthetic protocols for compounds in Chapter 4.....	144
6.4.1 Synthesis of compound 4-1 and 4-2	144
6.4.2 Cleavage of c-di-GMP and endo-S-c-di-GMP by RocR.....	149

6.4.3	Syntheses of compounds 4-52 and 4-53	151
6.4.4	Solid support synthesis (compounds 4-54 to 4-57).....	153
6.5	Details of computations.....	157
6.5.1	Ring-opening reactions.....	157
6.5.2	Calculation of the radii (volumes) of c-di-GMP polymorphs.....	157
6.6	NMR experiments for T1/T2 relaxation analysis (DOSY) and NOE.....	159
6.7	Biological assays.....	160
6.7.1	Minimal inhibitory concentration (MIC).....	160
6.7.2	Enzymatic assays.....	163
Appendix I.	Kinetics of the epimerization reaction.....	164
Appendix II.	Reaction conditions for dynamic ring-closing metathesis.....	167
Appendix III.	Introduction on pulsed gradient spin echo for DOSY experiment.....	171
Appendix IV.	NMR, IR spectra and HPLC chromatography.....	173
References	258

LIST OF TABLES

Table 1–1.	Structural classes, modes of action and antibiotic resistance mechanism of selected antibiotics.....	3
Table 1–2.	New antibiotics approved between 2004–2009	9
Table 1–3.	The antibiotic activities of type II FAS inhibitors.....	25
Table 1–4.	Known c-di-GMP adaptor proteins and RNAs.....	40
Table 2–1.	Microbiological and toxicity profiles of platensimycin, platencin and linezolid.....	44
Table 2–2.	MIC values of platensimycin/ platencin analogs against <i>S. aureus</i>	52
Table 3–1.	MIC values of compounds 3–6 to 3–22	68
Table 3–2.	MIC value of compounds 3–8 , 3–20 and 3–21	69
Table 4–1.	Backbone torsion angles for computed c-di-GMP and endo-S-c-di-GMP structures.....	77
Table 4–2.	Energy difference between “open” and “closed” forms of c-di-GMP and endo-S-c-di-GMP.....	79
Table 6–1.	The computed energies and other thermal parameters for the ring-opening reaction.....	157
Table 6–2.	Calculation of the radii and diffusion coefficients of c-di-GMP polymorphism.....	159

LIST OF FIGURES

Figure 1–1.	Chemical structures of antibiotics.....	4
Figure 1–2.	Chemical structures of recently approved antibiotics....	8
Figure 1–3.	a) The cell wall structure for Gram-positive bacteria; b) chemical structure of phospholipid; c) the cell wall structure for regular Gram-negative bacterium that contains an outer membrane; d) chemical structure of Kdo ₂ -lipid A; e) electron micrograph of the cell wall structure of a special bacteria strain: MTB and its chemical composition; f) the chemical structure of α -mycolic acid.....	12
Figure 1–4.	The catalytic mechanism of <i>S. pneumoniae</i> FabF.....	19
Figure 1–5.	The catalytic mechanism of <i>S. pneumoniae</i> FabG.....	20
Figure 1–6.	Catalytic mechanism of MTB FabI homolog, InhA.....	21
Figure 1–7.	The structures of fatty acid synthesis initiation module inhibitors.....	23
Figure 1–8.	Structures of condensing enzyme inhibitors.....	27
Figure 1–9.	Co-crystal structure of FabF/B proteins with their inhibitors. a) Cerulenin (CER) binding site of ecFabB; b) thiolactomycin (TLM) binding site of ecFabB; c) CER binding site of ecFabF; d) platensimycin binding site of ecFabF (C163Q); e) TLM binding site of MTB KasA, an FabF homolog.....	29
Figure 1–10.	The structures of KR and HD inhibitors.....	31
Figure 1–11.	Structures of FabI/K inhibitors.....	32
Figure 1–12.	a) Co-crystal structure of INH-NAD and InhA; b) benzodiazaborine-NAD and ecFabI; c) Triclosan-NAD and ecFabI.....	33

Figure 1–13.	a) Chemical structure of c-di-GMP and 5'-pGpG; b) proposed mechanism for the regulation of cellulose biosynthesis in <i>Gluconacetobacter xylinus</i>	37
Figure 1–14.	Structure of c-di-GMP and the related biological processes that it regulates.....	38
Figure 1–15.	Proposed catalytic mechanism for EAL domain-containing PDE.....	39
Figure 1–16.	Polymorphism of c-di-GMP. a) Lithium, sodium, ammonium and magnesium cations; b) potassium and aromatic intercalators. G-quadruplexes are formed in tetramolecular and octamolecular c-di-GMP polymorphism.....	42
Figure 1–17.	Co-crystal structures of a) P4397 (PilZ domain) with dimeric c-di-GMP; b) FimX (EAL domain) with monomeric c-di-GMP.....	42
Figure 2–1.	The structures of platensimycin and platencin.....	43
Figure 2–2.	Structure at 2.6 Å resolution of <i>E. coli</i> FabF (C163Q) in complex with platensimycin	45
Figure 2–3	Some critical binding interactions between platensimycin and amino acid residues in the active site of FabF. a) The interactions between the benzoic acid part of platensimycin and the FabF protein; b) Interactions of the tetracyclic ketolide core and the amide linker of platensimycin with the residues of FabF	46
Figure 2–4.	Structures of platencimycin A ₁ , platencin A ₁ and dihydroplatensimycin.....	48
Figure 2–5.	Superposition of the structures of platensimycin/platencin or their analogs to ecFabF (C163A).....	48

Figure 2–6.	The origin of the facial selectivity of reductive amination of compound 2–44 and 2–50	63
Figure 3–1.	Design of second generation of platensimycin/platencin analogs.....	67
Figure 3–2.	Synthesized analogs for the initial screening.....	68
Figure 3–3.	Second set of analogs and probes derived from (–)-myrtemycin.....	69
Figure 4–1.	a) Structures of c-di-GMP and endo-S-c-di-GMP monomer. The structure was optimized by Gaussian 09 software with HF/6-31G(d) basis set; b) two general conformers of c-di-GMP and analogs (open and closed).....	73
Figure 4–2.	¹ HNMR stacked spectra of 1.0 mM c-di-GMP in D ₂ O. Conditions: a) 100 mM KCl, 60 °C; b) 100 mM KCl, 20 °C; the peaks were assigned based on T ₁ /T ₂ relaxation analysis and ref 18; c) no metal cation, 20 °C; d) T ₁ /T ₂ relaxation analysis (from DOSY experiments) with 3 mM c-di-GMP in D ₂ O in 100 mM KCl (blue) or no KCl added (red) solution at 30 °C.....	81
Figure 4–3.	¹ HNMR stacked spectra of 1.0 mM endo-S-c-di-GMP in D ₂ O. Conditions: a) 100 mM KCl, 60 °C; b) 100 mM KCl, 20 °C; the peaks were assigned based on T ₁ /T ₂ relaxation analysis and NOE experiments (see Supporting Information); c) no metal cation, 20 °C; d) T ₁ /T ₂ relaxation analysis (from DOSY experiments) with 3 mM endo-S-c-di-GMP in D ₂ O in 100 mM KCl (blue) or no KCl added (green) solution at 30 °C.....	82
Figure 4–4.	CD spectra of c-di-GMP and endo-S-c-di-GMP.....	84
Figure 4–5.	a) Dimeric c-di-GMP, bound to WspR (DGC); b) dimeric c-di-GMP, bound to P4397 (PilZ domain); c) monomeric c-di-GMP bound to FimX (EAL domain); d) monomeric c-di-GMP bound to TBD1265 (EAL domain).....	86
Figure 4–6.	Inhibition of c-di-GMP synthesis by WspR with guanine-containing nucleotides. a) TLC of reaction mixture at different time points. Initial	

	reaction conditions; WspR, radio-labeled GTP and unlabeled c-di-GMP or endo-S-c-di-GMP or cGMP or no added nucleotide inhibitor); b) graph showing fraction of radio-labeled GTP that was converted into radio-labeled c-di-GMP in the presence of inhibitor.....	88
Figure 4–7.	Displacement of radio-labeled c-di-GMP from Alg44 (PilZ protein) by c-di-GMP, endo-S-c-di-GMP or cGMP. The value of “fraction bound” is inversely proportional to the binding affinity for Alg44.....	89
Figure 4–8.	a) Binding assays of RocR with c-di-GMP or endo-S-c-di-GMP in the presence of Ca ²⁺ ; b) RocR cleavage of endo-S-c-di-GMP only occurs at the natural phosphate site.....	89
Figure 4–9.	Sugar puckering modes in ribose and deoxyribose.....	92
Figure 4–10.	Chemical structures of designed c-di-GMP and endo-S-c-di-GMP analogs.....	93
Figure 5–1.	Structures of platensimycin (5–1), oxazinidinyI platensimycin (5–2) and myrtemycin (5–3).....	102
Figure 5–2	Selected natural products that carry a bicyclo[3.2.1] moiety.....	103
Figure 6–1.	The apparatus for solvent degassing.....	105
Figure 6–2.	a) A real photo of DNA/RNA synthesizer; b) detail illustration of a synthesis column.....	107
Figure 6–3.	HPLC analysis of cleavage of endo-S-c-di-GMP by RocR.....	149
Figure 6–4.	Sulfurization of the phosphonate on CPG beads.....	154
Figure 6–5.	The NOE of <i>syn</i> - and <i>anti</i> - guanosines.....	160
Figure 6–6.	MIC determination for platensimycin analogs against a) <i>S. aureus</i> , b) <i>S. agalactiae</i> and c) <i>B. subtilis</i>	161

LIST OF SCHEMES

Scheme 1–1. Fatty acid biosynthesis in <i>E. coli</i>	15
Scheme 1–2. Biosynthesis of α -mycolic acid.....	16
Scheme 2–1. Nicolaou's first total synthesis of platensimycin.....	50
Scheme 2–2. Snyder's synthesis strategy towards the core structure of platensimycin...	50
Scheme 2–3. Yamamoto's synthesis strategy towards the core structure of platensimycin.....	51
Scheme 2–4. Tiefenbacher and Mulzer's total synthesis strategy of platencin.....	51
Scheme 2–5. Synthetic strategy towards platensimycin analogs.....	54
Scheme 2–6. Retrosynthetic analysis of oxazolidinyl platensimycin.....	55
Scheme 2–7. 6-Exo-tet (pathway a) vs 5-exo-tet cyclization (pathway b).....	55
Scheme 2–8. The energy surfaces of pathway a and b for the epoxide ring-opening reaction.....	56
Scheme 2–9. Reaction conditions: a) LiCH_2OBn , THF, $-78\text{ }^\circ\text{C} \rightarrow \text{RT}$, 12 h, 84 %; b) LDA, HMPA, allyl iodide, THF, $-78\text{ }^\circ\text{C} \rightarrow \text{RT}$, 12 h, 62 % (67 % based on the starting material); c) $\text{Sn}(\text{CHCH}_2)_4$, n-BuLi, CuCN, $\text{BF}_3 \cdot \text{Et}_2\text{O}$, $-78\text{ }^\circ\text{C} \rightarrow \text{RT}$, 12 h, 85 %.....	58
Scheme 2–10. Stacked NMR spectra of epimerization reaction of compound <i>cis</i> - 2–34 and <i>trans</i> - 2–34 under the condition: 30 mol% DBU, 0.02 M substrate (pure <i>trans</i> -bis-alkene 2–34), $100\text{ }^\circ\text{C}$ in d_8 -toluene. The reaction was carried in a 5 mm NMR tube with oil bath and ^1H spectra were collected at room temperature within 5 min.....	58

Scheme 2–11. Dynamic ring-closing metathesis. Reaction conditions: Grubbs-Hoveyda II catalyst (2 % x 5), 50 % DDQ, 30% DBU, toluene, 0.02 M compound 2–34 , reflux, 6 h each loading, 69 %	59
Scheme 2–12. Reaction conditions: a) <i>m</i> -CPBA, dichloromethane, 0 °C→RT, 12 h, 64 %; b) MeLi, THF, –78 °C→RT, 5 h, 70%; c) Dess-Martin reagent, CH ₂ Cl ₂ , RT, 12 h, 95 %; d) 10 mol% Pd/C, H ₂ , MeOH, RT, 12 h, 90 %.....	59
Scheme 2–13. The product distribution of epoxide ring-opening reaction.....	60
Scheme 2–14. Epoxide ring-opening reaction and the stacked NMR spectra of a) reaction mixture in d ₆ -DMSO; b) epoxide ring-opening product 2–36 in CDCl ₃ ; c) epoxide ring-opening starting material 2–32 in CDCl ₃	61
Scheme 2–15. a) NIS, TFA, RT, 12 h, 100 %; b) MOMCl, Hunig base, CH ₂ Cl ₂ , RT, 12 h, 97 %; c) CNCO ₂ Me, PhMgBr, –78 °C → RT, THF, 12h, 78 %; d) MOMCl, Hünig base, CH ₂ Cl ₂ , RT, 12 h, 78 %; e) H ₂ , 10 mol% Pd/C, MeOH, 69%; f) pyridine, benzene, RT → 50 °C, 5 h, 95%; g) K ₂ CO ₃ , MeOH : H ₂ O = 3:1, RT, 10 h, 99 %.....	61
Scheme 2–16. Facial selectivity of reductive amination for a model reaction.....	63
Scheme 2–17. a) NaB(CN)H ₃ , MeOH, pH 4, RT, 5 h, 75%; b) carbonyl diimidazole, 20 mol % DMAP, benzene, 50 °C, 12 h, 76%; c) 1 N LiOH, MeOH: H ₂ O = 2:1, RT, 12 h, then, 2N HCl, MeOH: H ₂ O = 2:1, RT, 24 h, 80%; d) 2 N HCl, MeOH: H ₂ O = 3:1, RT, 24 h, 92%.....	64
Scheme 2–18. a) NaB(CN)H ₃ , MeOH, pH 4, RT, 5 h; then, carbonyl diimidazole, 20 mol% DMAP, benzene, 50 °C, 12 h, 70 %; b) 1 N LiOH, MeOH: H ₂ O = 2:1, RT, 12 h, then, 2N HCl, MeOH: H ₂ O = 2:1, RT, 24 h, 85 %.....	64
Scheme 3–1. A general pathway to generate bis-alkylamino-2,4-dihydroxybenzoic acid analog.....	67
Scheme 4–1. Synthesis of endo-S-c-di-GMP (4–2).....	76

Scheme 4–2. Cyclic di-UMP synthesis by Dennis and Jones.....	94
Scheme 4–3. Jones' H-phosphonate strategy for c-di-GMP synthesis.....	96
Scheme 4–4. Sintim's solid support synthesis of c-di-GMP.....	97
Scheme 4–5. Solid-support synthesis of dinucleotides and cyclization in solution phase.....	99
Scheme 4–6. a) Cleavage of nucleotide from CPG support, deprotection of cyanoethyl group and cyclization to afford endo-S-c-di-GMP analogs; b) the mechanism of sulfurization, using the Beaucage reagent.....	100
Scheme 6–1. Chemical synthesis of sulfonylethyl-ODMT beads.....	105
Scheme 6–2. General synthesis of platensimycin analogs: a) synthesis of <i>N</i> -di-alkyl analogs; b) synthesis of <i>N</i> -mono-alkyl analogs; c) synthesis of <i>N</i> -sulfonyl analogs; d) synthesis of acyl analogs.....	132
Scheme 6–3. Synthesis of compound 3–16	138
Scheme 6–4. Synthesis of compounds 4–52 and 4–53	152

LIST OF ABBREVIATIONS

ACC	acetyl-CoA carboxylases
ACP	acyl carrier protein
AcpS	ACP synthase
BSA	benzenesulfonic acid
CCCP	carbonyl cyanide <i>m</i> -chlorophenylhydrazone
CD	circular dichroism
CER	cerulenin
CPG	controlled pore glass
DBN	1,5-diazabicyclo[4.3.0]non-5-ene
DBU	1,8-diazabicyclo[5.4.0]undec-7-ene
DGC	diguanylate cyclases
DMAP	4-dimethylaminopyridine
DMF	dimethylformamide
DMT	dimethoxyl trityl
DNA	deoxyribonucleic acid
EGCG	Epigallocatechin gallate
ER	enoyl-ACP reductase
ETT	5-ethylthio-1 <i>H</i> -tetrazole
FAS	fatty acid synthase
FDA	Food and Drug Administration
GMP	guanosine monophosphate
GTP	guanosine triphosphate
G3P	glycerol-3-phosphate
HD	β -hydroxyacyl-ACP dehydrase
HIV	human immunodeficient virus
HMPA	hexamethylphosphoramide
INA	isoniazid
KAS	β -ketoacyl-acyl-carrier-protein synthase
KR	β -ketoacyl-ACP reductase
LDA	lithium diisopropylamine

LHDMS	lithium bis(trimethylsilyl)amide
MIC	minimal inhibitory concentration
MDR	multi-drug resistance
MOM	methoxymethyl
MRSA	methicillin-resistant <i>S. aureus</i> OR multi-drug-resistant <i>S. aureus</i>
MTB	<i>M. tuberculosis</i>
MTBD	7-methyl-1,5,7-triazabicyclo[4.4.0]dec-5-ene
NAD	nicotinamide adenine dinucleotide
NADP	nicotinamide adenine dinucleotide phosphate
NBO	2-nitrobenaldoxime
NIS	<i>N</i> -iodo succinimide
NMR	nuclear magnetic resonance
PAβND	L-phenylalanine-L-arginine-β-naphthylamide dihydrochloride
PDB	protein databank
PDE	phosphodiesterase
pGpG	5'-phosphoguanylyl-(3'-5')-guanosine
RNA	ribonucleic acid
rRNA	ribosomal RNA
TBD	1,5,7-triazabicyclo[4.4.0]dec-5-ene
TBS	<i>tert</i> -butyldimethylsilyl
TFA	trifluoroacetic acid
THF	tetrahydrofuran
TPSCI	2,4,6-triisopropyl-benzenesulfonylchloride
UMP	uridine monophosphate
VRE	vancomycin-resistant <i>Enterococci</i>

Chapter 1. Introduction

1.1 Bacterial antibiotic resistance problem

(The majority of this section was published in ref [1].)

The discovery of several antibiotics between the 1930s and 1960s led to effective management of previously lethal bacterial infections [2,3]. Several lethal epidemic diseases, caused by bacteria, were even considered extinct around 1980 in the western world (e.g. bubonic plague [4]). This success story did not last long, and soon multi-drug resistant bacteria (the so-called superbugs) emerged in hospital wards. It is hypothesized that the indiscriminate use of antibiotics in both hospitals [5,6] and animal farms [7] and pollution of the environment with antibiotics, which are added to general household products [8], contribute the rise of antibiotic resistance in bacteria.

Modern use of antibiotics probably began with the administration of sulfonamides (e.g. prontosil, compound **1–1** in **Figure 1–1**) and penicillins (e.g. penicillin G, compound **1–2**) to patients. Penicillin was once called the “magic drug”, and it contributed to reducing the number of deaths among soldiers in World War II, who were infected with *Streptococcus pneumonia* [9]. After early resistance to penicillin was observed [10–12], a new generation of β -lactam antibiotics, such as methicillin (**1–3**), cephalothin (**1–4**) and imipenem (**1–5**), were developed [13]. In 1964, a methicillin-resistant strain of *S. aureus* (MRSA) was isolated [14,15]. Sooner thereafter, other bacterial strains that were resistant to various antibiotics, e.g. streptomycin [16,17] (**1–8**), chloramphenicol [18] (**1–9**) and tetracycline [19,20] (**1–6**) were also identified. It is now widely recognized that bacteria can develop resistance to almost any antibiotic.

Table 1–1 lists several classical antibiotics and showcases the severity of the antibiotic resistance issue. With the exception of few antibiotics, e.g. vancomycin (**1–14**), bacteria developed resistance to most antibiotics within 15 years after their first clinical use. In the case of vancomycin [21], it took almost three decades, after the drug was first introduced into the US market, for scientists to observe the emergence of resistant bacteria strains (**Table 1–1**, Entry 7).

In the last few decades, scientists have put tremendous efforts into researching the mechanisms of antibiotic resistance. The three main strategies that are used by bacteria to develop resistance to antibiotics are:

- 1) Overexpression of enzymes that can modify the antibiotic to make it less effective.
- 2) Mutation of the antibiotic target site so that the target (e.g. enzymes) can maintain its function but not bind to the antibiotic.
- 3) Export of the antibiotic to the extracellular media by multidrug-resistant (MDR) efflux pumps or loss of porin channels resulting in lower permeability of the antibiotic.

Table 1–1. Structural classes, modes of action and antibiotic resistance mechanisms of selected antibiotics

Entry	Antibiotics	Structural class	Year introduced	Target process	Year resistance observed in hospital
1	Prontosil (1-1)	sulfonamides	1935	Inhibition of DNA/RNA synthesis (binds to dihydropteroate synthase)	1943[22]
2	Penicillin G (1-2)	β -lactams	1943	Inhibition of cell wall synthesis (binds to transpeptidase)	1945[11,12]
3	Streptomycin (1-8)	aminoglycosides	1943	Inhibition of protein synthesis (binds to the 16S site of 30S rRNA)	1945[16]
4	Chloramphenicol (1-9)	amphenicols	1947	Inhibition of protein synthesis (binds to the 23S site of 50S rRNA)	1950[18]
5	Tetracycline (1-6)	tetracycline	1948	Inhibition of protein synthesis (binds to the 16S site of 30S rRNA)	1963[19,20]
6	Erythromycin (1-7)	macrolides	1952	Inhibition of protein synthesis (binds to the 23S site of 50S rRNA)	1956[23]
7	Vancomycin (1-14)	glycopeptides	1956	Inhibition of cell wall synthesis (binds to D-Ala-D-Ala terminus of the peptidoglycan)	1984[21]
8	Polymyxin B (1-17)	polypeptides	1960s	Disrupt outer and inner membranes (binds to lipopolysaccharide)	1975[24]
9	Methicillin (1-3)	β -lactams	1960	Inhibition of cell wall synthesis (binds to transpeptidase)	1964[14,15]
10	Ciprofloxacin (1-13)	quinolones	1987 ^[a]	Inhibition of DNA replication (binds to bacterial DNA gyrase)	1990[25,26]
11	Cephalothin (1-4)	β -lactams	1964	Inhibition of cell wall synthesis (binds to transpeptidase)	1965[27]
12	Rifampicin (1-12)	rifamycins	1967	Inhibition of RNA synthesis (binds to RNA polymerase β subunit)	1968[28,29]
13	Clindamycin (1-16)	lincosamides	1969	Inhibition of protein synthesis (binds to the 23S site of 50S rRNA)	1970[30,31]
14	Imipenem (1-5)	β -lactams	1985	Inhibition of cell wall synthesis (binds to transpeptidase)	1988[32,33]
15	Quinupristin/dalfopristin (1-11)	streptogramin	1999 ^[b]	Inhibition of protein synthesis (binds to the 23S site of 50S rRNA)	1999[34,35]
16	Linezolid (1-10)	oxazolidinones	2000	Inhibition of protein synthesis (binds to the 23S site of 50S rRNA)	2001[36,37]
17	Daptomycin (1-15)	lipopeptides	2003	Depolarization of bacterial membrane	2005[38]

[a] Other quinolones were discovered in the 1960's; [b] other streptogramin antibiotics were developed prior to this year including virginiamycin and pristinamycin.

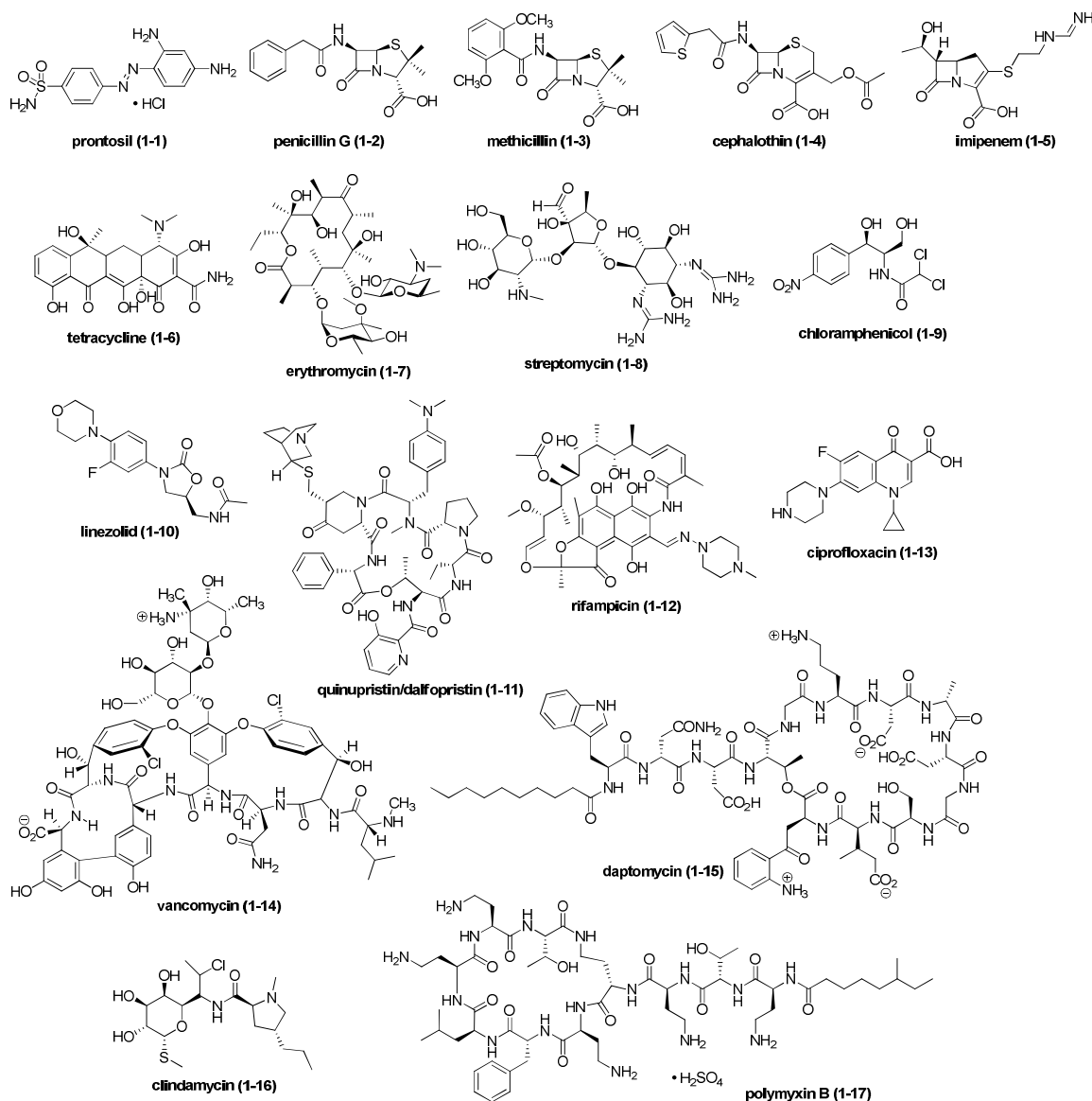


Figure 1–1. Chemical structures of antibiotics

β -Lactam drugs such as penicillin G (**Figure 1–1**, compound **1–2**), methicillin (**1–3**), cephalothin (**1–4**) and imipenem (**1–5**) are mainly inactivated via the overexpression of β -lactamases, which hydrolyze the antibiotics [39]. For an excellent review on the mechanism of action of β -lactamases, see ref [40]. Resistance to β -lactams via β -lactamase-mediated hydrolysis can be minimized when the β -lactam antibiotic is used in combination with β -lactamase inhibitors such as clavulanic acid [41], tazobactam[42] and

sulbactam [43]. Both clavulanic acid and sulbactam irreversibly inactivate β -lactamases [41,44]. Unfortunately there are documented cases where some bacterial strains have been shown to be resistant to these β -lactamase inhibitors – a very worrisome scenario [45,46].

Another antibiotic class, aminoglycosides, including streptomycin (**1–8**, **Figure 1–1**) and tobramycin, can inhibit bacterial ribosome function and hence inhibit protein synthesis [47,48]. Aminoglycosides are rendered ineffective by bacteria via the overexpression of antibiotic-modifying enzymes, such as nucleotidyltransferase or phosphotransferase, which transfer a monophosphate moiety from ATP to a hydroxyl on the ring of an aminoglycoside [49]. Other aminoglycoside modifying enzymes include *N*-acetyltransferases and *O*-adenyltransferases. These two enzymes catalyze acetyl CoA-dependent acetylation of the amino functionality (**1–8**) and ATP-dependent adenylation of the hydroxyl group (**1–8**), respectively [49]. Other protein synthesis inhibitor antibiotics, such as the streptogramins and oxazolidinones (e.g. linezolid), are made ineffective via the modification of the 23S site of 50S ribosomal RNA in bacteria [50,51].

Bacteria can also use multiple pathways to inactivate an antibiotic. For example, resistance to vancomycin (**1–14**) can occur via thickening of the bacterial cell wall [52], changing the peptidoglycan precursor [53,54] or expression of an ‘abnormal’ ligase that makes the unusual Ala-lactate peptide bond [55,56].

Efflux pump proteins such as AcrA and AcrB in *E. coli* [57,58], the MexA-MexB-OprM systems in *P. aeruginosa* [59,60] and NorA in *S. aureus* [61] export antibiotics out of bacterial cells, thereby raising the MIC (minimum inhibitory concentration) values of antibiotics. Proton motive force inhibitor (or commonly referred

to as energy uncoupler), carbonyl cyanide *m*-chlorophenylhydrazone (CCCP) [62,63] and MDR (multidrug-resistant) efflux pump inhibitors e.g. L-phenylalanine-L-arginine- β -naphthylamide dihydrochloride (PA β ND) [64,65], reserpine [66,67], biricodar [68] and timcodar [68] have been shown to potentiate the antibiotic activity of conventional antibiotics. The widespread use of MDR efflux inhibitors as combination therapeutics is probably not as popular as the use of β -lactamase inhibitors, due to the dearth of effective but non-toxic bacterial MDR efflux pump inhibitors.

After years of the development of second- and third-generation antibiotics, which ultimately suffered from bacterial resistance, two new drugs were introduced at the beginning of the new millennium: daptomycin (compound **1–15**, **Figure 1–1**) [69,70] and linezolid (**1–10**) [71,72]. Linezolid (**1–10**) is a synthetic oxazolidinone antibiotic, which was initially effective against vancomycin-resistant *Enterococci* (VRE) and MRSA [72]. Linezolid inhibits protein synthesis by binding to the 23S site of the 50S ribosome RNA [73]. Although its action is similar to the macrolides and amphenicols, no cross-resistance was observed [71]. Regretfully, linezolid resistance was reported in VRE and MRSA only a few years after it was introduced [36,74]. Daptomycin (**1–15**), a natural lipopeptide antibiotic, was also introduced in the early 21st century. Daptomycin kills bacteria via a novel mode of action involving binding to the bacterial cell wall and depolarizing the cell membrane [75]. Again, the early excitement regarding daptomycin's ability to kill MRSA and VRE was diminished upon the identification of strains of MRSA and VRE that were resistant to daptomycin (**1–15**) [76,77]. Only a handful of antibiotics have been approved by the United States FDA for clinical use in the past few years (see **Table 1–2** and **Figure 1–2**) [78-84]. Worryingly, these newer antibiotics (with

the exception of retapamulin) are merely derivatives of older generation antibiotics. Since the newer antibiotics are acting on the same targets, which have been shown to be evolvable, it would be naive to think that the newly introduced antibiotics will not ultimately suffer from bacterial resistance.

Retapamulin (compound **1–21**, **Figure 1–2**), introduced in 2007, belongs to a new class of antibiotics called pleuromutilins. It inhibits protein biosynthesis by binding to the peptidyl transferase center of the 23S ribosomal RNA, which is located on the 50S subunit and, thus, prevents peptide bond formation [85,86]. Retapamulin (**1–21**) may also destabilize transfer RNA in the P-site of the 50S subunit [86]. However, bacteria have shown in the past that ribosomal targets can be modified in order to abrogate antibiotic inhibition, and there is no reason to suggest that the 50S ribosome RNA is not evolvable.

The previous discussion highlights an unsavory truth: we are in a never-ending battle against pathogenic bacteria. The ability of bacteria to find several pathways to render a bacteriocidal or bacteriostatic antibiotic ineffective, coupled with the lack of newer druggable targets in bacteria and the paucity of new structural classes of antibiotics, implies that there might be a need for a paradigm shift in the strategies used to treat bacterial infections.

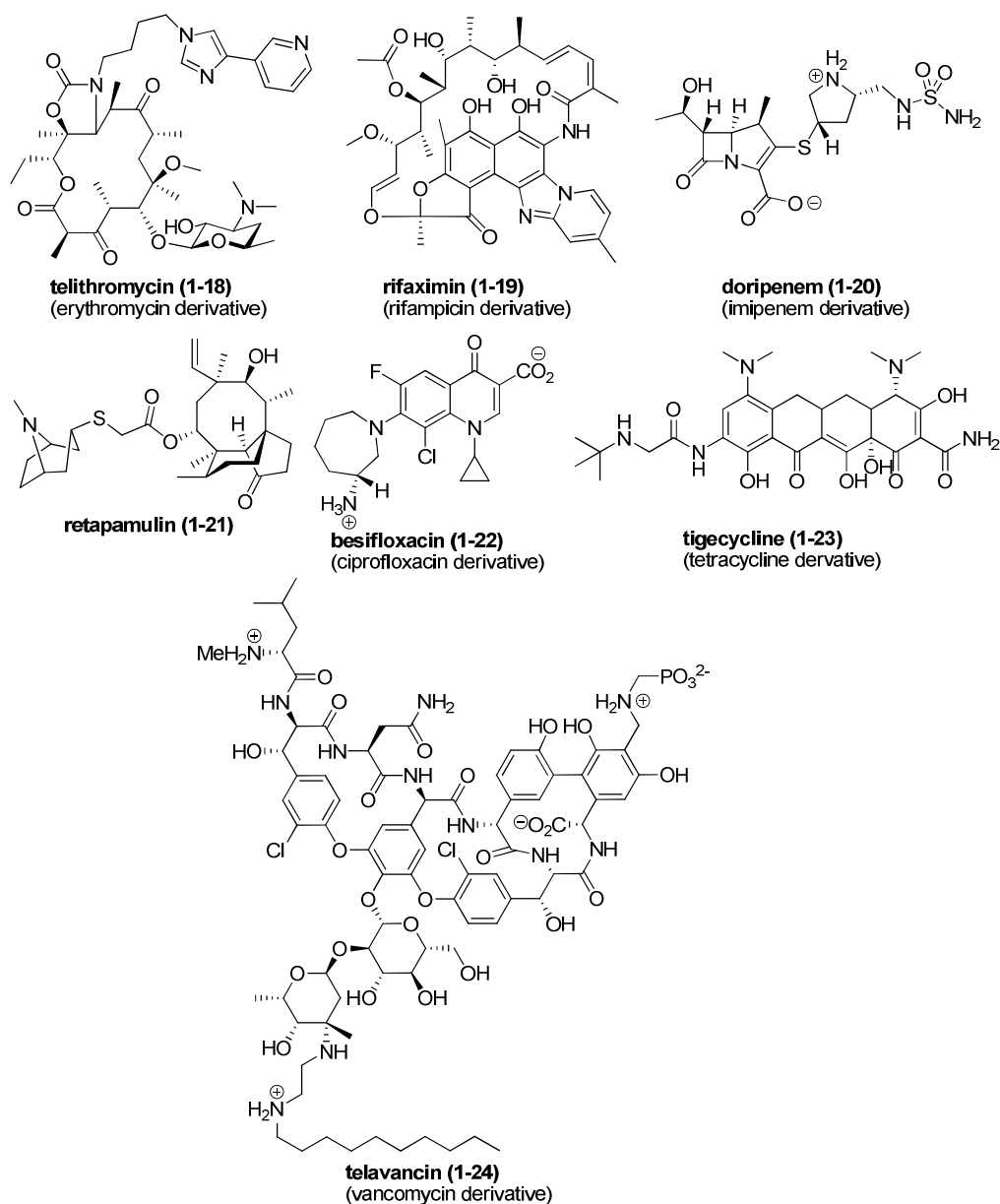


Figure 1–2. Chemical structures of recently approved antibiotics.

Table 1–2. New antibiotics approved between 2004–2009 [78-84].

Antibiotic	Structural class (lead compound)	Year Introduced into US market	Target process	Indication
Telithromycin (1–18)	macrolides (erythromycin)	2004	inhibition of protein synthesis (binds to 50S rRNA)	bronchitis, sinusitis, pneumonia etc.
Rifaximin (1–19)	rifamycins (rifampicin)	2004	inhibition of DNA-dependent RNA synthesis	travelers' diarrhea, gastrointestinal infections etc.
Tigecycline (1–23)	tetracyclines (tetracycline)	2005	inhibition of protein synthesis (binds to 30S rRNA)	skin and soft tissue infections etc.
Doripenem (1–20)	β -lactams (imipenem)	2007	inhibition of cell wall synthesis (binds to transpeptidase)	intra-abdominal, urinary tract infections etc.
Azithromycin ^[a]	macrolides (erythromycin)	2007	inhibition of protein synthesis (binds to 50S rRNA)	conjunctivitis etc.
Retapamulin (1–21)	pleuromutilin	2007	inhibition of protein synthesis (binds to 50S rRNA)	impetigo etc.
Amoxicillin ^[a]	β -lactams (penicillin)	2008	inhibition of cell wall synthesis (binds to transpeptidase)	tonsillitis, pharyngitis etc.
Besifloxacin (1–22)	quinolones (ciprofloxacin)	2009	inhibition of DNA replication (binds to bacterial DNA gyrase)	conjunctivitis etc.
Telavancin (1–24)	glycopeptides (vancomycin)	2009	inhibition of cell wall synthesis and depolarization of bacterial membrane	skin infections etc.

[a] These antibiotics were already in the market but were reintroduced for new indications.

1.2 Fatty acid biosynthesis – untapped opportunities to develop novel antibiotics

1.2.1 Introduction of fatty acid biosynthesis and its inhibition

Fatty acids play a key role in bacterial cellular structures and functions. Therefore, fatty acid synthases (FAS) are considered promising targets for the development of new antibiotics to resolve the rising drug resistant problem [87-91].

Fatty acids are key components of phospholipid and lipid A, important components of cell envelope in Gram-positive (e.g. *S. aureus*) and Gram-negative (e.g. *E. coli*) bacteria. Phospholipid (**Figure 1–3b**) is the major constituent of cellular membrane of almost all bacteria strains [92], whereas lipid A is mostly found in Gram-negative bacteria [93]. Unlike the cell wall of Gram-positive bacteria (**Figure 1–3a**), which mainly consists of peptidoglycan and teichoic acids, the cell wall of Gram-negative bacteria have a second membrane which contains lipopolysaccharides and lipoproteins (**Figure 1–3c**); and this lipid component is termed lipid A (**Figure 1–3d**). Among all the bacteria strains, the fatty acid biosynthesis of *E. coli* is the most extensively studied, and the biosynthesis pathways in this organism are summarized in **Scheme 1–1**.

The cell envelope (i.e. the cell membrane and cell wall) of *M. tuberculosis* (MTB) is distinct from either typical Gram-positive or -negative bacteria (**Figure 1–3d**). MTB infections are difficult to treat, and the World Health Organization reported in 2010 that there are still about two billion people in the world who carry MTB and that more than two million people die from MTB infections each year in the world [94,95]. This makes MTB the number one killer bacteria in the world. Fatty acids make up to approximately 60 % of the dry weight of a MTB bacterium. Among the MTB fatty acids, long-chain

mycolic acid (e.g. α -mycolic acid, **Figure 1–3f**), which is unique to MTB, is one of the best studied. The biosynthesis of α -mycolic acid is well characterized (**Scheme 1–2**).

In summary, the inhibition of fatty acid synthesis will disrupt bacterial cell envelope formation and function. The intermediates in the fatty acid biosynthesis pathways are also used in cellular regulation and metabolism. For example, in quorum sensing (bacterial communication) of *V. fischeri*, the signal molecule (acyl homoserine lactone) is synthesized from hexanoyl-ACP (ACP = acyl carrier protein) [96]. Also, lipid A in Gram-negative bacteria pathogens is not only used as a shield to the external chemical insult, but is also responsible for the toxic syndrome associated with bacterial infection by inhibiting the activation of human immune system [97].

The next section will focus on the mechanisms of the fatty acid biosynthesis in *E. coli* and mycolic acid biosynthesis in MTB. Some mechanisms (e.g. elongation steps) of FAS enzymes for many other bacteria strains (e.g. Gram-positive bacteria) are expected to be similar to these two strains.

Fatty acid biosynthesis can be classified into two categories, type I and type II, according to their genetic features. Type I fatty acid synthesis has mainly been found in eukaryotes (e.g. mammal, bird and yeast cell) and very rarely in prokaryotes (e.g. *Mycobacterium* cell). Type II fatty acid synthesis is mainly found in prokaryotes (bacteria) and some plants [101]. Type I FAS in most eukaryotes are encoded by one single gene, and the substrate does not fall off the multifunctional enzyme before synthesis is completed [102,103]. For example, the whole metabolic pathway for making 16-carbon fatty acids in yeast is carried out by a 2.6 MDa fatty acid synthase, which contains eight different active sites for catalysis [104]. On the other hand, the FAS enzymes of most prokaryotes are encoded by discrete genes, and these enzymes belong to type II.

MTB has both type I and type II FAS. During the biosynthesis of mycolic acid, type I FAS first synthesizes a 20-carbon fatty acid, and then type II FAS takes this 20-carbon substrate and continues with the synthesis of mycolic acid (**Scheme 1–2**).

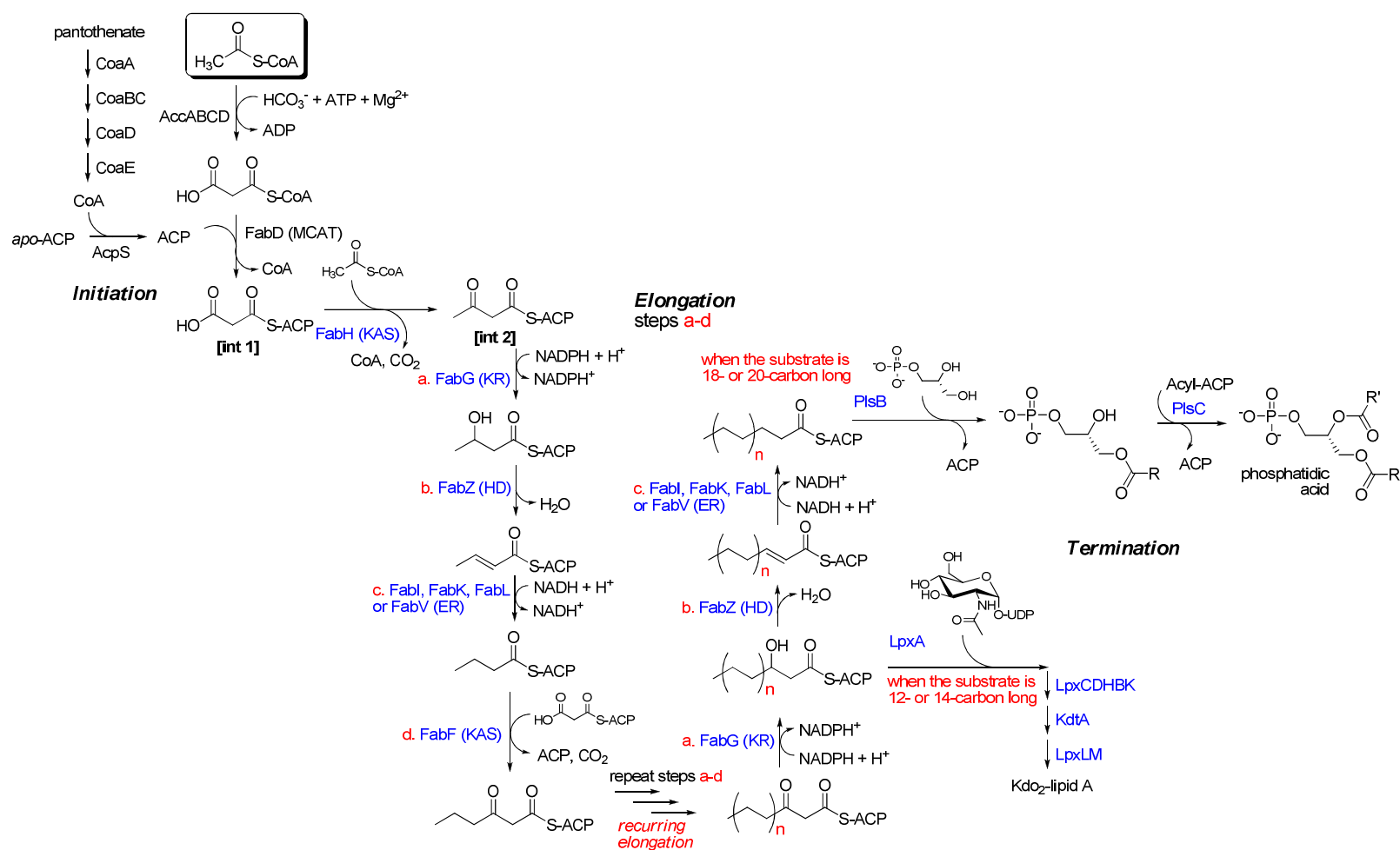
Generally speaking, type I FAS is more efficient than type II, and the products of type I are less diverse than type II [105,106]. Type II FAS can produce various chain lengths, unsaturated chains, branch chains, cyclic chains and hydroxy fatty acids [107]. Type I FAS (mostly in eukaryotes), on the other hand, usually only produces saturated, straight chain 16-carbon palmitic acid [105]. Despite the fact that the overall architectures of type I and II FAS enzymes are different, the catalytic mechanisms for the enzymatic reactions or the active site architectures of the enzymes are similar. Consequently, some small molecules can inhibit both type I and II FAS enzymes. For example, cerulenin is a potent inhibitor of bacterial type II FAS and can also inhibit type I FAS enzymes in

mammals [108]. Cerulenin is a transition-state mimetic and is bound to FAS enzymes via a covalent linkage [109,110].

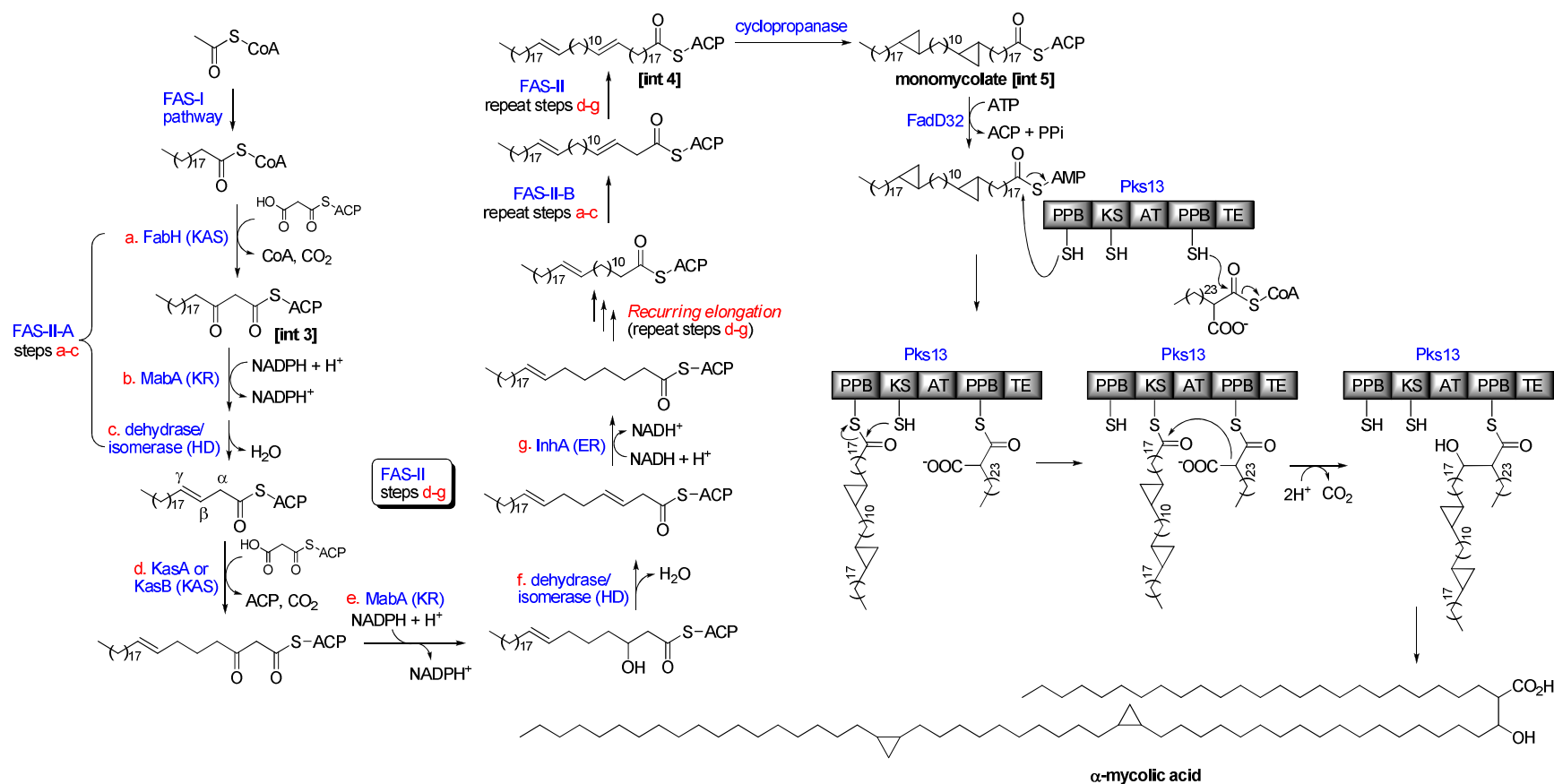
Some amino acid sequences of type II FAS enzymes are highly conserved. For example, the His-His-Cys catalytic triad is present in all of the condensing enzymes that are involved in the elongation steps (FabF and FabB) [111]. The conservation of the His-His-Cys catalytic triad in most FAS elongation enzymes presents a good opportunity to design small molecules that could inhibit FAS in diverse bacteria.

1.2.2 Modes of action of type II fatty acid biosyntheses

Bacterial fatty acid biosynthesis has three modules: initiation, elongation and termination (**Scheme 1–1** outlines the fatty acid biosynthesis in *E. coli*). It should be pointed out that in most bacteria, the strategies and/or mechanisms used to elongate fatty acids are similar to those used in *E. coli*, although alternative mechanisms may exist in some bacteria.



Scheme 1–1. Fatty acid biosynthesis in *E. coli*. During initiation step, acetyl-CoA is converted into malonyl-ACP (**int 1**), catalyzed by Acc protein and FabD. This is followed by a decarboxylative condensation, catalyzed by FabH to give acetoacetyl-ACP (**int 2**). During the elongation phase, two carbons are added in each cycle (step a–d). When a threshold chain length is reached, an intermediate in the elongation cycle is transferred to the termination pathway to produce phospholipid or lipid A.



Scheme 1–2. Biosynthesis of α -mycolic acid. Co-existence of type I and type II FAS system in bacteria is very rarely observed but occurs in mycobacteria. A 20-carbon long CoA thioester, synthesized by type I FAS system, is further extended by type II FAS to give an unsaturated 22-carbon CoA thioester (**int 3**). Subsequent elongations (recurring) then afford bis-alkene (**int 4**), which is then acted upon by cyclopropanase to give monomycolate (**int 5**). Monomycolate (**int 5**) is modified by FadD32 and a multidomain protein Pks13 to furnish the final product α -mycolic acid [112].

In *E. coli*, the initiation phase of fatty acid synthesis starts with the conversion of acetyl-CoA into malonyl-CoA, catalyzed by acetyl-CoA carboxylases (ACC). The ACC reaction requires four discrete enzymes, AccA, AccB, AccC and AccD, and the overall reaction is a biotin-dependent carboxylation of acetyl-CoA to form malonyl-CoA [113]. MTB has a similar initiation phase (not shown in **Scheme 1–2**). ACC is considered to be a promising target for antibiotic discovery. For example, NCI-65828 (see **Figure 1–7**; a small molecule belonging to the NCI small molecule diversity set) has a K_i value of 13 μM to AccD5 (i.e. $\beta 5$ subunit of AccD) of MTB [114].

One of the most abundant proteins in the bacterial cell is acyl carrier protein (ACP). ACP ($< 9,000$ Da in most cases) is a small and diffusible protein and is a necessary enzyme for the initiation step of fatty acid synthesis in all bacteria strains. ACP is converted from an inactive to an active form by ACP synthase (AcpS) from apo-ACP. Several inhibitors of AcpS that are effective in various bacterial strains have been discovered. For example, anthranilic acid and analogs have MICs around 32 μM against *S. aureus* (MRSA) and *B. subtilis* (168) [115]. The activated ACP then reacts with malonyl-CoA to form malonyl-ACP via a reaction that is catalyzed by transacylase (FabD, see **Scheme 1–1**). From this point on, the ACP will be a cofactor protein for all of the subsequent reactions until the acyl chain is transferred to the termination steps. For *E. coli*, malonyl-ACP can directly enter the elongation cycle by reacting with an acetyl-CoA catalyzed by FabH (**Scheme 1–1**). Whereas for MTB, malonyl-ACP first reacts with a 20-carbon ester, catalyzed by FabH, to give a 1,3-keto thioester, which is then converted to a β,γ -unsaturated ACP thioester by reductase, dehydrase and isomerase enzymes (FAS-II-A, **Scheme 1–2**). The mode of action of the dehydrase/isomerase in MTB FAS-II-A

pathway is still not clear. The resulting β,γ -unsaturated ACP thioester (22-carbon) then enters the elongation steps (FASII, **Scheme 1–2**). For either *E. coli* or MTB, four types of enzymes are involved in the elongation cycle: β -ketoacyl-ACP synthases (KAS), β -ketoacyl-ACP reductase (KR), β -hydroxyacyl-ACP dehydrase (HD) and enoyl-ACP reductase (ER) (**Scheme 1–1**). The acyl chain is elongated via the addition of two carbons during each cycle.

There are three known β -ketoacyl-ACP synthases (KAS) in *E. coli*, FabH, FabF and FabB. These three KAS enzymes all belong to the thiolase superfamily [111], which catalyze Claisen condensation reactions. Thus the KAS enzymes are also called condensing enzymes or KAS I–III in various literature reports (e.g. ref [116]). In MTB the three enzymes are referred to as FabH, KasA and KasB. FabH only catalyzes the first two condensation reactions in *E. coli*. For the first condensation, *E. coli* uses acetyl-CoA as the primer and malonyl-ACP as the acceptor to form the acetoacetyl-ACP as the product. For the second elongation cycle, the 4-carbon thioester ACP is used as primer instead [117]. Longer chains (C6 and up) require FabF and FabB for the condensation reactions. FabB is not efficient at elongating intermediates with long, saturated side chains, whereas FabF can elongate intermediates with both saturated and unsaturated side chains [116]. For MTB, FabH only catalyzes the first condensation reaction before the elongation (FASII, **Scheme 1–2**). The active site of FabH (both *E. coli* and MTB) contains a His-Asn-Cys catalytic triad, whereas those of both FabF and FabB have a His-His-Cys triad. **Figure 1–4** shows the catalytic mechanism of spFabF (sp means the protein was from *Streptococcus pneumoniae*) [118]. The thiol in the active site (Cys164) is activated into a thiolate, and the nucleophilic thiolate then attacks the carbonyl-ACP

substrate and transfers the acyl group. His303 and His337 are both protonated, and they stabilize the negative charge on the malonyl-ACP. After decarboxylation, the formed carbonanion will then attack the thioester on Cys164 [118]. It is also worth-noting that during the second thioester transfer, the amide bonds of Cys164 and Phe396 can stabilize the oxyanion intermediate via two hydrogen bonds, and this oxyanion binding site is usually refer as to an “oxyanion hole” in literature (**Figure 1–4**) [111]. The basic mechanisms of all the condensing enzymes are the same. For FabH, one of the histidines at the active site is replaced by an asparagine. In *E. coli*, FabF and FabB are homologous with 37 % sequence identity [87]. Consequently, FabB/F inhibitors often have similar structural features [87]. The best FabH and FabB/F inhibitors to Gram-positive bacteria discovered so far are platencin [119] and platensimycin [120] respectively. Platencin has an IC_{50} value of 16 μM against FabH [119], and platensimycin has an IC_{50} value of 0.048 μM against FabF in *S. aureus* [120]. In MTB, KasA and KasB are homologs of ecFabB and ecFabF (ec means *E. coli*), respectively [121].

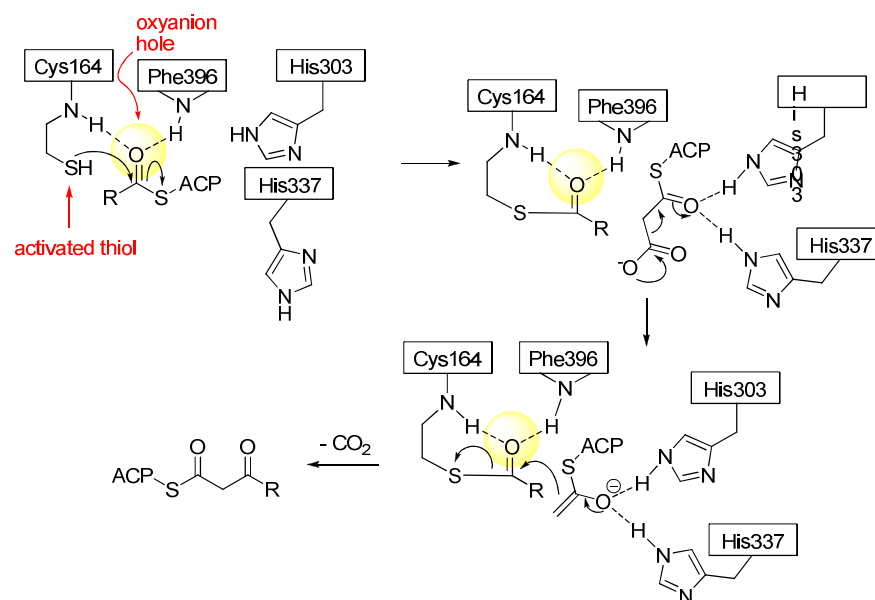


Figure 1–4. The catalytic mechanism of *S. pneumoniae* FabF [118].

KR (β -ketoacyl-ACP reductase, usually referred to as FabG) is a NADPH-dependent reductase that converts β -ketoacyl-ACP into β -hydroxyacyl-ACP [87]. Analysis of the X-ray crystal structure of KR (PDB code: 1Q7B) suggests that the hydride transfer from NADPH to the ketone carbon is probably facilitated by a Ser-Tyr-Lys hydrogen bonding relay (**Figure 1–5**). And this Ser-Tyr-Lys triad was found in various bacteria strains, including *Streptococcus pneumonia* [122], *E. coli* [123] and MTB (in MTB, KR is often referred to as MabA) [124].

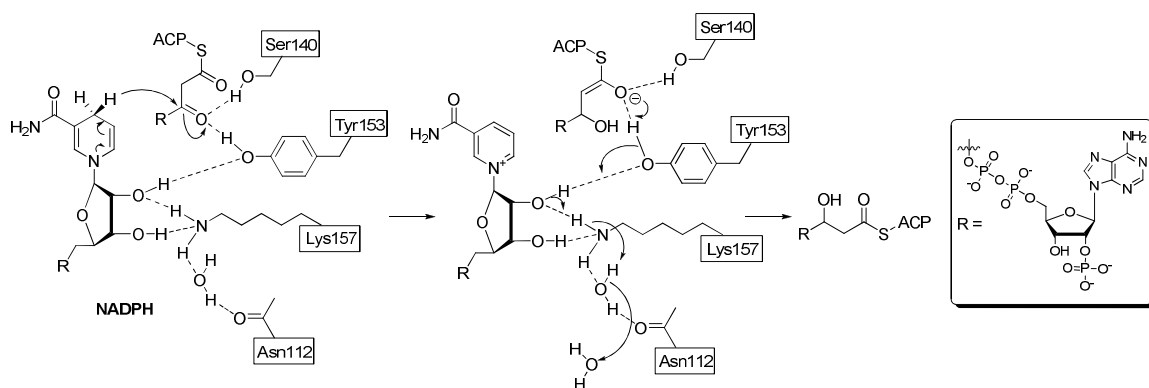


Figure 1–5. The catalytic mechanism of *S. pneumoniae* FabG [122].

In *E. coli*, β -hydroxyacyl ACP is dehydrated by HD (β -hydroxyacyl-ACP dehydrase), which is either FabZ or FabA. FabA is a bifunctional enzyme in *E. coli* that can dehydrate/ isomerize the substrate to give unsaturated intermediates or products. It is worth-noting that FabA is very narrow distributed in bacteria, and has only been observed in Gram-negative α - and γ -proteobacteria till today [125]. It is still unclear how MTB isomerize the double bonds via FAS-II-A and B (**Scheme 1–2**). Gram-positive bacteria do not have the homolog of ecFabA either. In *Enterococcus faecalis*, FabZ1 is the equivalent bifunctional isomerase/ dehydrase [125].

FabI, a NADH-dependent ER (enoyl-ACP reductase), is the last player to complete the elongation process of fatty acids in *E. coli*. Three other isoforms of ER in other bacteria strains, FabK, FabL and FabV, are also found [126]. Some bacteria strains can utilize more than one ER for fatty acid synthesis [127]. ER is a proven antibiotic target and isoniazid, which is an inhibitor of ER, has been used clinically to combat MTB since 1950's [87].

The catalytic mechanism of ER in MTB (referred to as InhA) is very similar to KR (**Figure 1–5, 1–6**). Instead of Ser-Tyr-Lys triad, InhA possesses a Phe-Tyr-Lys triad, where phenylalanine (Phe149) is probably used to direct the hydride transfer [128]. Studies utilizing isotopically enriched NADH (deuterated NADH) showed that Tyr158 probably does not act as a proton donor, but rather performs the role of an electrophilic catalyst [129]. In *E. coli*, FabI has a Tyr-Tyr-Lys triad, but the replacement of one of the tyrosines (Tyr158) with phenylalanine has no effect on catalysis [130]. This probably suggests that the catalytic mechanisms of ecFabI and InhA are similar.

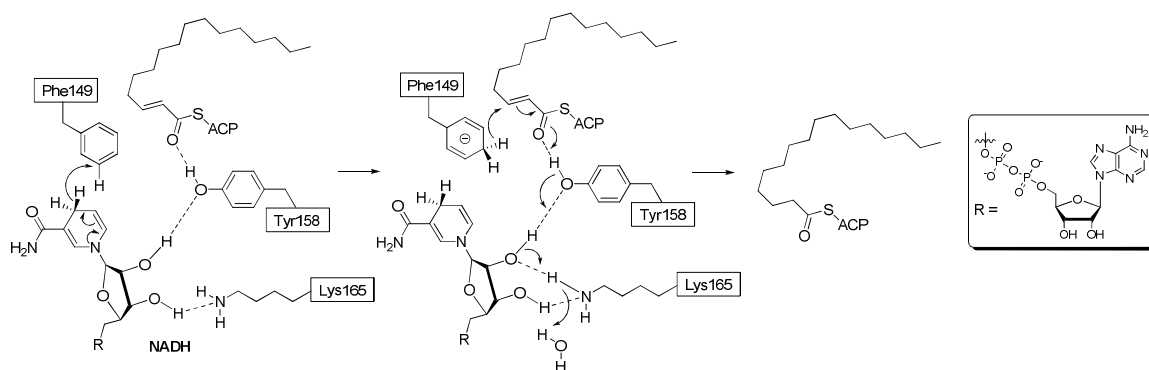


Figure 1–6. Catalytic mechanism of MTB FabI homolog, InhA [128].

In typical Gram-positive or Gram-negative bacteria, the final long-chain carbon acyl-ACP will then react with glycerol-3-phosphate (G3P) to start the phospholipid

biosynthesis (see **Scheme 1–1**) [131]. In Gram-negative bacteria β -hydroxyacyl-ACP is transported into the cell inner membrane and used for lipid A biosynthesis. The biosyntheses of both phospholipid and lipid A are beyond the scope of this thesis, and the interested reader should refer to recent reviews for more information [99,132]. In MTB mycolic acid biosynthesis the resulting 24 carbon acyl-ACP substrate will repeat the FAS-II-A (referred to as FAS-II-B) and the FAS-II process for 5 cycles, followed by cyclopropanation of the two double bonds (**Scheme 1–2**). For a further reading on mycolic acid synthesis in MTB see ref [112].

1.2.3 Type II FAS inhibitors

Small molecule inhibitors of FAS will be discussed in four sections: fatty acid synthesis initiation module inhibitors, condensing enzyme (KAS) inhibitors, β -ketoacyl-ACP reductase (KR) and β -hydroxyacyl-ACP dehydrase (HD) inhibitors, and, last but not least, enoyl-ACP reductase (ER) inhibitors. The antibiotic profiles of all the inhibitors are summarized in **Table 1–3**.

Initiation module inhibitors

As mentioned in the previous section 1.2.2, ACP is the one of the most abundant proteins in bacteria, and is an essential cofactor for quorum sensing [96]. The AcpS enzyme is required for the covalent attachment of 4'-phosphopantetheine (4'-PP) moiety to a conserved Ser36 on the apo-ACP to form the holo-ACP [133]. Apo-proteins are the proteins without a necessary cofactor bound, whereas proteins which are bound to cofactors are called holo-proteins. Both ACP and AcpS are essential to cellular viability. A high-throughput assay was devised to find inhibitors of AcpS by measuring the

incorporation of radio-labeled 4'-phospho-pantetheine moiety of CoA into preparations of apo-ACP [134].

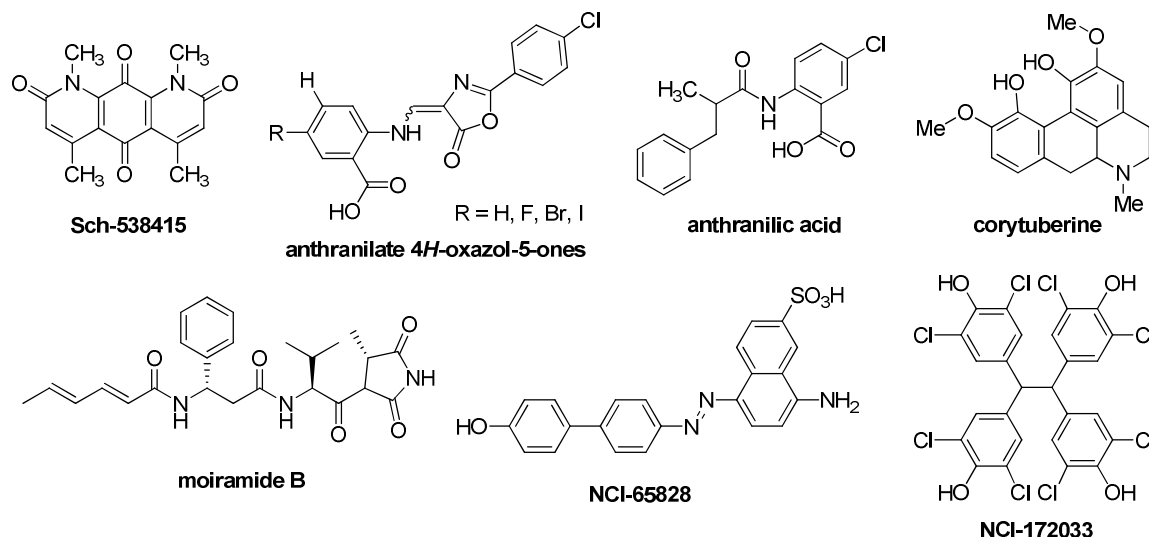


Figure 1–7. The inhibitors of fatty acid biosynthesis initiation phase.

The first small molecule inhibitor of AspS, Sch-538415 (**Figure 1–7**), was found in 2003 [134]. The IC_{50} value for Sch 538415 inhibition of the incorporation of radio-labeled 4'-phosphopantetheine (4'-PP) into AcpS is 4.2 μ M. Sch 538415 was also found to inhibit bacterial growth (determined using a cell-based agar diffusion assay) [134]. Anthranilate 4H-oxazol-5-one derivatives (**Figure 1–7**) were synthesized as AspS inhibitors [135]. Although anthranilate 4H-oxazol-5-ones were found to inhibit AcpS *in vitro* (**Table 1–3**), these molecules were not effective at killing bacteria. Anthranilic acid derivatives (**Figure 1–7**) were also found to be inhibitors of AspS, and these analogs were cytotoxic to bacteria with MIC values of 32–64 μ M to a number of Gram-positive strains. Gram-negative bacteria, however, were resistant to anthranilic acid derivatives [115].

Plants also have type II FAS, and many widely used herbicides target plant ACC (acetyl-CoA carboxylase) [136], validating ACC as a good antibacterial target [137]. Moiramide B (**Figure 1–7**) and andrimid were discovered in 1987 [138], and the first asymmetric synthesis of moiramide B was achieved in 1998 [139]. The mode of action of these pseudopeptide pyrrolidine dione antibiotics was not elucidated until 2004 [140]. Moiramide B is a selective inhibitor (nanomolar) of ACC of both Gram-positive and Gram-negative bacteria (see **Table 1–3**), but has an IC_{50} of $> 100 \mu M$ for eukaryotic acetyl-CoA carboxylase from rat liver [140]. Abundance of mycolic acids, a class of long fatty acids that usually contain 60–80 carbons (see **Figure 1–3f**), and multi-methyl-branched fatty acids are uniquely found in the cell envelope of all strains of *mycobacteria* [141]. Approximately 10 % of the genomes of *mycobacteria* are devoted to fatty acid biosynthesis [142]. NCI-65828 (see **Figure 1–7**), a lead compound that was originally identified via *in silico* inhibitor screening against AccD5 (one of the six known AccD in MTB), has a K_i value of $13 \mu M$ [143]. Further research also showed that NCI-172033 (see **Figure 1–7**), an analog of NCI-65828 (see **Figure 1–7**), has a K_i value of $1.8 \mu M$ to AccD6 from MTB [144,145].

To the best of our knowledge, the only FabD (MCAT; malonyl-CoA: acyl carrier protein transacylase) inhibitor discovered so far is corytuberine (**Figure 1–7**), which has an IC_{50} of $33 \mu M$ to the FabD of *Helicobacter pylori*. MCAT enzymatic assay also indicated that corytuberine probably inhibited the target in a non-competitive manner [146].

Table 1–3. The antibiotic activities of type II FAS inhibitors

protein	inhibitor	IC ₅₀ (μM)/ enzymatic assay	MIC (μM)/ strain name	References
AcpS	Sch-538415	4.2/ AcpS (<i>S. aureus</i>)	--	[134]
	4 <i>H</i> -oxazol-5-one	1.3/ AcpS (<i>B. subtilis</i>)	> 200/ <i>B. subtilis</i>	[135]
	anthranilic acid	2.8/ AcpS (<i>B. subtilis</i>)	32/ <i>S. aureus</i> (MRSA) 32/ <i>B. subtilis</i> (168)	[115]
ACC	moiramide B	0.015/ ACC (<i>E.coli</i>) 0.096/ ACC (<i>S. aureus</i>)	70/ <i>E. coli</i> (Neumann) 18/ <i>S. aureus</i> (133)	[140]
	NCI 65828	13 (<i>K_i</i>)/ AccD5 (MTB)	--	[143]
FabD	Corytuberine	33/ FabD (<i>Helicobacter pylori</i>)	--	[146]
FabH	1,2-dithiole-3-ones (HR12)	5.7/ FabH (<i>E. coli</i>) 1.9/ FabH (<i>S. aureus</i>)	17/ <i>E. coli</i> 38/ <i>S. aureus</i> (MRSA)	[147,148]
	YKAF02	0.042 (<i>K_d</i>) / FabH (<i>E. coli</i>)	16/ <i>E. coli</i> 32/ <i>S. aureus</i> (MRSA)	[149]
	YKAs3003	0.02 (<i>K_d</i>) / FabH (<i>E. coli</i>)	584/ <i>E. coli</i> 584/ <i>S. aureus</i> (MRSA)	[150]
	SB418001	1.2/ FabH (<i>E. coli</i>) 0.016/ FabH (<i>S. pneumonia</i>)	--	[151]
	benzoylamino-benzoic acids	0.004/ FabH (<i>E. faecalis</i>) 3.8/ FabH (<i>S. aureus</i>)	>106/ <i>E. faecalis</i> 52/ <i>S. aureus</i>	[152]
	Phomallenic acids (FabH/F)	52/ FASII ^[a] (<i>E.coli</i>) 21/ FASII (<i>S. aureus</i>)	>388/ <i>E.coli</i> (wild-type) 21/ <i>S. aureus</i> (wild-type)	[153]
	platencin (FabH/F)	4.6/ FabH (<i>S. aureus</i>) 9.2/ FabF (<i>S. aureus</i>)	2.4/ <i>S. aureus</i> (MRSA) >150/ <i>E.coli</i> (wild-type)	[119]
FabB/F	Cerulenin	3/ FabB (<i>K_d</i> , <i>E.coli</i>) 20/ FabF (<i>K_d</i> , <i>E.coli</i>) 700/ FabH (<i>K_d</i> , <i>E.coli</i>) 4.5/ FASII (<i>E.coli</i>) 6.7/ FASII (<i>S. aureus</i>)	425/ <i>E.coli</i> (wild-type) 287-573/ <i>S. aureus</i>	[154-156]
	Thiolactomycin	26/ FabB (<i>K_d</i> , <i>E.coli</i>) 60/ FabF (<i>K_d</i> , <i>E.coli</i>) 158/ FabH (<i>K_d</i> , <i>E.coli</i>) 61/ FASII (<i>S. aureus</i>)	476/ <i>E.coli</i> (No-9) 304-609/ <i>S. aureus</i> 238/ <i>B. subtilis</i> (PCI-219)	[155-158]
	thiotetromycin	63/ FASII (<i>S. aureus</i>)	269-538/ <i>S. aureus</i> 26/ <i>Bacteroides fragilis</i> (ATCC 23745)	[159]
	BABX	69/ FASII (<i>E.coli</i>) 21/ FASII (<i>S. aureus</i>)	>460/ <i>E.coli</i> (wild-type) 0.4/ <i>S. aureus</i> (wild-type)	[156]
	Platensimycin (FabF)	0.16/ FabF (<i>E.coli</i>) 0.048/ FabF (<i>S. aureus</i>) 67/ FabH (<i>S. aureus</i>) 0.5/ FASII (<i>S. aureus</i>)	>145/ <i>E.coli</i> (wild-type) 1.1/ <i>S. aureus</i>	[120]
FabG	Polyphenols (EGCG, FabG/I)	5/ FabG (<i>E.coli</i>) 15/ FabI (<i>E.coli</i>)	>200/ <i>E.coli</i>	[160]
FabA	3-decynoyl-NAC & Allenic acids (thioesters)	--	10/ <i>E.coli</i>	[161,162]
FabZ	NAS-91, NAS-21	0.6/ FabZ (<i>K_d</i> , <i>P. falciparum</i> , NAS-91)	--	[163]
FabI	isoniazid (INH-	0.00075/ FabI (<i>K_i</i> , MTB)	0.12/ MTB (wild-type)	[164-166]

	NAD)		>3,600/ <i>E.coli</i>	
	thionamides (ethionamide)	0.0007/ FabI (<i>K_i</i> , MTB)	5.9/ MTB (pMV261, PTH) >594/ <i>E.coli</i>	[164,167,168]
	triclosan	2.0/ FabI (<i>E. coli</i>)	1.7/ <i>E. coli</i> (wild-type)	[169]
	5-octyl-2- phenoxyphenol	0.005/ FabI (MTB)	6.7/ MTB (TN587)	[170]
	diazaborine (benzodiazaborine)	--	83/ <i>E. coli</i> (wild-type) 10/ <i>K. pneumoniae</i> 40/ MTB	[171,172]
	indole naphthyridinones (FabI/K)	<0.06/ FabI (<i>E. coli</i>) 0.05/ FabI (<i>S. aureus</i>) 0.13/ FabI (<i>H. influenzae</i>) 3.0/ FabK (<i>S. pneumoniae</i>)	1.3/ <i>E.coli</i> (120AcrAB) 0.04/ <i>S. aureus</i> (WCUH29) 2.6/ <i>H. influenzae</i> (Q1) 43/ <i>S. pneumoniae</i> (1629)	[173,174]

[a] The high through-put FASII inhibitory assay.

Condensing enzyme inhibitors

Cerulenin (CER) is a fungal mycotoxin, and was the first potent condensing enzyme inhibitor discovered [154]. The molecule is an irreversible inhibitor and mimics the transition state of the FabF/B catalyzed reaction (**Figure 1–9a**). FabH (the initiation condensing enzyme) is generally insensitive to cerulenin [155]. FabF is a homodimer, and Cys163 is located at the bottom of a mainly hydrophobic pocket at the dimer interface. Cerulenin is covalently attached to Cys163 via the opening of the epoxide ring by the Cys163 residue (**Figure 1–9a**). The amide carbonyl oxygen of cerulenin interacts with His340 and His303, and the hydroxyl group at C3 forms a hydrogen bond to the NH of Phe400 (**Figure 1–9a**) [175]. Cerulenin also inhibits the type I FAS. For example, it has IC₅₀ of 4.5 μ M to yeast KAS [176]. It is also worth-noting that cerulenin cannot be used for antibiotic therapy because it also inhibits human KAS. An analog of cerulenin C75 (**Figure 1–8**), however, has some clinical potential and was found to be cytotoxic to some human cancer cells [177].

Bacteria have developed resistance mechanisms to cerulenin [178]. Two resistance mechanisms to the action of cerulenin in *B. subtilis* have been reported: i) up-regulation of transcription of the *fabF* gene increases 8-fold in response to cerulenin; ii) spontaneous mutations of FAS enzymes lead to 10-fold increase in the MIC of cerulenin [178].

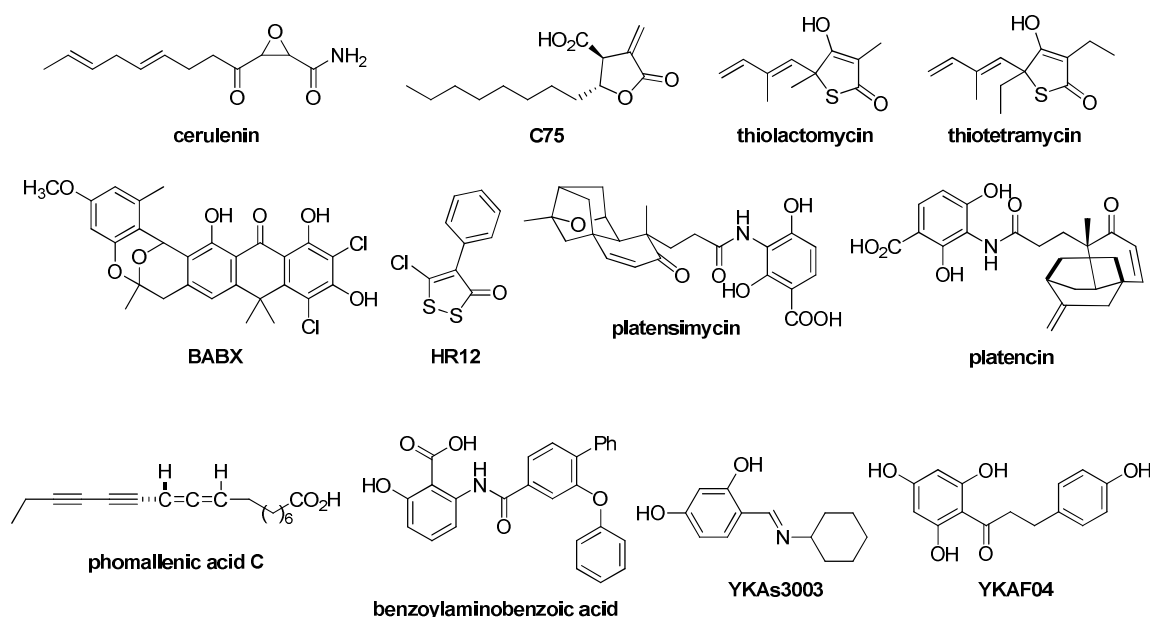


Figure 1–8. Structures of condensing enzyme inhibitors

Thiolactomycin (TLM, **Figure 1–8**) is a natural product isolated from a *Nocardia* strain in 1982 [157]. Unlike cerulenin (CER), the toxicity of TLM is weak in animal experiments, and it has a broad-spectrum antibiotic activity against both Gram-negative and Gram-positive bacteria *in vitro* and *in vivo* [179]. Several thiolactomycin analogs, such as thiotetramycin (**Figure 1–8**) [159], were isolated from *Streptomyces*. The variables of these analogs are limited on the alkyl substituents. Both CER and TLM have high affinities to FabB [155], whereas the binding affinity with FabH is very weak [155].

By changing the catalytic triad in FabB (His-His-Cys) into the His-Asn-Cys triad found in FabH, the mutated FabB showed significant resistance to both CER and TLM [155].

A Merck group designed a high through-put FASII inhibitory assay in 2005 by using an antisense silencing technology and changing the conventional substrates, acetyl-CoA and malonyl-CoA, into long-chain acyl-CoA (octanoyl-CoA or lauroyl-CoA) [156]. Using this method the inhibitors of the elongation steps in fatty acid synthesis were discovered [156]. Four potent FabB/F/H inhibitors were found by this modified FASII inhibitory assay, namely BABX [156], phomallenic acid C [153], platensimycin [120] and platencin [119] (see **Figure 1–8** and **Table 1–3**). All four compounds showed antibiotic activities *in vivo* only to Gram-positive but not Gram-negative bacteria. It was suggested that the action of efflux pumps in Gram-negative bacteria accounted for the poor activities of these compounds against Gram-negative bacteria. *E. coli* *lpxC* or *tolC* strains that did not have the efflux pumps could be inhibited with these new FAS inhibitors [120]. Platensimycin, isolated from *Streptomyces platensis*, is the best FabF inhibitor discovered so far, with an IC₅₀ of 48 and 160 nM for FabF of *S. aureus* and *E. coli*, respectively. The compound also showed a weak inhibition of *S. aureus* FabH, with an IC₅₀ of 67 μM [120]. Furthermore, platensimycin showed no toxicity issue to the human cell-line and no antibiotic cross-resistance to MRSA (methicillin-resistant *S. aureus*) and VRE (vancomycin-resistant *Enterococcus*) strains.

As previously mentioned, the FabF and FabB inhibitors usually share the same structural motifs because the binding sites these FabF/B inhibitors contain similar amino acids. **Figure 1–9** depicts the X-ray crystal structures of FabF/B and shows the binding modes of CER, TLM [155] and platensimycin [120] to FabF/B. A carbonyl group in all

three compounds plays an important role in their binding by interacting with the two histidines (His333 and His298 in **Figure 1–9a** and **1–9b**; His303 and His340 in **Figure 1–9c** and **1–9d**; His311 and His345 in **Figure 1–9e**) in the His-His-Cys triad. Apart from the nucleophilic addition of cysteine residue to the epoxide moiety on CER, the binding patterns of CER (**Figure 1–9a**, **1–9c**), TLM (**Figure 1–9b**, **1–9e**) and platensimycin (**Figure 1–9d**) in the active sites of the condensing enzymes are similar (**Figure 1–9**) [155].

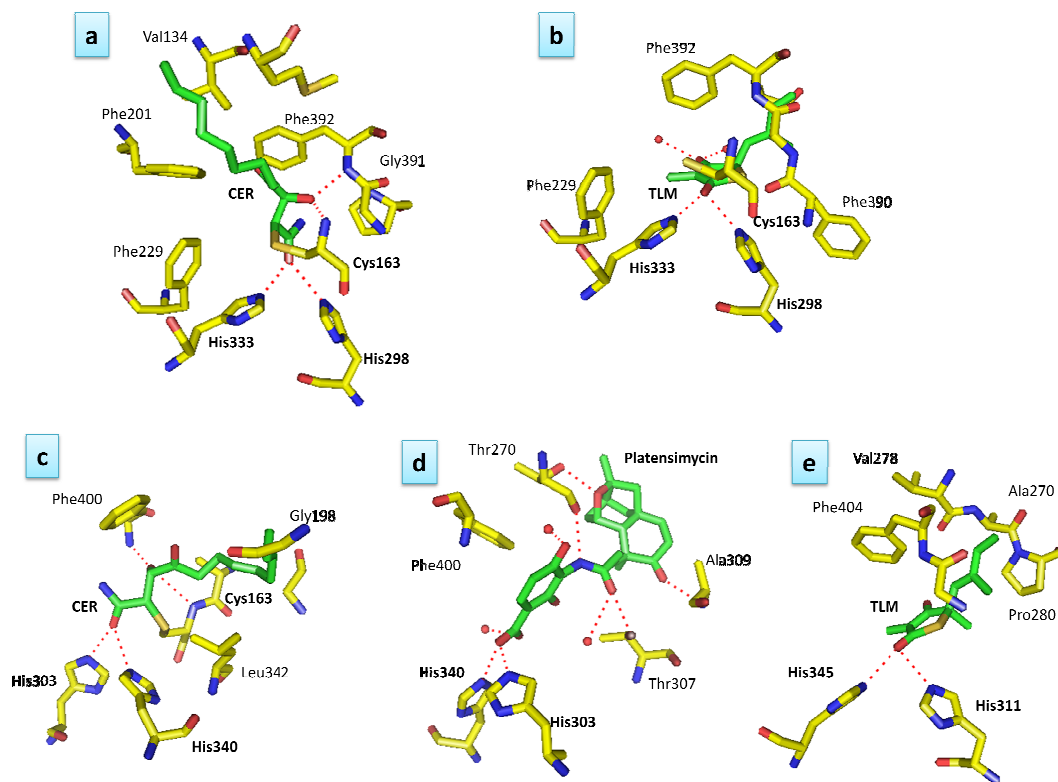


Figure 1–9. Co-crystal structure of FabF/B proteins with their inhibitors. a) Cerulenin (CER) binding site of ecFabB (PDB code 1FJ8); b) thiolactomycin (TLM) binding site of ecFabB (PDB code 1FJ4); c) CER binding site of ecFabF (PDB code 1B3N); d) platensimycin binding site of ecFabF (C163Q) (PDB code 2GFX); e) TLM binding site of MTB KasA, a FabF homolog (PDB code 2WGG). Amino acid residues (yellow); ligands bound to the proteins (CER, TLM or platensimycin: green); nitrogen, oxygen and sulfur atoms are colored blue, red and gold, respectively.

Besides FabF and FabB (or KasA and KasB in MTB), FabH is also a highly conserved protein. The amino acid sequence of FabH for *S. aureus* has 57, 40, and 34% sequence identity with the FabH of *B. subtilis*, *E. coli*, and *M. tuberculosis*, respectively [147]. Benzoylaminobenzoic acids (**Figure 1–8**) were discovered as FabH inhibitor in a structure-based drug design approach [152]. Many analogs of this class of compounds showed nanomolar inhibition activity against both Gram-positive and Gram-negative bacteria FabH [152]. Di- or tri- hydroxy benzene derivatives (e.g. YKAs3003, YKAF04; see **Figure 1–8**), which were discovered *in silico*, showed nanomolar inhibition to FabH [149,150]. However, the MIC values of these compounds are too high (16–584 μM) to be clinically useful (**Table 1–3**). Platencin, also isolated from *S. platensis* by the Merck group, is structurally similar to platensimycin with the only difference found in the tetracyclic moiety (**Figure 1–8**). Like platensimycin, platencin also has a broad-spectrum antibiotic activity against Gram-positive bacteria with no toxicity issue or antibiotic cross-resistance problem. However, platencin is 14-fold more active against FabH than platensimycin and maintains a similar inhibition activity to FabF, thus platencin is a dual FabF/H inhibitor. Also similar to platensimycin, platencin inhibited phospholipid biosynthesis in the whole-cell labeling experiments in *S. aureus* with IC_{50} values of 0.45 μM [119].

β -Ketoacyl-ACP reductase (KR) and β -hydroxyacyl-ACP dehydrase (HD) inhibitors

KR of *E. coli*, or FabG is a NAD(P)-dependant reductase. Only a handful of FabG inhibitors are currently known. Epigallocatechin gallate (EGCG) is the major component of green tea extracts. EGCG and other polyphenol green tea extracts, which contain the galloyl moiety, showed a potent dual inhibition of FabG and FabI, but a moderate *in vivo*

MIC value [160]. Other plant polyphenols were screened, and some of them had good FabG inhibition and antibacterial activities, but the mode of action of inhibition of both of the NAD(P)-dependant reductases is still unknown [160].

Little attention has been paid to the discovery of FabA inhibitors because not many bacterial strains have FabA as their β -hydroxyacyl-ACP dehydrase (e.g. *C. acetobutylicum* and *C. difficile*) [87]. The 3-decynoyl-*N*-acetylcysteamine, and its analogs, 2,3-decadienoyl-*N*-acetylcysteamine and 2,3-decadienoic acid were shown to inhibit β -hydroxydecanoyl thioester dehydrase of *E. coli* irreversibly (**Figure 1–10**) [161,162].

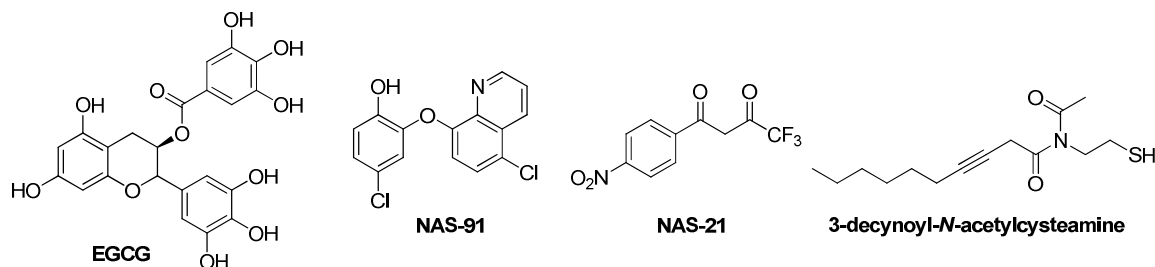


Figure 1–10. The structures of KR and HD inhibitors

The only FabZ (HD) inhibitors reported so far are two synthetic compounds, NAS-91 (**Figure 1–10**) and NAS-21. These two compounds showed binding constants (K_b) of 1.6×10^6 and $1.2 \times 10^6 \text{ M}^{-1}$ to FabZ, respectively [163].

Enoyl-ACP reductase (ER) inhibitors

Enoyl-ACP reductases, FabI/K/L/V (called InhA in MTB) are also validated antibiotic targets. At least four classes of ER inhibitors have been discovered so far: isoniazid (INH) [164], triclosan [169], diazaborine [171,172] and indole naphthyridinones [173,174] (see **Figure 1–11** for structures).

Isoniazid has been used as an anti-MTB drug since 1950's, and it still remains as the first-line antibiotic for MTB infections. Because of the drug-resistant problem, standard chemotherapy to treat MTB consists of at least four drugs: isoniazid, rifampin, ethambutol, and pyrazinamide. Although isoniazid has a very simple substituted pyridine structure (**Figure 1–11**), the mode of action of this pro-drug is complicated. It has been suggested that INH (isoniazid) is activated by KatG (catalaseperoxidase) and forms an adduct with NAD, and this INH-NAD adduct inhibits InhA (**Figure 1–12**) [180]. Inhibition of InhA results in the reduced synthesis of mycolic acid, which is required for the synthesis of *Mycobacteria* cell wall [180]. It should be pointed out that although it has become a common knowledge that isoniazid is a InhA inhibitor of MTB, there is still some evidence to suggest that there are more than one target of INH inside the MTB cell [181-183]. Bacterial resistance towards isoniazid is probably caused by mutations within the *katG* and *inhA* genes [180,184].

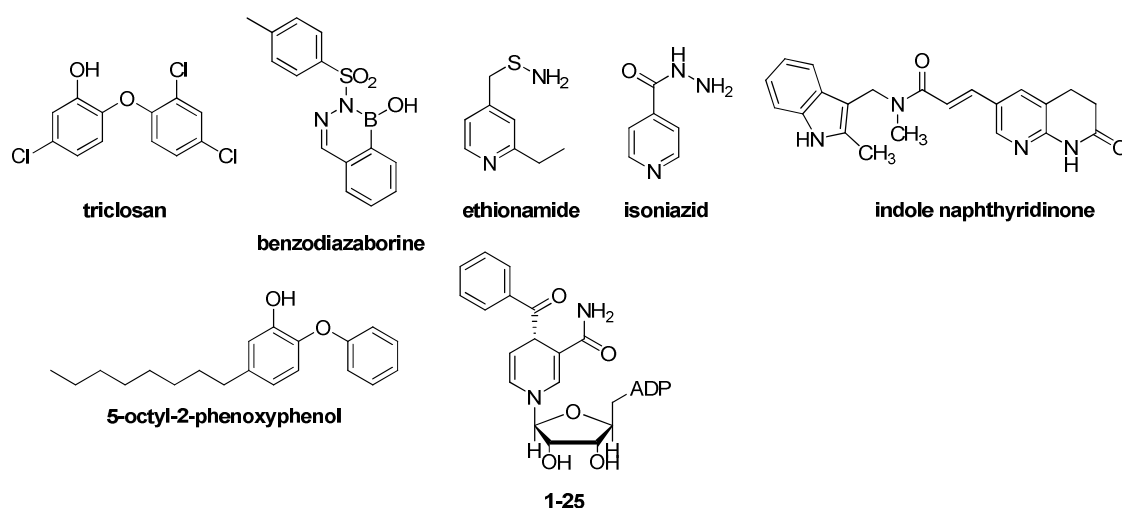


Figure 1–11. Structures of FabI/K inhibitors.

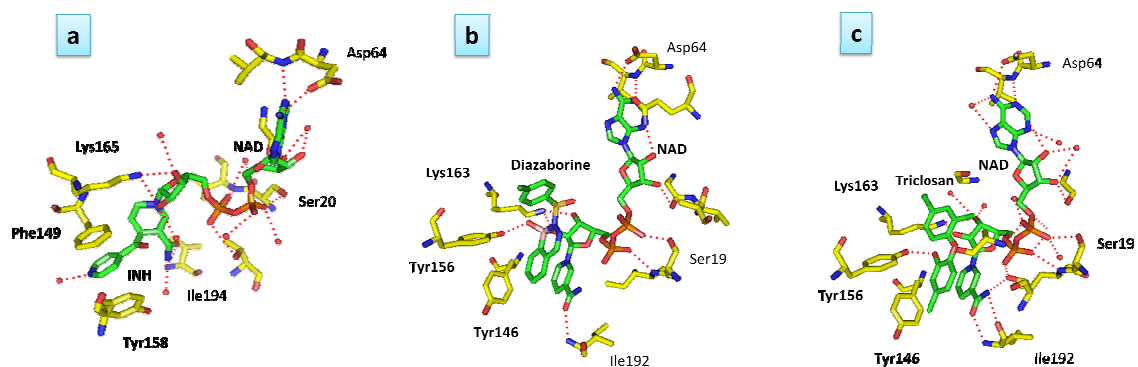


Figure 1–12. a) Co-crystal structures of INH-NAD and InhA (PDB code 1ZID) [185]; b) benzodiazaborine-NAD and ecFabI (PDB code 1DFG) [186]; c) Triclosan-NAD and ecFabI (PDB code 1QG6) [187]. Amino acid residues (yellow); ligands bound to the proteins (isoniazid, diazaborine or triclosan: green); nitrogen, oxygen, boron and phosphorous atoms are colored blue, red, pink and orange, respectively.

Ethionamide (**Figure 1–11**) and prothionamide are analogs of INH and are used as a second-line therapy for MTB infection. Their mode of action is similar to INH; ethionamide is activated by a putative mono-oxygenase (EtaA) to form a NAD adduct, whereas isoniazid is activated by the KatG [188]. Both isoniazid and ethionamide are narrow-spectrum antibiotics, and to the best of our knowledge, *Mycobacteria* are the only bacteria that are highly sensitive to these drugs (**Table 1–3**). Analogs of INH-NAD adduct have also been made (e.g. compound **1–25**, **Figure 1–11**) and these compounds inhibit InhA with K_i values that are similar to the K_i of INH (isoniazid) [189].

Diazaborine (**Figure 1–11**) is another FabI inhibitor, and is widely used in many commercial items, including hand soaps, mouthwash, etc [87]. However, this molecule contains a boron atom, and it is not suitable for human use due to issues associated with *in vivo* stability of the boron fragment. Analysis of the structures of complexes of *E. coli* ER with nicotinamide adenine dinucleotide and either thienodiazaborine or benzodiazaborine (**Figure 1–11**) revealed the formation of a covalent bond between the

2'-OH of the nicotinamide ribose and a boron atom in the drugs to generate a tightly bound adduct [186,190]. Mutational studies revealed that diazaborine binding to *E. coli* ER requires the presence of a glycine residue at position 93. Any other amino acid, other than glycine, at this position dramatically affected diazaborine binding to ER [191].

Triclosan (**Figure 1–11**) inhibits the ER with a dissociation constant of 7.1 pM [187]. Analysis of the co-crystal structure of triclosan and ER-NAD complex revealed that both triclosan and diazaborine inhibitors bind to the same site (**Figure 1–12**) [187]. Resistance to triclosan occurs via mutations to ER enzymes, such as FabI, akin to how mutations in INHA confer resistance to INH in MTB [169]. It should also be noted that many strains of bacteria do not possess FabI or have more than one ER. For such bacteria, triclosan is not a very effective antibiotic [127]. Additionally, the overexpression of the multidrug efflux pump locus *acrAB*, *marA* or *soxS* decreased susceptibility to triclosan in bacteria [192]. A detailed structure-activity relationship study of triclosan has been done by the Tonge group [170,193]. And they showed that many diphenyl ether analogs of triclosan (e.g. 5-octyl-2-phenoxyphenol) have similar or higher activity than triclosan to various bacteria, including *E. coli* and MTB [189].

Indole naphthyridinones (**Figure 1–11**) were discovered as ER inhibitors in 2003 [173]. This class of compounds showed potent antibiotic activity to various Gram-positive bacteria and some Gram-negative pathogens, including some multi-drug resistant pathogens (**Table 1–3**) [173]. Extensive SAR studies showed that some of the analogs have a dual inhibition of both FabI and FabK, and they have a promising oral *in vivo* efficacy in a *S. aureus* infection model in rats [174].

1.2.4 Other considerations when developing new antibiotics

As early as 1977, researchers noticed that in the presence of an inhibitory concentration of cerulenin, cells of *S. aureus* can resume growth when supplemented with either a saturated or an unsaturated fatty acid [194]. A very recent paper claimed that type II FAS is not a suitable antibiotic target for Gram-positive pathogens [195]. The uptake of exogenous fatty acids, which can be found in the human serum, would allow the bacteria to fully bypass the inhibition of the type II FAS process. Therefore the antibiotic activities of type II FAS inhibitors may be sensitive to the *in vivo* environment of the bacteria. It is therefore critical for the drug-developer to consider different scenarios whereby a therapeutic regimen will not work, when developing new antibiotics to solve the never-ending resistance problem.

1.3 Biofilm formation – another important antibiotic target

1.3.1 Introduction of c-di-GMP signaling

Biofilm is an aggregation of micro-organisms in bio-matrix on living and nonliving surfaces [1]. It has been noted that bacteria in biofilms are more resistant to antibiotics than free-living (planktonic) ones, and hence diseases related with biofilm-forming bacteria are usually chronic and difficult to treat [196]. Biofilm-forming bacteria have been implicated in several serious diseases, such as endocarditis, cystitis, cystic fibrosis pulmonary infections, and the infections of prosthetic devices [196]. Thus small molecules that can attenuate biofilm formation have the potential to solve the bacteria resistance problem. It is now known that a dinucleotide, cyclic diguanylic acid (c-di-

GMP, **Figure 1–13a**), appears to be a master regulator of several processes related to biofilm in various bacteria strains [197,198].

C-di-GMP was first discovered as a cellulose synthase activator in *Gluconacetobacter xylinus* (formally known as *Acetobactor xylinum*) by the Benziman group over two decades ago [199]. It was proposed by Benziman that c-di-GMP was synthesized by a membrane-bound protein diguanylate cyclase (DGC) from two molecules of GTP in the presence of Mg^{2+} (**Figure 1–13b**). C-di-GMP was shown to activate cellulose production in bacteria by binding to a cellulose synthase that is also a membrane protein. The degradation of c-di-GMP is catalyzed by phosphodiesterase A and B (PDE A/B), initially into pGpG by PDEA and then the pGpG is cleaved into two molecules of GMP by PDEB (**Figure 1–13b**).

Mg^{2+} is required for c-di-GMP degradation but Ca^{2+} can strongly inhibit hydrolysis [199]. DGCs are characterized by the GGDEF [200,201], whereas PDEs are characterized by the EAL domain [202]. These two domains have now been shown to be the most abundant in bacterial genomes [203]. The first identified receptor for c-di-GMP was the BcsB β -subunit of cellulose synthase [204,205]. However, after some debate about whether the BcsB β -subunit of cellulose synthase was indeed a c-di-GMP binding domain [206,207], Amikam and Galperin clarified that PilZ domain in the sequence of cellulose synthase was in fact the long-sought after c-di-GMP binding protein [208].

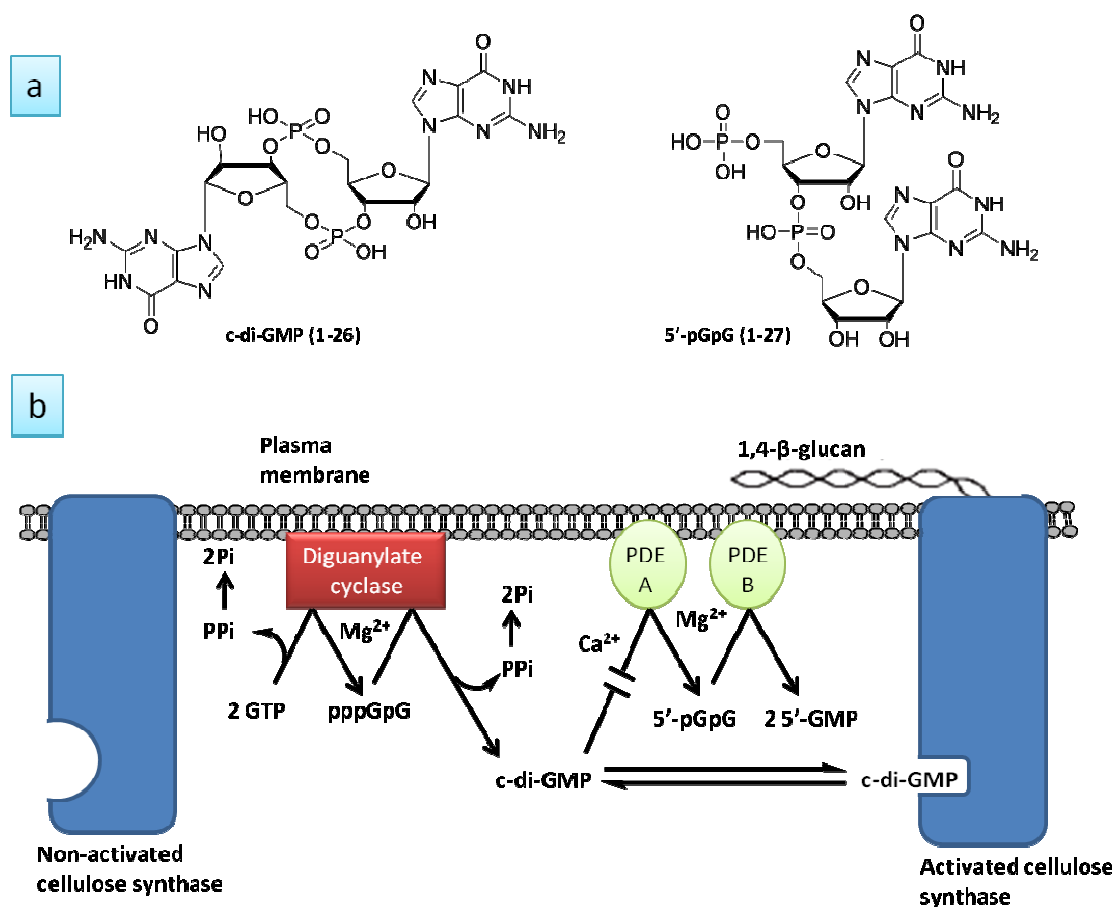


Figure 1–13. a) Chemical structure of c-di-GMP (1–26) and 5'-pGpG (1–27); b) proposed mechanism for the regulation of cellulose biosynthesis in *Gluconacetobacter xylinus* (reproduced from ref [199]).

C-di-GMP has now been shown to regulate diverse cellular processes in many bacteria strains (**Figure 1–14**) [203]. For example, several genes that are responsible for cell motility [209,210], virulence factors [211] and biofilm formation [212] are all under the control of c-di-GMP.

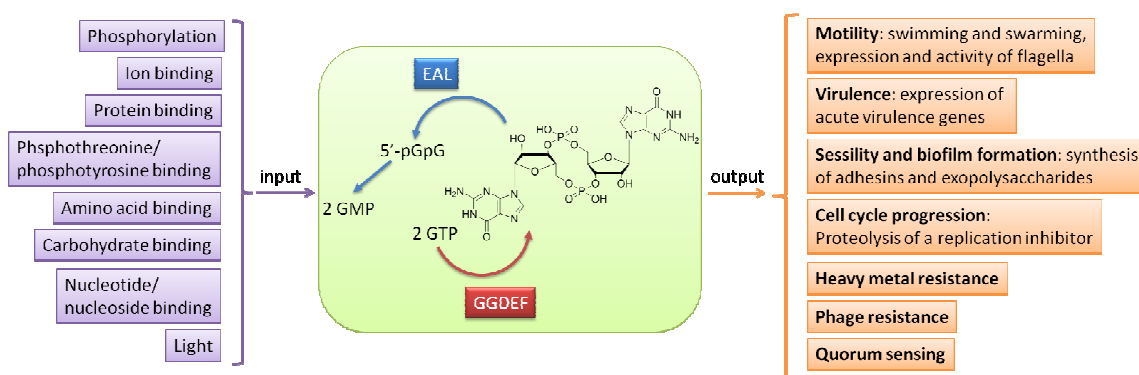


Figure 1–14. Structure of c-di-GMP and the related biological processes that it regulates (modified from ref [213] and [203]).

C-di-GMP also controls cell division and differentiation in bacteria [214,215]. Recently, it was also shown that c-di-GMP controls the growth and toxicity of *Legionella pneumophila* in their host cells [216]. C-di-GMP regulates mRNA translation as well, by binding to riboswitches [212,217]. A riboswitch is an mRNA molecule that binds to a specific small metabolite molecule, leading to conformational changes in the RNA. This conformational change in RNA structure ultimately affects gene translation or transcription. There are two types riboswitches found to bind c-di-GMP so far (**Table 1–4**), and they are named c-di-GMP-I riboswitch [212] and c-di-GMP-II riboswitch [217]. For example, c-di-GMP-II RNA riboswitch from *Clostridium difficile* (86 Cd) binds to c-di-GMP with a K_d value of 200 pM [217]. Upon binding to c-di-GMP, c-di-GMP-II riboswitch becomes a ribozyme and undergoes a self-splicing process [217].

The list of processes in bacteria that c-di-GMP apparently regulates keep increasing and a list of known c-di-GMP adaptor proteins, as well as processes that it regulates are shown in **Table 1–4** [213]. As already stated, c-di-GMP is produced by diguanylate cyclases (DGCs) from two GTPs and can be degraded into 5'-phosphoguanylyl-(3'-5')-guanosine (5'-pGpG, **Figure 1–13a**) by specific phosphor-

diesterases (PDEs). pGpG can be further degraded into two GMPs [199]. Some of the well characterized DGCs are WspR [200] and PleD [201]. These DGCs all contain a GGDEF domain [200,201] but the exact role played by this domain in DGC catalysis is not fully understood. Researchers have, however, postulated that the mechanism utilized by DGCs to make c-di-GMP from GTP could be similar to that of adenylyl cyclase [218,219]. PDE (e.g. FimX, RocR) contains an EAL domain [203]. Recent study showed that EAL domain can use one, two or three Mg^{2+} for catalysis but only one cation is essential [220]. Using RocR protein (from *Pseudomonas aeruginosa*) as a model, Liang's group further proposed that this key Mg^{2+} coordinates and polarizes the P–O bond of c-di-GMP, and lowers the pKa of the coordinated water to generate the nucleophilic hydroxide anion, with the assistance of Glu352 via a general acid/base mechanism (**Figure 1–15**) [220]. Proteins containing EAL domain specifically produce 5'-pGpG without the formation of 3'-pGpG.

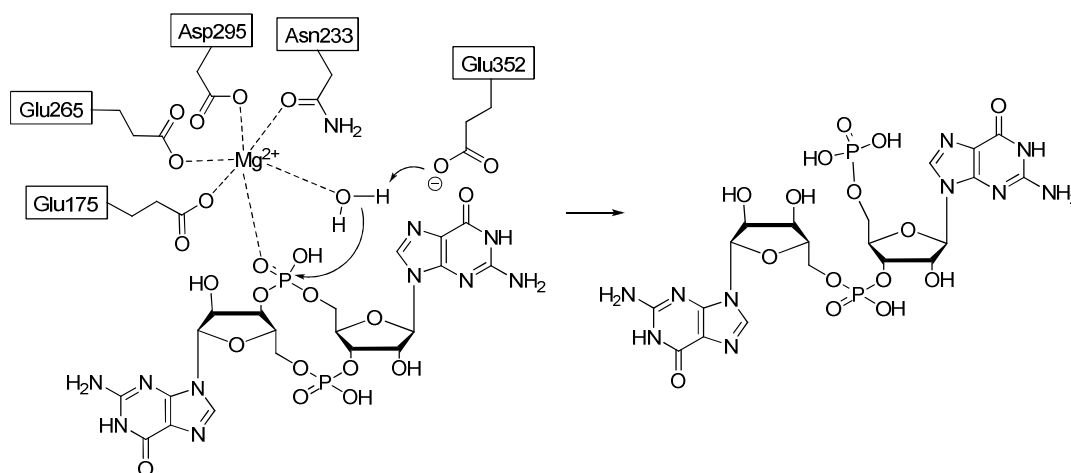


Figure 1–15. Proposed catalytic mechanism for EAL domain-containing PDE.

In the last few years, tremendous progress has been made towards identifying and understanding c-di-GMP metabolism proteins (PDEs and DGCs). However, very little is

known about the downstream proteins that bind to c-di-GMP and transmit the binding event into a biological response (the so-called adaptor proteins). **Table 1–4** shows known proteins that bind to c-di-GMP.

Table 1–4. Known c-di-GMP adaptor proteins and RNAs (modified from refs[213]).

Adaptor family	Example	Species	Functions controlled	Refs
Protein adaptors				
PilZ	Alg44	<i>Pseudomonas aeruginosa</i>	Alginate synthesis	[221]
	BcsA	Various Gram-negative bacteria	Cellulose synthesis	[207,208]
	DgrA	<i>Caulobacter crescentus</i>	Flagellar activity	[222]
	PilZ	<i>P. aeruginosa</i>	Twitching motility	[209]
	Plz proteins	<i>Vibrio cholerae</i>	Virulence gene expression	[211]
	YcgR	<i>Escherichia coli</i> and <i>Salmonella</i> spp.	Flagella activity	[223]
FleQ	FleQ	<i>P. aeruginosa</i>	Flagella expression and Pel synthesis	[224]
PelD	PelE	<i>P. aeruginosa</i>	Pel synthesis	[225]
I site effectors	PopA	<i>C. crescentus</i>	Cell cycle progression	[215]
RNA effectors				
c-di-GMP-I riboswitches (GEMM)	Vc1 (encoded by <i>gbpA</i>)	<i>V. cholerae</i>	Intestinal adhesion	[212]
	Vc2 (encoded by VC1722)	<i>V. cholerae</i>	Biofilm formation and rugosity	
	Cd1	<i>Clostridium difficile</i>	Flagella synthesis	
c-di-GMP-II riboswitches	84 Cd	<i>Clostridium difficile</i>	Bacterial virulence	[217]

1.3.2 Polymorphism of c-di-GMP

An interesting property of c-di-GMP is its ability to readily form dimers, tetraplexes and higher aggregates in the presence of cations at millimolar or even high micromolar concentration (**Figure 1–16**) [226,227]. Structural data analyses of proteins

that bind to c-di-GMP reveal that these proteins bind to either monomer (PDB code: 3HV8 [228]) and dimer c-di-GMP (PDB code: 3KYF [229]; **Figure 1–17**). Cations such as those of magnesium, sodium, lithium and ammonium promote dimer formation in c-di-GMP, whereas potassium ion promotes the formation of tetraplexes and octaplexes in c-di-GMP [226,227]. Recently the Sintim group also showed that higher aggregates of c-di-GMP, such as tetraplexes and octaplexes, can also form at physiological concentration (0–10 μ M) in the presence of aromatic intercalators [230].

This propensity of c-di-GMP to form tetraplexes or octaplexes (G-quadruplexes) at micromolar concentrations in the presence of cations (such as that of potassium) is intriguing because simple nucleotides (such as cGMP, GTP or pGpG) do not readily form G-quadruplex structures at micromolar concentrations. G-quadruplexes are formed by four guanine groups linked by eight H-bonds (**Figure 1–16**). In c-di-GMP, the near-planar G-quadruplex floors can stack with each other, stabilized by a face-face π – π stacking [227]. Not all bacterial c-di-GMP binding enzymes bind to the same c-di-GMP polymorphism. For example, P4397 (PilZ domain) binds to dimeric c-di-GMP (**Figure 1–17a**), whereas FimX (EAL domain) prefers monomeric c-di-GMP (**Figure 1–17b**). Therefore, the polymorphism of c-di-GMP should have biological implications. Plausibly, the facile interconversion of c-di-GMP into different aggregation states (especially in the presence of cations) could be a means whereby bacteria regulate biofilm formation in the presence of different metals.

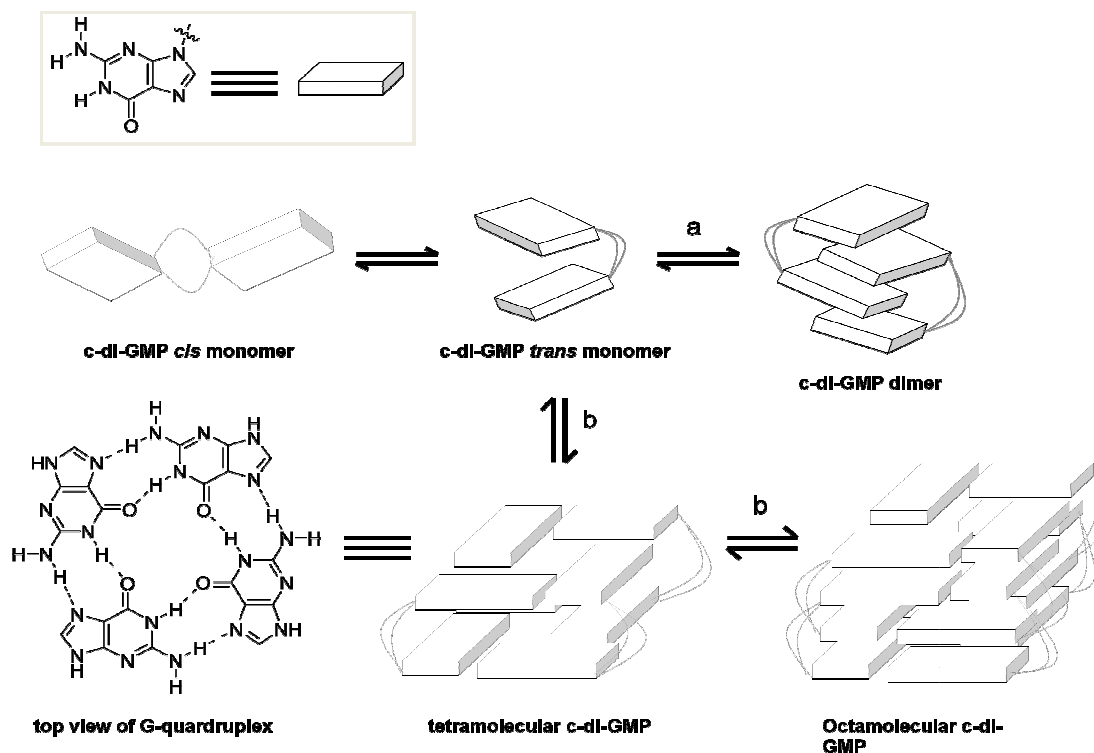


Figure 1–16. Polymorphism of c-di-GMP. a) Lithium, sodium, ammonium and magnesium cations; b) potassium and aromatic intercalators. G-quadruplexes are formed in tetramolecular and octamolecular c-di-GMP polymorphism.

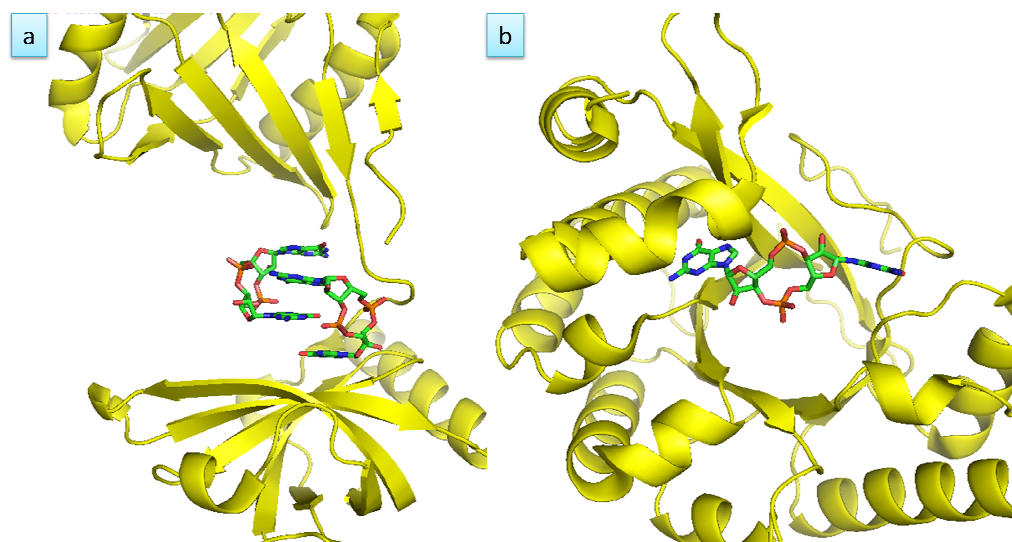


Figure 1–17. Co-crystal structures of a) P4397 (PilZ domain) with dimeric c-di-GMP (PDB 3KYF); b) FimX (EAL domain) with monomeric c-di-GMP (PDB 3HV8) (green, red, blue and orange represent carbon, oxygen, nitrogen and phosphorus atom on c-di-GMP, respectively; yellow represents the cartoon structure of the adaptor proteins).

Chapter 2. The synthesis and antibiotic activities of oxazinidinyl platensimycin

2.1 Syntheses of novel FAS inhibitors, platensimycin and platencin

In 2006, Merck reported a novel potent inhibitor of FabF, called platensimycin (**Figure 2–1**) [120], from a soil sample of *Streptomyces platensis* (MA7327) collected in South Africa. The yield of this natural product after extraction and HPLC purification was 0.6–1.3 mg/liter of the crude fermentation broth [120]. One year later, the same Merck team reported another compound called platencin (**Figure 2–1**), which is a good inhibitor of FabH, from a different strain of *Streptomyces platensis* (MA7339) from a soil sample collected in Spain with a similar purification method used for platensimycin discovery. Platencin was obtained in a yield of 1 mg/liter [119].

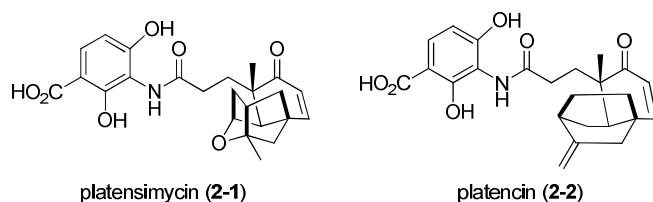


Figure 2–1. The structures of platensimycin and platencin.

Platensimycin (compound **2–1**, **Figure 2–1**) and platencin (compound **2–2**) both show a broad-spectrum Gram-positive activity *in vitro* and *in vivo* [119,120]. Single-enzyme catalytic assays showed that platensimycin is a superior inhibitor of saFabF (sa = *S. aureus*) with an IC_{50} of 0.048 μ M but a weak inhibitor of saFabH with an IC_{50} of 67 μ M [120], whereas platencin is a dual inhibitor of saFabF and saFabH with an IC_{50} of 0.11 and 16 μ M, respectively [119]. *In vivo*, platensimycin and platencin both showed an MIC (minimum inhibitory concentration) value range of 0.5–8 μ g/mL. These values

represent about 32-fold more antibiotic potency when compared to the commercial antibacterial drug, linezolid, on various antibiotic-resistant bacterial strains. Interestingly, both platensimycin and platencin do not exhibit significant cyto-toxicity (**Table 2–1**) [119,120].

FabH and FabF are condensing enzymes that are both necessary for the biosynthesis of the fatty acid component of bacterial cellular membrane, phospholipid. Thus a bacterium deficient in any of these two essential enzymes cannot survive [87]. Platensimycin and platencin are the most potent inhibitors of FabF/H reported to date, and because their modes of action are distinct from any current antibiotics, such as β -lactams, macrolides or oxazolidinones (e.g. linezolid), it was expected that platensimycin or platencin will not exhibit cross-resistance issue to these drugs (**Table 2–1**) [119,120].

Table 2–1. Microbiological and toxicity profiles of platensimycin, platencin and linezolid (adopted from ref [120] and [119])

Organism (genotype and description)	Platensimycin	Platencin	Linezolid
Antibacterial activity (MIC, $\mu\text{g/ml}$)			
<i>S. aureus</i> (MSSA, sensitive to methicilin)	0.5	0.5	4
<i>S. aureus</i> + serum	2	8	4
<i>S. aureus</i> (MRSA, resistant to methicilin)	0.5	1	2
<i>S. aureus</i> (MRSA, resistant to macrolide)	0.5	1	2
<i>S. aureus</i> (MRSA, resistant to linezolid)	1	1	32
<i>S. aureus</i> (VISA, resistant to vancomycin)	0.5	0.5	2
<i>E. faecalis</i> (resistant to macrolide)	1	2	1
<i>E. faecium</i> (VRE, resistant to vancomycin)	0.1	<0.06	2
<i>S. pneumoniae</i>	1	4	1
<i>E. coli</i> (wild-type)	>64	>64	>64
<i>E. coli</i> (tolC)	16	2	32
Toxicity ($\mu\text{g/ml}$)			
HeLa MTT (IC ₅₀)	>1,000	>100	>100
<i>Candida albicans</i> (MIC)	>64	>64	>64
Whole-cell activity (IC ₅₀ , $\mu\text{g/ml}$)			
Fatty acid synthesis (<i>S. aureus</i>)	0.1	0.19	ND
Fatty acid synthesis (<i>S. pneumoniae</i>)	0.8	2.7	ND

It is worth-noting that although platensimycin and platencin showed superior antibacterial activities to various commercial antibiotics against several antibiotic-resistant bacterial strains in *in vitro* assays, both drugs have poor pharmacokinetic profiles and did not display good *in vivo* activities because they were both inactivated by enzymes in the human serum.

2.1.1 KAS inhibition by platensimycin and platencin: mechanism of action

The crystal structure of a FabF mutant (C163Q), in complex with platensimycin, was disclosed in 2006 (**Figure 2–2**) [120]. Analysis of the crystal structure reveals the key hydrogen bonding interactions that are postulated to be vital for binding.

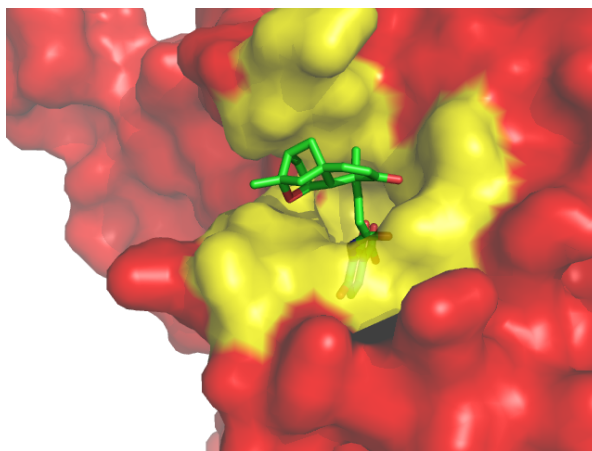


Figure 2–2. Structure at 2.6 Å resolution of *E. coli* FabF (C163Q) (active site residues: yellow; other residues: red) in complex with platensimycin (stick; green: carbon; red: oxygen; PDB code 2GFX) [120].

Platensimycin and platencin can be structurally divided into three moieties, the tetra- or tri- cyclic ketolide core, the benzoic acid, and the amide linker (**Figure 2–1**). For platencimycin, the carboxylate of the benzoic acid ring forms polar interactions with the

active-site histidine residues (His303 and His340). His303, His340 and Cys163 form the His-His-Cys catalytic triad, which plays an important role in the catalytic mechanism of FabF (see Section 1.2 for previous discussion on the mechanisms of FabF/H enzymes) [155]. The benzoic acid ring of platensimycin stacks with Phe400 of the FabF enzyme in an edge-to-face pattern of the FabF open conformation. Phe400 is the gatekeeper residue that separates the malonyl-binding and acyl binding subsites. In the apo-enzyme, in the closed conformation, Phe400 would sterically clash with the benzoic acid ring of platensimycin, and would not be able to make as favorable a stacking interaction with the inhibitor. This explains why platensimycin binds selectively to the acyl-enzyme intermediate [120]. The hydroxyl group *para* to the carboxylic acid group makes weak water-mediated hydrogen bonds to protein residue Asp265, which is part of the malonyl subsite (**Figure 2–3a**) [120].

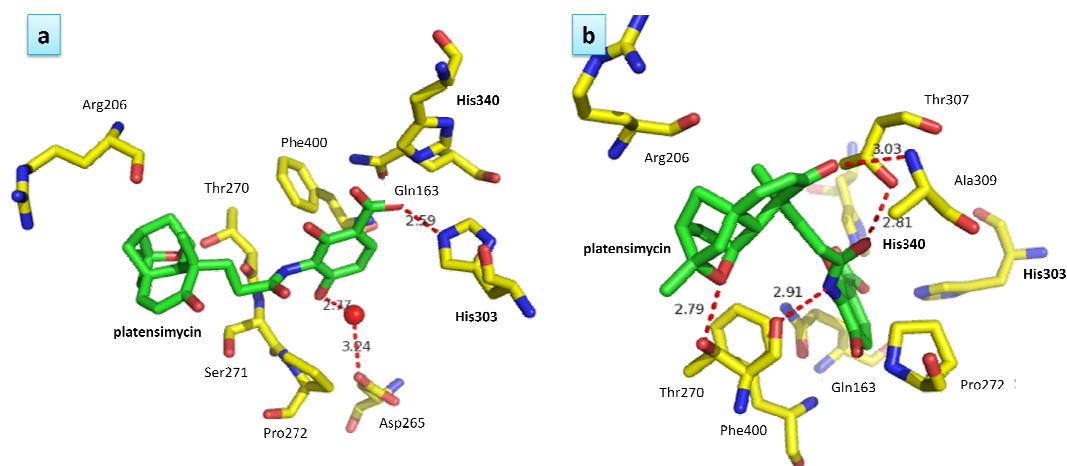


Figure 2–3. Some critical binding interactions between platensimycin (green backbone) and amino acid residues (yellow backbone) in the active site of FabF. a) The interactions between the benzoic acid part of platensimycin and the FabF protein; b) Interactions of the tetracyclic ketolide core and the amide linker of platensimycin with the residues of FabF (blue: nitrogen, red: oxygen).

The amide-linked, tetracyclic core of platensimycin is positioned in the mouth of the active site and is partly exposed to solvent (**Figure 2–2**) [120]. The amide linker makes two hydrogen bonds to the protein; the carbonyl oxygen hydrogen-bonds to the Thr307 side chain, and the amide nitrogen interacts with the backbone carbonyl of Thr270. The enone carbonyl oxygen of platensimycin makes a hydrogen bond to the backbone amide of Ala309, and the ether oxygen makes a hydrogen bond to the side-chain hydroxyl group of Thr270 (**Figure 2–3b**) [120].

More recent structural studies [231,232] showed that the binding modes of platencin, platensimycin A₁ (a hydroxy congener of platensimycin, **Figure 2–4**; compound **2–3**) and platencin A₁ (a hydroxy congener of platencin, compound **2–4**) are similar to platensimycin (**Figure 2–5**). The IC₅₀ values of platensimycin A₁ and platencin A₁ are also similar to that of platensimycin and platencin in cell-free FASII assays, respectively [231,232]. For platensimycin A₁, the hydroxylated tetracyclic core is slightly rotated and shifted compared to platensimycin in the binding site (**Figure 2–5**) [231]. For platencin and platencin A₁, the terpenoid ring of the tricyclic core lacks the ether oxygen atom found in platensimycin and therefore, both compounds cannot form a direct hydrogen bond to Thr270 (**Figure 2–3b**). This missing hydrogen bond probably accounts for the 6-fold weaker binding affinity to FabF compared to platensimycin [232]. However, the benzoic acid moieties and the amide linker are bound to the protein almost exactly the same way in all the cases. The hydrogenation product of platensimycin, whereby the enone moiety of the tetracyclic core is reduced, dihydroplatensimycin (compound **2–5**, **Figure 2–4**), binds to FabF with an affinity that is only 4-fold less than the natural platensimycin. The lower binding affinity of dihydroplatensimycin (compound **2–5**) to

FabF however suggests that the cyclohexenone ring probably plays a role in the binding of platensimycin to FabF by orienting the C-5 ketone for more favorable hydrogen-bonding interaction with Ala309 of the FabF backbone (**Figure 2–3b**) [233]. These observations make us conclude that because the core structure does not directly inhibit the His-His-Cys triad (around 10 Å away), interactions between the core structure of these inhibitors and the protein residues probably do not contribute as much to the binding energy as those between the benzoic acid moiety and the protein residues.

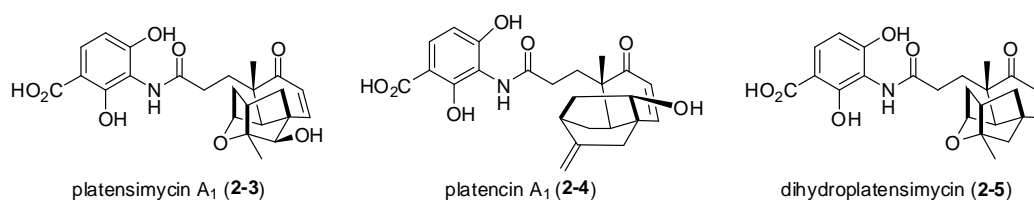


Figure 2–4. Structures of platencimycin A₁, platencin A₁ and dihydroplatensimycin.

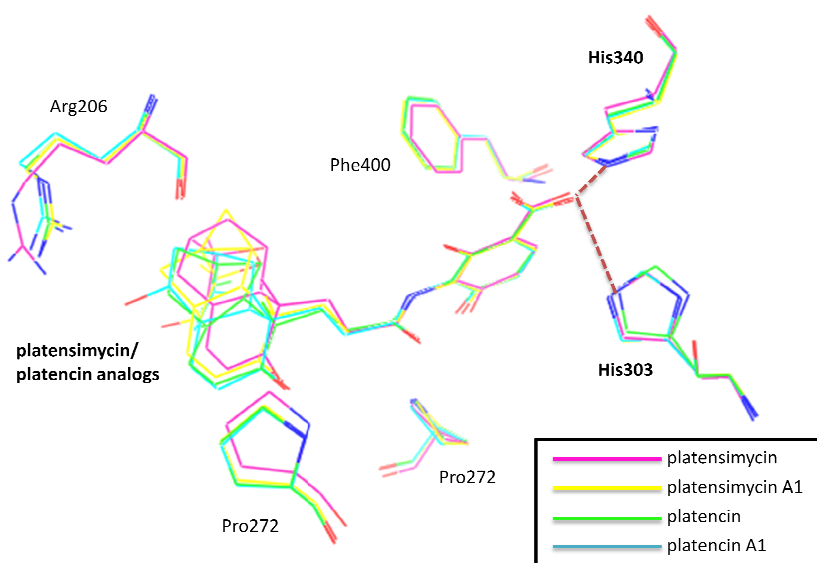
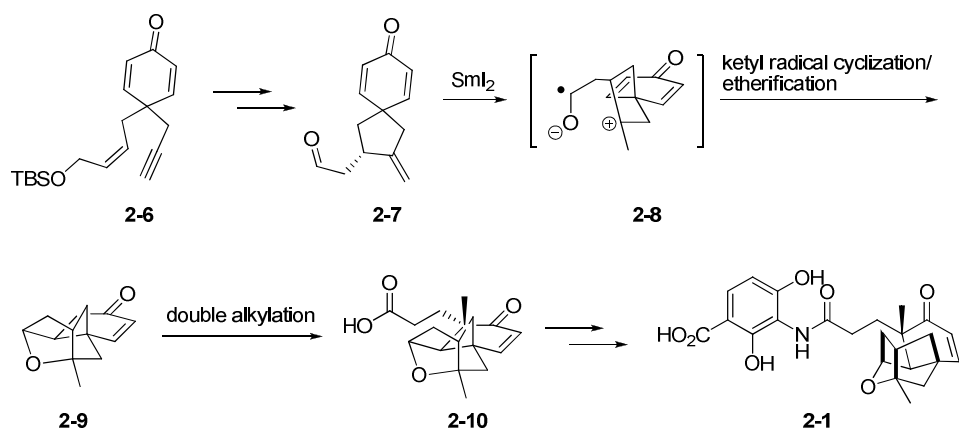


Figure 2–5. Superposition of the structures of platensimycin/platencin or their analogs to ecFabF (C163A). platensimycin: purple backbone (PDB code 3HNZ); platensimycin A₁: yellow backbone (PDB code 3IAP); platencin: green backbone (PDB code 3HO2); platencin A₁: blue backbone (PDB code 3HO9).

2.1.2 Previous total syntheses of platensimycin and platencin

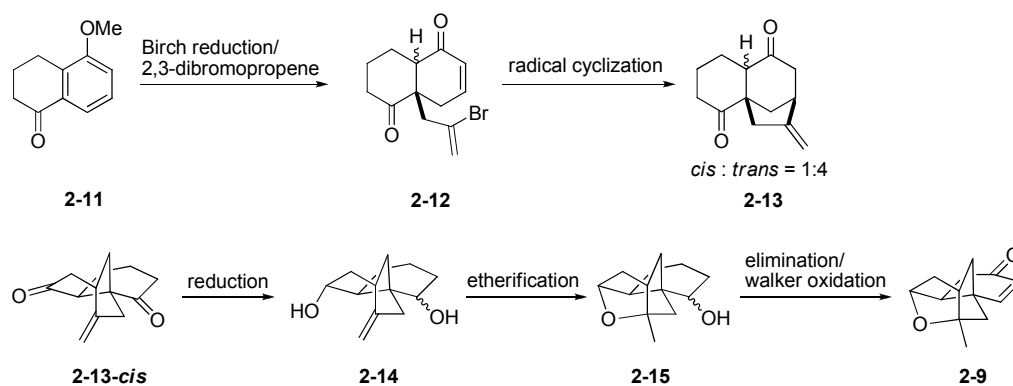
In only four years since the seminal report [120] by the Merck group, over 20 groups worldwide have reported the total syntheses of platensimycin [182,234-246] and platencin [247-257], or the enzymatic syntheses of platencimycin [258,259]. Additionally, several papers demonstrated various strategies to make analogs of these molecules [231,232,260-277], and the biological evaluations of these analogs [231,232,262-264,266-268,271-277] have also been reported. Several review articles [278-282] on these molecules have also been published, establishing the platensimycin family of antibiotics as one of the most intensely studied bioactive molecules in the last decade. Despite the intense research efforts directed at discovering newer analogs of platensimycin and family, the majority of the reported syntheses of platensimycin or analogs typically involve close to twenty total steps, with the shortest linear steps being around nine [256]. Most total syntheses of platensimycin or platencin have produced only a few milligrams of material. As most antibiotic pills used in the clinics typically contain from one to two hundred milligrams of active substances, the current chemical syntheses of platensimycin or analogs reported so far would not be economically viable.

Nicolaou's group first reported the total synthesis of platensimycin in 2006 [234] and platencin in 2008 [250]. Nicolaou's first platensimycin synthesis included 10 steps towards the core structure. The key step in Nicolaou's strategy is a ketyl radical cyclization step to construct the tetracyclic ring core of platensimycin (**Scheme 2–1**).

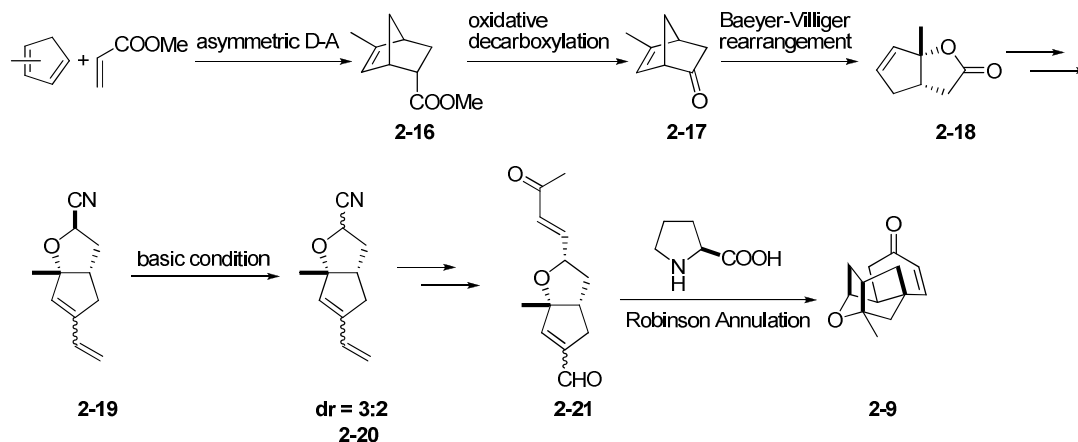


Scheme 2–1. Nicolaou's first total synthesis of platensimycin

Snider reported a 7-step synthesis of the core structure **2–9** of platensimycin (**Scheme 2–2**) [241], the major drawback of this approach is that many steps are low yielding and result in mixtures of undesired products. Therefore, for practical purposes, Snider's strategy is not ideal (**Scheme 2–2**). Yamamoto reported a 10-step asymmetric synthesis towards the core structure **2–9** of platensimycin in 2007 [237]. Yamamoto's synthesis started with an asymmetric Diels-Alder reaction, and ended with a stereoselective Robinson annulation as a key step (**Scheme 2–3**).

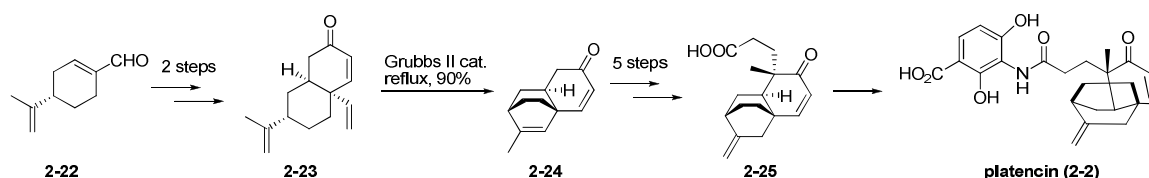


Scheme 2–2. Snyder's synthetic strategy towards the core structure of platensimycin



Scheme 2-3. Yamamoto's synthetic strategy towards the core structure of platensimycin

The core structure of platencin is less complicated than platensimycin. Instead of a tetracyclic moiety, the tricyclic moiety makes the platencin synthesis generally shorter than platensimycin. The shortest total synthesis of platencin so far is Tiefenbacher and Mulzer's synthesis reported in 2009 [256]. The synthesis started with a commercially available compound perillaldehyde. After the key ring-closing metathesis/ Diels-Alder cascade reaction, the tricyclic structure was readily formed in only three steps (**Scheme 2-4**). The total number of steps of Tiefenbacher and Mulzer's synthesis is nine, with an overall yield of 9.6 % [256].



Scheme 2-4. Tiefenbacher and Mulzer's total synthesis of platencin.

2.2 Design, syntheses and antibiotic activities of first generation platensimycin analog – oxazinidinyl platensimycin

(The majority of this section was published in ref [273])

2.2.1 The design of oxazinidinyl platensimycin

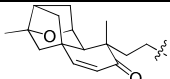
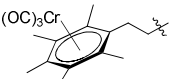
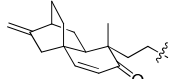
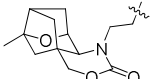
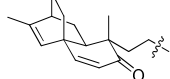
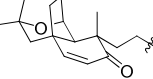
Although platensimycin shows an excellent antibacterial activity, there are still some issues that must be addressed:

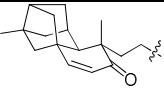
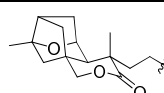
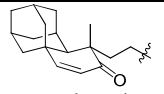
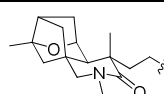
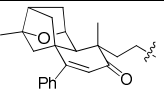
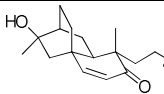
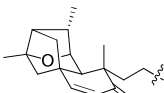
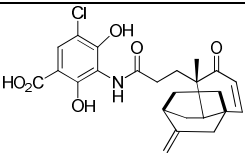
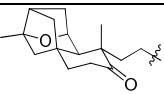
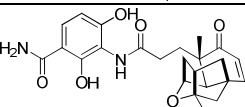
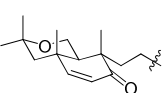
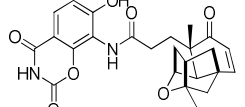
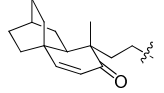
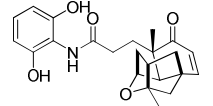
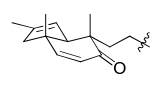
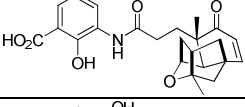
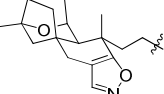
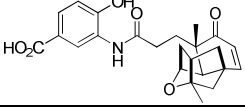
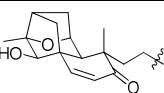
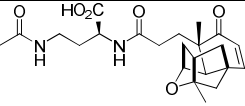
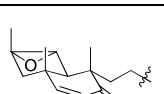
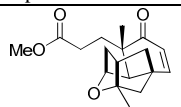
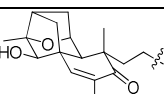
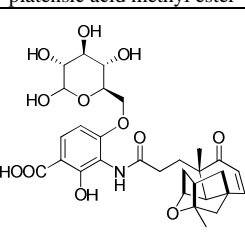
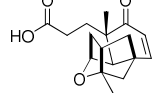
i) Platensimycin is 4-fold less effective in serum than that is in bacterial growth medium (**Table 2–1**). The instability of platensimycin in serum might be due to the hydrolysis of the amide group. Replacement of the amide moiety with stable isosteric groups might lead to a longer lasting drug.

ii) Practical chemical synthesis of platensimycin for mass usage is currently not feasible with the synthetic strategies reported so far.

Since the benzoic acid moiety is important, SAR studies of platensimycin have mainly been focused on the tetracyclic core structure of platensimycin, and any attempts to modify the benzoic acid moiety rendered the molecule inactive (**Table 2–2**). Interestingly, although the tetracyclic moiety of platensimycin is distal from the active site in FabF, modifications on the core does not always give an active compound (**Table 2–2**).

Table 2–2. MIC values of platensimycin/ platencin analogs against *S. aureus*. (Unless otherwise shown, analogs contain the benzoic acid moiety found in platensimycin)

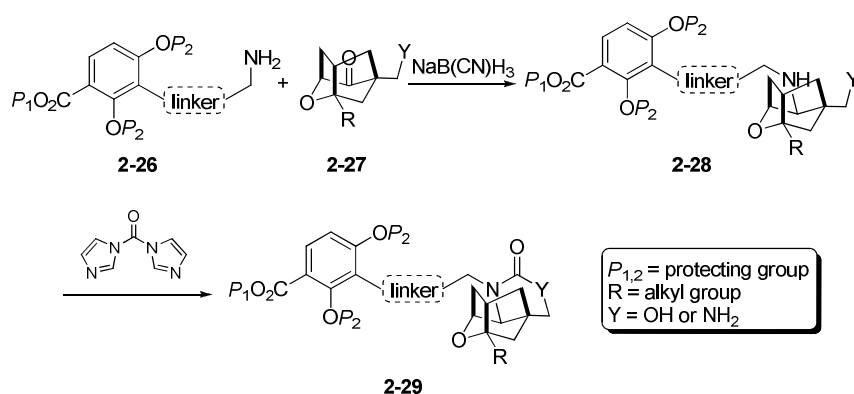
active analogs			inactive analogs		
core structures/ names	MIC	refs	core structures/ names	MIC	refs
 platensimycin	0.5 (2)	[120] [267]	 (OC) ₃ Cr	~78 (<i>B. subtilis</i>)	[271]
 platencin	0.5–1 (0.4–0.8)	[119] ([276])	 oxazinidinyl platensimycin	90 ^[a]	[273]
 iso-platencin	0.4–0.8	[276]	 iso-platensimycin	128	[268]

 carbaplatensimycin	1.1–2.2	[263]		>64	[272]
 adamantaplatensimycin	1.3–1.8	[262]		>64	[272]
 Ph	1	[267]		>1000	[274]
 CH ₃	1	[267]		>25.6	[276]
 dihydro-platensimycin	2	[233]		>64	[266]
 CH ₃	3.5–4.3	[264]		>64	[266]
 nor-platencin	4	[275]		>64	[266]
 CH ₃	8.0–10	[264]		>85	[264]
 CH ₃	16	[272]		>85	[264]
 platensimycin A ₁	16	[231]	 platensimide A	>1000	[274]
 CH ₃	17–20	[264]	 platensic acid methyl ester	>1000	[274]
 platensimycin A ₃	20	[274]	 platensimycin B ₃	>1000	[277]
 platensic acid	37–58 (>1000)	[264] ([274])			

[a] The molecule was synthesized and reported by Sintim group [273] and will be discussed in this dissertation.

Herein, we report the total synthesis and biological testing of oxazinidinyl platensimycin (2-30, **Scheme 2-6**) and a simplified oxazinidinyl analog (2-57, **Scheme 2-17**). This limited set of analogues was designed to answer two questions: a) Could the enone moiety of platensimycin be replaced with the oxazinidinyl ring to create a potential bioisostere compound 2? b) Could the tetracyclic core structure of platensimycin be replaced with other motifs that are synthetically easier to access?

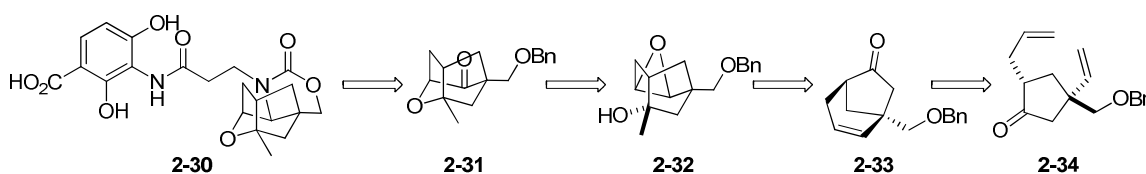
The choice of the oxazinidinyl moiety to replace the enone moiety was dictated by the observation by the Merck group that the enone functionality does not play a significant role in platensimycin inhibition of FabF [120]. Additionally, the replacement of the C4 atom (**Scheme 2-5**) with nitrogen will open up the possibility of synthesizing platensimycin analogs via reductive amination. Reductive amination reactions (**Scheme 2-5**), with sodium cyanoborohydride, do not require stringent inert or anhydrous conditions and are generally high yielding. Therefore the reaction is amenable for high-throughput synthesis; enabling the rapid syntheses of platensimycin analogs *via* the coupling of the aryl side chain with readily available 1,3-hydroxyketones to generate a library of oxazolidinyl platensimycin analogs with different core-structures for biological testing.



Scheme 2-5. Synthetic strategy towards platensimycin analogs.

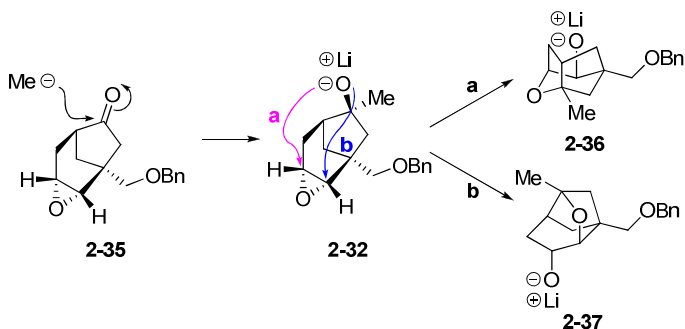
2.2.2 Synthesis of oxazinidinyl platensimycin

Scheme 2–6 outlines our retrosynthetic analysis for the core structure of platensimycin analogues. For the synthesis of the core structure of oxazolidinyl platensimycin **2–30**, bis-alkene **2–34** was chosen as a key intermediate that could be ring-closed with Grubb’s metathesis catalyst. Epoxidation of the resulting cyclic alkene would give compound **2–32**, after a nucleophilic addition to the ketone moiety.



Scheme 2–6. Retro-synthetic analysis of oxazinidinyl platensimycin.

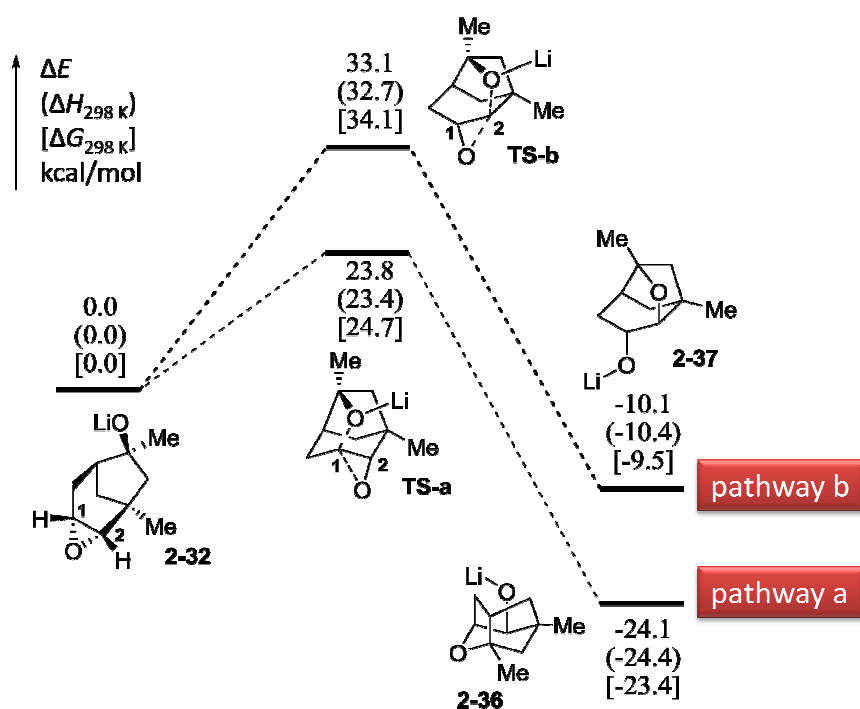
We reasoned that because the lone pairs of the hydroxyl oxygen anion of **2–32** overlapped with the π^* of the epoxide’s C-O bond, a facile 6-*exo-tet* ring closure should ensue to provide the tricyclic structure **2–36** (**Scheme 2–7**). Of concern was the possibility of obtaining the alternative diastereomer **2–37** via a 5-*exo-tet* ring closure.



Scheme 2–7. 6-*exo-tet* (pathway **a**) vs 5-*exo-tet* cyclization (pathway **b**).

DFT calculations, using the Gaussian 03 program, indicated that the activation energy of pathway **a** via the transition state structure **TS-a** was 9.8 kcal/mol lower than

that of pathway **b** via **TS-b**. This suggests that pathway **a** is more favorable than pathway **b** (**Scheme 2–8**). Diastereomer **2–37** contains a boat conformation and the ground state energy of **2–37** is 14.0 kcal/mol higher compared to **2–36** (**Scheme 2–8**). Also, for the optimized ground state geometry of compound **2–32**, the distance between the oxygen nucleophile and C1 atom (**Scheme 2–8**) was 3.2 Å whereas the oxygen nucleophile was 3.7 Å away from C2. Taken together, these analyses gave us the confidence that our key step towards the synthesis of oxazinidinyl platensimycin was viable and worth pursuing.

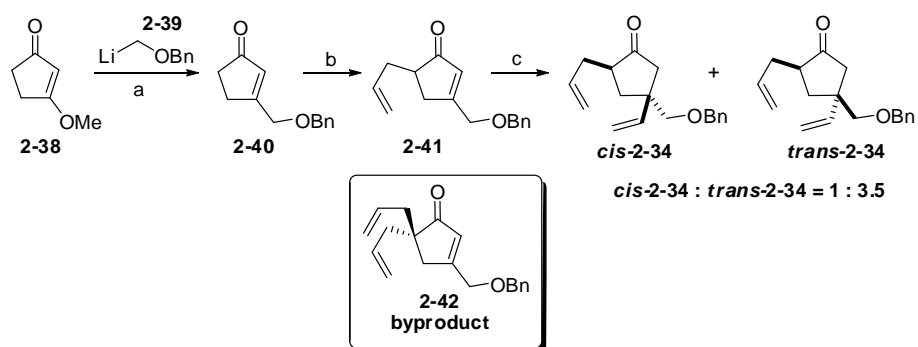


Scheme 2–8. The energy surfaces of pathway **a** and **b** for the epoxide ring-opening reaction

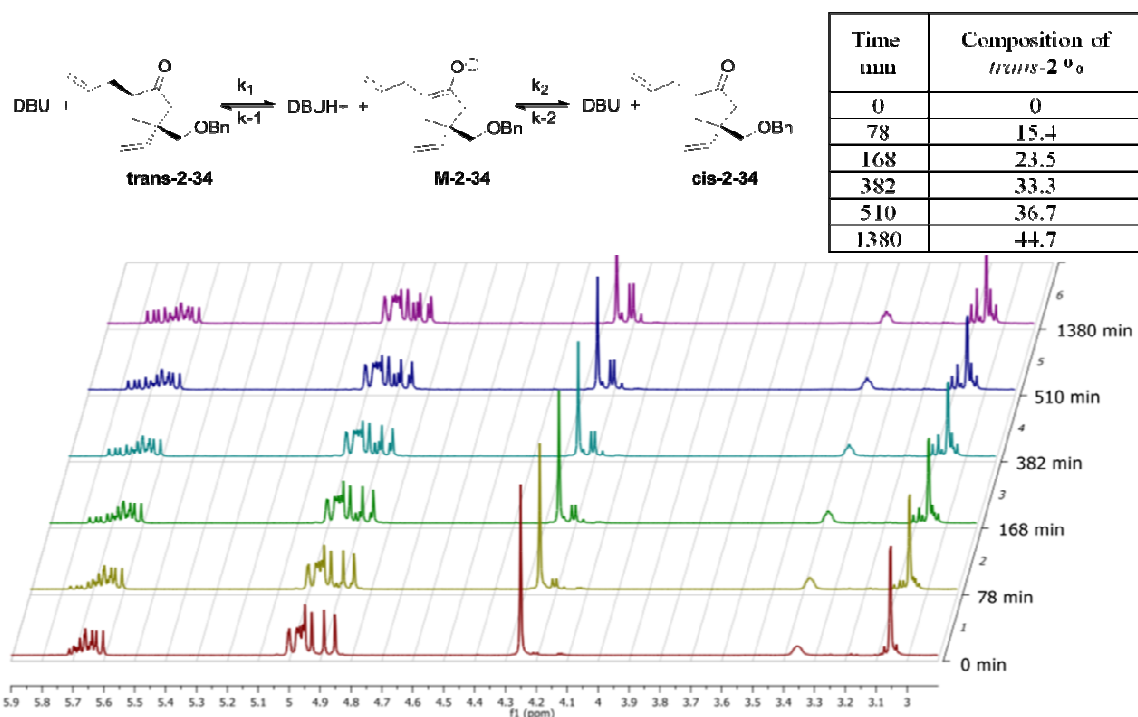
Initially, we set out to make bis-alkene **2–34**, the requisite substrate for the ring-closing metathesis reaction. Treatment of commercially available vinylgous ester **2–38** with anion **2–39**, generated from a stannane precursor *via* a lithium-tin exchange gave

enone **2-40** in good yield (84 %). The next step involved the allylation of enone **2-40** with an allyl halide. Allyl bromide only gave the desired product **2-41** in a meagre 34% yield accompanied by a substantial amount of diallylated product **2-42** (44 % yield). Interestingly, changing the allylation reagent to allyl iodide improved the yield to 62 % and the formation of the diallylated product was suppressed to 25 %. A conjugate addition of vinylolithium to enone **2-41**, in the presence of $\text{BF}_3 \cdot \text{Et}_2\text{O}$ resulted in a 1 : 3.5 mixture of *cis*-bis-alkene **2-34** and *trans*-bis-alkene **2-34** respectively. Unfortunately, the major product (*trans*-**2-42**) was not suitable for the subsequent ring-closing metathesis because the alkene moieties were *trans*- to each other (**Scheme 2-9**). The low overall yield of the desired *cis*-bis-alkene **2-34** led us to investigate the epimerization of compound *trans*-**2-34** to give *cis*-**2-34** (**Scheme 2-10**). Subjecting compound *trans*-**2-34** to 30 mol% DBU in toluene yielded an epimeric mixture of *trans*-**2-34**: *cis*-**2-34** in an 11: 9 ratio after 23 h (**Scheme 2-10**). It therefore appears that the undesired *cis*-bis-alkene **2-34** is both the kinetic and thermodynamic product.

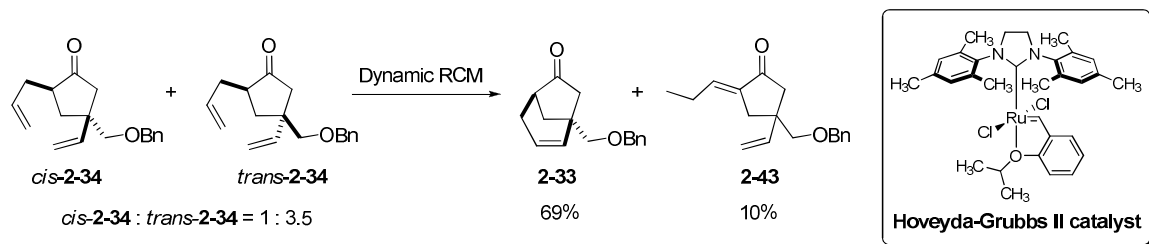
Under the experimental condition, *cis*-**2-34** and *trans*-**2-34** may reach 70 % of their equilibrium in about 6 hours (see **Appendix I**). We wondered if we could perform the ring-closing metathesis in the presence of DBU. Should the ruthenium catalyst be compatible with the amine base, then a dynamic ring-closing resolution should ensue and both diastereomers *cis*-**2-34** and *trans*-**2-34** would be suitable for the ring closing reaction. To the best of our knowledge, a dynamic ring-closing metathesis has not been reported in the literature. For the successful implementation of the dynamic ring-closing strategy, the ruthenium catalyst will have to survive the amine base for over 24 h at reflux conditions without being completely poisoned.



Scheme 2-9. Reaction conditions: a) LiCH_2OBn , THF, $-78\text{ }^\circ\text{C} \rightarrow \text{RT}$, 12 h, 84 %; b) LDA, HMPA, allyl iodide, THF, $-78\text{ }^\circ\text{C} \rightarrow \text{RT}$, 12 h, 62 % (67 % based on the starting material); c) $\text{Sn}(\text{CHCH}_2)_4$, *n*-BuLi, CuCN, $\text{BF}_3 \cdot \text{Et}_2\text{O}$, $-78\text{ }^\circ\text{C} \rightarrow \text{RT}$, 12 h, 85 %.

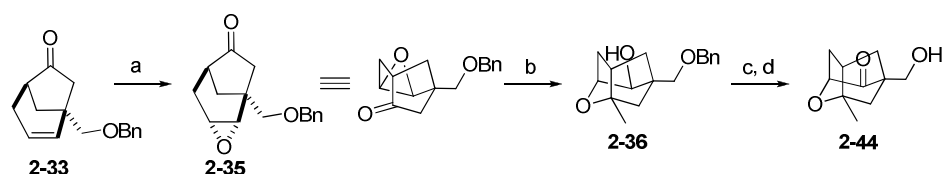


Scheme 2-10. Stacked NMR spectra of epimerization reaction of compound *cis-2-34* and *trans-2-34* under the condition: 30 mol% DBU, 0.02 M substrate (pure *trans*-bis-alkene **2-34**), $100\text{ }^\circ\text{C}$ in d_8 -toluene. The reaction was carried in a 5 mm NMR tube with oil bath and ^1H spectra were collected at room temperature within 5 min.



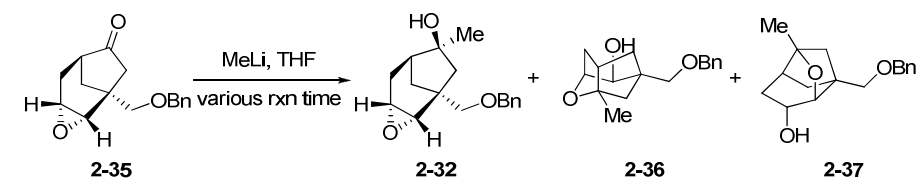
Scheme 2-11. Dynamic ring-closing metathesis. Reaction conditions: Hoveyda-Grubbs II catalyst (2 % x 5), 50 % DDQ, 30% DBU, toluene, 0.02 M compound **2-34**, reflux, 6 h each loading, 69 % (83 % based on the starting material). See Appendix II for more information.

Pleasingly, subjecting an epimeric mixture of compounds *cis-2-34*: *trans-2-34* (ratio of 1:3.5) to Hoveyda-Grubbs II catalyst in the presence of DBU and benzoquinone afforded the ring-closed product in 69 % yield (83 % based on the starting material, **Scheme 2-11**). In contrast, in the absence of DBU, the desired product could be obtained in a meager 20% yield. The benzoquinone additive was important for minimizing the formation of the enone by-product **2-43** [283]. For this protocol to work, it was important to add the ruthenium catalysts in 2 mol% portions five times over a 24 h period. The portion-wise addition of the catalyst was necessary because even though the catalyst was tolerant of the amine base to some extent, the ruthenium catalyst was decomposed under the experiment condition in a period of approximately one hour [284]. More reaction conditions screened for the dynamic ring-closing metathesis refer to Appendix II.



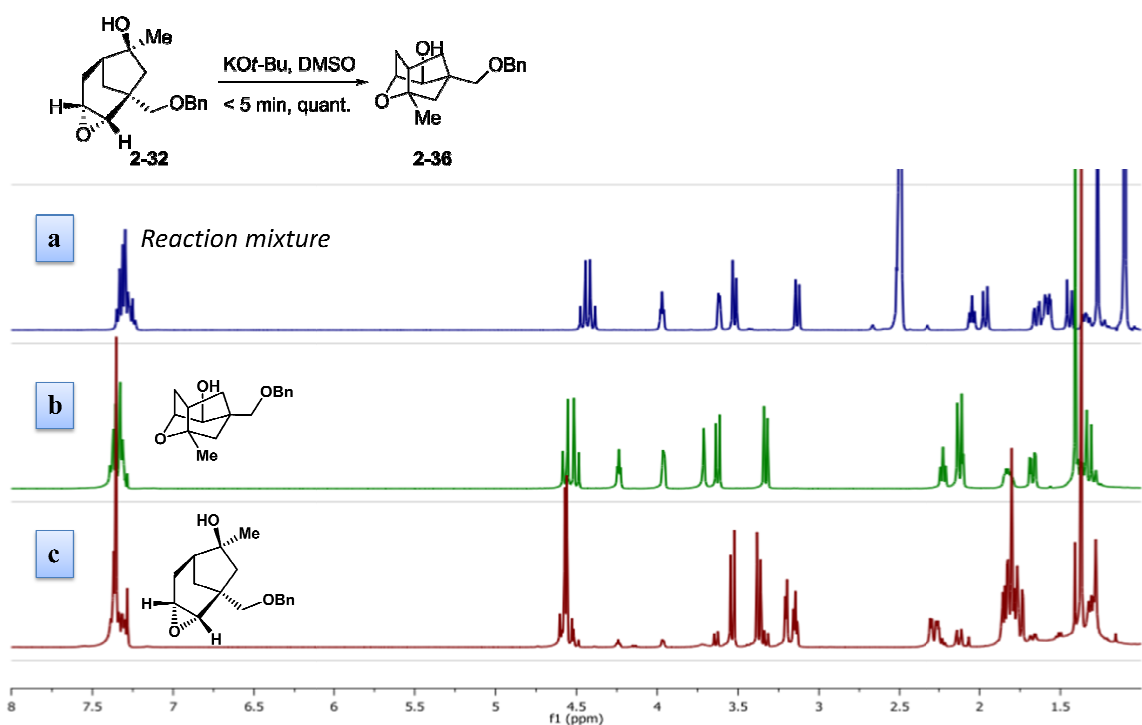
Scheme 2-12. Reaction conditions: a) *m*-CPBA, dichloromethane, 0 °C → RT, 12 h, 64 %; b) MeLi, THF, −78 °C → RT, 5 h, 70%; c) Dess-Martin reagent, CH₂Cl₂, RT, 12 h, 95 %; d) 10 mol% Pd/C, H₂, MeOH, RT, 12 h, 90 %.

With bicyclic compound **2–33** in hand, in gram quantities, we proceeded with the epoxidation reaction using *m*-CPBA. The epoxide **2–35**, obtained in 64 % yield, was then subjected to a tandem nucleophilic MeLi addition followed by a subsequent epoxide ring-opening to afford tricycle **2–36** in 70 % yield (**Scheme 2–13**). In line with our expectation, the 5-*exo-tet* pathway **b** product **2–37** was not observed (**Schemes 2–8** and **2–13**). Treatment of **2–32** with KO*t*-Bu (1.5 eq) in d₆-DMSO resulted in epoxide ring-opening product **2–36** within 5 minutes quantitatively (**Scheme 2–14**). Oxidation of compound **2–36** with Dess-Martin periodinane was followed by debenzylation with Pd/H₂ to afford **2–44** without any incident.

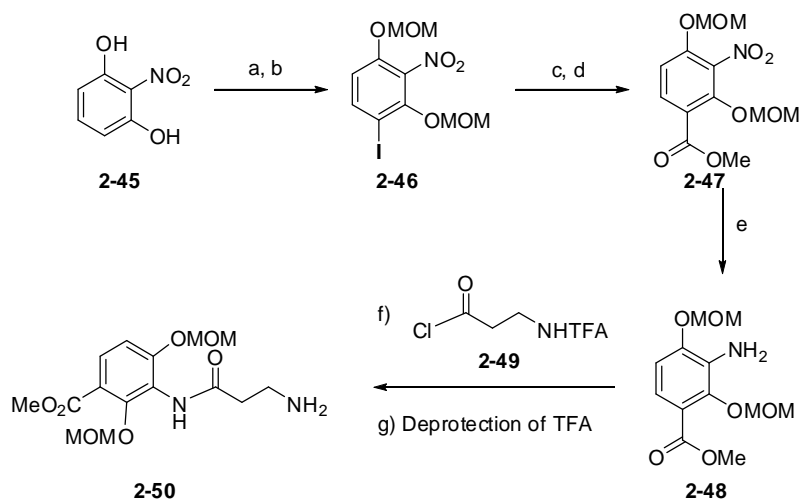


Entry	Temperature	Reaction time (h)	Product distribution
			2–32 : 2–36 : 2–37 (overall yield)
1	–78 → –10 °C	2	0.7 : 1 : 0 (87 %)
2	–78 → rt	6	0 : 1 : 0 (70 %)

Scheme 2–13. The product distribution of epoxide ring-opening reaction.



Scheme 2-14. Epoxide ring-opening reaction and the stacked NMR spectra of a) reaction mixture in d₆-DMSO; b) epoxide ring-opening product **2-36** in CDCl₃; c) epoxide ring-opening starting material **2-32** in CDCl₃.



Scheme 2-15. a) NIS, TFA, RT, 12 h, 100 %; b) MOMCl, Hunig base, CH₂Cl₂, RT, 12 h, 97 %; c) CNCO₂Me, PhMgBr, -78 °C → RT, THF, 12h, 78 %; d) MOMCl, Hünig base, CH₂Cl₂, RT, 12 h, 78 %; e) H₂, 10 mol% Pd/C, MeOH, 69%; f) pyridine, benzene, RT → 50 °C, 5 h, 95%; g) K₂CO₃, MeOH : H₂O = 3:1, RT, 10 h, 99 %.

The aromatic side chain of compound **5** was synthesized following the strategy shown in **Scheme 2–15**. The stage was now set to couple the aromatic side chain **2–50** with the tricyclic ring core **2–44**. The reductive amination intermediate **31** has two sterically similar faces (shown as faces **A** and **B** in **Figure 2–6**), and it appeared at first glance that a mixture of diastereomers would be obtained during the reductive amination step. We, however, postulated that because one face (face **B**) contained oxygen, subtle stereoelectronic factors could swing the selectivity towards the desired product. The Felkin-Anh model [285-287] is not suitable to interpret the stereoselectivity of this reaction. In Felkin-Anh model, the addition of nucleophiles to iminium **2–51** favors addition from face **A** (**Figure 2–6**) due to favorable interactions between the nucleophile and the low lying $\sigma^*_{\text{C-O}}$ bond. However, literature examples [288-291] indicated that, for tricyclic systems such as **2–51**, a Cieplak model [292,293] would be a more appropriate predictor for product distribution: A hydride approach from face **B** would lead to two $\sigma_{\text{C-C}}$ interacting favorably with the developing $\sigma_{\text{C-H}}$ bond whereas a hydride approach from face **A** will only lead to one $\sigma_{\text{C-C}}$ interacting favorably with the developing $\sigma^*_{\text{C-H}}$ bond. $\sigma_{\text{C-O}}$ bonds are low lying and not expected to make any significant hyperconjugative contribution. Additionally, transition-state dipole minimization between the C–O bond and the forming C–N bond dictates that approach from face **B** should predominate [294]. Together, these arguments strengthened our conviction that the desired product would be obtained via reductive amination. Model studies using a simplified side chain confirmed our prediction that hydride attack from face **B** predominates (**Scheme 2–16**).

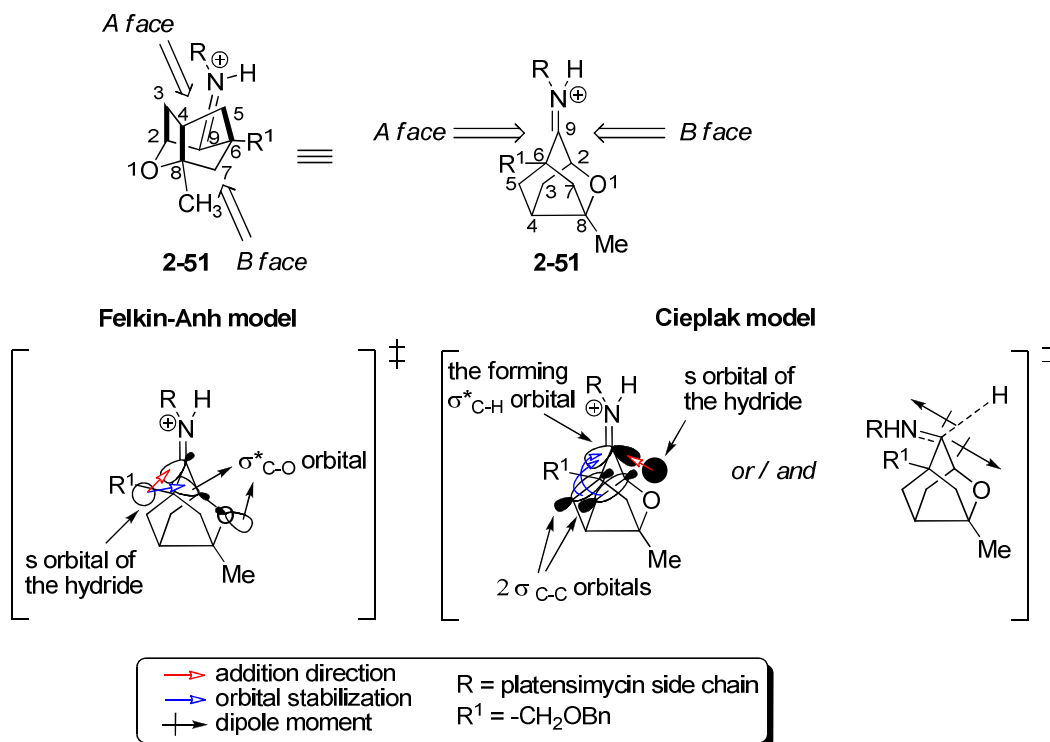
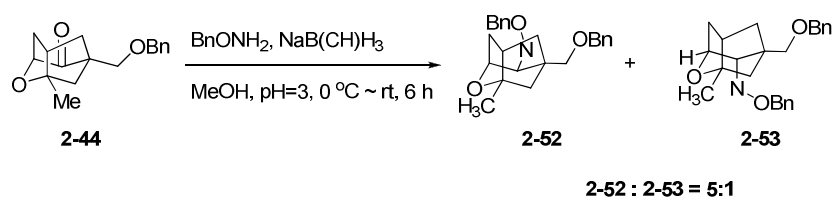


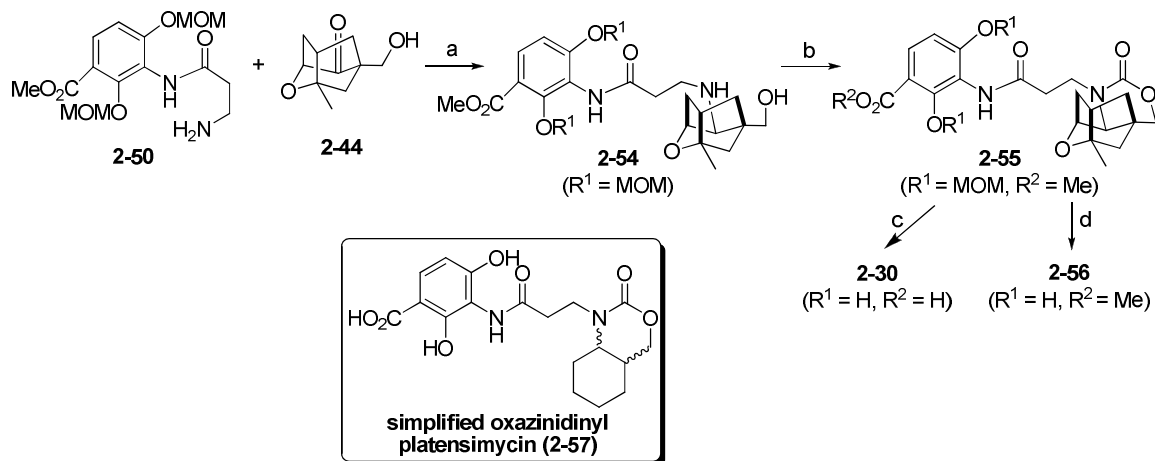
Figure 2–6. The origin of the facial selectivity of reductive amination of compound **2–44** and **2–50**. In Felkin-Anh model, the s orbital of the hydride is stabilized by interaction with the σ^* orbital of the C–O bond. In Cieplak model, the hyperconjugation of the forming $\sigma^*_{\text{C-H}}$ and the two $\sigma_{\text{C-C}}$ orbitals favors the nucleophilic addition from the B face. The dipole moment is also minimized in the transition state of B face addition.



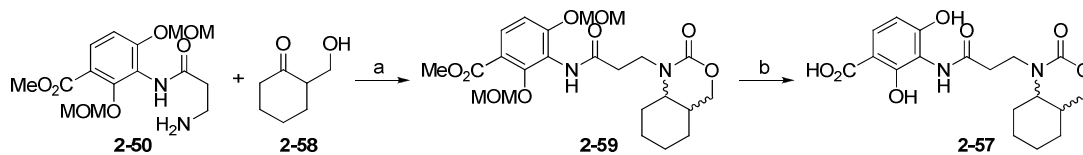
Scheme 2–16. Facial selectivity of reductive amination for a model reaction.

The end game of our synthesis proceeded smoothly. Reacting compounds **2-50** and **2-44** in methanol in the presence of sodium cyanohydride gave compound **2-54**; which was not purified but subjected to carbonyldiimidazole cyclization to afford **2-55** in 76% yield. Deprotection of the methyl ester and the MOM groups led to oxazinidinyl

platensimycin (**2-30**) in 80% yield over two steps. Oxazinidinyl cyclohexaplatensimycin (**2-57**) was synthesized following the strategy outlined in **Scheme 2-18**.



Scheme 2-17. a) $\text{NaB}(\text{CN})\text{H}_3$, MeOH, pH 4, RT, 5 h, 75%; b) carbonyl diimidazole, 20 mol % DMAP, benzene, 50°C , 12 h, 76%; c) 1 N LiOH, MeOH: H_2O = 2:1, RT, 12 h, then, 2N HCl, MeOH: H_2O = 2:1, RT, 24 h, 80%; d) 2 N HCl, MeOH: H_2O = 3:1, RT, 24 h, 92%.



Scheme 2-18. a) $\text{NaB}(\text{CN})\text{H}_3$, MeOH, pH 4, RT, 5 h; then, carbonyl diimidazole, 20 mol% DMAP, benzene, 50°C , 12 h, 70 %; b) 1 N LiOH, MeOH: H_2O = 2:1, RT, 12 h, then, 2N HCl, MeOH: H_2O = 2:1, RT, 24 h, 85 %.

2.2.3 The biological evaluation

Oxazinidinyl platensimycin (**2-30**) inhibited the growth of *Staphylococcus aureus* (Newman), *Streptococcus agalactiae* (2603V/R), and *Bacillus subtilis* (3160) at micromolar concentration (90 $\mu\text{g/mL}$). Despite its structural mimicry of platensimycin, oxazinidinyl platensimycin (**2-30**) is two orders of magnitude less potent.

Carbaplatensimycin (see **Table 2-2**), an analog that has the ethereal oxygen of platensimycin replaced with carbon, has an MIC of 3–4 μM (MRSA), which is close to that of the parent compound. It appears that the enone moiety of platensimycin is more important than the ethereal oxygen with regard to antibiotic activity. Oxazinidinyl platensinmycin methyl ester (**2-56**) did not inhibit bacterial growth at micromolar concentrations. We conclude, based on this work and others' [274] that bacterial esterases are unable to hydrolyze the ester analogs of platensimycin into active drugs.

Chapter 3. Syntheses and antibiotic activities of *N,N*-dialkylamino benzoic acids – second generation design of the platensimycin analogs

(The majority of the work was published in ref [295])

3.1 The design of dialkylamino benzoic acid analogs

Studies have shown that modifications on the 2,4-dihydroxybenzoic acid moiety of platensimycin diminish most of the antibiotic activity [264]. This is in agreement with the proposed mechanism whereby the dihydroxybenzoic acid subunit engages the His-His-Cys catalytic triad of the condensing enzymes (FabF/H) [120]. It therefore appears that efforts aimed at discovering simpler platensimycin analogs have a higher chance of success if the essential dihydroxybenzoic acid moiety is kept intact or minimally modified (**Table 2–2**).

Recently, several groups have focused their attention on the replacement of the “difficult-to-synthesize” tetracyclic core of platensimycin or platencin with moieties that are relatively easy to chemically prepare. For example the Metzler-Nolte group reported the synthesis and biological evaluation of a bioorganometallic analogs of platensimycin/platencin whereby the tetracyclic/tricyclic core of these antibiotics were replaced with a η^6 -arylCr(CO)₃ moiety [271]. Although the synthesis of the organometallic analogs of platensimycin took a total of nine linear steps, which was significantly shorter than the chemical synthesis of the parent platensimycin antibiotic, the MIC of these analogs were close to two orders of magnitude higher than platensimycin. Recently, Mulzer has reported a new analog that took only 7 total steps to make and which show antibiotic activity profile that is similar to those of platensimycin or platencin [276].

We rationalized that since FAS enzymes utilize substrates with long alkyl chains to make fatty acids [87] there ought to be a hydrophobic pocket at or near the active site of these enzymes. It is also known that dihydroxybenzoic acids bind to the catalytic triad in FAS enzymes [120]. In fact, other FAS inhibitors such as cerulenin [91], thiolactomycin [91] or alkyl disulfide [296] analogs contain hydrophobic alkyl or alkenyl side chains. Therefore we wondered if a combinatorial strategy whereby dihydroxybenzoic was coupled to a variety of commercially available alkyl chains would yield an active analog of platensimycin (**Figure 3–1**).

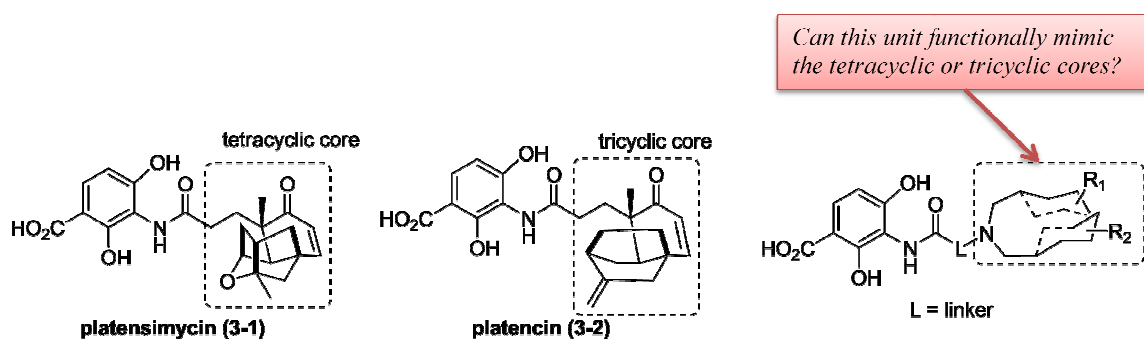
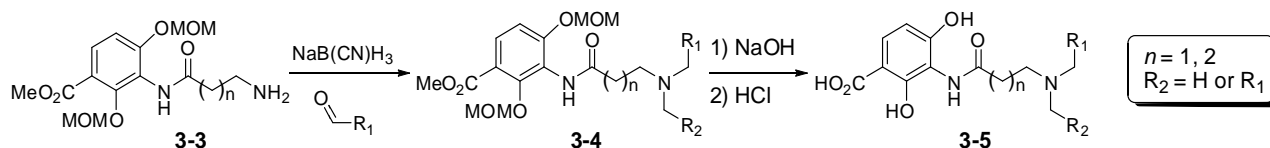


Figure 3–1. Design of second generation of platensimycin/platencin analogs.



Scheme 3–1. A general pathway to generate bis-alkylamino-2,4-dihydroxybenzoic acid analogs.

3.2 Synthesis and biological evaluation

En route to our reported synthesis of oxazinidinyll platensimycin [273], we demonstrated the facile synthesis of amine **3–3** (**Scheme 3–1**). This 2,4-dihydroxybenzoic acid ester with a terminal amino group **3–3** could be synthesized on gram-scale. A simple reductive amination with commercially available aldehydes

(**Scheme 3–3**) or reaction with acid chlorides or sulfonyl chlorides would then furnish myriads of easily accessible platensimycin/platencin analogs (see **Figures 3–2** and **3–3**).

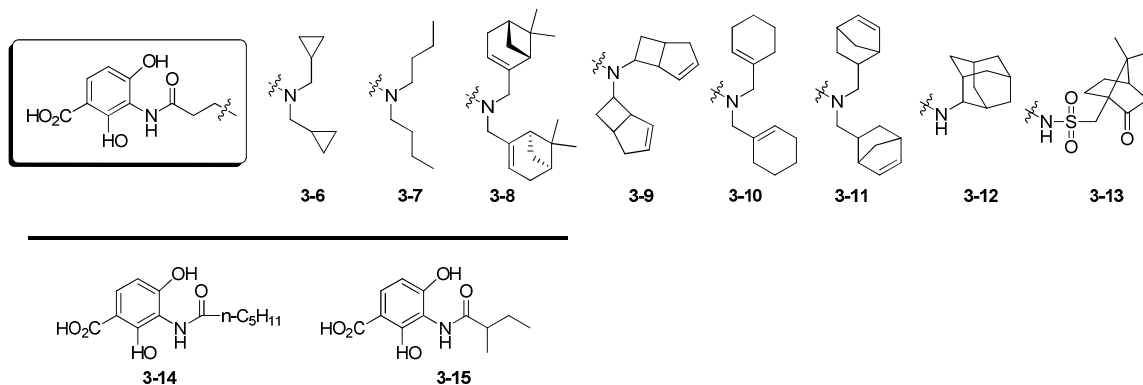


Figure 3–2. Synthesized analogs for the initial screening.

Table 3–1. MIC value of compounds **3–6** to **3–22**.

Compounds	MIC (μg/mL)	
	<i>B. subtilis</i> (3160)	<i>E. coli</i> K12 (1655)
platensimycin (1)	2	>32
3–6	>256	>256
3–7	128	>256
3–8	4	>256
3–9	>256	>256
3–10	>256	>256
3–11	>256	>256
3–12	>256	>256
3–13	>256	>256
3–14	>256	>256
3–15	>256	>256
3–16	>256	>256
3–17	>256	>256
3–18	8	>256
3–19	128	>256
3–20	2	>256
3–21	4	>256
3–22	>256	>256

Initial screening of analogs (**Table 3–1**), compounds **3–6** to **3–13**, revealed that compound **3–8** (a myrtenal derivative) had the most potency amongst the molecules

tested with MIC values of 4, 16 and 8 $\mu\text{g/mL}$ against *B. subtilis* (3160), methicillin-resistant *S. aureus* (MRSA) and vancomycin-resistant enterococci (VRE) respectively (Table 3–1, 3–2). The MIC of compound 3–8 against *B. subtilis* (4 $\mu\text{g/mL}$) compared favorably with the MIC of platensimycin against *B. subtilis* (2 $\mu\text{g/mL}$). The other bis-alkylamino analogs in Figure 3–2 were inactive and shows that the antibiotic activity of compound 3–8 is not just due to “greasiness”. Of note, compounds 3–10 and 3–11 which are structurally similar to compound 3–8 were found to be inactive. In line with earlier observation by the Merck group that platensimycin/platencin were ineffective against gram-negative bacteria [119,120], our new analog 8 was also ineffective against *E. coli* K12 (1655) (Table 3–1).

Table 3–2. MIC values of compounds 3–8, 3–20 and 3–21.

compounds	MIC, $\mu\text{g/mL}$		
	MRSA	VRE	<i>E. coli</i> + PA β ND
platensimycin (1)	0.5[120]	0.1[120]	>32
3–8	16	8	4
3–20	32	32	2
3–21	16	16	8

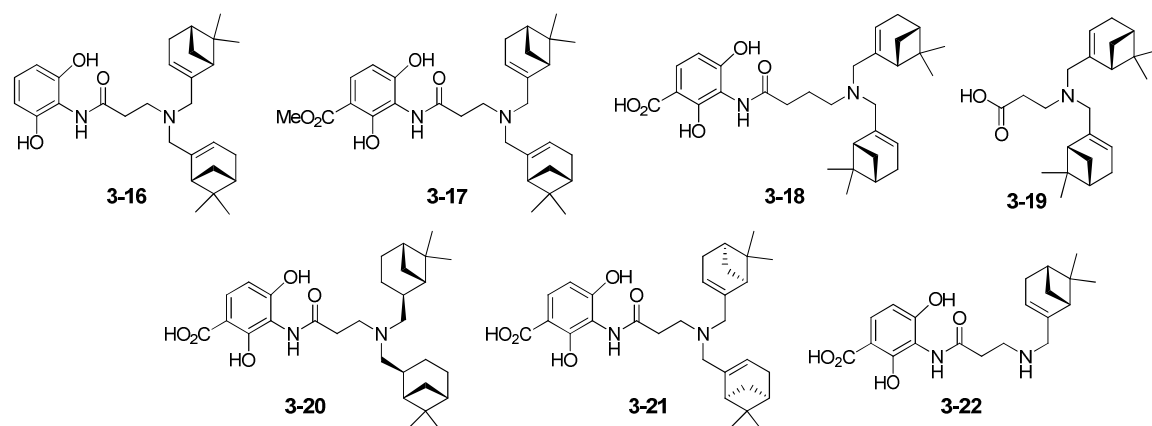


Figure 3–3. Second set of analogs and probes derived from (–)-myrtemycin.

We chose compound **3–8** as the lead structure and we designed a second set of structurally related compounds (**Figure 3–3**; compounds **3–16** to **3–22**). Compounds **3–16** and **3–17** tested the importance of the carboxylic acid moiety by either deleting or modifying as the methyl ester. Methyl esters can usually hydrolyze *in vivo* to produce carboxylic acids but we and others have previously shown that methyl esters of platensimycin are not good pro-drugs and do not hydrolyze into carboxylic acids under *in vivo* conditions [231,273,274]. This is not surprising because the presence of two phenolic hydroxyls on the benzoic acid core of platensimycin is expected to reduce the reactivity of the ester carbonyl towards hydrolysis. Compound **3–18** had one extra methylene group in the linker region between the benzoic acid core and the myrtenyl moiety and was designed to test the importance of the length of the linker unit. Compound **3–19** was designed to test if the benzoic acid moiety was as important in our analog as it is in the natural antibiotic. Compound **3–20** synthesized from saturated myrtanal, was designed to probe the importance of the alkene unit for biological activity. Compound **3–21** is the enantiomer of the lead compound **3–8** whereas compound **3–22** had only one (–)-myrtenyl group and was designed to test if both alkyl groups on nitrogen were needed for biological activity. The MIC values of the second-generation compounds **3–16** to **3–20** against *S. aureus* and *B. subtilis* are summarized in **Table 3–1**. From these results, we conclude that both carboxylic acid moiety and the di-myrtenyl/myrtyl groups are important for the antibiotic activity of compound **3–8**. Interestingly, the antibiotic activities of enantiomers (–)-**3–8** and (+)-**3–21** or the saturated form of (–)-**3–8**, compound (–)-**3–20** are similar (see **Table 3–1, 3–2**). Adding one carbon length between the benzoic acid moiety and the di-myrtenyl amino moiety

didn't change the MIC value significantly. However, analog **3–22** which had only one myrtenyl group attached to the nitrogen atom was inactive. The ineffectiveness of platensimycin/platencin against gram negative bacteria has been ascribed to efflux pumps in gram negatives that reduce the intracellular concentrations of this class of antibiotics [297]. Consequently, co-administration of efflux pump inhibitor, Phe-Arg- β -naphthylamide dihydrochloride (PA β ND), potentiated the effects of our new analogs on *E.coli*. In the presence of PA β ND at 128 μ g/mL, the MICs of compound **8** and analogs were 2–8 μ g/mL. Interesting, these MICs were even lower than that of platensimycin in the presence of PA β ND (see **Table 3–2**).

In summary, we illustrate that biological function can be replicated with moieties that are easier to install but which would not have been predicted based on structure homology design. Significantly, we report a new set of analogs, which are exceptionally simple to make (three linear steps from commercial materials) yet they maintain biological activities that are comparable to the natural compounds which are typically synthesized in over 15 linear steps. Ongoing work in our laboratory is currently focused on investigating if these new platensimycin analogs target the same biological targets as those of platensimycin and platencin.

Chapter 4. C-di-GMP mediated biofilm formation in bacteria and efforts towards anti-biofilm agents.

4.1 Endo-S-c-di-GMP, a conservative change to the phosphate moiety of c-di-GMP

4.1.1 Introduction

C-di-GMP signaling has become of interest in the development of anti-biofilm or anti-virulence drugs because it has recently been shown that it regulates diverse phenotypes in bacteria including biofilm formation [203]. Despite the central role that c-di-GMP plays in bacterial “lifestyle”, several aspects of this signaling molecule remain far from being understood. For example, the so-called adaptor proteins that bind to c-di-GMP and transmit this binding event into processes, which lead to biofilm formation, are poorly characterized. Most of the c-di-GMP adaptor proteins, which have been found so far (for example the PilZ family) do not have any enzymatic activities of their own, suggesting that they probably relay the c-di-GMP binding event into allosteric modulation of other enzymes that they associate with. However, these associated enzymes or factors of c-di-GMP adaptor proteins have largely not been found. An interesting property of c-di-GMP is its ability to readily form dimers, tetraplexes and higher aggregates in the presence of cations [226,227]. Divalent cations such as magnesium promote dimer formation in c-di-GMP whereas monovalent cations such as potassium promote the formation of tetraplexes and octaplexes in c-di-GMP [226,227]. This propensity of c-di-GMP to form tetraplexes or octaplexes (G-quadruplexes) at micromolar concentrations in the presence of cations (such as magnesium and potassium) is intriguing because simple nucleotides (such as cGMP, GTP or pGpG) do not readily form G-quadruplex structures at micromolar concentrations. Plausibly, the facile

interconversion of c-di-GMP into different aggregation states (especially in the presence of cations) could be a means whereby bacteria regulate biofilm formation in the presence of different metals.

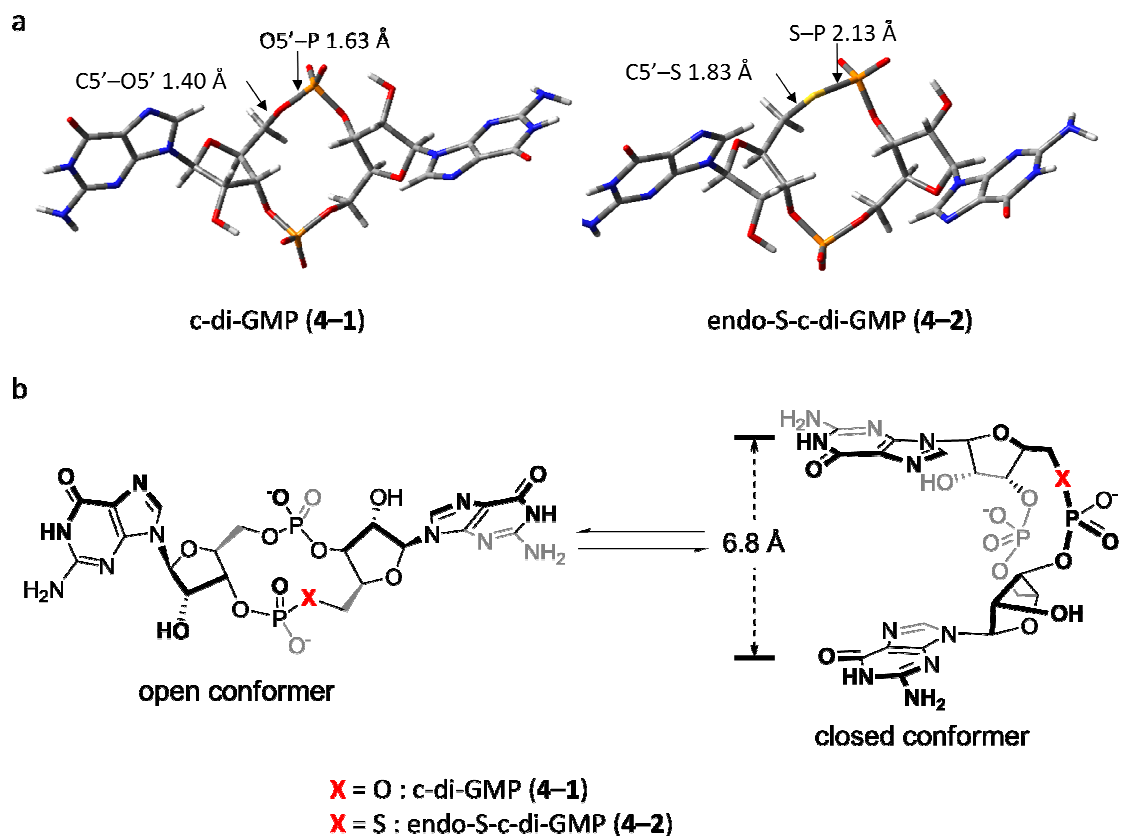


Figure 4-1. a) Structures of c-di-GMP (4-1, left) and endo-S-c-di-GMP (4-2, right) monomer. The structure was optimized by Gaussian 09 software[298] with HF/6-31G(d) basis set; b) two general conformers of c-di-GMP and analogs (open and closed).

Understanding the structural features which allow c-di-GMP to readily form aggregates is important for the fundamental understanding of how different nucleic acids adopt different architectures, as well as for providing insights into how this important bacterial signaling molecule (c-di-GMP) achieves its interesting polymorphism. We have been particularly interested in G-quadruplex formation by c-di-GMP and how this is so

readily achieved when the dinucleotide pGpG does not so readily form intermolecular G-quadruplexes. As both c-di-GMP and pGpG contain guanine bases, which are required for the formation of the G-tetrad plane found in G-quadruplexes, it is reasonable to assume that other structural features found in c-di-GMP, but not in the linear pGpG, are responsible for the enhancement of G-quadruplex formation. Herein, we reveal that small changes to the phosphodiester backbone of c-di-GMP (0.92 Å increase in the circumference of the backbone ring; **Figure 4–1a**) remarkably decrease the propensity to form G-quadruplexes. We show that a c-di-GMP analog which has one of the oxygens in the 5'-bridging phosphodiester linkages replaced by sulfur (endo-S-c-di-GMP (**4–2**), **Figure 4–1b**) has altered biophysical and biochemical properties, distinct from those of c-di-GMP.

One general strategy that is typically used by drug developers to discover antagonists of signaling molecules is to modify the signaling molecule to afford analogs [299] that still maintain the ability to bind to the receptors that the signaling molecule binds to but unable to activate the receptors for biological function. In order to develop effective c-di-GMP analogs, which will be used to antagonize the actions of c-di-GMP, it is of interest to determine which functionalities on c-di-GMP could be modified to maintain binding to c-di-GMP processing proteins, without triggering processes that lead to biofilm formation. The aggregation of a c-di-GMP antagonist into higher aggregates would reduce its effective molarity. Therefore, we initiated a program to determine which moieties on c-di-GMP facilitate aggregate formation. C-di-GMP is a twelve-membered ring with limited conformational flexibility. The crystal structure of c-di-GMP reveals that the torsion angles found in this macrocycle are similar to those found in standard

linear RNAs, implying that the ring structure imposes little to no torsional stress to this molecule [300].

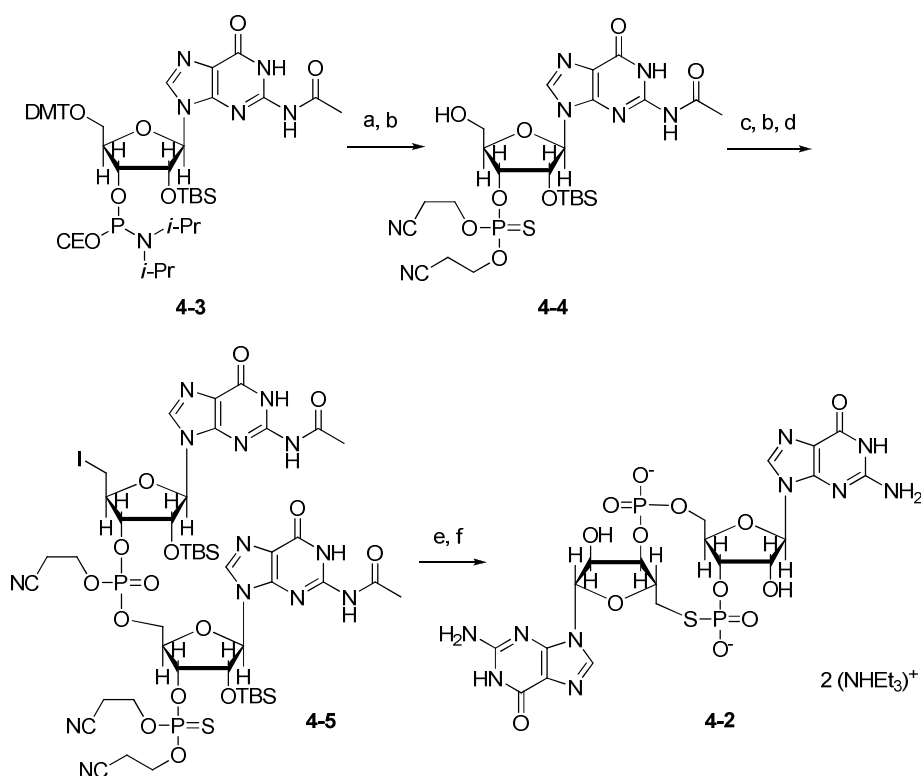
The ability of c-di-GMP but not linear pGpG, to readily form dimers and G-quadruplexes at micromolar concentrations prompted us to hypothesize that the lack of conformational flexibility in c-di-GMP, coupled with the low torsional stress in the macrocycle poise this molecule to make aggregates, such as G-quadruplexes or dimers (**Figure 1–16**). As a starting point to determine if the 12-membered ring of c-di-GMP is critical to its biophysical (aggregate formation) as well as biochemical (binding to receptors) properties, we chose to study a very close analog of c-di-GMP, referred in this thesis as endo-S-c-di-GMP (**4–2**).

The replacement of oxygen at the bridging positions in phosphate linkages in nucleic acids can be considered conservative; Kool has shown that the thermal stabilities of DNAs containing phosphodiester linkages have similar thermal stabilities as native DNAs [301]. Enzymes, such as Klenow DNA polymerase or T7 RNA polymerase, can utilize templates containing phosphothioates as effectively as those containing native phosphodiester linkages and no pauses were observed at the phosphothioester sites when these replicative enzymes were used [301].

4.1.2 Synthesis of endo-S-c-di-GMP.

The synthesis of endo-S-c-di-GMP (**4–2**) is summarized in **Scheme 4–1** (22% overall yield from commercially available phosphoramidite **4–3**). The key step for the synthesis of **4–2** is the phosphothioate–iodide macro-ring closure, developed by Kool [302]. It has been shown by several researchers that the “bridging” positions in the phosphate linkages of both DNA [303–307] and RNA [308–311] can be replaced by sulfur

to give phosphothioester linkages. In DNA, 5'-phosphorothioester linkages are stable [301] whereas for RNAs, 5'-phosphorothioesters are about six fold more labile than the natural phosphodiester linkages at pH 7 [308]. Although endo-S-c-di-GMP (**4-2**) also contains 2'-OH (the functionality that is responsible for facilitating hydrolysis in RNA) it is stable at neutral pH because the cyclic structure positions the phosphate moiety more than 3.3 Å away from the 2'-OH, making it impossible for the 2'-OH in endo-S-c-di-GMP to participate in an in-line cleavage reaction [312].



Scheme 4-1. Synthesis of endo-S-c-di-GMP (**4-2**). Conditions: a) cyanoethyl alcohol (5.0 eq.), imidazolium perchlorate (3.6 eq.), 6 h, then Beacauge reagent (2.5 eq.), 1 h, MeCN, RT; b) dichloroacetic acid (11–14 eq.), CH₂Cl₂, 10 min, 60 % over two steps; c) phosphoramidite **4-3** (1.5 eq.), imidazolium perchlorate (4.7 eq.), then *t*-BuOOH (9.3 eq.), MeCN, RT, 6 h; d) Me(PhO)₃P⁺I⁻ (5.3 eq.), 2,6-lutidine (20 eq.), DMF, RT, 1 h, 61 % over three steps; e) ammonia, RT, 24 h; f) NEt₃·3HF (20 eq.), MeCN, RT, 12 h, 59 % over two steps. DMF = dimethylformamide.

4.1.3 Polymorphism of c-di-GMP and endo-S-c-di-GMP

C-di-GMP can exist in myriads of conformations. These conformations can be generally categorized as “closed” (the two guanine bases are on the same face) or “open” (the two guanines are on opposite faces). Calculations using Gaussian 09 software with HF/6-31G(d) basis set revealed that the ground state conformer of c-di-GMP is an open conformer whereby the C5s of the two guanines are 13.5 Å apart. The “closed” conformer of c-di-GMP, where the two guanines are parallel and separated by 6.8 Å, is biologically relevant and found in the active site of many c-di-GMP binding proteins (for recent examples see protein databank (PDB) crystal structures 3KYF [229], 3KLO [313] and 3I5A [314]). Computational studies revealed that the torsion angle [300] of endo-S-c-di-GMP is different from that of the native c-di-GMP (**Table 4–1**). From these computational studies, we predicted that the aggregative behavior of endo-S-c-di-GMP would be different from that of c-di-GMP.

Table 4–1. Backbone torsion angles for computed c-di-GMP and endo-S-c-di-GMP structures.

		Angle, degrees					
		α	β	γ	δ	ε	ζ
c-di-GMP ^a	open ^d	72.3	–163.9	50.4	96.1	–161.5	63.6
	closed ^e	79.7	–151.9	55.1	83.2	–179.4	64.9
endo-S-c-di-GMP ^b	open ^f	63.9	–146.6	58.9	94.3	–164.1	64.8
	closed ^e	68.5	–137.6	64.5	80.6	–179.9	65.9
linear RNA ^c		73.8	–168.2	62.2	81.6	–147.1	63.9

The dihedral angular notations are determined as follows: a) O3'–P ^{α} –O5'–C5' ^{β} –C5' ^{γ} –C4' ^{δ} –C3' ^{ε} –O3' ^{ζ} –P–O5'; b) O3'–P ^{α} –S ^{β} –C5' ^{γ} –C4' ^{δ} –C3' ^{ε} –O3' ^{ζ} –P–O5'; c) These are average values, taken from PDB 3MXH; d) C5–C5 of the guanines are 13.5 Å apart; e) C5–C5 of the guanines are 6.8 Å apart; f) C5–C5 of the guanines are 11.7 Å apart as the most stable conformer.

It is expected that the “closed conformer” of c-di-GMP (**4-1**) or endo-S-c-di-GMP (**4-2**) would more readily form dimers or G-quadruplexes than the open conformers of c-di-GMP and endo-S-c-di-GMP (**Figure 1-16**). This is because in the closed conformation of both c-di-GMP and endo-S-c-di-GMP, the two guanines are suitably positioned for mutual intercalation (dimer, **Figure 1-16**) or for forming G-quadruplexes (**Figure 1-16**). One can therefore reliably predict the relative aggregative property of a c-di-GMP analog by comparing the relative energy difference between the “closed” and “open” conformers of an analog to that of c-di-GMP.

Computational studies done on both c-di-GMP and endo-S-c-di-GMP (both gas phase and using a solvent model) revealed that c-di-GMP is more likely (~ three times) to form a “closed” conformer than endo-S-c-di-GMP (see Table 2). This prediction was verified experimentally; the ¹HNMR spectra of triethylammonium c-di-GMP and endo-S-c-di-GMP show that both compounds exist as monomeric forms at 20 °C in the absence of monovalent cations such as K⁺ (see **Figure 4-2c** and **4-3c**). The ¹HNMR spectrum of c-di-GMP (which is C₂ symmetric) shows two singlets at 5.87 and 7.96 ppm, assigned to the anomeric H1' and guanine H8 protons, respectively (**Figure 4-2c**). Endo-S-c-di-GMP is not C₂ symmetric, due to the presence of one “bridging” sulfur atom in the phosphothioate moiety and therefore the two anomeric H1' as well as the two guanine H8 in endo-S-c-di-GMP are chemically non-equivalent and have different chemical shifts (**Figure 4-3c**). The guanine H8 in endo-S-c-di-GMP appears as two singlets of equal intensities at 7.90 and 8.02 ppm, and the anomeric H1' in endo-S-c-di-GMP appears as a singlet at 5.95 and a doublet at 5.85 ppm (**Figure 4-3c**). Upon the addition of 100 mM K⁺ to c-di-GMP, the intensities of the peaks at 7.96 and 5.87 ppm are reduced and other

peaks appear around 7.96 and 5.87 ppm (**Figure 4–2b**). These peaks are attributed to the different aggregates of c-di-GMP because upon heating the sample to 60 °C (which will break all aggregates), the multiple peaks disappear and new singlet peaks at 8.39 and 6.30 ppm appear (corresponding to the guanine H8 and the anomeric H on c-di-GMP respectively, **Figure 4–2a**). The shift in ppm values for monomeric c-di-GMP is expected as temperature affects ppm values [315]. Based on integration of the peaks in the ¹H NMR spectrum of c-di-GMP in a buffer containing 100 mM potassium cations at 20 °C, we estimate that only 14 % of c-di-GMP exists in the monomeric form under this condition (**Figure 4–2b**). On the other hand, upon the addition of 100 mM K⁺ to endo-S-c-di-GMP, 43 % of the monomeric form still remains in the solution (compare **Figures 4–2** and **4–3**). It therefore appears that c-di-GMP has a higher propensity to form aggregates than endo-S-c-di-GMP and it is remarkable that a single conservative substitution in the phosphate moiety can result in such drastic consequences.

Table 4–2. Energy difference between “open” and “closed” forms of c-di-GMP and endo-S-c-di-GMP.

	ΔE^{gas} (open–closed) ^a kcal/mol	ΔE^{sol} (open–closed) ^b kcal/mol	ratio (open : closed) ^c	
			gas phase	solution phase
c-di-GMP	–1.9	1.9	24: 1	1: 25
endo-S-c-di-GMP	–2.8	1.3	113: 1	1: 9

a) The electronic energy (in the gas phase) was computed with Gaussian 09 software [298] with HF/6-31G(d) basis set; b) The solvent effect in H₂O was calculated with Onsager’s model in a self-consistent reaction field (see Supporting Information for details); c) the ratio was determined from the equilibrium constant K , obtained from the equation $\Delta E = -RT \ln K$ ($T = 298$ K).

In order to determine the nature of the aggregation states of both c-di-GMP and endo-S-c-di-GMP, DOSY experiments were conducted (see Appendix II for a brief introduction). Following literature precedent, the diffusion constants of the various c-di-GMP/endo-S-c-di-GMP aggregates were obtained via analysis of T_1/T_2 relaxation [316]. According to the Stokes-Einstein equation, the hydrodynamic frictional coefficients or the diffusion constant $D = k T / (6 \pi \eta R)$, where k is the Boltzmann constant, T is the temperature, η is the solvent viscosity and R is the radius of the molecular sphere. It therefore follows that the diffusion constant is inversely proportional to the radius of the molecule (or aggregate). The diffusion constants of c-di-GMP and endo-S-c-di-GMP in their monomeric forms can be obtained via DOSY experiments, in the absence of added metal cations (**Figures 4-2c, 4-2d, 4-3c and 4-3d**). Based on the obtained diffusion constant for monomeric c-di-GMP or endo-S-c-di-GMP, the diffusion constants for the dimeric, tetrameric and octameric forms can be predicted, using calculated radii of these aggregates (**Figures 4-2d, 4-3d** and Section 6.5.2). The monomer, dimer, tetramer and octamer of c-di-GMP or endo-S-c-di-GMP are denoted as M, B (Bimolecular, consistent with previous report ref [227]), T and O, respectively in **Figures 4-2b** and **4-3b**. For c-di-GMP, the majority of the aggregates in the presence of K^+ are tetrameric (T) and octameric (O) [227], with predicted diffusion constants at 2.01×10^{-10} and $1.62 \times 10^{-10} \text{ m}^2/\text{s}$; the experimental diffusion constants of the tetramer and octamer forms of c-di-GMP (obtained from the DOSY experiment) are 1.91×10^{-10} and $1.60 \times 10^{-10} \text{ m}^2/\text{s}$, respectively. For endo-S-c-di-GMP, the only identified aggregate state in the presence of K^+ was dimers (B), with the predicted and experimental diffusion constants at 2.07×10^{-10} and $1.93 \times 10^{-10} \text{ m}^2/\text{s}$, respectively (Section 6.5.2).

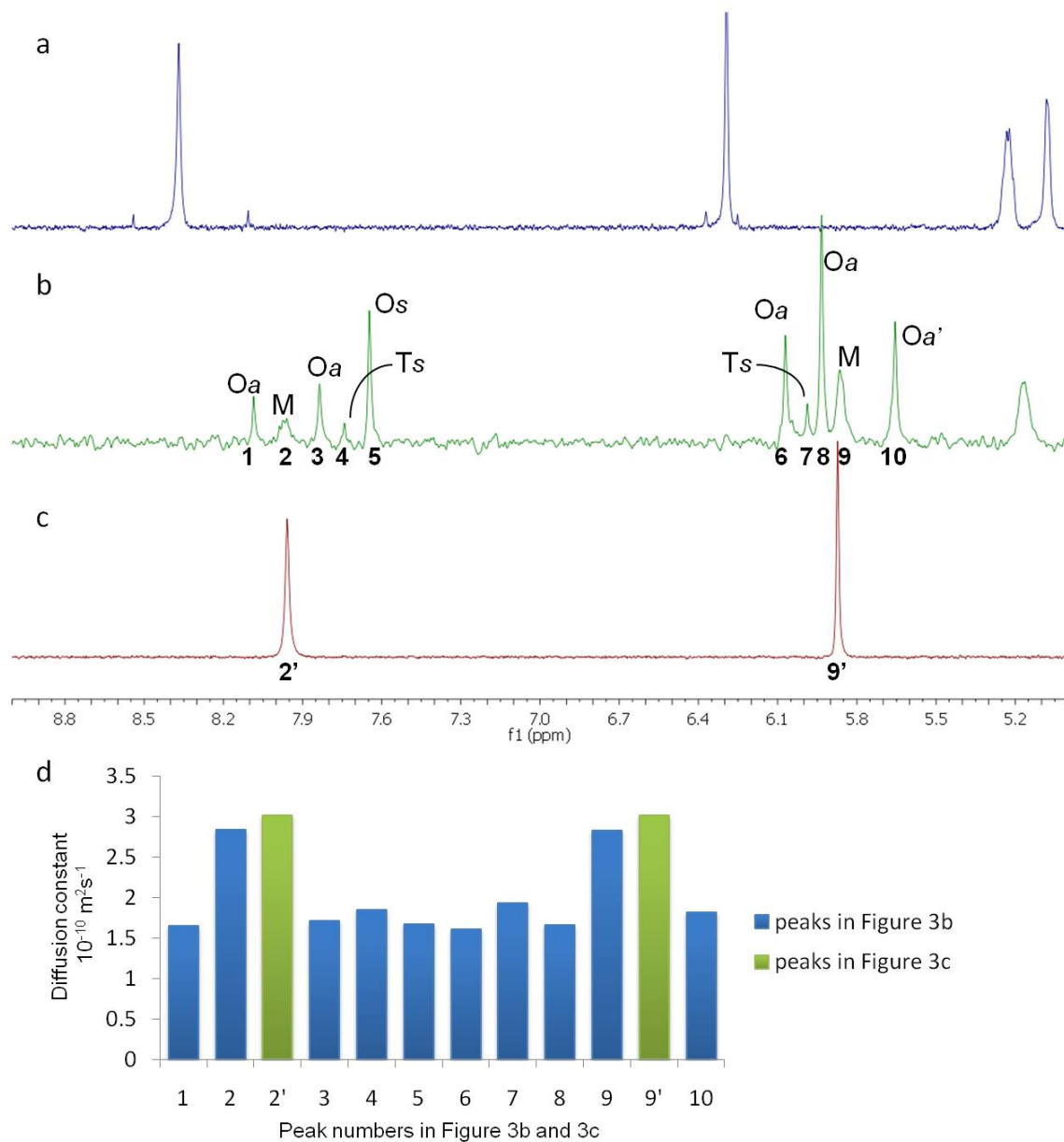


Figure 4-2. ¹H NMR stacked spectra of 1.0 mM c-di-GMP in D₂O. Conditions: a) 100 mM KCl, 60 °C; b) 100 mM KCl, 20 °C; the peaks were assigned based on T₁/T₂ relaxation analysis and ref 18; c) no metal cation, 20 °C; d) T₁/T₂ relaxation analysis (from DOSY experiments) with 3 mM c-di-GMP in D₂O in 100 mM KCl (blue) or no KCl added (red) solution at 30 °C.

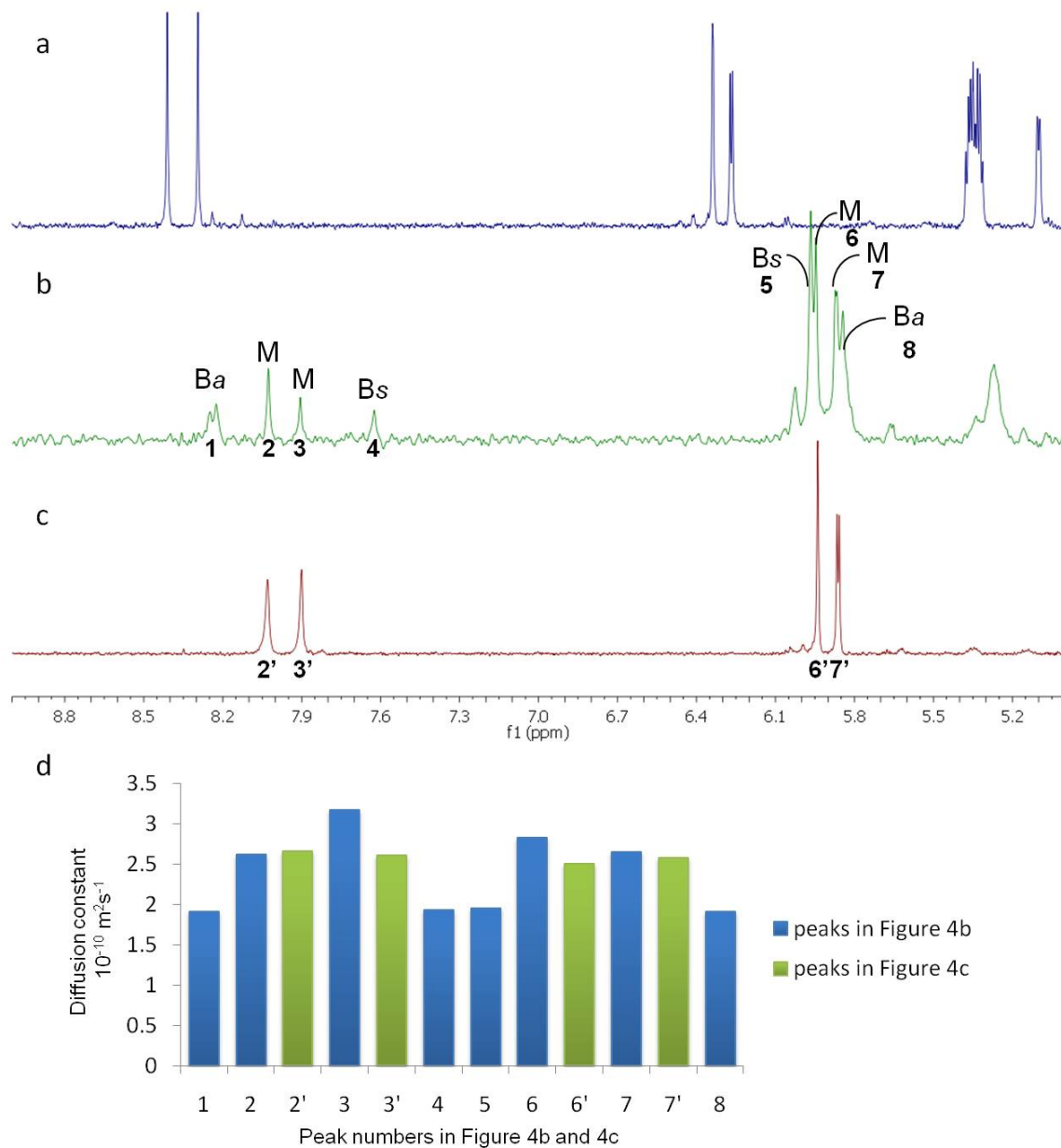


Figure 4–3. ¹H NMR stacked spectra of 1.0 mM endo-S-c-di-GMP in D₂O. Conditions: a) 100 mM KCl, 60 °C; b) 100 mM KCl, 20 °C; the peaks were assigned based on T₁/T₂ relaxation analysis and NOE experiments (see Supporting Information); c) no metal cation, 20 °C; d) T₁/T₂ relaxation analysis (from DOSY experiments) with 3 mM endo-S-c-di-GMP in D₂O in 100 mM KCl (blue) or no KCl added (green) solution at 30 °C.

The relative conformations of the guanine H8 and anomeric H1' were determined, following previous reported method [227]. Guanine H8 and anomeric H1, in the *syn* conformation, are expected to exhibit strong positive NOE effects; whereas guanine H8, in the *anti* conformation, is expected to show a much weaker NOE effect with the anomeric H1 (Section 6.6.1). The *syn* or *anti* relation was denoted as “s” or “a” in **Figures 4–2b** and **4–3b**, respectively. For example, Ba represents a dimeric endo-S-c-di-GMP with the H1' and H8 in an *anti* conformation in **Figure 4–3b**.

Circular dichroism (CD) is a powerful tool for identifying the aggregation state of nucleic acids [227,317,318]. Although CD cannot give detailed molecular structure of G-quadruplex (tetramolecular or octamolecular complexes), it can be used to qualitatively determine if a G-quadruplex is present in solution. Jones has shown that a positive CD peak at around 310 nm is indicative of tetramolecular or octamolecular complex formation by c-di-GMP [227]. This CD signature which indicates the presence of c-di-GMP tetramolecular or octamolecular complexes was corroborated with NMR studies by Jones group.

The CD (circular dichroism) spectra of c-di-GMP (under different conditions) are also remarkably different from that of endo-S-c-di-GMP (**Figure 4–4**). In the presence of potassium cation, c-di-GMP (100 μ M) forms G-quadruplexes (a positive CD peak around 310 nm is indicative of G-quadruplex formation in c-di-GMP, see **Figure 4–4a** and also reference [227]). However, the CD spectra of endo-S-c-di-GMP (100 μ M) in the presence of various monovalent cations (Na^+ , K^+ , Li^+) do not show any sign of G-quadruplex formation (no positive peak around 310 nm, see **Figure 4–4b**). Even when

the concentration of endo-S-c-di-GMP is increased to 200 μM , no G-quadruplex formation is observed (Figure 4–4c).

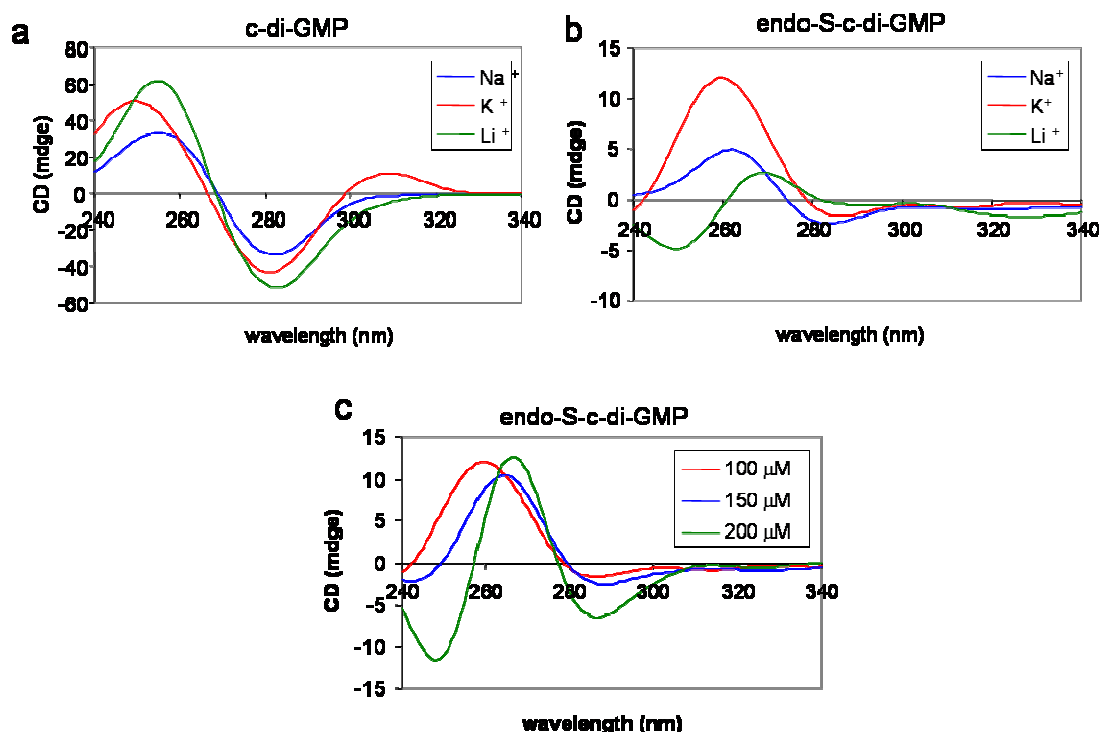


Figure 4–4. CD spectra of c-di-GMP and endo-S-c-di-GMP. Conditions: 10 °C, [MCl; M is Li, Na or K] = 1.0 M, 10 mM Tris-HCl (pH 7.5). a) 100 μM c-di-GMP; b) 100 μM endo-S-c-di-GMP; c) 100, 150 and 200 μM of endo-S-c-di-GMP in 1.0 M of KCl.

4.1.4 C-di-GMP and endo-S-c-di-GMP binding to metabolism and “adaptor” proteins

Having established via NMR and CD studies that endo-S-c-di-GMP has a lower propensity to form aggregates (dimers and tetraplexes), we proceeded to investigate if endo-S-c-di-GMP would bind to proteins that have been previously shown to bind to the native c-di-GMP. Most of the crystal structures of c-di-GMP, bound to various proteins, reveal extensive interactions between the protein residues and the phosphate and

nucleobase moieties of c-di-GMP. For example, the phosphate moieties of c-di-GMP interact with Arg479 and Gln596 of the EAL domain of FimX [202,228] (from *Pseudomonas aeruginosa*, and binds monomeric c-di-GMP, **Figure 4–5c**) The majority of c-di-GMP binding proteins, whose crystal structures have been deposited in the protein databank (pdb), bind to dimeric c-di-GMP. In the majority of these structures, the protein residues interact with the phosphate moiety of c-di-GMP. The crystal structure of dimeric c-di-GMP bound to VpsT [313,319] (a transcriptional regulator from *V. cholerae*) reveal that Thr133 and Arg134 as well as other residues make specific interactions with the phosphate groups of c-di-GMP. Similarly, Arg123 and Asn124 of P4397 (a c-di-GMP “adaptor” protein containing the PilZ domain [209,229]) interact with the phosphate moiety in dimeric c-di-GMP (**Figure 4–5b**). Most diguanylate cyclases contain an inhibitory site (I-site) that allosterically modulates the synthesis of c-di-GMP [320]. WspR, a DGC from *Pseudomonas aeruginosa* also contains the I-site and analysis of a crystal structure of WspR bound to dimeric c-di-GMP (**Figure 4–5a**) [314] reveals specific interactions between the protein and the phosphate group found in c-di-GMP (**Figure 4–5d**) [321].

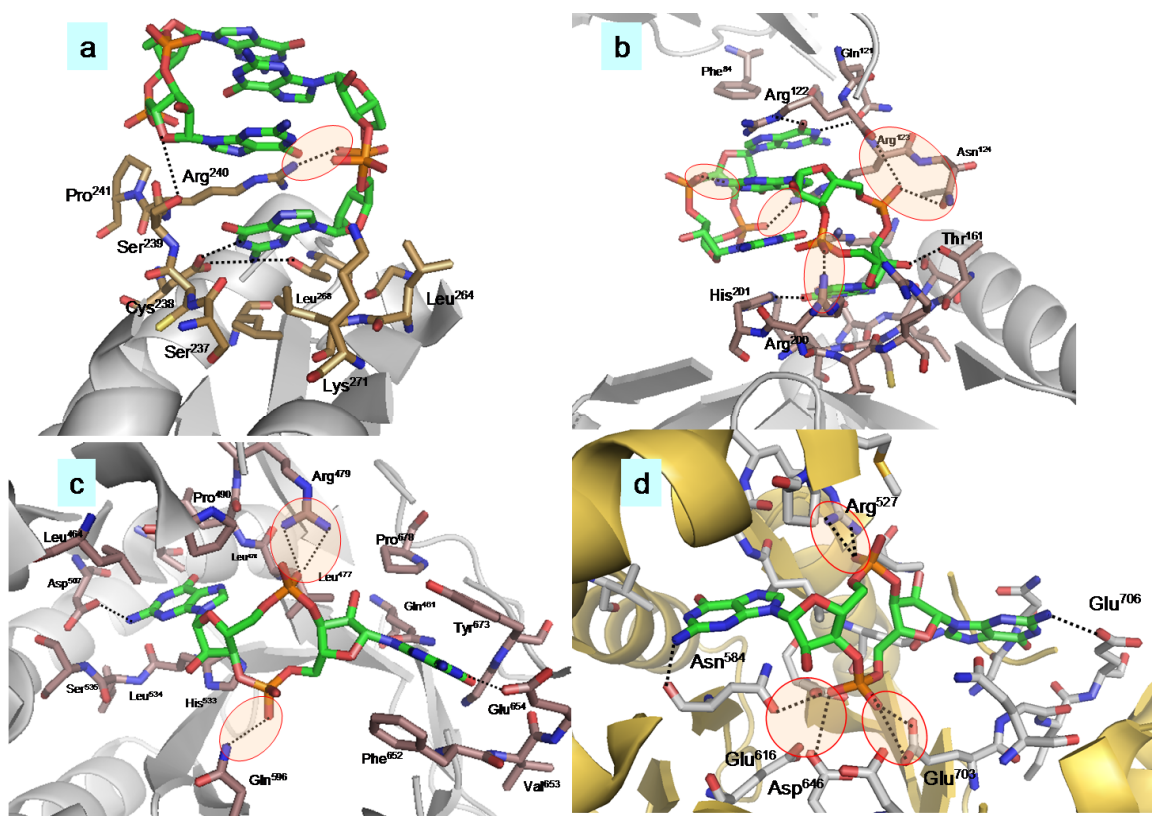


Figure 4–5. a) Dimeric c-di-GMP, bound to WspR (DGC) (PDB code: 315A); b) dimeric c-di-GMP, bound to P4397 (PilZ domain) (PDB code: 3KYF); c) monomeric c-di-GMP, bound to FimX (EAL domain) (PDB code: 3HV8); d) monomeric c-di-GMP, bound to TBD1265 (EAL domain) (PDB code: 3N3T).

Are these phosphate–protein residue interactions important for c-di-GMP binding and how much do these interactions contribute to the overall binding of c-di-GMP to metabolism and processing proteins? To answer the above question, we investigated the biological profile of endo-S-c-di-GMP binding towards well-characterized c-di-GMP interacting proteins from *P. aeruginosa*, including WspR (a DGC protein) [322], RocR (a PDE protein) [220] and PilZ-domain containing protein Alg44 [323]. WspR has been shown to be a potent DGC that promote biofilm formation via synthesis of c-di-GMP. As with a number of DGC, WspR has an I-site that binds c-di-GMP on the opposite face

from the catalytic site to inhibit the diguanylate cyclase activity. RocR is a potent PDE that has been shown to inhibit the expression of chaperone-usher pili that participate in biofilm formation [324]. Alg44 is a gene encoded in the *alg* operon that binds c-di-GMP and this binding is required for the production of the alginate polysaccharide. The interaction of Alg44 to c-di-GMP is well studied through isothermal calorimetry and filter binding assays [221]. To assess the effect of endo-S-c-di-GMP, the compound was tested for its ability to inhibit the DGC activity of WspR, to compete for cleavage by the PDE activity of RocR and to compete for binding to Alg44 by thin layer chromatography (TLC) or filter binding assay. The effect of endo-S-c-di-GMP was compared to c-di-GMP, which blocks all three protein activities, and cGMP, which does not affect any of the proteins. In the presence of endo-S-c-di-GMP (1 mM), WspR (5 μ M) in Tris buffer converted 70 % of GTP (8 nM) into c-di-GMP. 1 mM of c-di-GMP was however able to inhibit WspR from converting GTP into c-di-GMP (**Figure 4–6**). Similarly endo-S-c-di-GMP failed to displace radio-labeled c-di-GMP from Alg44 whereas c-di-GMP was able to displace radio-labeled c-di-GMP from Alg44 (**Figure 4–7**). Endo-S-c-di-GMP did however bind to RocR, evident by the inhibition of RocR cleavage of radio-labeled c-di-GMP in the presence of endo-S-c-di-GMP (**Figure 4–8**). In the case of RocR, endo-S-c-di-GMP was almost as effective at competing with radio-labeled c-di-GMP as c-di-GMP. In the presence of Ca^{2+} [199], PDEs do not cleave c-di-GMP. Therefore, to determine the binding constant for c-di-GMP/endo-S-c-di-GMP and RocR, we added Ca^{2+} (5 mM) to the binding buffer. Unlabeled c-di-GMP could compete with radio-labeled c-di-GMP (5 nM) binding to RocR (5 μ M) with an IC_{50} of 236 nM, whereas endo-S-c-di-GMP competed with radio-labeled c-di-GMP with an IC_{50} of 431 nM (**Figure 4–8a**). The

cleavage site of endo-S-c-di-GMP was exclusively observed at the natural phosphate but not the endo-S-phosphothioate bridge (**Figure 4–8b** and Section 6.4.2). And the fact that the RocR enzymatic cleavage occurred also proves that the binding of endo-S-c-di-GMP with RocR protein.

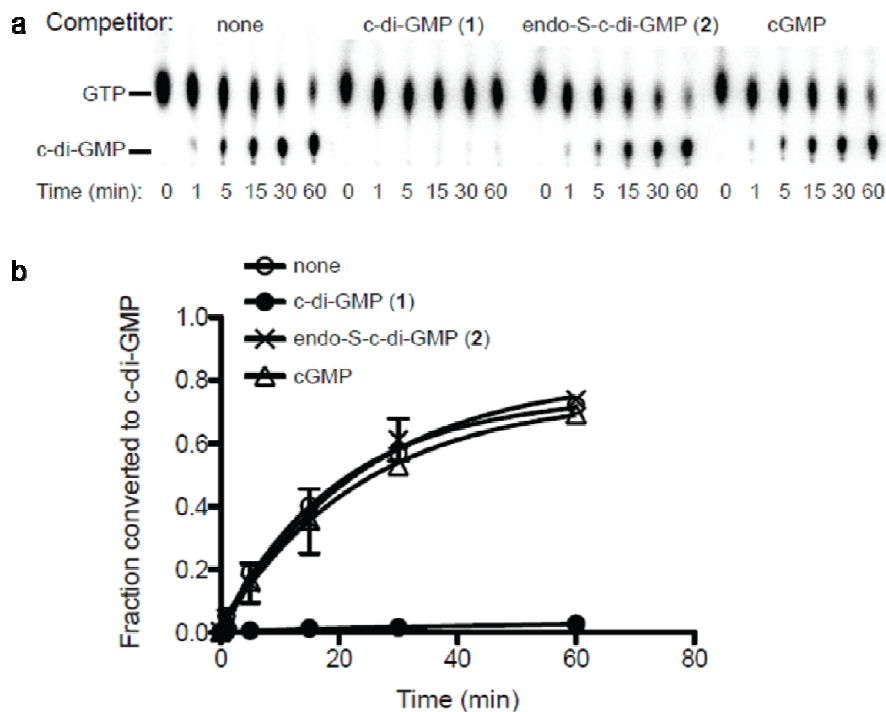


Figure 4–6. Inhibition of c-di-GMP synthesis by WspR with guanine-containing nucleotides. a) TLC of reaction mixture at different time points. Initial reaction conditions; WspR, radio-labeled GTP and unlabeled c-di-GMP or endo-S-c-di-GMP or cGMP or no added nucleotide inhibitor); b) graph showing fraction of radio-labeled GTP that was converted into radio-labeled c-di-GMP in the presence of inhibitor.

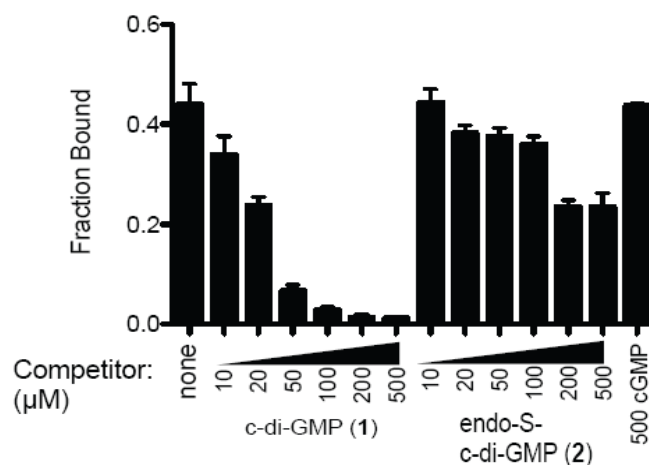


Figure 4-7. Displacement of radio-labeled c-di-GMP from Alg44 (PilZ protein) by c-di-GMP, endo-S-c-di-GMP or cGMP. The value of “fraction bound” is inversely proportional to the binding affinity for Alg44.

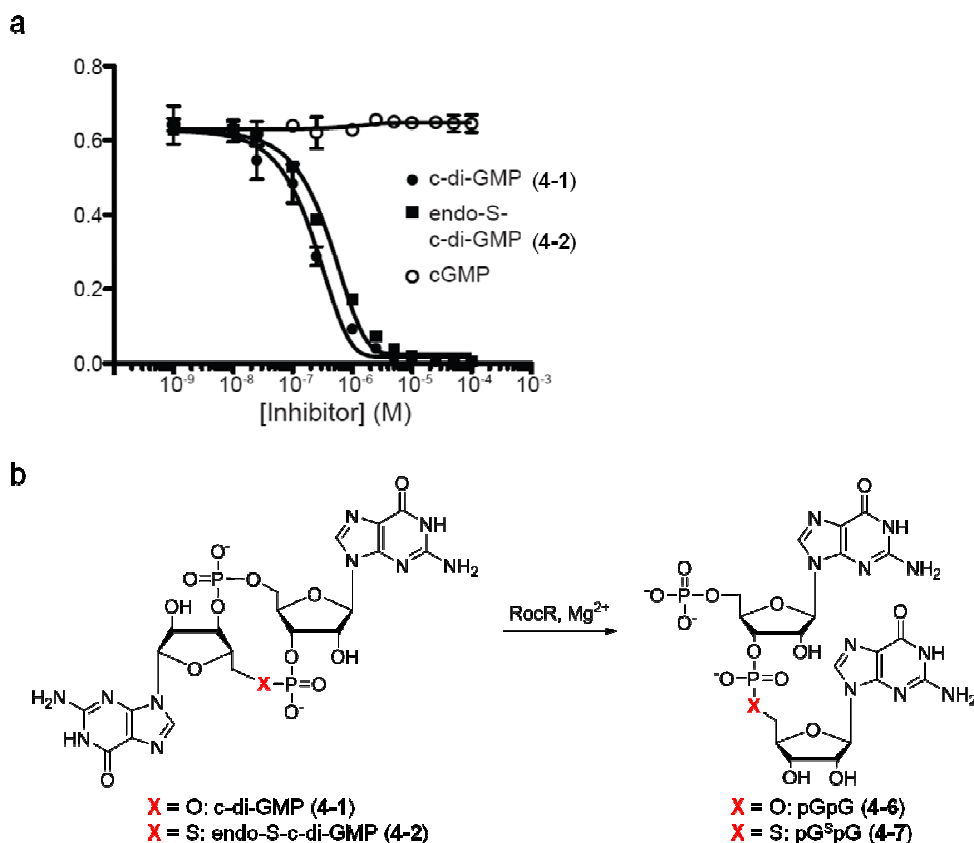


Figure 4-8. a) Binding assays of RocR with c-di-GMP or endo-S-c-di-GMP in the presence of Ca^{2+} ; b) RocR enzymatic cleavage reactions on c-di-GMP and endo-S-c-di-GMP (see Section 6.4.2).

The studies presented herein reveal that proteins that bind to c-di-GMP utilize the phosphate moiety of c-di-GMP as an important recognition element. The crystal structure of c-di-GMP bound to the EAL domain of FimX shows the dinucleotide bound in the “open” conformer (Figure 6c and d) whereas c-di-GMP is bound to most DGCs and PilZ proteins in the “closed” conformer (see Figure 6a and b). RocR has been crystallized but its structure not solved [325]. However, Rao *et al.* have computed the structure of RocR and shown that the computed structure binds to monomeric c-di-GMP, which is in the “open” conformer [326]. Interestingly, endo-S-c-di-GMP (**4–2**) (which has a lower propensity to form a “closed” conformer) could only inhibit an EAL containing protein, RocR, and not DGC or PilZ containing proteins (WspR and Alg44 respectively).

4.1.5 Conclusion

C-di-GMP analogs that can selectively inhibit c-di-GMP metabolism or “adaptor” proteins will become useful tools for modulating c-di-GMP signaling in bacteria. To readily cross the bacterial cell membrane, it is desirable that such analogs are not charged. In this work, a conservative modification of one of the phosphate moieties in c-di-GMP (by replacing only one of the “bridging” oxygens in the phosphate linkages in c-di-GMP with sulfur) gives an analog, endo-S-c-di-GMP, which is remarkably different (biophysically and biochemically) from c-di-GMP. This suggests that the phosphate moieties in c-di-GMP play important roles in aggregate formation as well as the binding of c-di-GMP to metabolism and processing proteins. It appears that the interactions between proteins’ residues and the phosphate moieties in c-di-GMP are important for binding. Therefore, it is tempting to speculate that the amino acids that contact the phosphate moieties are partial determinants of c-di-GMP binding to the so-called adaptor

proteins. Future directions are aimed at mutating these residues in c-di-GMP proteins to determine if they are indeed determinants of c-di-GMP binding to adaptor proteins. These experiments are beyond the scope of this current Ph.D work. Adaptor proteins that bind to c-di-GMP are poorly characterized but they are thought of as mediators of c-di-GMP action. Understanding the determinants of c-di-GMP binding to proteins will aid in the prediction of c-di-GMP binding proteins as well as providing design principles for the construction of c-di-GMP antagonists.

C-di-GMP interacts with numerous proteins and has pleiotropic effects on the bacterial cell. The effect of endo-S-c-di-GMP allows selective inhibition of proteins that bind the open form of c-di-GMP. This provides the basis for rationale design of small molecular inhibitors that only act on specific proteins in the c-di-GMP pathway. Future studies may also reveal selective inhibition of the proteins that bind the closed form of c-di-GMP.

4.2 Design and syntheses of c-di-GMP analogs

4.2.1 The design of the c-di-GMP analogs

The previous section highlighted that conservative changes to the phosphate moiety of c-di-GMP remarkably affect structure and biological profile. To gain more insights into which of the functionalities in c-di-GMP are important for binding to c-di-GMP signaling proteins, we extended our studies to look at how modifications to the 2'-OH of c-di-GMP could affect the structure and biological profile of these analogs. Four sugar puckering conformations of ribose and deoxyribose can exist in equilibrium (**Figure 4–9**, [327]). The ribose unit in c-di-GMP adopts a 3'-endo, 2'-exo puckering; the 3'-carbon and the nucleobase lie on the same face, whereas the 2'-carbon lies in the

opposite face [328]. The electronic properties and the size of the 2'-functionalities have a great effect on the sugar puckering modes [329]. The 2'-OH can also partake in hydrogen bonding interactions with the macromolecular receptor that binds to c-di-GMP (e.g. PDB code: 3HV8). Six analogs (**4-52** to **4-57**) were synthesized following Jones' protocol (**Figure 4-10**) [330].

In compounds **4-52** and **4-53**, the 2'-OH group in c-di-GMP is replaced with 2'-OMe and 2'-H, respectively. **4-52** is expected to adopt a 3'-endo, 2'-exo puckering (similar to c-di-GMP) but the OMe group can only act as a hydrogen bond acceptor and not donor (unlike c-di-GMP, for which the 2'-OH can act as a hydrogen bond acceptor or donor). Also the 2'-OMe group is bigger than the native 2'-OH. Consequently analog **4-52** is ideal for probing the effect of the 2'OH group in c-di-GMP. In compound **4-53**, the 2'-OH is replaced with a 2'-H. It was expected that **4-53** would adopt all puckering modes available to it (similar to the puckering modes in 2'-deoxynucleotides [329]). Compound **4-53** would, therefore, be ideal for investigating how the sugar puckering mode affects the biophysics as well as the biology of c-di-GMP. We have already mentioned that the conservative substitution of the phosphate moiety of c-di-GMP affords an analog that has a lower propensity to form aggregates (Section 4.1). To arrive at c-di-GMP sugar analogs that also have a lower propensity to form aggregates, we designed compounds **4-54** to **4-57** in which both the 2'-OH and one of the bridging oxygens in the phosphodiester are modified (**Figure 4-10**).

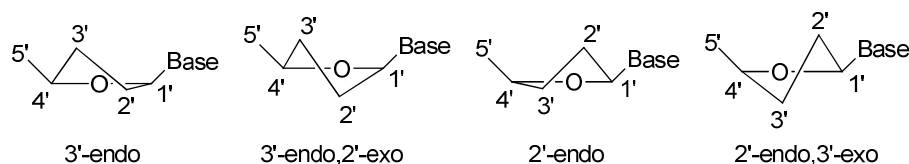


Figure 4–9. Sugar pucker modes in ribose and deoxyribose.

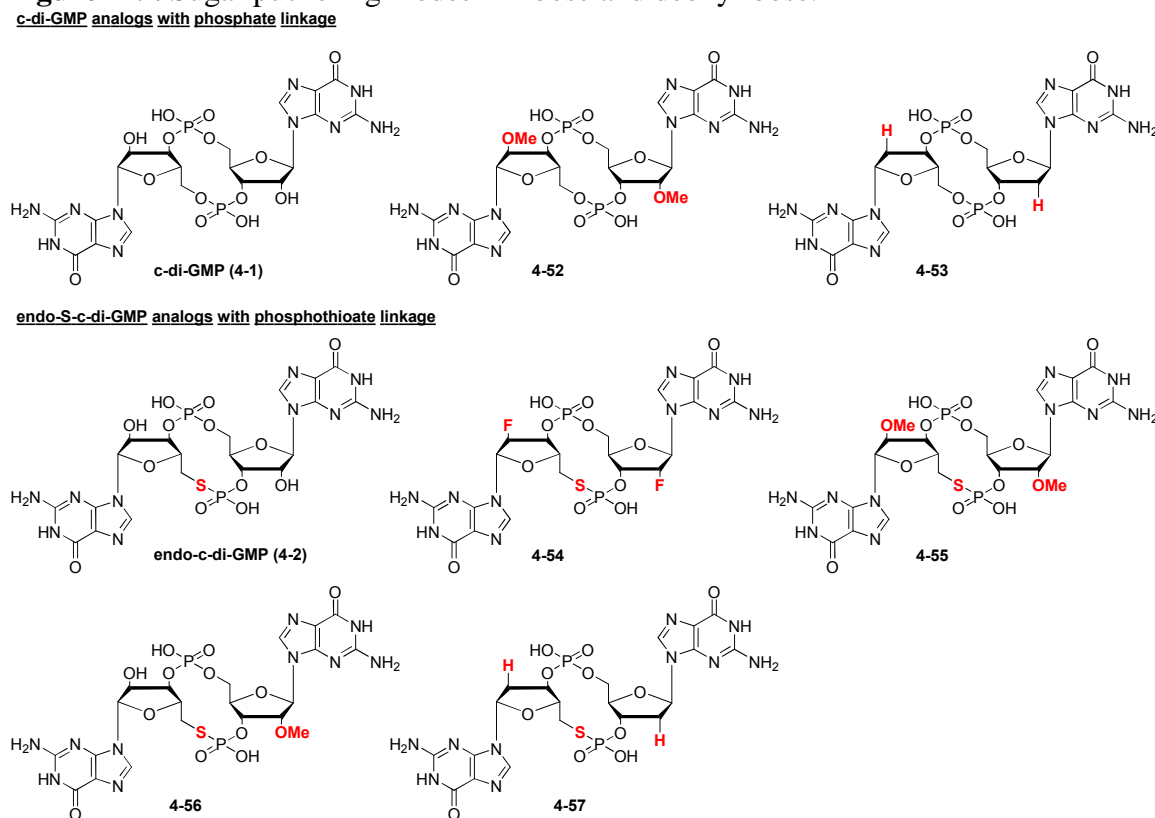
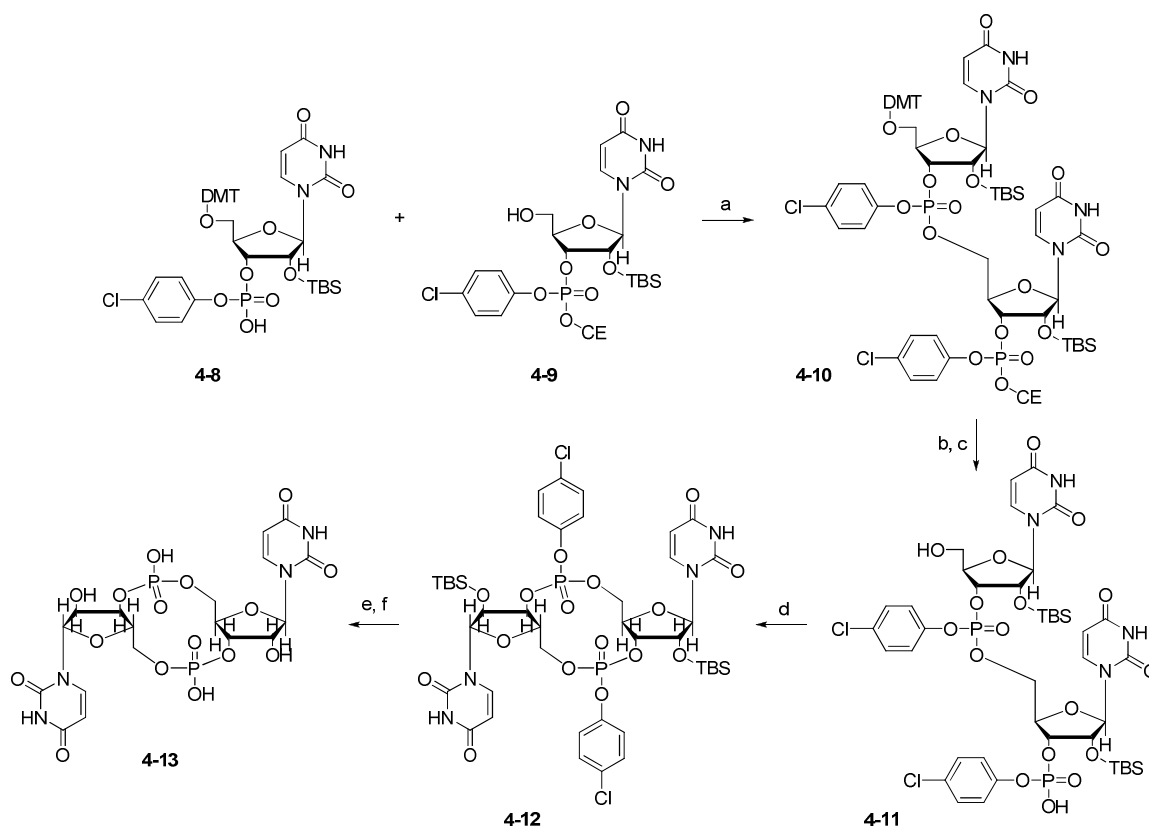


Figure 4–10. Chemical structures of designed c-di-GMP and endo-S-c-di-GMP analogs.

4.2.2 Previous syntheses of c-di-GMP

The synthesis of c-di-GMP is non-trivial. The first preparative synthesis of c-di-GMP was probably reported by Dennis and Jones groups in 1985 with a phosphotriester strategy [331]. Dennis and Jones prepared cyclic di-UMP (**Scheme 4–2**), cyclic di-AMP and cyclic UMP-AMP and investigated their inhibitory activity against RNA synthesis [331]. The highlight of their synthesis is a sulfonyl chloride (TPSCl) mediated coupling of an alcohol and a phosphate. This was followed by deprotection of the cyanoethyl group on phosphate with Et₃N and a cyclization step, utilizing the same TPSCl for an intramolecular reaction of a 3'-phosphate with a 5'-OH of a dinucleotide to afford a

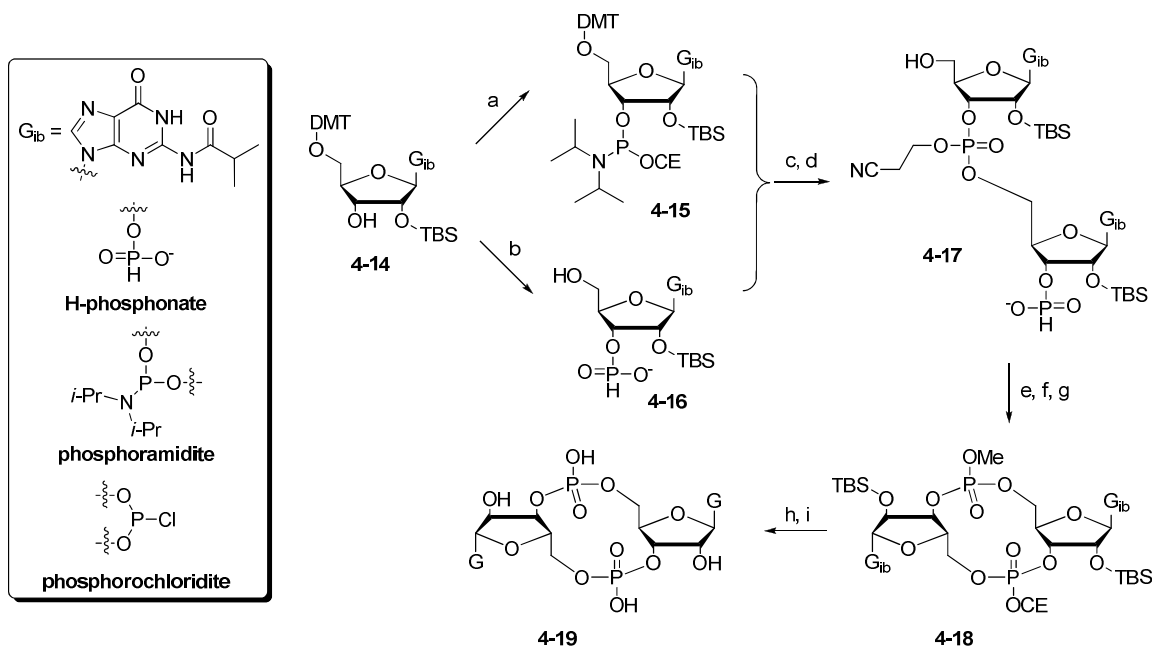
cyclized product (**4-12**). After global deprotections with 2-nitrobenaldoxime (NBO) and ammonia, cyclic dinucleotides (such as **4-13**) were obtained. Later, in 1987, the Benziman et al. adapted this chemical synthetic strategy for synthesizing cyclic di-GMP, and they published a modified c-di-GMP chemical synthesis method using a different cyclization reagent (triisopropylbenzenesulfonyl nitrotriazole) and protecting groups [332]. In the following decades, Hayakawa [333], Jones [330], Sintim [334] and others all contributed to a better chemical synthesis of c-di-GMP. Recently an enzymatic synthesis of c-di-GMP using DGC from *E. coli* also reported [335].



Scheme 4-2. Cyclic di-UMP synthesis by Dennis and Jones [331]. Conditions: a) TPSCl (3 eq), tetrazole (9 eq) in pyridine, RT, 2 h; b) NEt₃, pyridine, RT, 2 h; c) BSA (2 %), CHCl₃: MeOH (7: 3), 0 °C , 20 min; d) TPSCl (6 eq), tetrazole (18 eq), RT, 5 h; e) tetramethylguanidine (TMG), *p*-nitrobenzaldoxime (NBO), in dioxane: H₂O (1: 1), RT,

12 h, then, ammonia (37 %, aq), RT→50 °C , 12 h; f) TBAF in pyridine, RT, 3 h, then pyridinium Dowex 50-X8, RT, 1 h.

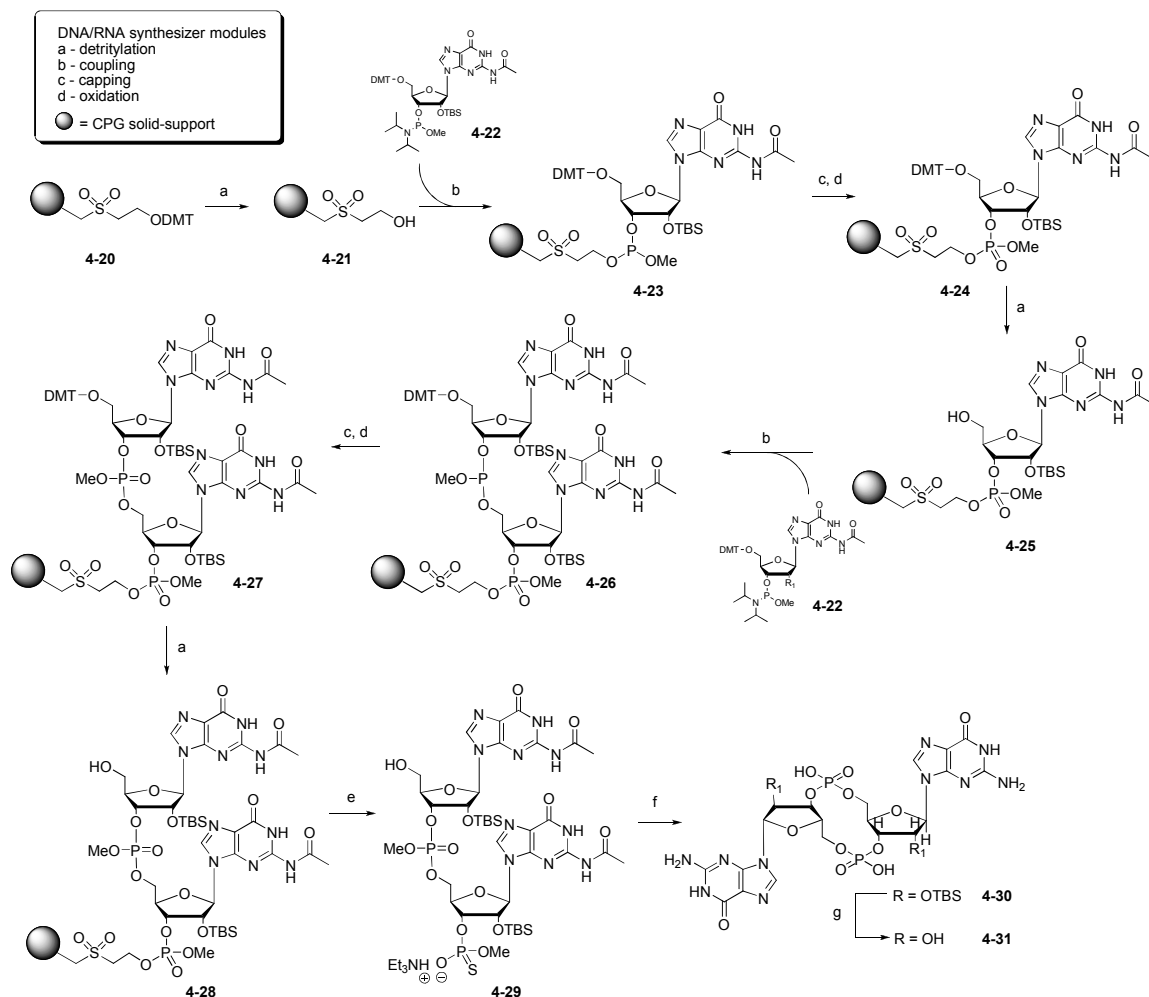
Hayakawa's synthesis was a modified procedure of the Dennis and Jones' strategy. The yield of the cyclization step was claimed to improve, up to 75 %, by changing the protecting groups on the phosphate [333]. We and others have however not managed to obtain a high yield in the cyclization step [336]. Jones' group also introduced an H-phosphonate strategy [226] (**Scheme 4-3**). Firstly, guanosine phosphoramidite **4-15** and phosphonate **4-16** were prepared by coupling a common starting material **4-14** with phosphoramidite and phosphorochloridite, respectively. The resulting phosphoramidite (**4-15**) and H-phosphonate (**4-16**) were then coupled and oxidized, followed by cyclization with an acid chloride (**4-18**). The final product (**4-19**) was achieved by removal of the TBS group with $\text{NEt}_3 \cdot 3\text{HF}$ and global deprotection of the *iso*-butyrate and the cyanoethyl groups on the nucleobase and phosphate groups respectively with ammonia. Recently, the Jones' group reported a gram scale synthesis of c-di-GMP and phosphothioate analog by using a modified H-phosphonate strategy that was originally reported by the group [316,330].



Scheme 4-3. Jones' H-phosphonate strategy for c-di-GMP synthesis. Conditions: a) bis(diisopropylamino)cyclohexyl phosphoramidite, pyridinium trifluoroacetate; b) 2-chloro-4H-1,3,2-benzodioxaphosphorin-4-one; c) pyridinium trifluoroacetate; d) *tert*-butylhydroperoxide; e) sulfonic acid resin; f) adamantoylcarbonyl chloride; g) NBS, MeOH; h) pyridine: ammonia (37 %, aq) (1:1); i) $NEt_3 \cdot 3HF$.

Taking advantage of solid-support synthesis, Sintim group proposed a miniscale synthesis of c-di-GMP synthesis (**Scheme 4-4**) [334]. The synthesis is programmed (steps a–d, **Scheme 4-4**) by DNA/RNA synthesizer and can be achieved automatically before the macro-ring is closed. The DNA/RNA synthesizer can perform four standard commands: detritylation with an acid, coupling reaction with a phosphoramidite (**4-22**), capping the trace amount of unreacted hydroxyl groups with an acid anhydride, and an oxidation reaction to convert phosphines into phosphates (**Scheme 4-4**). The synthesis start from an ODMT modified CPG bead **4-20** (for synthesis see Section 6.1), and after two complete cycles of synthesis with DMT-off mode (a–b–c–d–a–b–c–d–a, **Scheme 4-4**; DMT-off mode means the product is DMT deprotected when the programmed cycles finish), a 5'-OH diguanosine (**4-28**) was produced on the CPG beads. After the CPG linker was cleaved by Et_3N , the ring was cyclized with a sulfonyltriazole (1-

mesitylenesulfonyl-3-nitro-1,2,4-triazole) followed by a global deprotection with ammonia and $\text{NEt}_3 \cdot 3\text{HF}$ in sequence to yield the final product.

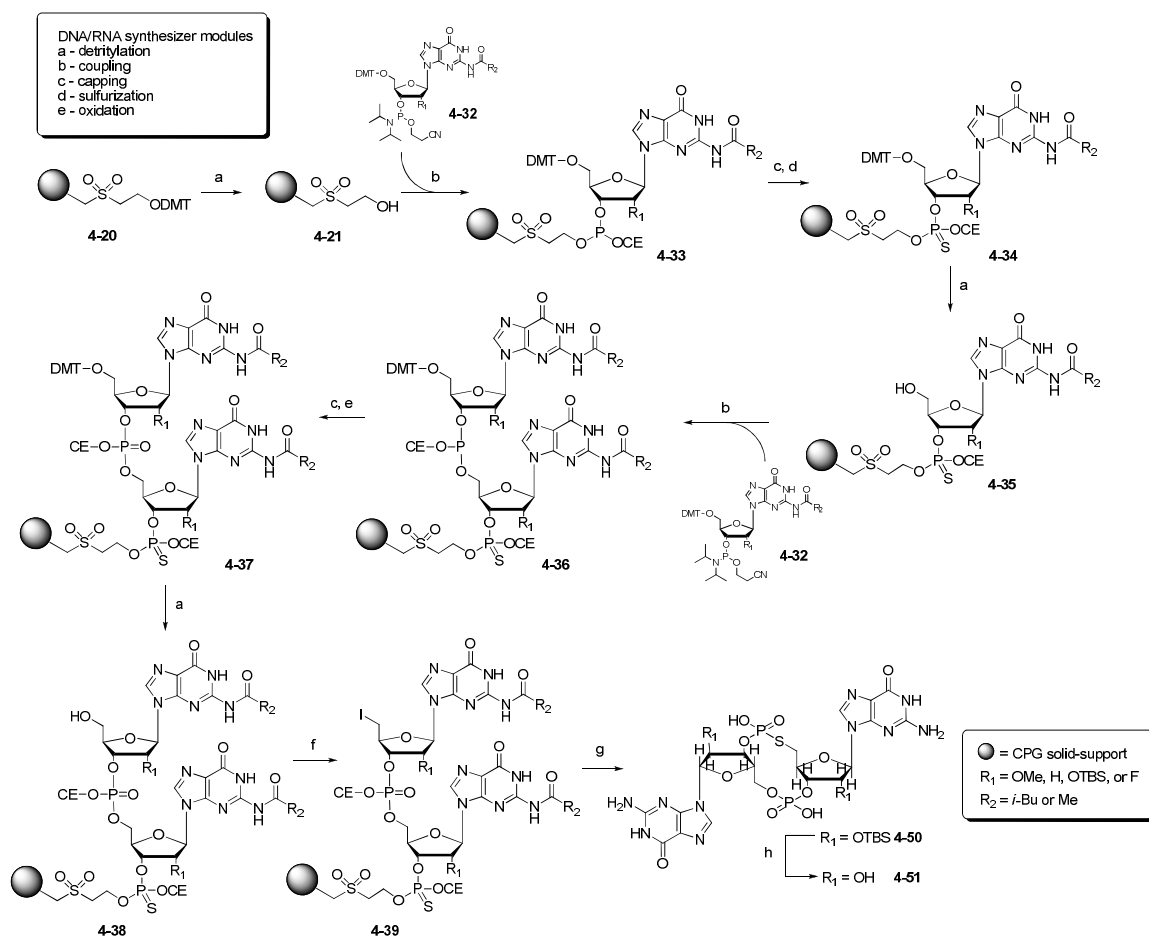


Scheme 4-4. Sintim's solid support synthesis of c-di-GMP. Steps a–d were conducted on the DNA/RNA synthesizer with a standard program. Reaction conditions: a) detritylation: 6 % dichloroacetic acid in CH_2Cl_2 , RT, 45 s; b) coupling: phosphoramidite (0.1 g/mL), ETT (0.25 M) in CH_3CN , RT, 90 s; c) capping: Ac_2O (10 v%), 2,6-lutidine (10 v%) in THF (Cap A solution), then *N*-methylimidazole (10 v%) in THF (Cap B solution), RT, 30 s; d) oxidation: I_2 (0.02 M) in water: pyridine: THF (1: 2: 7), RT, 30 s; e) TEA in acetonitrile, then 1-mesitylenesulfonyl-3-nitro-1,2,4-triazole (0.1 M) in pyridine, RT, 48 h, then filtered; g) NH_4OH (28 %), RT or 40 °C , 14 h, then filtered; h) $\text{NEt}_3 \cdot 3\text{HF}$ (20 eq.) in pyridine, 40 °C , 4 h. HPLC purification was conducted for the final products.

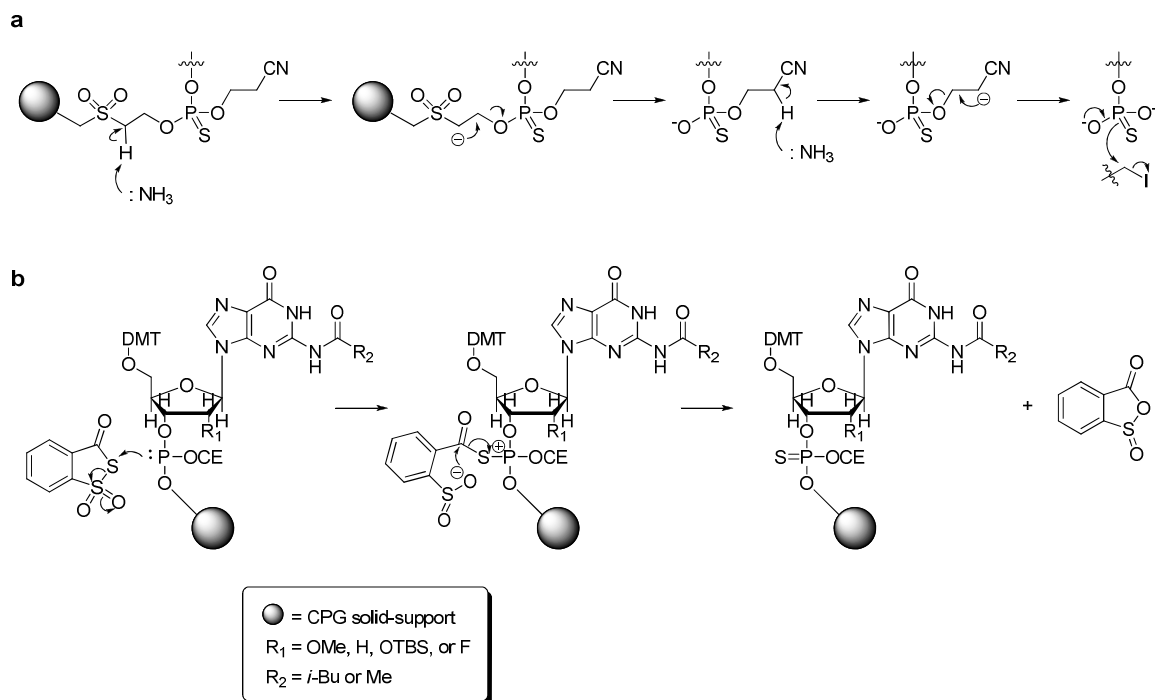
4.2.3 The synthesis of the designed c-di-GMP analogs

We choose the solid-supported strategy [334] for synthesizing endo-S-c-di-GMP analogs (see **Scheme 4–5**) and solution phase strategy [330] for synthesizing natural c-di-GMP analogs. The advantages of preparing c-di-GMP analogs on a solid-support are numerous: i) the intermediate can be simply purified by washing off unreacted reagents with organic solvents, rather than by using tedious column chromatography or HPLC purification; and ii) most reactions can be pre-programmed in a DNA/RNA synthesizer and, hence, easier to execute. For the synthesis of endo-S-c-di-GMP analogs, sulfurization was achieved using Beaucage reagent. The mechanism for phosphothioate using Beaucage reagent, or 3*H*-1,2-benzodithiole-3-one 1,1-dioxide is illustrated in **Scheme 4–6b** [337].

In summary, eight c-di-GMP analogs (including the natural c-di-GMP, **Figure 4–9**) were synthesized without incident. The characterization of the c-di-GMP analogs are referred to Section 6.4. The ongoing work by a new Ph.D student in the Sintim laboratory is to characterize the synthesized c-di-GMP analogs, using both biophysical and biochemical techniques. These experiments are expected to provide more insights regarding the pharmacophore units on c-di-GMP that are important for binding to the different classes of c-di-GMP binding proteins.



Scheme 4–5. Solid-support synthesis of dinucleotides and cyclization in solution phase. Steps a–e were conducted on the DNA/RNA synthesizer with a standard program. Reaction conditions: a) detritylation: 6 % dichloroacetic acid in CH₂Cl₂, RT, 45 s; b) coupling: phosphoramidite (0.1 g/mL), ETT (0.25 M) in CH₃CN, RT, 90 s; c) capping: Ac₂O (10 v%), 2,6-lutidine (10 v%) in THF (Cap A solution), then *N*-methylimidazole (10 v%) in THF (Cap B solution), RT, 30 s; d) sulfuration: Beaucage reagent (10 mg/mL) in CH₃CN, RT, 15 min; e) oxidation: I₂ (0.02 M) in water: pyridine: THF (1: 2: 7), RT, 30 s; f) methyltriphenoxyposphonium iodide (20 eq.) in DMF, RT, 45 min, then filtered; g) NH₄OH (37 %), RT or 40 °C , 14 h, then filtered; h) NEt₃·3HF (20 eq.) in pyridine, 40 °C , 4 h. HPLC purification was conducted for the final products.



Scheme 4–6. a) Cleavage of nucleotide from CPG support, deprotection of cyanoethyl group and cyclization to afford endo-S-c-di-GMP analogs; b) the mechanism of sulfurization, using the Beaucage reagent.

Chapter 5. Conclusions and future directions

5.1 FAS inhibitors

In this dissertation we have highlighted an unsavory truth that we are in a never-ending battle with bacterial pathogens. Solving this bacterial resistance problem demands the combination of several disciplines, from synthetic organic chemistry to biochemical characterization of ligand protein interactions and then to microbiology. Fatty acids are important building units in both human and bacterial cells. However the enzymes that are responsible for fatty acids in humans are different from those found in bacteria, presenting a great opportunity to target FAS enzymes for antibiotic development. Platensimycin and platencin are newly discovered potent bacterial FAS inhibitors. In the early part of this dissertation, we demonstrated concise synthetic strategies to access platensimycin-like molecules (such as compound **5-2**, **Figure 5-1**) and showed that although the tetracyclic core of platensimycin was initially thought of as not been important for the drug's action, conservative modifications to this ring can sometimes abrogate the drug's affinity for the FabF enzyme. Interestingly, using function-oriented synthetic approach [338-343], we also demonstrate that analogs whereby the tetracyclic core unit of platensimycin is drastically altered (such as compound **5-3**, **Figure 5-1**) can also have good antibiotic profile. We have therefore identified a new class of antibiotic class, called *N,N*-dialkylamine benzoic acids (such as compound **5-3**).

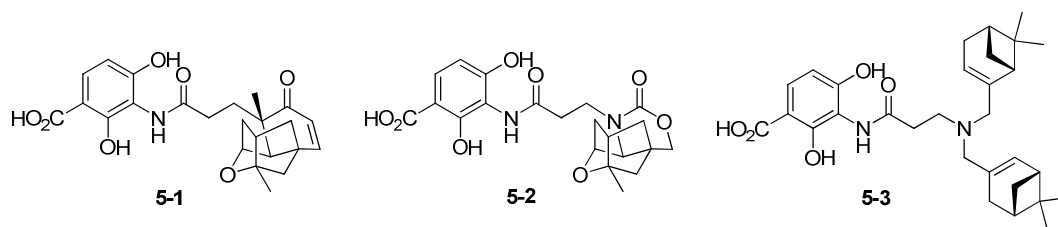


Figure 5–1. Structures of platensimycin (**5–1**), oxazinidinyl platensimycin (**5–2**) and myrtemycin (**5–3**).

5.2 Development of dynamic ring-closing metathesis

En route to making platensimycin-like compounds, we uncovered conditions that allowed for ring-closing metathesis, under dynamic conditions. The dynamic ring-closing metathesis is a one-pot reaction in the presence of both ruthenium and a compatible base. The dynamic ring-closing metathesis (RCM) permitted the use of either diastereomers *cis*-**2–34** or *trans*-**2–34** to be used for a ring-closing reaction. Normally RCM requires that both alkenes on cyclic structures to be on the same side, but a dynamic RCM combines epimerization and the ring-closing reaction in one pot and thereby obviating the need to have both alkenes on cyclic structures to be on the same side, see **Scheme 2–11**). The product obtained from our dynamic RCM procedure, **2–33**, contains a bicyclo[3.2.1] moiety that is not only found in platensimycin but also in many other biologically active molecules (**Figure 5–2**). Thus the dynamic ring-closing metathesis would be a general way to construct these molecules. Future development of the dynamic RCM to shorten the reaction time as well as reduce the catalyst loading will make this methodology attractive for others to use for the synthesis of complex molecules.

Chapter 6. Experimental Section

6.1 General procedure

6.1.1 General reaction conditions

Air and moisture sensitive reactions are explicitly indicated in the reaction procedures. Reactions were carried out in oven-dried glassware and sealed with rubber septa under a positive pressure of anhydrous argon or nitrogen. All solution phase reactions were all stirred with teflon-coated magnetic stir bars. Elevated temperatures were obtained using silicone oil baths and monitored by a thermometer. Low temperatures were obtained by ice bath or by solid CO₂ (dry ice) mixed with organic solvents such as acetone and acetonitrile. Organic solutions were all concentrated using a Büchi rotary evaporator with an aspirator pump. Trace amount of solvent or high boiling point solvent was removed by treatment under high vacuum for 0.5–5 hours.

6.1.2 Preparation of the solvents

Anhydrous tetrahydrofuran was obtained by distillation over metallic sodium or using a PureSolvent™ system prior to use. Dry dichloromethane, toluene and pyridine were distilled from CaH₂ prior to use. Acetonitrile was first distilled over CaH₂ and then dried overnight with activated molecular sieves (4Å). DMF was distilled over CaCl₂ under a reduced pressure before stored with activated molecular sieves (4Å) overnight. Anhydrous benzene was purchased from Sigma-Aldrich and used “as is”. Degassed solvent was obtained by bubbling argon through the solvent (5–10 bubbles per second) and venting with a needle for 30 min (**Figure 6–1**).

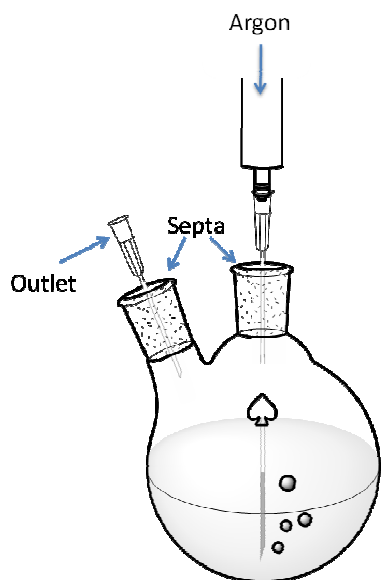
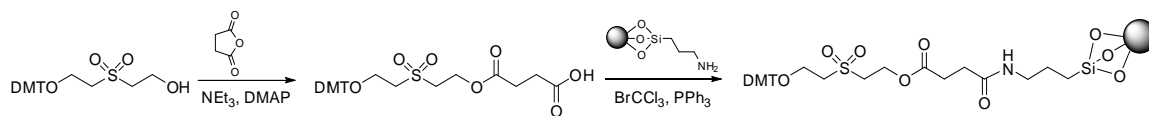


Figure 6–1. The apparatus for solvent degassing.

6.1.3 Reagents

Hoveyda-Grubbs II catalyst and anhydrous Hünig's base (diisopropylethylamine) was purchased from Sigma-Aldrich. Triethylamine was dried over activated molecular sieves overnight prior to use. Chloro(methoxy)methane was purchased from TCI America. Phosphoramidites and Beaucage reagent were purchased from Glen Research or Azco Biotech. Sulfonylethyl-ODMT modified CPG beads were synthesized by reported procedure [344] from the inexpensive 3-aminopropyl CPG on a 100 g scale (**Scheme 6–1**). Solvents for silica-gel chromatography (ACS grade) and HPLC (HPLC grade) were purchased from VWR. Other reagents were all purchased from Sigma-Aldrich or Acros.



Scheme 6–1. Chemical synthesis of sulfonylethyl-ODMT beads [344].

6.1.4 Instrument

Thin-layer chromatography (TLC) was performed on Merck Kieselgel 60 F₂₅₄ plates with a 365 nm fluorescent indicator. The TLC was visualized by UV light, KMnO₄ stain or acidic *p*-anisaldehyde stain followed by gentle heating. The crude reaction mixtures were purified by flash chromatography on silica gel (230-400 mesh) with slow elution of a mixture of organic solvents, or by HPLC. A Varian 210 system was used with a UV detector for all HPLC analysis and purification. The samples were all filtered by a 0.2 μ m syringe filter (PVDF or PTFE) prior to the injection.

NMR spectra were measured on Bruker AV-400, Bruker DRX-400, Bruker DRX-500 or Bruker AVIII-600. Data for ¹H-NMR spectra are reported as follows: chemical shift (ppm, relative to residual solvent peaks or indicated external standards; s = singlet, d = doublet, t = triplet, q = quartet, dd = doublet of doublets, td = triplet of doublets, dt = doublet of triplets, ddd = doublet of doublet of doublets, tdd = triplet of doublet of doublets, dddd = doublet of doublet of doublet of doublets, m = multiplet), coupling constant (Hz), and integration. Coupling constants were rounded to 0.5 Hz. Data for ¹³C-NMR are reported in terms of chemical shift (ppm) relative to residual solvent peak. HSQC (Heteronuclear Single Quantum Coherence), COSY (COrrrelation SpectroscopY) and selective NOE (Nuclear Overhauser effect) were also reported for the structural elucidation purpose. DOSY (Diffusion Ordered Spectroscopy) experiment conditions refer to Section 6.6.1.

Mass spectra (MS) were recorded by JEOL AccuTOF-CS (ESI positive and negative modes) or Varian GC-MS (EI, 70 eV). High resolution mass spectra (HRMS) for ESI spectrometer were calibrated with an aqueous solution of CsI. The aggregated

cation $[\text{Cs}_2\text{I}]^+$ and anion $[\text{CsI}_2]^-$ peaks were used as standard for ESI positive and negative mode, respectively.

UV absorbance spectra were obtained on a JASCO V-630 spectrophotometer with 1 cm path length cuvette, and CD experiments were performed on a JASCO J-81 spectropolarimeter with 1 cm path length cuvette. The concentration of a stock solution of c-di-GMP and endo-S-c-di-GMP was determined by the measuring of absorbance at 260 nm for c-di-GMP and endo-S-c-di-GMP, using $21,600 \text{ M}^{-1}\text{cm}^{-1}$ as a molar extinction coefficient for both compounds.

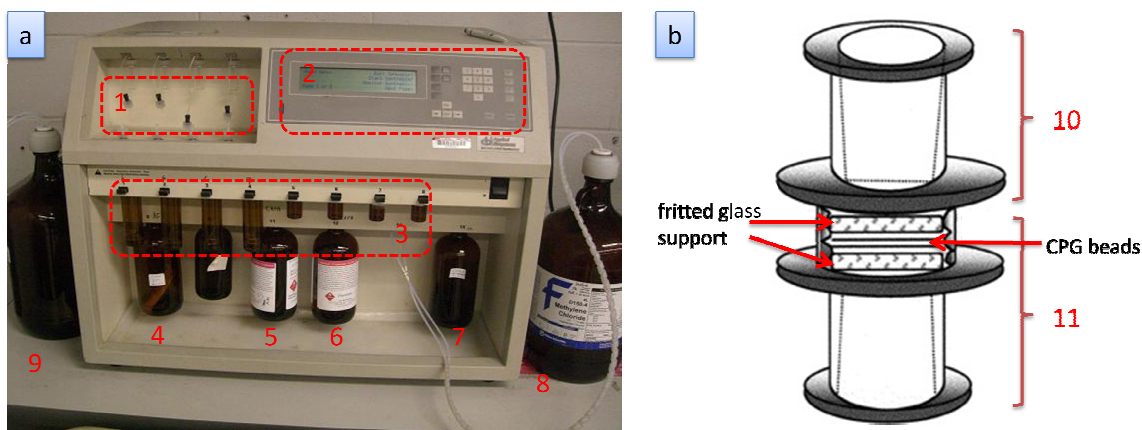
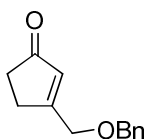


Figure 6–2. a) A real photo of DNA/RNA synthesizer (photo credit: Dr. Shizuka Nakayama). 1 – synthesis columns (up to four columns can be installed); 2 – control panel; 3 – phosphoramidites; 4 – ETT (0.25 M) in CH_3CN with 4 Å molecular sieves; 5 – Cap A solution (Ac_2O (10 v%), 2,6-lutidine (10 v%) in THF); 6 – Cap B solution (*N*-methylimidazole (10 v%) in THF); 7 – I_2 (0.02 M) in water: pyridine: THF (1: 2: 7); 8 – 6 % dichloroacetic acid in CH_2Cl_2 ; 9 – anhydrous acetonitrile (with 4 Å molecular sieves). b) detail illustration of a synthesis column. The column contains two separate parts 10 and 11, and each part contains a fritted glass support that can hold the CPG beads and allow the liquid reagents to pass through. Around 0.1 g CPG beads can be loaded in between the two fritted glass supports. Bigger scale synthesis columns can also be used. (The figure is modified from www.abrf.org/jbt/2000/September00/sep00bintzler.html)

DNA/RNA synthesizer (ABI Applied Biosynthesis 392) was used to conduct the pre-programmed synthesis of nucleotides (**Figure 6–2**). Regular 1.0 μmol synthesis program was used for all CPG-supported reactions.

6.2 Synthetic protocols for compounds in Chapter 2

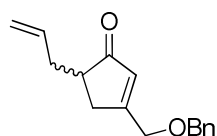
3-(Benzyloxymethyl)cyclopent-2-enone (2–39)



(Benzyloxymethyl)tributylstannane was prepared (50 g scale) using the reported literature method [345]. This reaction was air and moisture sensitive. To a solution of (benzyloxymethyl)tributylstannane (13.0 g, 31.6 mmol) in dry THF (130 mL) at $-78\text{ }^{\circ}\text{C}$ under argon, *n*-BuLi (1.6 M in hexane, 17.0 mL, 27.2 mmol) was added via syringe. After stirring for 15 min, 3-methoxycyclopent-2-enone **2–38** (2.20 g, 19.6 mmol) in dry THF (15 mL) was added dropwise within 10 min. A precipitate sometimes forms before addition is complete. After stirring for 1 h, the reaction mixture was allowed to warm to room temperature and stirred at room temperature for an additional 4 h before the mixture was quenched with NH_4Cl (saturated aqueous solution, 50 mL). The aqueous layer was then extracted with EtOAc (30 mL x 3). The combined organic layer was dried over MgSO_4 and was concentrated *in vacuo*. The crude material was purified by silica gel column chromatography ($R_f = 0.35$, hexane/EtOAc = 3:1) to afford product **2–39** (3.35 g, 84 %) as a pale yellow crystal. Product **2–39** showed black on TLC after staining with *p*-anisaldehyde followed by gentle heating.

^1H NMR (400 MHz, CDCl_3) δ ppm 7.52-7.15 (m, 5H), 6.17 (m, 1H), 4.56 (s, 2H), 4.28 (s, 2H), 2.61-2.46 (m, 2H), 2.40-2.35 (m, 2H). ^{13}C NMR (100 MHz, CDCl_3) δ ppm 208.7, 177.7, 137.1, 128.7, 128.1, 127.5, 127.2, 72.7, 69.0, 34.4, 28.0. GCMS (EI): 202 (M^+), 173, 107, 91. IR (cm^{-1}): 3072 (w), 2852 (w), 1699 (s), 1677 (s), 1625 (m), 1498 (w), 1437 (m), 1402 (w), 1265 (s), 1240 (w), 1143 (s), 1105 (m), 1024 (m), 971 (w), 868 (w), 735 (s), 699 (s), 628 (w).

(\pm)-5-Allyl-3-(benzyloxymethyl)cyclopent-2-enone (2–40)

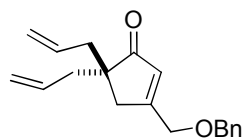


This reaction was air and moisture sensitive. To a solution of diisopropylamine (2.0 mL, 15 mmol) in dry THF (50 mL) at $-78\text{ }^{\circ}\text{C}$ under argon, *n*-BuLi (1.6 M in hexane, 8.2 mL, 13 mmol) was added dropwise within 10 min. After stirring for 30 min, the reaction mixture was allowed to warm to $0\text{ }^{\circ}\text{C}$. After stirring for another 1 h, dry HMPA (1.5 mL, 8.6 mmol) was added via syringe, and the reaction mixture was cooled to $-78\text{ }^{\circ}\text{C}$. Enone **2–39** (2.44 g, 12.1 mmol) in dry THF (10 mL) was added dropwise within 5 min. The reaction mixture was stirred for 1 h at $-78\text{ }^{\circ}\text{C}$ before allyl iodide (1.4 mL, 15 mmol) in dry THF (10 mL) was added dropwise within 30 min. After stirring for another 30 min, the reaction mixture was allowed to warm to room temperature overnight. The reaction mixture was quenched with NH_4Cl (saturated aqueous solution, 30 mL), the water layer was extracted with EtOAc (20 mL x 3). The combined organic layer was dried over MgSO_4 and was concentrated *in vacuo*. The crude material was purified by silica gel column chromatography ($R_f = 0.40$, hexane/EtOAc = 5:1) to afford product **2–40** (1.83 g, 62 %) as a colorless oil. Some starting material enone **2–39** was recovered

(0.15 g, 8 %). The product **2-40** showed black on TLC after staining with *p*-anisaldehyde followed by gentle heating. Byproduct **2-41** was obtained (~ 25 %) as a colorless oil.

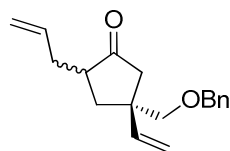
^1H NMR (400 MHz, CDCl_3) δ ppm 7.43-7.27 (m, 5H), 6.22-6.17 (m, 1H), 5.74 (tdd, $J = 17.0, 10.0, 7.0$ Hz, 1H), 5.07 (ddd, $J = 17.0, 3.0, 1.5$ Hz, 1H), 5.05-5.01 (m, 1H), 4.60 (s, 2H), 4.30 (d, $J = 0.5$ Hz, 2H), 2.72 (tdd, $J = 19.0, 7.0, 1.0$ Hz, 1H), 2.61-2.46 (m, 2H), 2.31 (d, $J = 19.0$ Hz, 1H), 2.20-2.10 (m, 1H). ^{13}C NMR (100 MHz, CDCl_3) δ ppm 210.3, 176.6, 137.3, 135.2, 128.5, 128.4, 127.9, 127.6, 116.8, 73.0, 69.3, 44.8, 35.3, 34.2. GCMS (EI): 242 (M^+), 136, 121, 91. IR (cm^{-1}): 1695 (s), 1627 (m), 1440 (m), 1370 (w), 1265 (m), 1144 (s), 1106 (m), 1027 (m), 1000 (w), 913 (s), 854 (w), 740 (s), 697 (m).

5,5-Diallyl-3-(benzyloxymethyl)cyclopent-2-enone (2-41)



^1H NMR (400 MHz, CDCl_3) δ ppm 7.42-7.28 (m, 5H), 6.28 (t, $J = 2.0$ Hz, 1H), 5.63 (dddd, $J = 17.0, 10.0, 8.0, 7.0$ Hz, 2H), 4.98-4.90 (m, 4H), 4.78 (s, 2H), 2.66 (dd, $J = 13.0, 7.0$ Hz, 2H), 2.41-2.28 (m, 4H), 2.19 (m, 2H). ^{13}C NMR (100 MHz, CDCl_3) δ ppm 222.1, 140.8, 137.3, 134.4, 128.4, 127.9, 127.3, 118.2, 117.4, 73.9, 57.0, 40.5, 39.0, 23.5. GCMS (EI): 281 (M-H^+), 251, 214, 173, 91. IR (cm^{-1}): 2861 (w), 1737 (s), 1641 (w), 1454 (w), 1270 (w), 1093 (s), 997 (m), 915 (s), 737 (m), 698 (s).

(\pm)-2-Allyl-4-(benzyloxymethyl)-4-vinylcyclopentanone (2-34)

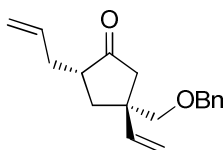


This reaction is air and moisture sensitive. In a 250 mL round bottom flask, CuCN (2.6 g, 29 mmol) was added and dried under high vacuum at 100 °C for 1 h. After the mixture had been cooled to room temperature, the flask was flushed with argon before tetravinyltin (3.5 mL, 19 mmol) in dry THF (100 mL) was added. The mixture was then cooled to -78 °C, and *n*-BuLi (18.0 mL, 1.6 M in hexane, 28.8 mmol) was added dropwise within 15 min. After stirring for 30 min, the reaction mixture turned greenish. BF₃·Et₂O (11.4 mL, 90.0 mmol) was then added via syringe and stirring continued for 10 min before enone **2-40** (1.14 g, 4.70 mmol) in dry THF (10 mL) was added dropwise within 10 min. After stirring for another 1 h, the reaction mixture was allowed to warm to room temperature overnight, and it slowly turned black. The reaction mixture was quenched with NH₄Cl (saturated aqueous solution, 20 mL), whereupon the black color disappeared to give a clear brown solution, and the water layer was extracted with EtOAc (15 mL x 3). The combined organic layer was dried over MgSO₄ and was concentrated *in vacuo*. The crude material was purified by silica gel column chromatography (*R*_f = 0.40, hexane/EtOAc = 10:1) to afford product (a mixture of *cis*- and *trans*- **2-34**, 1.08 g, 85 %) as a colorless oil. The product **2-34** mixture showed black on TLC after staining with *p*-anisaldehyde followed by gentle heating. The product ratio was determined by GCMS and ¹H NMR. *cis*-**2-34**: *trans*-**2-34** = 1: 3.7.

¹H NMR (400 MHz, CDCl₃) δ ppm 7.40-7.23 (m, 5H for *trans*, 5H for *cis*), 5.95 (dd, *J* = 18.0, 11.0 Hz, 1H for *cis*), 5.9 (dd, *J* = 18.0, 11.0 Hz, 1H for *trans*), 5.79-5.66 (m, 1H for *trans*, 1H for *cis*), 5.15 (d, *J* = 11.0 Hz, 1H for *trans*), 5.03 (m, 3H for *trans*, 3H for *cis*), 4.54 (s, 2H for *trans*), 4.51 (d, *J* = 7.0 Hz, 2H for *cis*), 3.38 (s, 2H for *trans*), 3.35 (dd, *J* = 24.0, 9.0 Hz, 2H for *cis*), 2.57-2.44 (m, 1H for *trans*, 1H for *cis*), 2.43-2.22 (m, 3H for

trans, 3H for *cis*), 2.07 (m, 2H for *trans*, 2H for *cis*), 1.77 (t, $J = 12.0$ Hz, 1H for *trans*, 1H for *cis*). ^{13}C NMR (100 MHz, CDCl_3) δ ppm 218.8, 218.5, 142.7, 141.6, 138.1, 137.9, 135.7, 135.7, 128.3, 128.3, 127.6, 127.5, 127.4, 127.3, 127.2, 116.5, 116.4, 114.5, 113.1, 76.3, 75.9, 73.3, 73.2, 47.0, 46.8, 46.6, 45.5, 44.9, 44.4, 37.4, 36.0, 35.2, 34.0, 31.8, 29.6, 29.6, 29.3, 27.8, 27.6, 26.8, 26.6, 22.6, 17.4, 14.1, 13.5, 13.5. GCMS (EI): 179, 149, 136, 121, 107, 91.

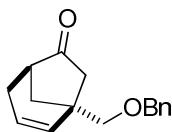
(\pm)-(2S,4R)-2-Allyl-4-(benzyloxymethyl)-4-vinylcyclopentanone (*trans*-2-34)



Analytically pure **2-34** was obtained by subjecting the *cis*-/ *trans*- mixture to Hoveyda-Grubbs II catalyst. With this approach, only the *cis*-isomer ring-closed. The crude material was purified by flash chromatography, silica gel ($R_f = 0.40$, hexane/EtOAc = 10:1).

^1H NMR (400 MHz, CDCl_3) δ ppm 7.39-7.27 (m, 5H), 5.85 (dd, $J = 18.0, 11.0$ Hz, 1H), 5.73 (tdd, $J = 18.0, 11.0, 7.0$ Hz, 1H), 5.15 (d, $J = 11.0$ Hz, 1H), 5.06 (d, $J = 18.0$ Hz, 1H), 5.04 (ddd, $J = 18.0, 3.5, 1.5$ Hz, 1H), 5.01 (tdd, $J = 11.0, 2.0, 1.0$ Hz, 1H), 4.54 (s, 2H), 3.37 (s, 2H), 2.56-2.45 (m, 1H), 2.42 (dd, $J = 2.0, 1.5$ Hz, 1H), 2.40-2.30 (m, 2H), 2.12-2.01 (m, 2H), 1.77 (d, $J = 15.0$ Hz, 1H). ^{13}C NMR (100 MHz, CDCl_3) δ ppm 218.5, 141.6, 138.1, 135.7, 128.3, 127.6, 127.4, 116.4, 114.5, 75.9, 73.2, 46.6, 45.5, 44.9, 36.0, 34.0. GCMS (EI): 179, 149, 136, 121, 107, 91.

(±)-1-(Benzyloxymethyl)bicyclo[3.2.1]oct-2-en-6-one (2-33)

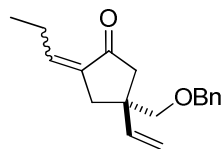


This reaction was air sensitive. Dry toluene (250 mL) was transferred into a 500 mL round bottom flask containing bis-alkene **2-34** (0.680 g, 2.50 mmol), dichlorodicyano quinone (0.11 g, 0.48 mmol), and DBU (0.17 mL, 1.14 mmol) under argon. The resulting black red solution was cooled to -78 °C and degassed under high vacuum for 1 h. The reaction mixture was heated to 100 °C and Hoveyda-Grubbs II catalyst (50 mg, 0.080 mmol, 3.2 mol %) in degassed dry toluene (1 mL) was added via syringe. A black precipitate was observed in the reaction mixture. More Hoveyda-Grubbs II catalyst (same quantity as previously) was added every 6 h interval. A total of 16 mol% of catalyst was added. 30 min after the last catalyst portion was added, the reaction mixture was allowed to cool to room temperature, and the solvent was removed *in vacuo*. The crude material was purified by silica gel column chromatography (hexane/EtOAc = 10:1) to afford recovered starting material bis-alkene **2-34** (R_f = 0.40, 0.120 g, 18%) and product **2-33** (R_f = 0.35, 0.420 g, 69 %, 83 % based on the starting material) as a colorless oil. The product **2-33** showed blue on TLC after staining with *p*-anisaldehyde followed by gentle heating. The major byproduct (10 %) was enone **2-43**, which resulted from alkene migration.

^1H NMR (400 MHz, CDCl_3) δ ppm 7.46-7.15 (m, 5H), 5.89 (ddd, J = 9.5, 4.0, 2.0 Hz, 1H), 5.55 (td, J = 9.5, 3.0 Hz, 1H), 4.58 (s, 2H), 3.48 (q, J = 9.0 Hz, 2H), 2.68 (t, J = 4.5 Hz, 1H), 2.48-2.39 (m, 1H), 2.33-2.29 (m, 2H), 2.28-2.19 (m, 1H), 2.06 (dd, J = 11.0, 5.5 Hz, 1H), 1.94 (dd, J = 11.0, 2.5 Hz, 1H). ^{13}C NMR (100 MHz, CDCl_3) δ ppm 220.3,

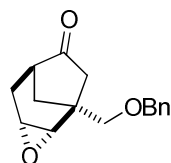
138.2, 135.3, 128.3, 127.6, 127.4, 124.7, 74.5, 73.3, 51.6, 46.4, 42.7, 36.4, 32.4. GCMS (EI): 242 (M^+), 136, 91. IR (cm^{-1}): 1722 (s), 1452 (w), 1270 (s), 1112 (m), 1025 (m), 712 (s).

(\pm) 4-(benzyloxymethyl)-2-propylidene-4-vinylcyclopentanone (2–43)



^1H NMR (400 MHz, CDCl_3) δ ppm 7.35-7.21 (m, 5H), 6.51 (tt, $J = 7.5, 2.5$ Hz, 1H), 5.88 (dd, $J = 18.0, 11.0$ Hz, 1H), 5.06 (d, $J = 11.0$ Hz, 1H), 5.01 (d, $J = 18.0$ Hz, 1H), 4.49 (s, 2H), 3.34 (s, 2H), 2.61 (dd, $J = 73.0, 17.0$ Hz, 2H), 2.42 (dd, $J = 53.0, 18.0$ Hz, 2H), 2.15-2.05 (m, 2H), 1.02 (t, $J = 7.5$ Hz, 3H). GCMS (EI): 270 (M^+), 240, 149, 136, 107, 91. IR (cm^{-1}): 2928 (w), 2857 (w), 1736 (s), 1652 (w), 1454 (w), 1407 (w), 1271 (w), 1206 (w), 1096 (s), 735 (s), 698 (s), 1027 (m), 918 (m).

(\pm) Compound 2–35

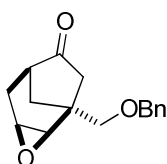


To a solution of alkene **2–33** (0.388 g, 1.60 mmol) in dichloromethane (5 mL) at 0 °C, *m*CPBA (0.46 g, 70 %, 2.6 mmol) was added quickly under the protection of nitrogen. After stirring for 1 h, the reaction mixture was allowed to warm to room temperature overnight. The solvent was removed *in vacuo* and the crude material was immediately purified by silica gel column chromatography (hexane/EtOAc = 3:1) to afford the desired product **2–35** ($R_f = 0.40$, 0.232 g, 64 %) and diastereomer byproduct **2–**

35b ($R_f = 0.30$, 0.045 g, 12 %). The products **2–35** and **2–35b** showed blue on TLC after staining with *p*-anisaldehyde followed by gentle heating.

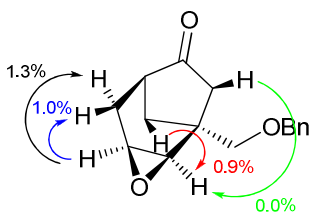
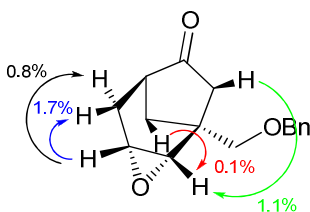
^1H NMR (500 MHz, CDCl_3) δ ppm 7.39-7.21 (m, 5H), 4.62-4.51 (m, 2H), 3.65 (d, $J = 9.0$ Hz, 1H), 3.53 (d, $J = 9.0$ Hz, 1H), 3.19 (d, $J = 3.0$ Hz, 1H), 3.04 (t, $J = 4.0$ Hz, 1H), 2.31 (s, 2H), 2.19 (t, $J = 5.5$ Hz, 1H), 2.09 (dd, $J = 15.0, 5.5$ Hz, 1H), 2.03-1.96 (m, 1H), 1.93 (ddd, $J = 16.0, 4.5, 1.5$ Hz, 1H), 1.54 (dd, $J = 11.0, 5.5$ Hz, 1H). ^{13}C NMR (125 MHz, CDCl_3) δ ppm 219.1, 137.9, 128.2, 127.4, 127.2, 73.6, 73.2, 56.6, 48.8, 45.4, 43.7, 43.0, 30.0, 27.7. ESI^+/MS for $[\text{C}_{16}\text{H}_{19}\text{O}_3]^+$: 259 (m/z).

(±) Compound 2–35b

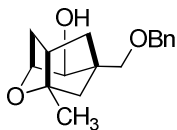


^1H NMR (500 MHz, CDCl_3) δ ppm 7.40-7.27 (m, 5H), 4.60 (s, 2H), 3.65 (d, $J = 9.0$ Hz, 1H), 3.57 (d, $J = 11.0$ Hz, 1H), 3.38 (d, $J = 4.0$ Hz, 1H), 3.10 (t, $J = 3.0$ Hz, 1H), 2.51 (dd, $J = 17.0, 3.0$ Hz, 1H), 2.43 (d, $J = 15.0$ Hz, 1H), 2.28 (t, $J = 5.5$ Hz, 1H), 2.08 (ddd, $J = 15.0, 6.0, 3.0$ Hz, 1H), 1.81-1.77 (m, 3H). ^{13}C NMR (125 MHz, CDCl_3) δ ppm 218.4, 137.9, 128.4, 127.7, 127.6, 74.8, 73.4, 58.8, 50.0, 44.5, 42.9, 41.6, 36.2, 33.2. ESI^+/MS for $[\text{C}_{16}\text{H}_{19}\text{O}_3]^+$: 259 (m/z). IR (cm^{-1}): 2920 (w), 2858 (w), 1742 (s), 1455 (w), 1364 (w), 1258 (w), 1102 (s), 1075 (m), 1012 (w), 838 (w), 750 (m), 700 (m).

NOE of compound 2–35 and 2–35b



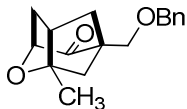
(±) Compound 2–36



This reaction was air and moisture sensitive. To a solution of epoxide **2–35** (88 mg, 0.340 mmol) in dry THF (3 mL) at $-78\text{ }^{\circ}\text{C}$ under argon, *n*-BuLi (0.30 mL, 1.6 M in hexane, 0.48 mmol) was added dropwise within 1 min via a syringe. After stirring for 1 h, the reaction was allowed to warm to $0\text{ }^{\circ}\text{C}$ and stirred at $0\text{ }^{\circ}\text{C}$ for another 2 h. The reaction was quenched with NH_4Cl (saturated aqueous solution, 1 mL). The water layer was extracted with EtOAc (2 mL x 3). The combined organic layer was dried over MgSO_4 and was concentrated *in vacuo*. The crude material was purified by silica gel column chromatography ($R_f = 0.25$, hexane/EtOAc = 3:1) to afford product **2–36** (65 mg, 70 %) as a colorless oil. The product **2–36** showed purple on TLC after staining with *p*-anisaldehyde followed by gentle heating. See Section 6.5.1 for the details of computational study of this reaction.

^1H NMR (400 MHz, CDCl_3) δ ppm 7.41-7.26 (m, 5H), 4.51 (dd, $J = 27.5, 12.0$ Hz, 2H), 4.21 (t, $J = 4.0$ Hz, 1H), 3.94 (d, $J = 3.5$ Hz, 1H), 3.69 (s, 1H), 3.60 (d, $J = 9.0$ Hz, 1H), 3.30 (d, $J = 9.0$ Hz, 1H), 2.20 (t, $J = 6.5$ Hz, 1H), 2.10 (d, $J = 11.5$ Hz, 1H), 2.09 (d, $J = 11.5$ Hz, 1H), 1.86-1.74 (m, 1H), 1.65 (dd, $J = 11.5, 3.5$ Hz, 1H), 1.38 (s, 3H), 1.35 (tdd, $J = 11.5, 7.0, 2.0$ Hz, 1H), 1.30 (d, $J = 11.5$ Hz, 1H). ^{13}C NMR (125 MHz, CDCl_3) δ ppm 137.6, 128.4, 127.7, 127.4, 85.6, 78.6, 77.2, 73.5, 73.2, 49.1, 47.3, 44.4, 39.5, 37.4, 22.6. ESI $^+$ /MS for $[\text{C}_{17}\text{H}_{23}\text{O}_3]^+$: 275 (m/z).

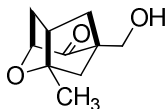
(±) Compound 2–31



To a solution of alcohol **2–36** (36mg, 0.131 mmol) in wet dichloromethane [346] (1 mL) at 0 °C under nitrogen, Dess-Martin reagent (15 wt% in dichloromethane, 0.90 mL, 0.20 mmol) was added dropwise within 1 min via a syringe. The reaction was allowed to warm to room temperature overnight. After the removal of the solvent *in vacuo*, the crude material was purified by silica gel column chromatography (R_f = 0.35, hexane/EtOAc = 5:1) to afford product **2–31** (34 mg, 95 %) as a colorless oil. The product **2–31** showed black on TLC after staining with *p*-anisaldehyde followed by gentle heating.

^1H NMR (500 MHz, CDCl_3) δ ppm 7.36-7.25 (m, 5H), 4.53 (d, J = 1.0 Hz, 2H), 4.24 (d, J = 4.5 Hz, 1H), 3.59 (dd, J = 25.0, 10.0 Hz, 2H), 2.57 (t, J = 6.0 Hz, 1H), 2.25 (tdd, J = 11.0, 6.0, 4.5 Hz, 1H), 2.21-2.15 (m, 2H), 2.05 (d, J = 12.0 Hz, 1H), 1.85 (d, J = 12.0 Hz, 1H), 1.58 (dd, J = 12.0, 3.5 Hz, 1H), 1.53 (s, 3H). ^{13}C NMR (125 MHz, CDCl_3) δ ppm 208.5, 138.4, 128.2, 127.4, 127.4, 86.9, 83.7, 73.3, 68.6, 58.8, 51.1, 44.6, 44.2, 42.5, 22.3. ESI^+ /MS for $[\text{C}_{17}\text{H}_{21}\text{O}_3]^+$: 273 (m/z).

(±) Compound 2–44

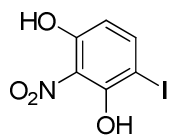


This reaction was air sensitive. To a solution of benzyl protected alcohol **2–31** (27 mg, 0.100 mmol) in MeOH (1 mL), Pd/C (5 % on activated carbon, 20 mg, 0.095 mmol) was added. The flask was evacuated and flushed with hydrogen, and the mixture was

stirred at room temperature overnight. The crude material was filtered through a pad of silica gel and the solvent was evaporated to afford product **2–44** (16 mg, 90 %) as a colorless oil. The product **2–44** showed purple on TLC after staining with *p*-anisaldehyde followed by gentle heating ($R_f = 0.25$, hexane/EtOAc = 1:1).

^1H NMR (500 MHz, CDCl_3) δ ppm 4.24 (d, $J = 4.5$ Hz, 1H), 3.64 (ddd, $J = 18.0, 12.0, 5.5$ Hz, 2H), 2.61 (t, $J = 6.0$ Hz, 1H), 2.33 (t, $J = 6.5$ Hz, 1H), 2.29 (dd, $J = 12.0, 3.5$ Hz, 1H), 2.22–2.28 (m, 1H), 1.93 (ddd, $J = 12.0, 6.5, 4.0$ Hz, 1H), 1.86 (d, $J = 12.0$ Hz, 1H), 1.79 (d, $J = 12.0$ Hz, 1H), 1.77 (dd, $J = 12.0, 3.5$ Hz, 1H), 1.54 (s, 3H). ^{13}C NMR (125 MHz, CDCl_3) δ ppm 211.4, 87.1, 83.5, 64.3, 60.3, 51.5, 44.8, 44.2, 42.5, 22.2. HRMS (ESI+, m/z) calculated for $\text{C}_{10}\text{H}_{15}\text{O}_3$ [$M + \text{H}$] $^+$ 183.1033, found 183.1040. IR (cm^{-1}): 3426 (br, m), 1721 (s), 1381 (m), 1079 (s), 1033 (s), 993 (s), 961 (m), 918 (w), 830 (m), 735 (m).

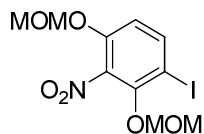
4-Iodo-2-nitrobenzene-1,3-diol (**2–45b**)



To a solution of 2-nitroresorcinol **2–45** (5.36 g, 34.6 mmol) in TFA (150 mL) at 0 °C, *N*-iodosuccinimide (NIS, 7.60 g, 33.8 mmol) was added in aliquots. The resulting solution was warmed to room temperature and stirred at 25 °C overnight. The reaction mixture was poured into ice-water (60 mL) and extracted with toluene (3 x 30 mL). The combined organic extract was washed with saturated aqueous sodium hydrosulfite and dried (MgSO_4). The solvent was removed under reduced pressure to afford product **2–45b** (9.70 g, 99 %) as an orange crystalline.

^1H NMR (500 MHz, CDCl_3) δ ppm 11.45 (s, 1H), 10.69 (s, 1H), 7.88 (d, $J = 9.0$ Hz, 1H), 6.54 (d, $J = 9.0$ Hz, 1H). ^{13}C NMR (125 MHz, CDCl_3) δ ppm 156.7, 154.6, 147.5, 123.8, 111.6, 72.5.

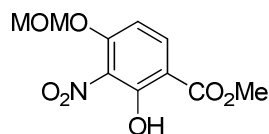
1-Iodo-2,4-bis(methoxymethoxy)-3-nitrobenzene (2–46)



This reaction was moisture sensitive. To a solution of 2-nitroresorcinol derivative **2–45b** (9.27 g, 33.0 mmol) in anhydrous dichloromethane (100 mL) at 0 °C, Hünig's base (11.0 g, 85.1 mmol) was added. After stirring for 30 min, MOMCl (6.6 g, 82 mmol) was added to the resulting brown solution and stirred at 25 °C overnight. After the removal of the solvent *in vacuo*, the crude material was purified by silica gel column chromatography ($R_f = 0.40$, hexane/EtOAc = 5:1) to afford product **2–46** (11.8 mg, 97 %) as a yellow solid.

^1H NMR (500 MHz, CDCl_3) δ ppm 7.76 (d, $J = 9.0$ Hz, 1H), 6.86 (d, $J = 9.0$ Hz, 1H), 5.19 (s, 2H), 5.11 (s, 2H), 3.51 (s, 3H), 3.44 (s, 3H). ^{13}C NMR (125 MHz, CDCl_3) δ ppm 149.5, 149.3, 140.3, 138.1, 113.7, 100.7, 95.0, 82.0, 57.8, 56.6. IR (cm^{-1}): 2980 (w), 1538 (s), 1464 (m), 1368 (m), 1259 (w), 1125 (m), 1029 (s), 937 (m), 879 (s), 807 (m).

Methyl 2-hydroxy-4-(methoxymethoxy)-3-nitrobenzoate (2–46b)

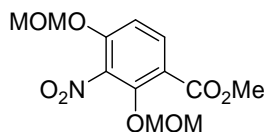


This reaction was air and moisture sensitive and the procedure was modified from ref [347]. To a solution of iodobenzene derivative **2–46** (4.20 g, 11.3 mmol) in anhydrous THF (300 mL) at –78 °C, PhMgBr (11 mL, 3.0 M, 33 mmol) was added, maintaining

rigorous stirring. Stirring was continued for 30 min before methyl carbonocyanide (3.5 mL, 40 mmol) was added dropwise to the resulting green viscous reaction mixture. After stirring for another 1 h at $-78\text{ }^{\circ}\text{C}$, the reaction mixture was allowed to warm to room temperature overnight. The reaction mixture was quenched with NH_4Cl (saturated aqueous solution, 60 mL) and the water layer was extracted with EtOAc (30 mL x 3). The combined organic layer was dried over MgSO_4 and was concentrated *in vacuo*. The crude material was purified by silica gel column chromatography ($R_f = 0.30$, hexane/EtOAc = 5:1) to afford product **2-46b** (2.26 g, 85 %) as a yellow solid. It appears that the reaction or the work-up conditions lead to the deprotection of one of the MOM groups.

^1H NMR (500 MHz, CDCl_3) δ ppm 11.41 (s, 1H), 7.87 (d, $J = 9.0$ Hz, 1H), 6.77 (d, $J = 9.0$ Hz, 1H), 5.28 (s, 2H), 3.96 (s, 3H), 3.49 (s, 3H). ^{13}C NMR (125 MHz, CDCl_3) δ ppm 169.3, 154.4, 153.9, 132.2, 131.4, 107.5, 105.7, 94.7, 56.8, 52.7.

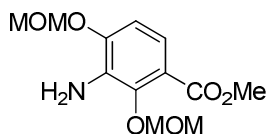
Methyl 2,4-bis(methoxymethoxy)-3-nitrobenzoate (**2-47**)



This reaction was air sensitive. To a solution of compound **2-46b** (1.85 g, 7.20 mmol) in anhydrous dichloromethane (50 mL) at $0\text{ }^{\circ}\text{C}$, Hünig's base (1.30 g, 10.1 mmol) was added. The reaction mixture was warmed to room temperature and stirred for 30 min before MOMCl (0.70 g, 8.7 mmol) was added. The reaction mixture was then stirred overnight. After the removal of the solvent *in vacuo*, the crude material was purified by silica gel column chromatography ($R_f = 0.30$, hexane/EtOAc = 5:1, overlap with **2-46b**) to afford product **2-47** (1.70 mg, 78 %) as a yellow solid.

^1H NMR (500 MHz, CDCl_3) δ ppm 7.96 (d, $J = 9.0$ Hz, 1H), 7.06 (d, $J = 9.0$ Hz, 1H), 5.26 (s, 2H), 5.13 (s, 2H), 3.88 (s, 3H), 3.47 (s, 3H), 3.47 (s, 3H). ^{13}C NMR (125 MHz, CDCl_3) δ ppm 164.2, 152.2, 150.6, 138.4, 133.8, 118.0, 110.6, 102.1, 94.9, 57.7, 56.8, 52.3. IR (cm^{-1}): 3313 (w), 1668 (m), 1608 (w), 1503 (w), 1435 (s), 1308 (s), 1249 (m), 1134 (s), 1041 (s), 997 (s), 920 (m), 736 (m).

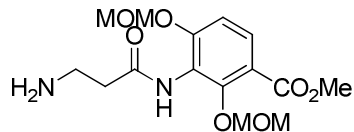
Methyl 3-amino-2,4-bis(methoxymethoxy)benzoate (2–48)



This reaction was air sensitive. To a solution of nitrobenzene **2–47** (1.50 g, 4.98 mmol) in MeOH (25 mL) and trace of toluene (0.5 mL), Pd/C (5 % on activated carbon, 1.1 g, 0.52 mmol; wet with MeOH before adding) was added. The flask was evacuated and flushed with hydrogen, and the mixture was stirred at room temperature overnight. After the removal of the solvent *in vacuo*, the crude material was purified by silica gel column chromatography ($R_f = 0.30$, hexane/EtOAc = 2:1) to afford product **2–48** (0.94 g, 70 %) as a colorless oil.

^1H NMR (500 MHz, CDCl_3) δ ppm 7.24 (d, $J = 8.5$ Hz, 1H), 6.85 (d, $J = 8.5$ Hz, 1H), 5.24 (s, 2H), 5.10 (s, 2H), 4.25 (s, br, 2H), 3.86 (s, 3H), 3.61 (s, 3H), 3.49 (s, 3H). ^{13}C NMR (125 MHz, CDCl_3) δ ppm 166.2, 148.5, 145.4, 131.7, 120.0, 118.0, 109.5, 101.1, 94.8, 57.6, 56.3, 51.7. HRMS (ESI+, m/z) calculated for $\text{C}_{12}\text{H}_{18}\text{NO}_6$ [$M + \text{H}$] $^+$ 272.1134, found 272.1134. IR (cm^{-1}): 2269 (w), 2925 (w), 1716 (m), 1595 (m), 1459 (m), 1295 (m), 1198 (m), 1128 (s), 1079 (m), 1032 (s), 992 (s), 920 (s), 742 (m).

Methyl 3-(3-aminopropanamido)-2,4-bis(methoxymethoxy)benzoate (2–50)

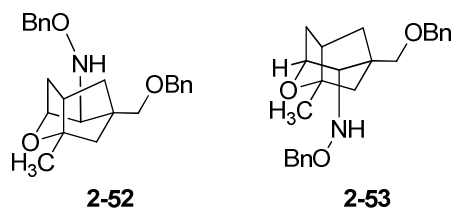


3-(2,2,2-Trifluoroacetamido)propanoic acid was prepared following literature ref [348]. The reaction was moisture sensitive. To a mixture of 3-(2,2,2-trifluoroacetamido)propanoic acid (1.48 g, 8.00 mmol) and 2 drops of dry pyridine in anhydrous benzene (20 mL), oxalyl chloride (1.0 mL, 11.7 mmol) was added dropwise (effervescence was observed). After stirring at 50 °C for another 30 min, the solvent was removed *in vacuo*. The resulting viscous black oil (acid chloride **2–49**) was diluted with anhydrous dichloromethane (10 mL) and was added into a solution of amine **2–48** (0.76 g, 2.80 mmol) in anhydrous dichloromethane (10 mL), followed by the addition of pyridine (1.5 mL, 18.6 mmol). The mixture was stirred for 5 h at room temperature and the solvent was removed *in vacuo* (R_f = 0.40, hexane/EtOAc = 2: 1). MeOH (10 mL), H₂O (3 mL) and K₂CO₃ (0.76 g, 5.50 mmol) was then added, and the mixture was stirred at room temperature for 7 h. The crude material was concentrated at reduced pressure and the residue was purified by silica gel column chromatography (R_f = 0.40, CHCl₃: MeOH: 28% NH₄OH = 35: 7: 1) to afford product **2–50** (0.91 g, 95 %) as a colorless solid. The products **2–50** showed purple on TLC after staining with ninhydrin followed by gentle heating.

¹H NMR (500 MHz, CDCl₃) δ ppm 7.70 (d, J = 8.5 Hz, 1H), 6.93 (d, J = 8.5 Hz, 1H), 5.16 (s, 2H), 4.99 (s, 2H), 3.80 (s, 3H), 3.47 (s, 3H), 3.41 (s, 3H), 3.05 (s, br, 2H), 2.51 (s, br, 2H). ¹³C NMR (125 MHz, CDCl₃) δ ppm 170.8, 165.3, 156.6, 154.1, 130.3, 121.4, 117.8, 110.3, 100.9, 94.5, 57.3, 56.3, 51.8, 38.3, 37.9. HRMS (ESI+, m/z) calculated for

$C_{15}H_{23}N_2O_7$ $[M + H]^+$ 343.1492, found 343.1485. IR(cm^{-1}): 2952 (w), 1692 (m), 1596 (w), 1460 (m), 1294 (m), 1199 (m), 1152 (m), 1033 (m), 994 (s), 922 (m), 750 (m).

(±) **Compound 2-52 and 2-53**



To a mixture of ketone **2-31** (20 mg, 0.073 mmol) and *O*-benzylhydroxylamine (18 mg, 0.146 mmol) in MeOH (0.3 mL, pH 3, adjusted by HCl) at 0 °C, NaB(CN)H₃ (7.0 mg, 0.111 mmol) was added. After stirring for 5 h, the solvent was removed *in vacuo* and the crude material was purified by silica gel column chromatography (hexane: EtOAc = 10:1) to afford product **2-52** (20 mg, 72%) and **2-53** (6 mg, 14 %) as colorless oil.

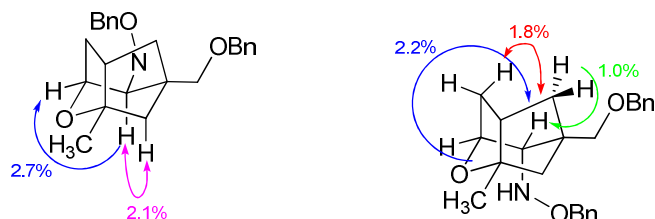
2-52: ¹H NMR (400 MHz, CDCl₃) δ ppm 7.41-7.24 (m, 10H), 4.67 (s, 2H), 4.48 (dd, J = 12.0 Hz, 2H), 4.49-4.47 (m, 1H), 3.34-3.33 (m, 1H), 3.40 (d, J = 9.5 Hz, 1H), 3.28 (d, J = 9.5 Hz, 1H), 2.21 (t, J = 6.5 Hz, 1H), 2.13 (d, J = 11.0 Hz, 1H), 1.83-1.79 (m, 3H), 1.41 (s, 3H), 1.37-1.33 (m, 2H). ¹³C NMR (100 MHz, CHCl₃) δ ppm 138.2, 137.8, 128.4, 128.3, 128.2, 127.7, 127.4, 127.2, 86.0, 77.7, 76.5, 75.6, 73.2, 63.4, 49.4, 48.1, 44.7, 39.8, 37.7, 22.9. ESI⁺/MS for [C₂₄H₃₀NO₃]⁺: 380 (m/z). IR (cm^{-1}): 2927 (w), 2855 (w), 1454 (w), 1270 (w), 1096 (m), 1028 (w), 914 (w), 828 (w), 734 (s), 698 (s).

2-53: ¹H NMR (400 MHz, CDCl₃) δ ppm 7.39-7.27 (m, 10 H), 4.66 (s, 2H), 4.55 (d, J = 4.5 Hz, 1H), 4.48 (s, 2H), 3.60 (d, J = 9.0 Hz, 1H), 3.18 (d, J = 9.0 Hz, 1H), 3.04 (s, 1H), 2.23 (t, J = 6.0 Hz, 1H), 2.00 (tdd, J = 8.0, 5.5, 2.0 Hz, 1H), 1.67-1.59 (m, 4H), 1.35 (s, 3H), 1.20 (d, J = 11.0 Hz, 1H). ¹³C NMR (100 MHz, CHCl₃) δ ppm 138.7, 138.2, 128.3, 128.2, 128.2, 127.5, 127.3, 127.3, 86.3, 77.2, 75.9, 73.7, 73.2, 61.3, 48.7, 45.0, 44.2, 43.9,

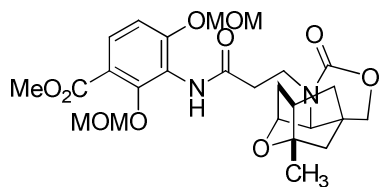
39.7, 23.1. ESI⁺/MS for [C₂₄H₃₀NO₃]⁺: 380 (m/z). IR (cm⁻¹): 2927 (w), 2853 (w), 1721 (w), 1453 (w), 1269 (m), 1098 (m), 1026 (m), 965 (w), 919 (w), 735 (s), 711 (m), 697 (s).

Stereochemistry of **2-52** and **2-53** was determined based on NOE experiments.

(±) Compound **2-52** and **2-53**

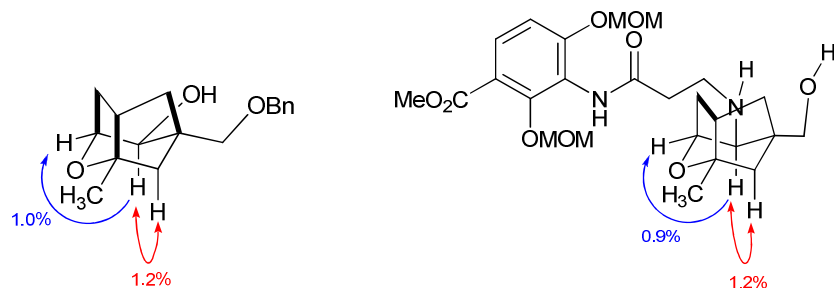


(±) Compound **2-55**



To a mixture of ketone **2-44** (12 mg, 0.066 mmol) and amine **2-50** (90 mg, 0.26 mmol) in MeOH (0.3 mL, pH 4, adjusted by HCl) at 0 °C, NaB(CN)H₃ (7.0 mg, 0.111 mmol) was added in 3 portions within 1 h. After stirring for another 5 h, the solvent was removed *in vacuo* and the crude material was redissolved in CHCl₃: MeOH (20:1). This solution was then filtered through a pad of silica gel and washed with CHCl₃: MeOH (20:1, 5 mL x 2). This procedure removes the unreacted amine starting material from the filtrate. The stereochemistry of crude product **2-54** was determined by NOE experiment.

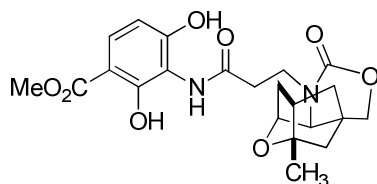
(±) Compound **2-36** and **2-54**



The filtrate (crude compound **2-54**) was concentrated at a reduced pressure and then further dried under high vacuum for 2 h before it was diluted with anhydrous benzene (1 mL). Carbonyl diimidazole (50 mg, 0.31 mmol) and DMAP (8.0 mg, 0.066 mmol) were sequentially added to the reaction mixture and stirred at 50 °C for 24 h. The reaction mixture was concentrated at reduced pressure and the residue was purified by silica gel column chromatography (hexane: acetone = 1:1) to afford product **2-55** (20 mg, 56 %) as a colorless oil and as a single diastereomer. A major side reaction was the reduction of the ketone **2-44**. Also when the concentration of ketone **2-44** was < 0.2 M, the yield of product **2-55** was generally low.

^1H NMR (500 MHz, CHCl_3) δ ppm 7.79 (d, $J = 7.5$ Hz, 1H), 7.62 (s, 1H), 7.04 (d, $J = 9.0$ Hz, 1H), 5.29-5.20 (m, 2H), 5.10-5.04 (m, 2H), 4.71 (s, 1H), 4.19 (d, $J = 11.0$ Hz, 1H), 4.06-3.94 (m, 1H), 3.86 (s, 3H), 3.77 (d, $J = 11$ Hz, 1H), 3.67 (s, 1H), 3.58 (s, 3H), 3.50 (s, 3H), 3.47-3.37 (m, 1H), 2.93-2.72 (br, 1H), 2.68-2.58 (br, 1H), 2.32 (t, $J = 6.5$ Hz, 1H), 1.98 (dd, $J = 12.0, 3.0$ Hz, 2H), 1.80 (d, $J = 11.0$ Hz, 1H), 1.68 (dd, $J = 11.0, 3.5$ Hz, 1H), 1.56 (dd, $J = 11.0, 7.5$ Hz, 1H), 1.49 (d, $J = 11.0$ Hz, 1H), 1.43 (s, 3H). ^{13}C NMR (125 MHz, CHCl_3) δ ppm 169.0 (br), 165.2, 156.8, 154.3 (br), 153.4, 130.5 (br), 121.5, 117.8, 111.0, 101.8, 94.8, 86.8, 76.3, 72.4, 58.4, 57.4, 56.4, 51.9, 45.8, 43.8, 43.2, 40.6, 40.1, 37.7, 34.9 (br), 22.6. HRMS (ESI+, m/z) calculated for $\text{C}_{26}\text{H}_{35}\text{N}_2\text{O}_{10}$ [$M + \text{H}$] $^+$ 535.2291, found 535.2216.

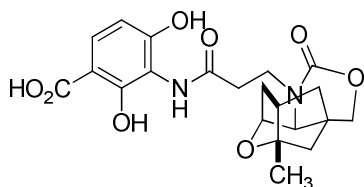
(±) Compound 2-56



To a solution of compound **2–55** (10 mg, 0.0187 mmol) in MeOH (0.3 mL), 6 M HCl aqueous solution (0.1 mL) was added. After stirring at room temperature for 24 h, the reaction mixture was extracted with CHCl₃: *i*-PrOH = 3: 1 (0.3 mL x 5). The organic layer was concentrated *in vacuo* and under high vacuum and the residue was purified by silica gel column chromatography (hexane: acetone = 1:1) to afford product **2–56** (7.8 mg, 92 %) as a colorless solid.

¹H NMR (500 MHz, CHCl₃) δppm 11.65 (s, 1H), 10.71 (s, 1H), 8.11 (s, 1H), 7.58 (d, *J* = 9.0 Hz, 1H), 6.52 (d, *J* = 9.0 Hz, 1H), 4.67 (t, *J* = 3.5 Hz, 1H), 4.19 (d, *J* = 11.0 Hz, 1H), 3.99 (ddd, *J* = 14.0, 7.0, 6.0 Hz, 1H), 3.92 (s, 3H), 3.79 (d, *J* = 11.0 Hz, 1H), 3.64 (d, *J* = 3.5 Hz, 1H), 3.46 (td, *J* = 14.0, 7.0 Hz, 1H), 2.99 (td, *J* = 15.0, 7.0 Hz, 1H), 2.78 (td, *J* = 15.0, 6.5 Hz, 1H), 2.34 (t, *J* = 6.5 Hz, 1H), 2.03-1.95 (m, 1H), 1.99 (dd, *J* = 12.0, 3.5 Hz, 1H), 1.82 (d, *J* = 12.0 Hz, 1H), 1.72 (dd, *J* = 11.0, 3.5 Hz, 1H), 1.63-1.56 (m, 1H), 1.50 (d, *J* = 11.0 Hz, 1H), 1.44 (s, 3H). ¹³C NMR (125 MHz, CHCl₃) δppm 171.4, 170.6, 155.0, 153.9, 153.7, 127.7, 114.0, 111.3, 104.2, 86.9, 76.4, 72.5, 59.0, 52.2, 45.8, 43.7, 43.3, 40.9, 40.1, 37.7, 35.1, 22.5. HRMS (ESI+, *m/z*) calculated for C₂₂H₂₇N₂O₈ [*M* + H]⁺ 447.1777, found 447.1760.

(±) Compound 2–30

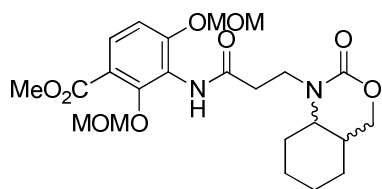


To a solution of compound **2–55** (5.0 mg, 0.0096 mmol) in MeOH (0.3 mL), LiOH (1.6 M in MeOH: H₂O = 3: 1, 0.2 mL) was added. HCl (4 M in MeOH: H₂O, 0.3 mL) was added before the reaction mixture was stirred for 12 h at room temperature.

After stirring at room temperature for another 24 h, the reaction mixture was extracted with CHCl_3 : *i*-PrOH = 3: 1 (0.3 mL x 5). The organic layer was concentrated *in vacuo* and under high vacuum and the residue was purified by silica gel column chromatography (acetone: hexane: AcOH = 1: 1: 0.1) to afford product **2–30** (3.3 mg, 80 %) as a colorless solid.

^1H NMR (600 MHz, d_4 -MeOD) δ ppm 7.68 (d, J = 9.0 Hz, 1H), 6.45 (d, J = 9.0 Hz, 1H), 4.72 (t, J = 3.0 Hz, 1H), 4.31 (d, J = 11.0 Hz, 1H), 4.05 (td, J = 13.0, 6.0 Hz, 1H), 3.88-3.82 (m, 1H), 3.83 (d, J = 11.0 Hz, 1H), 3.44 (td, J = 15.0, 7.0 Hz, 1H), 2.89 (td, J = 15.0, 7.0 Hz, 1H), 2.66 (td, J = 14.0, 6.5 Hz, 1H), 2.35 (t, J = 6.5 Hz, 1H), 1.98-1.94 (m, 1H), 1.90 (dd, J = 12.0, 3.0 Hz, 1H), 1.87 (d, J = 12.0 Hz, 1H), 1.70 (dd, J = 11.0, 3.0 Hz, 1H), 1.68-1.62 (m, 1H), 1.60 (d, J = 11.0 Hz, 1H), 1.42 (s, 3H). ^{13}C NMR (150 MHz, d_4 -MeOD) δ ppm 176.7, 175.4, 175.2, 161.4, 157.8, 132.5, 114.8, 110.6, 108.1, 89.9, 79.2, 75.2, 60.9, 48.0, 46.6, 45.9, 43.5, 42.3, 40.2, 36.6, 24.3. HRMS (ESI+, m/z) calculated for $\text{C}_{21}\text{H}_{25}\text{N}_2\text{O}_8$ [$M + \text{H}$] $^+$ 433.1611, found 433.1590.

Compound 2–59



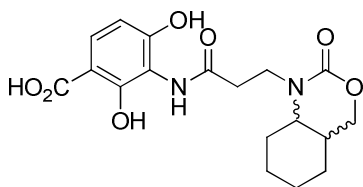
To a mixture of 2-(hydroxymethyl)cyclohexanone (256 mg, 2.00 mmol) and amine **2–50** (342 mg, 1.00 mmol) in MeOH (5 mL, pH 3-4, adjusted by HCl) at 0 °C, $\text{NaB}(\text{CN})\text{H}_3$ (140 mg, 2.22 mmol) was added in 3 portions within 1 h. After stirring for another 5 h, the solvent was removed *in vacuo* and the crude material was redissolved in CHCl_3 : MeOH (20:1). This solution was then filtered through a pad of silica gel and

washed with CHCl₃: MeOH (20: 1, 5 mL x 2). This procedure removes the unreacted amine starting material from the filtrate. The filtrate was concentrated at a reduced pressure and then further dried under high vacuum for 2 h before it was diluted with anhydrous benzene (5 mL). Carbonyl diimidazole (200 mg, 1.24 mmol) and DMAP (80 mg, 0.66 mmol) were sequentially added to the reaction mixture and stirred at 50 °C for 24 h. The reaction mixture was concentrated at reduced pressure and the residue was purified by silica gel column chromatography (hexane: acetone = 1:1) to afford product **2-59** (336 mg, 70 %) as a colorless oil.

¹H NMR (400 MHz, CHCl₃) δppm 7.80 (s, 1H for *trans*, 1H for *cis*), 7.71 (d, *J* = 9.0 Hz, 1H for *trans*, 1H for *cis*), 6.95 (d, *J* = 9.0 Hz, 1H for *cis*), 6.94 (d, *J* = 9.0 Hz, 1H for *trans*), 5.16 (s, 2H for *trans*, 2H for *cis*), 4.98 (s, 2H for *trans*, 2H for *cis*), 4.32 (dd, *J* = 11.0, 11.0 Hz, 1H for *cis*), 3.99 (dd, *J* = 11.0, 11.0 Hz, 1H for *trans*), 3.98 (dd, *J* = 11.0, 11.0 Hz, 1H for *cis*), 3.79 (dd, *J* = 11.0, 11.0 Hz, 1H for *trans*), 3.78 (s, 3H for *trans*, 3H for *cis*), 3.75-3.57 (m, 2H for *trans*, 1H for *cis*), 3.51 (s, 3H for *cis*), 3.50 (s, 3H for *trans*), 3.41 (s, 3H for *cis*), 3.40 (s, 3H for *trans*), 3.40-3.30 (m, 2H for *cis*), 3.01 (t, *J* = 8.5 Hz, 1H for *trans*), 2.94-2.71 (m, 1H for *trans*, 1H for *cis*), 2.70-2.60 (m, br, 1H for *cis*), 2.58-2.46 (m, br, 1H for *trans*), 2.45-2.38 (m, br, 1H for *cis*), 2.34-2.21 (m, 1H for *trans*, 1H for *cis*), 1.94 (d, *J* = 12.0 Hz, 1H for *cis*), 1.81 (d, *J* = 8.0 Hz, 1H for *trans*), 1.76-1.51 (m, 3H for *trans*, 3H for *cis*), 1.51-1.31 (m, 2H for *cis*), 1.30-1.10 (m, 2H for *trans*, 3H for *cis*), 1.10 (dd, *J* = 14.0, 8.5 Hz, 1H for *trans*), 0.94 (ddd, *J* = 13.0, 3.5, 3.5 Hz, 1H for *trans*). ¹³C NMR (100 MHz, CHCl₃) δppm 169.3 (br, *trans* / *cis*), 165.1 (*trans* / *cis*), 156.6 (*trans*), 156.5 (*cis*), 154.5 (br, *trans* / *cis*), 153.7 (*trans*), 153.0 (*cis*), 130.5 (br, *trans* / *cis*), 121.3 (*trans* / *cis*), 117.7 (*cis*), 117.6 (*trans*), 110.5 (*cis*), 110.4

(*trans*), 101.3 (*cis*), 101.2 (*trans*), 94.5 (*trans* / *cis*), 70.0 (*trans*), 66.7 (*cis*), 59.5 (*cis*), 57.1 (*trans*), 56.3 (*cis*), 56.2 (*trans*), 51.7 (*trans* / *cis*), 44.0 (br, *cis*), 40.4 (br, *trans*), 38.6 (*trans* / *cis*), 35.2 (br, *trans*), 34.9 (br, *cis*), 31.3 (*trans*), 30.6 (*cis*), 30.2 (*trans*), 27.6 (*cis*), 25.9 (*trans*), 25.1 (*cis*), 24.3 (*trans*), 24.1 (*trans*), 23.5 (*cis*), 20.8 (*cis*). HRMS (ESI+, m/z) calculated for C₂₃H₃₃N₂O₉ [*M* + H]⁺ 481.2189, found 481.2169.

Compound 2–57

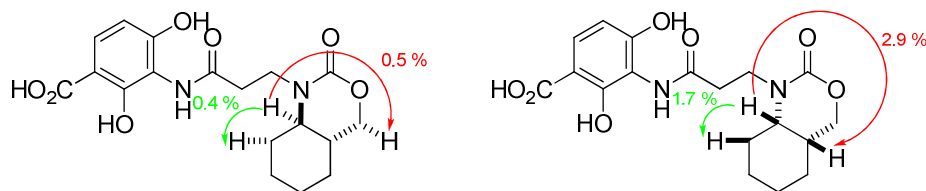


To a solution of compound **2–59** (240 mg, 0.50 mmol) in MeOH (1 mL), LiOH (1.6 M in MeOH: H₂O = 3: 1, 0.8 mL) was added. HCl (4 M in MeOH: H₂O, 1.6 mL) was added before the reaction mixture was stirred for 12 h at room temperature. After stirring at room temperature for another 24 h, the reaction mixture was extracted with CHCl₃: *i*-PrOH = 3: 1 (2 mL x 5). The organic layer was concentrated *in vacuo* and under high vacuum and the residue was purified by silica gel column chromatography (acetone: hexane: AcOH = 1: 1: 0.1) to afford product **2–57** (161 mg, 85 %) as a colorless solid. The ratio of *cis*-4 and *trans*-4 is 2:3, determined by ¹H NMR. The stereochemistry of product **2–57** was determined by NOE experiment.

¹H NMR (500 MHz, d₄-MeOD) δ ppm 7.63 (d, *J* = 8.5 Hz, 1H for *cis*, 1H for *trans*), 6.41 (d, *J* = 8.5 Hz, 1H for *cis*, 1H for *trans*), 4.43 (dd, *J* = 11.0, 11.0 Hz, 1H for *cis*), 4.07 (dd, *J* = 11.0, 11.0 Hz, 1H for *cis*), 4.06 (dd, *J* = 11.0, 11.0 Hz, 1H for *trans*), 3.92 (dd, *J* = 11.0, 11.0 Hz, 1H for *trans*), 3.90-3.78 (m, 1H for *cis*, 1H for *trans*), 3.72-3.58 (m, 1H, *trans*), 3.59-3.50 (m, 1H, *cis*), 3.46 (td, *J* = 14.0, 6.5 Hz, 1H, *cis*), 3.22 (t, *J* = 9.5 Hz, 1H,

trans), 2.88-2.74 (m, 1H for *cis*, 1H for *trans*), 2.69-2.48 (m, 1H for *cis*, 1H for *trans*), 2.40-2.26 (m, 1H for *cis*, 1H for *trans*), 1.99 (d, $J = 12.0$ Hz, 1H, *cis*), 1.84 (d, $J = 5.5$ Hz, 1H, *trans*), 1.78-1.58 (m, 3H for *trans*, 3H for *cis*), 1.53 (dd, $J = 23.0, 12.0$ Hz, 1H, *cis*), 1.50-1.36 (m, 1H, *cis*), 1.42-1.22 (m, 2H for *cis*, 2H for *trans*), 1.17 (dd, $J = 23.0, 13.0$ Hz, 1H, *trans*), 1.03 (dd, $J = 21.0, 12.0$ Hz, 1H, *trans*). ^{13}C NMR (125 MHz, $\text{d}_4\text{-MeOD}$) δ ppm 173.9 (*cis*), 173.8 (*trans*), 173.6 (*cis* / *trans*), 159.9 (*cis*), 159.8 (*trans*), 156.7 (*cis* / *trans*), 156.0 (*cis* / *trans*), 130.9 (*cis* / *trans*), 113.4 (*trans*), 113.4 (*cis*), 109.2 (*trans*), 109.2 (*cis*), 106.5 (*cis* / *trans*), 71.6 (*trans*), 68.6 (*cis*), 60.5 (*trans*), 57.4 (*cis*), 45.3 (*cis*), 41.6 (*trans*), 40.1 (*trans*), 35.9 (*trans*), 35.7 (*cis*), 33.0 (*cis*), 31.3 (*trans*), 28.6 (*cis*), 27.2 (*trans*), 26.3 (*cis*), 25.7 (*trans*), 25.5 (*trans*), 24.9 (*cis*), 22.1 (*cis*). HRMS (ESI+, m/z) calculated for $\text{C}_{18}\text{H}_{23}\text{N}_2\text{O}_7$ [$M + \text{H}$] $^+$ 379.1505, found 379.1525.

Compound *trans*-2–57 and *cis*-2–57



6.3 Synthetic protocols for compounds in Chapter 3.

6.3.1 Synthetic strategies

All the analogs in Chapter 3 are generated from four methods (**Scheme 6–2**) except for compound **3–16**. The synthesis of compound **3–16** refers to **Scheme 6–3**.

Method A

Experimental details for the synthesis of compound **6-1** refer to Section 6.2 (compound **2-50**). The reactions were performed at 1.0–10 mmol scale. Amine **6-1** (1.0 eq.), acetic acid (3.0 eq.) and aldehyde/ ketone (3.0 eq.) were stirred in MeOH ([**6-1**] = 0.2 M) at RT for 15 min. Sodium cyanoborohydride (1.5 eq.) was added in five aliquots over 1 h. The reaction mixture was stirred at RT for another 2 h and then quenched with 1 M NaOH. The mixture was extracted with CHCl₃ (x 3) and then concentrated under vacuum. The crude product was purified on silica-gel with hexane: EtOAc to give pure product **6-2** in up to 85% yield.

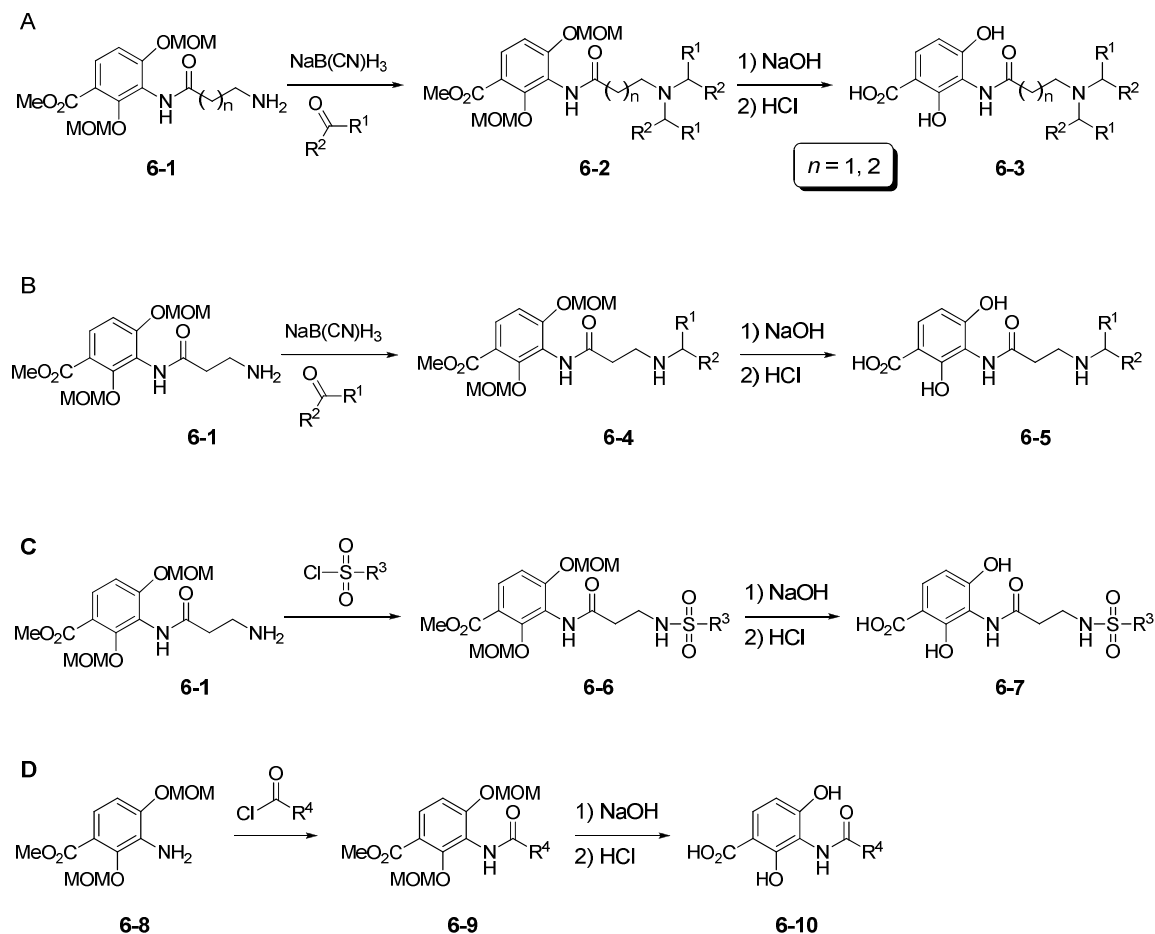
Intermediate **6-2** was stirred with NaOH (5.0 eq.) in MeOH: H₂O (3: 1, [**6-2**] = 0.2 M) for 5–14 h, at which point the starting material disappeared on TLC. HCl (6 M in H₂O, 20.0 eq.) was then added to the cloudy reaction mixture to form a clear solution at RT. The reaction was heated to 40 °C and stirred overnight before quenching with saturated NaHCO₃. The mixture was extracted with CHCl₃: *i*-PrOH (3: 1) three times. The crude product was concentrated under vacuum and purified on silica-gel with CHCl₃: MeOH (5% NH₄OH), or using HPLC C18 reverse phase column (Nacalai tesque 5C18-MS II column) to give product **6-3** in up to 69% yield. The product displayed a distinctive blue color under UV light (365 nm) on TLC (F₂₅₄). For gram-scale syntheses, the products can be recrystallized with 2:1 MeOH: 2 M HCl aqueous solution.

Method B

The procedure was the same as method A with the only exception being the use of 1 equiv. of aldehyde used instead of the 3 equiv. used in method A.

Method C

Sulfonyl chloride (2.0 eq.) was added to a solution of amine **6-1** (1.0 eq.) and NEt_3 (2.5 eq.) in anhydrous CH_2Cl_2 and the reaction was stirred at RT for overnight. The crude product was concentrated under vacuum and purified on silica-gel (hexane: EtOAc) to give the product **6-6** in 57% yield.



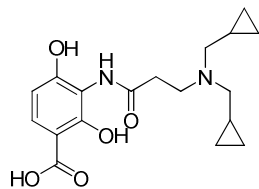
Scheme 6-2. General synthesis of platensimycin analogs: a) synthesis of *N*-di-alkyl analogs; b) synthesis of *N*-mono-alkyl analogs; c) synthesis of *N*-sulfonyl analogs; d) synthesis of acyl analogs.

Method D

For experimental details for the synthesis of compound **6–8**, refer to Section 6.2 (compound **2–48**). This reaction is moisture sensitive. The acid chloride (1.5 eq.) was added to a solution of **6–8** (1.0 eq.) and NEt₃ (2.0 eq.) in CH₂Cl₂ and the reaction was stirred at RT for 1 h. The reaction mixture was washed with saturated NaHCO₃ and the aqueous layer was extracted with CHCl₃ (x 2). The crude product was concentrated under vacuum and purified on silica-gel (hexane: EtOAc) to give the product S9 in up to 90% yield.

6.3.2 Physical data of the analogs

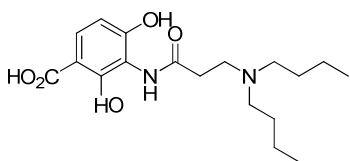
3-(3-(Bis(cyclopropylmethyl)amino)propanamido)-2,4-dihydroxybenzoic acid (**3–6**)



The compound was synthesized with an overall yield of 13% from **2–50** and 10 mg material was obtained. $R_f = 0.30$, NH₃•H₂O (28% aq.)/ MeOH/ CHCl₃ = 1/7/55.

¹H NMR (500 MHz, MeOD) δ 7.68 (d, $J = 8.5$ Hz, 1H), 6.36 (d, $J = 8.5$ Hz, 1H), 3.70 (t, $J = 6.5$ Hz, 2H), 3.20 (t, br, $J = 6.5$ Hz, 4H), 3.01 (t, $J = 6.5$ Hz, 2H), 1.29 – 1.13 (m, 2H), 0.87 – 0.71 (m, 4H), 0.56 – 0.44 (m, 4H). ¹³C NMR (125 MHz, MeOD) δ 175.8, 172.2, 159.8, 157.4, 132.2, 131.1, 112.6, 107.3, 59.6, 50.0, 30.5, 6.9, 5.2. HRMS (ESI+, m/z) calculated for C₁₈H₂₅N₂O₅ [$M + H$]⁺ 349.1763, found 349.1758.

3-(3-(Dibutylamino)propanamido)-2,4-dihydroxybenzoic acid (**3–7**)

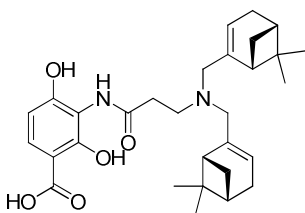


The compound was synthesized with an overall yield of 13% from **2-50** and 14 mg material was obtained. The major byproduct is the benzoic acid methyl ester (50%).

$R_f = 0.35$, $\text{NH}_3 \cdot \text{H}_2\text{O}$ (28% aq.)/ MeOH/ $\text{CHCl}_3 = 1/7/55$.

^1H NMR (500 MHz, CDCl_3) δ 9.14 (s, br, 1H), 7.62 (d, $J = 9.0$ Hz, 1H), 6.39 (d, $J = 9.0$ Hz, 1H), 3.45 – 3.39 (m, 2H), 3.05 – 3.00 (m, 6H), 1.75 – 1.68 (m, 4H), 1.40 (q, $J = 7.5$ Hz, 4H), 0.98 (t, $J = 7.5$ Hz, 6H). ^{13}C NMR (125 MHz, CDCl_3) δ 174.9, 170.1, 155.8, 153.2, 128.9, 113.7, 110.8, 108.8, 52.5, 49.7, 32.3, 25.4, 20.4, 13.8. HRMS (ESI+, m/z) calculated for $\text{C}_{18}\text{H}_{29}\text{N}_2\text{O}_5$ [$M + \text{H}$] $^+$ 353.2076, found 353.2069.

(–)-Myrtemycin (**3-8**)

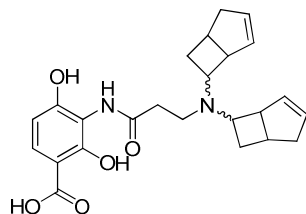


The compound was synthesized with an overall yield of 68% from **2-50** and 18 mg material was obtained. $R_f = 0.40$, $\text{NH}_3 \cdot \text{H}_2\text{O}$ (28% aq.)/ MeOH/ $\text{CHCl}_3 = 1/7/55$.

$[\alpha]_D^{20} = -10.6^\circ$ ($c = 1.0$ in MeOH). ^1H NMR (600 MHz, [D5] pyridine) δ 10.84 (s, 1H), 8.12 (d, $J = 8.5$ Hz, 1H), 6.88 (d, $J = 8.5$ Hz, 1H), 5.56 (s, 2H), 3.42 (d, $J = 12.5$ Hz, 2H), 3.35 – 3.25 (m, br, 1H), 3.23 – 3.08 (m, 4H), 3.08 – 2.90 (m, br, 1H), 2.64 (s, 2H), 2.36 (dt, $J = 8.5, 5.5$ Hz, 2H), 2.24 (d, $J = 17.5$ Hz, 1H), 2.15 (d, $J = 17.5$ Hz, 1H), 1.96 (s, 2H), 1.24 (s, 6H), 1.20 (d, $J = 8.5$ Hz, 2H), 0.85 (s, 6H). ^{13}C NMR (126 MHz, [D5] pyridine) δ 175.8, 174.5, 159.0, 158.8, 146.2, 130.4, 123.9, 116.3, 111.2, 108.1, 61.0,

51.4, 45.8, 42.1, 39.1, 34.6, 33.2, 32.9, 27.4, 22.3. HRMS (ESI+, m/z) calculated for $C_{30}H_{41}N_2O_5$ [$M + H$]⁺ 509.3015, found 509.3014.

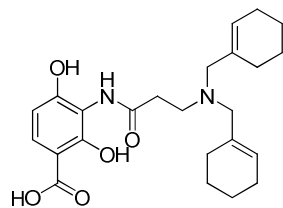
Compound 3-9



The compound was synthesized with an overall yield of 21% from **2-50** and 23 mg material was obtained. $R_f = 0.40$, $NH_3 \cdot H_2O$ (28% aq.)/ MeOH/ $CHCl_3 = 1/7/55$.

1H NMR (500 MHz, MeOD) δ 7.48 (d, $J = 8.5$ Hz, 1H), 6.22 (dd, $J = 8.5, 1.5$ Hz, 1H), 5.75 – 5.42 (m, 4H), 3.14 – 2.93 (m, 5H), 2.93 – 2.67 (m, 4H), 2.57 (d, $J = 37.5$ Hz, 1H), 2.49 – 2.18 (m, 5H), 2.18 – 1.99 (m, 1H), 1.99 – 1.74 (m, 2H). ^{13}C NMR (125 MHz, MeOD) δ 173.8, 171.5, 156.0, 153.9, 133.6, 130.7, 128.9, 113.7, 109.4, 108.2, 63.7, 57.3, 46.2, 42.5, 41.0, 40.0, 39.2. HRMS (ESI+, m/z) calculated for $C_{24}H_{29}N_2O_5$ [$M + H$]⁺ 425.2076, found 425.2066.

Compound 3-10

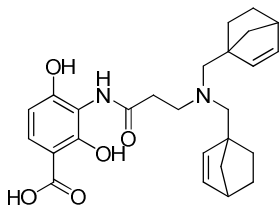


The compound was synthesized with an overall yield of 40% from **2-50** and 8 mg material was obtained. $R_f = 0.35$, $NH_3 \cdot H_2O$ (28% aq.)/ MeOH/ $CHCl_3 = 1/7/55$.

1H NMR (500 MHz, $CDCl_3$) δ 7.55 (d, $J = 8.5$ Hz, 1H), 6.33 (d, $J = 8.5$ Hz, 1H), 5.69 (s, 2H), 3.16 (s, br, 4H), 3.05 (s, br, 2H), 2.85 (s, br, 2H), 2.06 – 1.86 (m, br, 8H), 1.60 – 1.40 (m, br, 8H). ^{13}C NMR (125 MHz, $CDCl_3$) δ 174.4, 172.1, 156.0, 154.2, 131.8, 130.3,

129.1, 113.3, 110.0, 108.7, 61.1, 50.1, 31.6, 27.5, 25.8, 22.7, 22.2. HRMS (ESI+, m/z) calculated for C₂₄H₃₃N₂O₅ [*M* + H]⁺ 429.2389, found 429.2383.

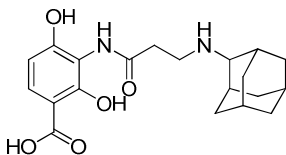
Compound **3-11**



The compound was synthesized with an overall yield of 58% from **S1** and 13 mg material was obtained. *R*_f = 0.40, NH₃•H₂O (28% aq.)/ MeOH/ CHCl₃ = 1/7/55.

¹H NMR (500 MHz, CDCl₃) δ 7.63 (d, *J* = 8.5 Hz, 1H), 6.39 (d, *J* = 8.5 Hz, 1H), 6.17 (s, 2H), 5.95 (s, 2H), 3.53 – 3.12 (m, 2H), 3.12 – 2.87 (m, 2H), 2.87-2.79 (m, 4H), 2.70 – 2.50 (m, 2H), 2.55-2.35 (m, 4H), 1.98 (s, br, 2H), 1.55 – 1.36 (m, 2H), 1.34 – 1.23 (m, 2H), 0.63 (dd, *J* = 23.0, 12.0 Hz, 2H). ¹³C NMR (125 MHz, CDCl₃) δ 174.4, 170.9, 155.7, 153.7, 139.0, 131.7, 129.1, 113.4, 109.9, 108.9, 58.4, 50.3, 50.0 (covered by the solvent peak), 45.9, 42.8, 34.9, 34.6, 32.6. HRMS (ESI+, m/z) calculated for C₂₆H₃₃N₂O₅ [*M* + H]⁺ 453.2389, found 453.2402.

2,4-Dihydroxy-3-(3-(adamantylamino)propanamido)benzoic acid (**3-12**)

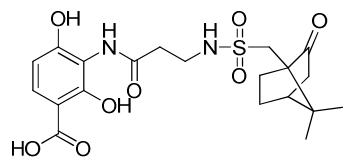


The compound was synthesized with an overall yield of 46% from **S1** and 27 mg material was obtained. *R*_f = 0.30, NH₃•H₂O (28% aq.)/ MeOH/ CHCl₃ = 1/7/55.

¹H NMR (500 MHz, MeOD) δ 7.69 (d, *J* = 8.5 Hz, 1H), 6.39 (d, *J* = 8.5 Hz, 1H), 3.48 – 3.42 (m, 3H), 3.10 – 3.00 (m, 2H), 2.26 (s, br, 2H), 2.08 – 1.98 (m, 4H), 1.96 – 1.86 (m, 4H), 1.84 (s, br, 2H), 1.77 (d, *J* = 8.0 Hz, 2H). ¹³C NMR (125 MHz, MeOD) δ 175.8 (br),

172.0, 159.0, 157.1, 130.4, 111.6, 106.7, 63.5, 42.5, 37.4, 37.0, 31.0, 30.1, 27.4. HRMS (ESI+, m/z) calculated for $C_{20}H_{27}N_2O_5$ [$M + H$]⁺ 375.1920, found 375.1900.

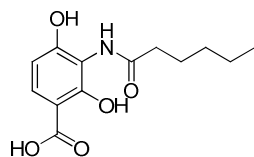
Compound 3–13



The compound was synthesized with an overall yield of 20% from **S1** and 12 mg material was obtained. $R_f = 0.40$, MeOH/ $CHCl_3 = 1/10$.

1H NMR (500 MHz, $CDCl_3$) δ 7.57 (d, $J = 9.0$ Hz, 1H), 6.43 (d, $J = 9.0$ Hz, 1H), 3.49 (qd, $J = 13.5, 7.0$ Hz, 2H), 3.42 (d, $J = 15.0$ Hz, 1H), 2.88 (d, $J = 15.0$ Hz, 1H), 2.79 (t, $J = 6.0$ Hz, 2H), 2.32 (ddd, $J = 18.5, 7.5, 7.5$ Hz, 1H), 2.25 (ddd, $J = 14.5, 12.0, 3.5$ Hz, 1H), 2.06 (t, $J = 4.5$ Hz, 1H), 2.03 – 1.92 (m, 1H), 1.87 (d, $J = 18.5$ Hz, 1H), 1.77 (ddd, $J = 14.0, 9.5, 4.5$ Hz, 1H), 1.38 (ddd, $J = 13.0, 9.5, 4.0$ Hz, 1H), 0.98 (s, 3H), 0.82 (s, 4H). ^{13}C NMR (126 MHz, $CDCl_3$) δ 216.8, 174.0, 171.9, 155.3, 155.1, 128.8, 113.7, 110.5, 104.9, 58.9, 49.6, 42.8 (2 carbons), 39.5, 36.8, 27.0, 25.8, 19.7, 19.5. HRMS (ESI+, m/z) calculated for $C_{20}H_{27}N_2O_8S$ [$M + H$]⁺ 455.1488, found 455.1502.

3-Hexanamido-2,4-dihydroxybenzoic acid (3–14)

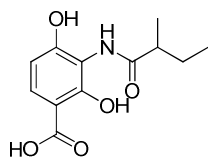


The compound was synthesized with an overall yield of 41% from **2–48** and 14 mg material was obtained.

1H NMR (500 MHz, Acetone) δ 7.65 (d, $J = 9.0$ Hz, 1H), 6.49 (d, $J = 9.0$ Hz, 1H), 2.64 (t, $J = 7.5$ Hz, 2H), 1.83 – 1.64 (m, 2H), 1.45 – 1.31 (m, 4H), 0.93 (t, $J = 7.0$ Hz, 3H). ^{13}C

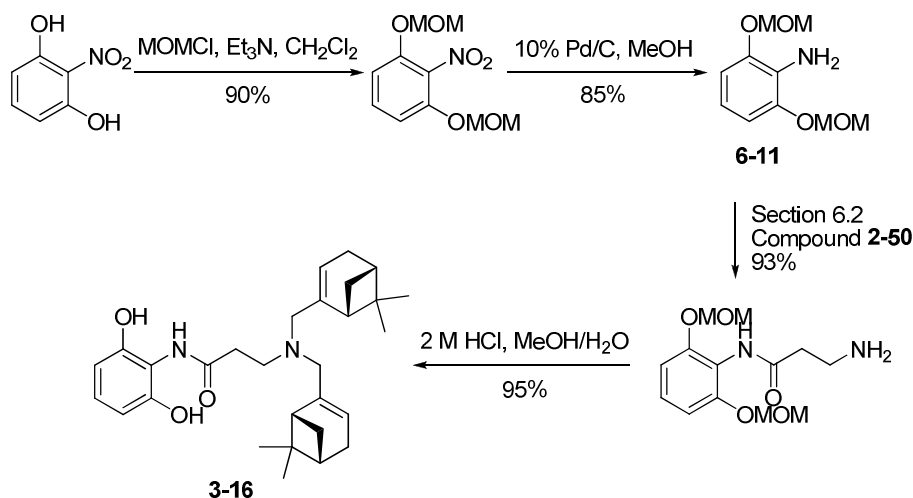
NMR (126 MHz, Acetone) δ 175.8, 172.7 (br), 156.8, 156.3, 129.0, 115.4, 111.3, 105.2, 30.3, 30.1, 26.3, 23.1, 14.2. HRMS (ESI+, m/z) calculated for $C_{13}H_{18}NO_5$ [$M + H$]⁺ 268.1185, found 268.1197.

2,4-Dihydroxy-3-(2-methylbutanamido)benzoic acid (**3-15**)



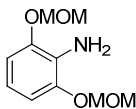
The compound was synthesized with an overall yield of 54% from **2-48** and 15 mg material was obtained.

¹H NMR (500 MHz, CDCl₃) δ 11.55 (s, br, 1H), 11.35 (s, br, 1H), 7.97 (s, 1H), 7.66 (d, J = 9.0 Hz, 1H), 6.58 (d, J = 9.0 Hz, 1H), 2.61 – 2.43 (m, 1H), 1.90 – 1.70 (m, 1H), 1.70 – 1.52 (m, 1H), 1.31 (d, J = 7.0 Hz, 3H), 1.02 (t, J = 7.5 Hz, 3H). ¹³C NMR (125 MHz, CDCl₃) δ 177.7, 174.2, 156.1, 154.5, 128.6, 114.6, 112.0, 103.1, 43.8, 27.7, 17.7, 11.9. HRMS (ESI+, m/z) calculated for $C_{12}H_{16}NO_5$ [$M + H$]⁺ 254.1028, found 254.1020.



Scheme 6-3. Synthesis of compound **3-16**.

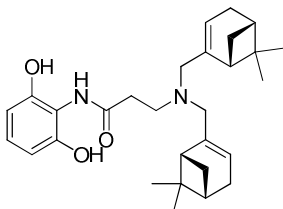
1,3-bis(methoxymethoxy)-2-nitrobenzene (**6–11**)



The reaction procedure refers to Section 6.2 (compound **2–46**). The compound was synthesized with an overall yield of 83% from 2-nitroresorcinol and 0.16 g material was obtained.

^1H NMR (400 MHz, CDCl_3) δ 6.79 (d, $J = 8.5$ Hz, 2H), 6.64 (AA'BB', $J = 8.5, 7.5$ Hz, 1H), 5.20 (s, 4H), 3.95 (s, br, 2H), 3.51 (s, 6H). ^{13}C NMR (100 MHz, CDCl_3) δ 145.2, 127.4, 116.9, 109.0, 95.2, 56.0. HRMS (ESI+, m/z) calculated for $\text{C}_{10}\text{H}_{16}\text{NO}_4$ [$M + \text{H}$] $^+$ 214.1079, found 214.1079.

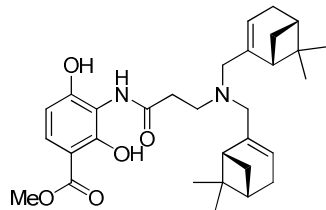
Compound **3–16**



The compound was synthesized with an overall yield of 17% from **6–11** and 26 mg material was obtained.

$[\alpha]_{\text{D}}^{22} = -13.5^\circ$ ($c = 0.5$ in MeOH : $\text{CHCl}_3 = 1 : 20$). ^1H NMR (500 MHz, CDCl_3) δ 10.32 (s, 1H), 6.96 (t, $J = 8.0$ Hz, 1H), 6.51 (d, $J = 8.0$ Hz, 2H), 5.44 (s, 2H), 3.21 (dd, $J = 13.5, 1.5$ Hz, 2H), 3.06 – 2.96 (m, 1H), 2.85 (d, $J = 13.5$ Hz, 2H), 2.76 – 2.64 (m, 1H), 2.64 – 2.50 (m, 2H), 2.42 – 2.10 (m, 8H), 2.03 (s, br, 2H), 1.16 (s, 6H), 1.05 (d, $J = 8.5$ Hz, 2H), 0.81 (d, $J = 4.0$ Hz, 6H). ^{13}C NMR (125 MHz, CDCl_3) δ 173.4, 149.7, 145.1, 126.8, 122.4, 115.5, 109.8, 60.2, 49.8, 44.8, 40.8, 38.0, 33.3, 31.8 (2 carbons), 26.4, 21.2. HRMS (ESI+, m/z) calculated for $\text{C}_{29}\text{H}_{41}\text{N}_2\text{O}_3$ [$M + \text{H}$] $^+$ 465.3117, found 465.3109.

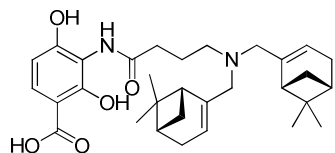
(-)-Myrtemycin methyl ester (**3-17**)



The compound was synthesized with an overall yield of 65% from **2-50** and 15 mg material was obtained. $R_f = 0.40$, MeOH/ CHCl₃ = 1:10.

$[\alpha]_D^{22} = -9.4^\circ$ ($c = 0.5$ in MeOH: CHCl₃ = 1 : 20). ¹H NMR (500 MHz, CDCl₃) δ 11.59 (s, 1H), 10.75 (s, 1H), 10.52 (s, 1H), 7.61 (d, $J = 9.0$ Hz, 1H), 6.53 (d, $J = 9.0$ Hz, 1H), 5.43 (s, 2H), 3.94 (s, 3H), 3.23 (d, $J = 12.5$ Hz, 2H), 3.10 – 2.92 (m, 1H), 2.80 (d, $J = 13.0$ Hz, 2H), 2.75 – 2.63 (m, 1H), 2.63 – 2.46 (m, 2H), 2.28 (dd, $J = 11.5, 5.0$ Hz, 4H), 2.20 (dd, $J = 18.0, 2.5$ Hz, 2H), 2.14 (dt, $J = 8.5, 5.5$ Hz, 2H), 2.09 – 1.94 (m, 2H), 1.14 (s, 6H), 1.04 (d, $J = 8.5$ Hz, 2H), 0.80 (s, 6H). ¹³C NMR (126 MHz, CDCl₃) δ 173.8, 171.1, 156.0, 155.1, 145.3, 127.7, 122.3, 115.1, 111.5, 104.2, 60.4, 52.3, 50.0, 44.6, 40.7, 37.9, 33.3, 31.7 (2 carbons), 26.2, 21.2. HRMS (ESI+, m/z) calculated for C₃₁H₄₃N₂O₅ [$M + H$]⁺ 523.3172, found 523.3172.

(-)-Homo-myrtemycin (**3-18**)

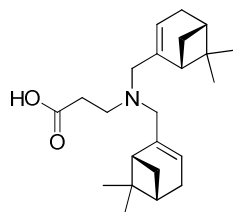


The compound was synthesized with an overall yield of 45% from **2-50** and 25 mg material was obtained. $R_f = 0.45$, NH₃•H₂O (28% aq.)/ MeOH/ CHCl₃ = 1/7/55.

$[\alpha]_D^{22} = -7.4^\circ$ ($c = 0.5$ in MeOH: CHCl₃ = 1 : 20). ¹H NMR (600 MHz, CDCl₃/MeOD = 20/1) δ 7.65 (d, $J = 8.5$ Hz, 1H), 6.33 (d, $J = 8.5$ Hz, 1H), 5.73 (s, 2H), 3.48 (d, br, $J = 11.5$ Hz, 2H), 3.41 – 3.21 (m, covered by the solvent residue peak, 2H), 3.05 (s, br, 1H),

2.88 (s, br, 1H), 2.74 – 2.55 (m, 2H), 2.45 (dt, $J = 9.0, 5.5$ Hz, 2H), 2.42 – 2.19 (m, 6H), 2.19 – 1.97 (m, 4H), 1.26 (s, 6H), 1.14 (d, $J = 9.0$ Hz, 2H), 0.83 (s, 6H). ^{13}C NMR (150 MHz, $\text{CDCl}_3/\text{MeOD} = 20/1$) δ 176.0 (br), 175.3, 159.0, 156.6, 142.3 (br), 130.6, 128.6 (br), 113.4, 112.5, 107.8, 71.5, 60.1, 54.4, 45.7, 41.8, 39.1, 34.9, 32.7 (2 carbons), 26.6, 21.6. HRMS (ESI+, m/z) calculated for $\text{C}_{31}\text{H}_{43}\text{N}_2\text{O}_5$ [$M + \text{H}$] $^+$ 523.3172, found 523.3164.

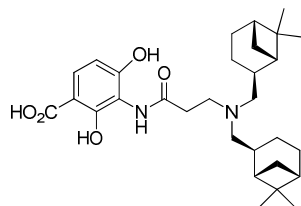
Compound 3–19



The compound was synthesized with an overall yield of 67% from β -alanine and (–)-myrtenal and 0.30 g material was obtained.

$[\alpha]_{\text{D}}^{27} = -8.3^\circ$ ($c = 3.0$ in $\text{MeOH}:\text{CHCl}_3 = 1 : 20$). ^1H NMR (400 MHz, CDCl_3) δ 5.52 (s, 2H), 3.24 (d, $J = 12.0$ Hz, 2H), 3.08 – 2.94 (m, 1H), 2.89 (d, $J = 13.0$ Hz, 2H), 2.67 – 2.45 (m, 3H), 2.42 (dt, $J = 9.0, 5.5$ Hz, 2H), 2.29 (d, br, $J = 18.0$ Hz, 2H), 2.21 (dd, br, $J = 18.0, 2.5$ Hz, 2H), 2.14 (t, br, $J = 5.0$ Hz, 2H), 2.16 – 1.98 (m, 2H), 1.25 (s, 6H), 1.06 (d, $J = 9.0$ Hz, 2H), 0.78 (s, 6H). ^{13}C NMR (100 MHz, CDCl_3) δ 174.0, 142.3, 125.1, 58.9, 48.9, 44.3, 40.3, 38.0, 31.7, 31.6, 29.4, 26.1, 21.1. HRMS (ESI+, m/z) calculated for $\text{C}_{23}\text{H}_{36}\text{NO}_2$ [$M + \text{H}$] $^+$ 358.2746, found 358.2743. IR (cm^{-1}): 2916 (s), 1718 (s), 1383 (s), 1195 (s), 1038 (m), 752 (m).

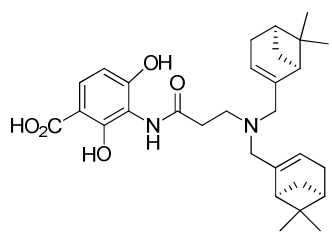
(–)-Myrtamycin (3–20)



(-)-Myrtanal was prepared by Corey-Kim oxidation [349] from (1*S*,2*S*,5*S*)-(-)-myrtanol (99 % ee). And the crude material was used for pathway 1 without further purification. The compound (**3–20**) was synthesized with an overall yield of 63% from **2–50** and 0.40 g material was obtained. $R_f = 0.35$, $\text{NH}_3 \cdot \text{H}_2\text{O}$ (28% aq.)/ MeOH/ $\text{CHCl}_3 = 1/7/55$.

$[\alpha]_D^{21} = -9.6^\circ$ ($c = 0.6$ in MeOH: $\text{CHCl}_3 = 1 : 20$). ^1H NMR (500 MHz, [D5] pyridine) δ 8.25 (d, $J = 8.5$ Hz, 1H), 6.80 (d, $J = 8.5$ Hz, 1H), 3.05 – 2.88 (m, 1H), 2.87 – 2.65 (m, 3H), 2.22 – 2.12 (m, 4H), 2.11 – 2.02 (m, 4H), 1.85 – 1.65 (m, 6H), 1.63 (d, $J = 6.5$ Hz, 2H), 1.62 – 1.50 (m, 2H), 1.36 – 1.26 (m, 4H), 1.22 (s, 6H), 0.83 (s, 6H). ^{13}C NMR (126 MHz, [D5] pyridine) δ 175.9, 174.4, 158.9, 155.5, 129.6, 123.8, 115.9, 109.2, 61.2, 53.4, 44.5, 42.2, 40.0, 34.0, 31.2, 27.6, 25.5, 24.3, 21.5, 20.9. HRMS (ESI+, m/z) calculated for $\text{C}_{30}\text{H}_{45}\text{N}_2\text{O}_5$ $[M + \text{H}]^+$ 513.3328, found 513.3326. IR(cm^{-1}): 2916 (m), 1556 (m), 1384 (s), 1266 (m), 736 (s).

(+)-Myrtemycin (**3–21**)

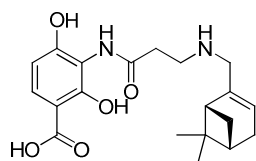


The compound was synthesized with an overall yield of 69% from **2–50** and 0.75 g material was obtained. (+)-Myrtenal was synthesized by literature method [350] from (+)-pinene (99 % ee). $R_f = 0.40$, $\text{NH}_3 \cdot \text{H}_2\text{O}$ (28% aq.)/ MeOH/ $\text{CHCl}_3 = 1/7/55$.

$[\alpha]_D^{20} = +10.8^\circ$ ($c = 1.0$ in MeOH). ^1H NMR (600 MHz, [D5] pyridine) δ 10.84 (s, 1H), 8.12 (d, $J = 8.5$ Hz, 1H), 6.88 (d, $J = 9.0$ Hz, 1H), 5.56 (s, 2H), 3.42 (d, $J = 12.4$ Hz, 2H), 3.35 – 3.25 (M, BR, 1H), 3.23 – 3.08 (m, 4H), 3.08 – 2.90 (m, br, 1H), 2.64 (s, 2H), 2.36

(dt, $J = 8.5, 5.5$ Hz, 2H), 2.20 (dd, $J = 50.0, 17.5$ Hz, 4H), 1.96 (s, 2H), 1.24 (s, 6H), 1.20 (d, $J = 8.5$ Hz, 2H), 0.85 (s, 6H). ^{13}C NMR (126 MHz, [D5] pyridine) δ 175.8, 174.5, 159.0, 158.8, 146.2, 130.4, 123.9, 116.3, 111.2, 108.1, 61.0, 51.4, 45.8, 42.1, 39.1, 34.6, 33.2, 32.9, 27.4, 22.3. HRMS (ESI+, m/z) calculated for $\text{C}_{30}\text{H}_{41}\text{N}_2\text{O}_5$ [$M + \text{H}$] $^+$ 509.3015, found 509.3015. IR(cm^{-1}): 2917 (s), 1654 (s), 1447 (m), 1366 (m), 1312 (s), 1181 (s), 1051 (s), 891 (m), 792 (s).

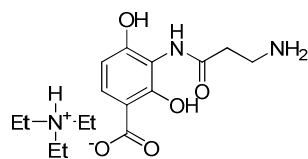
Compound 3–22



The compound was synthesized with an overall yield of 20% from **2–50** and 26 mg material was obtained. $R_f = 0.30$, $\text{NH}_3 \cdot \text{H}_2\text{O}$ (28% aq.)/ MeOH/ $\text{CHCl}_3 = 1/7/55$.

^1H NMR (600 MHz, MeOD) δ 7.65 (d, $J = 8.5$ Hz, 1H), 6.34 (d, $J = 8.5$ Hz, 1H), 5.78 (s, 1H), 3.56 (d, br, $J = 5.0$ Hz, 2H), 3.40 – 3.30 (m, covered by the solvent residue peak, 2H), 2.92 (t, $J = 6.0$ Hz, 2H), 2.50 (dt, $J = 9.0, 5.5$ Hz, 1H), 2.35 (q, br, $J = 18.0$ Hz, 2H), 2.27 – 2.18 (m, 1H), 2.12 (s, 1H), 1.32 (s, 3H), 1.22 (d, $J = 8.5$ Hz, 1H), 0.87 (s, 3H). ^{13}C NMR (151 MHz, MeOD) δ 176.0, 172.3, 159.6, 157.2, 140.8, 131.0, 127.0, 112.8, 112.7, 107.4, 58.4, 53.3, 45.4, 44.7, 41.8, 39.2, 32.3 (2 carbons), 26.5, 21.5. HRMS (ESI+, m/z) calculated for $\text{C}_{20}\text{H}_{27}\text{N}_2\text{O}_5$ [$M + \text{H}$] $^+$ 375.1920, found 375.1919.

3-(3-aminopropanamido)-2,4-dihydroxybenzoic acid (as TEAA salt, 3–23)



The compound was synthesized with an overall yield of 15% from **2-50** and 5 mg material was obtained. The product was purified on HPLC (RP-C18 column), 1 % → 15 % B in 0 → 20 min (A: 0.1 M TEAA in water, B: acetonitrile).

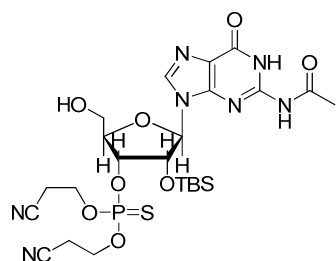
^1H NMR (500 MHz, MeOD) δ 7.69 (d, J = 9.0 Hz, 1H), 6.47 (d, J = 9.0 Hz, 1H), 3.28 (t, J = 6.5 Hz, 2H), 2.89 (t, J = 6.5 Hz, 2H). ^{13}C NMR (126 MHz, MeOD) δ 173.7, 172.2, 160.2, 131.3, 113.0, 109.0, 106.4, 40.6, 37.1. HRMS (ESI+, m/z) calculated for $\text{C}_{10}\text{H}_{13}\text{N}_2\text{O}_5$ [$M + \text{H}$] $^+$ 241.0824, found 241.0801.

6.4 Synthetic protocols for compounds in Chapter 4

6.4.1 Synthesis of compound 4-1 and 4-2

For the synthesis of natural c-di-GMP, see ref [330]. The synthesis of endo-S-c-di-GMP is outlined in **Scheme 4-1** in Section 4.1.1, and the detailed procedure was described below.

2'-OTBS, *N*-acetyl guanosine-3'-dicyanoethylphosphorothioate (**4-4**)



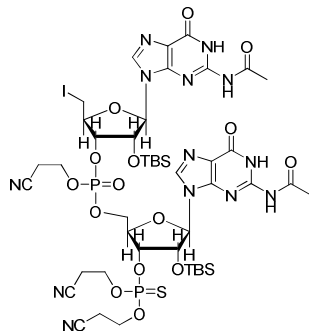
Standard guanosine phosphoramidite **4-3** (1.03 g, 1.09 mmol) and cyanoethyl alcohol (0.40 mL 5.5 mmol) were dissolved in anhydrous acetonitrile (15 mL) at RT under argon and stirred for 15 min. After the addition of imidazolium perchlorate [351] (0.70 g, 4.0 mmol), the reaction mixture was stirred for 6 h at RT. Because reagent (3*H*-1,2-benzodithiole-3-one 1,1-dioxide, 0.55 g, 2.8 mmol) was then added, and the reaction

mixture was stirred for an extra 1 h before an aqueous solution of $\text{Na}_2\text{S}_2\text{O}_3$ (1 M, 30 mL) was poured into the reaction vessel to quench the reaction and CH_2Cl_2 (30 mL) was added. The two layers were immediately separated and the organic layer was collected. The aqueous layer was then extracted with CH_2Cl_2 (50 mL x 2) and the combined organic layer was concentrated with a rotary evaporator to dryness.

The crude material was re-dissolved in CH_2Cl_2 (20 mL), and dichloroacetic acid (1.00 mL, 12.2 mmol) was added dropwise over 5 min to form a red/orange solution. After stirring for 10 min at RT, an aqueous solution of NaHCO_3 (saturated solution, 30 mL) was poured into the reaction mixture to quench the reaction. The two layers were separated and the organic layer was collected. The aqueous layer was then extracted with CH_2Cl_2 (50 mL x 2) and the combined organic layer was concentrated at a reduced pressure. The crude product was immediately purified with a silica-gel (40 g, 400-mesh) column with gradient elution (2–10 % MeOH in CH_2Cl_2 , $R_f = 0.45$, 10 % MeOH in CH_2Cl_2). Product (60 % from phosphoramidite **4–3**) was collected as a pale yellow glacial solid.

^1H NMR (500 MHz, CDCl_3) δ 12.33 (s, 1H), 9.96 (s, br, 1H), 7.89 (s, 1H), 5.76 (d, $J = 7.0$ Hz, 1H), 5.12 (dd, $J = 10.5, 4.5$ Hz, 1H), 5.04 (d, $J = 5.0$ Hz, 1H), 4.87 (d, $J = 5.0$ Hz, 1H), 4.40 – 4.22 (m, 4H), 3.99 (d, $J = 12.5$ Hz, 1H), 3.90 – 3.71 (m, 1H), 2.95 – 2.71 (m, 4H), 2.31 (s, 3H), 0.73 (s, 9H), –0.09 (s, 3H), –0.28 (s, 3H). ^{31}P NMR (202 MHz, CDCl_3) δ 67.7. ^{13}C NMR (126 MHz, CDCl_3) δ 173.0, 155.6, 147.9, 139.5, 122.4, 116.8, 89.3, 84.6, 78.9, 73.5, 63.0, 61.9, 53.6, 31.0, 25.6, 24.5, 19.7, 18.0, –4.7, –5.2. ESI $^+$ /MS for $[\text{C}_{24}\text{H}_{37}\text{N}_7\text{O}_8\text{PSSi}]^+$: calculated 642.1931, found 642.1902.

Compound 4-5



A solution containing guanosine phosphothioate **4-4** (0.27 g, 0.42 mmol) and phosphoramidite **4-3** (0.59 g, 0.63 mmol) in anhydrous acetonitrile (15 mL) was stirred at RT under argon for 15 min. After the addition of imidazolium perchlorate (0.35 g, 2.0 mmol), the reaction mixture was stirred for 6 h at RT. *t*-BuOOH (70 % aqueous solution, 0.50 mL, 3.9 mmol) was then added, and the reaction mixture was stirred for an extra 10 min before an aqueous solution of Na₂S₂O₃ (1 M, 30 mL) was poured into the reaction vessel to quench the reaction and CH₂Cl₂ (30 mL) was added. The two layers were immediately separated and the organic layer was collected. The aqueous layer was then extracted with CH₂Cl₂ (50 mL x 2) and the combined organic layer was concentrated with a rotary evaporator to dryness.

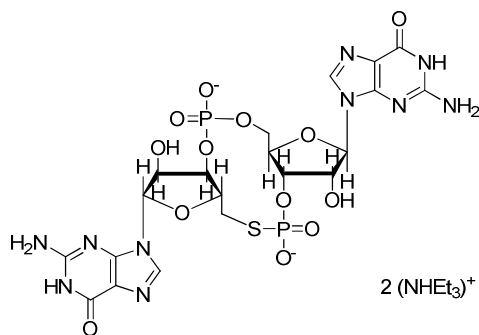
The crude material was re-dissolved in CH₂Cl₂ (20 mL), and dichloroacetic acid (0.50 mL, 6.1 mmol) was added dropwise over 5 min to form a red/orange solution. After stirring for 10 min at RT, an aqueous solution of NaHCO₃ (saturated solution, 30 mL) was poured into the reaction mixture to quench the reaction. The two layers were separated and the organic layer was collected. The aqueous layer was then extracted with CH₂Cl₂ (50 mL x 3) and the combined organic layer was concentrated at a reduced pressure. The crude product was passed through a short silica-gel column (10 g) with

elution of 2:1 acetone: hexane (100 mL) to remove the byproduct. The desired product could be eluted with 1:10 MeOH: CH₂Cl₂ (R_f = 0.25) and then dried thoroughly under high vacuum.

A mixture of the crude material, methyltriphenoxyposphonium iodide (0.95 g, 2.10 mmol) and 2,6-lutidine (1.00 mL, 8.61 mmol) was dissolved in anhydrous DMF (10 mL) under argon. The reaction was stirred for 1 h at RT before an aqueous solution of Na₂S₂O₃ (1 M, 30 mL) and CH₂Cl₂ (30 mL) was poured into the reaction mixture. The two layers were separated and the organic layer was collected. The aqueous layer was then extracted with CH₂Cl₂ (50 mL x 3) and the combined organic layer was concentrated at a reduced pressure. The crude product was immediately purified with a silica-gel (40 g) column with gradient elution (1–8 % MeOH in CH₂Cl₂, R_f = 0.30, 5 % MeOH in CH₂Cl₂). 0.42 g product (61 % from intermediate **4-4**) was collected as a pale yellow glacial solid.

¹H NMR (500 MHz, CDCl₃) δ 12.28 (s, 1H), 12.15 (s, 1H), 10.75 (d, J = 7.0 Hz, 2H), 7.84 (s, 1H), 7.72 (s, 1H), 5.76 (dd, J = 22.0, 7.0 Hz, 2H), 5.41 – 5.15 (m, 2H), 5.15 – 4.89 (m, 2H), 4.74 – 4.49 (m, 2H), 4.49 – 4.12 (m, 8H), 3.62 (dd, J = 10.5, 8.0 Hz, 1H), 3.46 (dd, J = 10.5, 5.0 Hz, 1H), 2.84 – 2.69 (m, 6H), 2.24 (d, J = 2.5 Hz, 6H), 0.74 (s, 9H), 0.73 (s, 9H), –0.05 (s, 3H), –0.06 (s, 3H), –0.23 (s, 3H), –0.29 (s, 3H). ³¹P NMR (202 MHz, CDCl₃) δ 67.9, –2.9. ¹³C NMR (126 MHz, CDCl₃) δ 173.1, 155.9, 155.7, 148.5, 148.1, 139.7, 138.8, 122.8, 122.3, 116.9, 116.7, 89.3, 88.8, 82.5, 81.4, 79.7, 72.8, 71.9, 67.8, 63.3, 63.0, 29.7, 25.6, 24.3, 19.8, 18.0, 5.5, –4.57, –4.79, –5.15, –5.18. ESI⁺/MS for [C₄₅H₆₇IN₁₃O₁₅P₂SSi₂]⁺: calculated 1306.2659, found 1306.2570.

Endo-S-c-di-GMP (**4–2**, as a triethylammonium salt)



5'-Iodo guanosine phosphothioate **4–5** (50 mg, 0.038 mmol) was stirred with ammonia (30 % NH_4OH in water, 5 mL) at RT for 24 h. The solvent was removed with a rotary evaporator and the crude material was thoroughly dried under high vacuum. Anhydrous pyridine (1.0 mL) and $\text{NEt}_3 \cdot 3\text{HF}$ (0.25 g, 1.6 mmol; *caution! the chemical is highly toxic*) were added carefully into the plastic reaction vessel, and the mixture was stirred vigorously at 50 °C for 6 h. Upon the immediate addition of acetone (20 mL), a white precipitate formed. The solid was filtered by a powder funnel with a piece of cotton, and was washed with acetone (5 mL x 4). The collected crude product was then re-dissolved in water (10 mL), purified by HPLC (Nacalai tesque 5C18-MS II column), concentrated at a reduced pressure, and washed with acetone (2 mL x 5) to remove the excess of TEAA (triethylammonium acetate) buffer. 16 mg product was collected as a white solid (59 % from **4–5**).

^1H NMR (500 MHz, D_2O , with water suppression) δ 8.25 (s, 1H), 8.10 (s, 1H), 6.12 (s, 1H), 6.05 (d, $J = 4.5$ Hz, 1H), 5.22 – 5.02 (m, 3H), 4.87 (d, $J = 5.0$ Hz, 1H), 4.59 – 4.53 (m, 2H), 4.50 (d, $J = 12.5$ Hz, 1H), 4.24 (d, $J = 12.5$ Hz, 1H), 3.42 (ddd, $J = 13.0, 12.5, 7.5$ Hz, 1H), 3.30 (q, $J = 7.5$ Hz, 12H), 3.22 (ddd, $J = 14.0, 12.0, 3.0$ Hz, 1H), 1.38 (t, $J = 7.5$ Hz, 18H). ^{31}P NMR (202 MHz, D_2O) δ 19.9, –0.4. ^{13}C NMR (151 MHz, D_2O) δ 158.9

(2 carbons), 153.9, 153.8, 151.6, 150.9, 138.1, 137.1, 116.5 (2 carbons), 89.2, 88.0, 81.1, 79.6, 74.3, 73.5, 72.0, 70.8, 62.4, 46.7, 31.4, 8.2. ESI[−]/MS for [C₂₀H₂₃N₁₀O₁₃P₂S][−]: calculated 705.0647, found 705.0620.

6.4.2 Cleavage of c-di-GMP and endo-S-c-di-GMP by RocR

The RocR enzymatic reaction was scaled up to 500 μM endo-S-c-di-GMP in a total volume of 0.50 mL, and other conditions remained the same as indicated in Section 6.6.2. At three time points: 30 min, 2 h and 18 h, aliquots of the reaction were taken and the reaction was stopped by adding a final concentration of 5 mM EDTA and cooling on ice. RocR was then removed by running through a size exclusion column. The samples were subsequently stored at −20 °C until HPLC analysis (**Figure 6–3**).

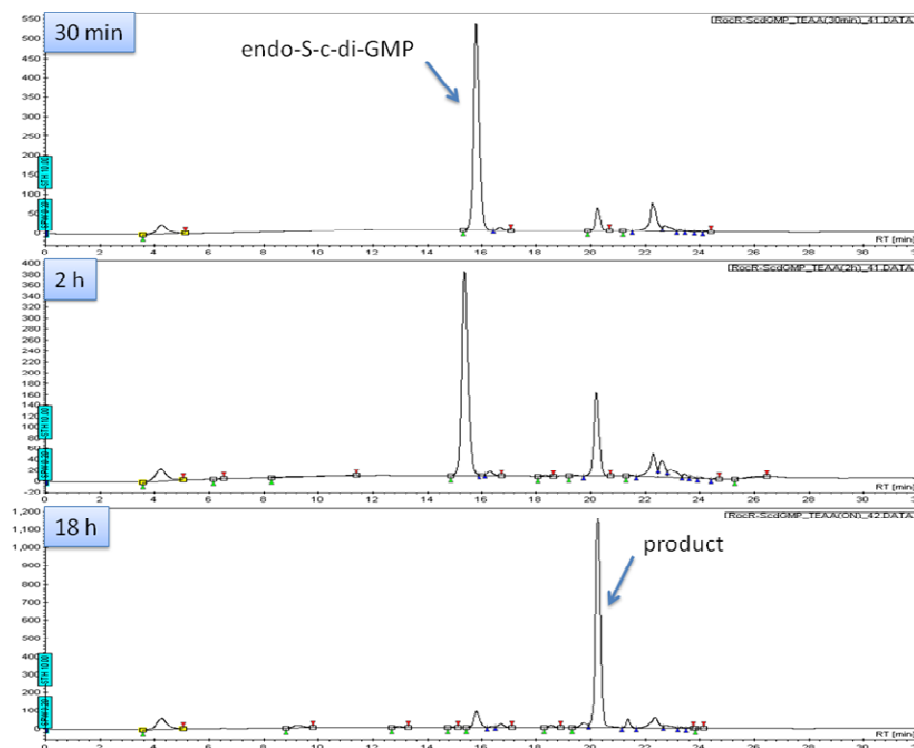


Figure 6–3. HPLC analysis of cleavage of endo-S-c-di-GMP by RocR. Condition: 1 → 11 % B, 0 → 16 min (A: 100 mM TEAA buffer in water; B: acetonitrile), RT.

The HPLC chromatography (**Figure 6–3**) clearly showed that endo-S-c-di-GMP (at 15.5 min) was converted to a product (at 20.3 min) almost quantitatively after 18 h. Mass spectrometry and NMR analysis both indicated that 5'-pG^SpG was the product (terminal phosphothioates usually give a ³¹PNMR signal at 16–17 ppm [352,353], whereas the endo-sulfur phosphothioates have signals around 20 ppm [354]. Additionally terminal phosphates (dianionic) have ³¹PNMR peaks around 1 ppm (see NMR data for pGpG (**4–7**)), whereas phosphodiester (monoanionic) have ³¹PNMR signals around –1 pm [333]. The ³¹PNMR of the product of the RocR cleavage reaction has peaks at –0.5 and 20.3 ppm (characteristic of a phosphodiester and a terminal phosphothioate respectively); therefore we conclude that cleavage of endo-S-c-di-GMP exclusively occurred at the natural phosphate site.

5'-pG^SpG (**4–6**)

¹H NMR (600 MHz, D₂O) δ 7.82 (s, 1H), 7.78 (s, 1H), 6.00 (d, *J* = 3.0 Hz, 1H), 5.63 (d, *J* = 5.0 Hz, 1H), 5.33 (td, *J* = 7.5, 3.5 Hz, 1H), 5.13 (ddd, *J* = 11.0, 7.0, 5.0 Hz, 1H), 4.62 – 4.51 (m, 2H), 4.47 – 4.37 (m, 1H), 4.20 (ddd, *J* = 11.5, 4.5, 2.5 Hz, 1H), 4.12 (dt, *J* = 11.0, 5.5 Hz, 1H), 4.06 (dt, *J* = 6.0, 4.5 Hz, 1H), 3.08 (q, *J* = 7.5 Hz, 9H), 2.60 (ddd, *J* = 20.5, 14.5, 5.5 Hz, 2H), 1.15 (t, *J* = 7.5 Hz, 15H). ³¹P NMR (162 MHz, D₂O) δ 20.3, –0.5. ESI[–]/MS for [C₂₀H₂₃N₁₀O₁₃P₂S][–]: calculated 705.0647 [M–H₃O][–], found 705.0622.

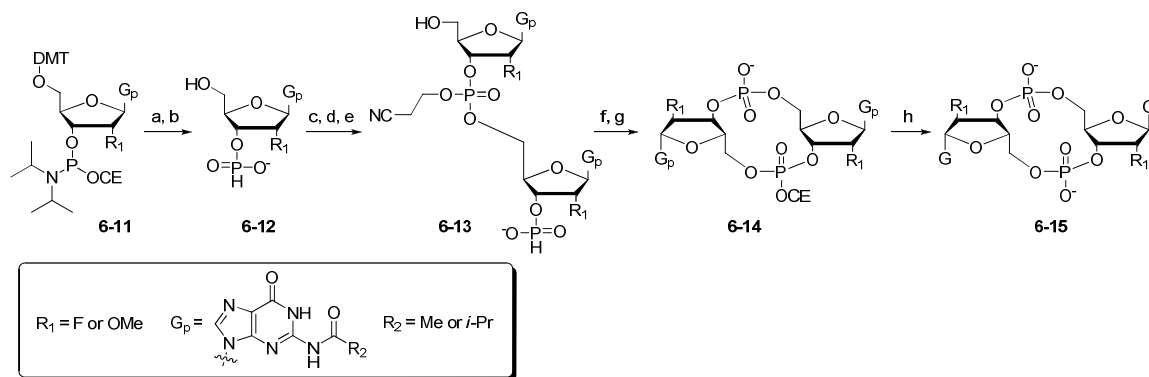
pGpG bis(triethylammonium) salt (**4–7**)

¹H NMR (600 MHz, D₂O) δ 7.93 (s, 1H), 7.86 (s, 1H), 5.74 (d, *J* = 5.5 Hz, 1H), 5.69 (d, *J* = 5.5 Hz, 1H), 4.48 – 4.33 (m, 1H), 4.30 (s, 1H), 4.21 (s, 1H), 4.13 (dt, *J* = 11.5, 3.0 Hz, 1H), 4.05 (dt, *J* = 11.5, 4.0 Hz, 1H), 3.99 – 3.77 (m, 2H), 3.07 (q, *J* = 7.5 Hz, 12H), 1.15

(t, $J = 7.5$ Hz, 18H). ^{31}P NMR (243 MHz, D_2O) δ 1.1, -0.6. ESI $^-$ /MS for $[\text{C}_{20}\text{H}_{25}\text{N}_{10}\text{O}_{15}\text{P}_2]^-$: calculated 707.0982, found 707.0989.

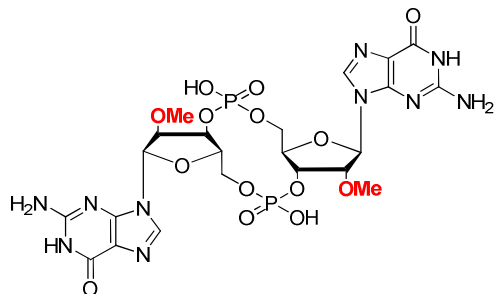
6.4.3 Syntheses of compounds **4-52** and **4-53**

Jones' strategy for the synthesis of c-di-GMP [330] was adopted for the synthesis of c-di-GMP analogs containing natural phosphate linkages, **4-52** and **4-53**. Crude materials were used for the steps up until intermediate **6-14** before the first purification was done (**Scheme 6-4**). 2.0 g of starting phosphoramidite **6-11** was used. After mono-cyanoethyl protected **6-14** was obtained, the solvent was removed from the reaction mixture by high-vacuum to yield a sticky yellow solid. This crude material was transferred to a centrifuge tube and was sequentially washed with EtOAc (50 mL x 2), MeOH (50 mL x 3) and centrifuged each time. The EtOAc layer was extracted with H_2O (25 mL x 2), and the aqueous layer combined with the MeOH layer and was concentrated and subjected to HPLC purification. HPLC condition: 10 \rightarrow 25% B, 0 \rightarrow 20 min (A: 0.1 M TEAA in water; B: acetonitrile). The product was identified by ESI-MS (negative mode) before the global deprotection step. Procedures for global deprotection, using ammonium hydroxide, and HPLC purification of the final compound were similar to those used for preparing compound **4-2**.



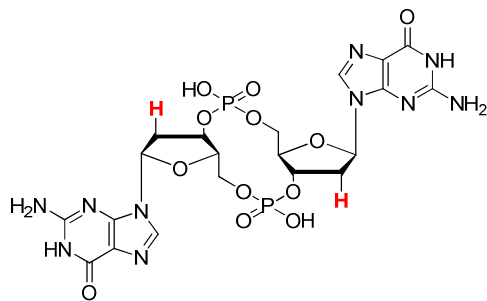
Scheme 6-4. Synthesis of compounds **4-52** ($R_1 = \text{Me}$) and **4-53** ($R_1 = \text{F}$). Modified conditions from ref [330] were used: a) pyridinium trifluoroacetate, H_2O , then $t\text{-BuNH}_2$; b) dichloroacetic acid, then quenched with pyridine; c) compound **6-11**; d) $t\text{-BuOOH}$; e) dichloroacetic acid, then quenched with pyridine; f) 5,5-dimethyl-2-oxo-2-chloro-1,3,2-dioxaphosphinane (DMOCP); g) I_2 , H_2O , then HPLC purification; h) ammonia, then HPLC purification.

2',2'-di-OMe c-di-GMP bis(triethylammonium) salt (**4-52**)



^1H NMR (500 MHz, D_2O) δ 7.93 (s, 2H), 5.88 (d, $J = 6.0$ Hz, 2H), 4.81 (td, $J = 8.5$, 4.5 Hz, 2H), 4.44 (t, $J = 5.5$ Hz, 2H), 4.33 (d, $J = 3.0$ Hz, 2H), 3.81 (dd, $J = 13.0$, 2.5 Hz, 2H), 3.76 (dd, $J = 13.0$, 3.5 Hz, 2H), 3.39 (s, 6H), 3.10 (q, $J = 7.5$ Hz, 12H), 1.18 (t, $J = 7.5$ Hz, 18H). ^{31}P NMR (202 MHz, D_2O) δ 0.1. ^{13}C NMR (126 MHz, D_2O) δ 158.7, 153.7, 151.3, 138.0, 116.6, 86.0, 85.0, 81.2, 72.1, 61.1, 58.1, 46.6, 8.1. ESI $^-$ /MS for $[\text{C}_{22}\text{H}_{27}\text{N}_{10}\text{O}_{14}\text{P}_2]^-$: calculated 717.1189, found 717.1150.

C-di-dGMP bis(triethylammonium) salt (**4-53**)



^1H NMR (400 MHz, D_2O) δ 7.96 (s, 2H), 6.21 (s, 2H), 5.07 – 4.86 (m, 1H), 4.15 (s, 2H), 4.00 (dd, J = 40.0, 10.5 Hz, 3H), 3.06 (q, J = 7.5 Hz, 12H), 2.99 – 2.77 (m, 2H), 2.63 (dt, J = 14.0, 7.0 Hz, 2H), 1.14 (t, J = 7.5 Hz, 18H). ^{31}P NMR (161 MHz, D_2O) δ –0.5. ESI $^-$ /MS for $[\text{C}_{20}\text{H}_{23}\text{N}_{10}\text{O}_{12}\text{P}_2]^-$: calculated 657.0978, found 657.0998.

6.4.4 Solid support synthesis (compounds **4-54** to **4-57**)

Sulfonylethyl-ODMT CPG (10 $\mu\text{mol/g}$) was prepared following literature [344] (see **Scheme 6-1**, credit: Andrew Shurer). The solid support was loaded (0.1 g) into the synthesis column (**Figure 6-2b**) and sealed tightly. A DNA/RNA synthesizer was used for making the dinucleotide and was set up as described in Section 6.1.4 (**Figure 6-2**). Two cycles of standard 1.0 μmol RNA program (DMT-off) were performed with an interruption before the oxidation step during the first cycle and the oxidation step was done manually, using a solution of Beaucage reagent (1 mg/mL in anhydrous acetonitrile, 1 mL) for 30 min using the apparatus shown in **Figure 6-4**. A white precipitate might be observed in the syringes in the sulfurization step, and after the reaction was finished, the synthesis column was put back on to the DNA/RNA synthesizer for the rest of the synthesis cycles.

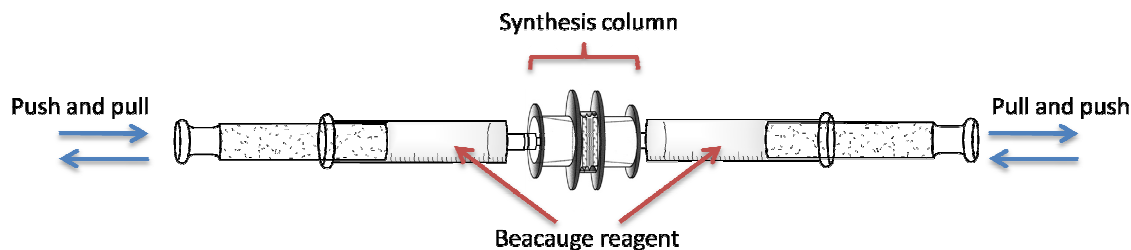
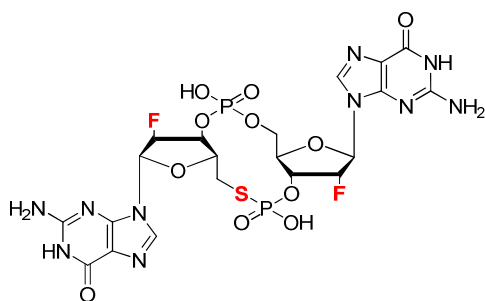


Figure 6–4. Sulfurization of the phosphonate on CPG beads. An empty syringe and another one with 1 mL Beacauge reagent (1 mg/mL in anhydrous acetonitrile) were attached on each side of the synthesis column. The liquid was passed through the column by pushing and pulling the two syringes simultaneously. This liquid transfer was repeated three times during the 30 min.

When the two synthesis cycles were completed, the synthesis column was washed with anhydrous acetonitrile for another 60 s on the DNA/RNA synthesizer before the CPG beads in the synthesis column were dried by blowing through with argon. The DNA/RNA synthesizer can handle four synthesis columns simultaneously and a total of 24 columns were synthesized for each analog. The argon-dried CPG beads were collected in a round-bottom flask (theoretically contained 24 μmol nucleotides). The CPG beads were then further dried under the high vacuum for 5 h while gently stirring. Anhydrous DMF (10 mL) was transferred to the flask containing the dried CPG beads with a cannula, followed by a rapid transfer of methyltriphenoxyposphonium iodide (0.95 g, 2.10 mmol) and 2,6-lutidine (1.00 mL, 8.61 mmol) under the protection of argon. The reaction was stirred for 1 h at RT before an aqueous solution of $\text{Na}_2\text{S}_2\text{O}_3$ (1 M, 30 mL) was poured into the reaction mixture. The CPG beads were washed with H_2O (10 mL x 3) and methanol (10 mL x 3) in a Buchner funnel before transferred into a round-bottom flask and stirred with ammonia (30 % NH_4OH in water, 15 mL) at 40 °C for overnight. The reaction mixture was then filtered and rinsed with H_2O (10 mL x 3). The combined

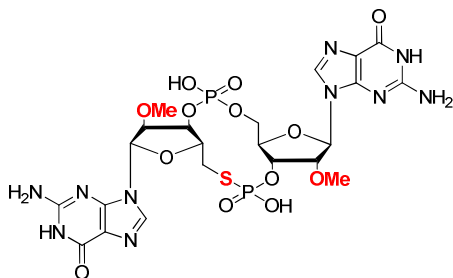
filtrate was concentrated and for analogs **4-54**, **4-55** and **4-57** the crude products were directly subjected to HPLC purification. For the procedure of OTBS group deprotection of analog **4-56** and HPLC conditions refer to the preparation of compound **4-2**. The fractions collected from HPLC were concentrated at a reduced pressure, and washed with acetone (2 mL x 5) to remove the excess of TEAA (triethylammonium acetate) buffer. 3–14 mg product of compounds **4-54** to **4-57** was collected as a white solid (estimated yields of 18–83 % were obtained, based on the estimated loading of the CPG beads).

2',2'-difluoro-endo-S-c-di-GMP bis(triethylammonium) salt (**4-54**)



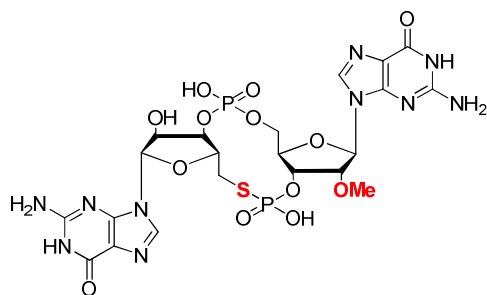
^1H NMR (500 MHz, D_2O , water suppression, 50 $^\circ\text{C}$) δ 8.28 (s, 1H), 8.15 (s, 1H), 6.51 (d, $J = 19.0$ Hz, 1H), 6.42 (d, $J = 19.0$ Hz, 1H), 5.98 (dd, $J = 52.0, 3.5$ Hz, 1H), 5.80 (dd, $J = 52.0, 3.5$ Hz, 1H), 5.50 (tdd, $J = 13.0, 8.5, 5.0$ Hz, 1H), 5.35 (dt, $J = 22.5, 9.0$ Hz, 1H), 4.63 (d, $J = 12.5$ Hz, 1H), 4.33 (d, $J = 11.0$ Hz, 1H), 3.69 (dt, $J = 13.5, 5.0$ Hz, 1H), 3.30 (t, $J = 11.0$ Hz, 1H). ^{31}P NMR (202 MHz, D_2O , 50 $^\circ\text{C}$) δ 19.3, -0.5 . ESI $^-$ /MS for $[\text{C}_{20}\text{H}_{21}\text{F}_2\text{N}_{10}\text{O}_{11}\text{P}_2\text{S}]^-$: calculated 709.0561, found 709.0596.

2',2'-di-OMe-endo-S-c-di-GMP bis(triethylammonium) salt (**4-55**)



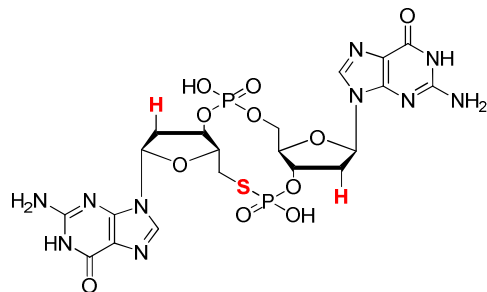
^1H NMR (500 MHz, D_2O , 50 °C) δ 8.31 (s, 1H), 8.18 (s, 1H), 6.30 (s, 1H), 6.19 (d, J = 4.5 Hz, 1H), 5.35 (dt, J = 10.0, 5.0 Hz, 1H), 5.21 (td, J = 9.0, 5.0 Hz, 1H), 4.91 (t, J = 4.5 Hz, 1H), 4.66 – 4.52 (m, 4H), 4.39 – 4.23 (m, 1H), 3.87 (s, 3H), 3.76 (s, 3H), 3.52 (ddd, J = 14.0, 11.5, 7.5 Hz, 1H), 3.38 (q, J = 7.5 Hz, 12H), 3.32 (ddd, J = 14.0, 11.5, 3.0 Hz, 1H), 1.47 (t, J = 7.5 Hz, 18H). ^{31}P NMR (202 MHz, D_2O , 50 °C) δ 18.9, –0.7. ^{13}C NMR (126 MHz, D_2O , 50 °C) δ 159.9 (2 carbons), 154.9, 154.8, 152.6, 152.0, 139.1, 138.2, 117.6 (2 carbons), 88.1, 87.7, 83.7, 82.3, 81.8, 80.8, 74.1, 71.3, 71.2, 63.3, 59.9, 47.9, 32.4, 9.30. ESI $^-$ /MS for $[\text{C}_{22}\text{H}_{27}\text{N}_{10}\text{O}_{13}\text{P}_2\text{S}]^-$: calculated 733.0960, found 733.0981.

2',2'-OMe-OH-endo-S-c-di-GMP (**4-56**)



^1H NMR (500 MHz, D_2O , water suppression, 50 °C) δ 8.32 (s, 1H), 8.18 (s, 1H), 6.29 (s, 1H), 6.12 (d, J = 4.5 Hz, 1H), 5.35 – 5.06 (m, 3H), 4.74 – 4.48 (m, 3H), 4.31 (d, J = 13.0 Hz, 1H), 3.84 (d, J = 3.0 Hz, 3H), 3.50 (ddd, J = 13.5, 11.5, 7.5 Hz, 1H), 3.35 – 3.17 (m, 1H). ^{31}P NMR (202 MHz, D_2O , 50 °C) δ 19.1, –0.2. ESI $^-$ /MS for $[\text{C}_{21}\text{H}_{25}\text{N}_{10}\text{O}_{13}\text{P}_2\text{S}]^-$: calculated 719.0804, found 719.0793.

Endo-S-c-di-dGMP triethylammonium salt (**4-57**)



^1H NMR (500 MHz, D_2O , water suppression, 50 °C) δ 8.26 (s, 1H), 8.23 (s, 1H), 6.65 – 6.43 (m, 2H), 5.41 (s, 2H), 4.69 – 4.48 (m, 2H), 4.46 – 4.27 (m, 2H), 3.42 (q, J = 7.5 Hz, 6H), 3.33 (dd, J = 13.5, 5.5 Hz, 2H), 3.23 (ddd, J = 20.5, 13.5, 6.0 Hz, 2H), 3.02 (dt, J = 13.5, 6.0 Hz, 1H), 2.92 (ddd, J = 11.0, 5.5, 5.0 Hz, 1H), 1.51 (t, J = 7.5 Hz, 9H). ^{31}P NMR (202 MHz, D_2O , 50 °C) δ 19.7, –0.3. ESI $^+$ /MS for $[\text{C}_{20}\text{H}_{23}\text{N}_{10}\text{O}_{11}\text{P}_2\text{S}]^-$: calculated 673.0749, found 673.0702.

6.5 Computational details

All of the calculations were performed with the Gaussian 03/09 program [298].

6.5.1 Ring-opening reaction

For ring-opening reaction in Chapter 2 (**Scheme 2–8**), density functional B3LYP [355,356] was used to locate all the transition structures and intermediates. Frequency calculations at the same level have been performed to confirm each stationary point to be either a minimum or a transition structure. 6-31G basis set is applied for all elements. The reported energies (**Table 6–1**) are zero-point energy-corrected electronic energies (ΔE_0 K), enthalpies ($\Delta H_{298\text{ K}}$) and free energies ($\Delta G_{298\text{ K}}$).

Table 6–1. The computed energies and other thermal parameters for the ring-opening reaction (in Hartree).^[a]

Structures	E_{ele}	$E_0\text{ K}$	$H_{298\text{ K}}$	$G_{298\text{ K}}$
2–32	–547.920343986	–547.681748	–547.668910	–547.718623
TS-a	–547.879565801	–547.643849	–547.631576	–547.679279
2–36	–547.960483826	–547.720075	–547.707858	–547.755868
TS-b	–547.864745024	–547.629002	–547.616869	–547.664266
2–37	–547.938092690	–547.697860	–547.685563	–547.733836

[a] For the Cartesian coordinates of the computed structures, see the Supporting Information of ref [273].

6.5.2 Calculation of the radii (volumes) of c-di-GMP polymorphism

Hartree-Fock method and Onsager's model (Gaussian keyword: SCRF = dipole) in the self-consistent reaction field (SCRF) were used to calculate the radius of the solute cavity (Gaussian keyword: volume; parameters: H₂O dielectric constant $\epsilon = 78.4$, $a_0 = 1000$ Å). The 3-21G basis set was used for atom C, N, O, and H, and 6-31G(d) basis set was used for atom P, S and K.

According to Stokes-Einstein equation, $D = k T / (6 \pi \eta R)$, where k is the Boltzmann constant, T is the temperature, η is the solvent viscosity and R is the radius of the molecular sphere. The diffusion constants in solution phase are inversely proportional to the radii of the particles. The diffusion constant of monomeric c-di-GMP and endo-S-c-di-GMP were measured with previous reported method [227,316]. The diffusion constants for other c-di-GMP aggregation states can be predicted from the calculated radii. Due to the low symmetry of endo-S-c-di-GMP aggregates, the radii calculation requires higher computing resource. However, we assume that the ratios of different aggregates of endo-S-c-di-GMP are similar to that of c-di-GMP. Thus we applied the ratio of calculated radii for c-di-GMP aggregates, and the measured monomeric endo-S-c-di-GMP diffusion constant to predict other diffusion constants for endo-S-c-di-GMP aggregates. The results of the calculation were summarized in the **Table 6-2** (See Supporting Information of ref [357] for the Cartesian coordinates of the c-di-GMP aggregate structures).

Table 6–2. Calculation of the radii and diffusion coefficients of c-di-GMP polymorphism

Aggregates	Calculate radii (Å)	Symmetry of the structures	Calculated diffusion constant (10^{-10} m/s ²)
c-di-GMP			
Monomeric c-di-GMP (closed)	6.41	C2	3.01 ^a
Monomeric c-di-GMP (open)	6.34	C2	--
Dimeric c-di-GMP	7.91	-- ^b	2.45
Tetrameric c-di-GMP	9.61	D4	2.01
Octameric c-di-GMP	11.92	D4	1.62
endo-S-c-di-GMP			
Monomeric endo-S-c-di-GMP (closed)	6.50	C1	2.55 ^a
Monomeric endo-S-c-di-GMP (open)	6.27	C1	--
Dimeric endo-S-c-di-GMP	--	--	2.07
Tetrameric endo-S-c-di-GMP	--	--	1.70
Octameric endo-S-c-di-GMP	--	--	1.37

a) The diffusion constants of monomeric form of c-di-GMP and endo-S-c-di-GMP were measured from DOSY T_1/T_2 relaxation analysis with no metal cation added (average value; see **Figure 4–2, 4–3** and Section 6.6.1 for detail); b) The dimeric c-di-GMP structure was adapted from x-ray crystal structure (PDB code: 315A)

6.6 NMR experiments for T_1/T_2 relaxation analysis (DOSY) and NOE

The Bruker AV III 600 MHz spectrometer was used to determine the diffusion constants and the NOE effect. The concentration of the samples was controlled at 3 mM in D₂O (with or without K⁺) using UV analysis ($\epsilon_{260\text{ nm}} = 21600$). The samples with 100 mM KCl was incubated at 90 °C for 5 min, cooled down to RT, and stored at 4 °C for overnight before use. Shigemi NMR tubes (D₂O) were used for all experiments, in which 0.30 mL sample solution was applied. A temperature control module was used for all experiments at 30.0 °C [316].

DOSY was measured with the stimulated echo pulse sequence (Bruker pulse program `stebpgp1s19`) using bipolar gradient pulses and watergate 3-9-19 to subpressed the solvent. Key aquisition parameters for the DOSY experiment include the big delta (Δ)

at 0.10 s, the number of scans at 8, relaxation delay at 2.5 s, and the gradient strength was varied 32 times linearly from 5 to 95% . The gradient pulse length (small delta δ) within the range of 1.4–1.8 ms was optimized under the experiment condition upon the point that the region of 5.5–9.0 ppm showed a good decay for the major peaks. The data were processed with TopSpin 2.1 software with T_1/T_2 relaxation analysis. Exponential function was applied for the raw data and the curve-fitting of the decays was based on the area of the peaks.

The condition of NOE experiment was referred to previous report [227], where a short mixing time (150 ms) was applied. The **Figure 6–5** illustrates that the *syn* conformer of guanine H8 and anomeric H showed a significantly stronger positive NOE (> 35 %) compared to *anti* conformer (< 8 %).

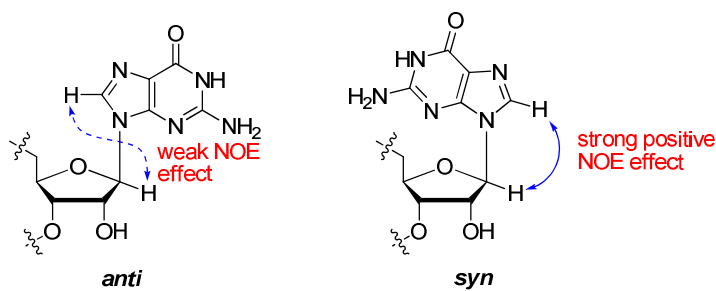


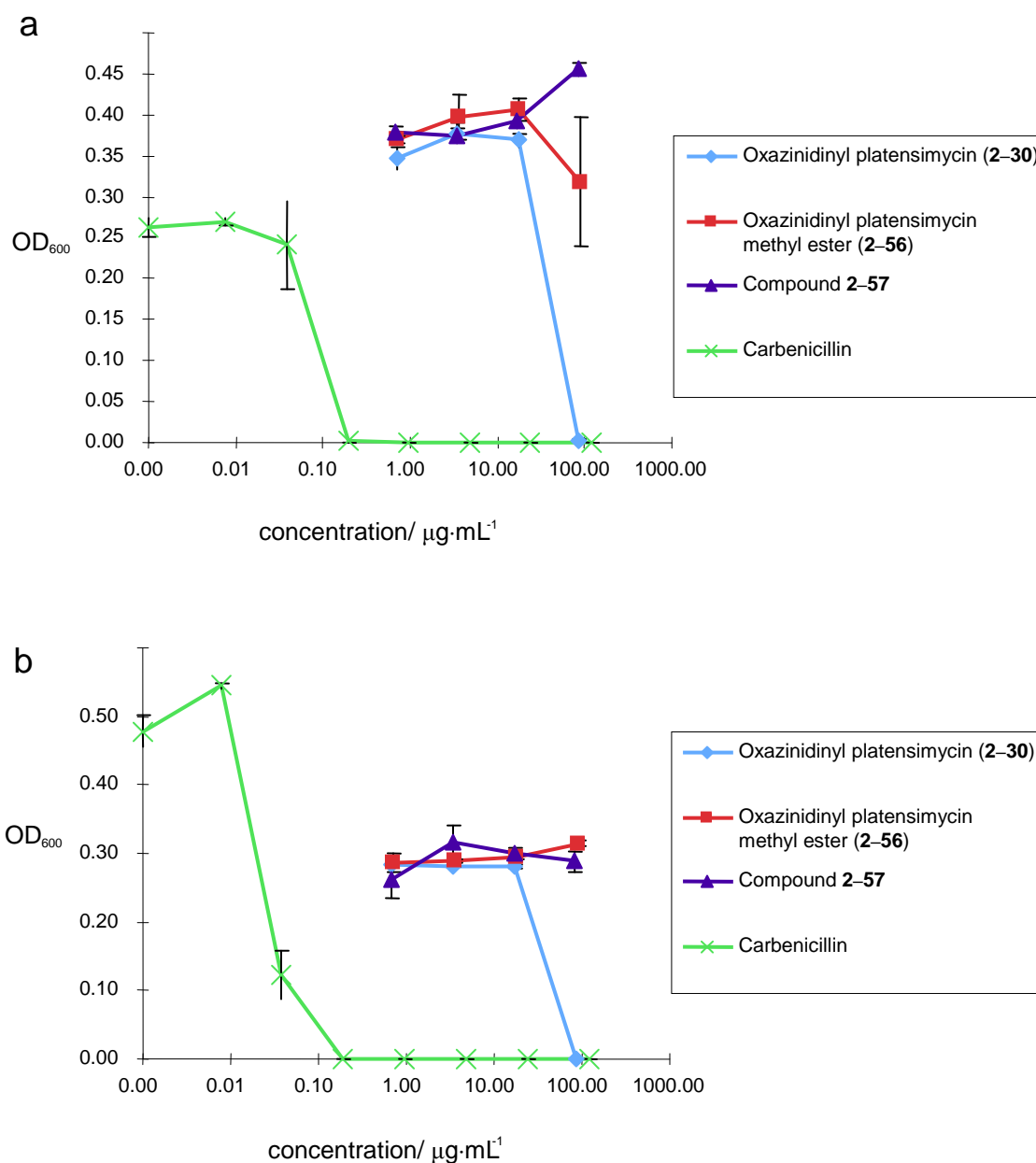
Figure 6–5. The NOE of *syn*- and *anti*- guanosines.

6.7 Biological assays

6.7.1 Minimal inhibitory concentration (MIC)

In Chapter 2, *Staphylococcus aureus* (Newman), *Streptococcus agalactiae* (2603V/R), and *Bacillus subtilis* (3160) were routinely grown in tryptic soy broth, Todd Hewitt broth and Luria Broth, respectively. For minimal inhibitory concentration determination, each of the strains was diluted to 5×10^5 cfu/mL and 98 μ L was added to

2 μL of diluted compounds or known antibacterial agent (carbenicillin or platensimycin) at the indicated concentration in sterile 96-well plate. The plates were shaken for 24 hours at 37 $^{\circ}\text{C}$ in a humidified chamber. The MIC was determined as the lowest concentration at which no bacteria were observed to grow as determined by OD_{600} (**Figure 6–6**). All experiments were performed in triplicate.



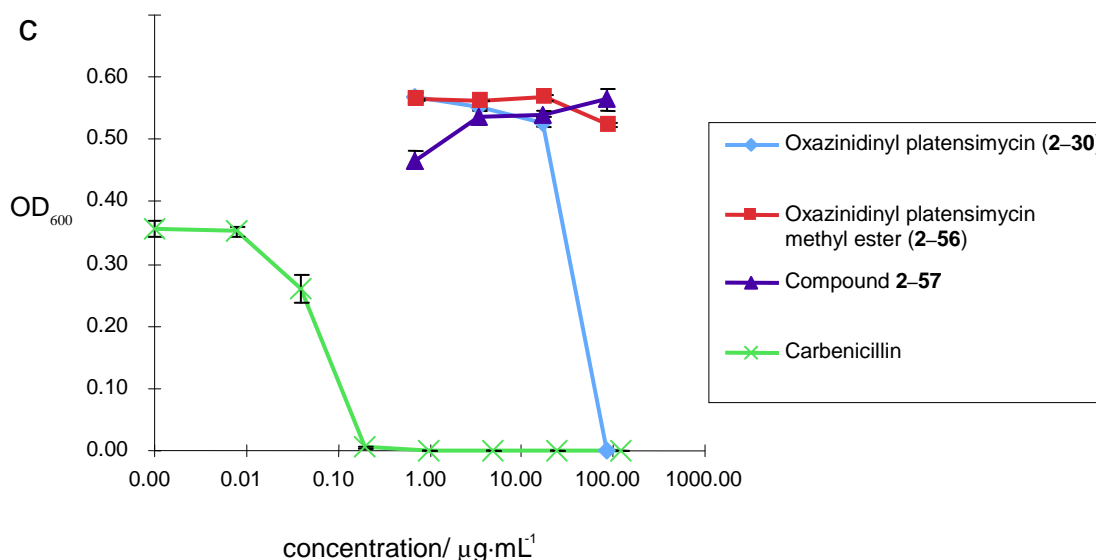


Figure 6-6. MIC determination for platensimycin analogs against a) *S. aureus*, b) *S. agalactiae* and c) *B. subtilis*.

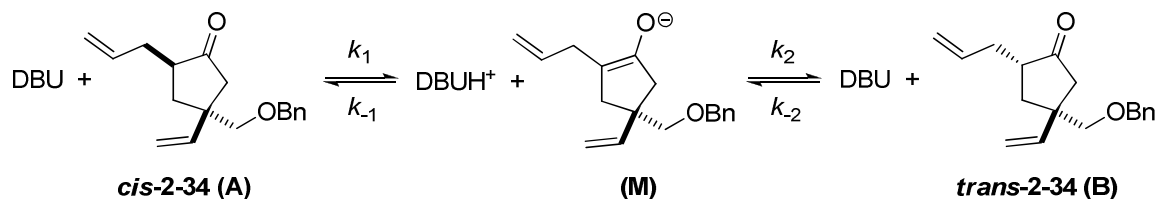
In Chapter 3, each of the strains of *Bacillus subtilis* (3160) and *Escherichia coli* K12 (1655) were grown in Luria Broth. The strains were diluted to 3×10^5 cfu/mL and 98 μ L was added to 2 μ L of diluted compounds or known antibacterial agent (FAS inhibitors: platensimycin or cerulenin) at the indicated concentration in a sterile 96-well plate. When MDR inhibitor Phe-Arg β -naphthylamide dihydrochloride (PA β ND) was added, 97 μ L bacterial broth, 2 μ L antibacterial solution and 1 μ L MDR inhibitor solution was mixed in each well of a 96-well plate. The plates were shaken for 24 hours at 37 °C. The minimum inhibitory concentration (MIC) was determined as the lowest concentration at which no bacteria were observed to grow as determined by OD₆₀₀. All experiments were performed in triplicate. The MIC testing against MRSA and VRE strains were done by Accugen Laboratories and AntiMicrobial Test Laboratories.

6.7.2 Enzymatic assays

Alg44, RocR, and WspR were purified by histidine chromatography followed by Q-sepharose anion exchange column. Proteins were dialyzed into a 10 mM Tris, 100 mM NaCl solution. α - 32 P-c-di-GMP was generated from purified WspR as described in Lee *et al.*'s previous report [225]. For binding assay of Alg44, 5 μ M protein was mixed with 1 μ M α - 32 P-c-di-GMP and indicated competitor (c-di-GMP or endo-S-c-di-GMP) in a buffer containing 10 mM Tris (pH 8.0), 100 mM KCl, and 5 mM MgCl₂. This mixture was allowed to equilibrate for 10 min. The binding assay was analyzed using pulldown assay with Ni-NTA agarose beads [225]. For RocR and WspR enzymatic assays, 5 μ M enzyme was added to 8 nM α - 32 P-c-di-GMP (for RocR) or 8 nM α - 32 P-GTP (for WspR) and 1 mM of the indicated competitor in reaction buffer (10 mM Tris pH 8.0, 100 mM NaCl, 5 mM MgCl₂). 1 μ L of sample were spotted on polyethyleneimine cellulose TLC plates at indicated times after addition of the enzyme. Samples were dried and separated using a mobile phase consisting of 1: 1.5 of saturated (NH₄)₂SO₄ and 1.5 M KH₂PO₄. TLC plates were dried, exposed on a phosphorimager screen and visualized with a Fujifilm FLA-7000.

Appendix I. Kinetic study of the epimerization reaction

Assuming the reaction pathway is as described in **Scheme S1**.



Scheme S1. Proposed mechanism for DBU catalyzed epimerization of bis-alkene (2–34).

$$\frac{d[\text{DBUH}^+]}{dt} = k_1[\text{DBU}][\text{A}] - k_{-1}[\text{DBUH}^+][\text{M}^-] - k_2[\text{DBUH}^+][\text{M}^-] + k_{-2}[\text{DBU}][\text{B}]$$

From the *Steady State Approximation*: $\frac{d[\text{DBUH}^+]}{dt} = 0$

Thus, $[\text{DBUH}^+][\text{M}^-] = [\text{DBU}] \frac{k_1[\text{A}] + k_{-2}[\text{B}]}{k_{-1} + k_2}$ (S3)

The kinetic equation of B is $\frac{d[\text{B}]}{dt} = k_2[\text{DBUH}^+][\text{M}^-] - k_{-2}[\text{DBU}][\text{B}]$

Substitute Eq. S3 into the above equation:

$$\frac{d[\text{B}]}{dt} = k_2[\text{DBU}] \frac{k_1[\text{A}] + k_{-2}[\text{B}]}{k_{-1} + k_2} - k_{-2}[\text{DBU}][\text{B}] \quad (\text{S4})$$

At the equilibrium point (> 1380 min),

Let $[\text{B}]_\infty = \xi([\text{A}] + [\text{B}]) = \xi[\text{A}]_0$, so, $[\text{A}]_\infty = (1 - \xi)[\text{A}]_0$.

Substitute into Eq. S4,

$$\left. \frac{d[\text{B}]}{dt} \right|_{t=\infty} = 0 = k_2[\text{DBU}] \frac{k_1[\text{A}]_\infty + k_{-2}[\text{B}]_\infty}{k_{-1} + k_2} - k_{-2}[\text{DBU}][\text{B}]_\infty$$

Thus, $k_{-1}k_{-2} = k_1k_2 \frac{1-\xi}{\xi}$ (S5)

Substitute Eq. S5 into Eq. S4,

$$\frac{d[B]}{dt} = [DBU] \frac{k_1k_2}{k_{-1} + k_2} ([A]_0 - \frac{1}{\xi}[B])$$

Let $K = [DBU] \frac{k_1k_2}{k_{-1} + k_2}$

So, the kinetic equation of B becomes, $r = \frac{d[B]}{dt} = K[A]_0 - \frac{K}{\xi}[B]$

Using the initial condition: $[B]_{t=0} = 0$,

$$[B] = \xi[A]_0(1 - e^{-Kt/\xi}) \quad (\text{S6})$$

Transform Eq. S6 into: $1 - \frac{[B]}{\xi[A]_0} = -\frac{K}{\xi}t$

Take logarithm on both sides: $\ln(1 - \frac{[B]}{\xi[A]_0}) = -\frac{K}{\xi}t \quad (\text{S7})$

A plot of $\ln(1 - \frac{[B]}{\xi[A]_0})$ versus t gives: $\xi = 0.447$ ($R^2 = 0.987$) (**Figure S1**)

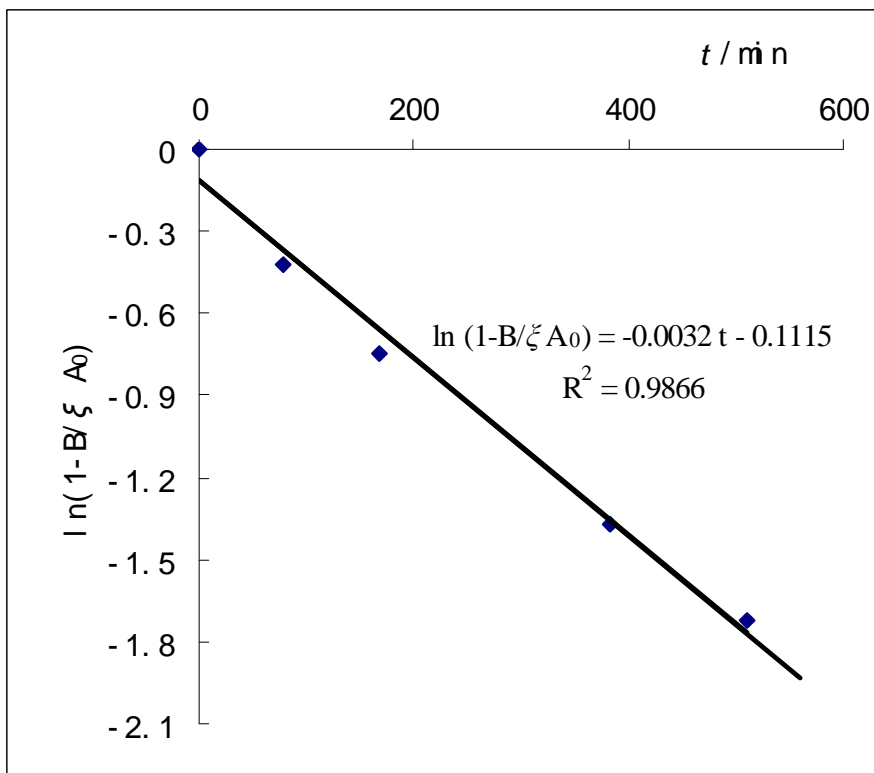


Figure S1. The scatter plot and the trend line of $\ln(1 - \frac{[B]}{\xi[A]_0})$ over t .

$$\text{Thus, } \frac{k_1 k_2}{k_{-1} + k_2} = 0.24 \text{ L} \cdot \text{mol}^{-1} \cdot \text{min}^{-1}$$

Consider 70% conversion towards the equilibrium, *i.e.* $[B]_{70\%} = 0.7 \times \xi[A]_0$,

$$\text{Then: } t_{70\%} = -\frac{K}{\xi} \ln 0.3 = 374 \text{ min} \approx 6 \text{ h} \quad (\text{S8})$$

Thus, 70 % of the equilibrium is reached in 6 h.

Appendix II. Reaction conditions for dynamic ring-closing metathesis

Dynamic ring-closing metathesis (DRCM) was performed by combining the ruthenium catalyst and an epimerization base in the same flask. Other than Hoveyda-Grubbs II catalyst, two other ruthenium catalysts, Grubbs I and Grubbs II catalyst (Figure S2), were also screened. In the case of Grubbs I catalyst, no reaction occurred with the bis-alkene substrate **2-34** and the starting material was recovered. For Grubbs II catalyst, the yield of the reaction (23 %) was significantly lower than the reaction that was catalyzed by Hoveyda-Grubbs II catalyst (69 %). Significant side products (a complicated mixture) were also obtained when Grubbs II catalyst was used (Scheme S2).

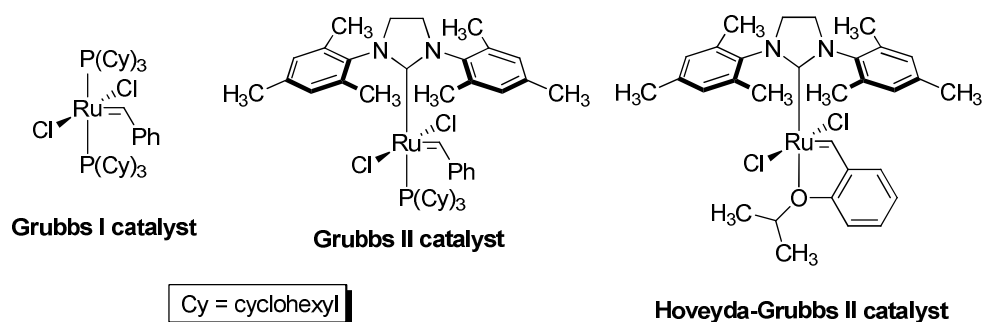
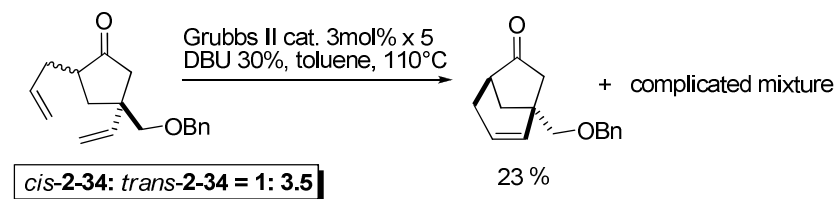


Figure S2. The structures of Grubbs I, Grubbs II and Hoveyda-Grubbs II catalyst.

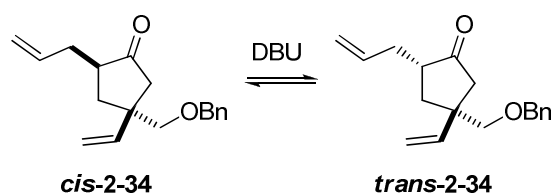


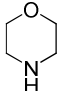
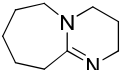
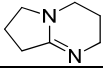
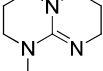
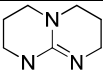
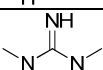
Scheme S2. The unsuccessful ring-closing metathesis reactions that were catalyzed by Grubbs I and Grubbs II catalyst. Reaction condition: 0.05 M *cis*-**2-34**: *trans*-**2-34** (1: 3.5), 16 h.

The rate-limiting step of the dynamic ring-closing metathesis (see Section 2.2.2) is the DBU catalyzed epimerization, with an apparent rate constant of $0.24 \text{ M}^{-1}\text{min}^{-1}$ (see Appendix I). Since the ruthenium catalyst is deactivated over time in the presence of alkenes [283,284] ($t_{1/2} \sim 1 \text{ h}$ under the experiment condition), the catalyst needs to be repeatedly added every other 3 h during the slow epimerization process. We envisaged that a base with better epimerization ability would reduce the loading of the ruthenium catalyst. Ideally, if the epimerization equilibrium can be rapidly reached before the catalyst is deactivated, the ruthenium catalyst can be added at the beginning of the reaction (one time loading). Therefore we screened other amine and alkoxide bases for the epimerization ability and the compatibility with Hoveyda-Grubbs II catalyst (**Table S1**). The epimerization reaction was performed with 30 mol% of various bases and a mixture of *cis*-**2–34**: *trans*-**2–34** (1: 5.7) at 75 °C. To test the compatibility of the bases and the ruthenium catalyst, a simpler bis-alkene, diallyl dimethylmalonate was used with 3 mol% Hoveyda-Grubbs catalyst and 30 mol% indicated base. No ring-closure product can form if the ruthenium catalyst is poisoned (**Scheme S2**). Among all the amine bases that are screened, 1,5,7-triazabicyclo[4.4.0]dec-5-ene, solid-supported and solution phase DBU (entry 7, 9 and 4, **Table S1**) had the best epimerization abilities. In the case of 1,5,7-triazabicyclo[4.4.0]dec-5-ene, the epimerization reaction was significantly more rapid than the reactions catalyzed by other bases, and the reaction almost reaches equilibrium after 1 h (at equilibrium, *cis*-**2–34**: *trans*-**2–34** = 1.0: 1.2 in toluene). This amine, however, poisons the Hoveyda-Grubbs II catalyst, and is, therefore, not ideal for DRCM. Most of the amines or imines bearing an N–H moiety were not compatible with the ruthenium catalyst. Bulky tertiary amines, such as Hünig's base (entry 2, **Table S1**)

and DBU are therefore most ideal for DRCM because they can epimerize ketone substrates and do not readily poison the ruthenium catalyst. Surprisingly, KO*t*-Bu (entry 10, **Table S1**) was also compatible with Hoveyda-Grubbs II catalyst in protic solvent, *t*-BuOH, and the epimerization ability was similar to DBU (entry 4 and 9, **Table S1**).

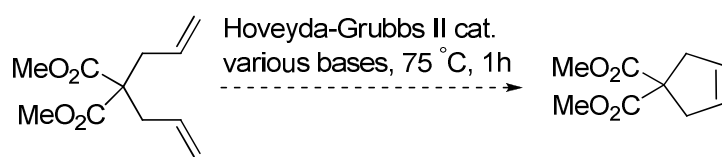
Table S1. Epimerization of ketone **2–34** by various bases (the initial mixture of **2–34** consisted of 1: 5.7 *cis*: *trans*)



Entry	Bases	<i>cis</i> - 2–34 : <i>trans</i> - 2–34 ^[a]
1	Et ₃ N	1.0: 5.5
2	Et(<i>i</i> -Pr) ₂ N	1.0: 5.1
3		1.0: 5.5
4		1.0: 4.9
5		1.0: 5.2
6		1.0: 5.6
7		1.0: 1.4
8		1.0: 5.4
9	solid support- DBU ^[b]	1.0: 4.2
10	KO <i>t</i> -Bu ^[c]	1.0: 4.2
11	(no base)	1.0: 5.7

[a] The reaction condition for the epimerization reaction: 30 mol% base and 0.05 M *cis*-**2–34**: *trans*-**2–34** (1: 5.7) was heated at 75 °C in (CH₂Cl)₂; [b] the concentration of substrate was 0.20 M; [c] the reaction was performed in *t*-BuOH.

To test if the various bases in **Table S1** can poison the ruthenium catalyst, a model reaction (**Scheme S3**) on a small scale was performed and monitored by TLC. In the absence of any added amine base, the reaction proceeded to completion, as judged by the disappearance of starting material and the appearance of a product. Initial TLC screening indicated that in the presence of Et₃N, Hünig's base, 7-methyl-1,5,7-triazabicyclo[4.4.0]dec-5-ene, solid-support DBU and KO^{*t*}-Bu (entries 1, 2, 6, 9 and 10 in **Table S1**), the starting material was mostly consumed after 1 h, and the product band appeared on the TLC. For the bases DBU (solution phase) and 2,3,4,6,7,8-hexahydropyrrolo[1,2-*a*]pyrimidine (entries 4 and 5 in **Table S1**), some starting material remained after 1 h, therefore we conclude that these two bases partially inhibited the ruthenium catalyst. For bases morpholine, 1,5,7-triazabicyclo[4.4.0]dec-5-ene and *N,N,N',N'*-tetramethylguanidine (entries 3, 7 and 8 in **Table S1**), no product band was observed and the starting material band remained on TLC after 1 h. Therefore, we conclude that these bases poisoned the catalyst.



Scheme S3. Determination of which bases are compatible with the ruthenium catalyst.

Appendix III. Introduction on pulsed gradient spin echo for DOSY experiment

DOSY (Diffusion Orded SpectroscopY) experiment is a NMR technique based on Pulsed Gradient Spin Echo (PGSE), a method for measuring translational diffusion rate of each component in a mixture of various aggregates [357]. PGSE NMR is commonly used to determine the size of oligomerization of biomolecules in aqueous solution [358].

In the magnetic spin vector model, the magnetization vector of the atoms precesses (Larmor precession) when they are applied a magnetic field. Because a 90° radiofrequency (RF) pulse is applied, the magnetization precession rotates from the z-axis to the x-y plane [359]. When a linear gradient field is applied at t_1 along the z-axis of the NMR tube in DOSY experiment (G in a duration of δ , **Figure S3a**), the magnetic field strength of each point along the z-axis is different from the others [359]; therefore the precession angles of the magnetization vector (Ω , **Figure S3a**) are shown as linear distribution along the z-axis (**Figure S3b, S3c**). After a period of time (Δ), a second magnetic gradient field is applied to offset the previously generated precession (the precession is on a opposite direction due to the 180° RF pulse, see **Figure S3a**). If no translational diffusion occurs along the z-axis, the precession is completely cancelled out; therefore a maximum echo signal is obtained (**Figure S3b**). However, if the translation diffusion occurs, the spin precession cannot offset; therefore, the larger the diffusion, the poorer the spins are refocused and the smaller the echo signal is obtained [359].

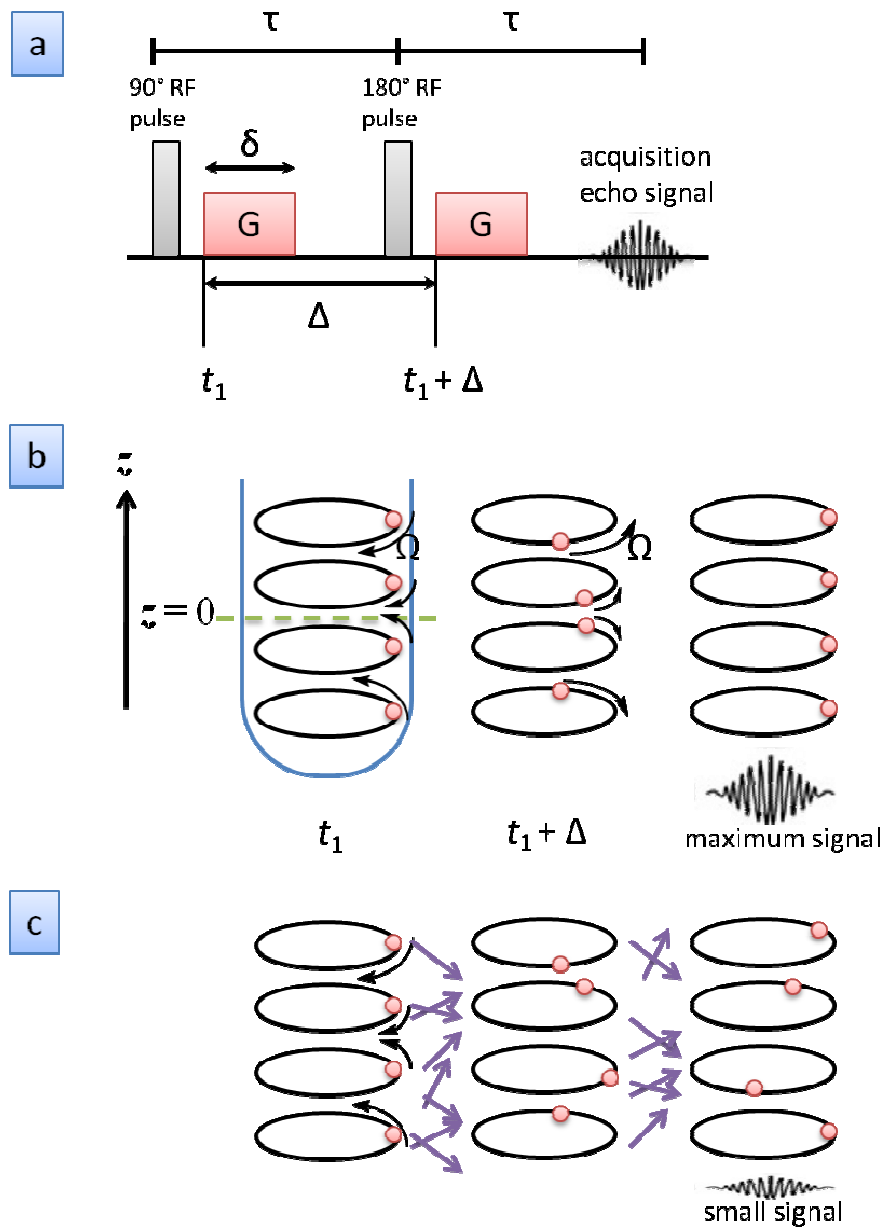
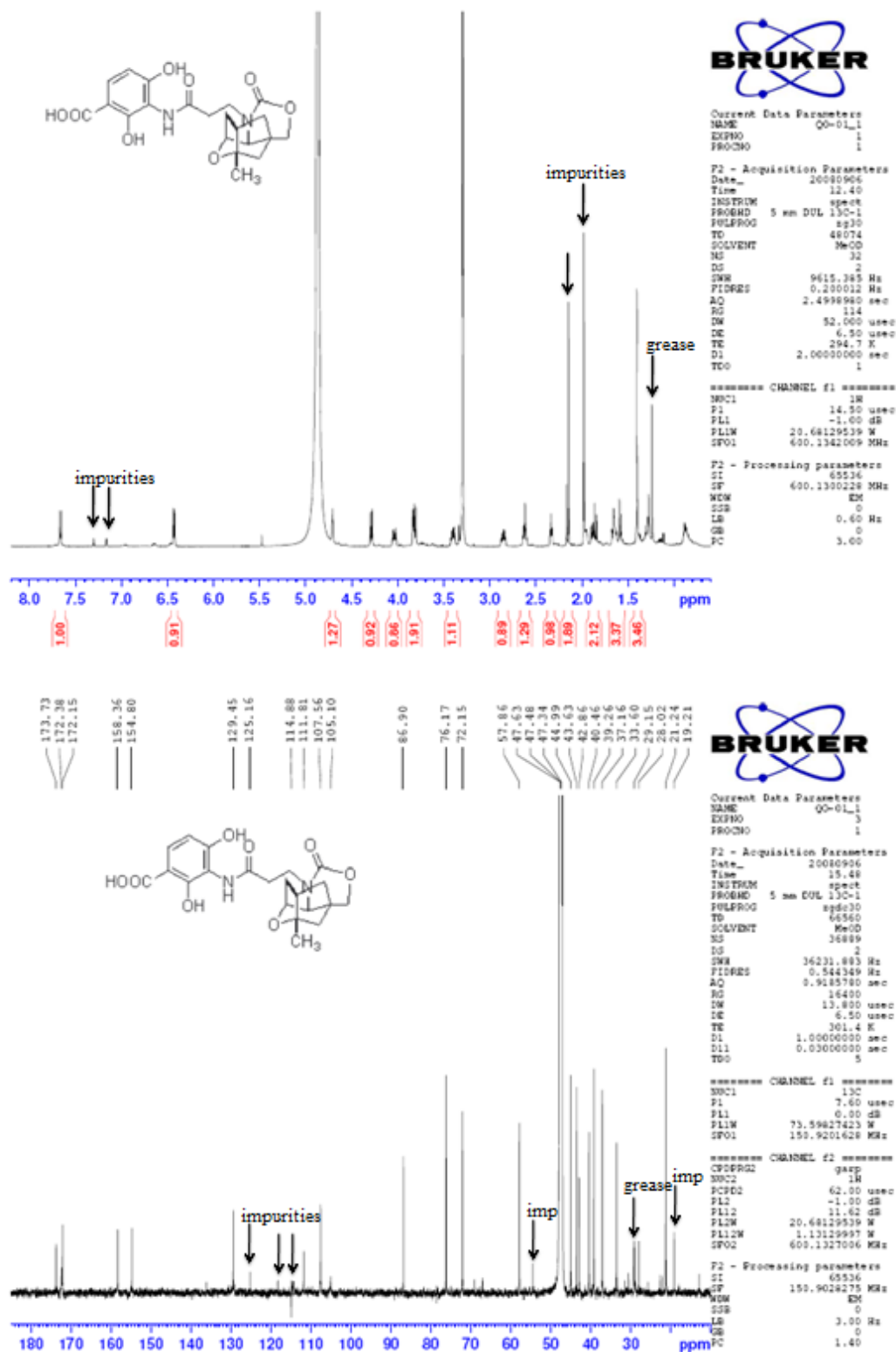


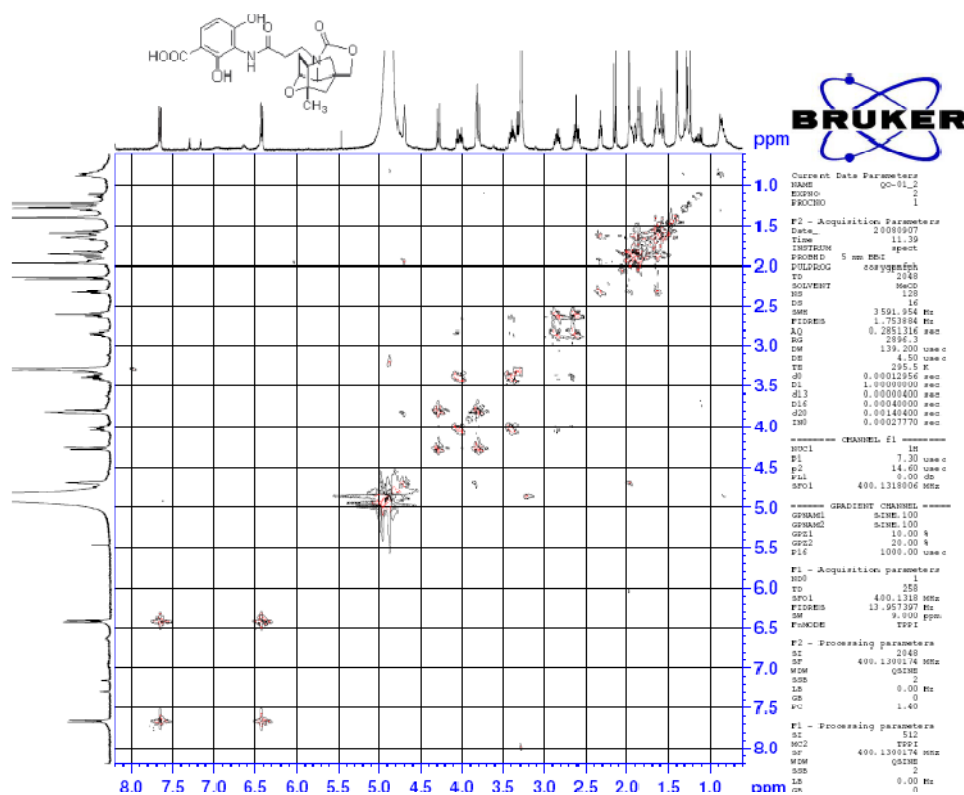
Figure S3. a) The Pulsed Gradient Spin Echo (PGSE) pulse sequence. G is the amplitude of the pulsed gradient (in duration δ), Δ is the interval between two pulsed gradients. Also shown are the magnetic.

Appendix IV. NMR, IR spectra and HPLC chromatography

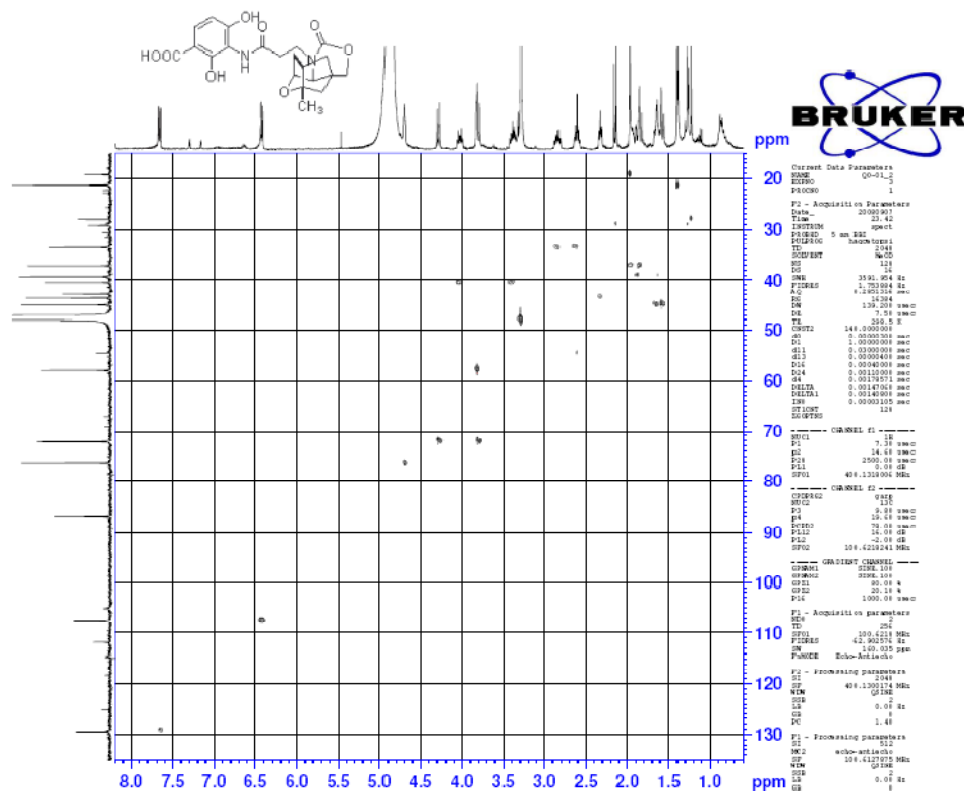
Compound 2-30



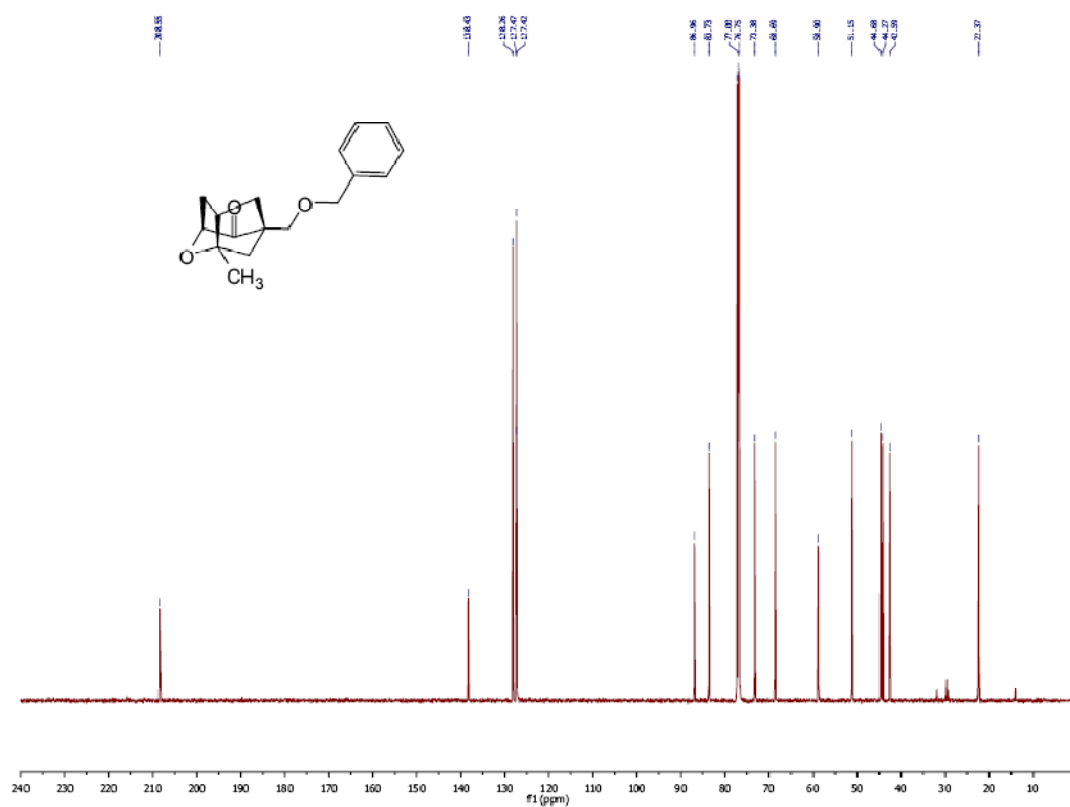
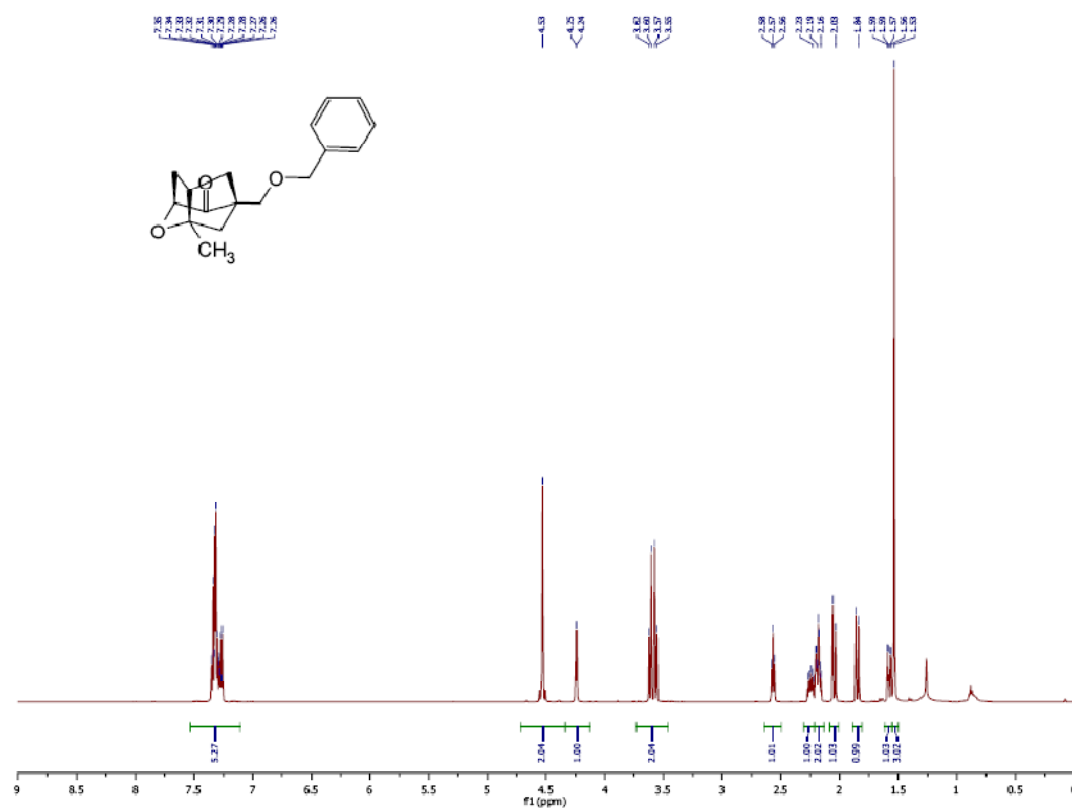
COSY



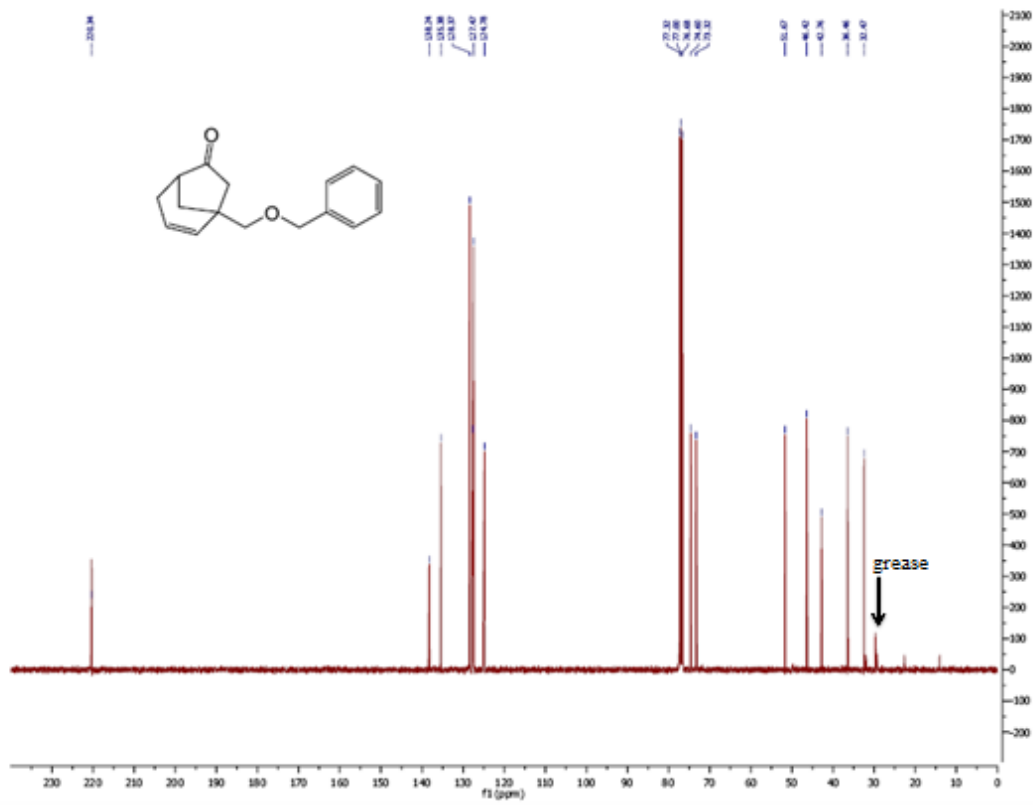
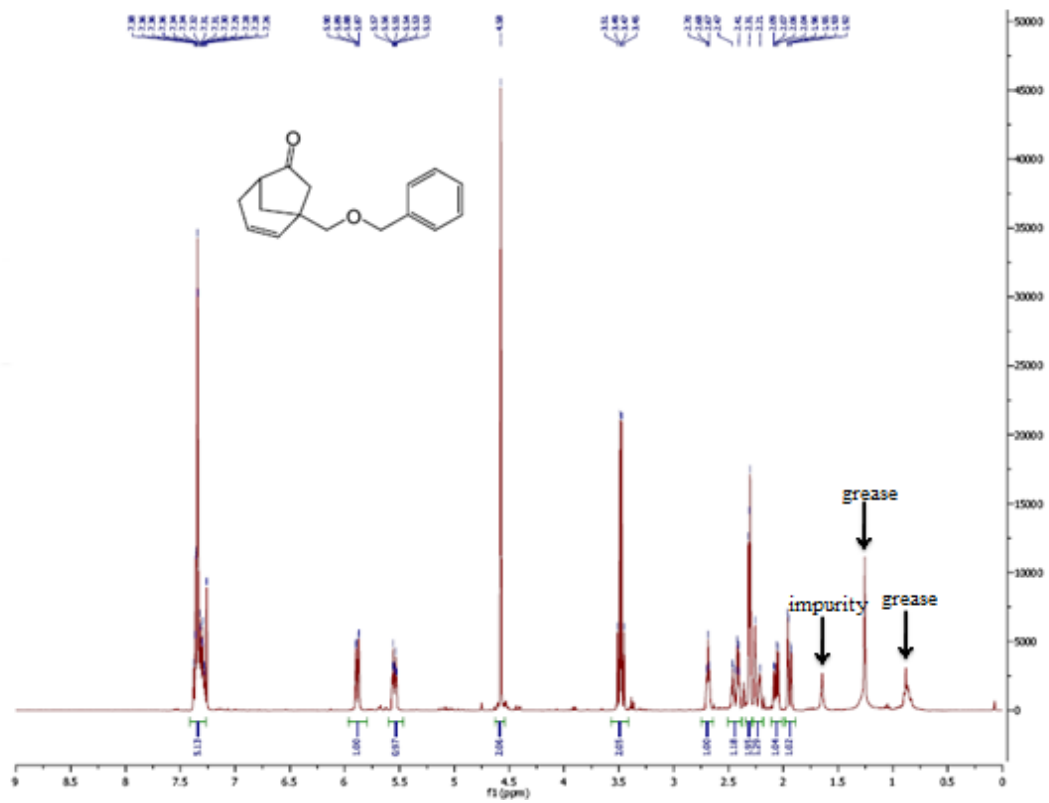
HSQC

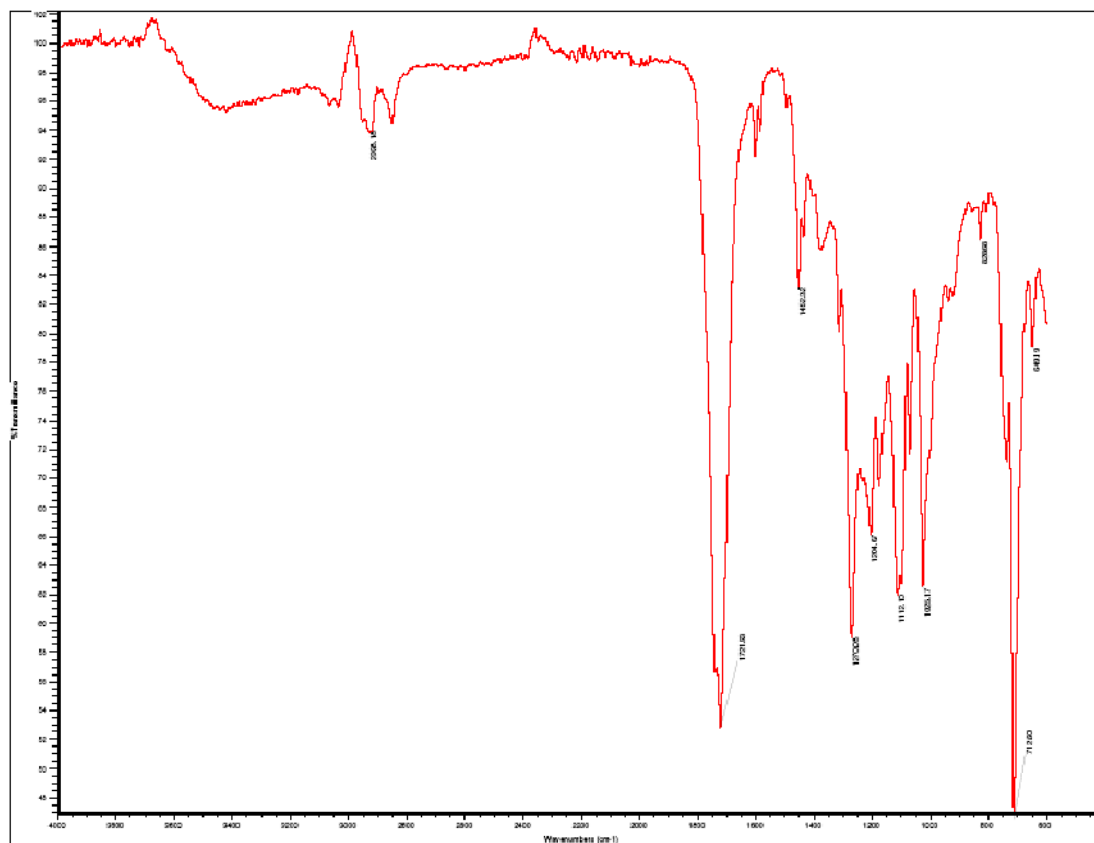


Compound 2-31

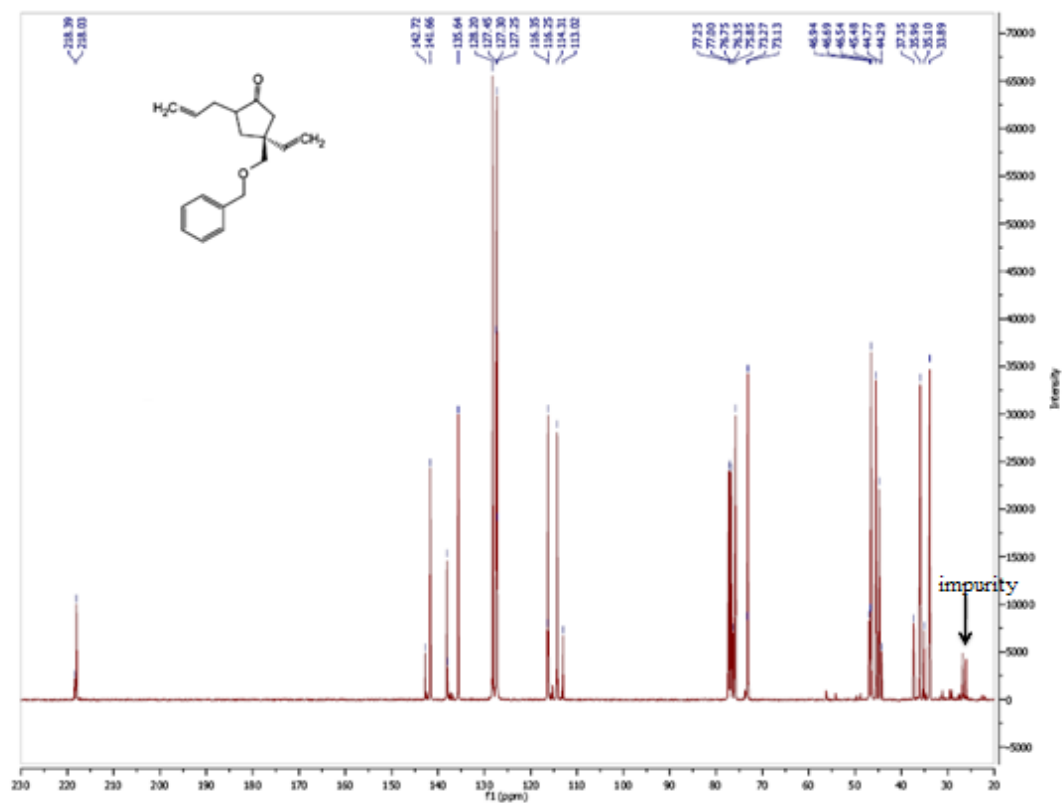
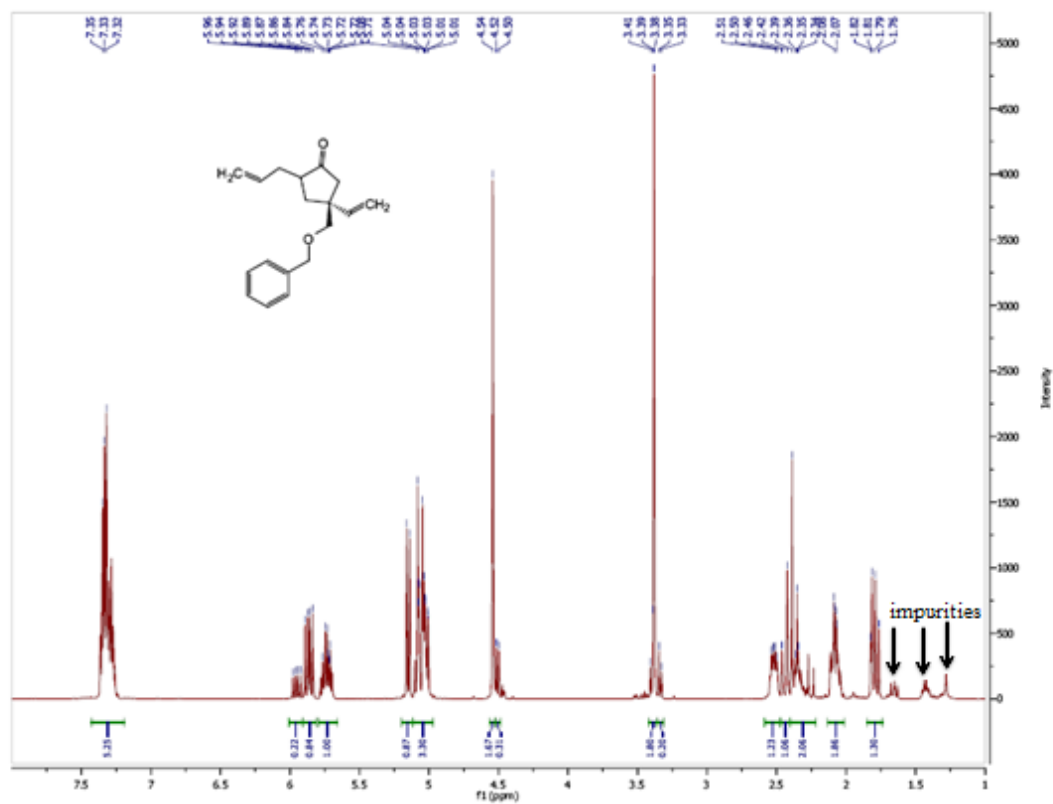


Compound 2-33

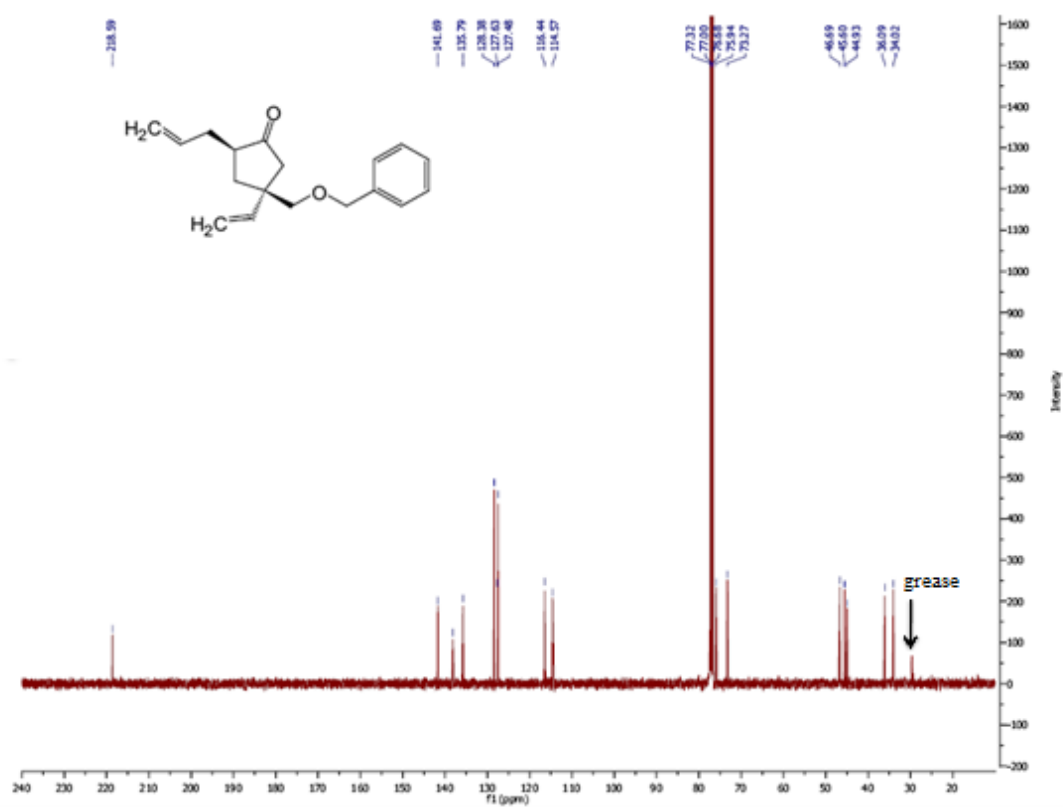
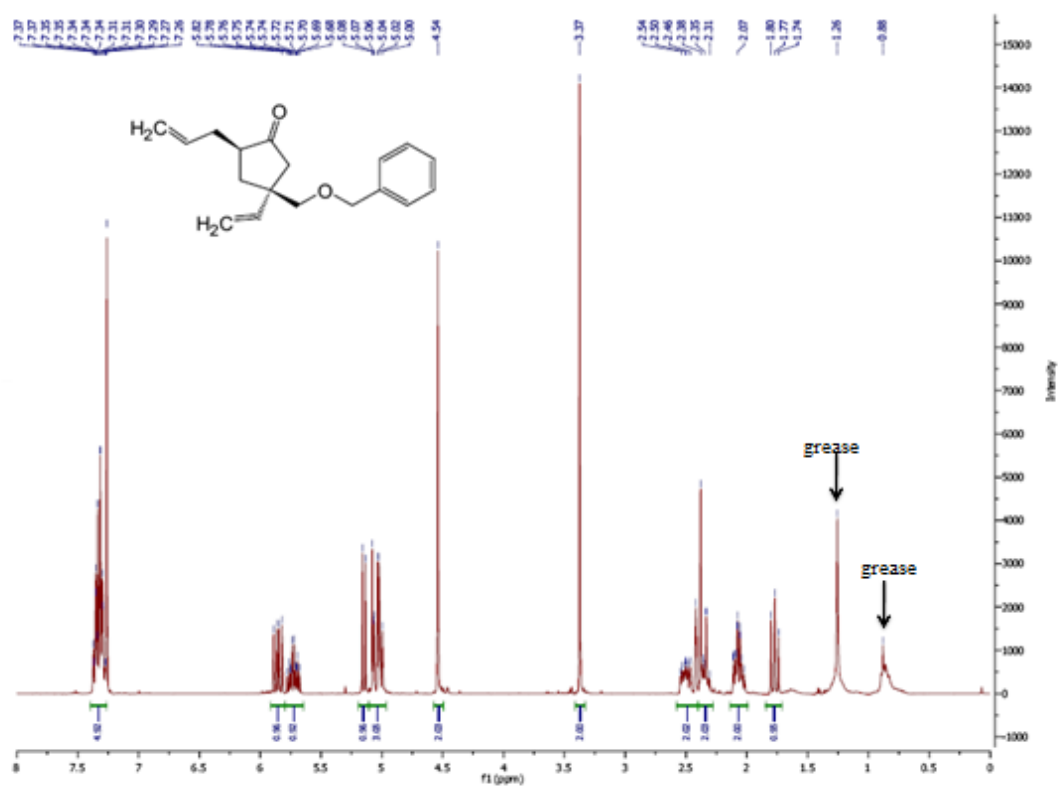




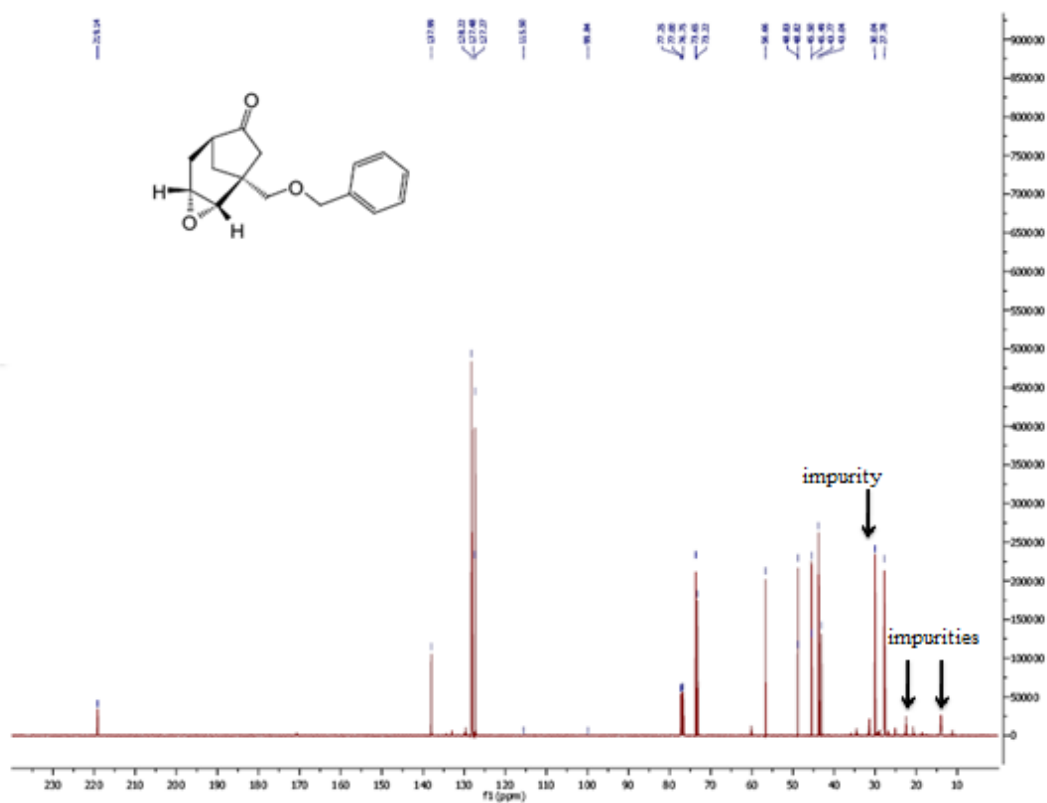
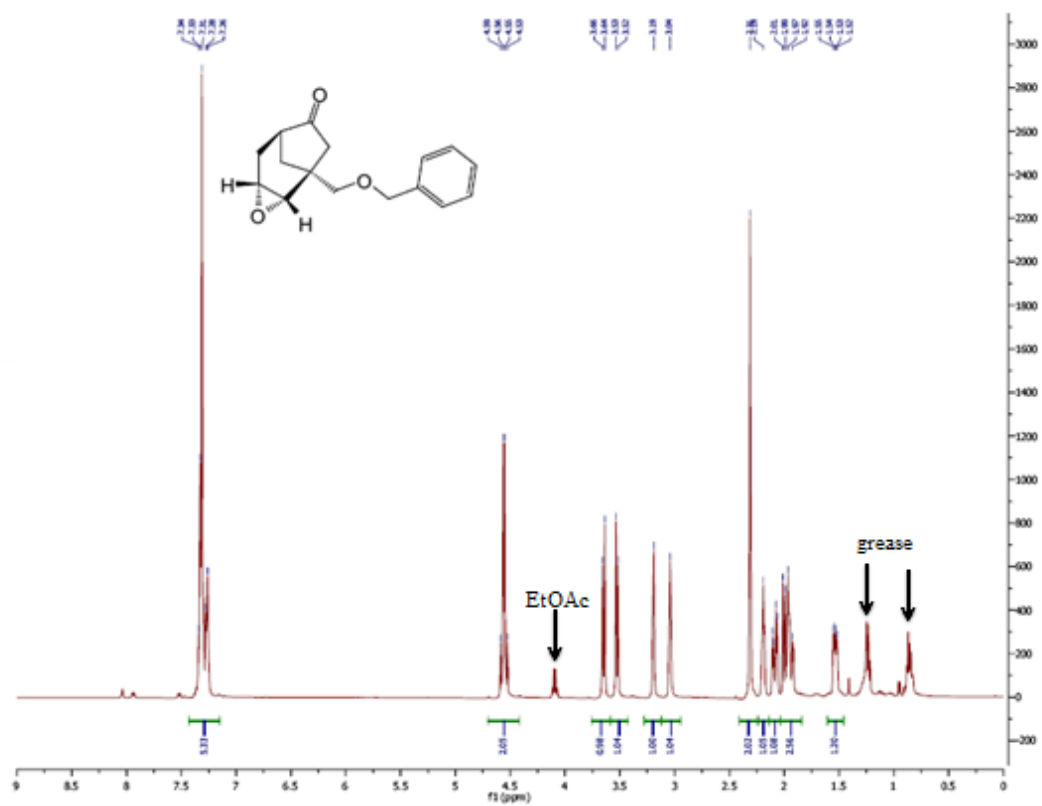
Compound *cis-/ trans*-2-34



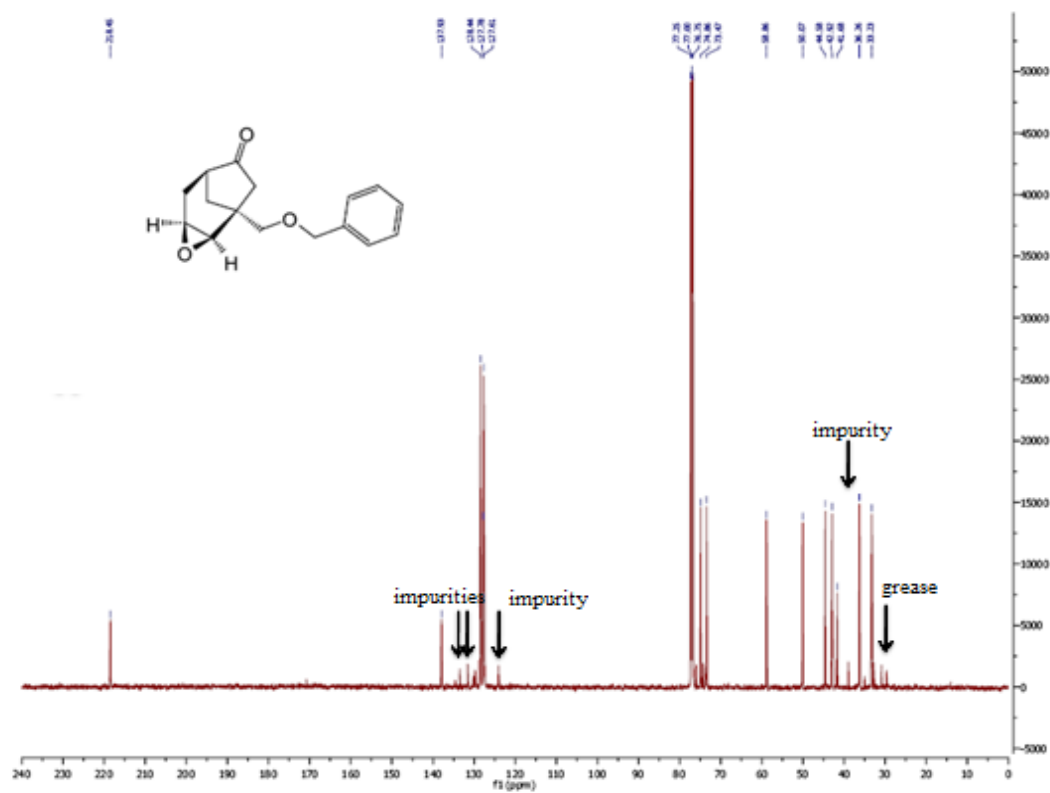
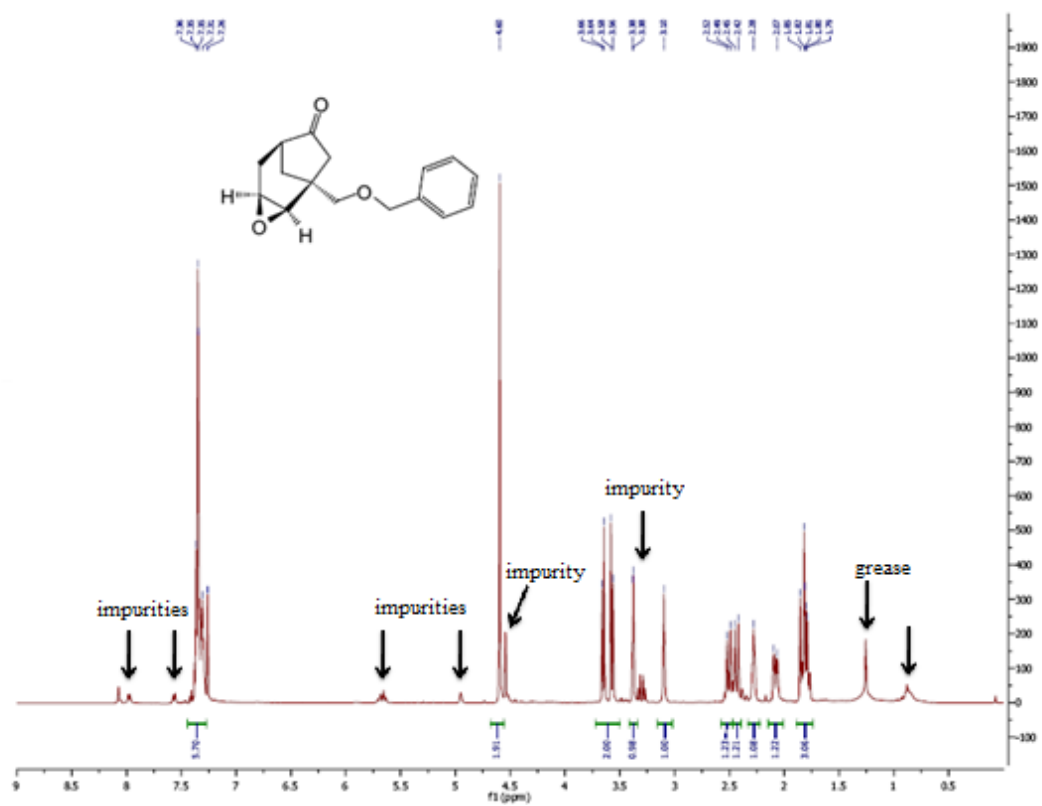
Compound *trans*-2-34

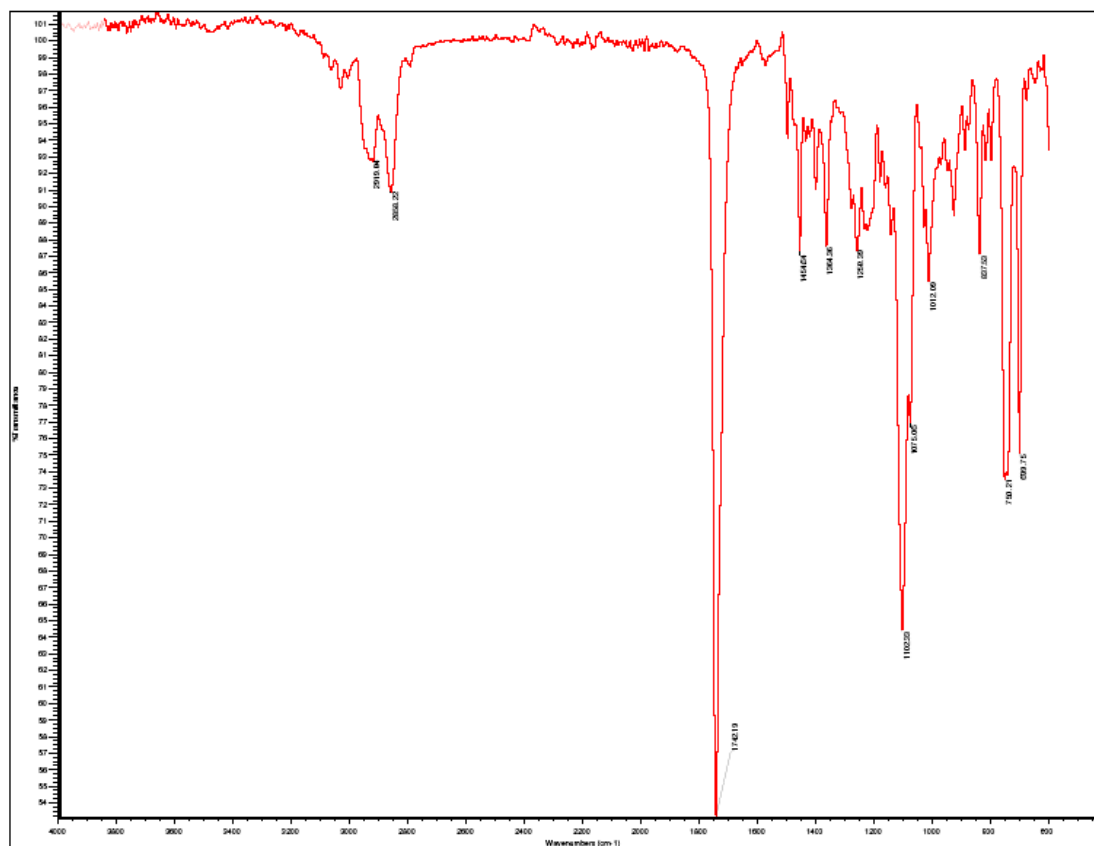


Compound 2-35

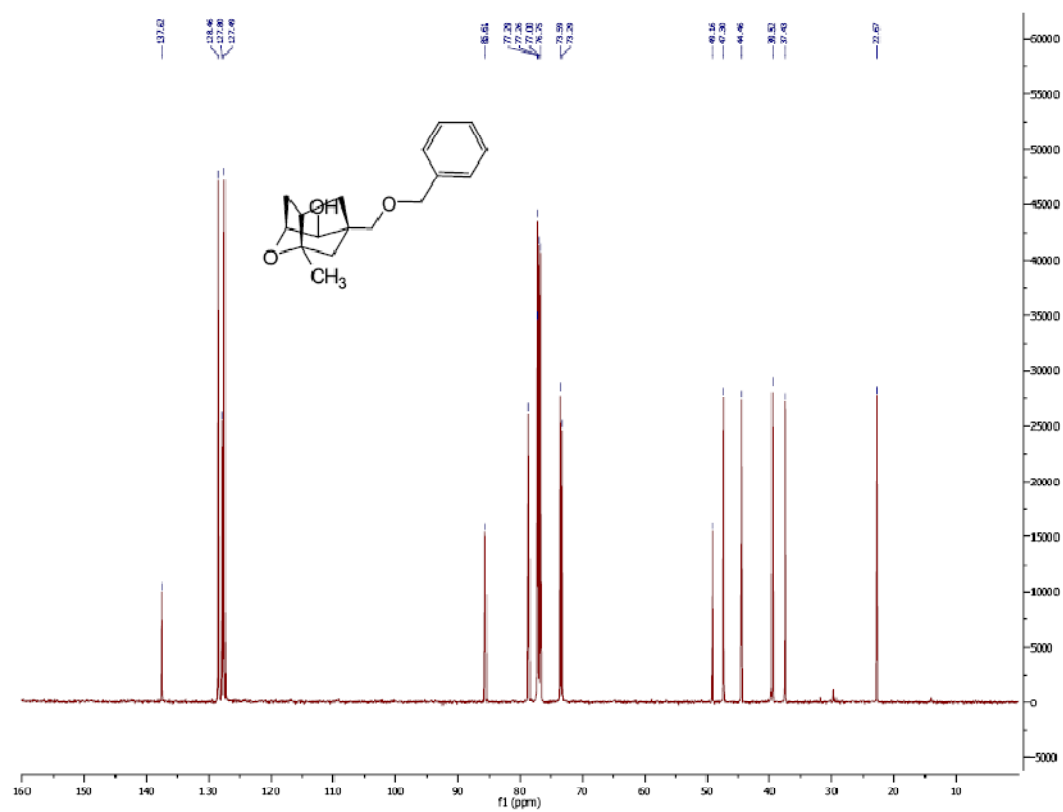
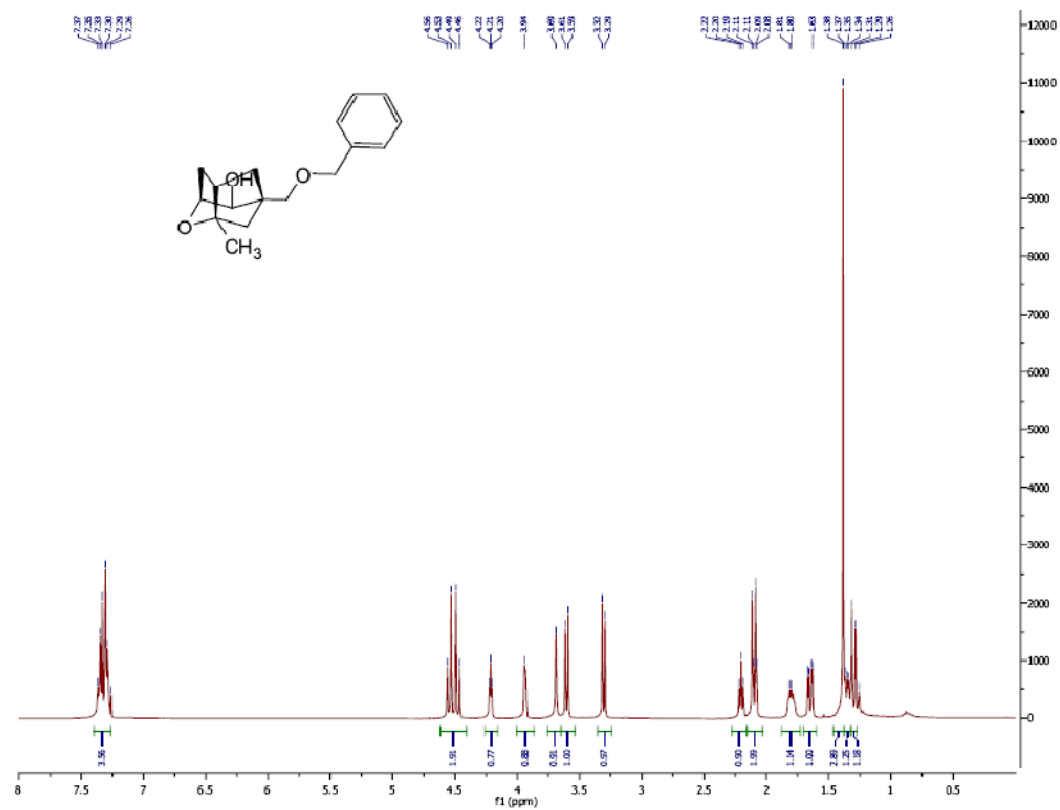


Compound 2-35b

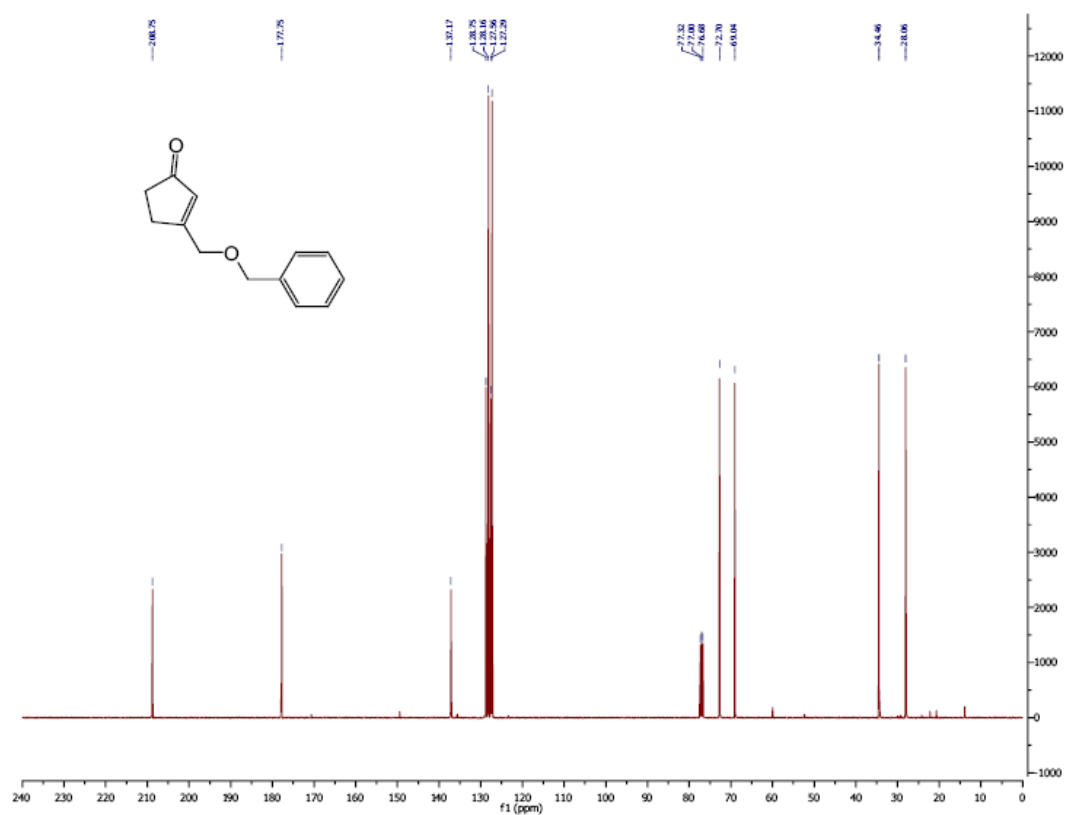
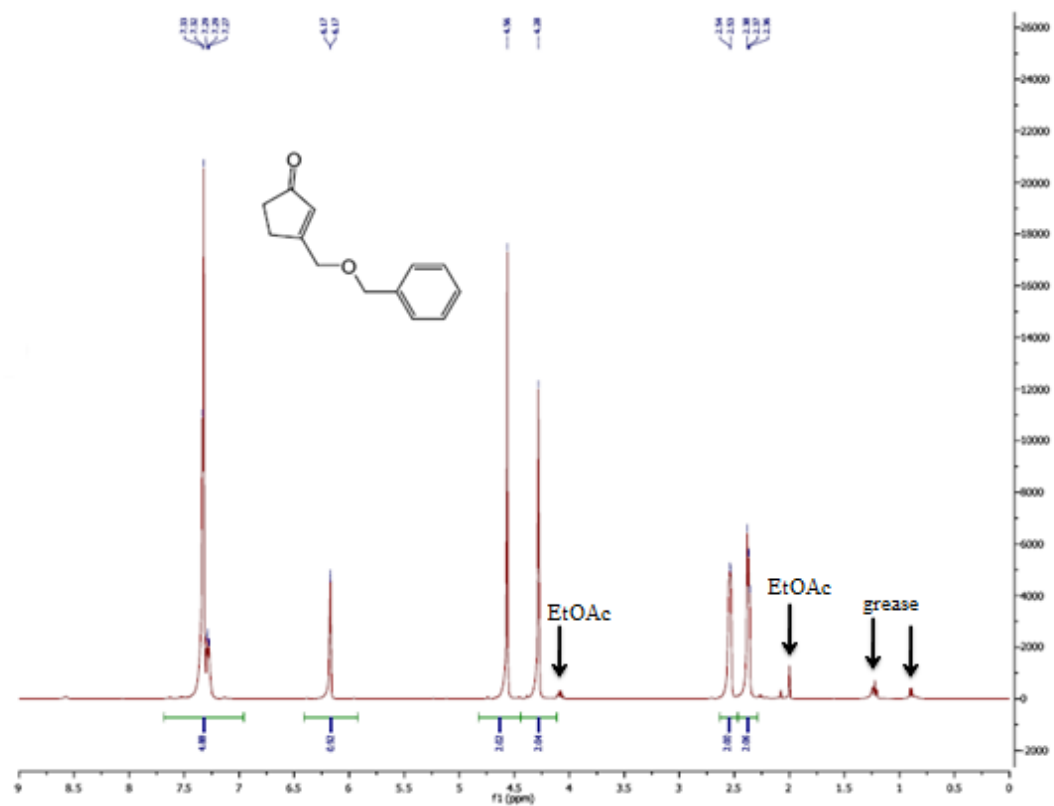


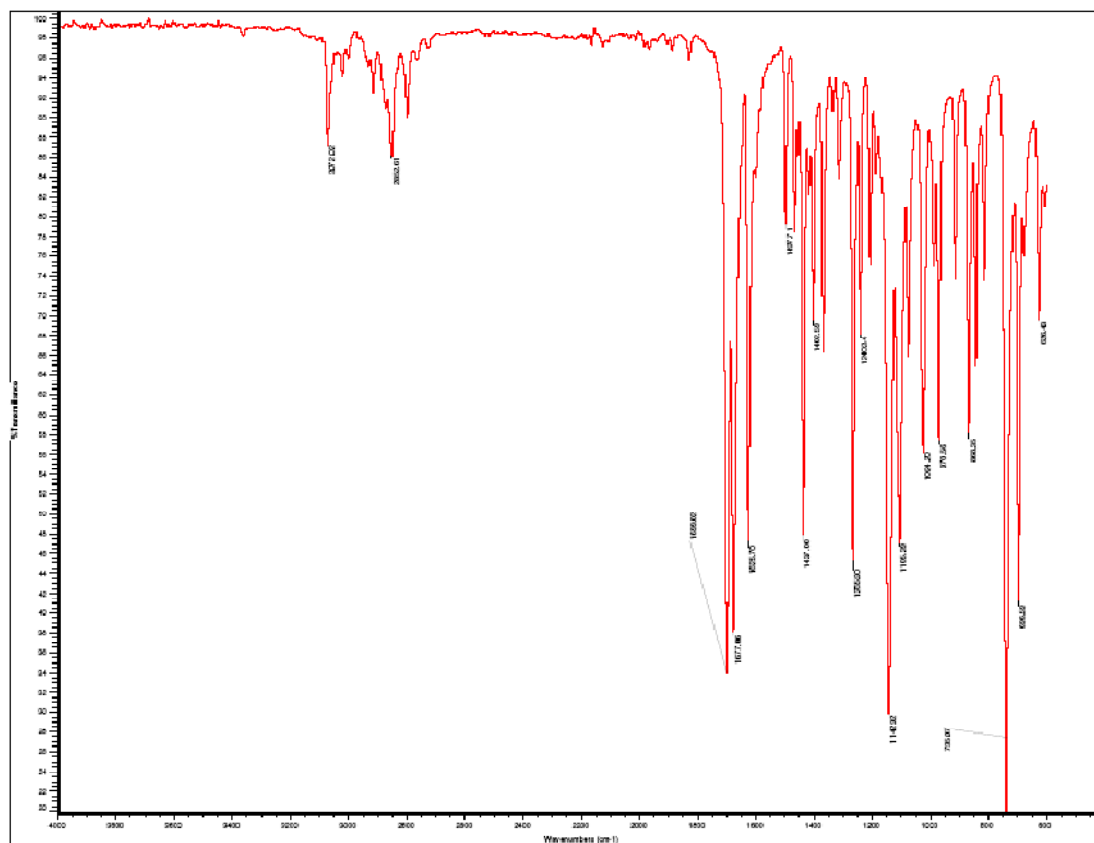


Compound 2-36

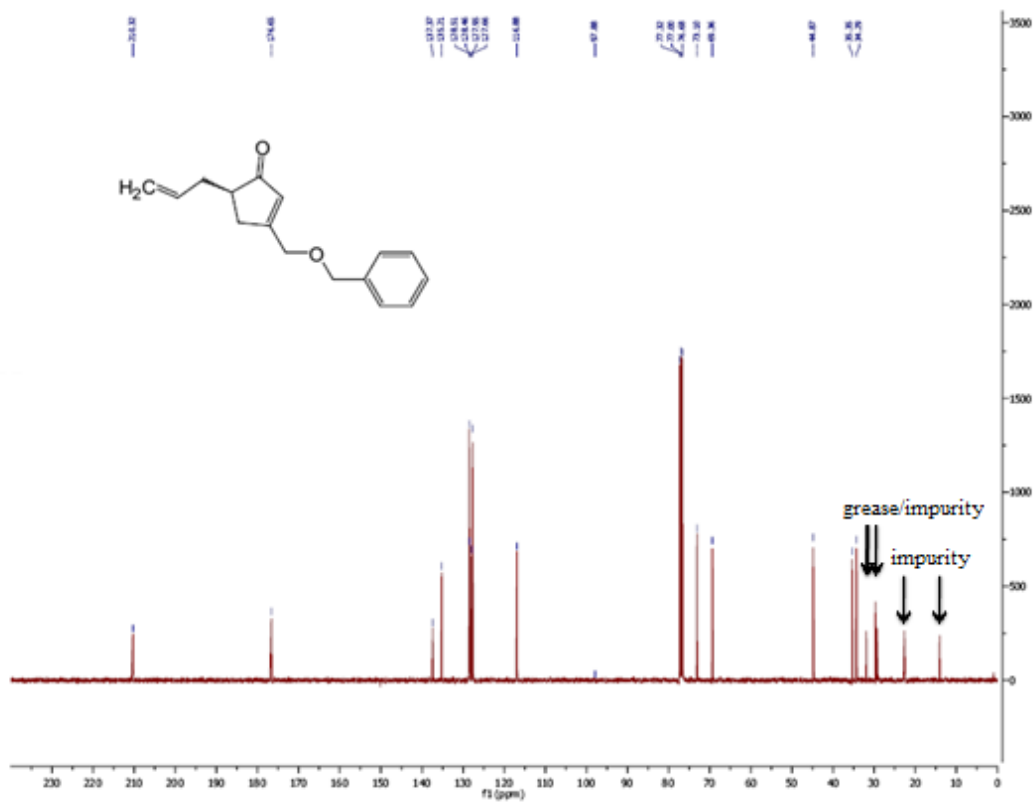
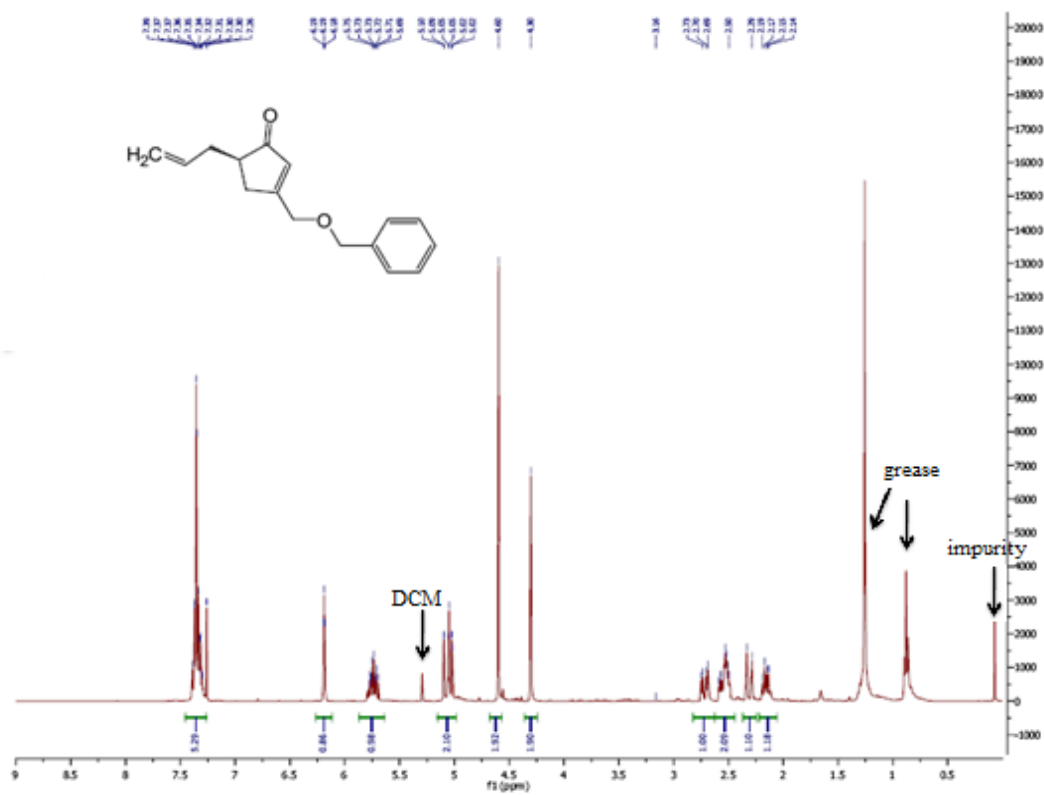


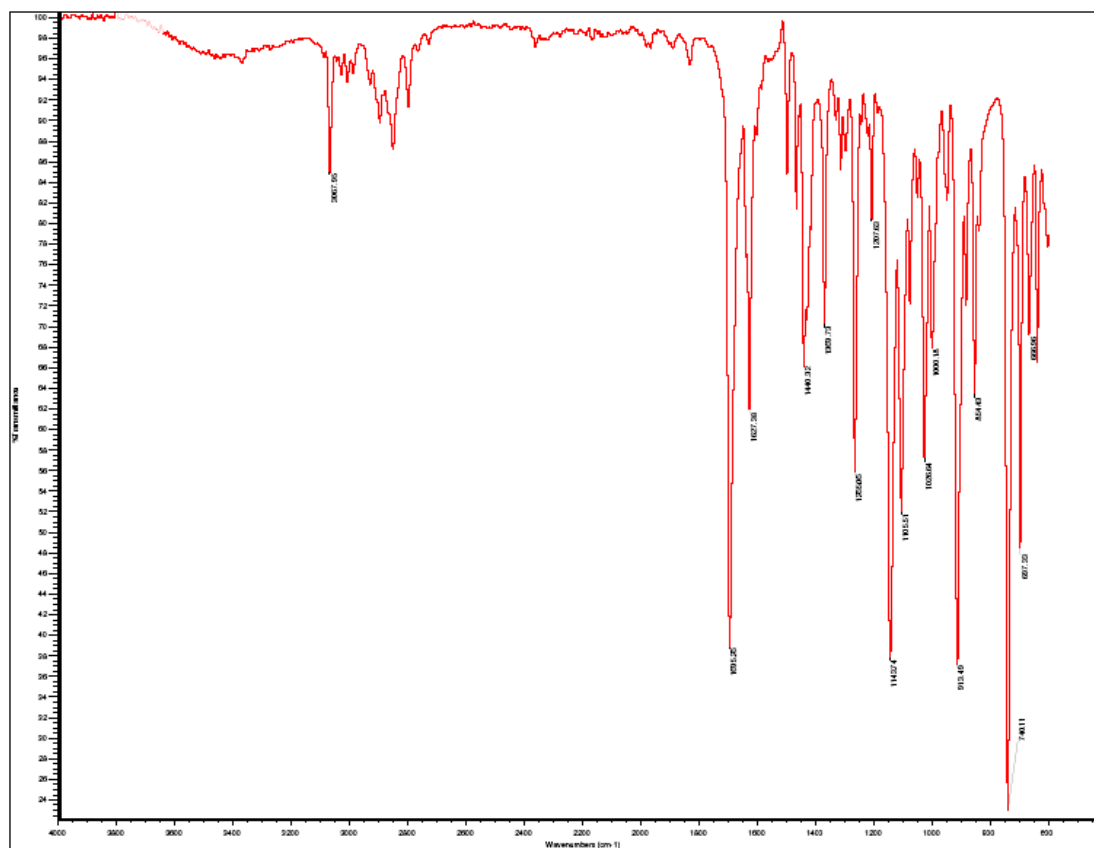
Compound 2-39



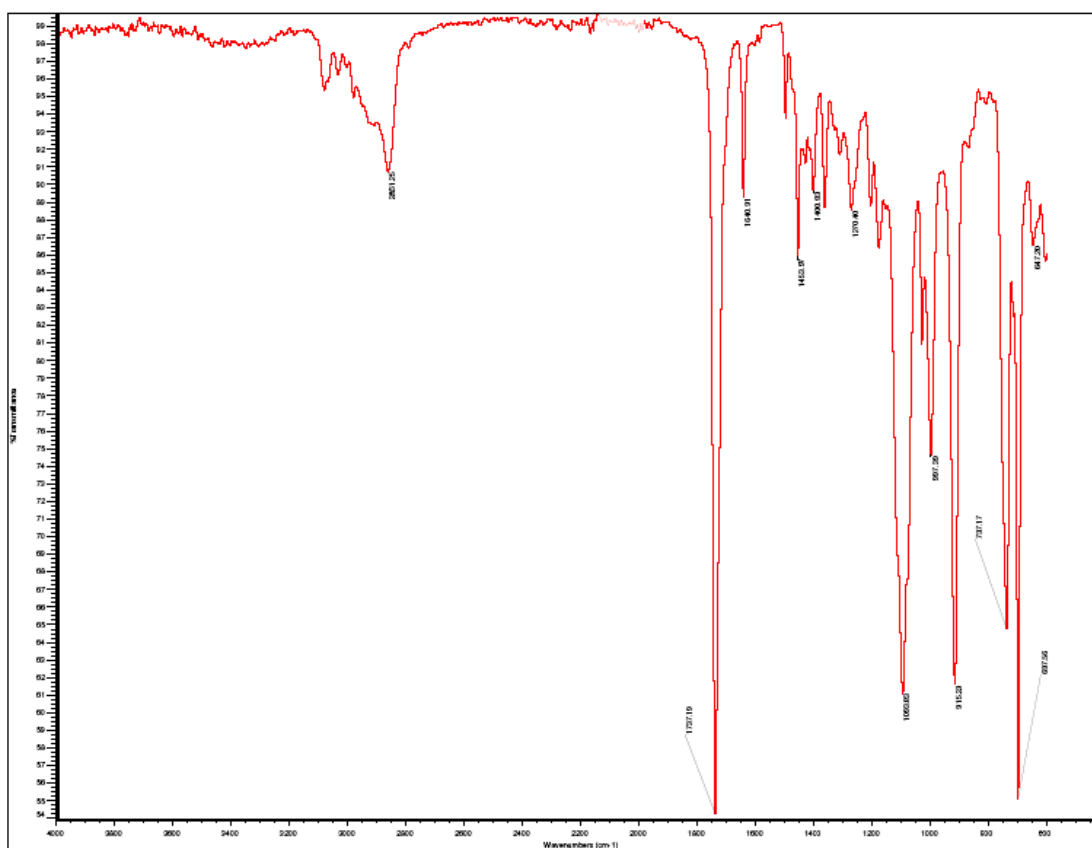
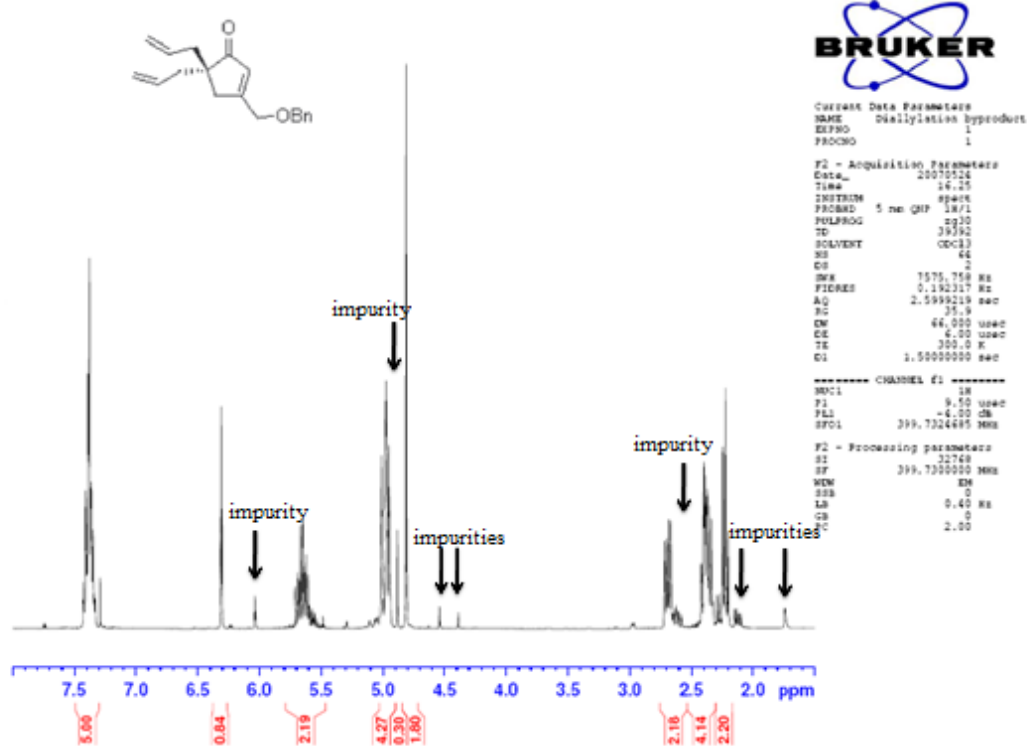


Compound 2-40

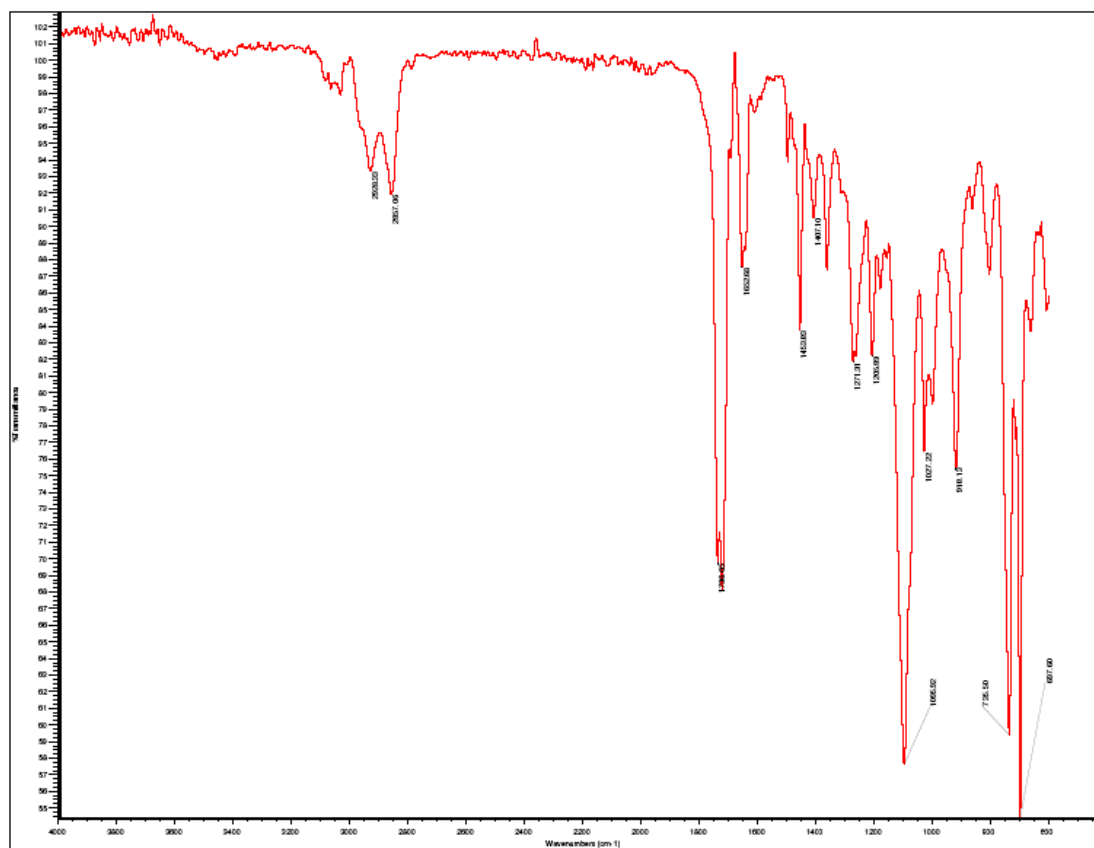
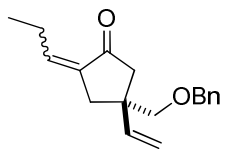




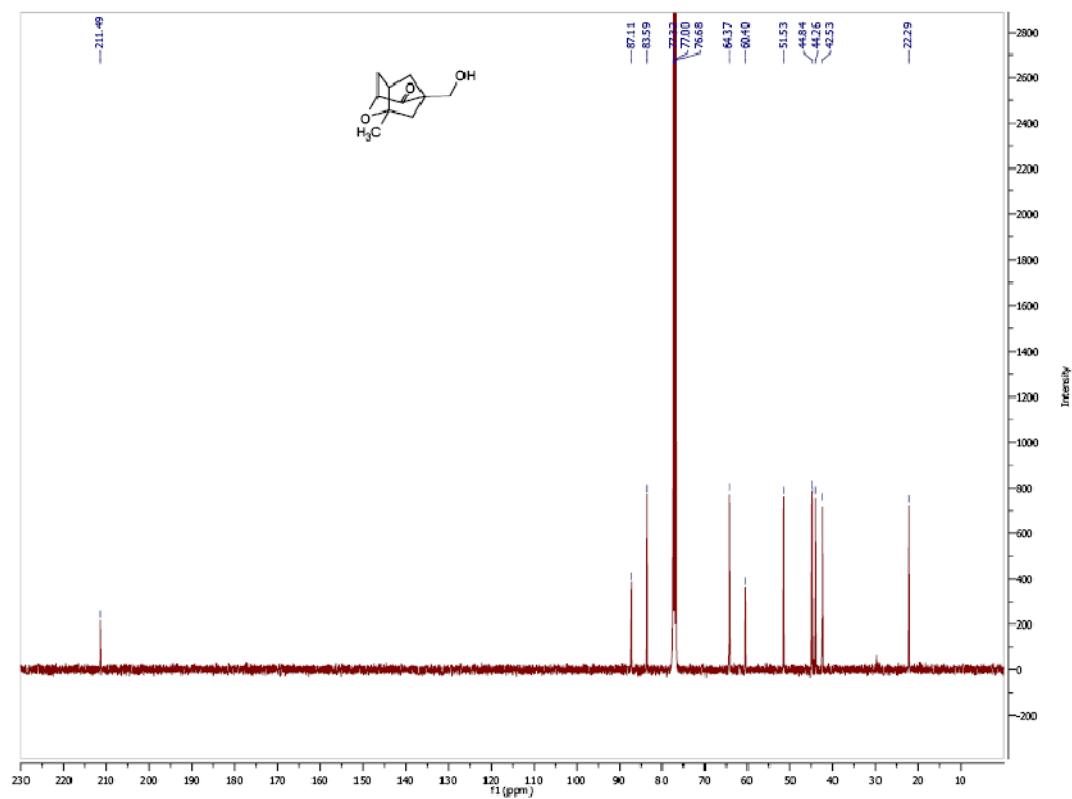
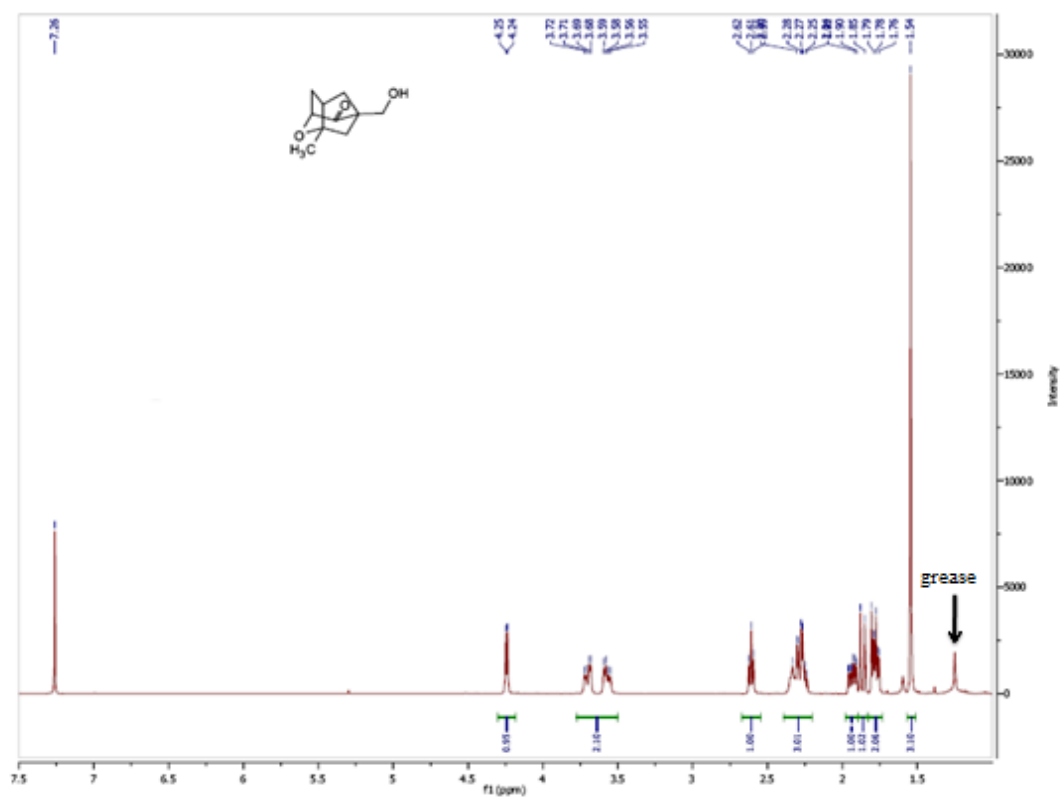
Compound 2-41

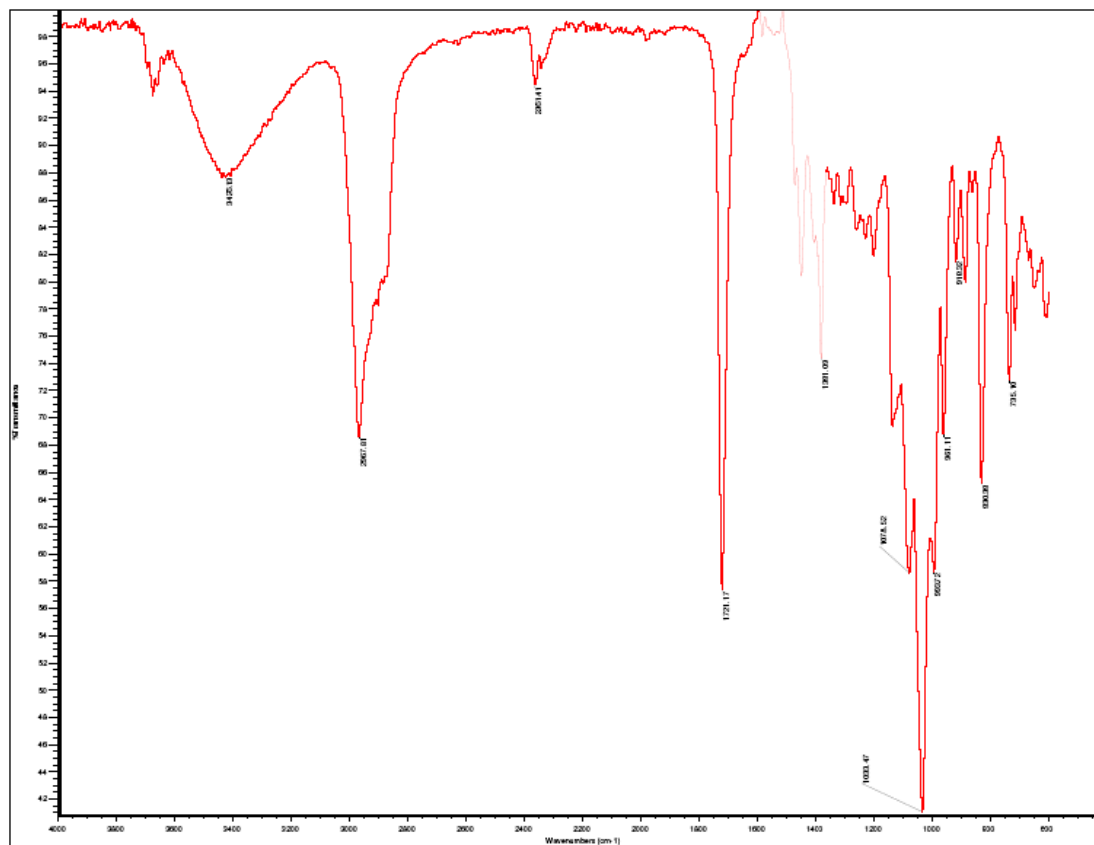


Compound 2-43

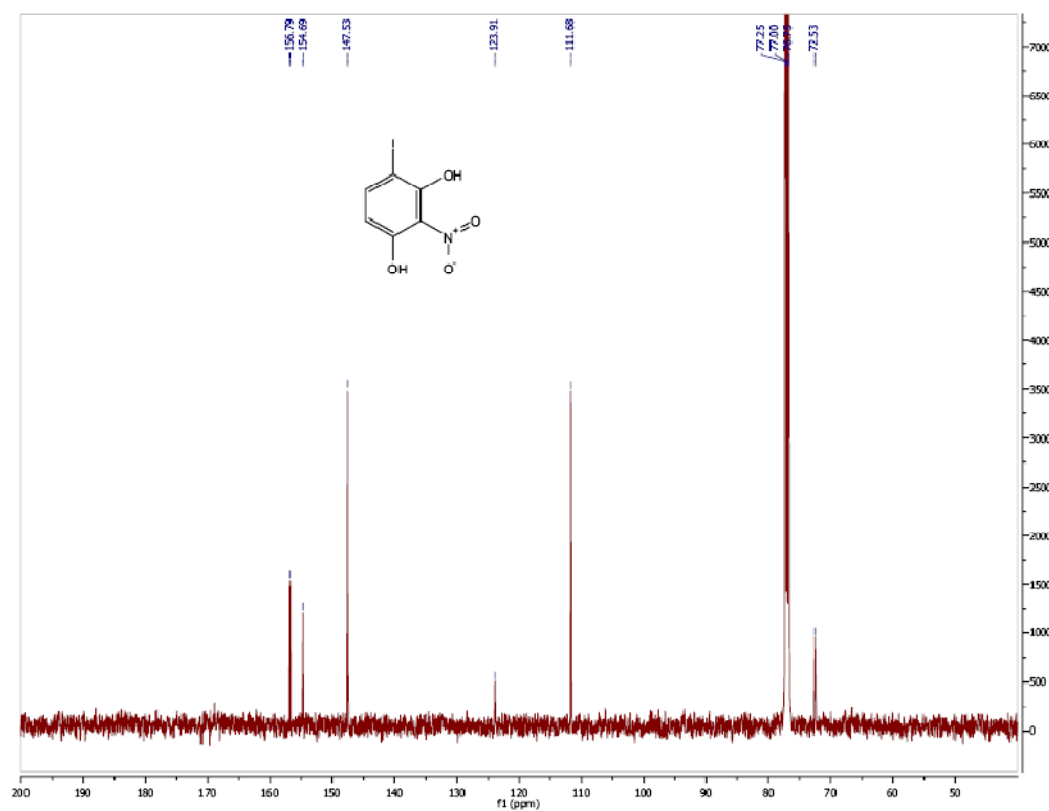
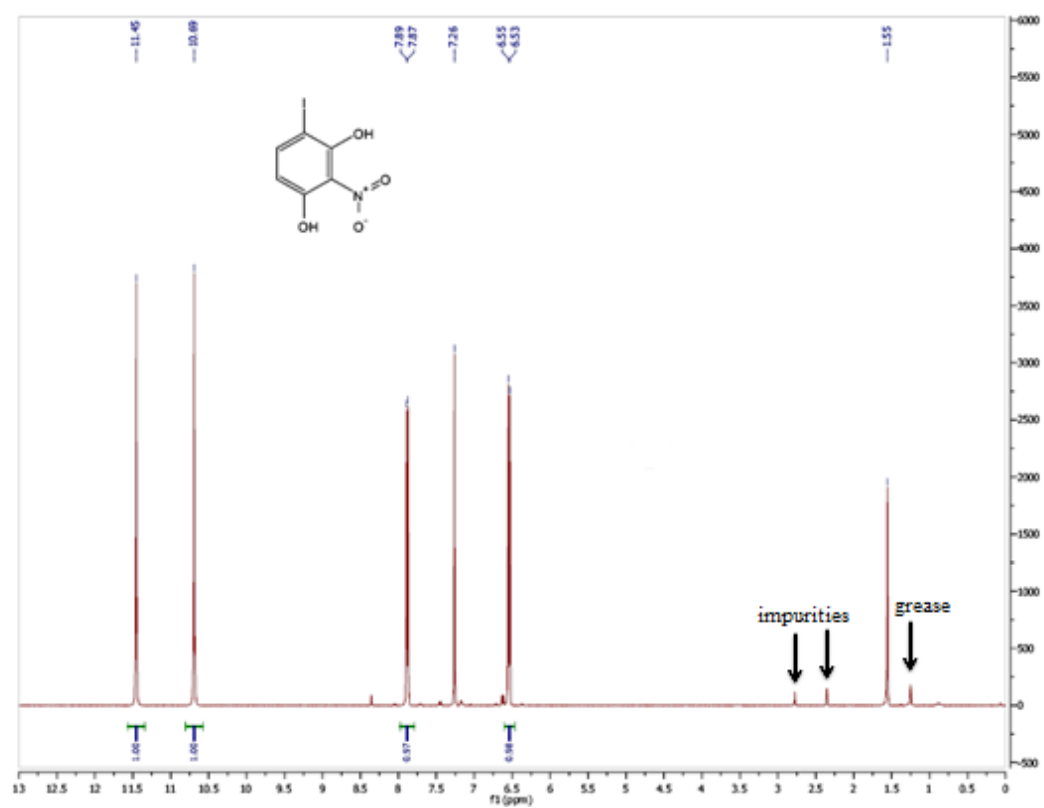


Compound 2-44

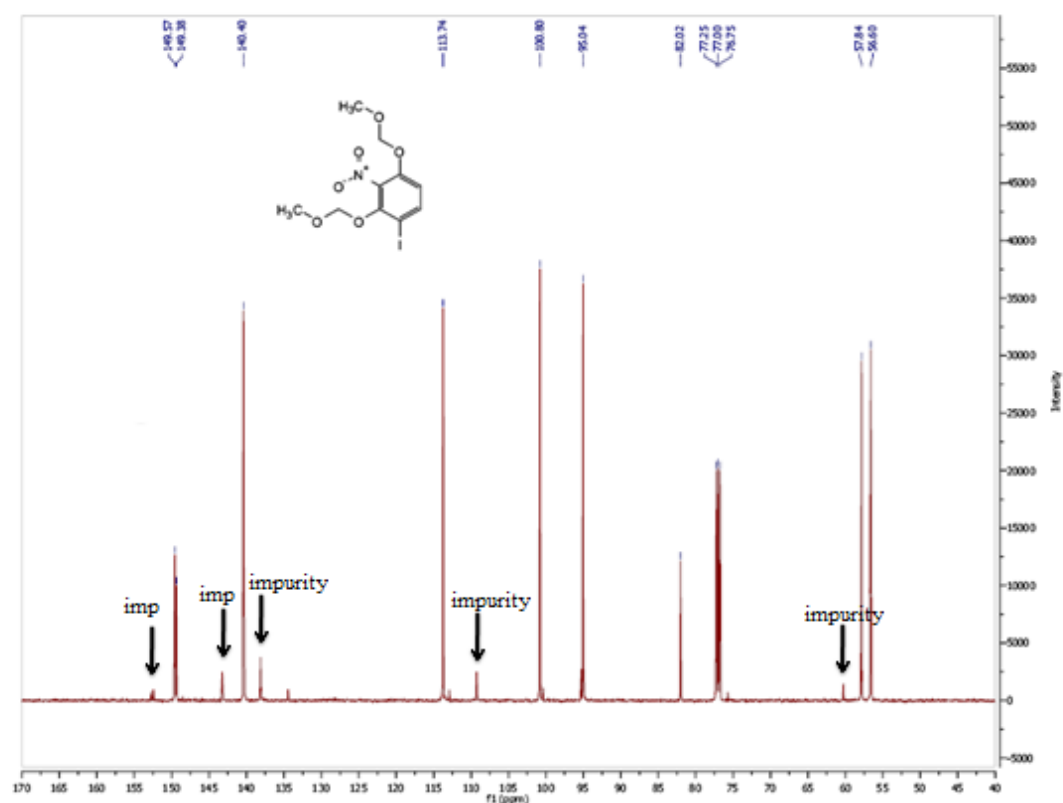
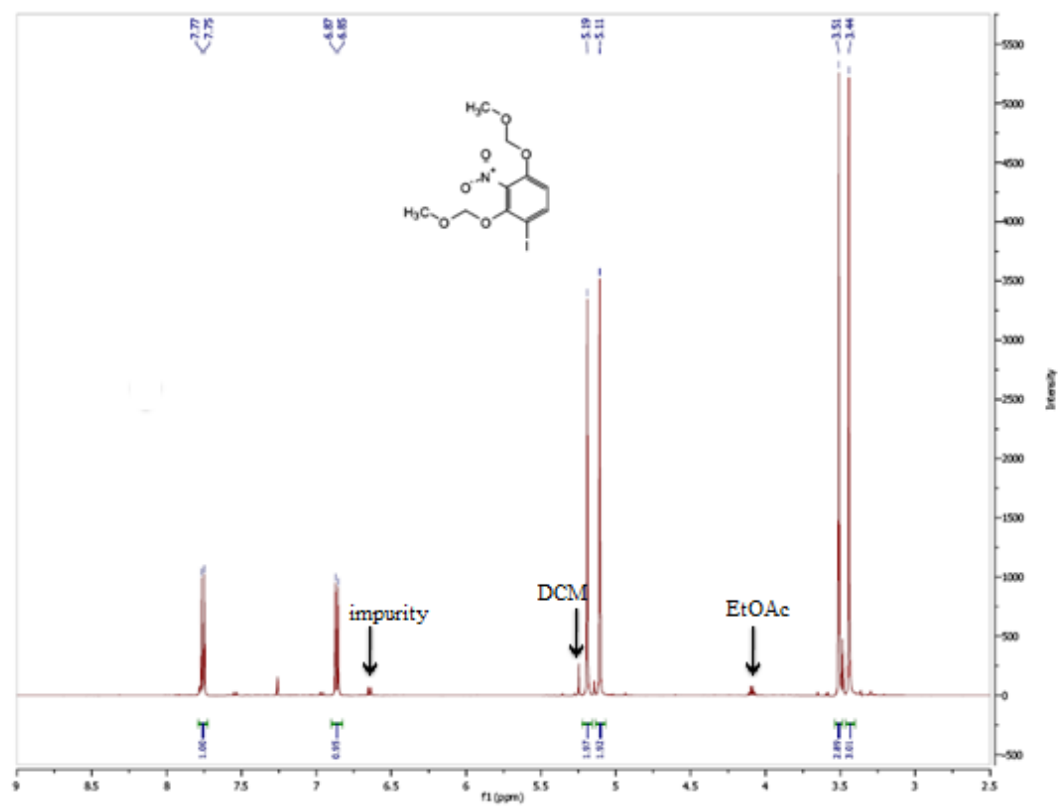


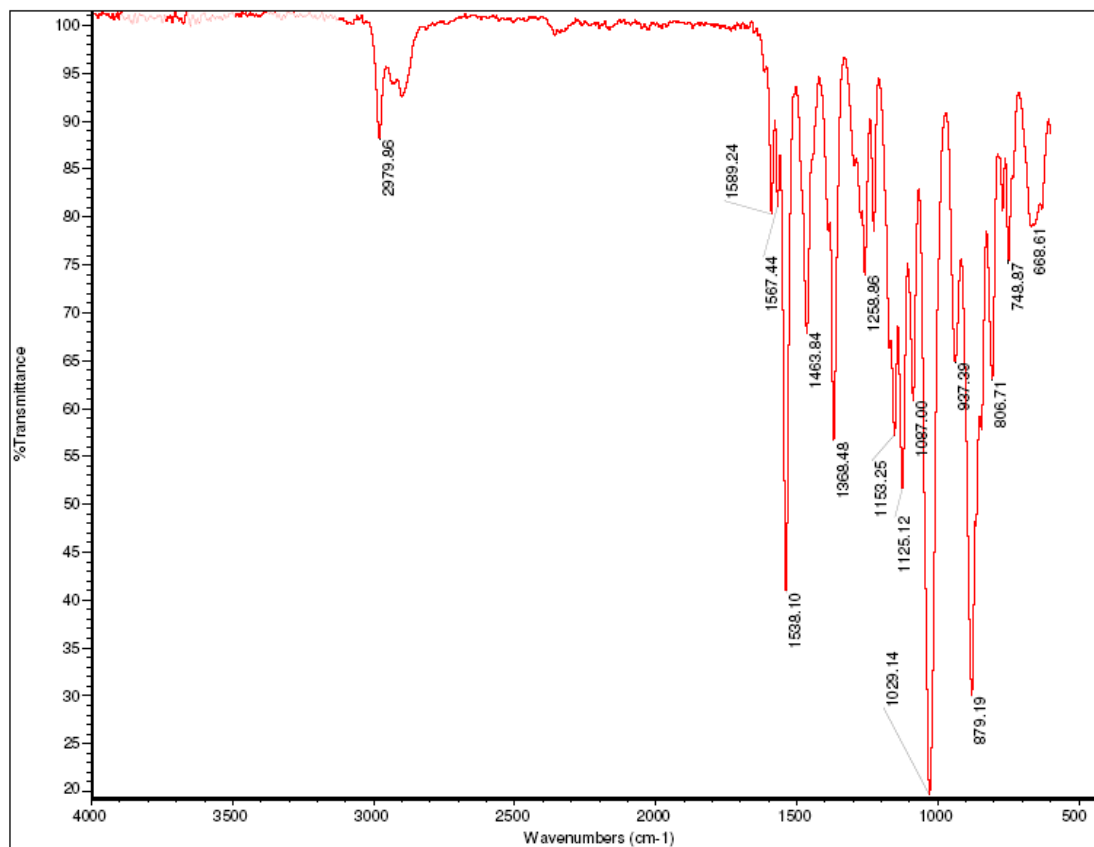


Compound 2-45b

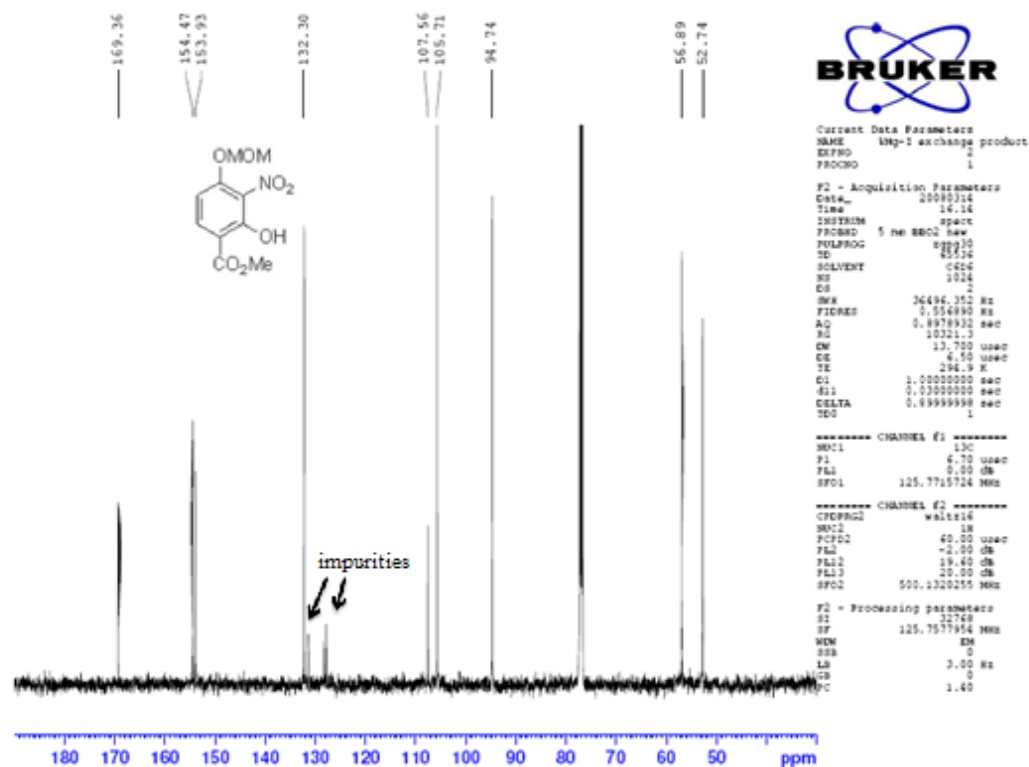
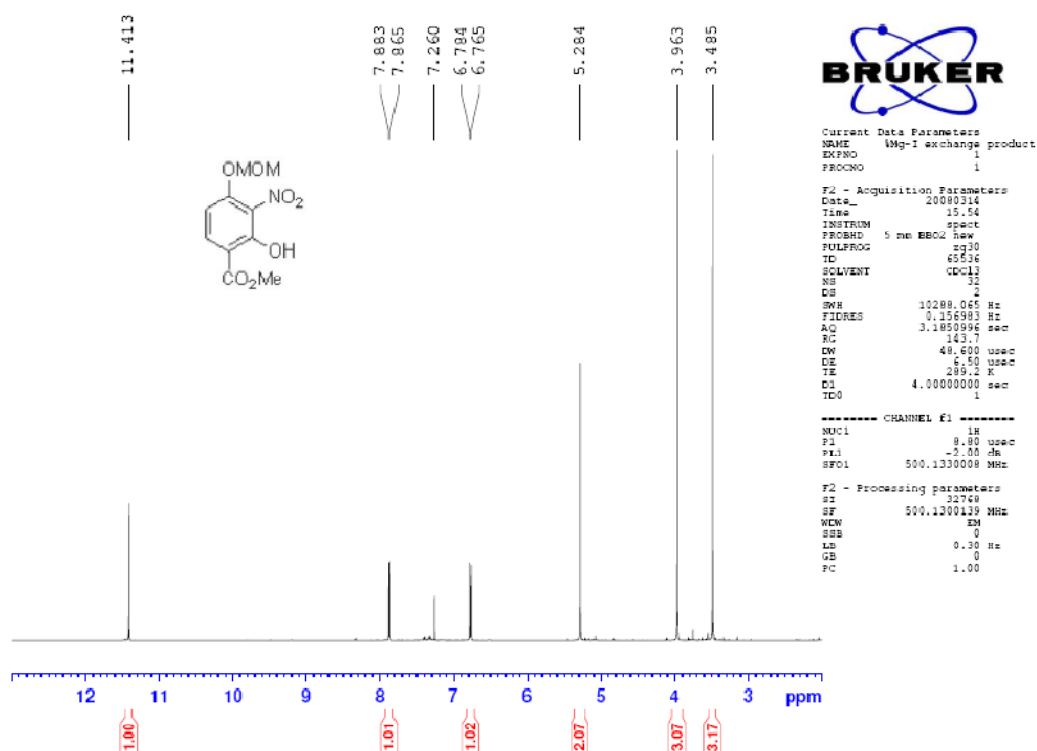


Compound 2-46

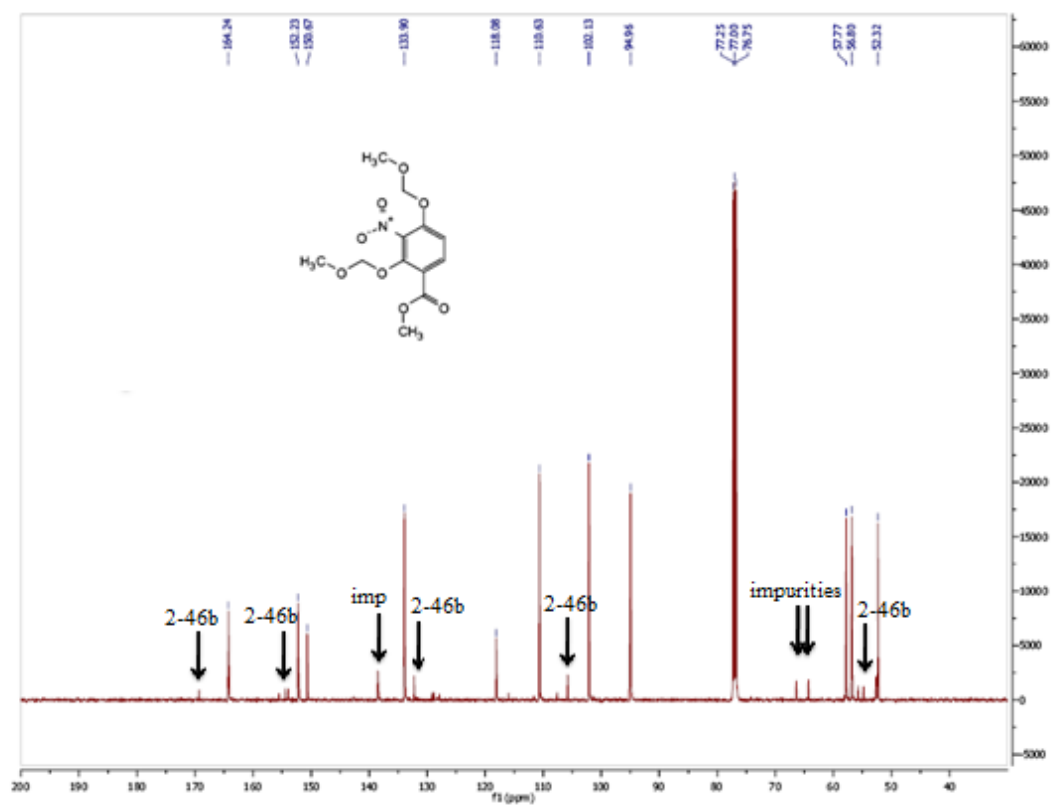
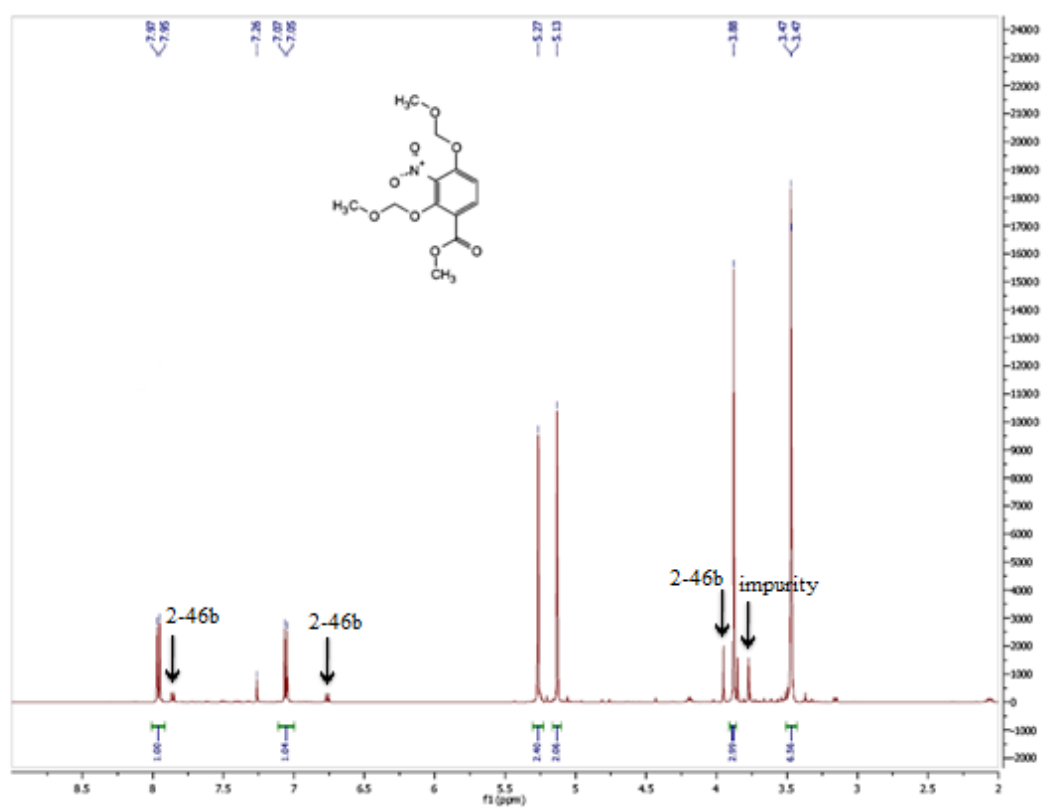


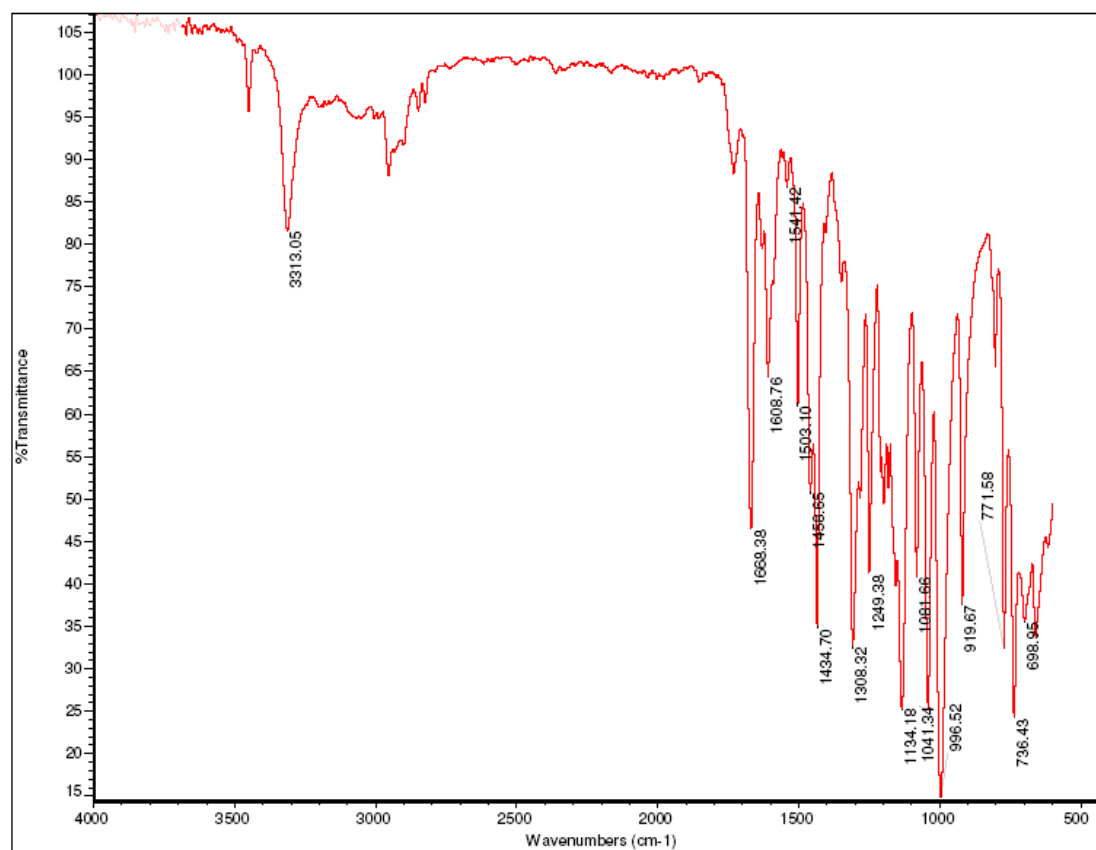


Compound 2-46b

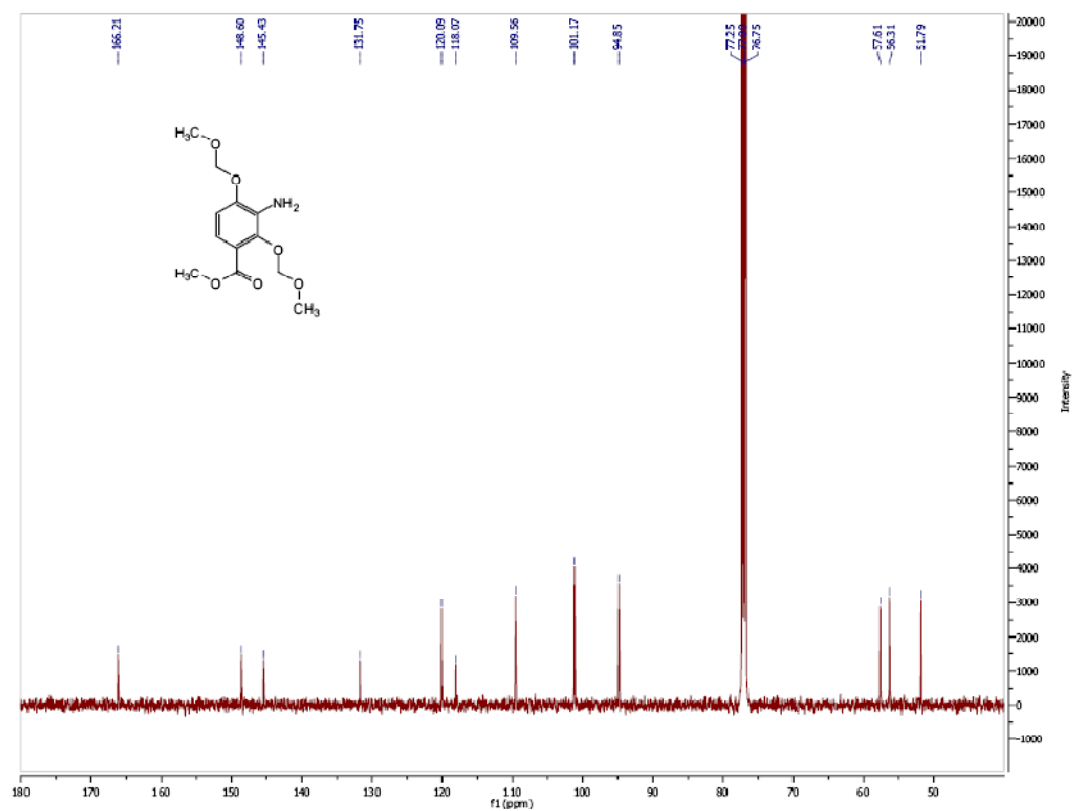
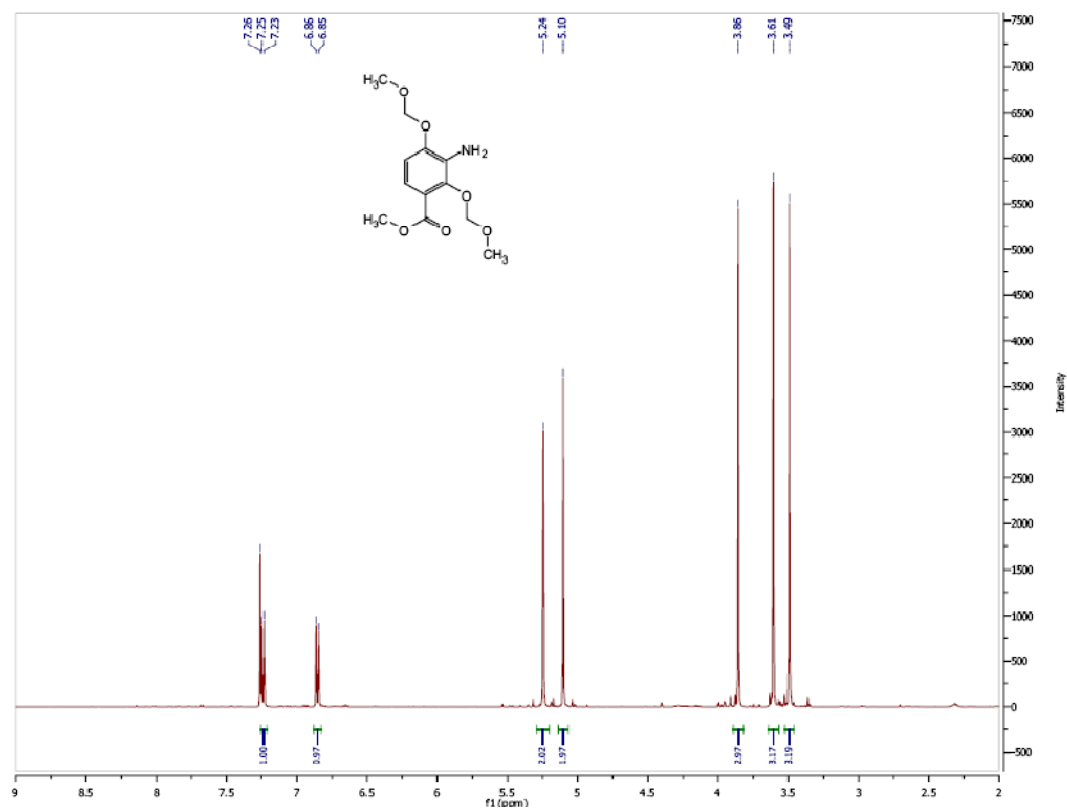


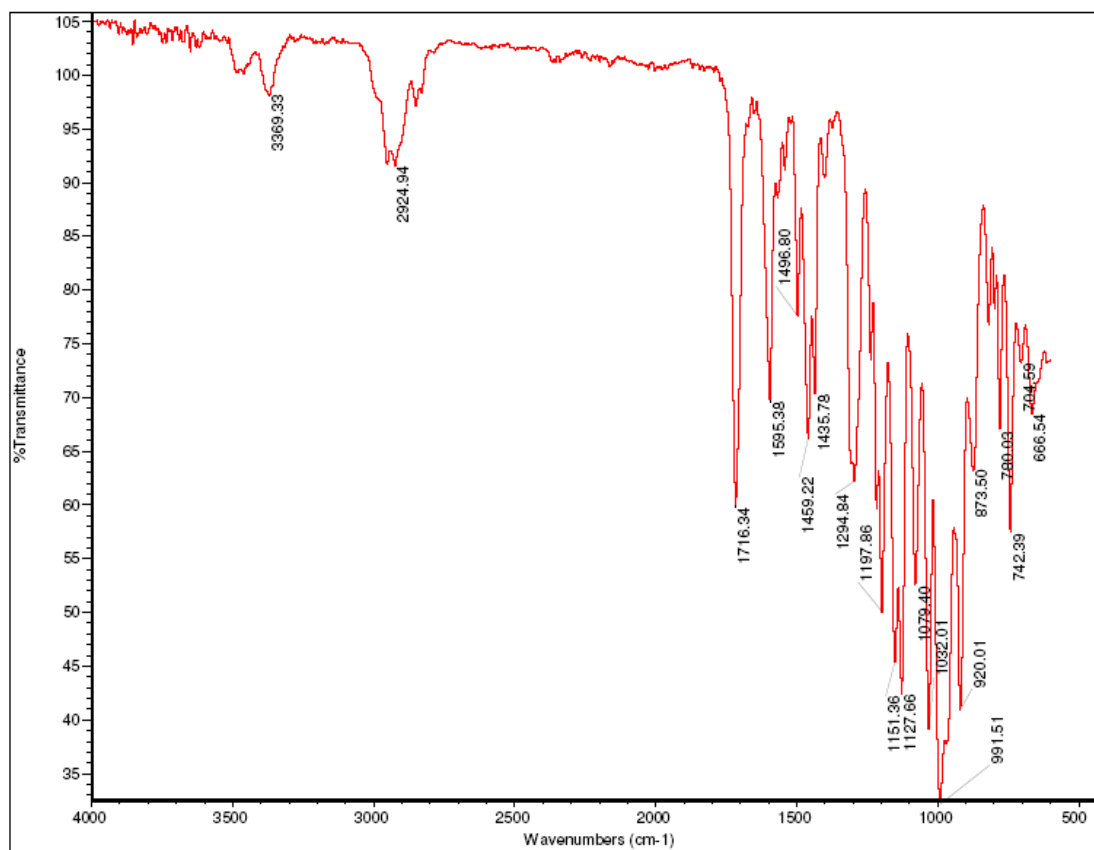
Compound 2-47



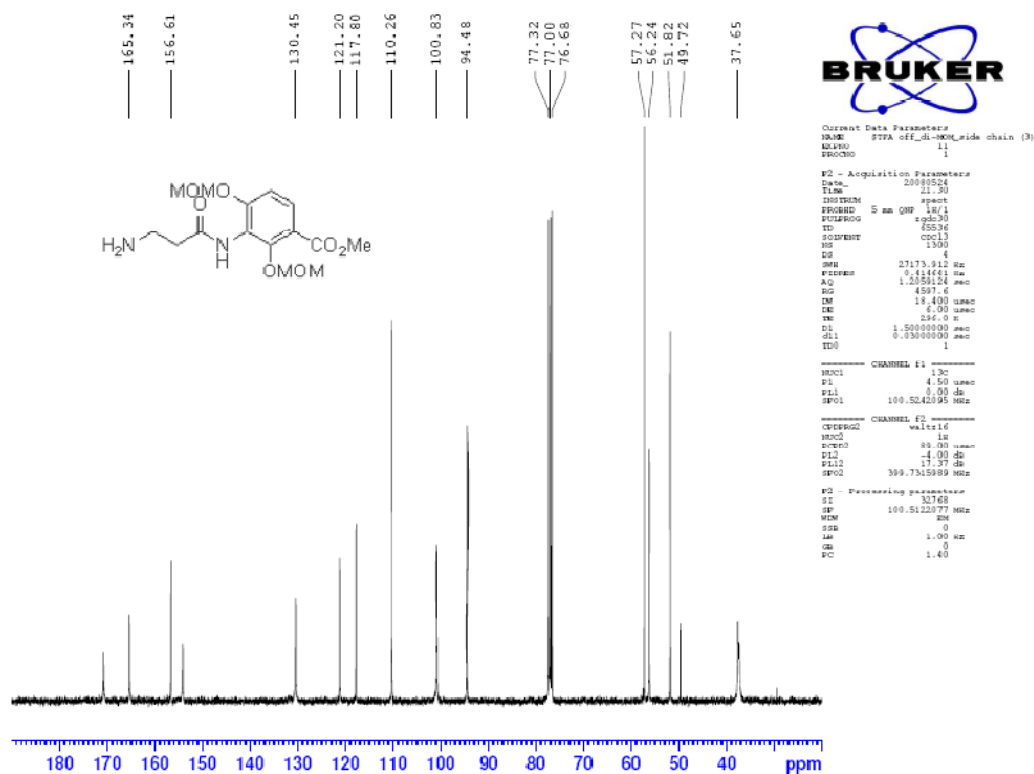
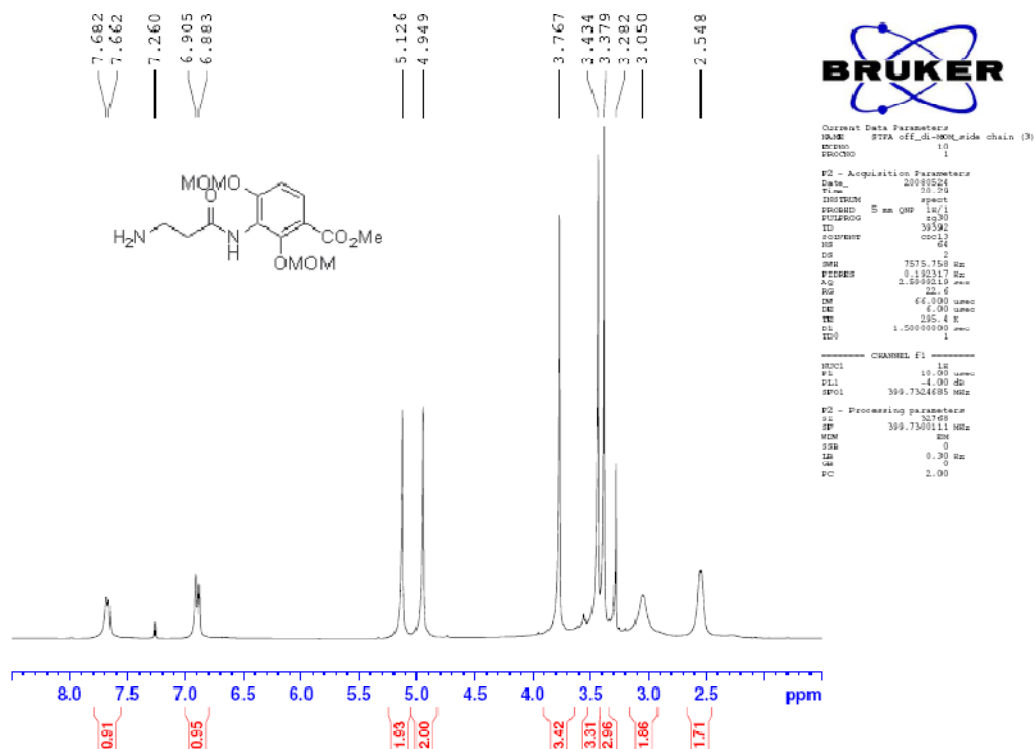


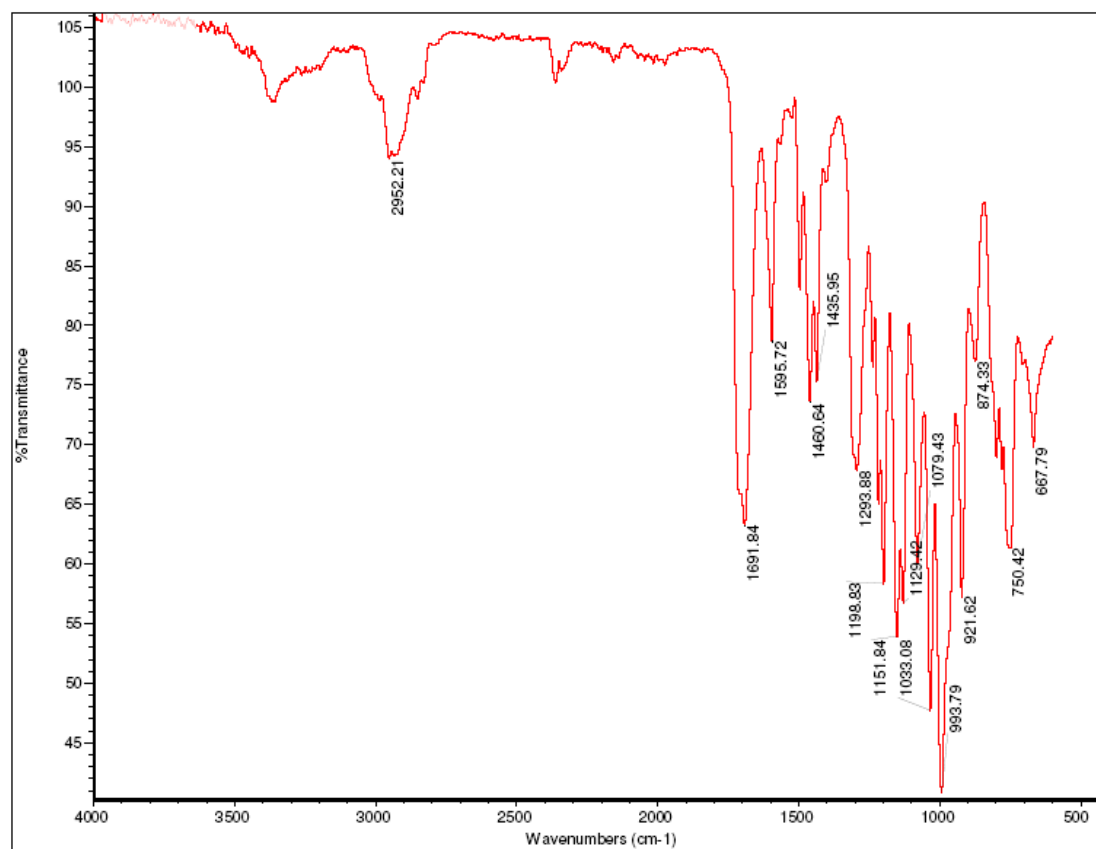
Compound 2-48



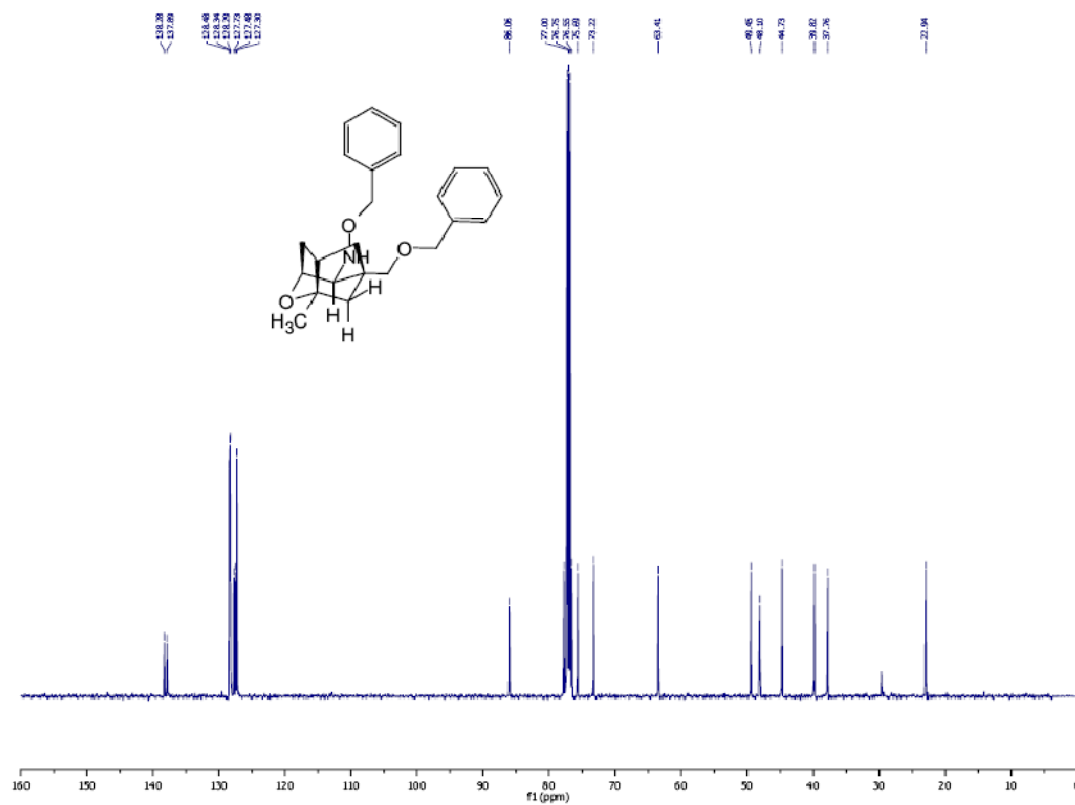
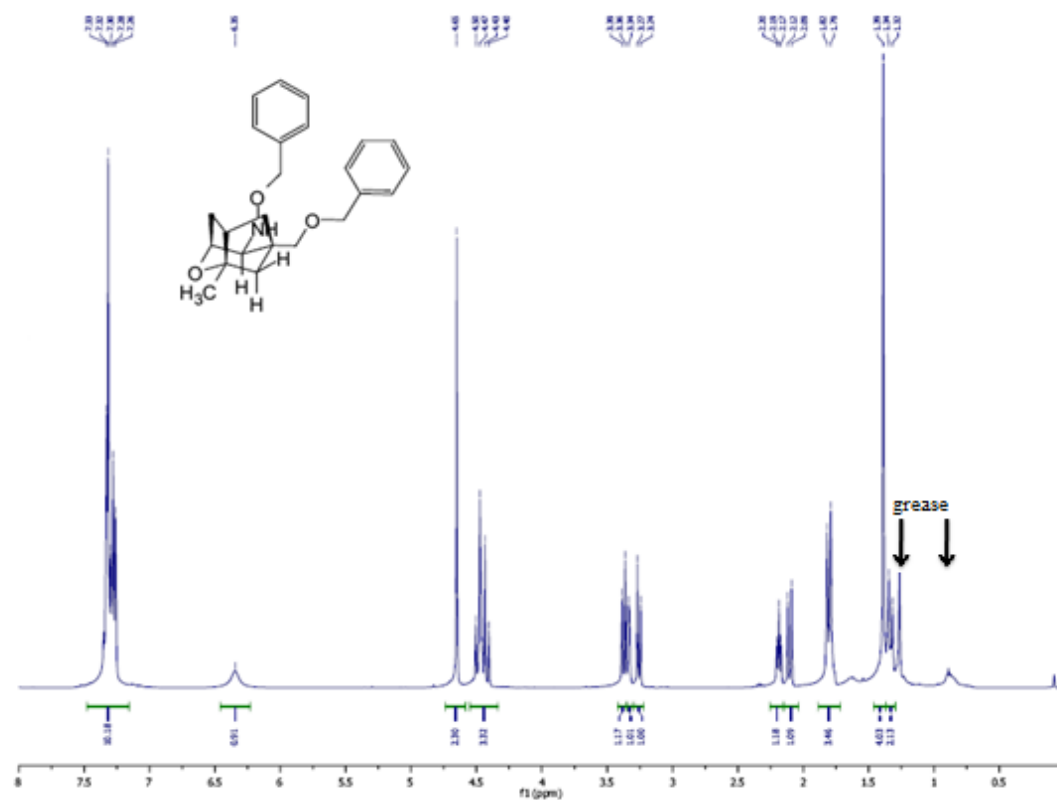


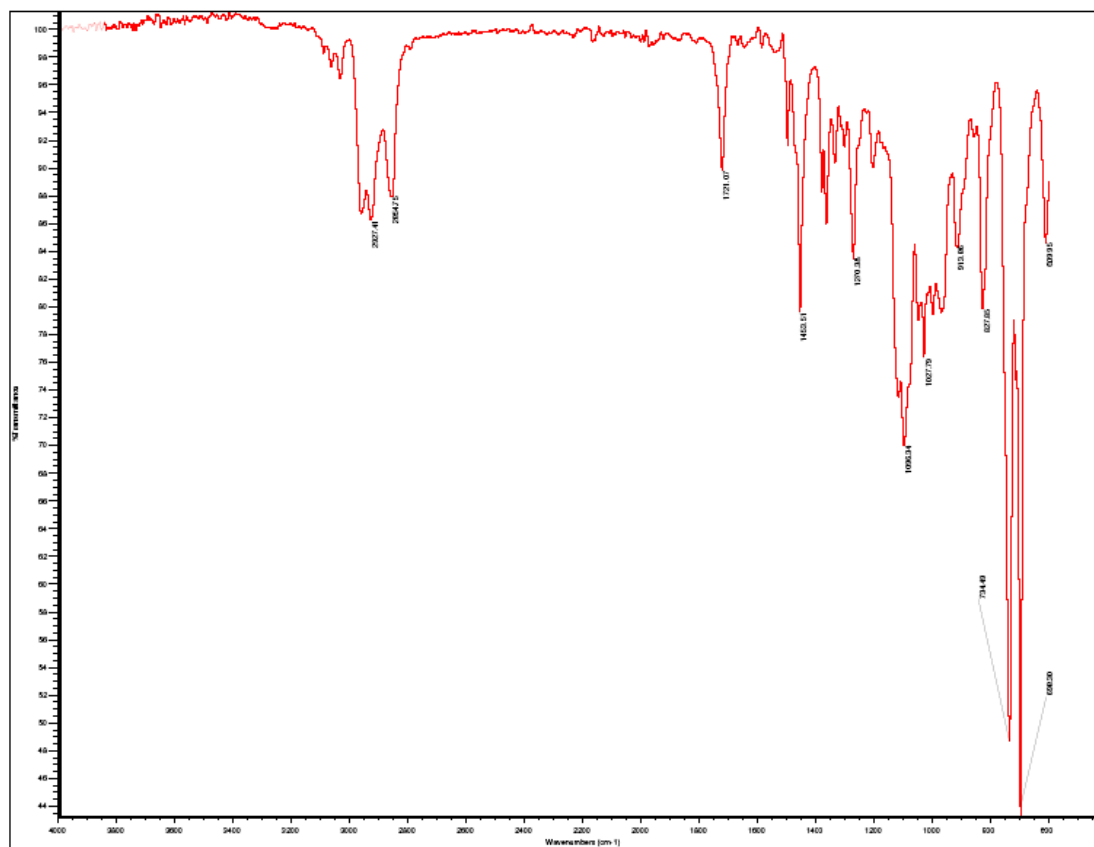
Compound 2-50



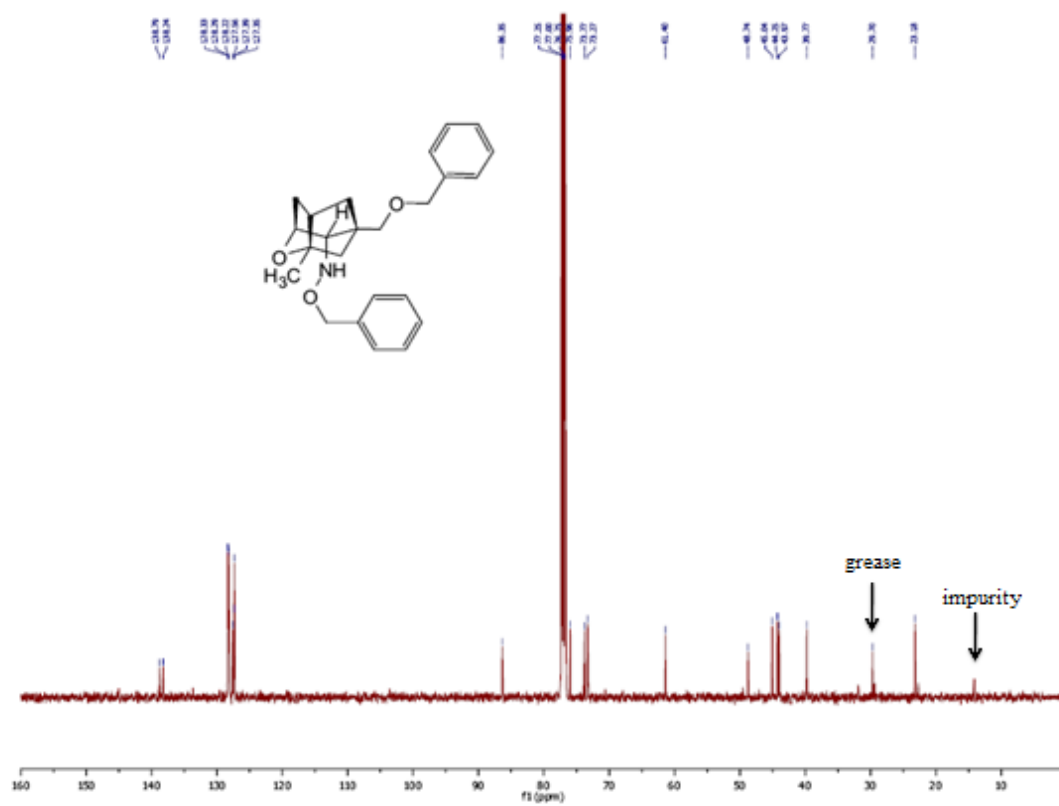
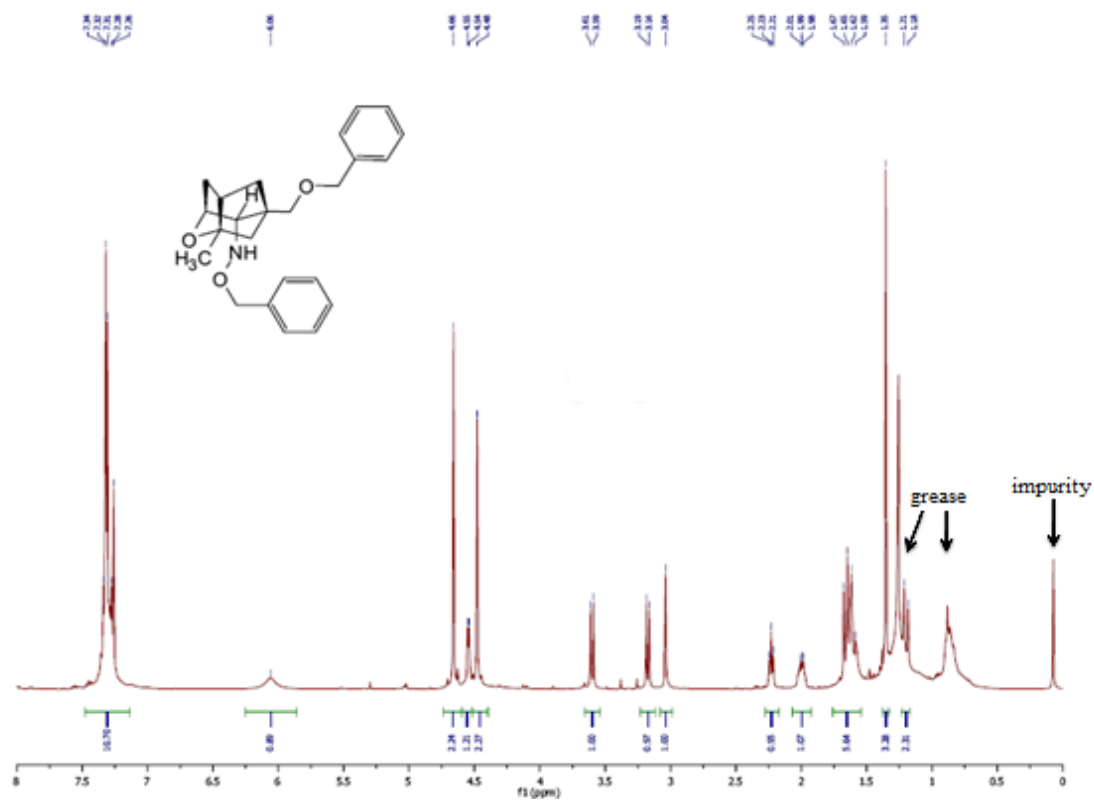


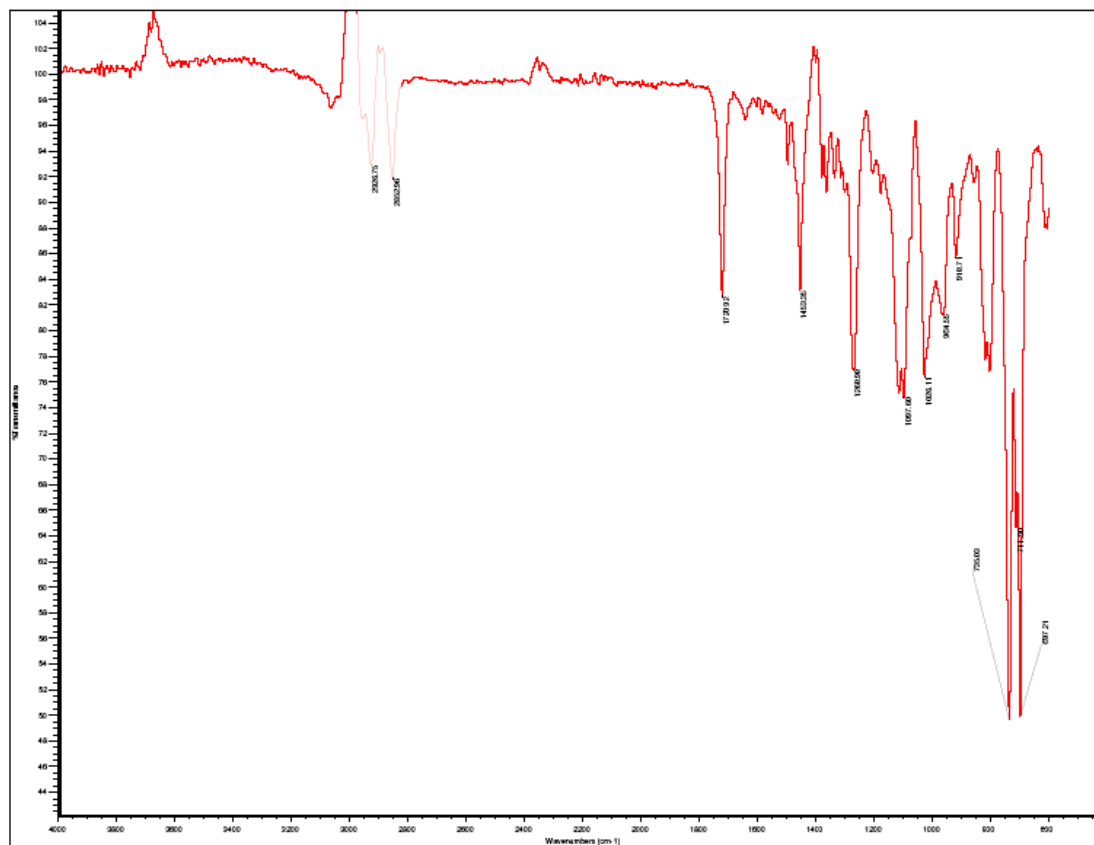
Compound 2-52



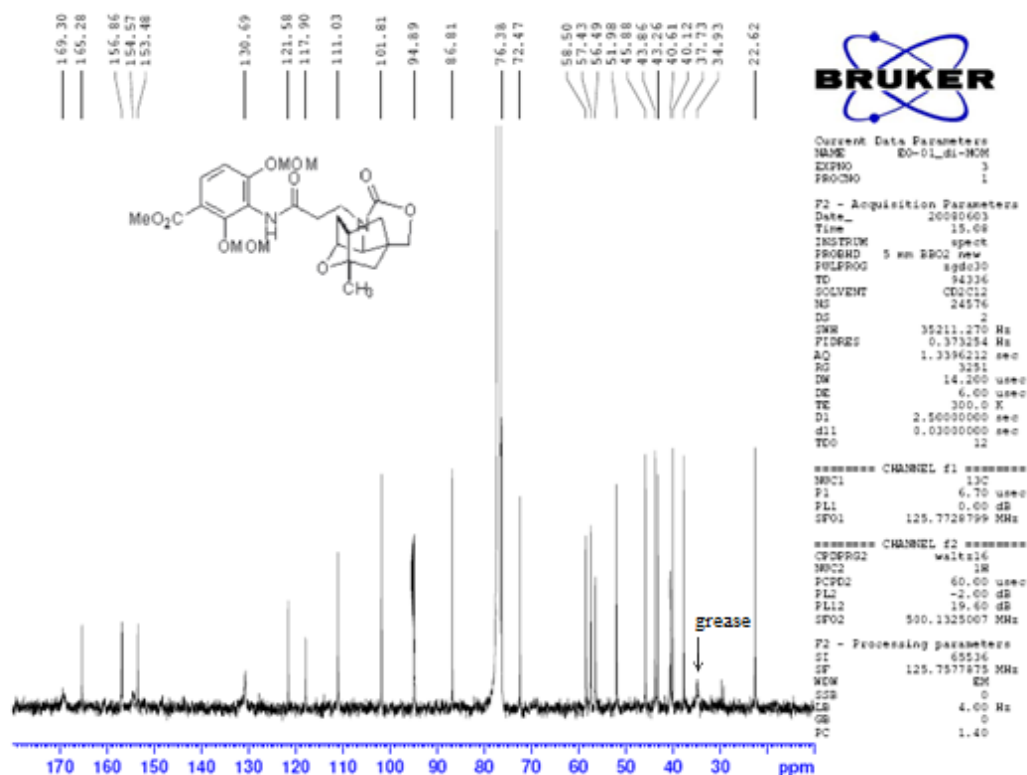
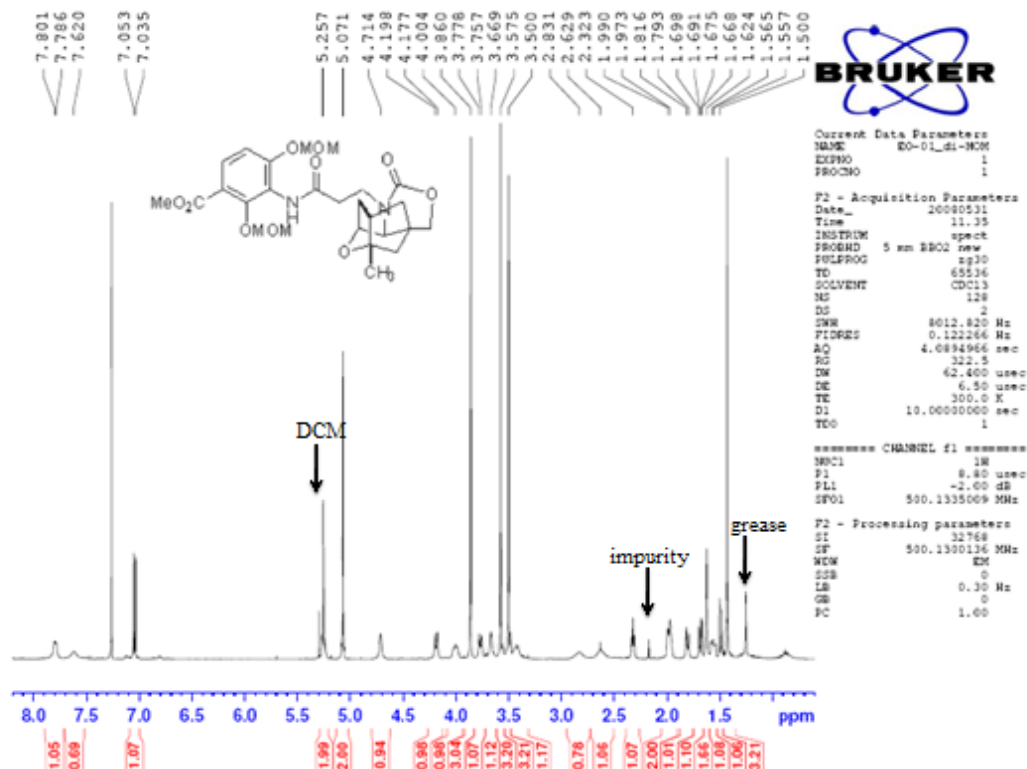


Compound 2-53

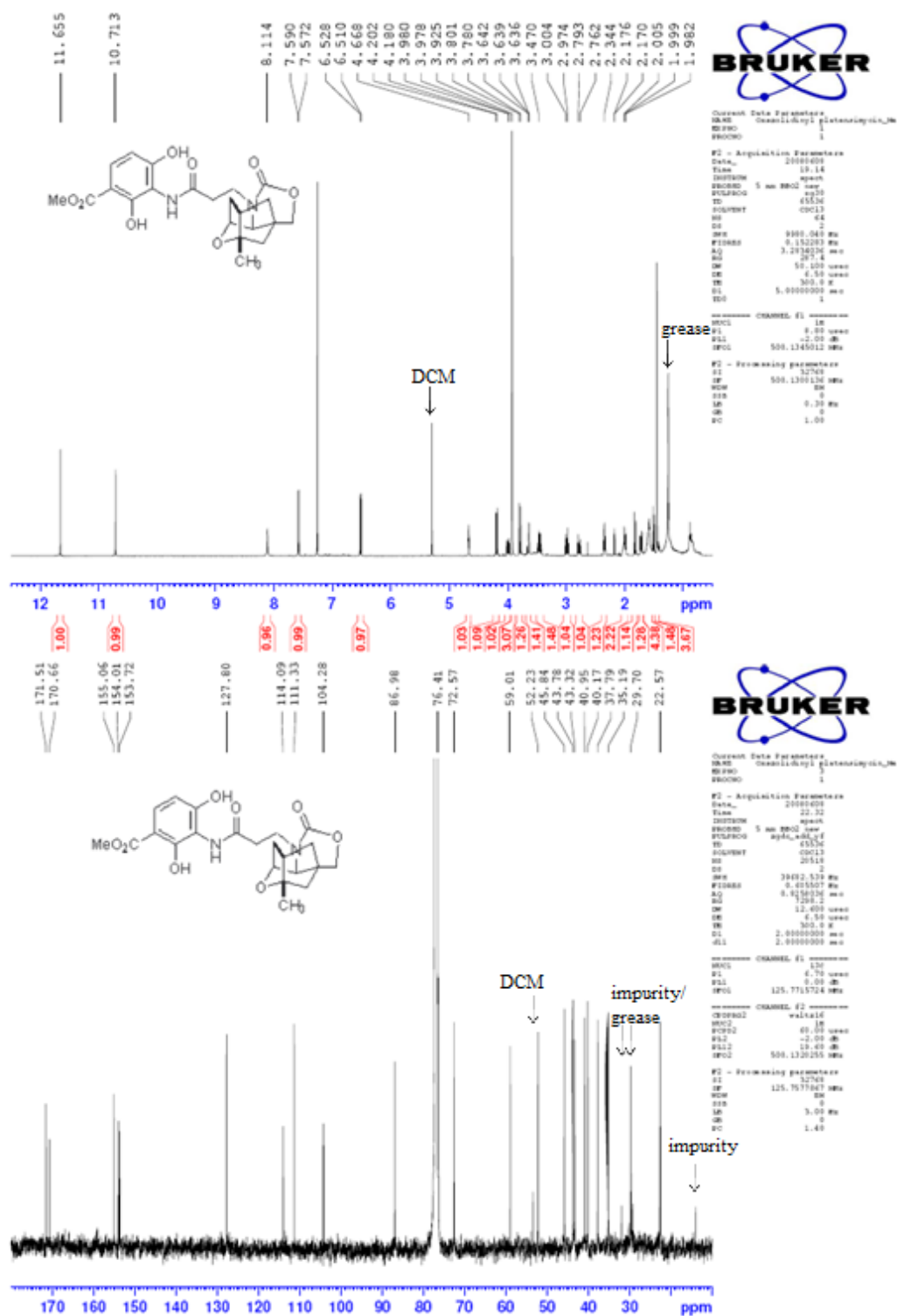




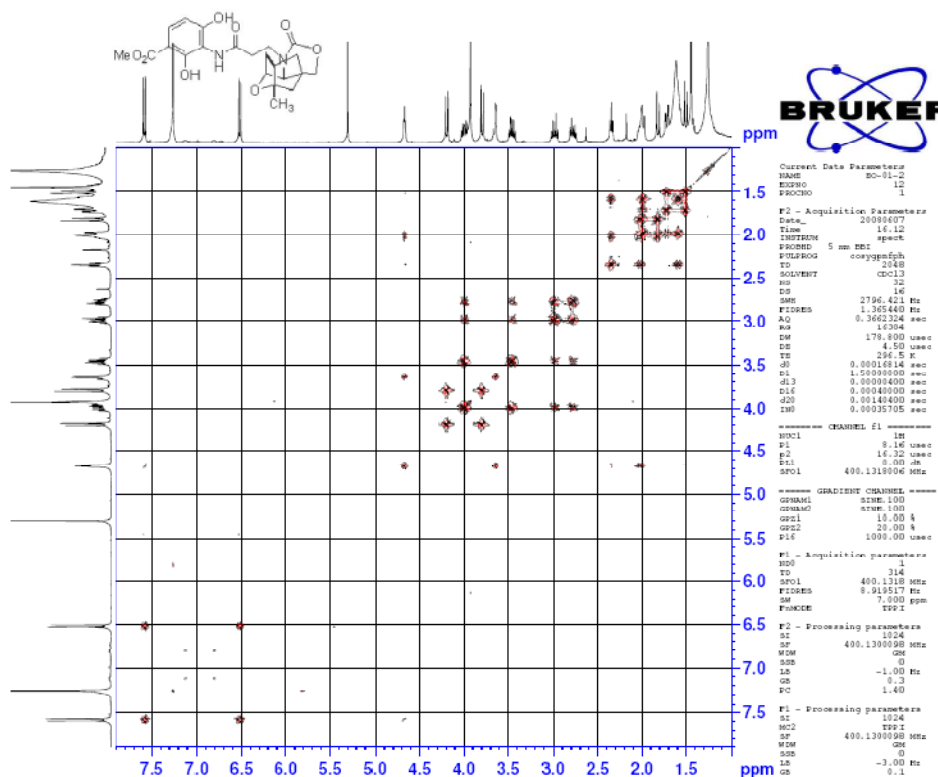
Compound 2-55



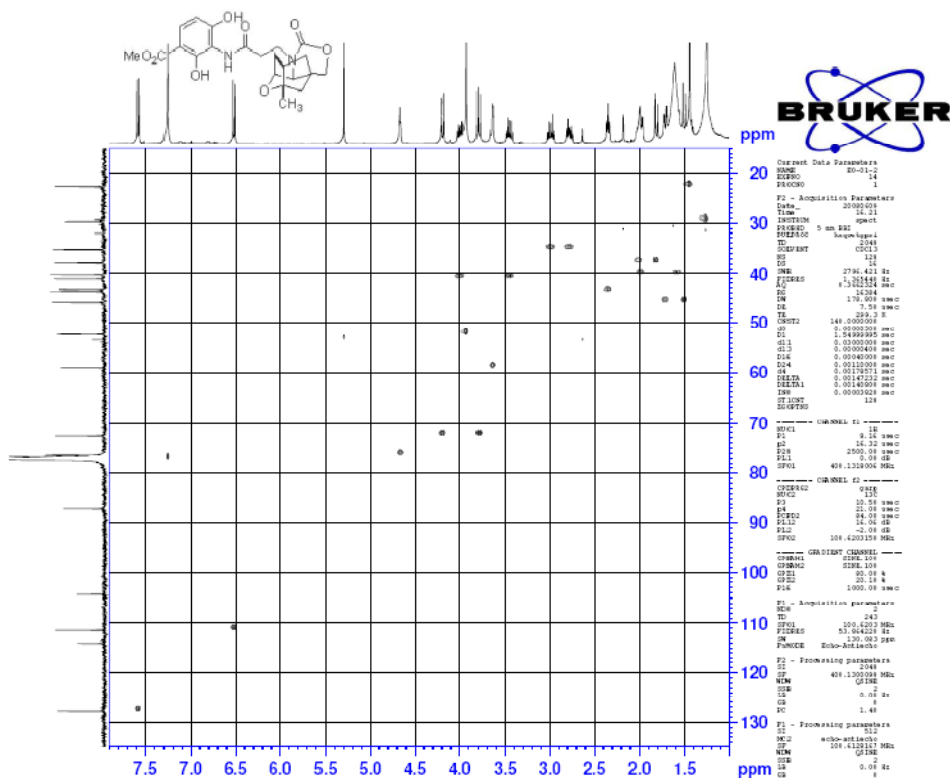
Compound 2-56



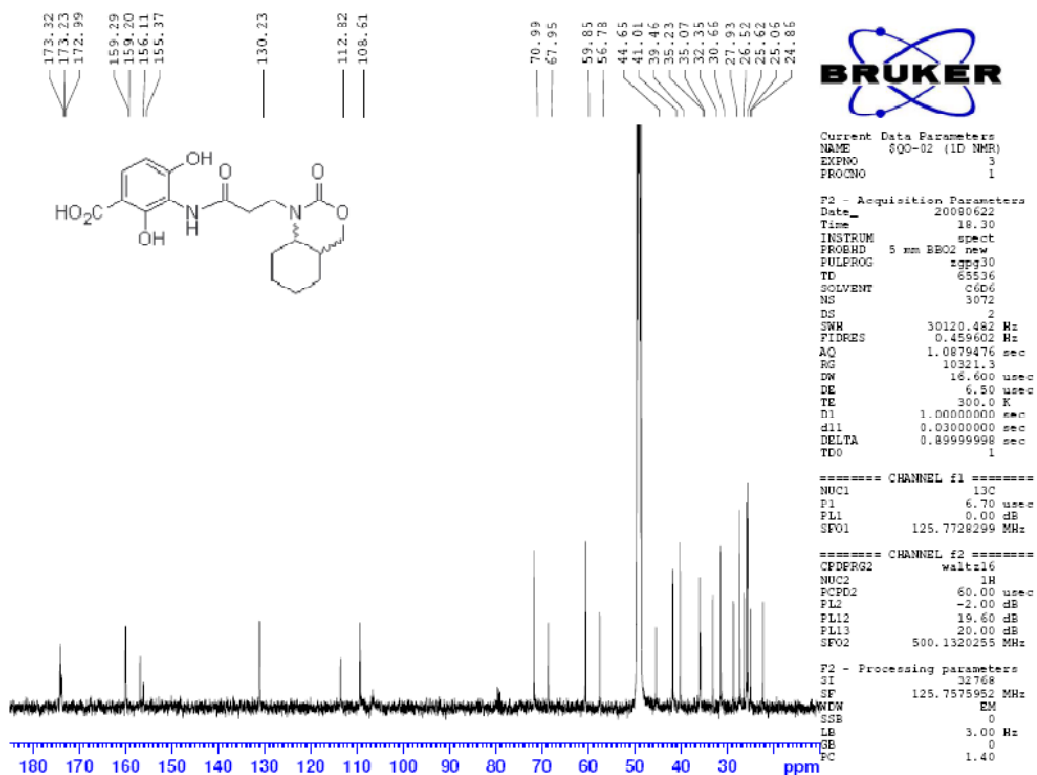
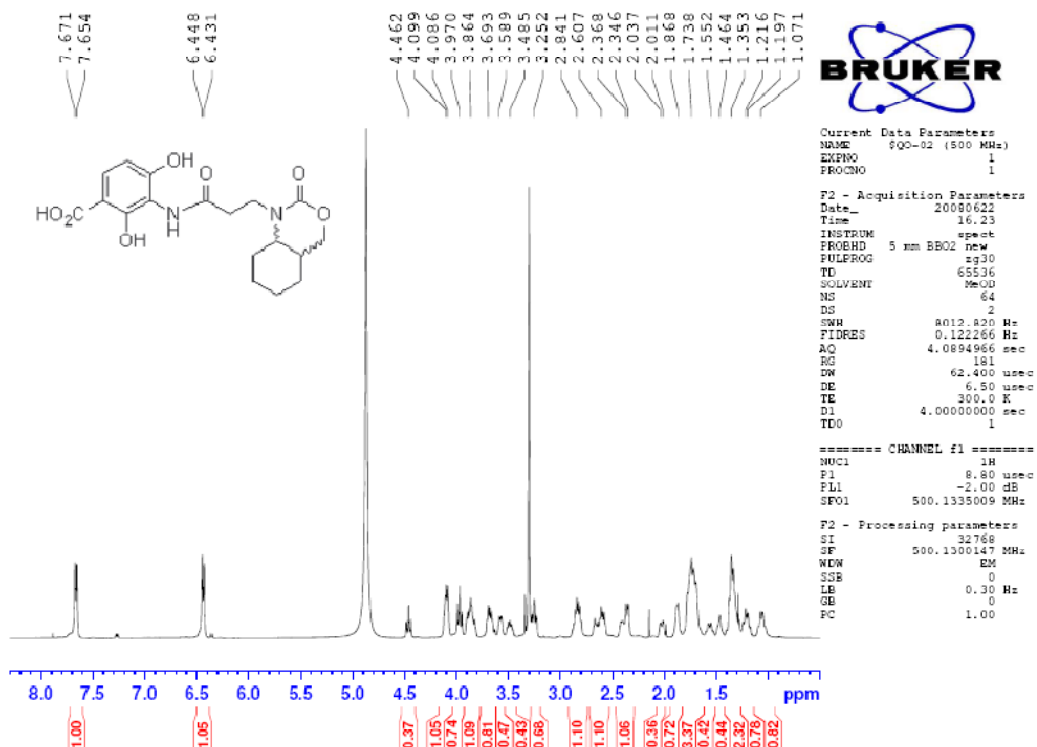
COSY



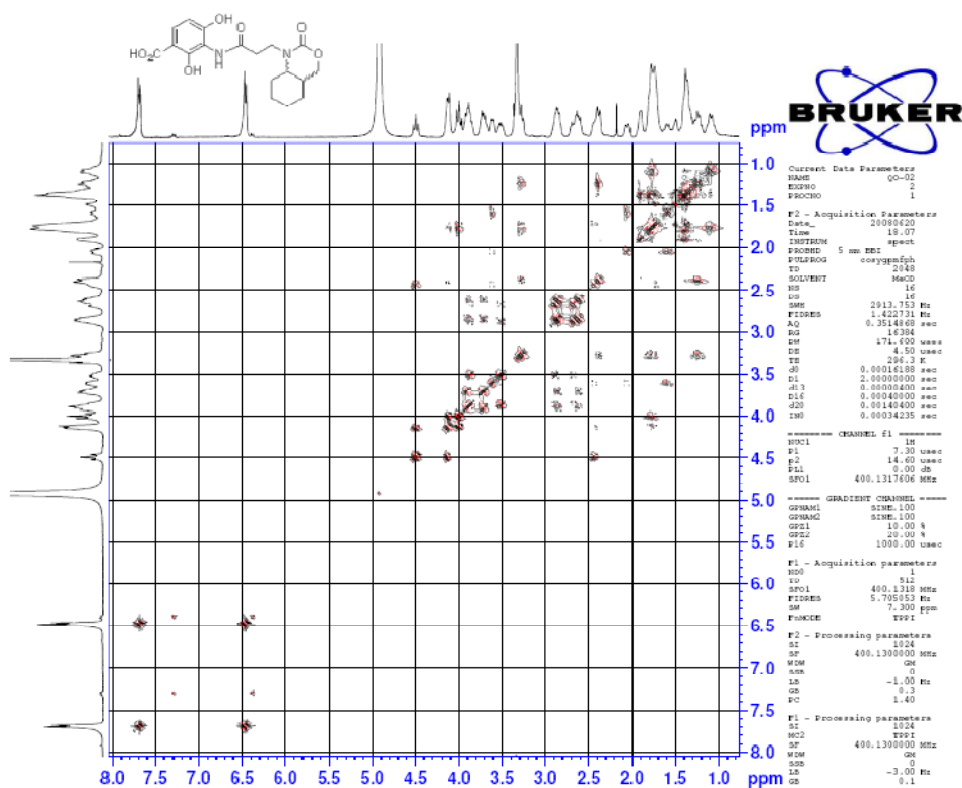
HSQC



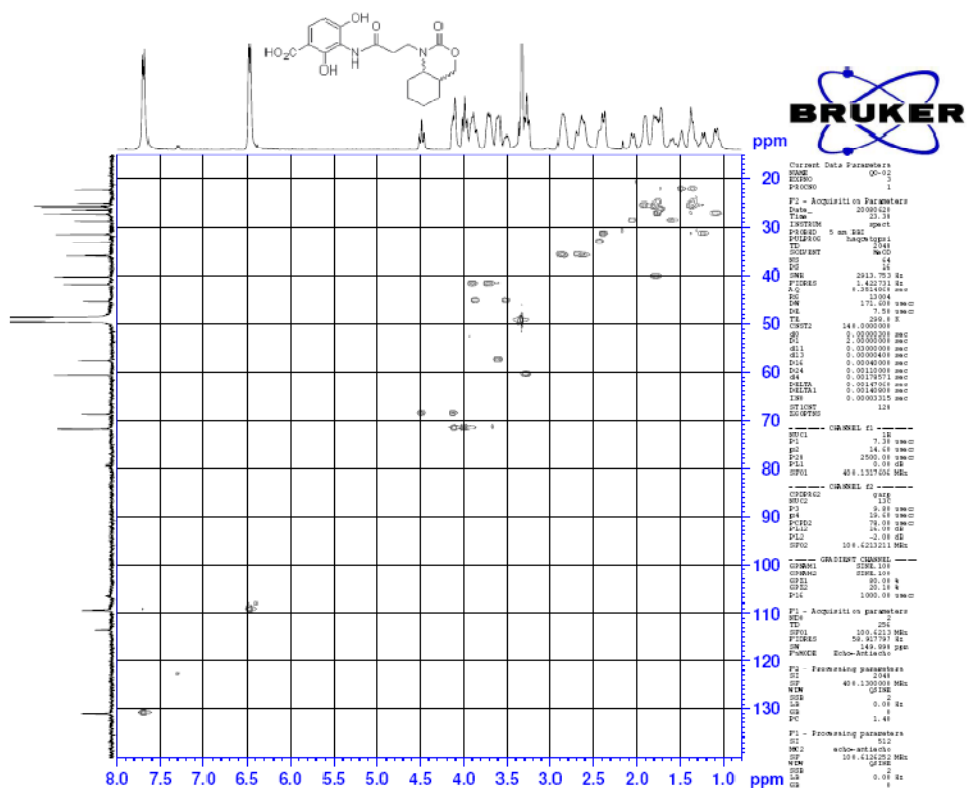
Compound 2-57



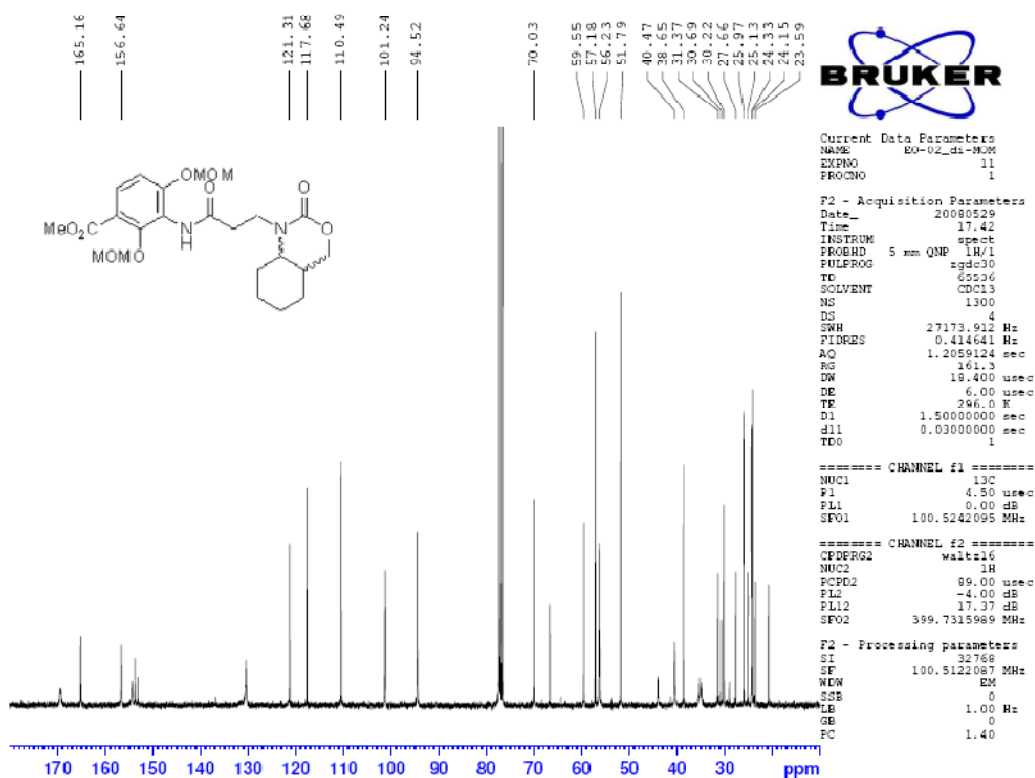
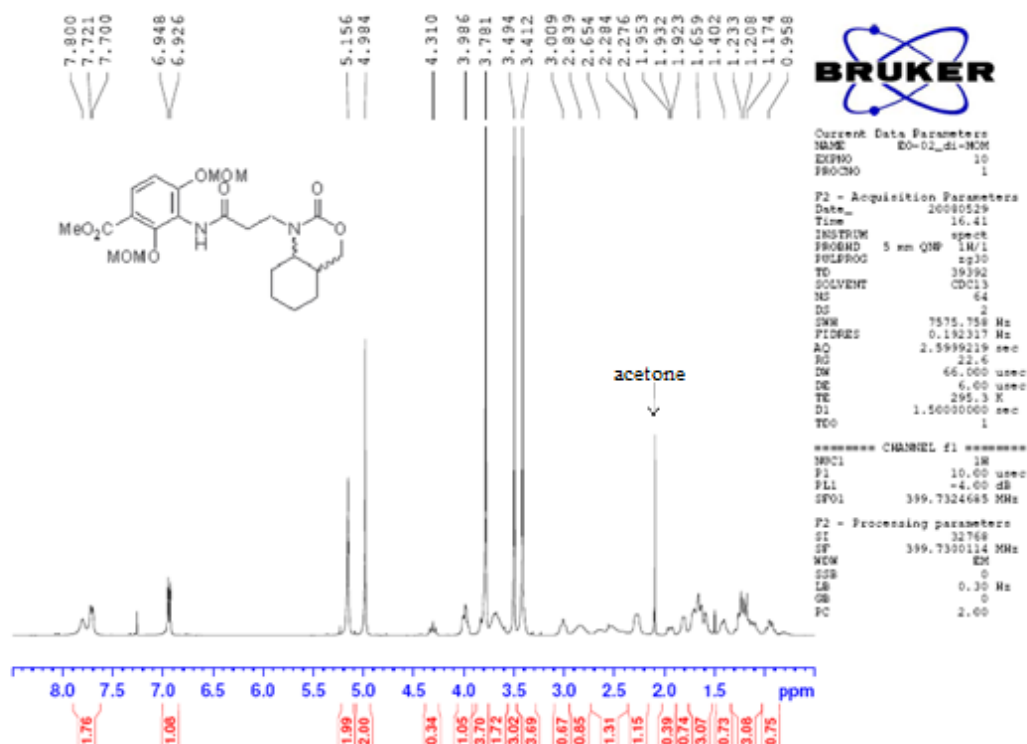
COSY



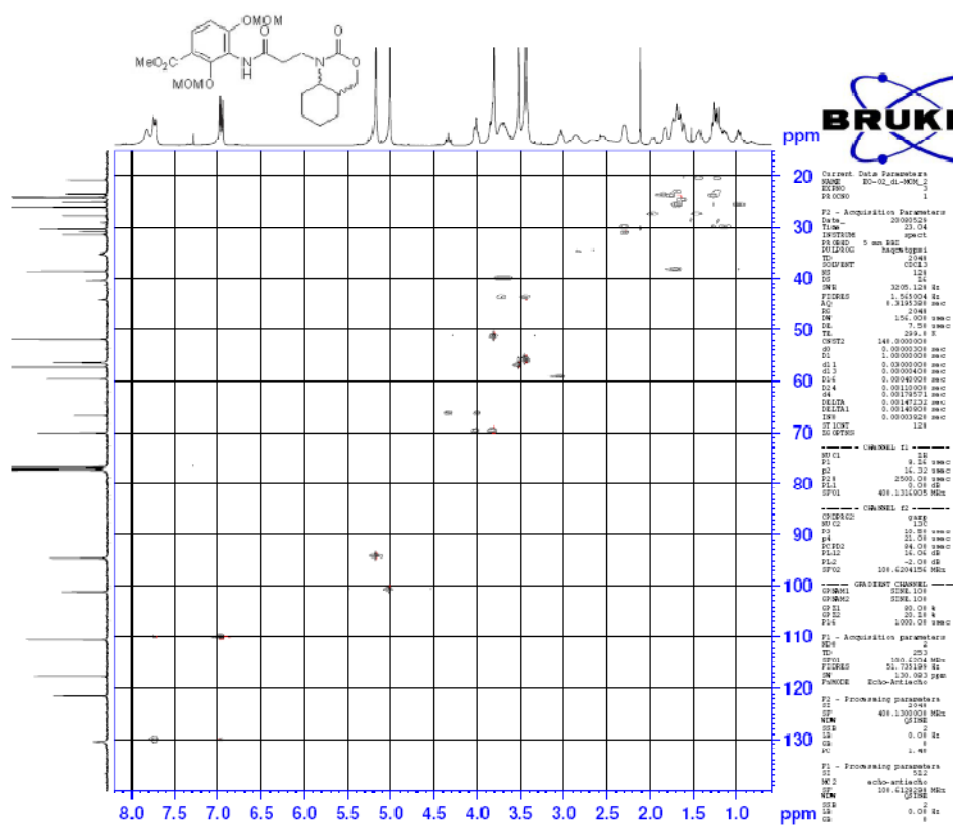
HSQC



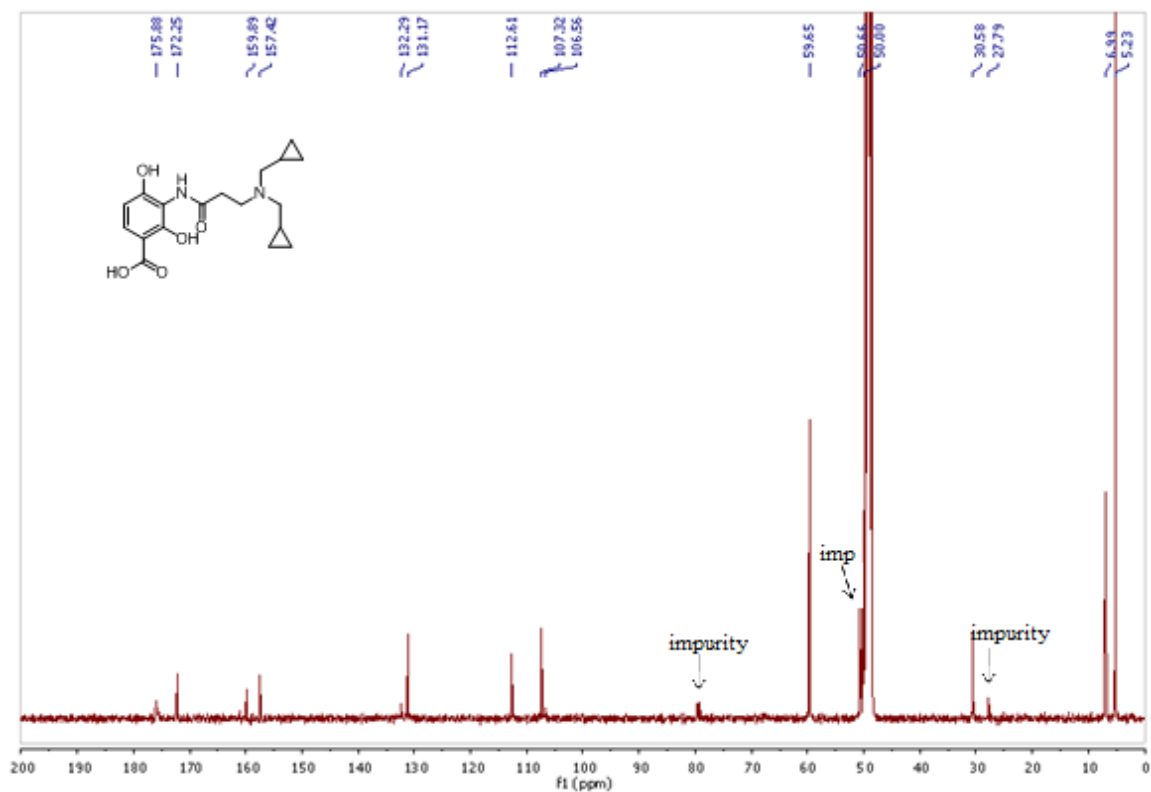
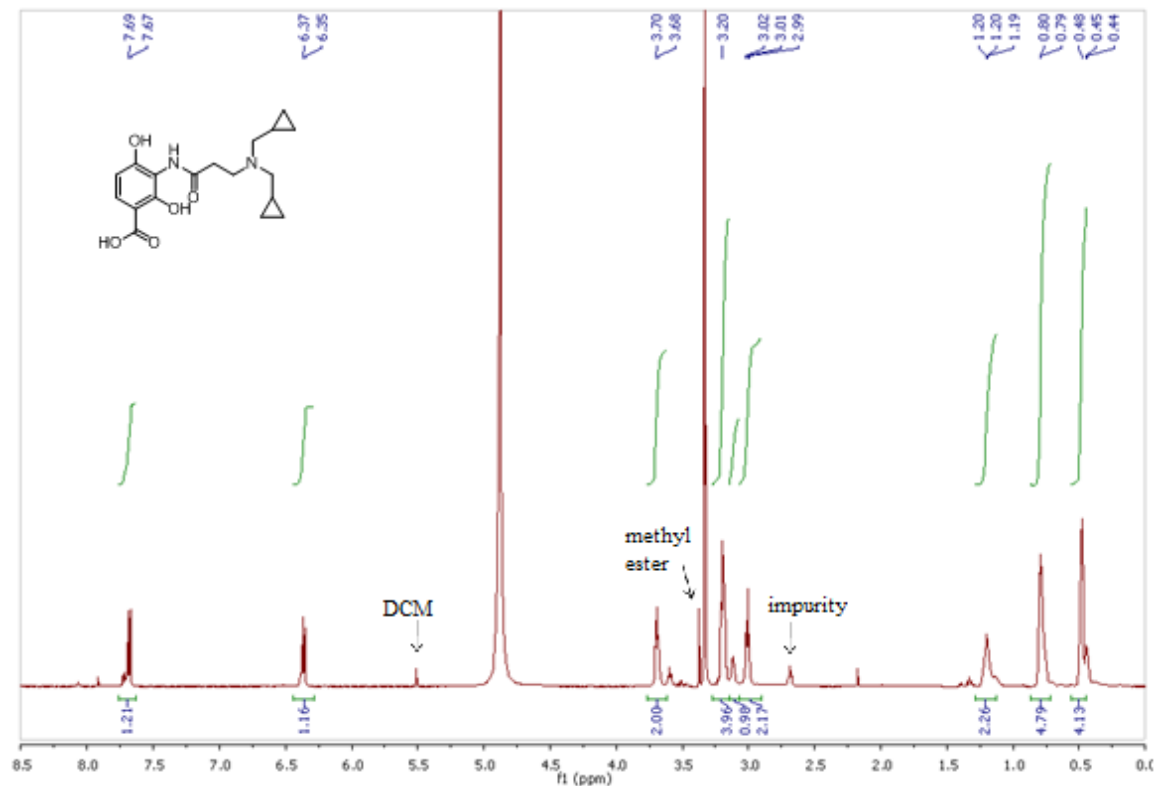
Compound 2-59



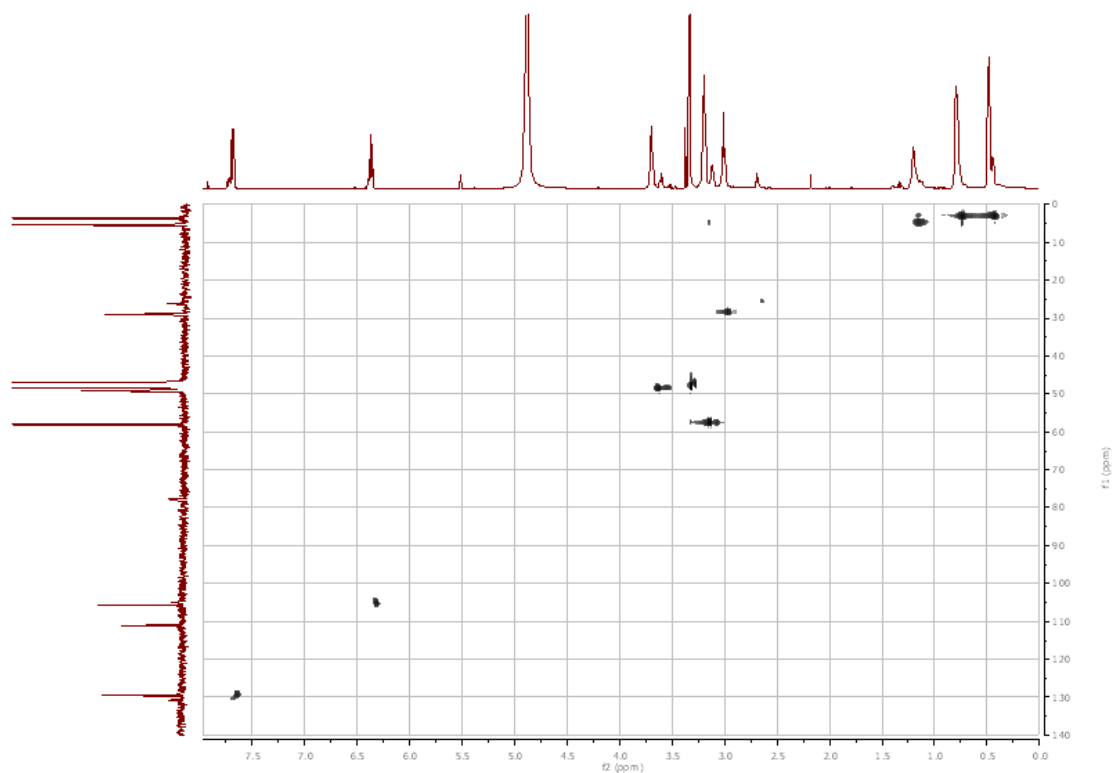
HSQC



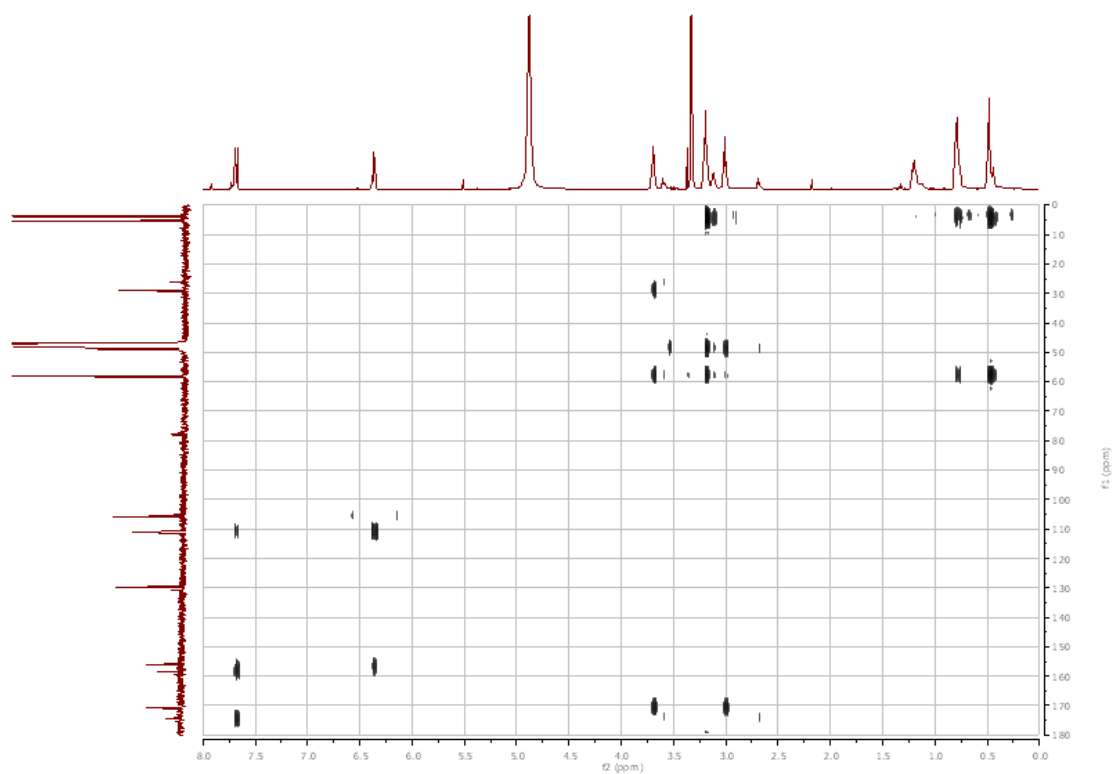
Compound 3-6



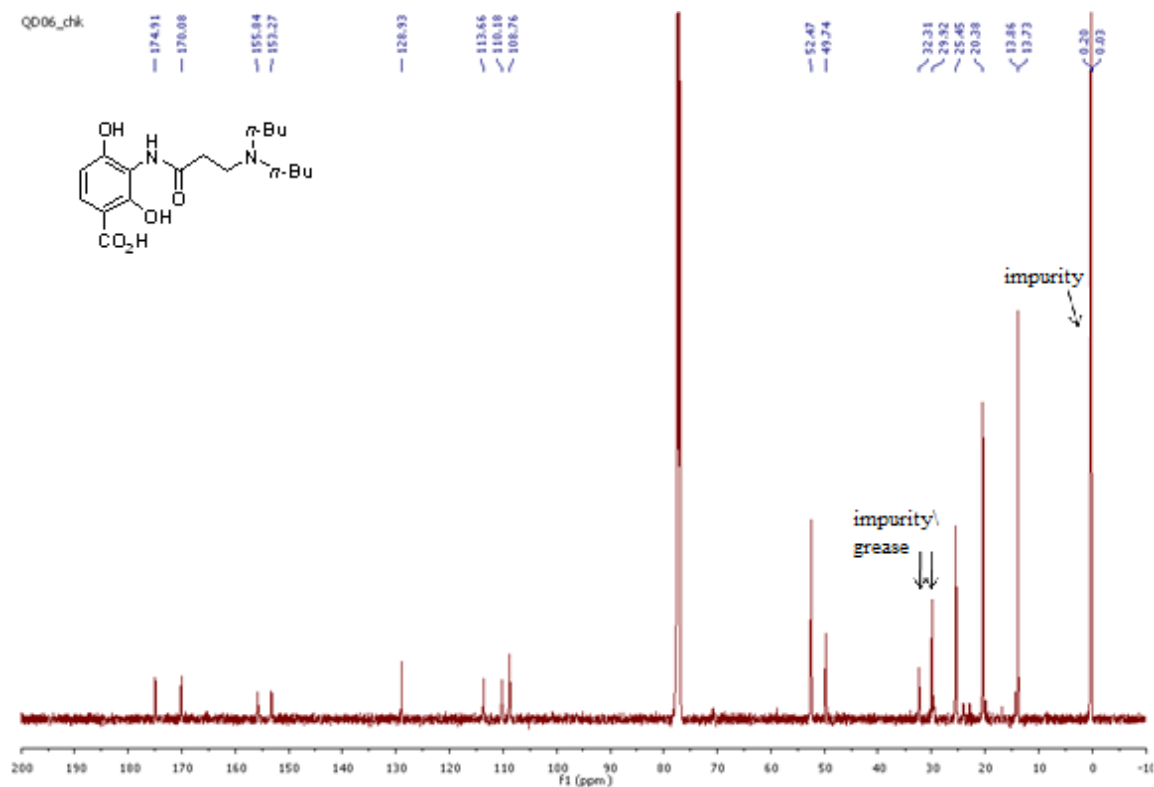
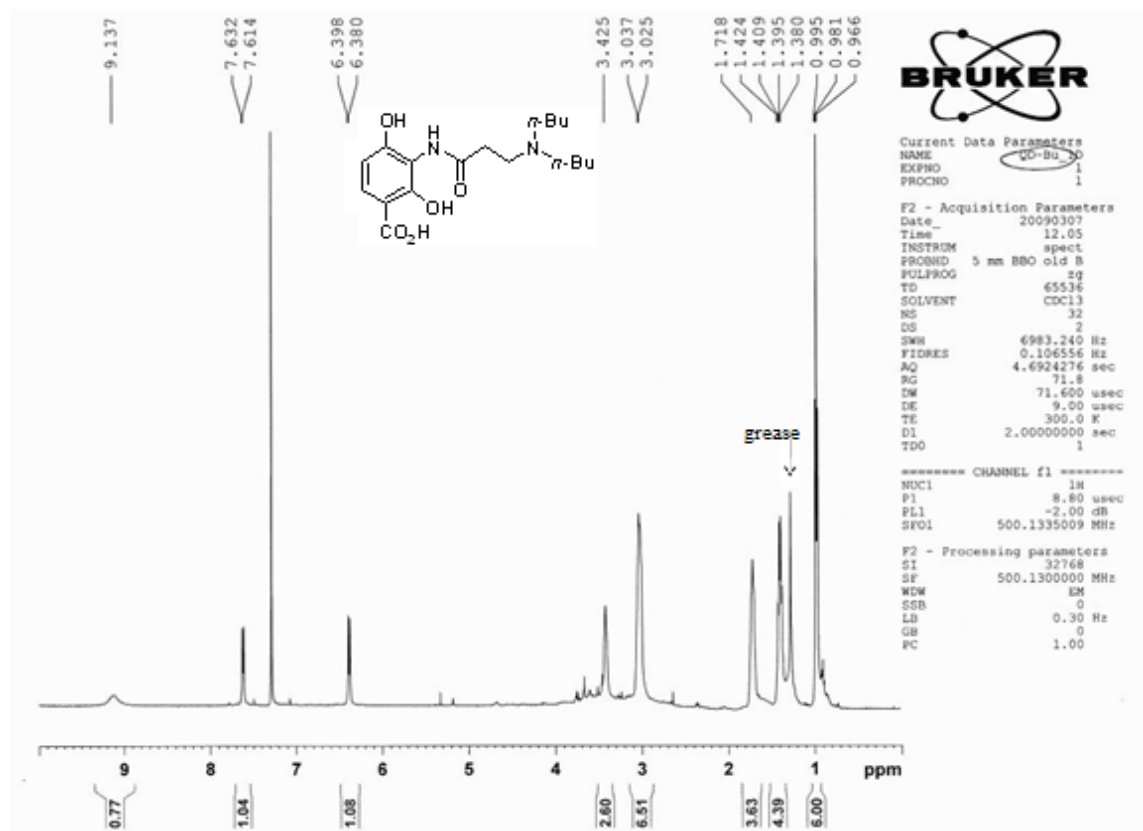
HSQC



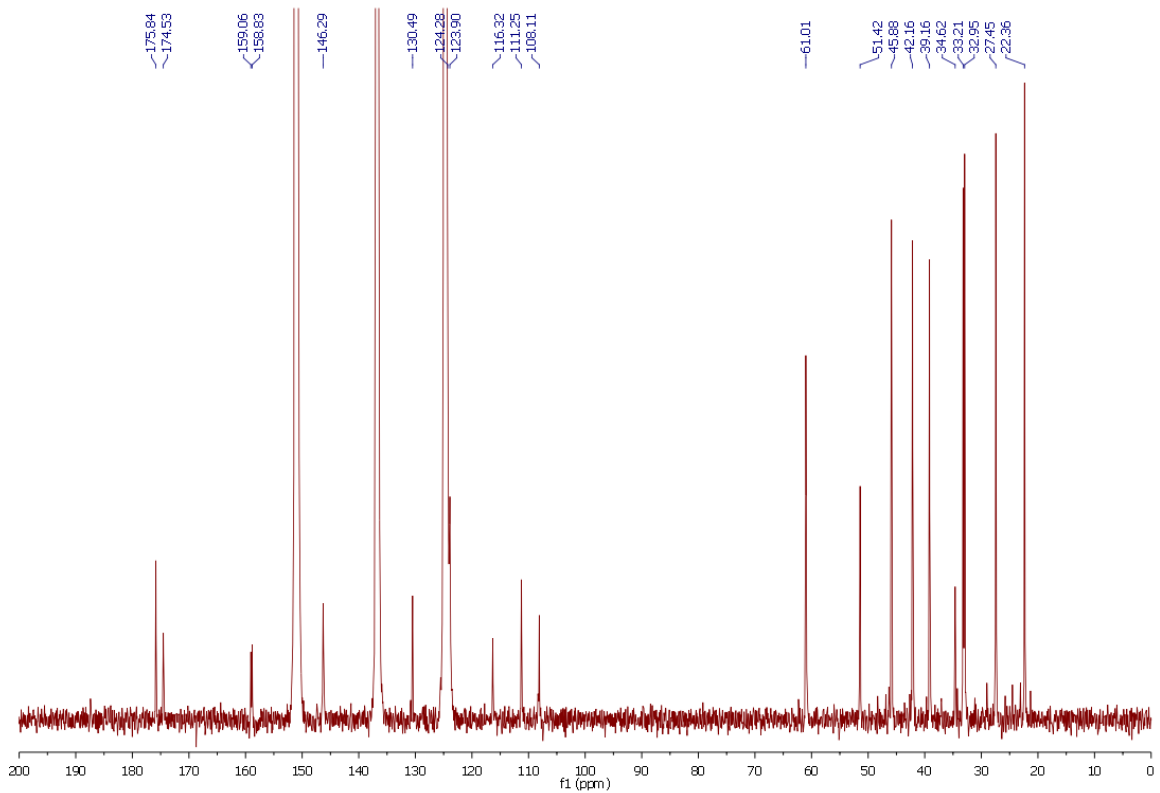
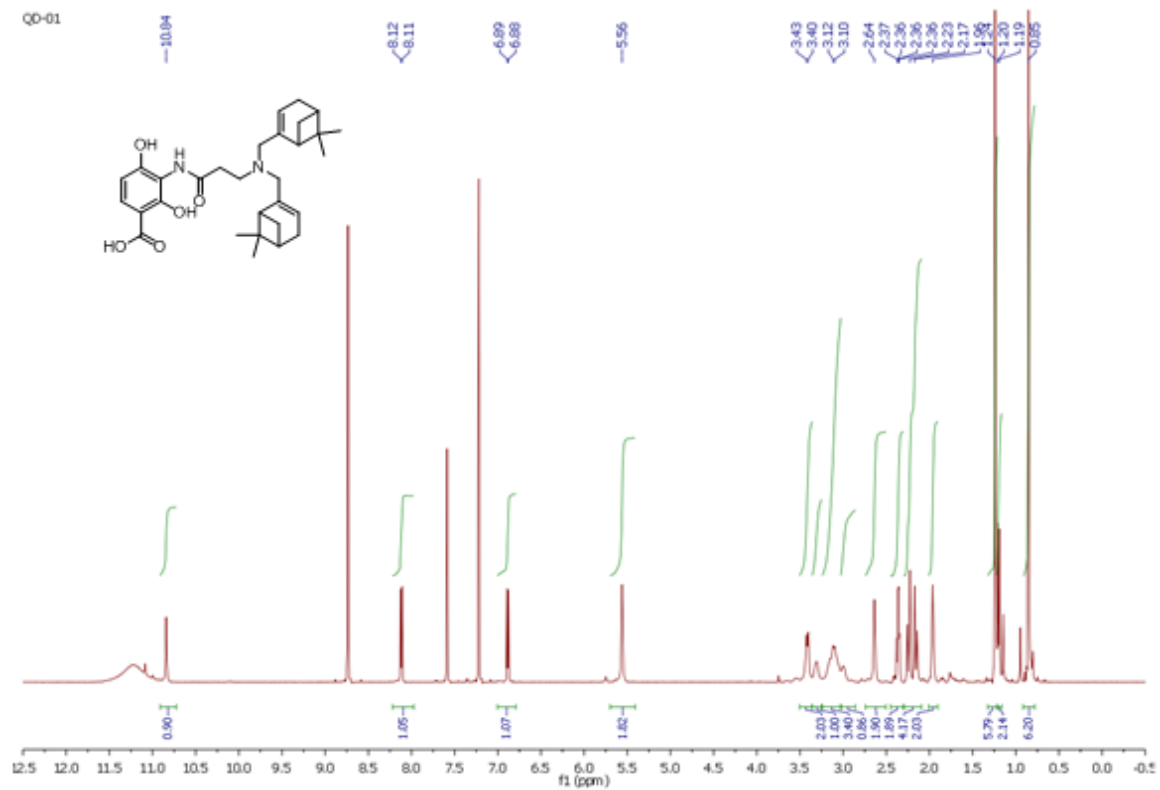
HMBC



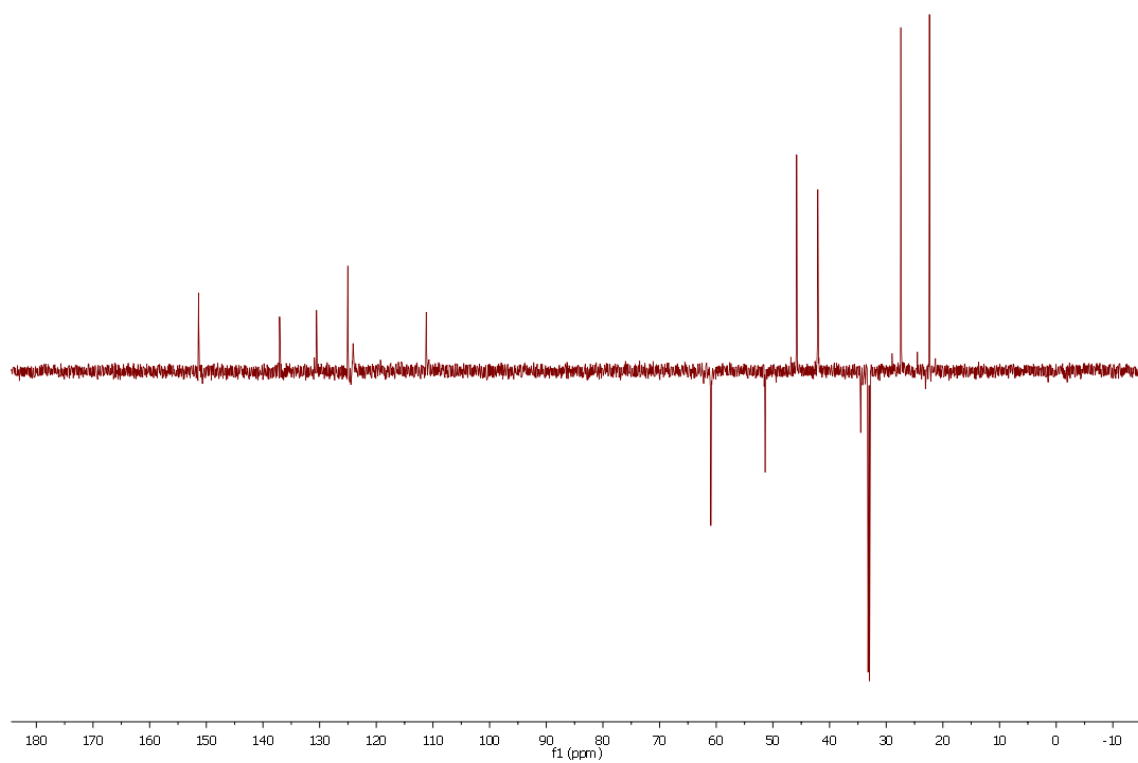
Compound 3-7



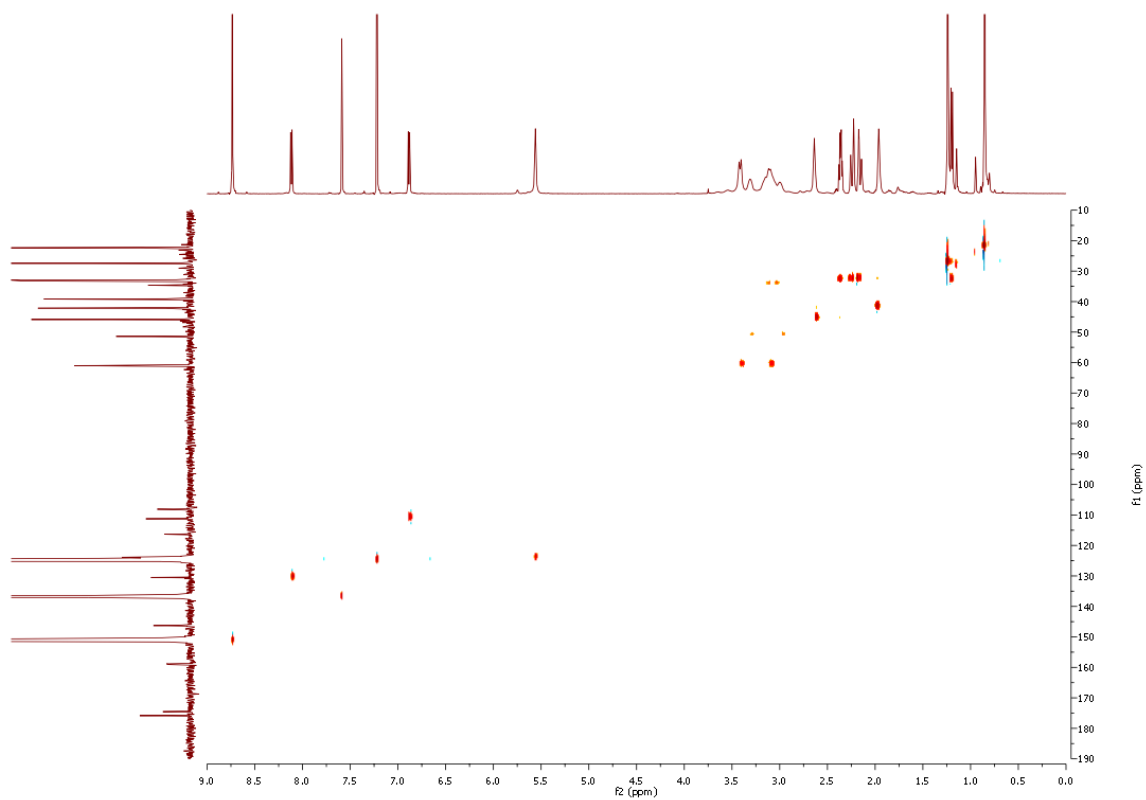
(-)-myrtemycin (3-8)



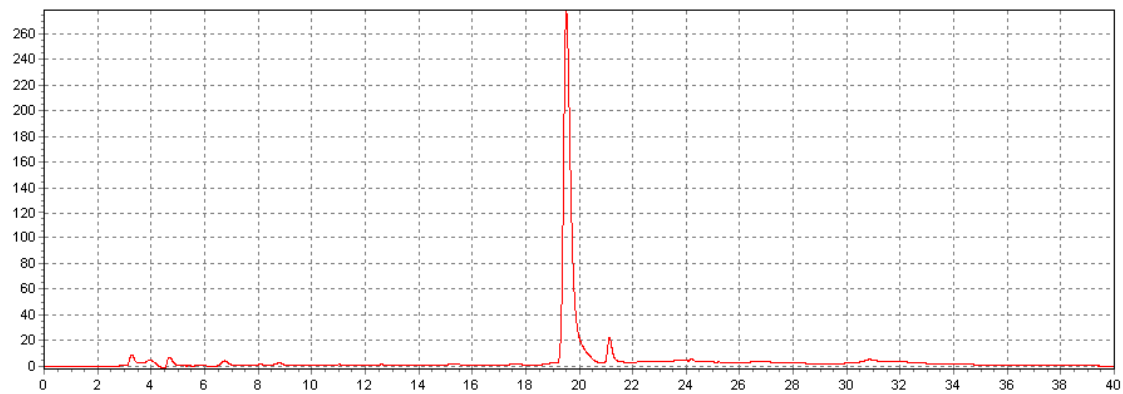
DEPT135



HSQC

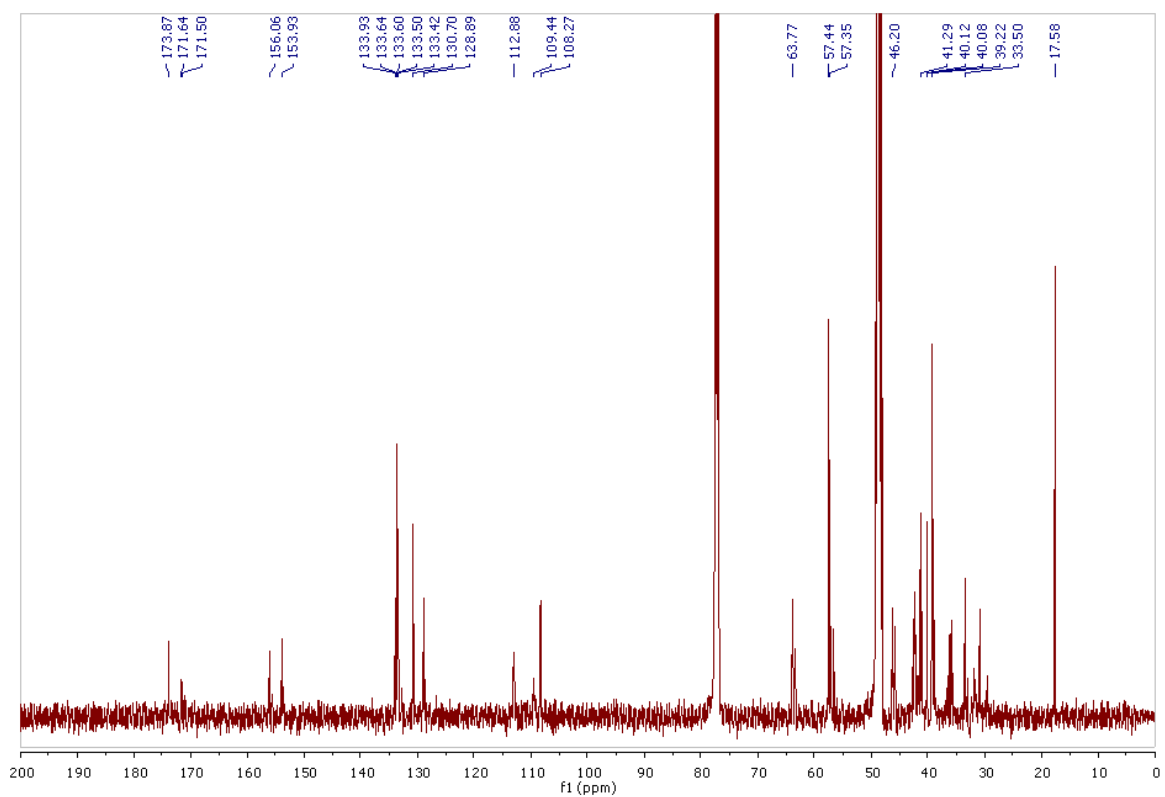
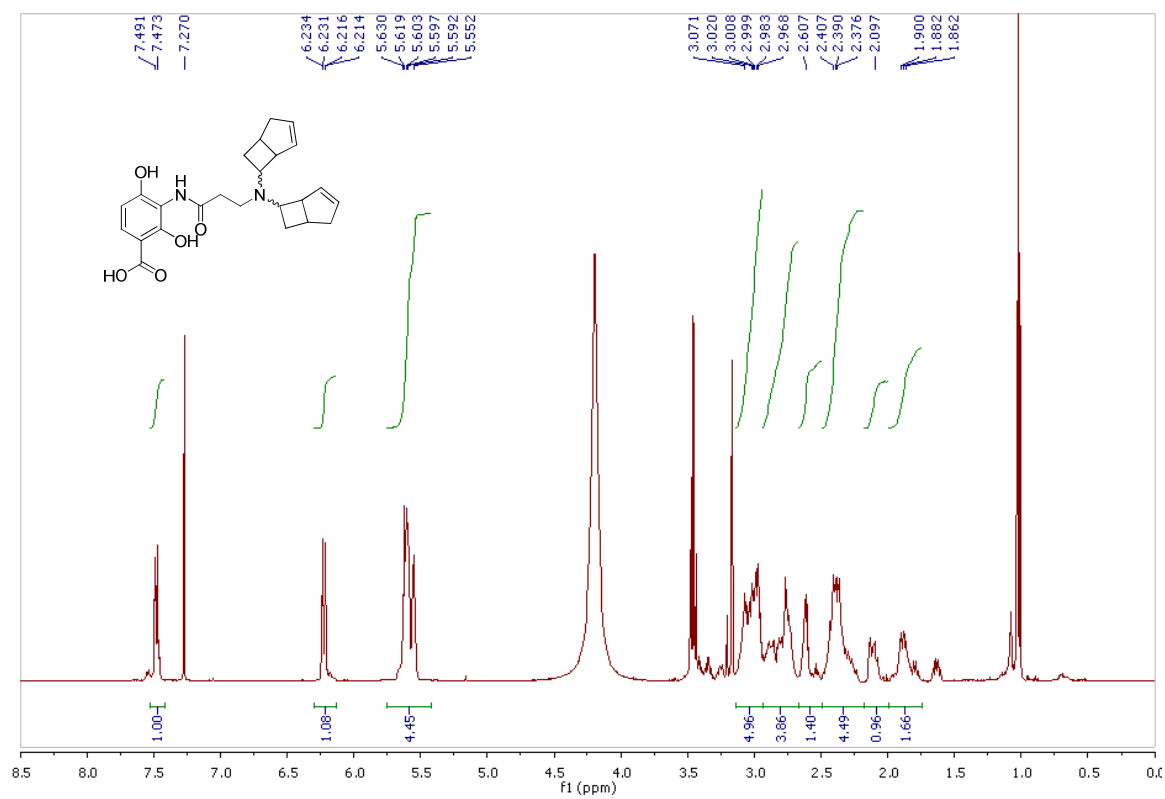


HPLC chromatography

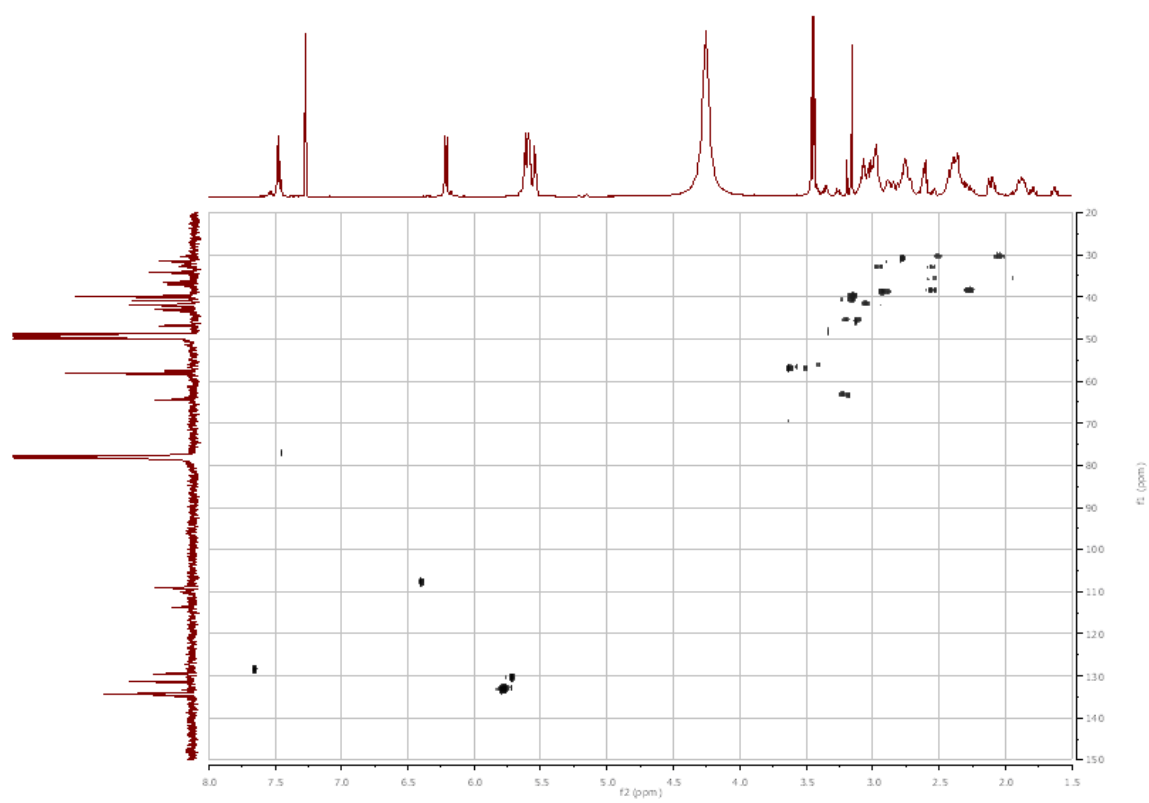


HPLC condition: A: 0.1 % TFA in H₂O; B: 0.1 % TFA in acetonitrile. 1 → 20 min: 33
→ 63 % B.

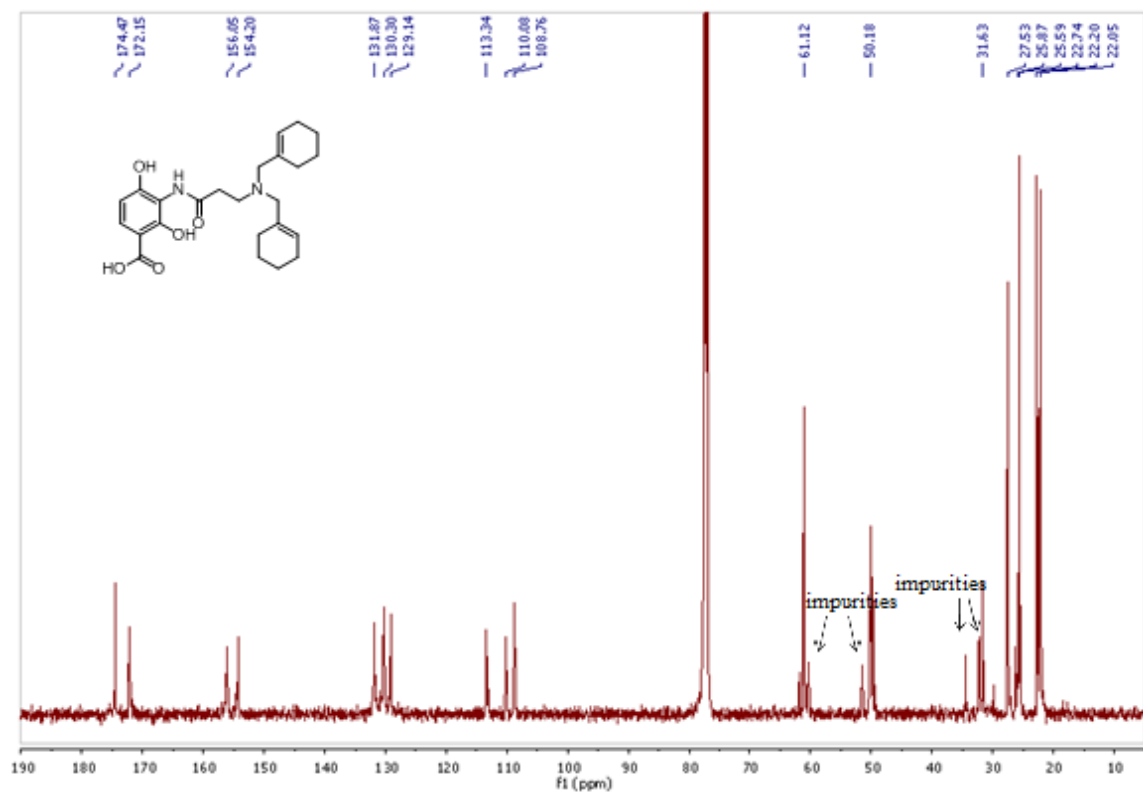
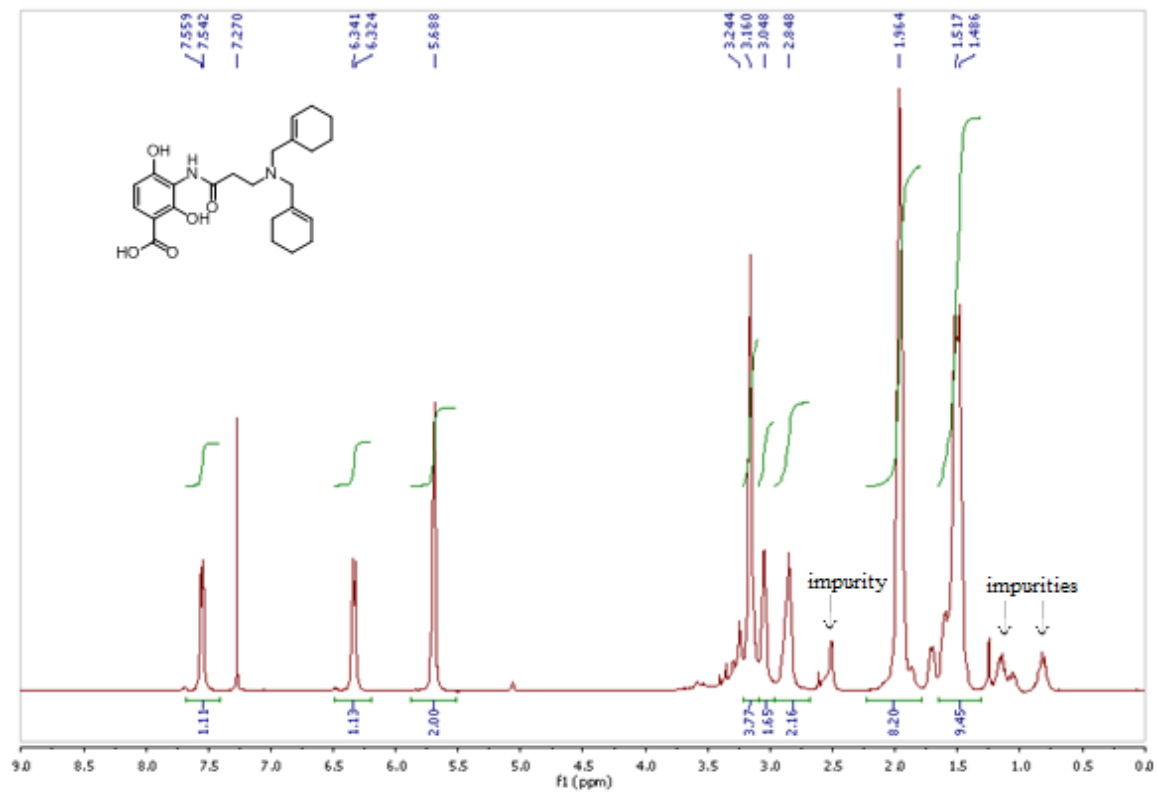
Compound 3-9



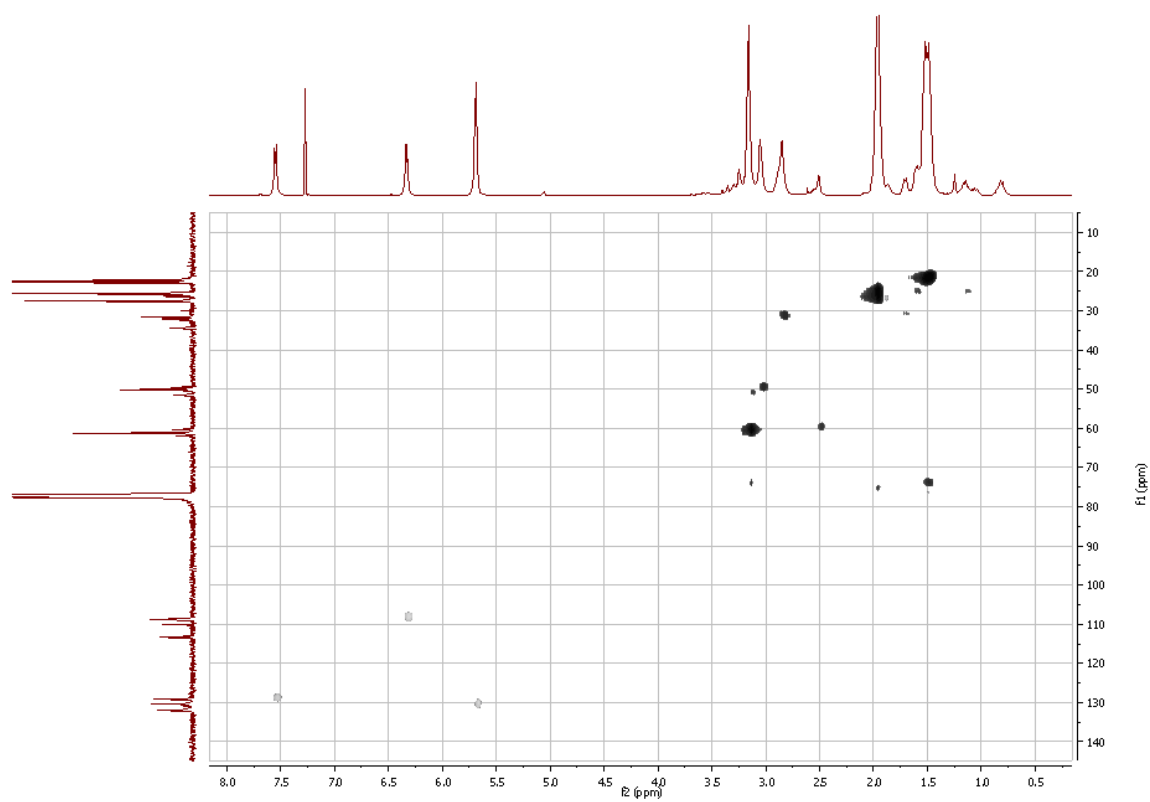
HSQC



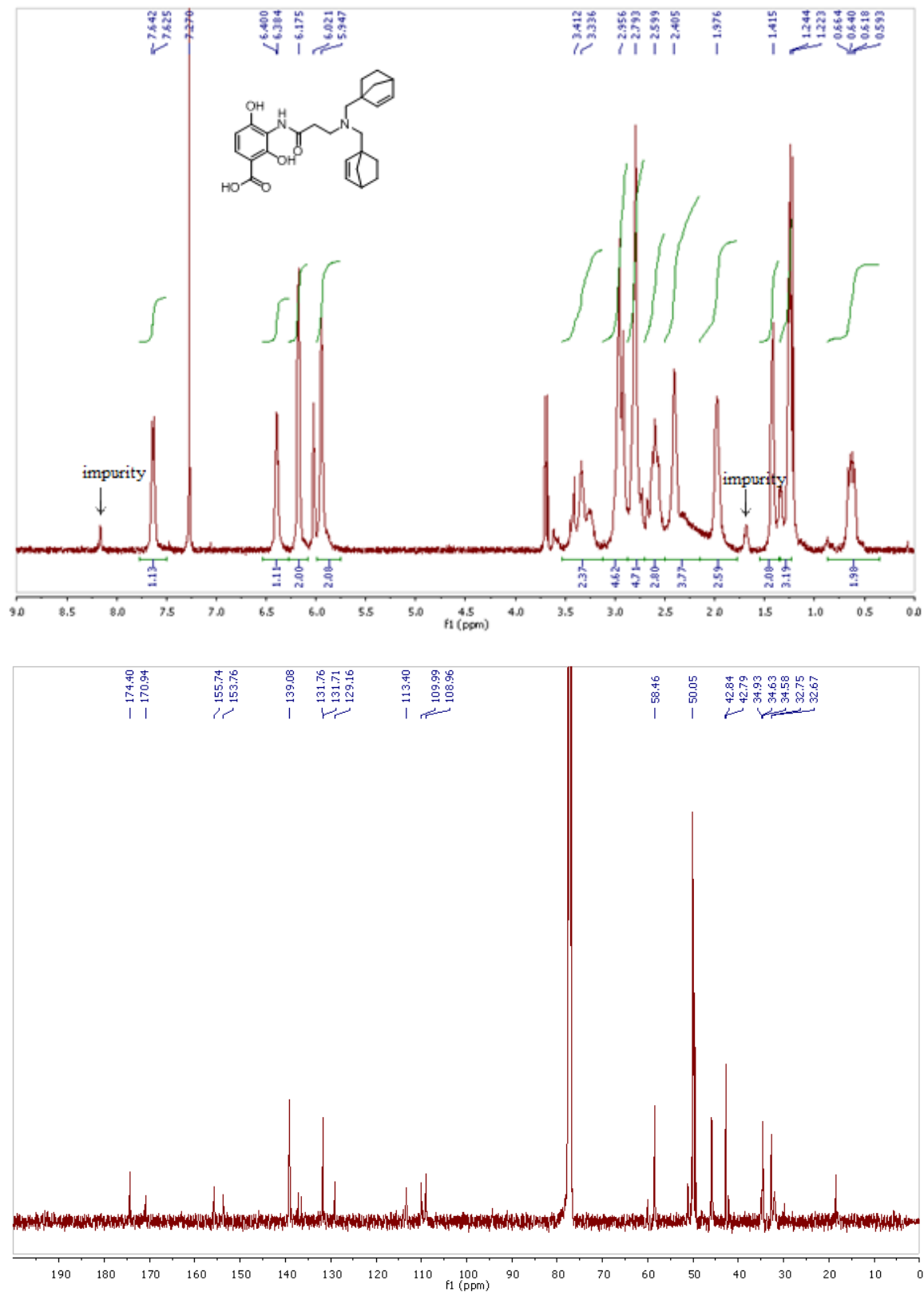
Compound 3–10 (the peaks are broadened possibly due to the protonation of the amino group)



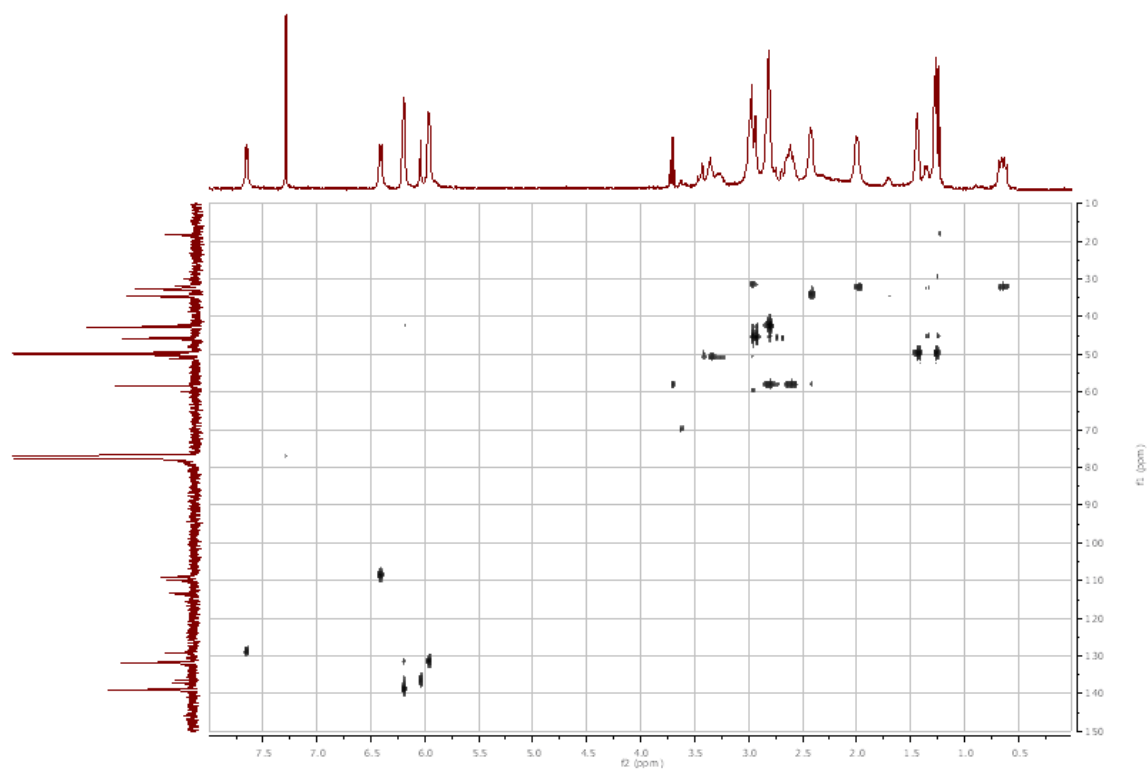
HSQC



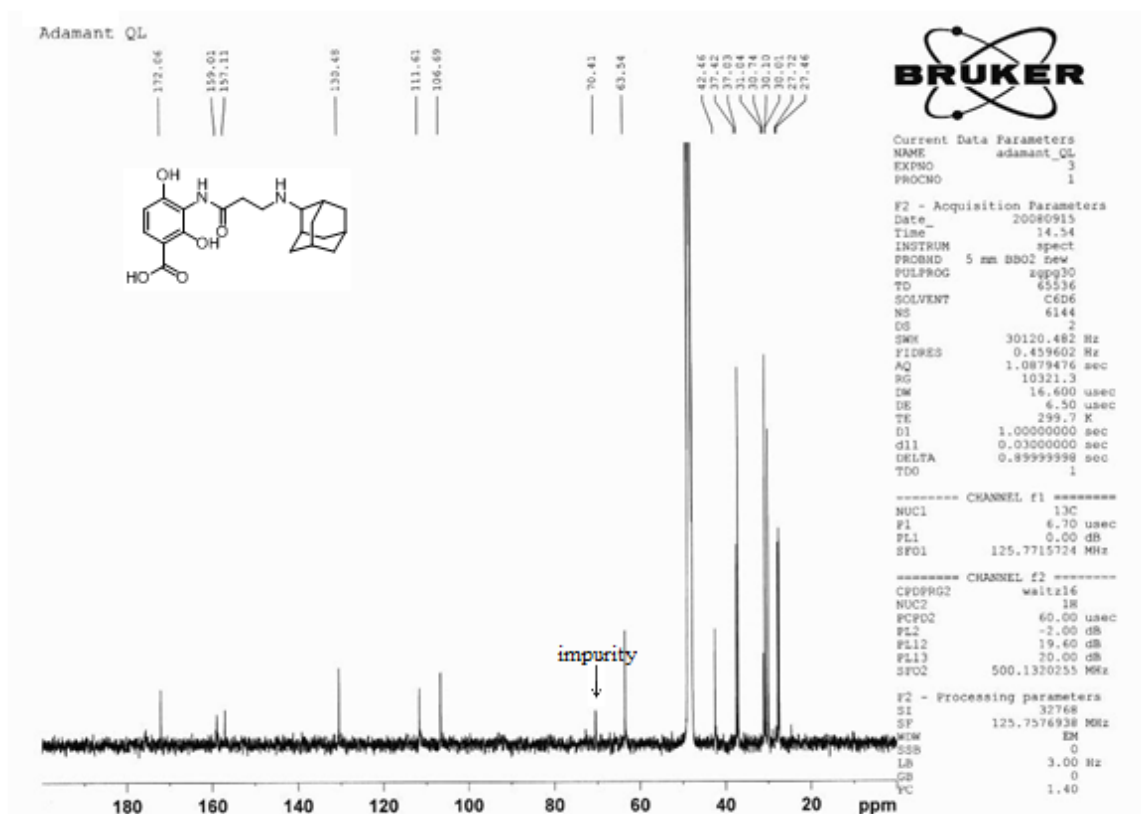
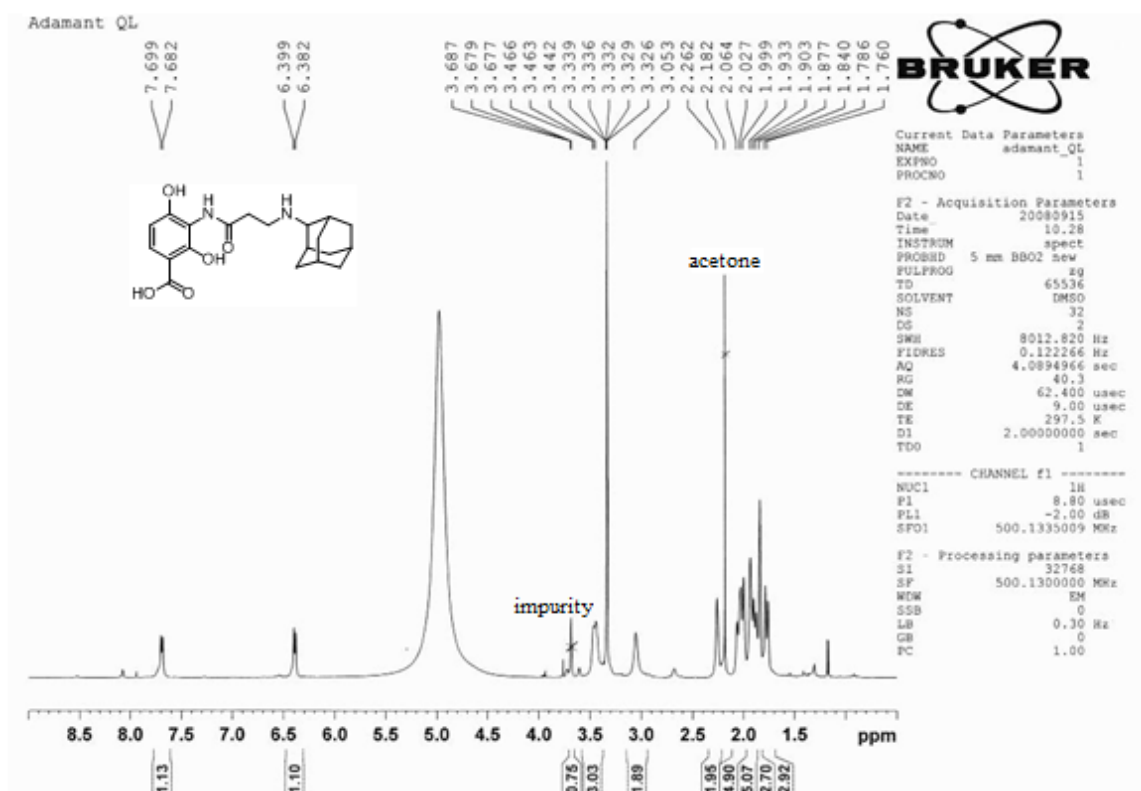
Compound 3–11 (the peaks are broadened possibly due to the protonation of the amino group)



HSQC



Compound 3-12



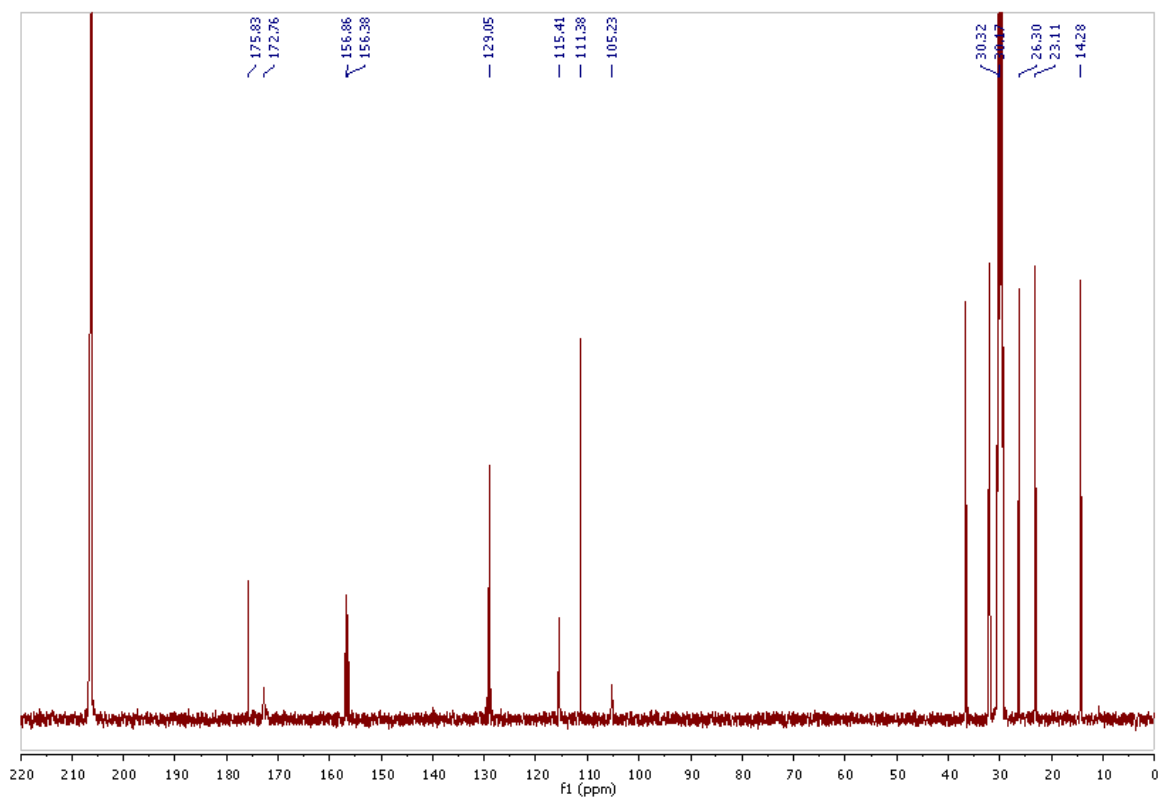
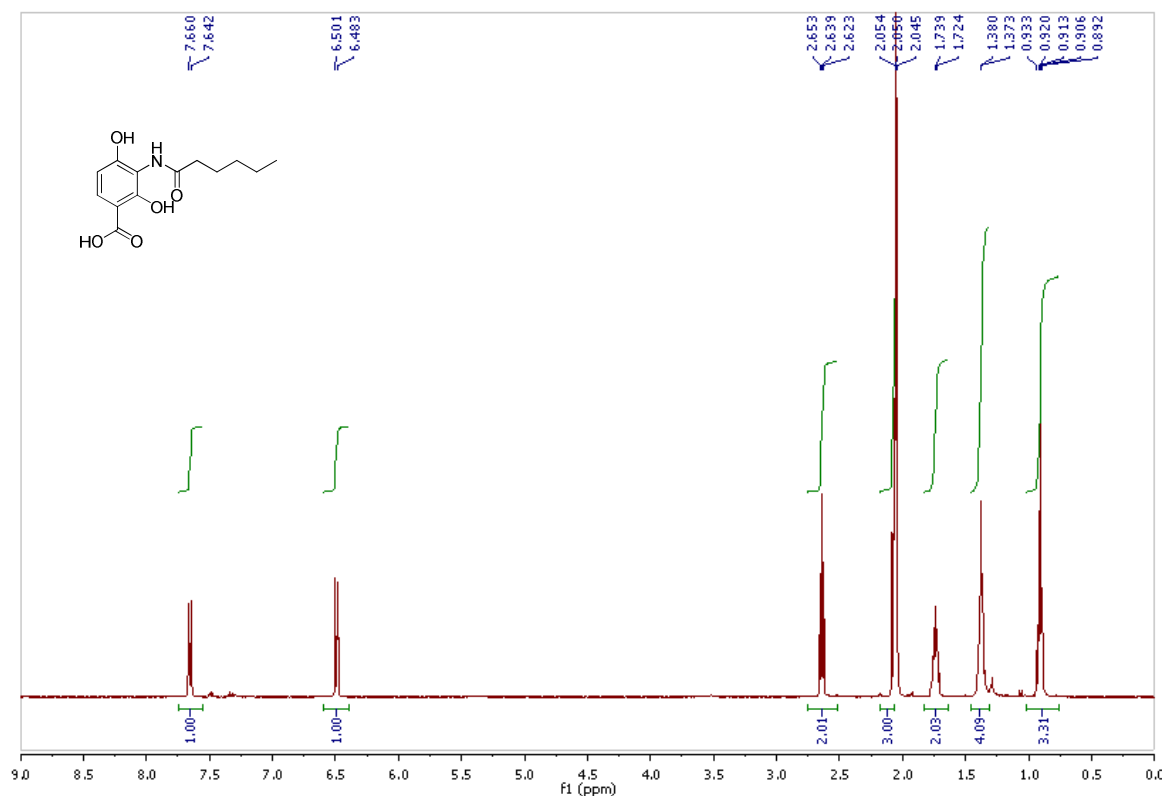
Chemical structure of compound 10 is shown. The ^{13}C NMR spectrum (ppm) displays the following peaks:

- 216.83
- 174.07
- 171.94
- 155.30
- 155.17
- 128.85
- 113.73
- 110.51
- 104.93
- 50.96
- 49.66
- 42.84
- 39.50
- 27.00
- 19.76
- 19.52

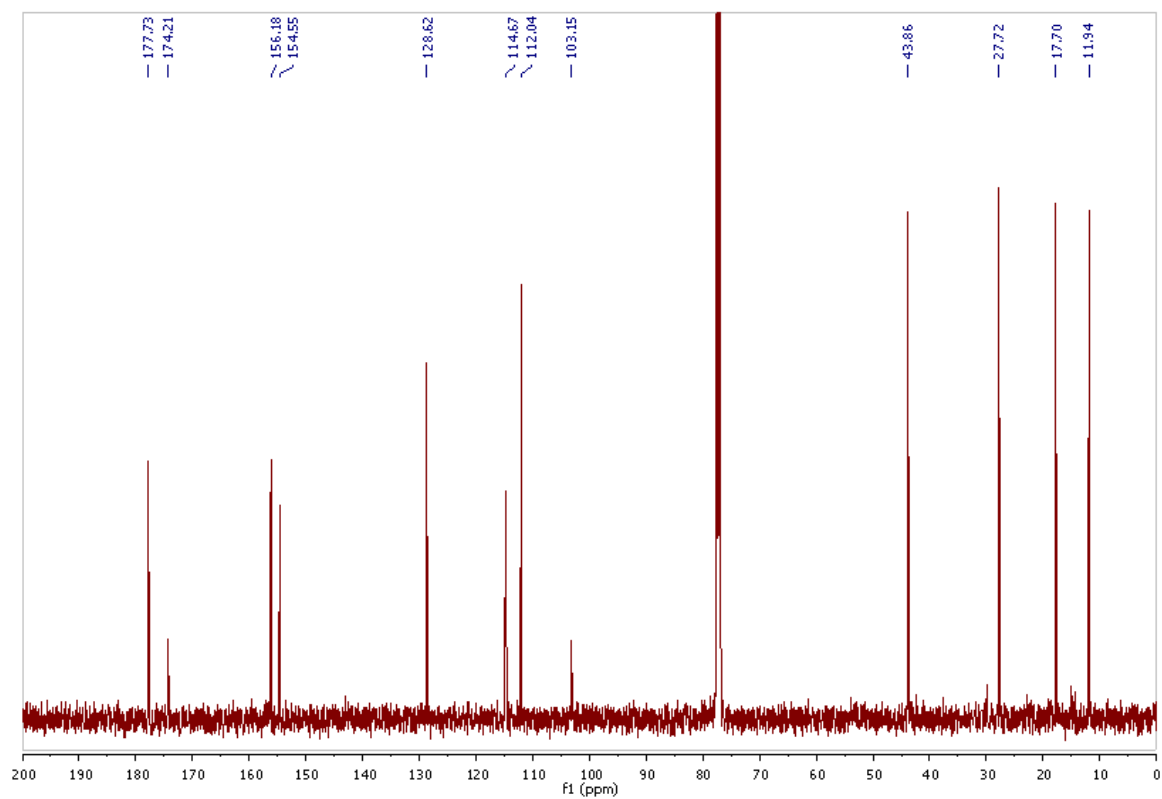
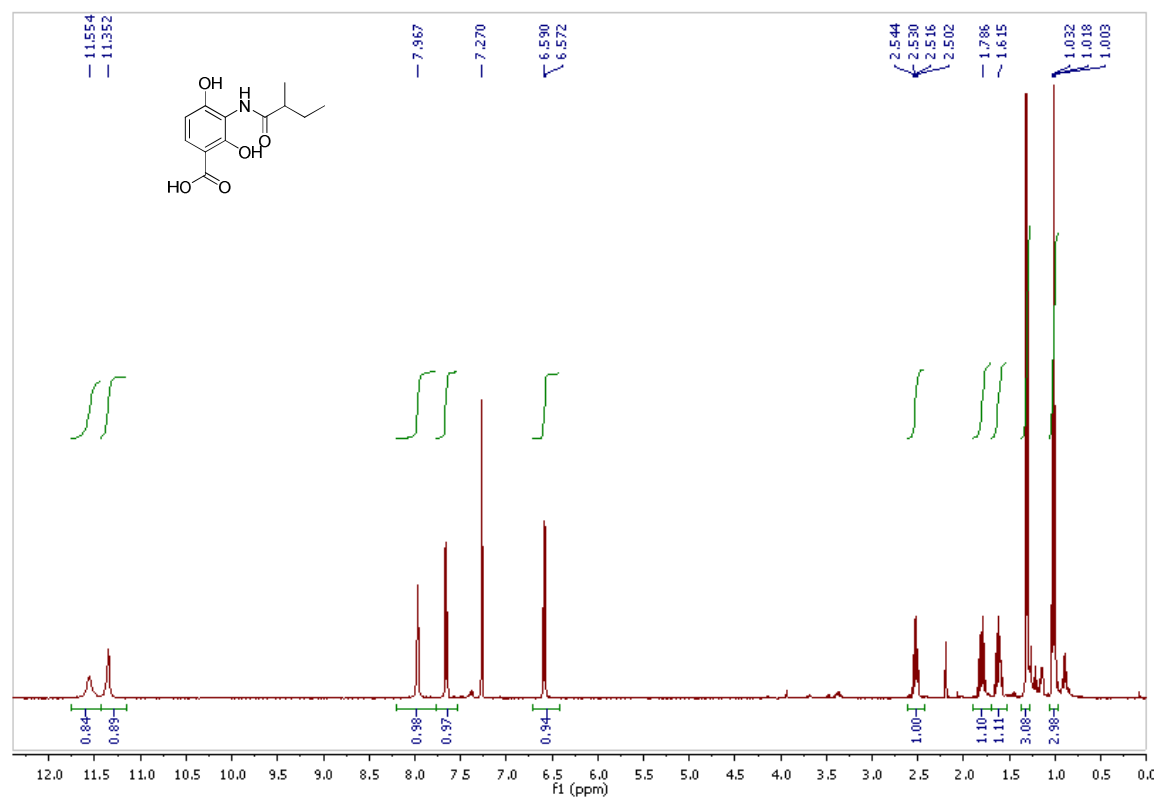
A peak at approximately 30 ppm is labeled "grease".



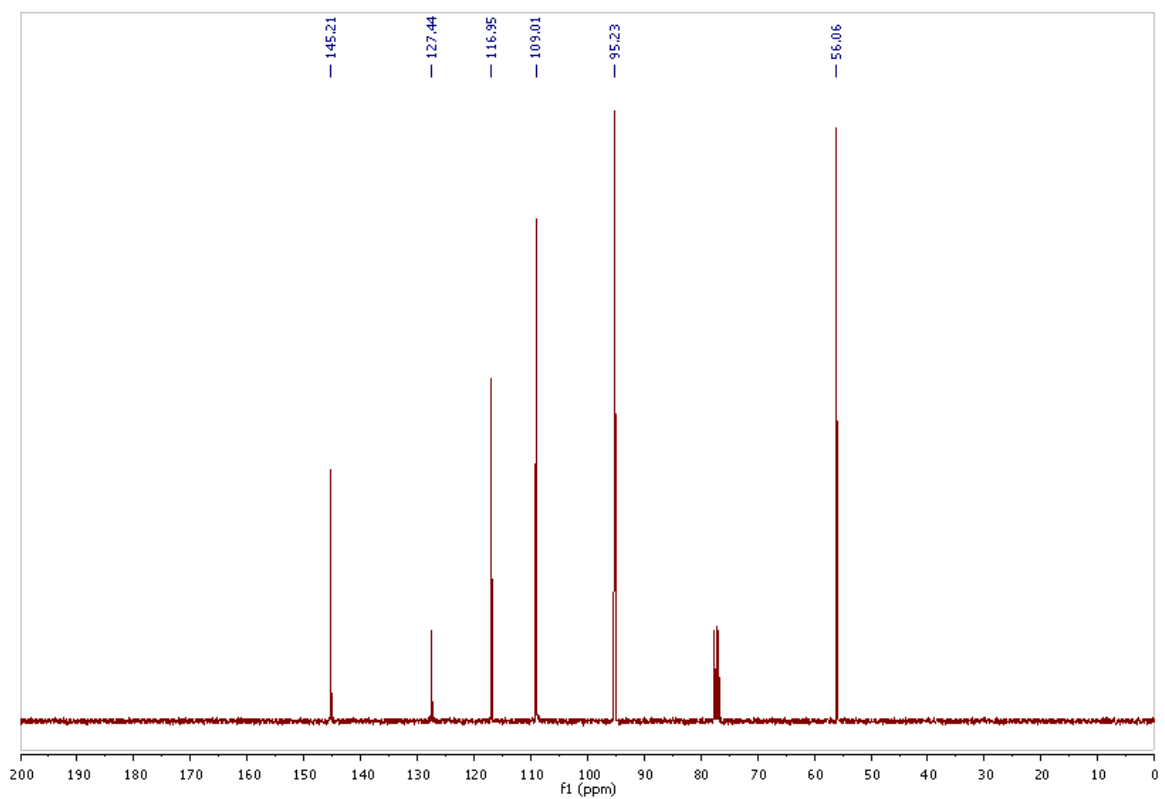
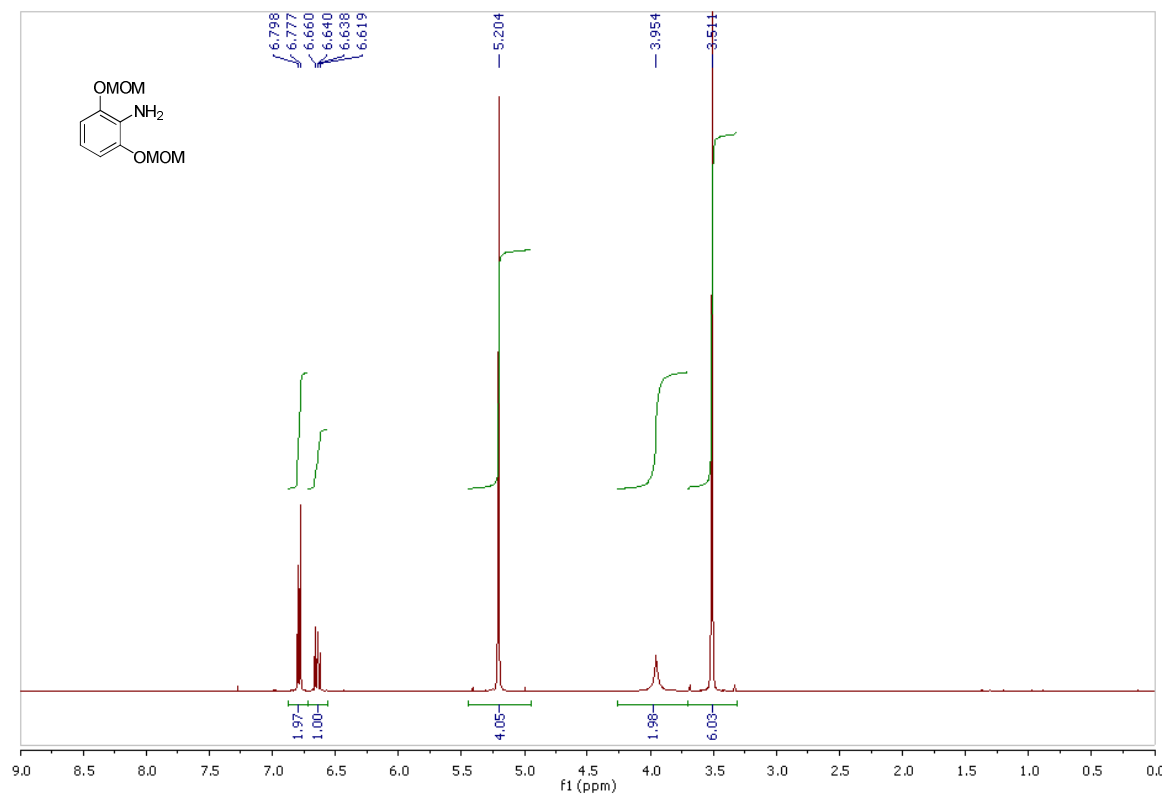
Compound 14



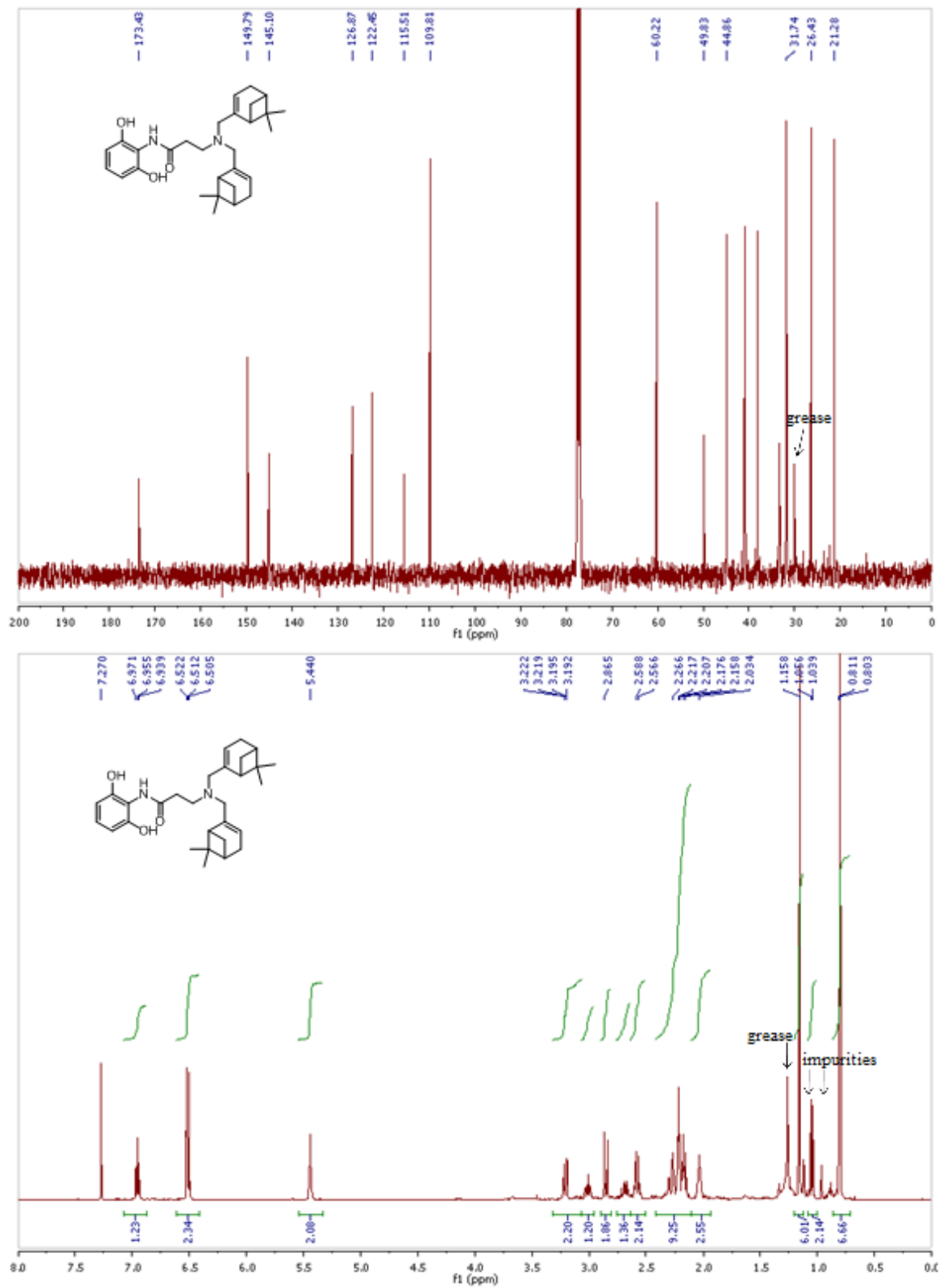
Compound 3-15



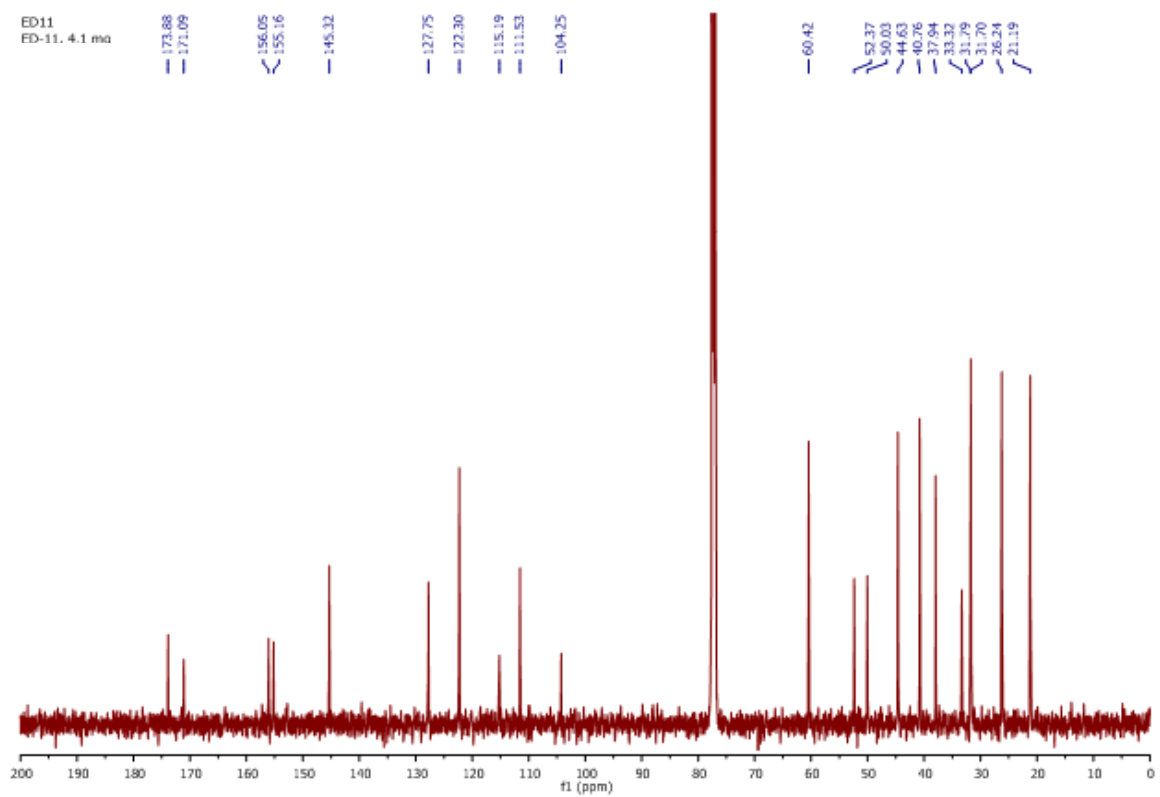
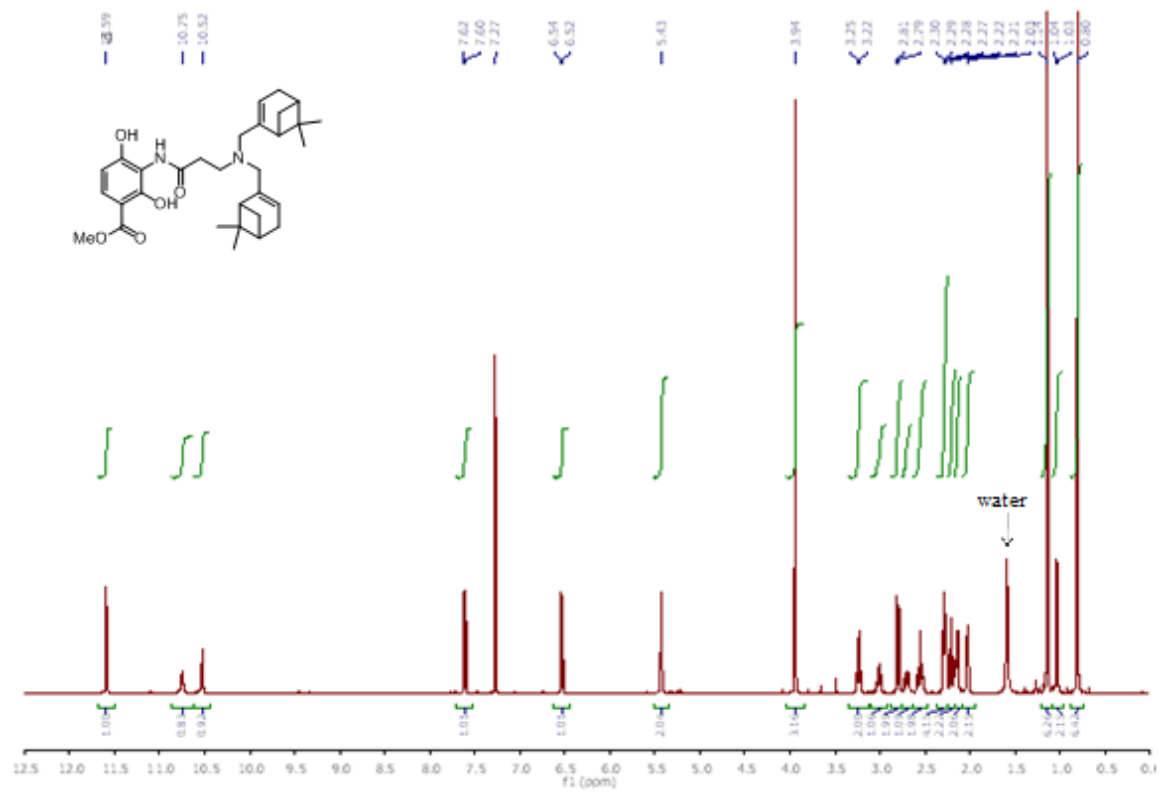
Compound 6-11



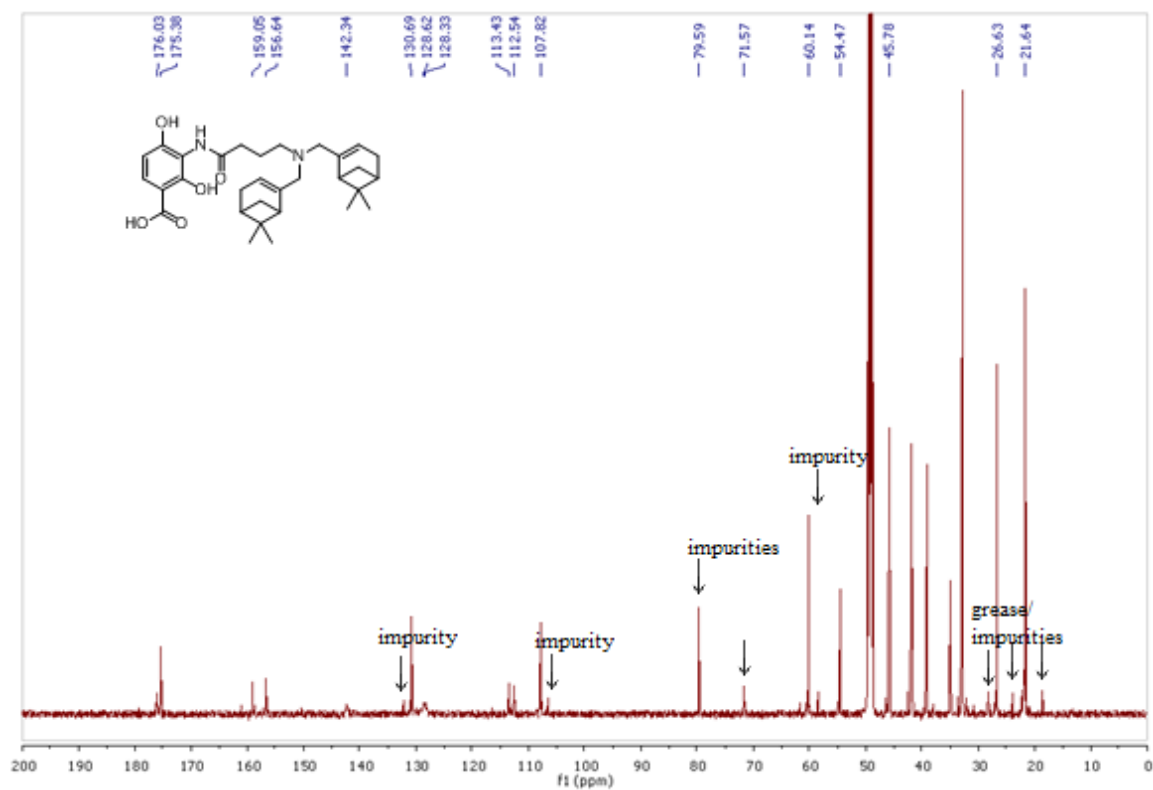
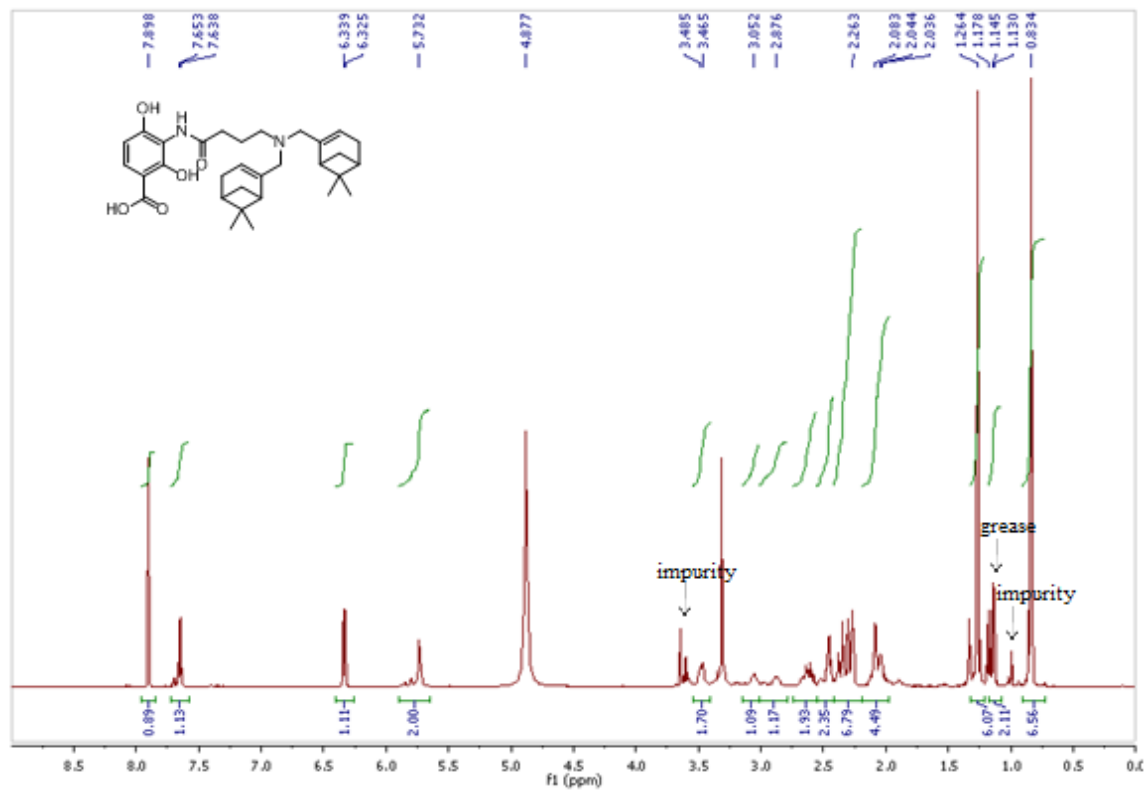
Compound 3-16



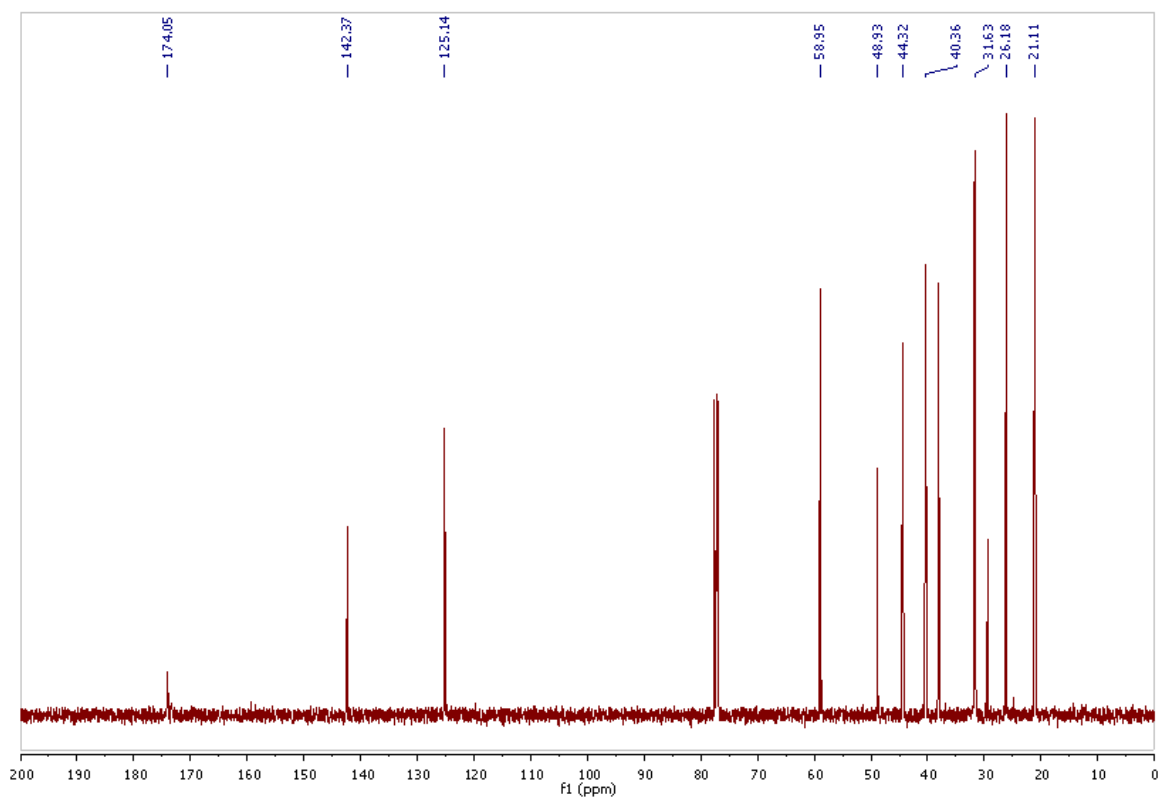
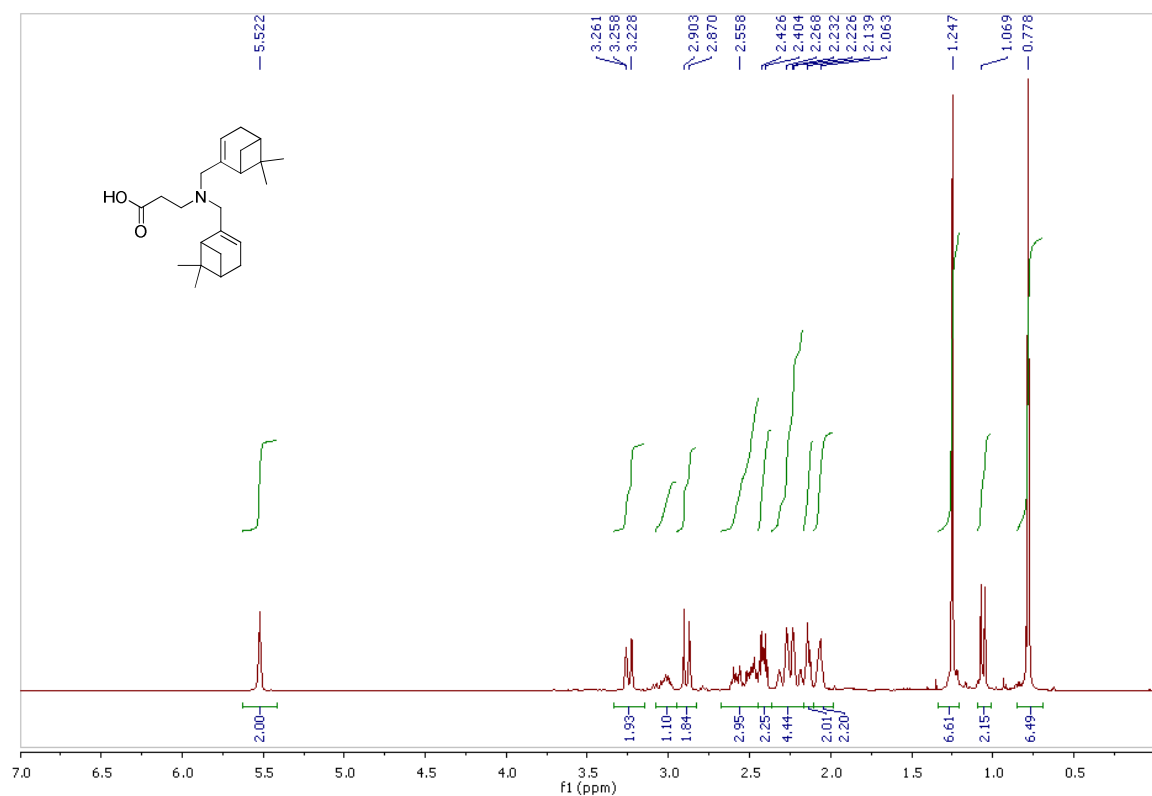
Compound 3-17

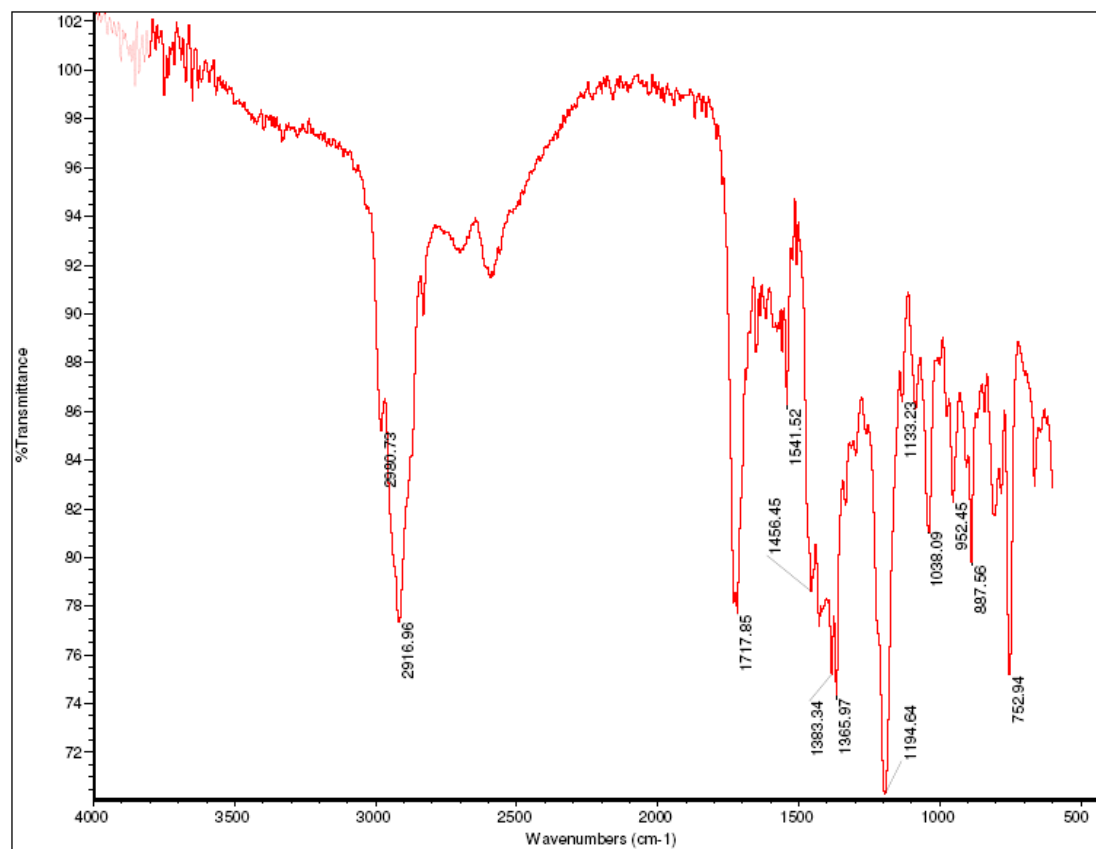


(-)-Homo-myrtemycin (3-18)

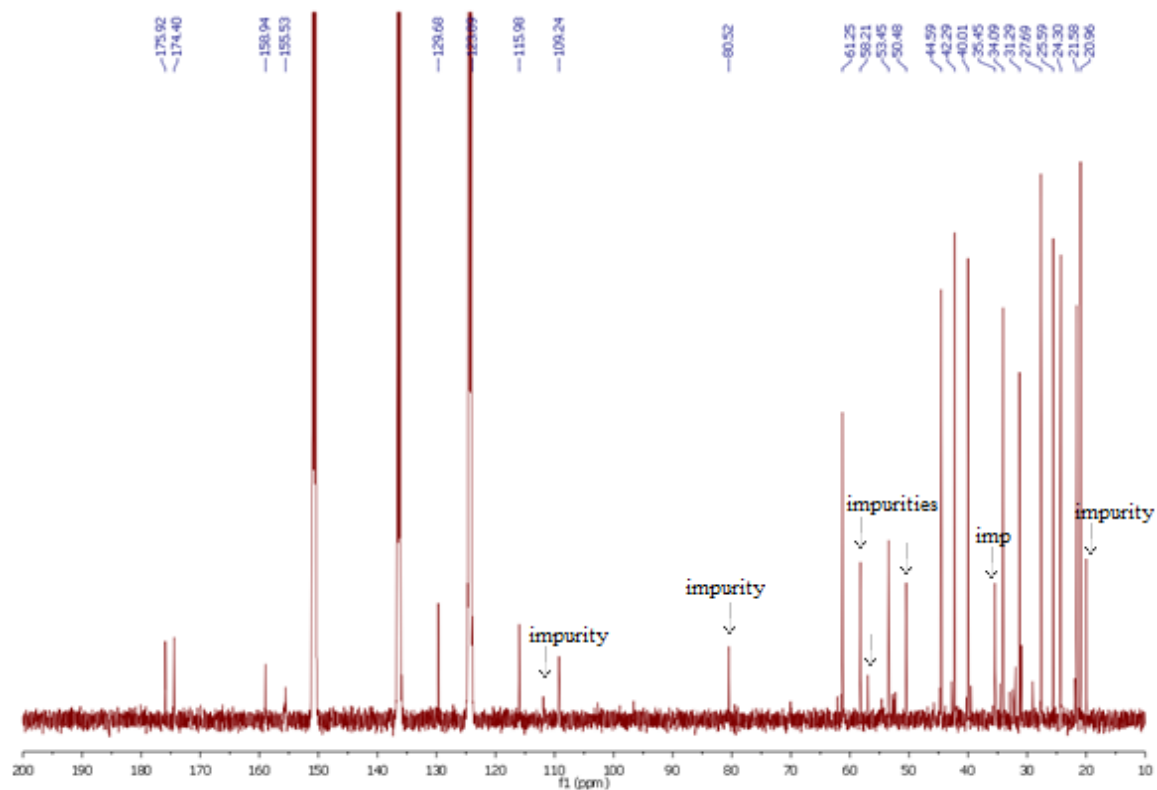
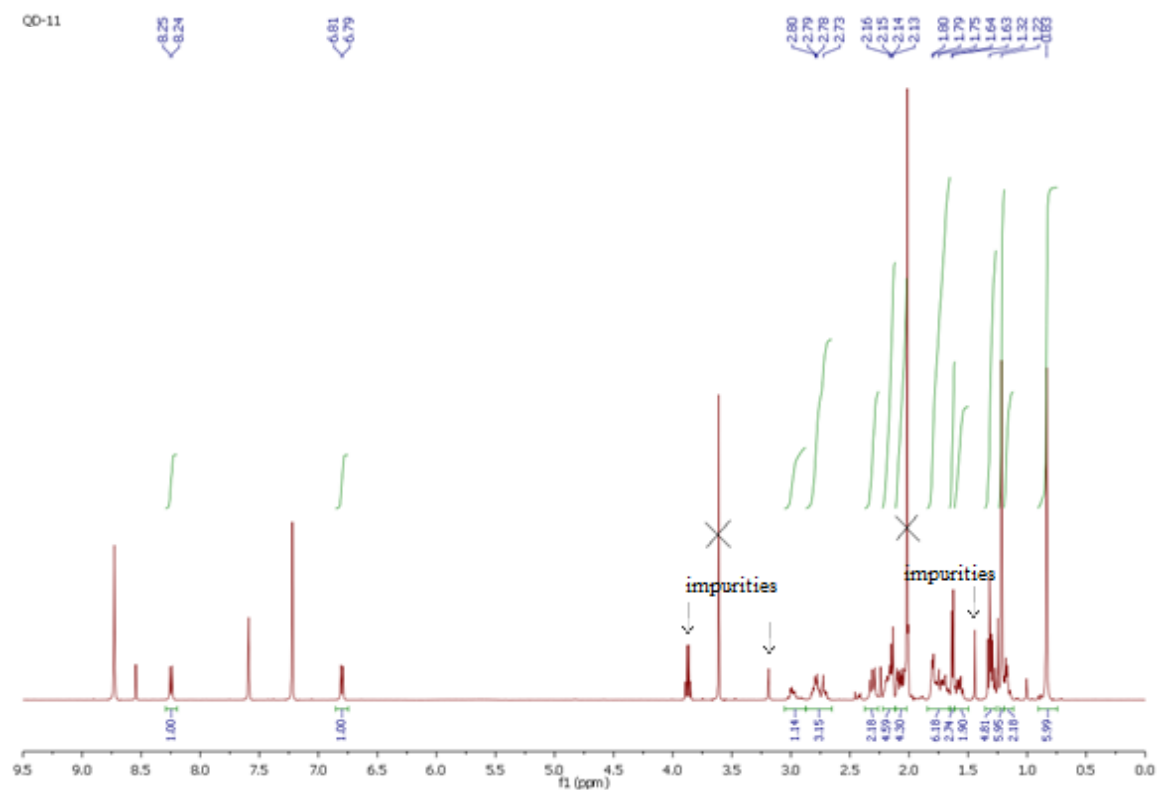


Compound 3-19

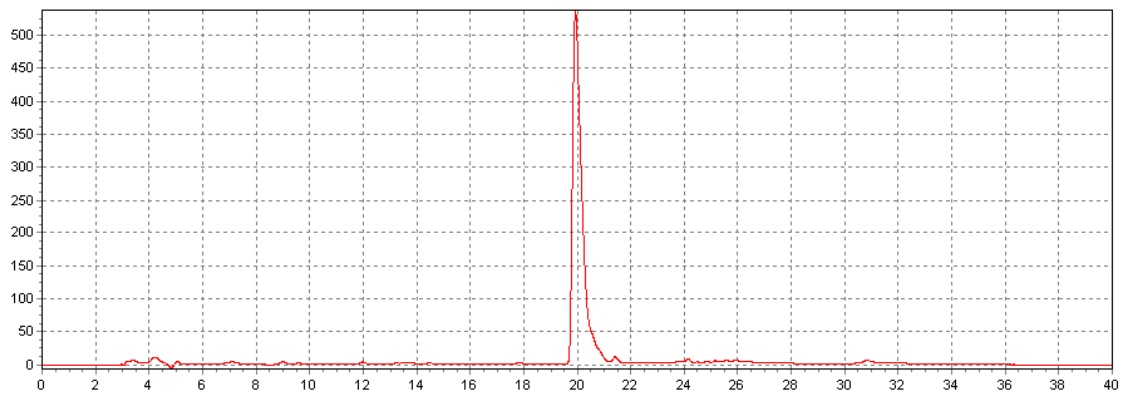




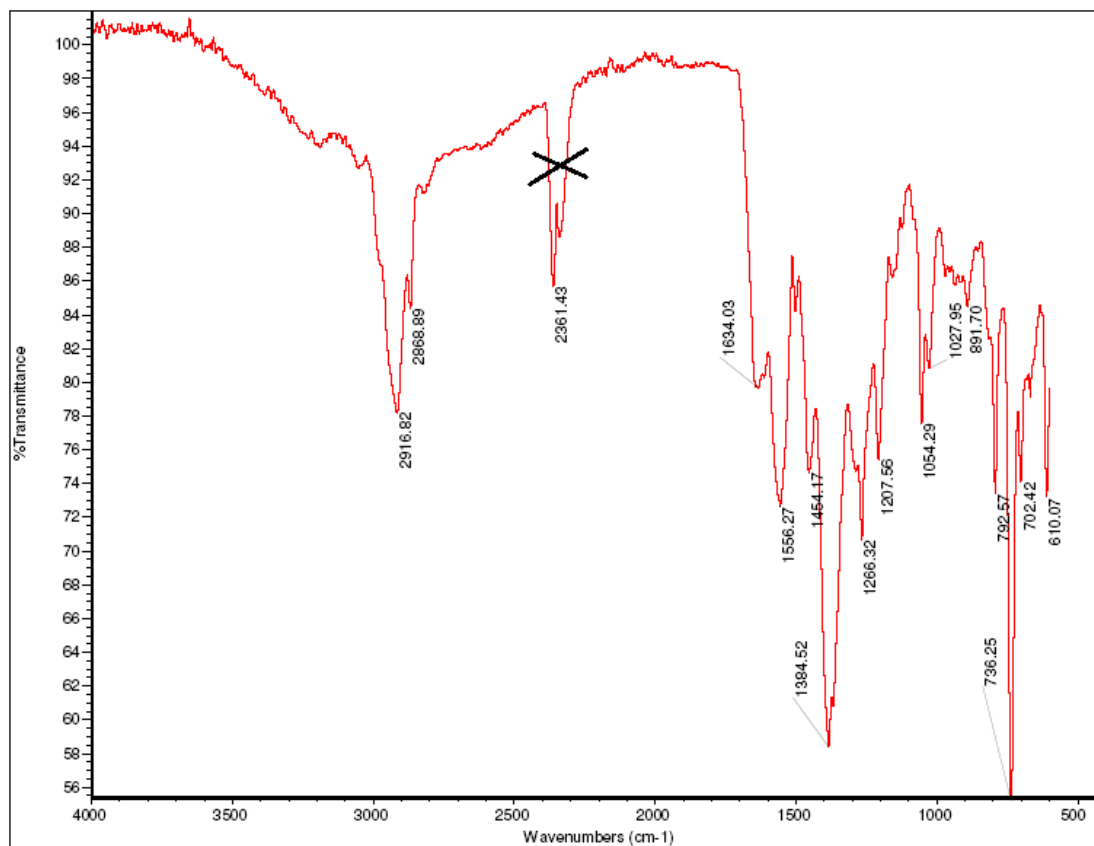
(-)-Myrtamycin (3-20)



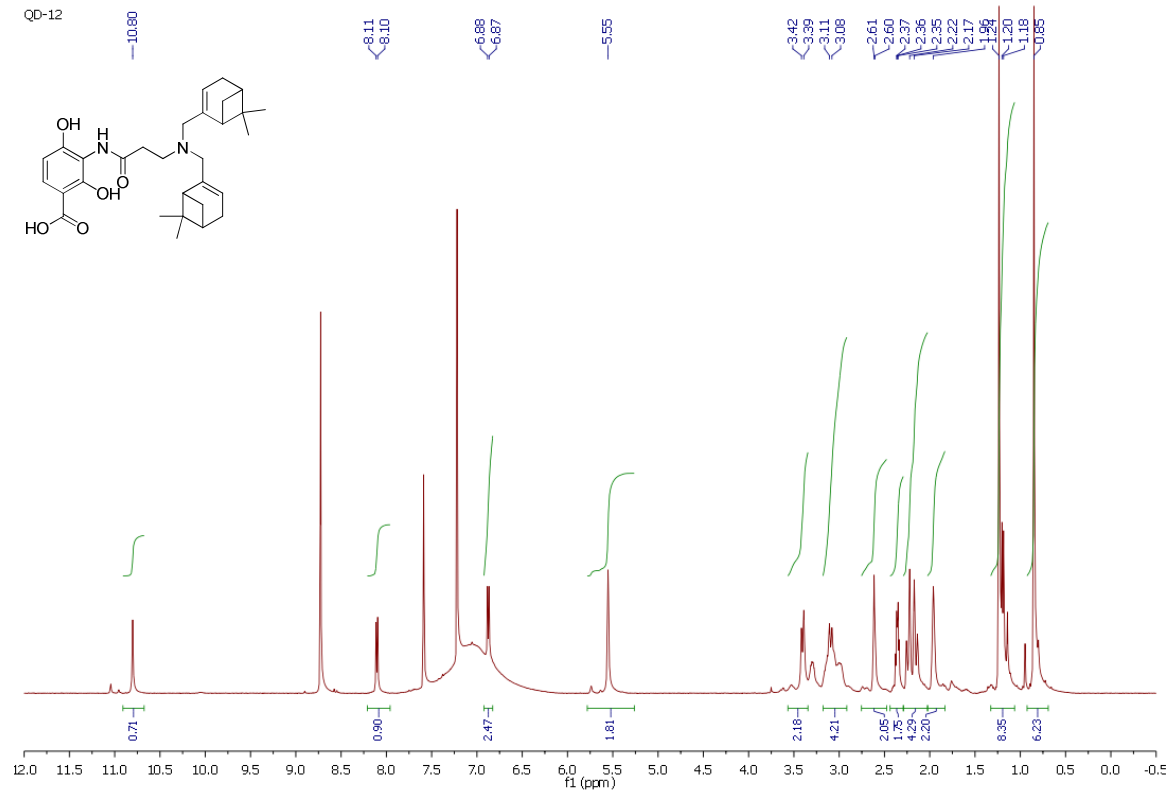
HPLC chromatography



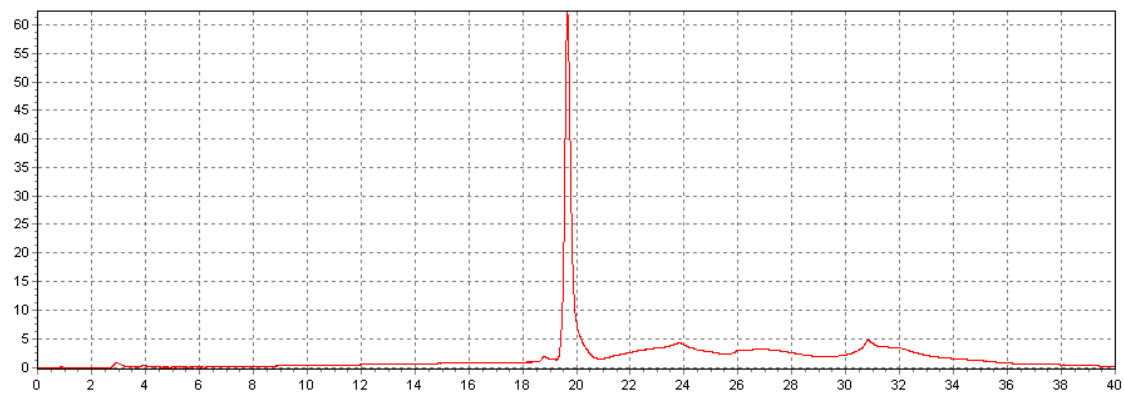
HPLC condition: A: 0.1 % TFA in H₂O; B: 0.1 % TFA in acetonitrile. 1 → 20 min: 33 → 63 % B.



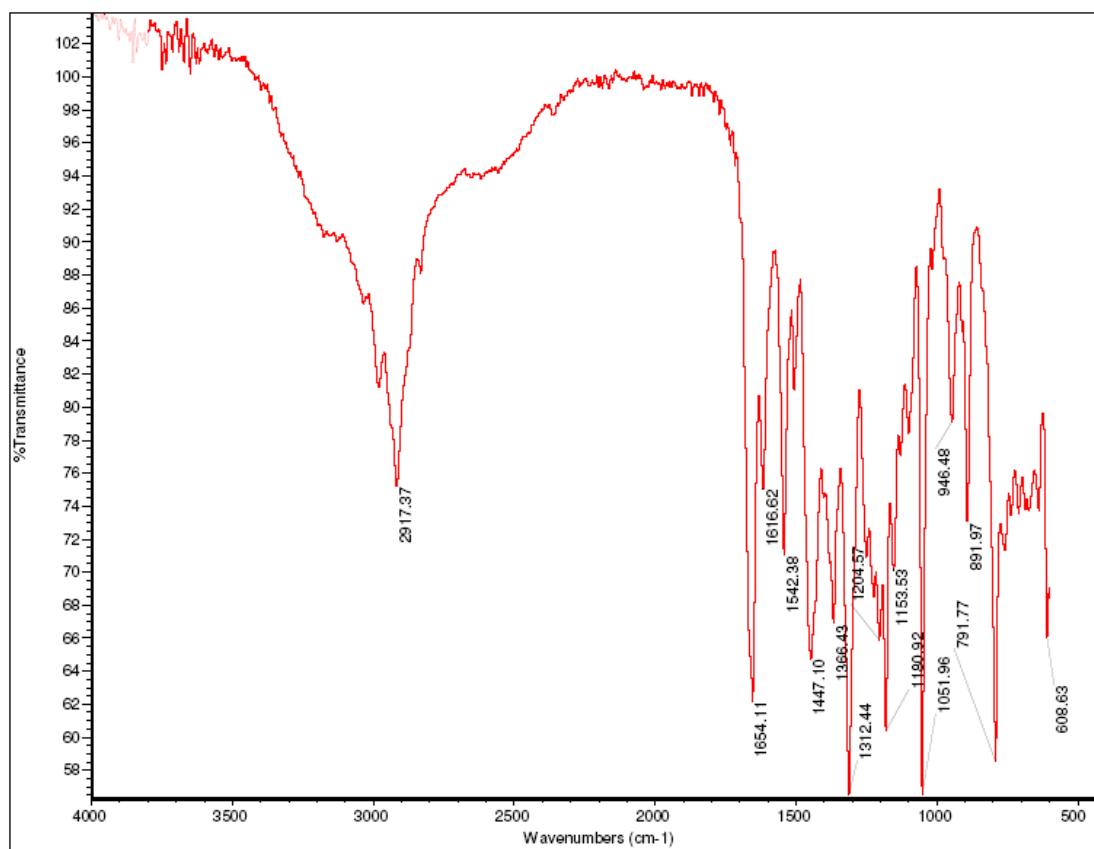
Compound 3-21



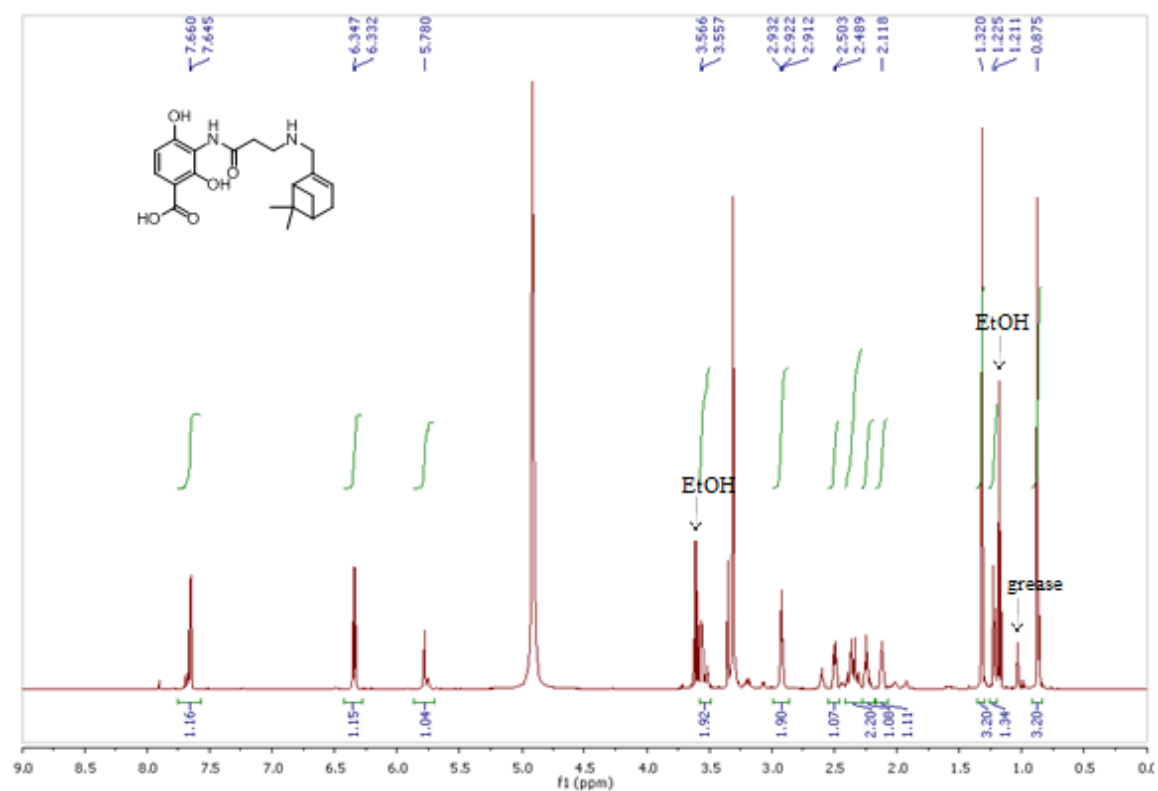
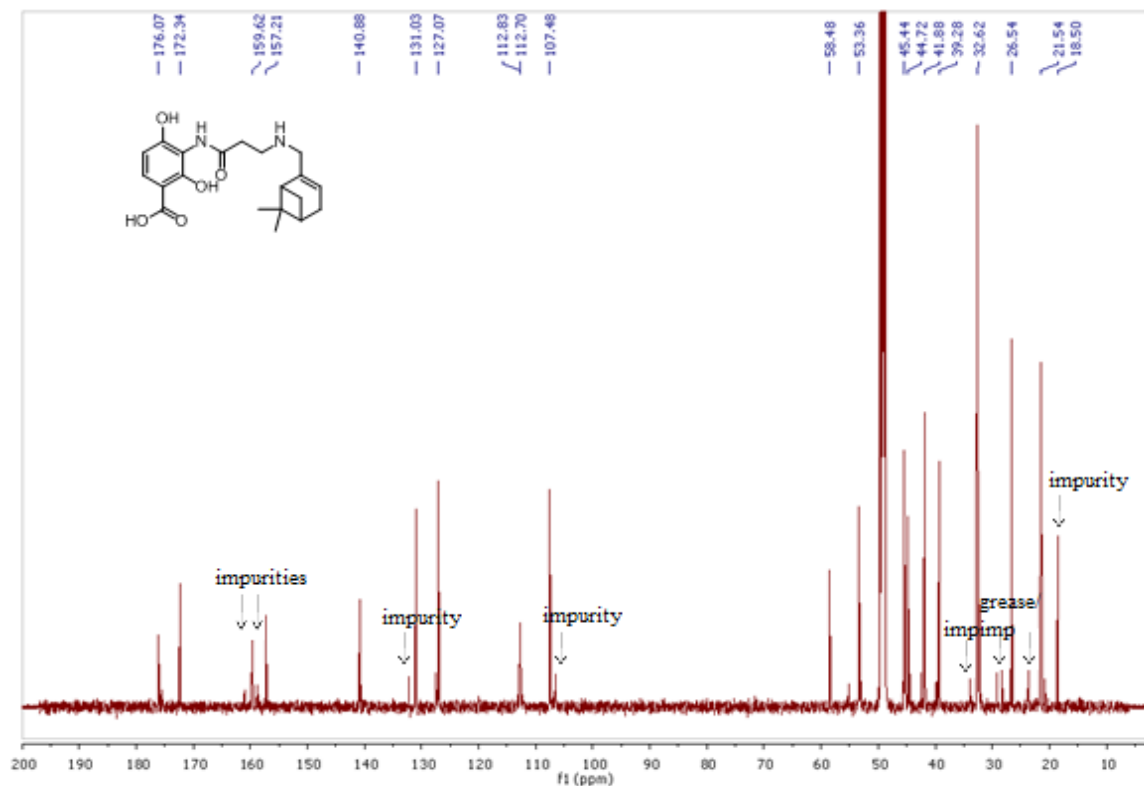
HPLC chromatography



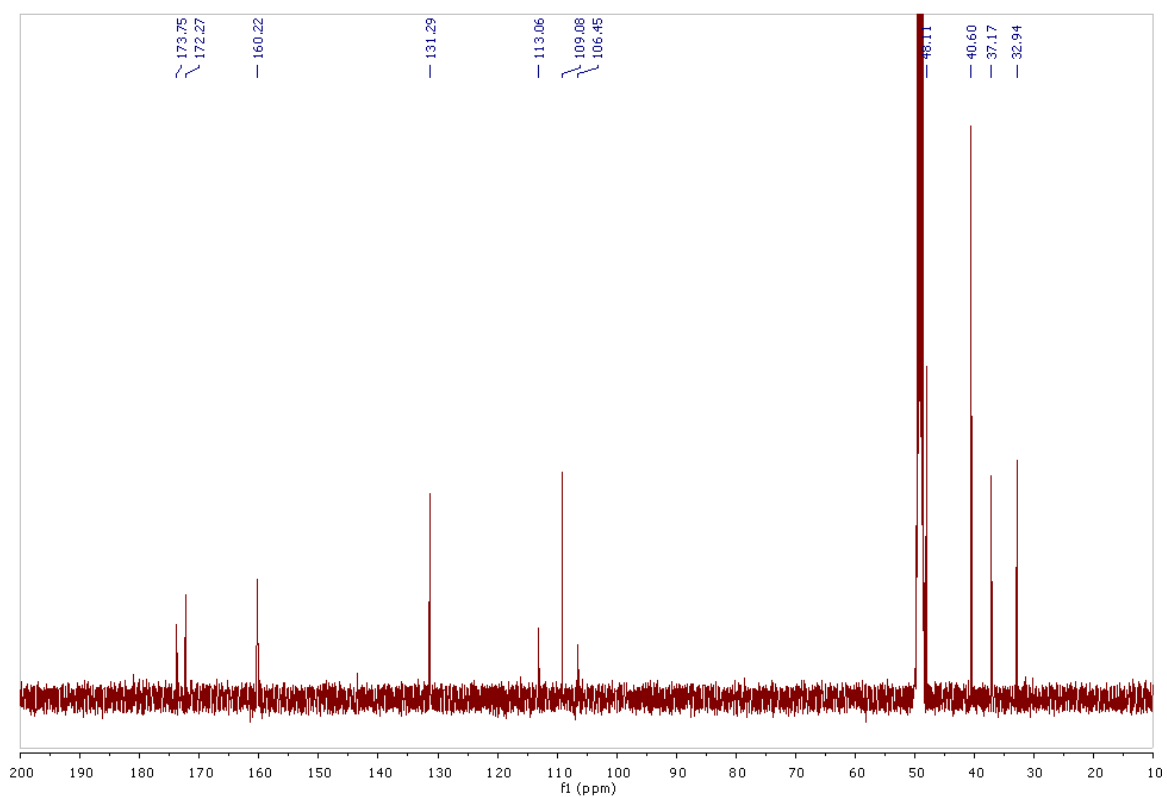
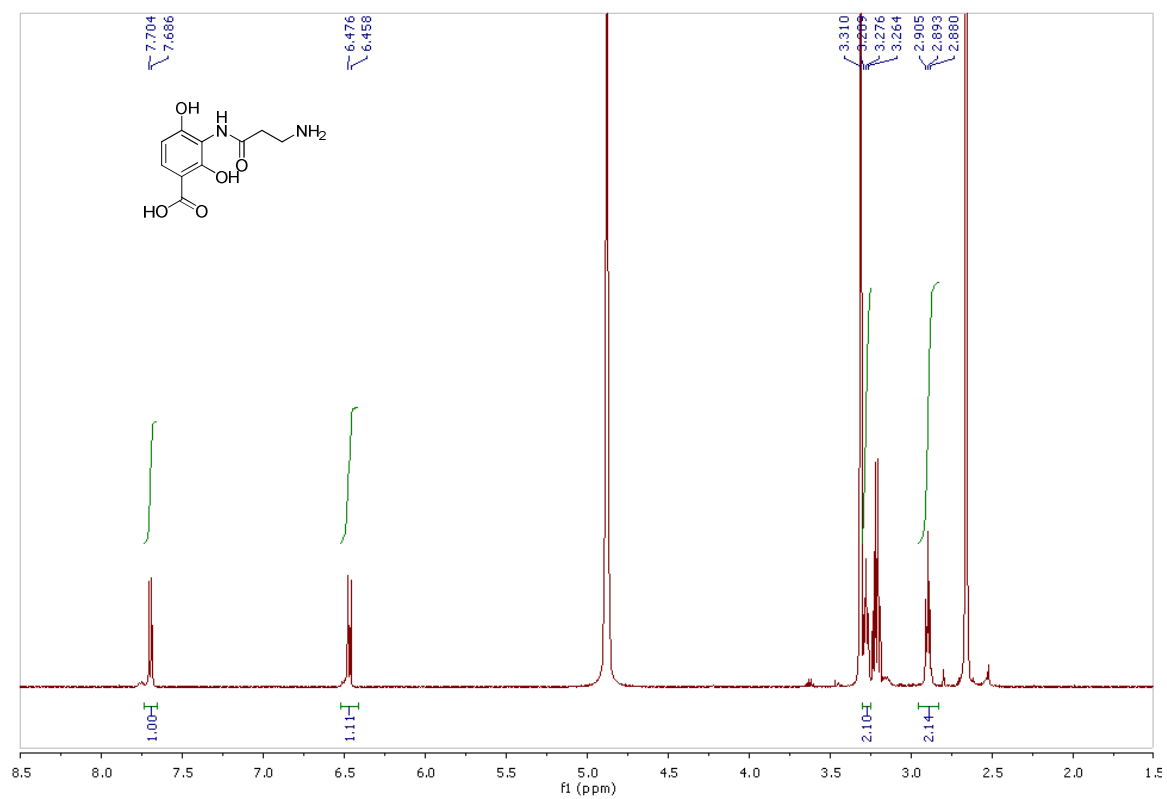
HPLC condition: 0.1 % TFA in H₂O; B: 0.1 % TFA in acetonitrile. 1 → 20 min: 33 → 63 % B.

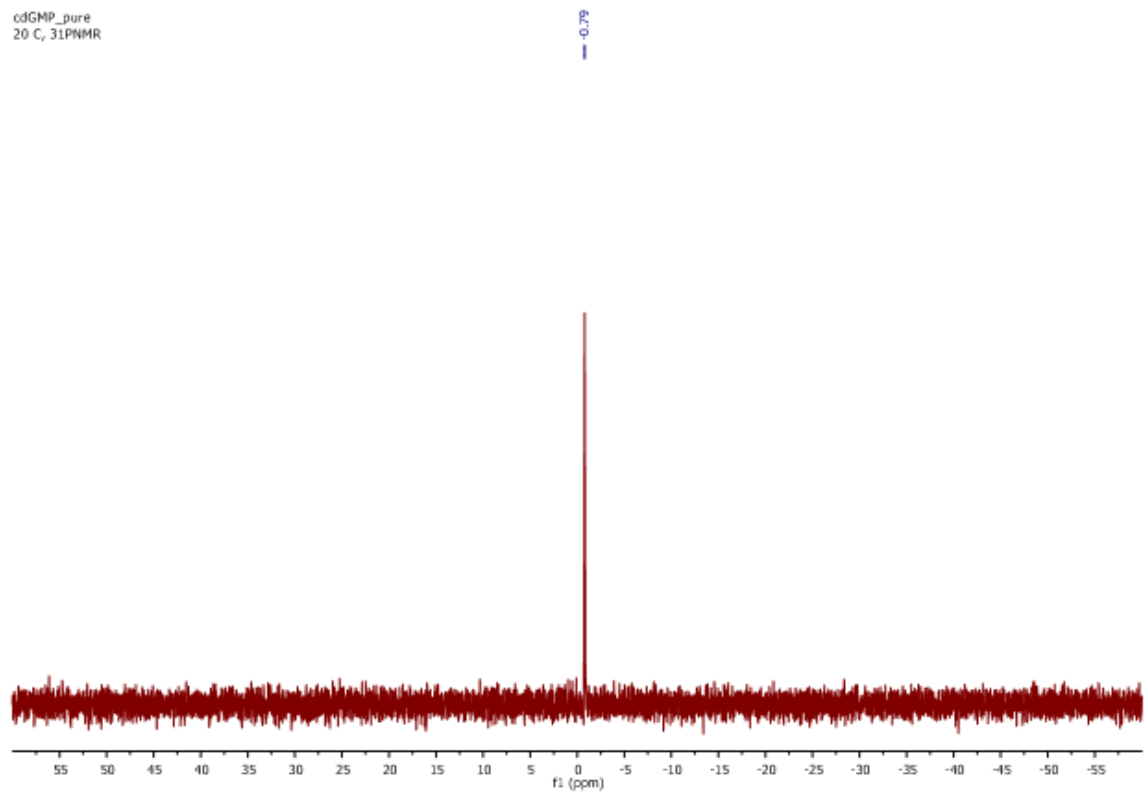
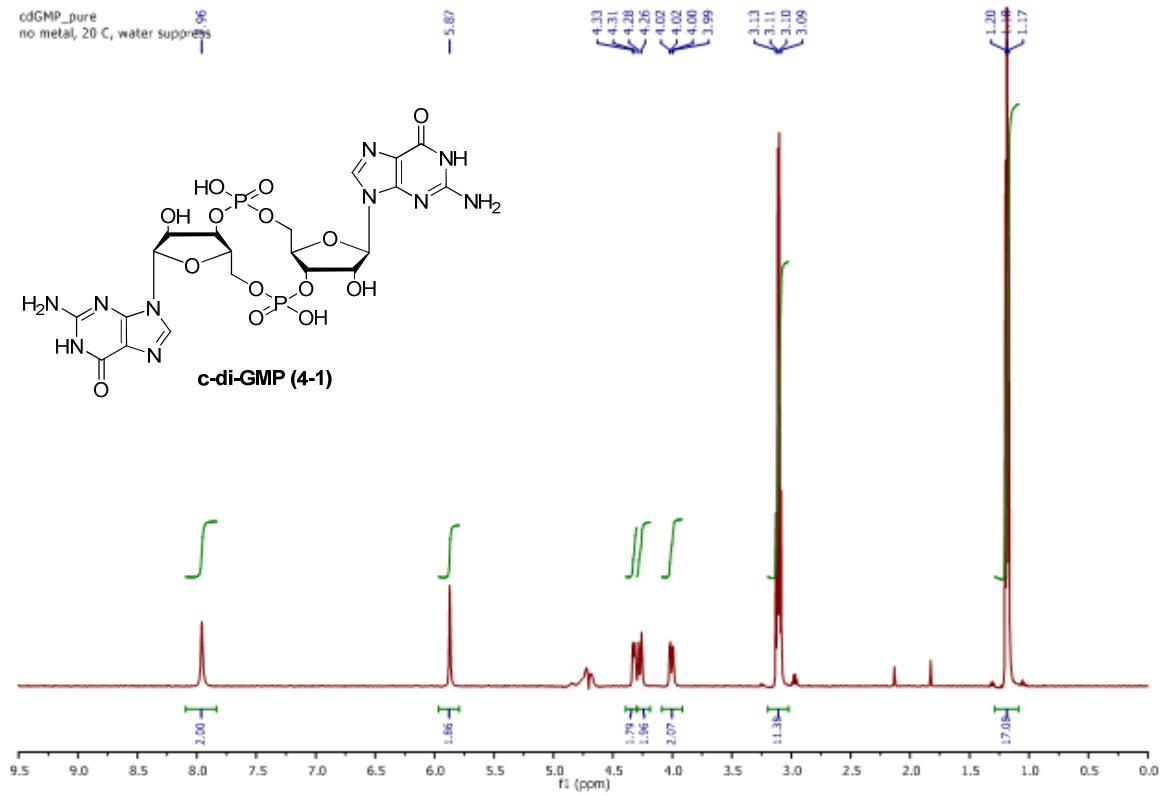


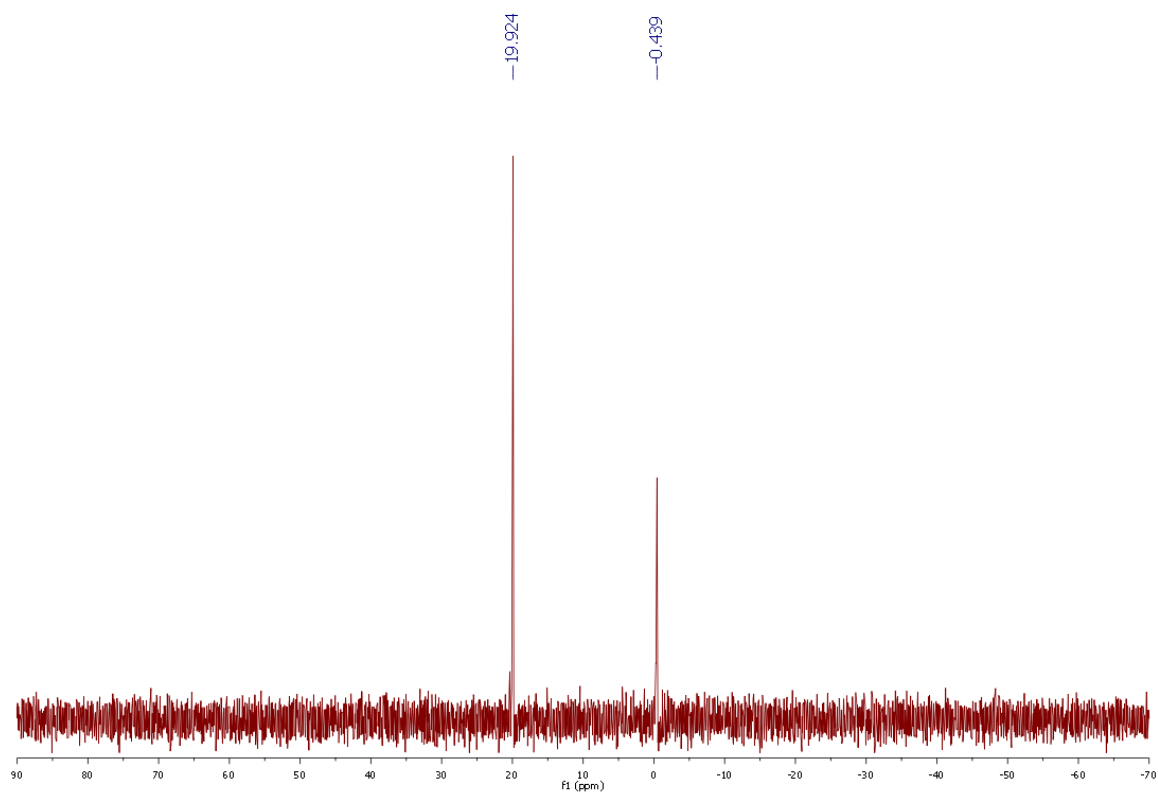
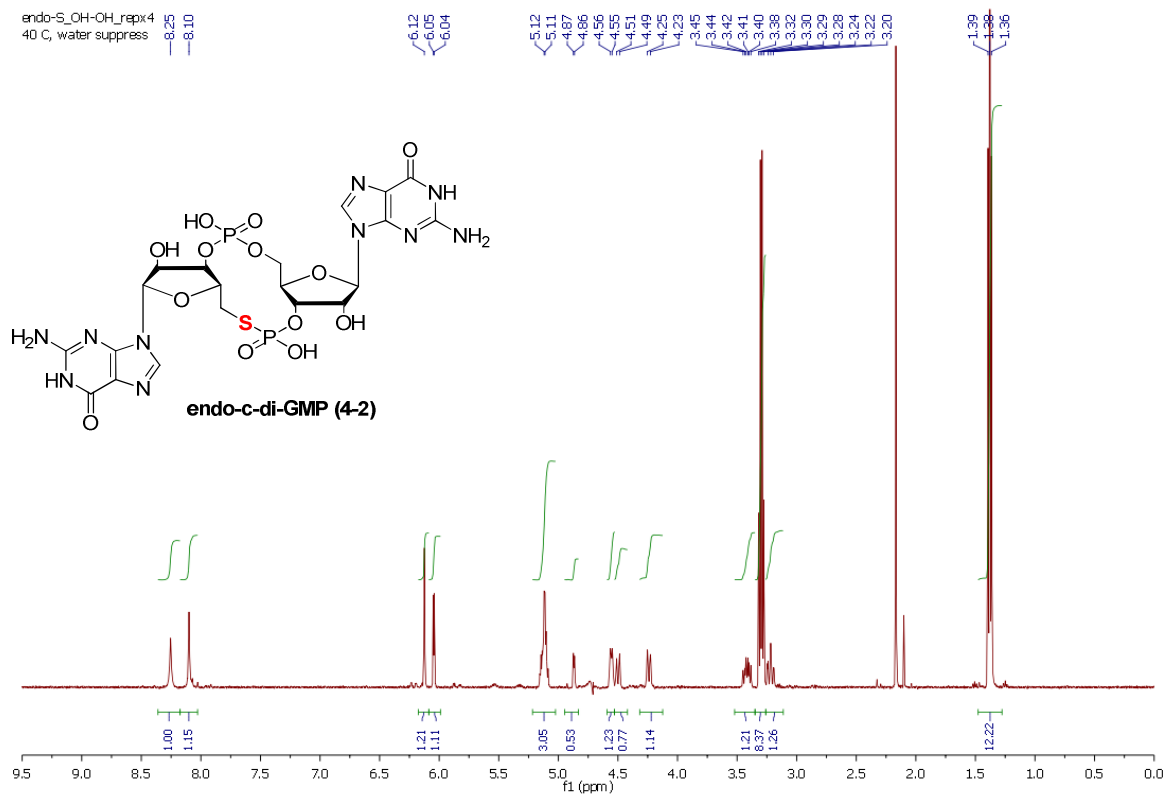
Compound 3-22

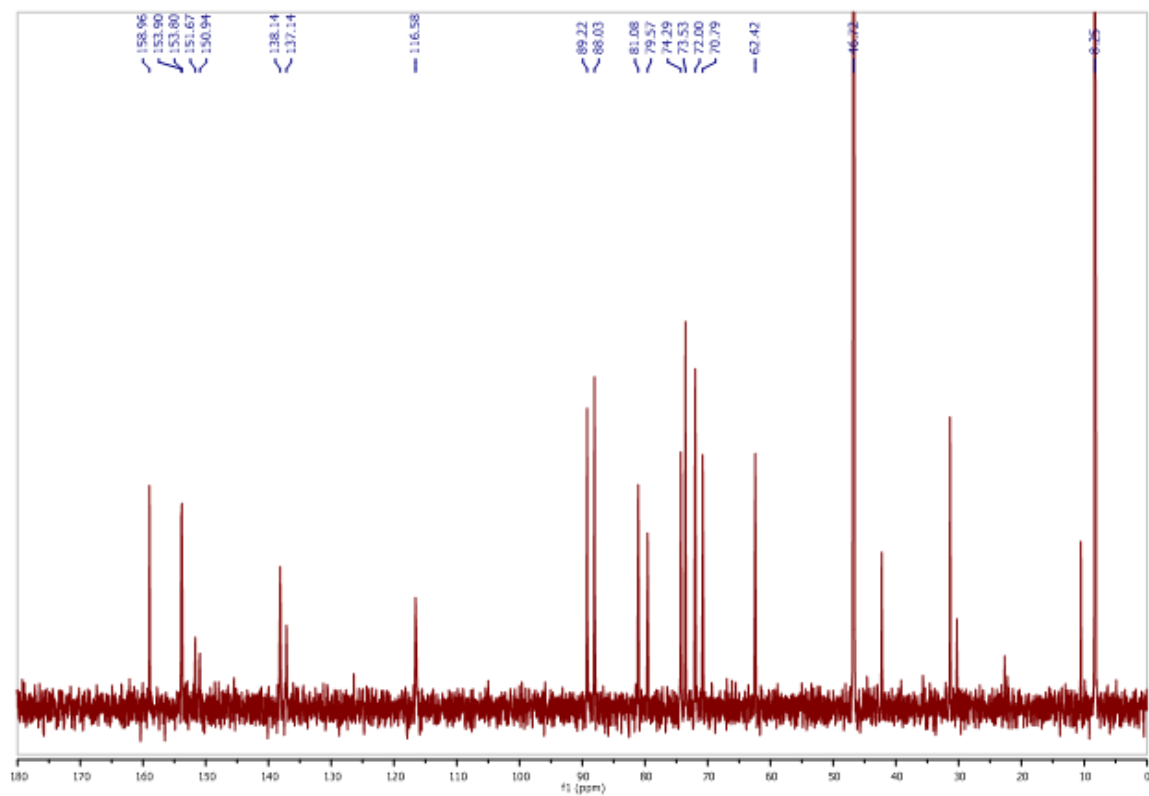


Compound 3-23

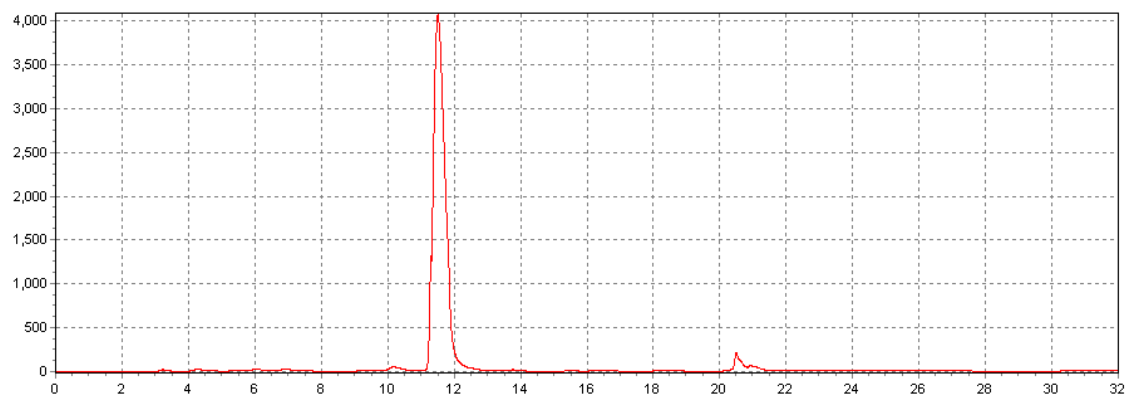




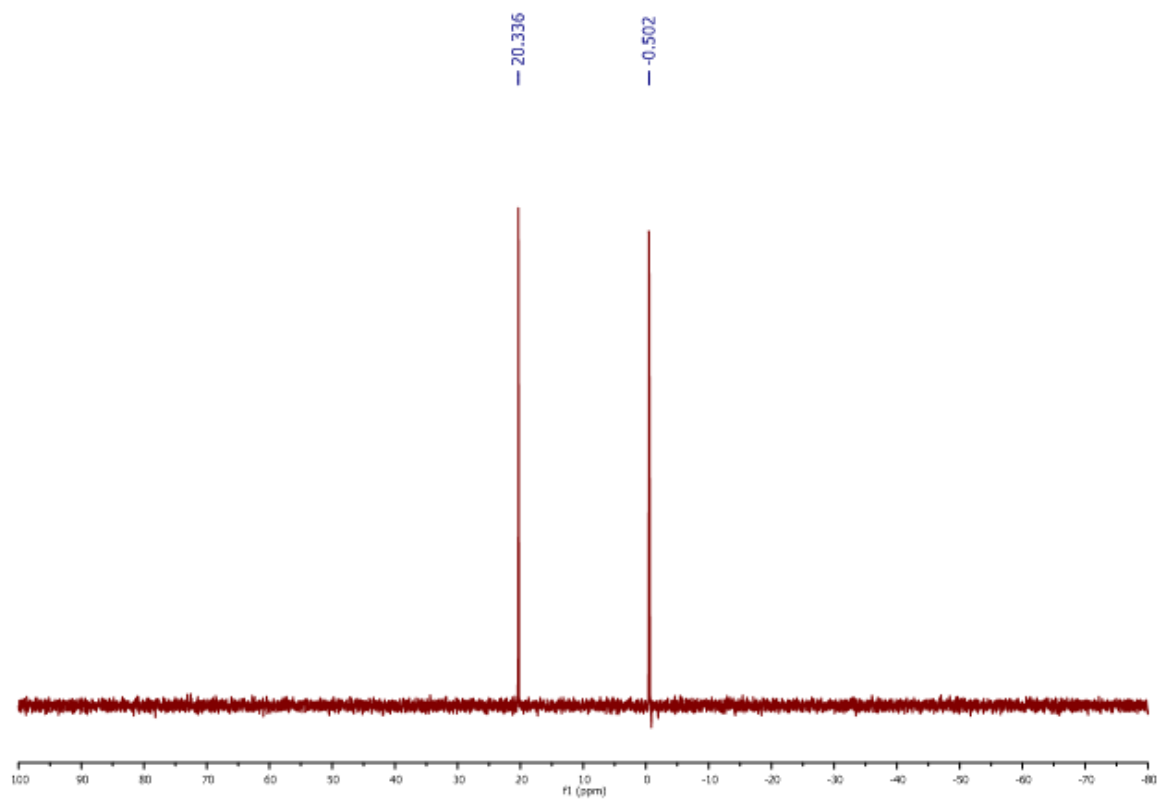
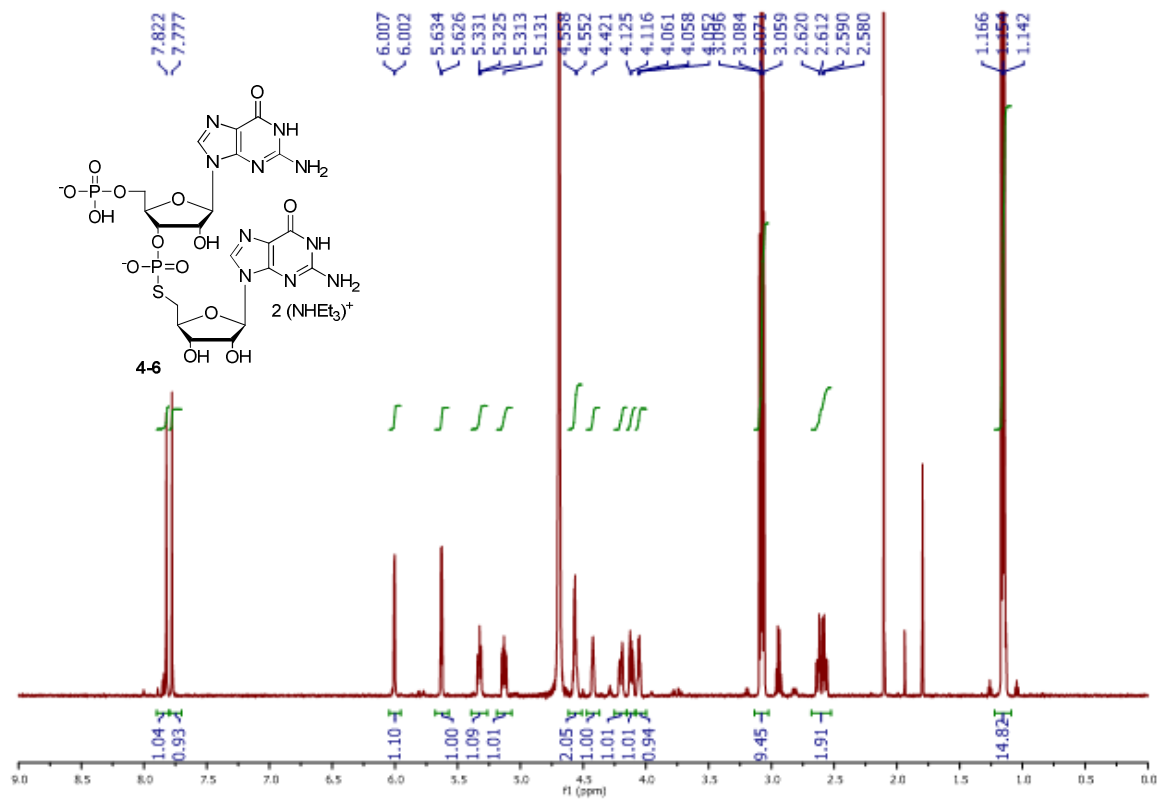


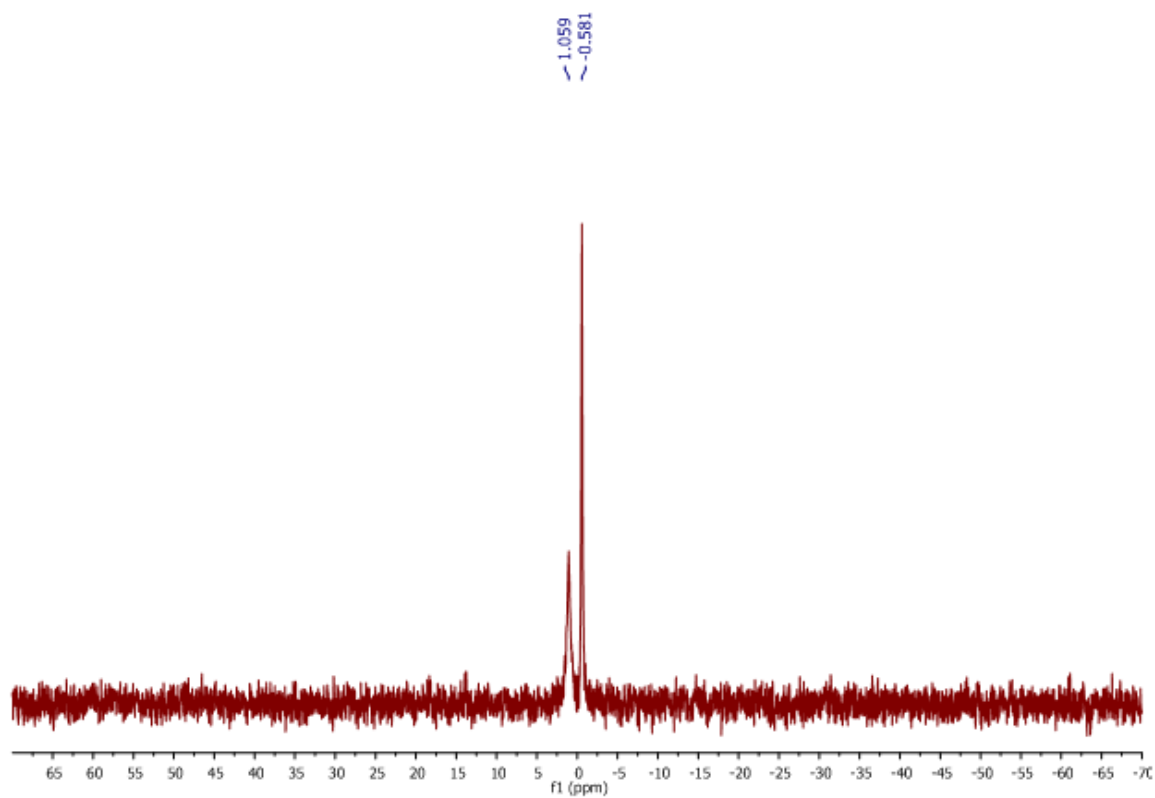
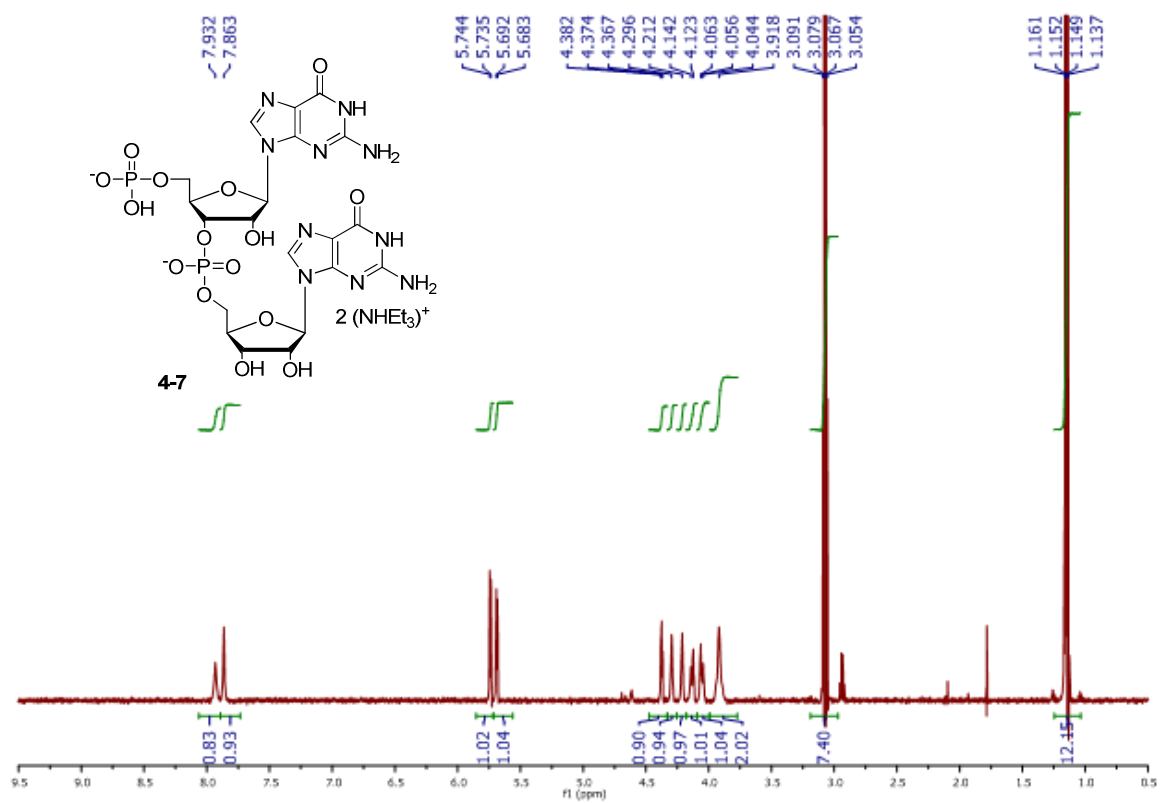


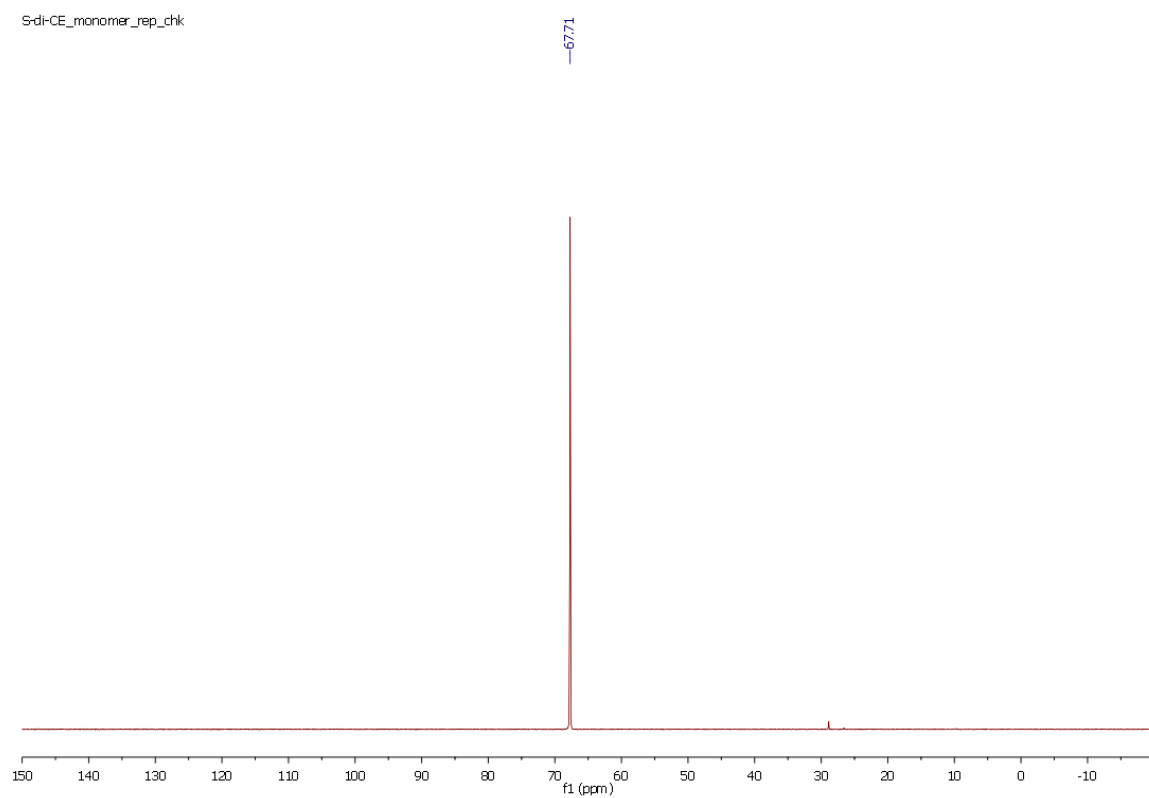
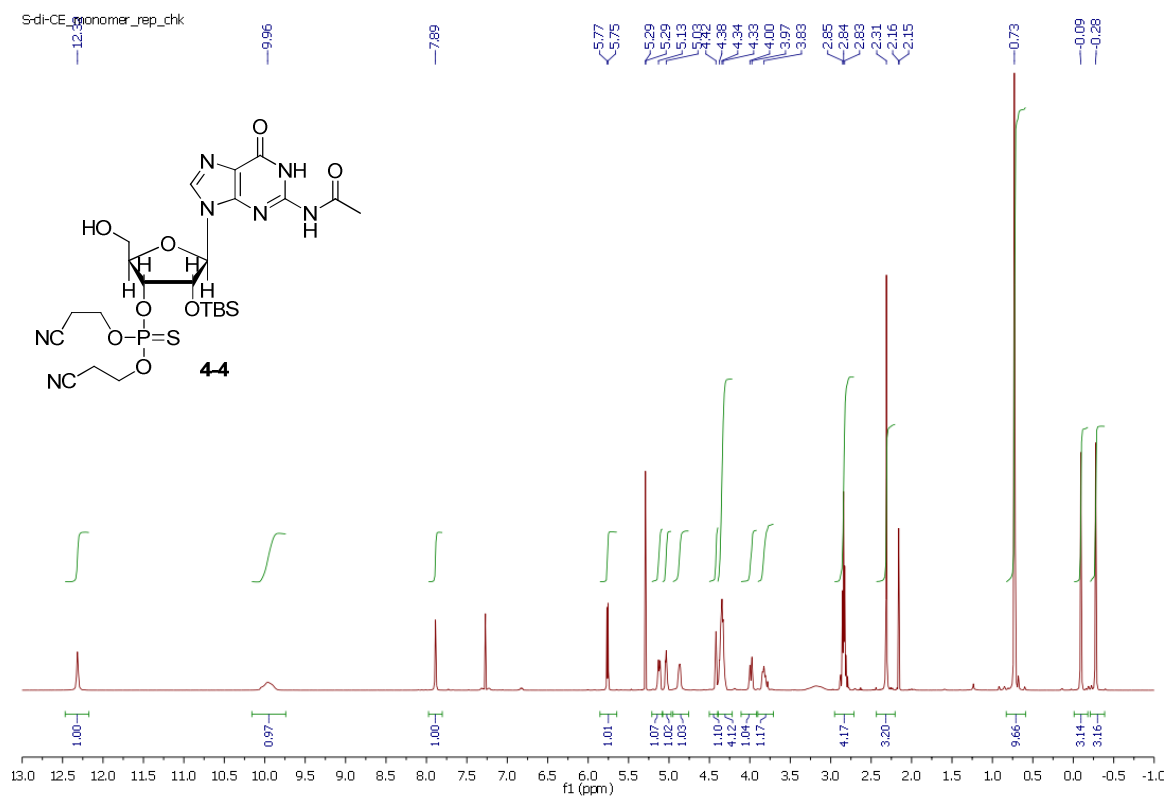
HPLC chromatography

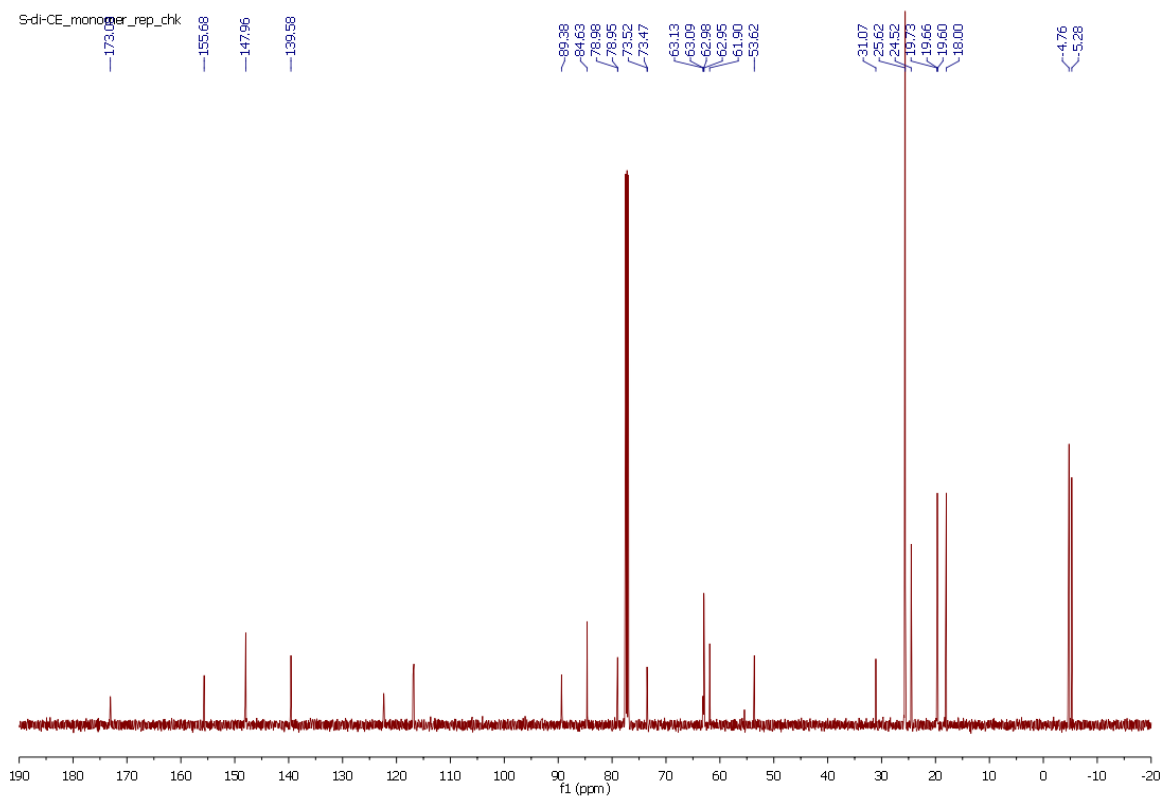


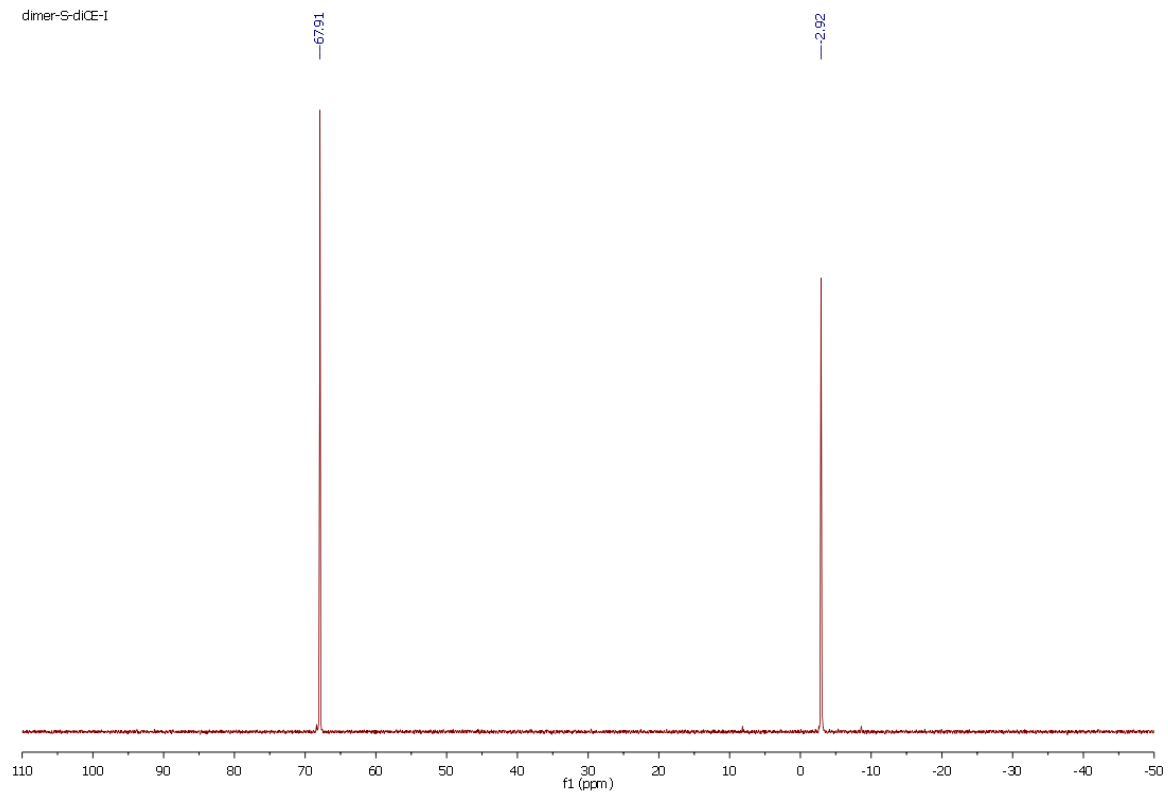
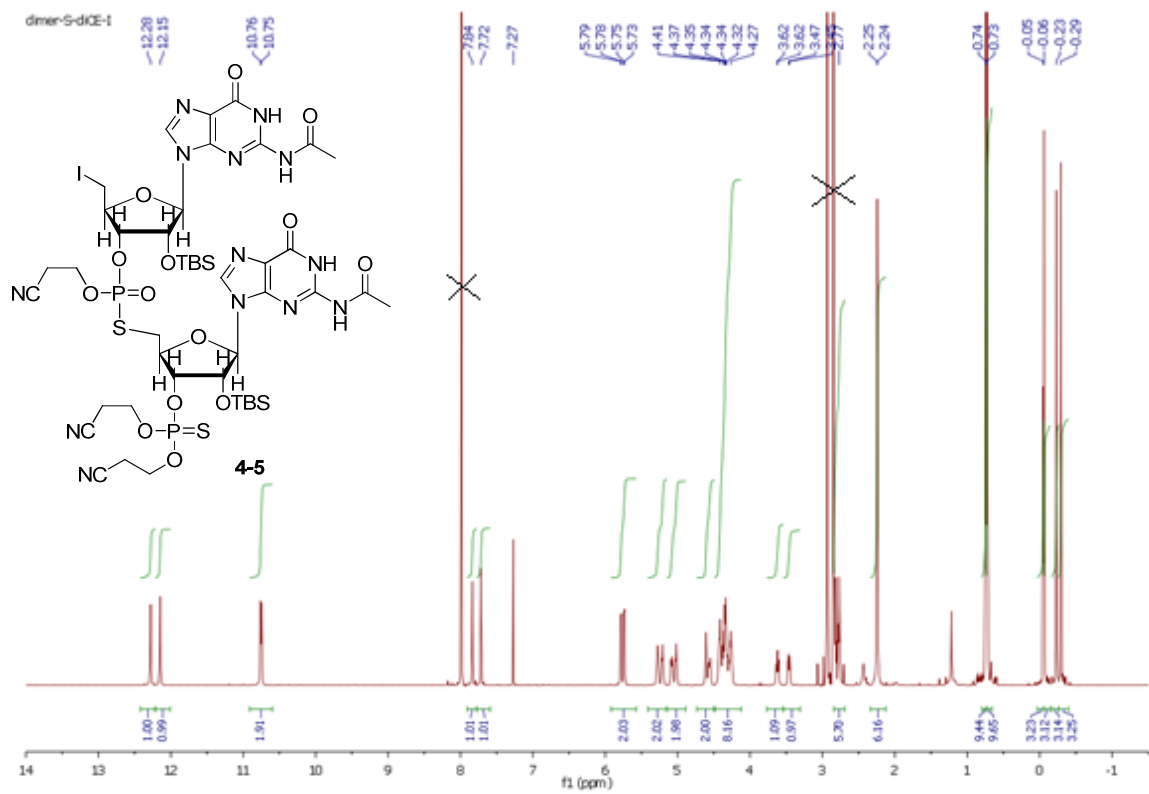
HPLC condition: A: 100 mM TEAA buffer with 2% MeOH in water; B: acetonitrile; 0
 → 4 % B, 0 → 14 min, 50 °C.

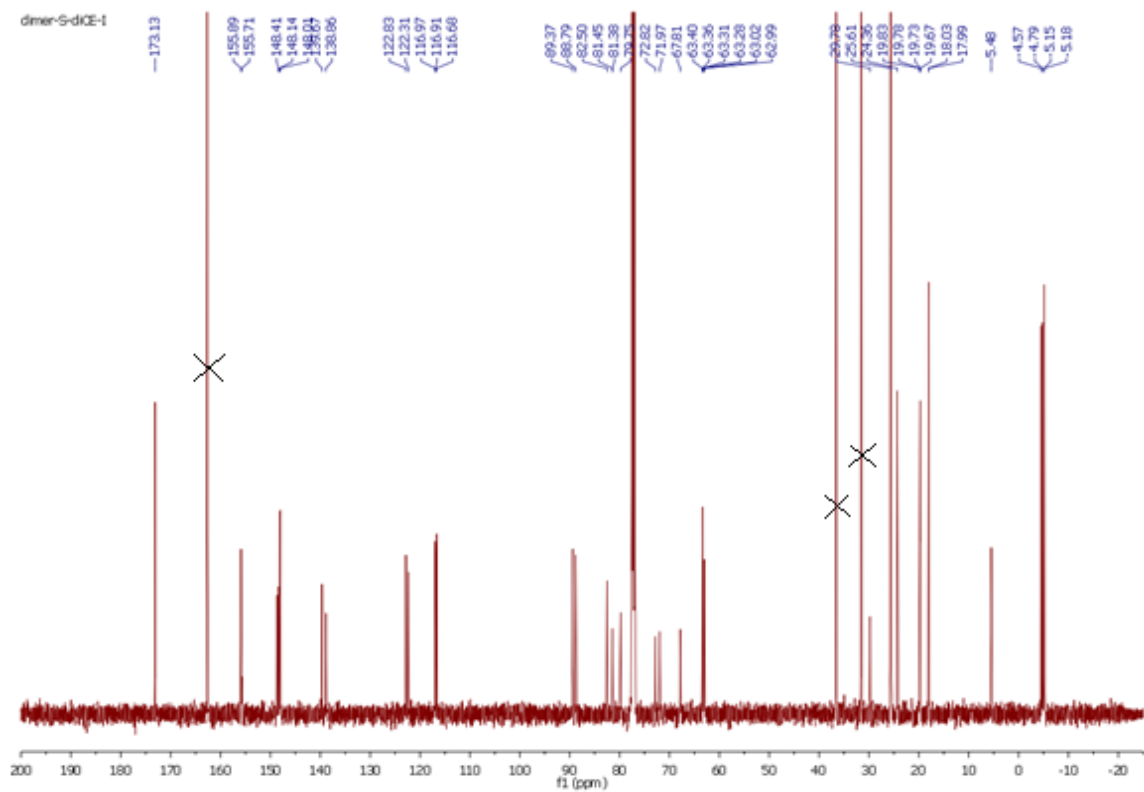


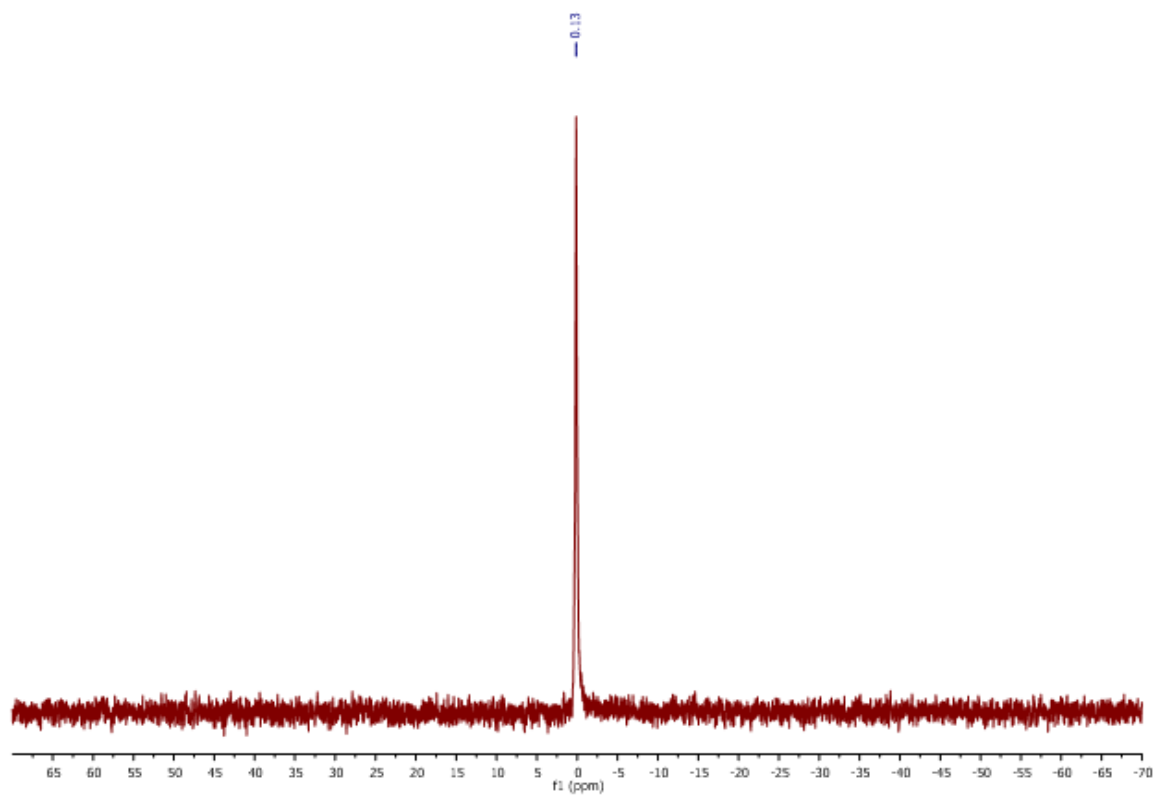
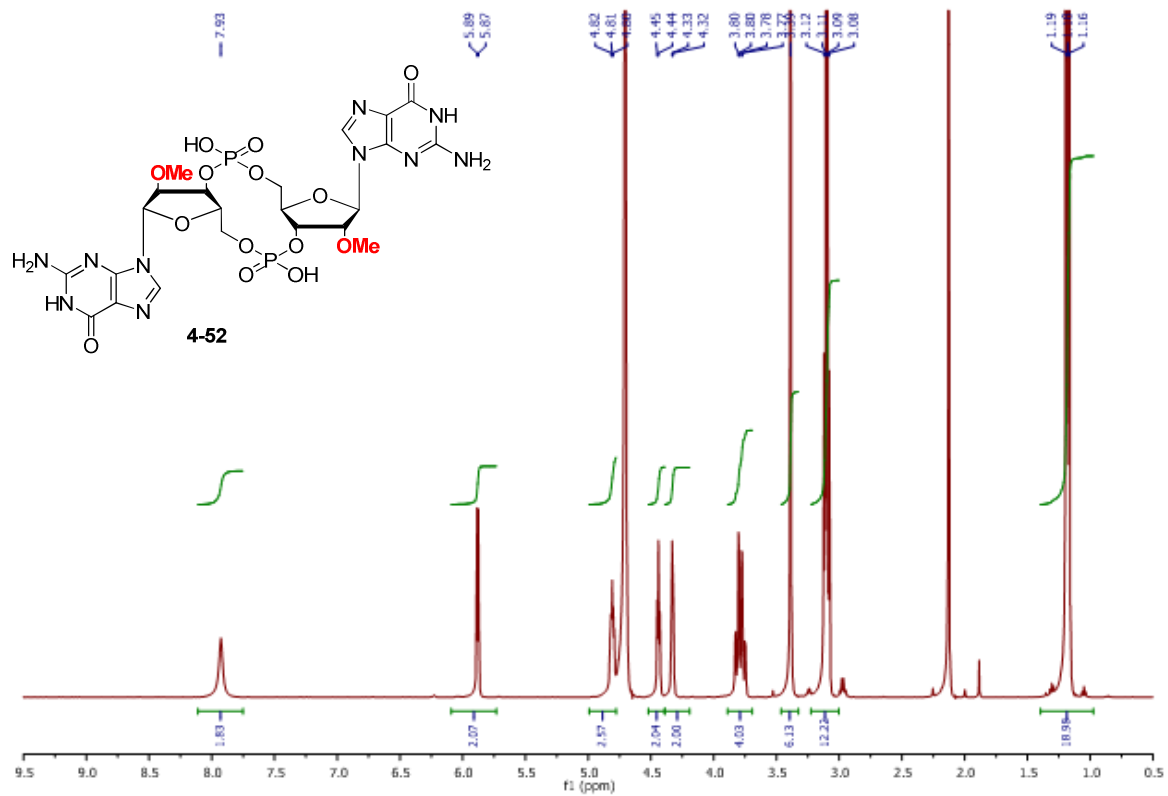


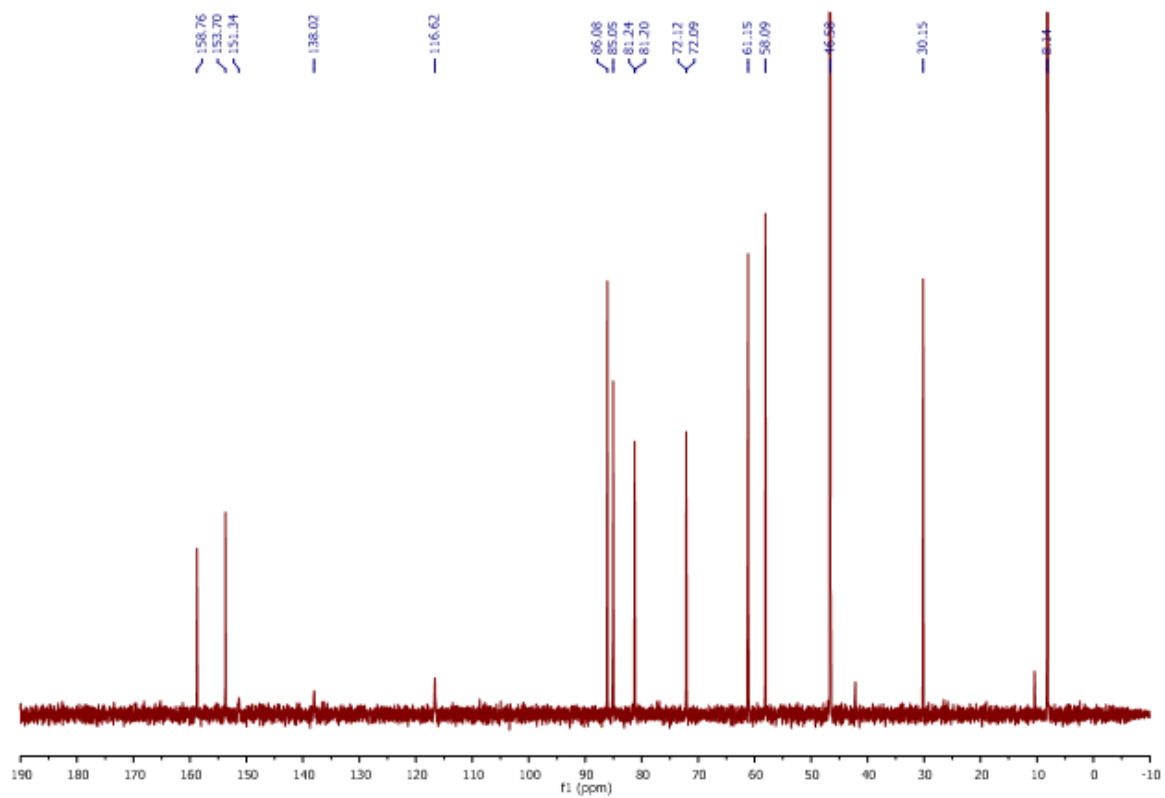


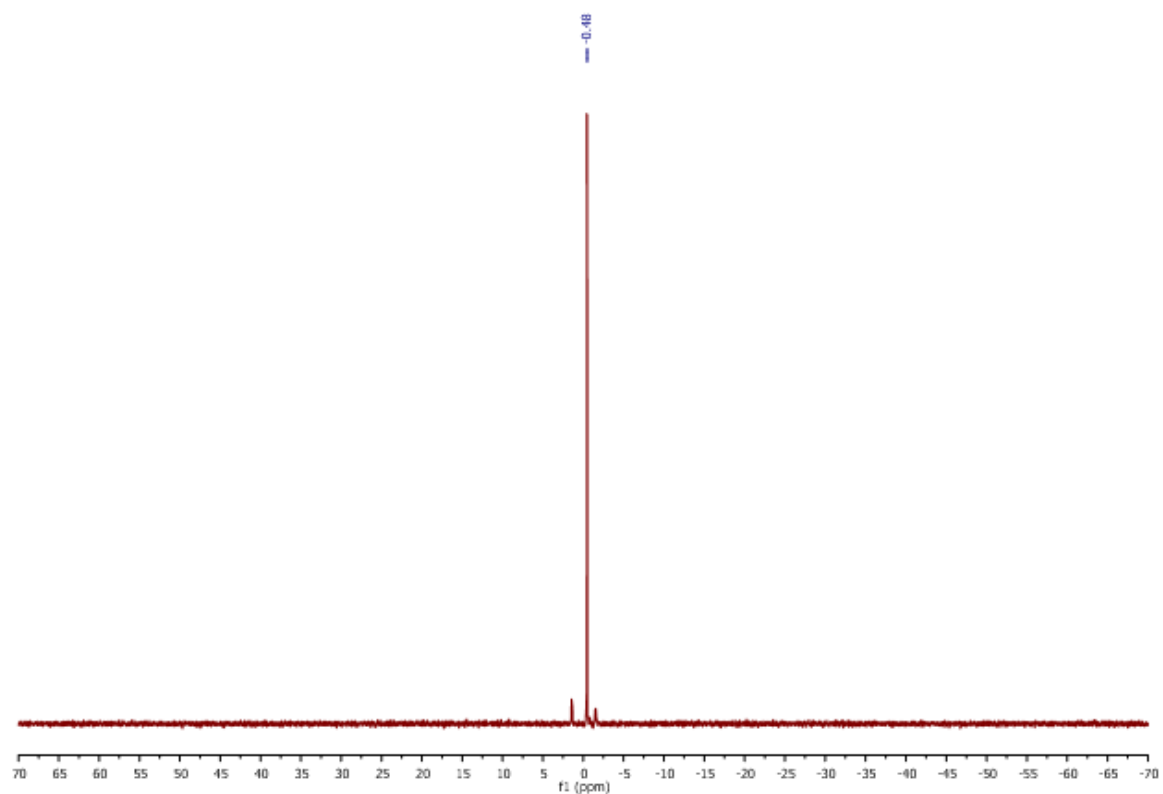
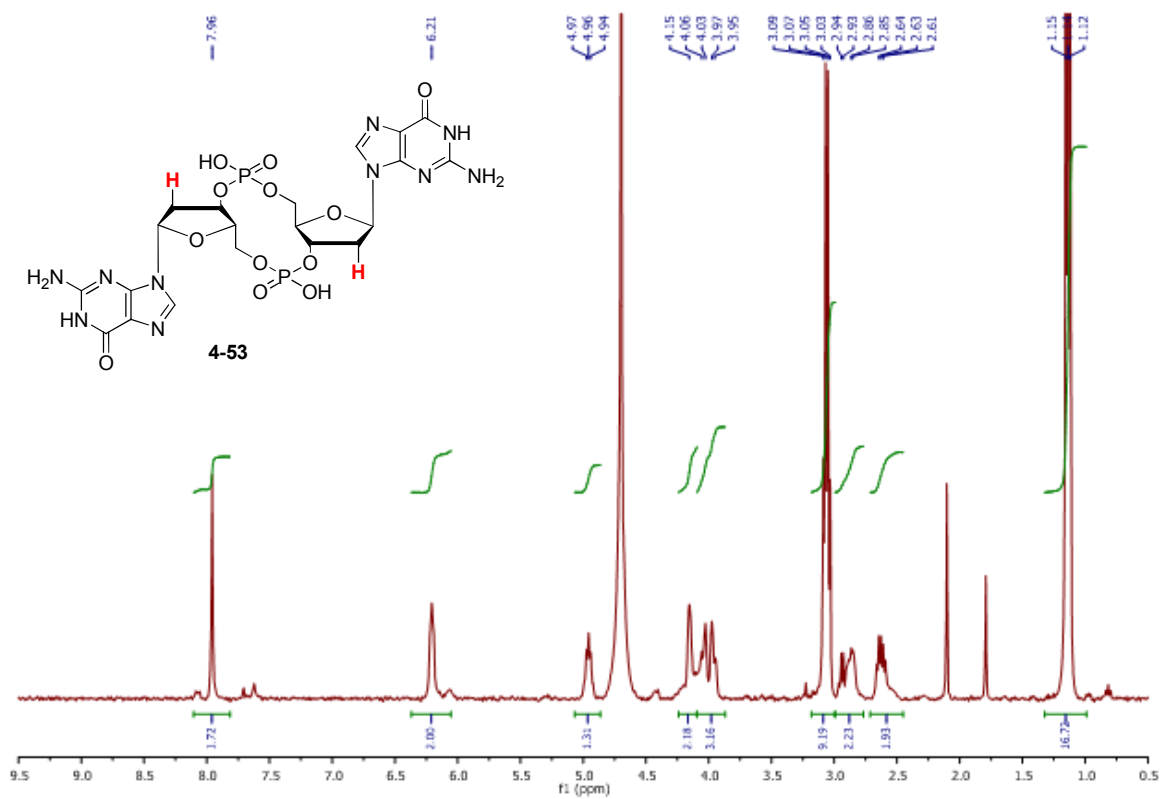


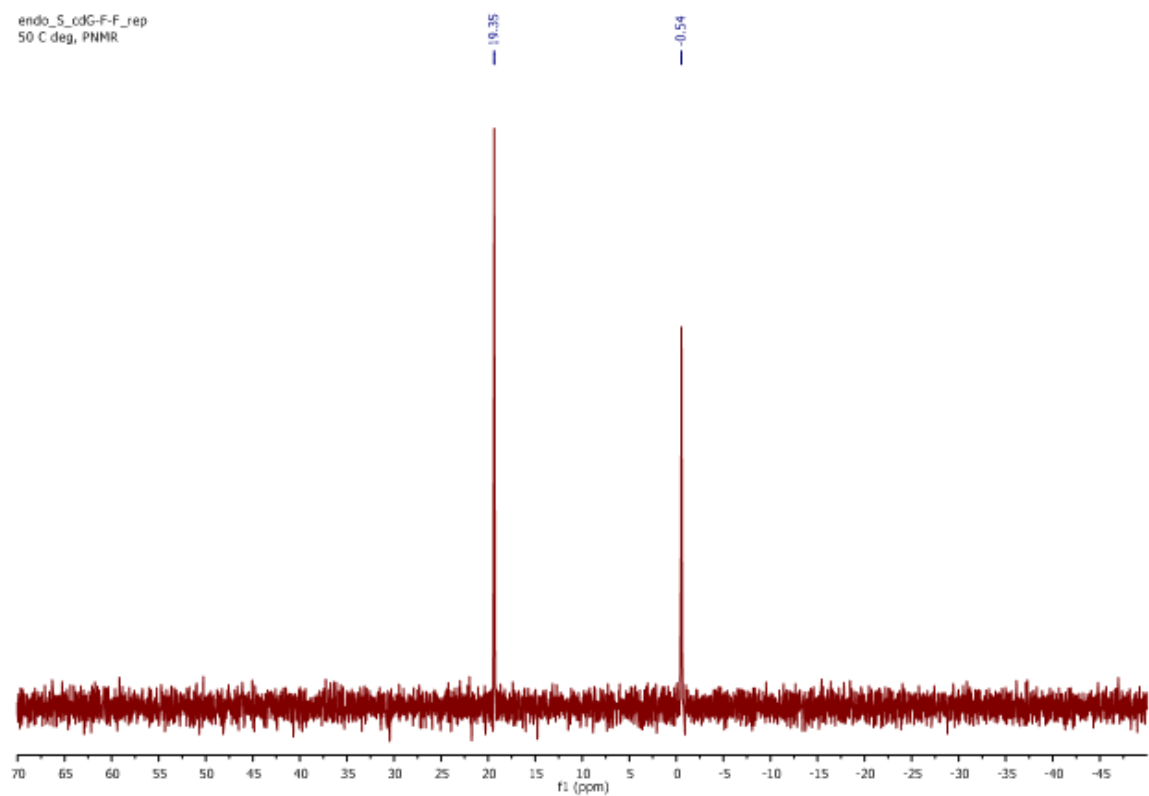
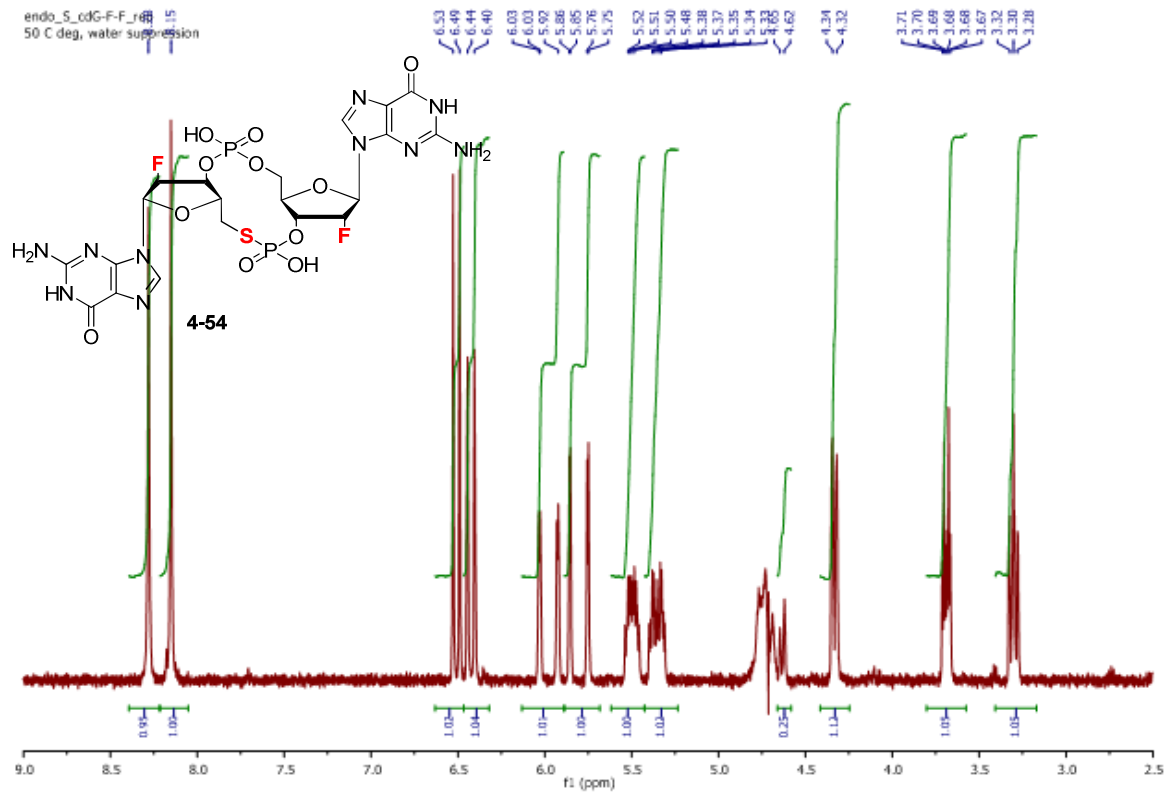


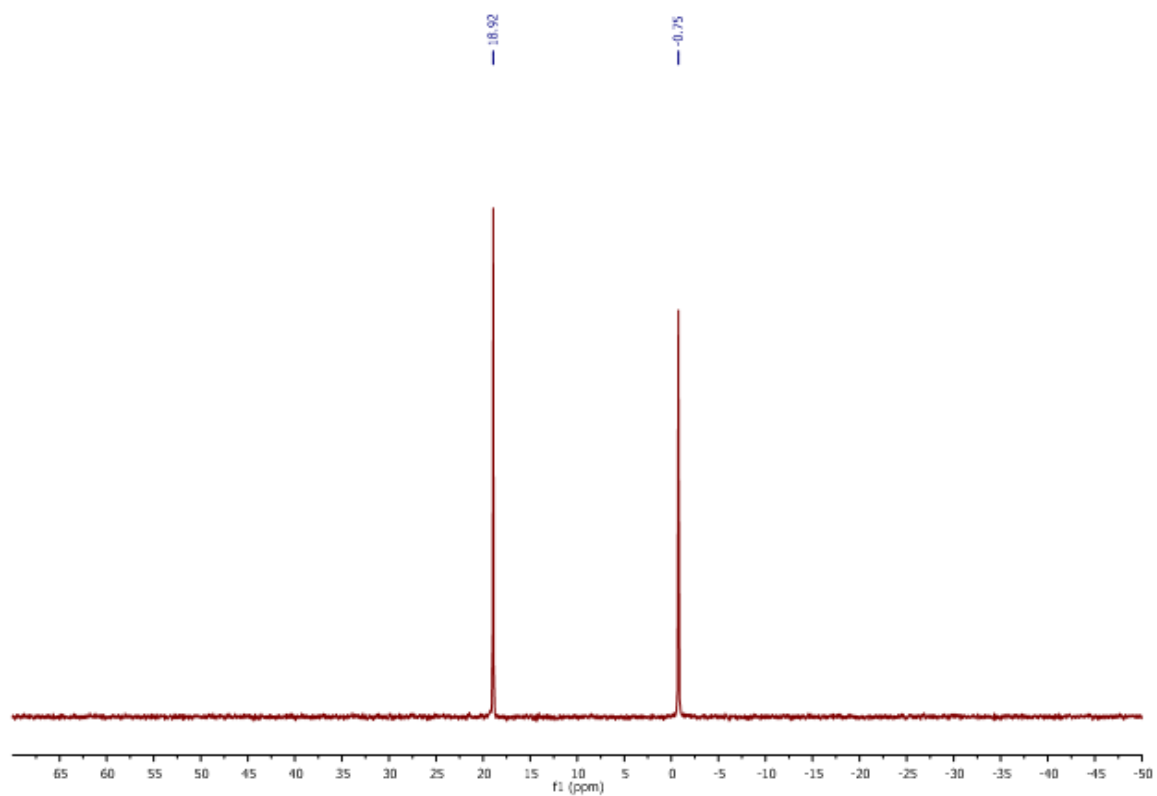
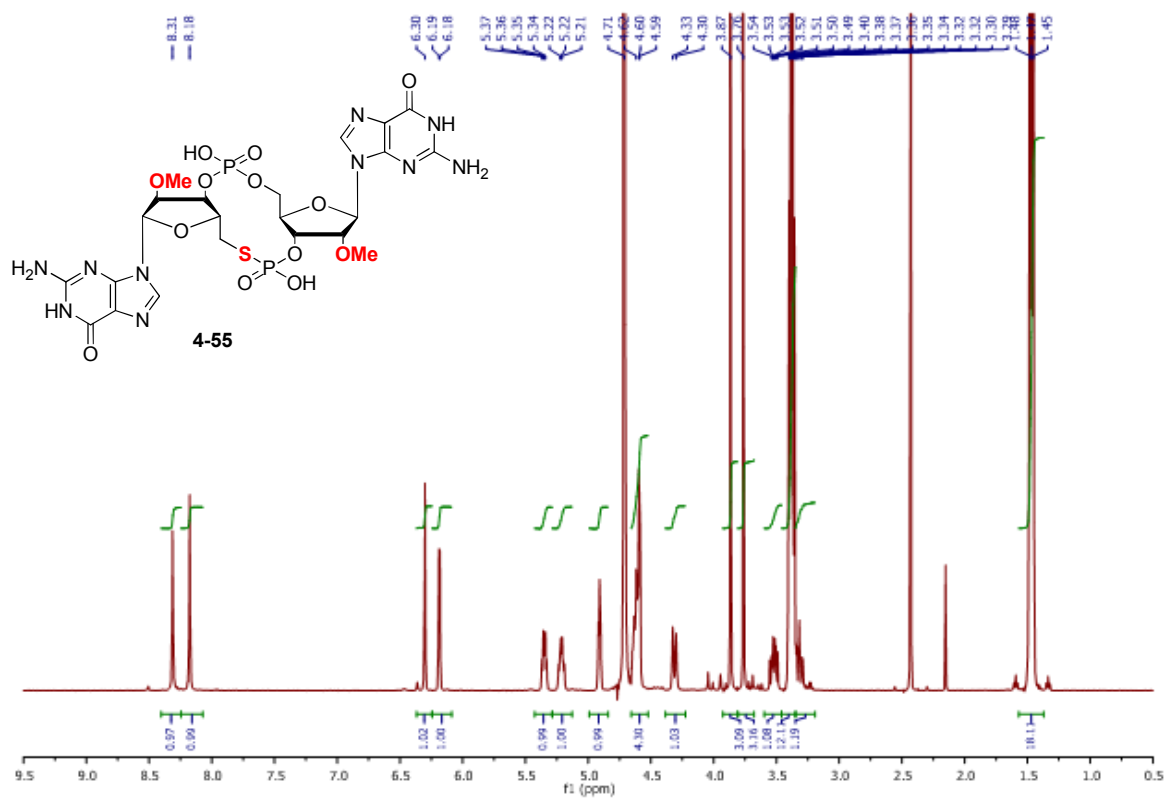


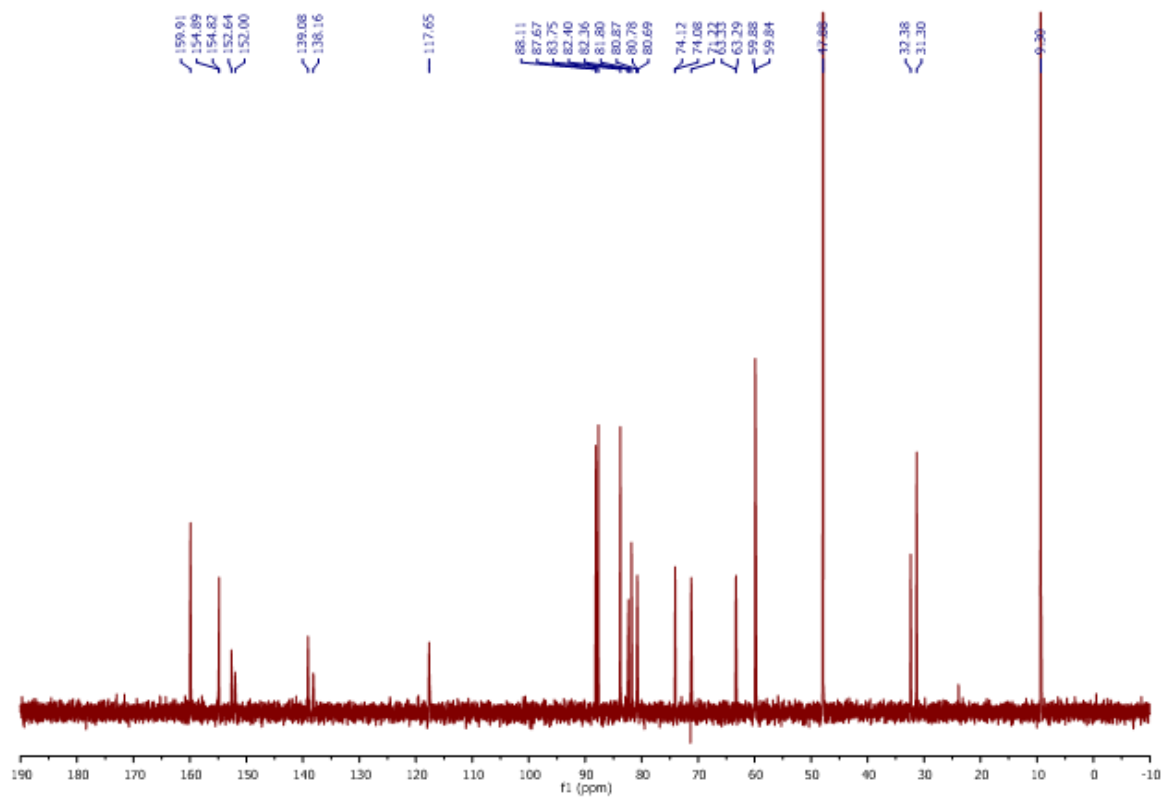


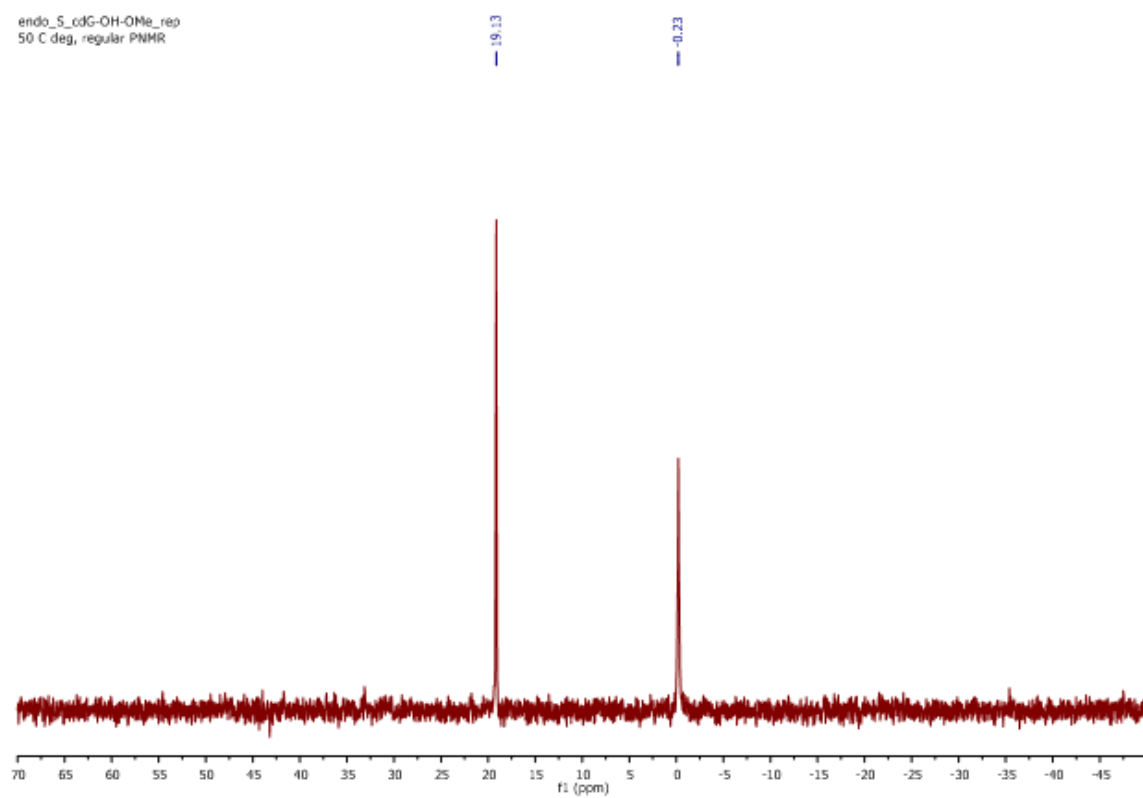
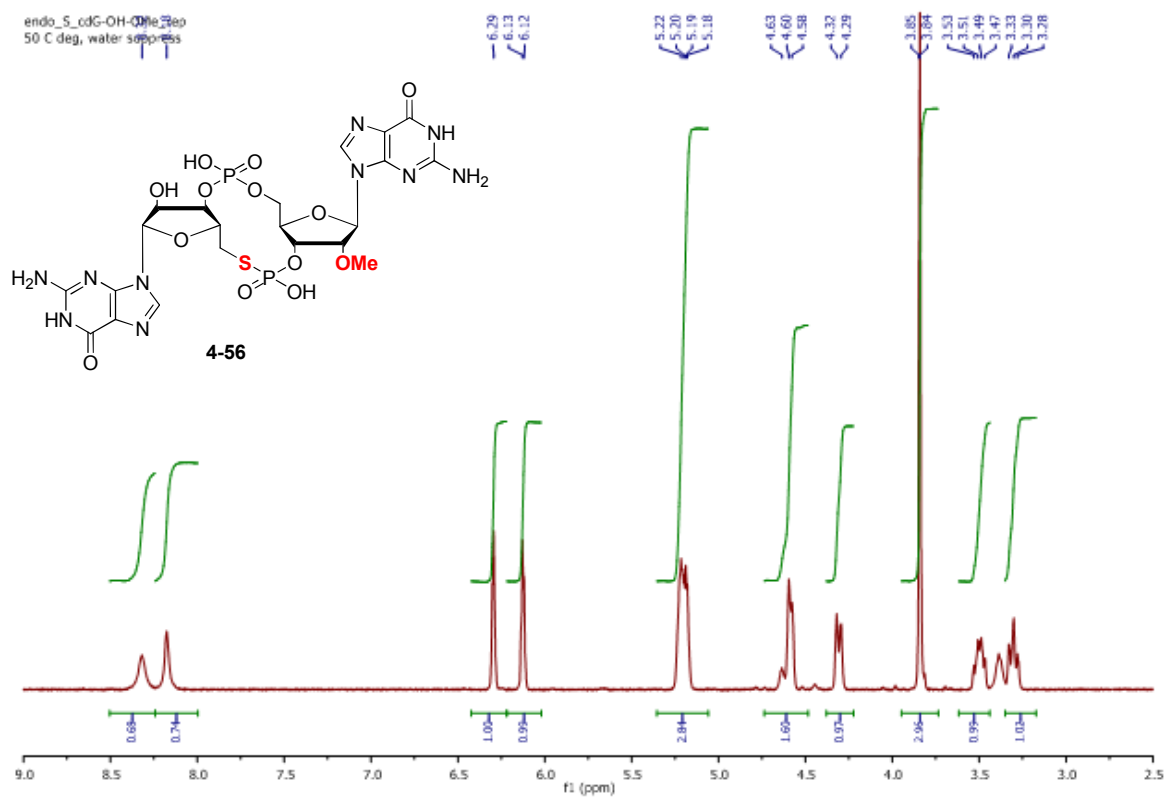


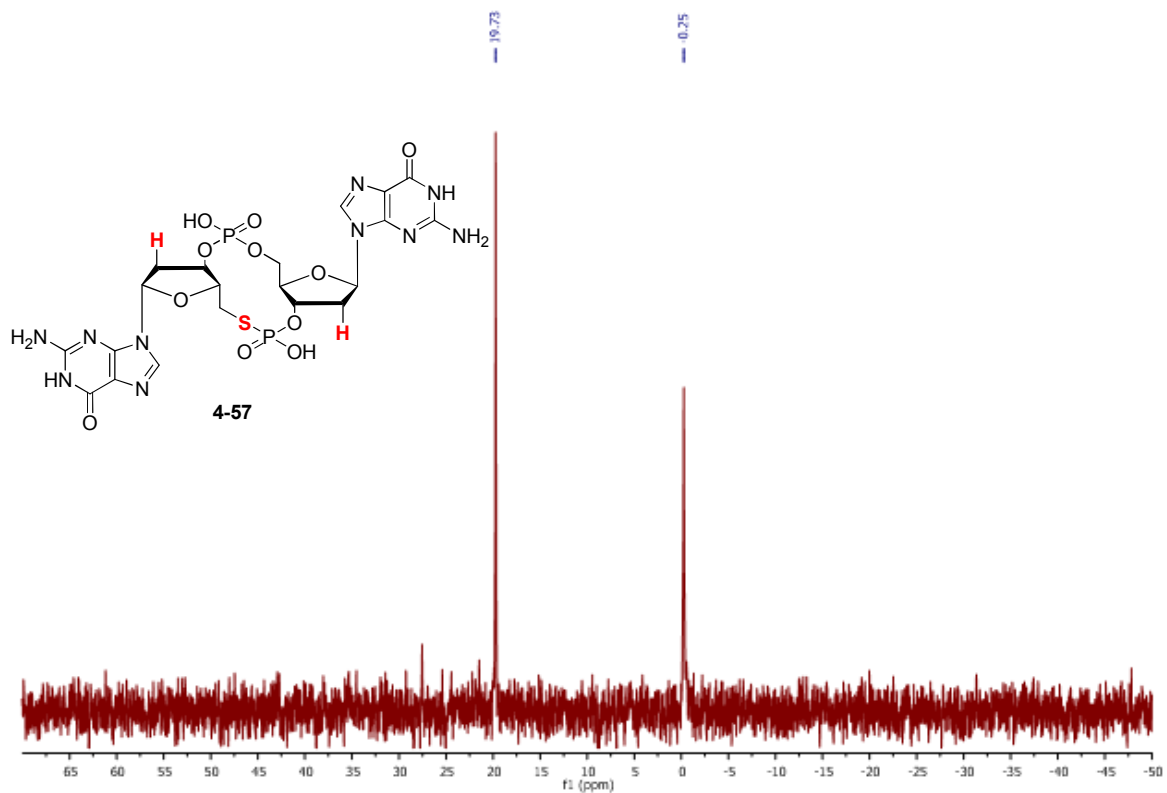
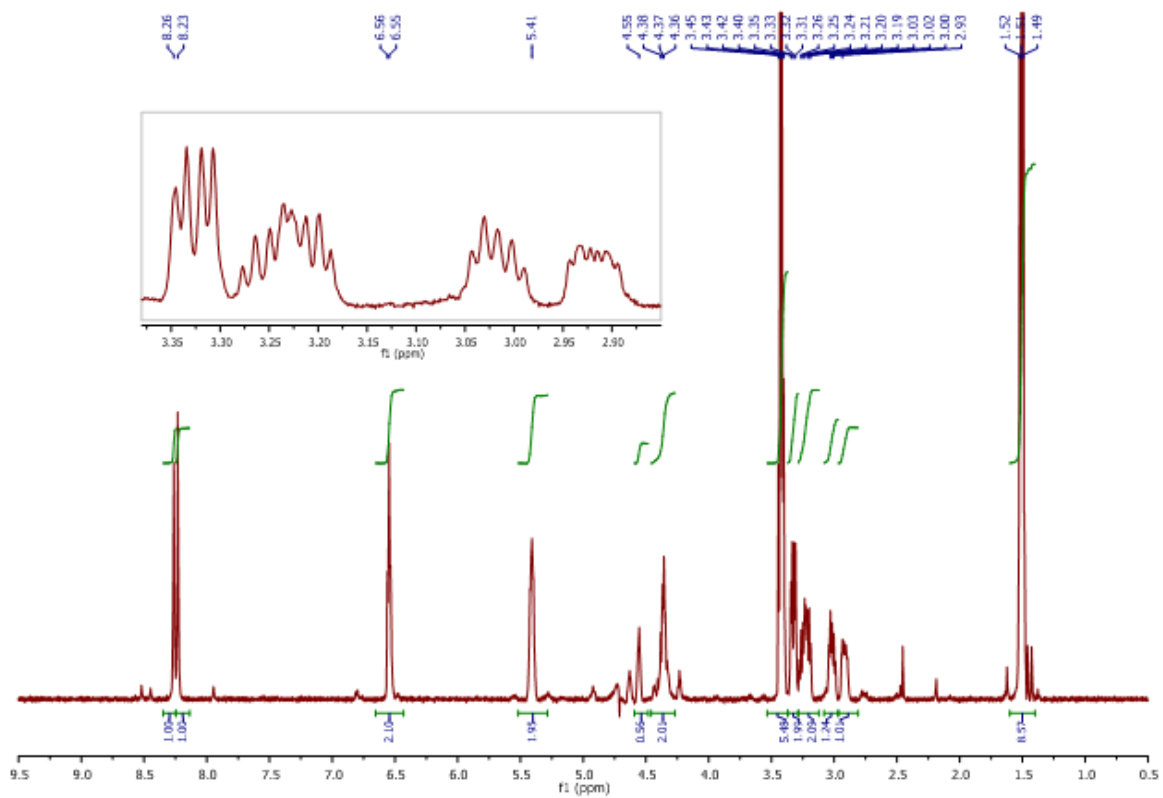












References

1. Sintim HO, Al Smith J, Wang JX, Nakayama S, Yan L. Paradigm shift in discovering next-generation anti-infective agents: targeting quorum sensing, c-di-GMP signaling and biofilm formation in bacteria with small molecules. *Fut. Med. Chem.*, 2(6), 1005-1035 (2010).
2. von Nussbaum F, Brands M, Hinzen B, Weigand S, Habich D. Antibacterial natural products in medicinal chemistry--exodus or revival? *Angew. Chem. Int. Ed.*, 45(31), 5072-5129 (2006).
3. Arias CA, Murray BE. Antibiotic-resistant bugs in the 21st century – a clinical super-challenge. *New Engl. J. Med.*, 360(5), 439-443 (2009).
4. Lawrence C. Bubonic plague – extinct disease or present danger? *Nurs. Mirror*, 145(21), 13-16 (1977).
5. Hiramatsu K, Aritaka N, Hanaki H *et al.* Dissemination in Japanese hospitals of strains of *Staphylococcus aureus* heterogeneously resistant to vancomycin. *Lancet*, 350(9092), 1670-1673 (1997).
6. Nicolau DP. Current challenges in the management of the infected patient. *Curr. Opin. Infect. Dis.*, 24 Suppl 1, S1-10 (2011).
7. van Rijen MM, Van Keulen PH, Kluytmans JA. Increase in a Dutch hospital of methicillin-resistant *Staphylococcus aureus* related to animal farming. *Clin. Infect. Dis.*, 46(2), 261-263 (2008).
8. Levy SB. Antibacterial household products: cause for concern. *Emerg. Infect. Dis.*, 7(3 Suppl), 512-515 (2001).
9. Henrichsen J. Typing of *Streptococcus pneumoniae*: past, present, and future. *Am. J. Med.*, 107(1A), 50S-54S (1999).
10. Abraham EP, Chain E. An enzyme from bacteria able to destroy penicillin. *Nature*, 46, 837 (1940).
11. Miller CP, Bohnhoff M. Studies on the action of penicillin; development of penicilli resistance by gonococcus. *Proc. Soc. Exp. Biol. Med.*, 60, 354-356 (1945).
12. Plough HH. Penicillin resistance of *Staphylococcus aureus* and its clinical implications. *Am. J. Clin. Pathol.*, 15, 446-451 (1945).
13. Medeiros AA. Evolution and dissemination of beta-lactamases accelerated by generations of beta-lactam antibiotics. *Clin. Infect. Dis.*, 24 Suppl 1, S19-45 (1997).

14. Barber M. Methicillin-resistant staphylococci and hospital infection. *Postgrad. Med. J.*, 40, Suppl:178-181 (1964).
15. Eriksen KR. Methicillin-resistance in *Staphylococcus aureus* apparently developed during treatment with methicillin. *Acta Pathol. Microbiol. Scand.*, 61, 154-155 (1964).
16. Finland M, Murray R, et al. Development of streptomycin resistance during treatment. *J. Am. Med. Assoc.*, 132, 16-21 (1946).
17. Klein M, Kimmelman LJ. Development of streptomycin resistance of the shigellae. *J. Bacteriol.*, 51, 581 (1946).
18. Colquhoun J, Weetch RS. Resistance to chloramphenicol developing during treatment of typhoid fever. *Lancet*, 2(6639), 621-623 (1950).
19. Rountree PM, Bulteau VG. Hospital infection with tetracycline-resistant haemolytic streptococci. *Med. J. Aust.*, 2(11), 446-448 (1965).
20. Turner GC. Tetracycline-resistant pneumococci in a general hospital. *Lancet*, 2(7321), 1292-1295 (1963).
21. Shlaes DM, Marino J, Jacobs MR. Infection caused by vancomycin-resistant *Streptococcus sanguis* II. *Antimicrob. Agents. Chemother.*, 25(4), 527-528 (1984).
22. Landy M, Larkum NW, Oswald EJ, Streightoff F. Increased synthesis of *p*-aminobenzoic acid associated with the development of sulfonamide resistance in *Staphylococcus aureus*. *Science*, 97(2516), 265-267 (1943).
23. Clapper WE, Secrest RR, January HL. Clinical results and resistance of organisms remaining after treatment with erythromycin. *Antibiot. Annu.*, 616-622 (1956).
24. Galizzi A, Cacco G, Siccardi AG, Mazza G. Mode of action of polymyxin B: physiological studies with *Bacillus subtilis*-resistant mutant. *Antimicrob. Agents. Chemother.*, 8(3), 366-369 (1975).
25. Raviglione MC, Boyle JF, Mariuz P, Pablos-Mendez A, Cortes H, Merlo A. Ciprofloxacin-resistant methicillin-resistant *Staphylococcus aureus* in an acute-care hospital. *Antimicrob. Agents. Chemother.*, 34(11), 2050-2054 (1990).
26. Tebas P, Martinez Ruiz R, Roman F *et al.* Early resistance to rifampin and ciprofloxacin in the treatment of right-sided *Staphylococcus aureus* endocarditis. *J. Infect. Dis.*, 163(1), 204-205 (1991).
27. Ayliffe GA. Cephalosporinase and penicillinase activity of Gram-negative bacteria. *J. Gen. Microbiol.*, 40(1), 119-126 (1965).
28. Ezekiel DH, Hutchins JE. Mutations affecting RNA polymerase associated with rifampicin resistance in *Escherichia coli*. *Nature*, 220(5164), 276-277 (1968).

29. Lukas W. Analytical study of the treatment of 18 cases of chronic open pulmonary tuberculosis with secondary resistance to rifampicin. *Respiration*, 28, Suppl:70-83 (1971).
30. Kohn J, Evans AJ. Group A streptococci resistant to clindamycin. *Br. Med. J.*, 2(5706), 423 (1970).
31. Borges JS, Schleider M, Roberts RB. In vivo development of resistance to clindamycin by *Staphylococcus aureus*. *Postgrad. Med. J.*, 58(1), 153-154 (1975).
32. Sze EH, Osborne NG, Adelson MD, Granato P. Emergence of imipenem-resistant *Pseudomonas aeruginosa* during treatment of intra-abdominal infection in a patient with ovarian carcinoma. *J. Natl. Med. Assoc.*, 80(10), 1133-1135 (1988).
33. Krcmery V, Antal M, Menkyna R, Knothe H, Schafer V. Differential resistance of hospital *Pseudomonas aeruginosa* to ceftazidime, imipenem or aztreonam. *J. Chemother.*, 1(4 Suppl), 364-365 (1989).
34. Schmitz FJ, Sadurski R, Stattfeld A, Kray A, Verhoef J, Fluit AC. Cross-resistance analyses and molecular typing of *Staphylococcus aureus* and *Streptococcus* spp. isolates resistant to quinupristin/dalfopristin. *J. Antimicrob. Chemother.*, 44(6), 847-849 (1999).
35. Soltani M, Beighton D, Philpott-Howard J, Woodford N. Mechanisms of resistance to quinupristin-dalfopristin among isolates of *Enterococcus faecium* from animals, raw meat, and hospital patients in Western Europe. *Antimicrob. Agents Chemother.*, 44(2), 433-436 (2000).
36. Tsiodras S, Gold HS, Sakoulas G *et al.* Linezolid resistance in a clinical isolate of *Staphylococcus aureus*. *Lancet*, 358(9277), 207-208 (2001).
37. Richter E, Rusch-Gerdes S, Hillemann D. First linezolid-resistant clinical isolates of *Mycobacterium tuberculosis*. *Antimicrob. Agents Chemother.*, 51(4), 1534-1536 (2007).
38. Lewis JS, 2nd, Owens A, Cadena J, Sabol K, Patterson JE, Jorgensen JH. Emergence of daptomycin resistance in *Enterococcus faecium* during daptomycin therapy. *Antimicrob. Agents Chemother.*, 49(4), 1664-1665 (2005).
39. Bush K, Jacoby GA, Medeiros AA. A functional classification scheme for beta-lactamases and its correlation with molecular structure. *Antimicrob. Agents Chemother.*, 39(6), 1211-1233 (1995).
40. Fisher JF, Meroueh SO, Mobashery S. Bacterial resistance to beta-lactam antibiotics: compelling opportunism, compelling opportunity. *Chem. Rev.*, 105(2), 395-424 (2005).
41. Finlay J, Miller L, Poupard JA. A review of the antimicrobial activity of clavulanate. *J. Antimicrob. Chemother.*, 52(1), 18-23 (2003).

42. Schoonover LL, Occhipinti DJ, Rodvold KA, Danziger LH. Piperacillin/tazobactam: a new beta-lactam/beta-lactamase inhibitor combination. *Ann. Pharmacother.*, 29(5), 501-514 (1995).
43. Benson JM, Nahata MC. Sulbactam/ampicillin, a new beta-lactamase inhibitor/beta-lactam antibiotic combination. *Drug Intell. Clin. Pharm.*, 22(7-8), 534-541 (1988).
44. Imtiaz U, Billings EM, Knox JR, Mobashery S. A structure-based analysis of the inhibition of class A beta-lactamases by sulbactam. *Biochemistry*, 33(19), 5728-5738 (1994).
45. Henquell C, Sirot D, Chanal C *et al.* Frequency of inhibitor-resistant TEM beta-lactamases in *Escherichia coli* isolates from urinary tract infections in France. *J. Antimicrob. Chemother.*, 34(5), 707-714 (1994).
46. Chaibi EB, Sirot D, Paul G, Labia R. Inhibitor-resistant TEM beta-lactamases: phenotypic, genetic and biochemical characteristics. *J. Antimicrob. Chemother.*, 43(4), 447-458 (1999).
47. Le Goffic F, Capmau ML, Tangy F, Baillarge M. Mechanism of action of aminoglycoside antibiotics. Binding studies of tobramycin and its 6'-N-acetyl derivative to the bacterial ribosome and its subunits. *Eur. J. Biochem.*, 102(1), 73-81 (1979).
48. Borovinskaya MA, Pai RD, Zhang W *et al.* Structural basis for aminoglycoside inhibition of bacterial ribosome recycling. *Nat. Struct. Mol. Biol.*, 14(8), 727-732 (2007).
49. Shaw KJ, Rather PN, Hare RS, Miller GH. Molecular genetics of aminoglycoside resistance genes and familial relationships of the aminoglycoside-modifying enzymes. *Microbiol. Rev.*, 57(1), 138-163 (1993).
50. Lai CJ, Weisblum B, Fahnestock SR, Nomura M. Alteration of 23 S ribosomal RNA and erythromycin-induced resistance to lincomycin and spiramycin in *Staphylococcus aureus*. *J. Mol. Biol.*, 74(1), 67-72 (1973).
51. Morales G, Picazo JJ, Baos E *et al.* Resistance to linezolid is mediated by the cfr gene in the first report of an outbreak of linezolid-resistant *Staphylococcus aureus*. *Clin. Infect. Dis.*, 50(6), 821-825 (2010).
52. Hanaki H, Kuwahara-Arai K, Boyle-Vavra S, Daum RS, Labischinski H, Hiramatsu K. Activated cell-wall synthesis is associated with vancomycin resistance in methicillin-resistant *Staphylococcus aureus* clinical strains Mu3 and Mu50. *J. Antimicrob. Chemother.*, 42(2), 199-209 (1998).

53. Allen NE, Hobbs JN, Jr., Richardson JM, Riggin RM. Biosynthesis of modified peptidoglycan precursors by vancomycin-resistant *Enterococcus faecium*. *FEMS Microbiol. Lett.*, 77(1-3), 109-115 (1992).
54. Billot-Klein D, Gutmann L, Sable S, Guittet E, van Heijenoort J. Modification of peptidoglycan precursors is a common feature of the low-level vancomycin-resistant VANB-type *Enterococcus* D366 and of the naturally glycopeptide-resistant species *Lactobacillus casei*, *Pediococcus pentosaceus*, *Leuconostoc mesenteroides*, and *Enterococcus gallinarum*. *J. Bacteriol.*, 176(8), 2398-2405 (1994).
55. Park IS, Walsh CT. D-Alanyl-D-lactate and D-alanyl-D-alanine synthesis by D-alanyl-D-alanine ligase from vancomycin-resistant *Leuconostoc mesenteroides*. Effects of a phenylalanine 261 to tyrosine mutation. *J. Biol. Chem.*, 272(14), 9210-9214 (1997).
56. Kuzin AP, Sun T, Jorczak-Baillass J, Healy VL, Walsh CT, Knox JR. Enzymes of vancomycin resistance: the structure of D-alanine-D-lactate ligase of naturally resistant *Leuconostoc mesenteroides*. *Structure*, 8(5), 463-470 (2000).
57. Ma D, Cook DN, Alberti M, Pon NG, Nikaido H, Hearst JE. Genes *acrA* and *acrB* encode a stress-induced efflux system of *Escherichia coli*. *Mol. Microbiol.*, 16(1), 45-55 (1995).
58. Husain F, Nikaido H. Substrate path in the AcrB multidrug efflux pump of *Escherichia coli*. *Mol. Microbiol.*, 78(2), 320-330 (2010).
59. Li XZ, Nikaido H, Poole K. Role of *mexA-mexB-oprM* in antibiotic efflux in *Pseudomonas aeruginosa*. *Antimicrob. Agents Chemother.*, 39(9), 1948-1953 (1995).
60. Ziha-Zarifi I, Llanes C, Kohler T, Pechere JC, Plesiat P. In vivo emergence of multidrug-resistant mutants of *Pseudomonas aeruginosa* overexpressing the active efflux system MexA-MexB-OprM. *Antimicrob. Agents Chemother.*, 43(2), 287-291 (1999).
61. Neyfakh AA, Borsch CM, Kaatz GW. Fluoroquinolone resistance protein NorA of *Staphylococcus aureus* is a multidrug efflux transporter. *Antimicrob. Agents Chemother.*, 37(1), 128-129 (1993).
62. Mallea M, Chevalier J, Eyraud A, Pages JM. Inhibitors of antibiotic efflux pump in resistant *Enterobacter aerogenes* strains. *Biochem. Biophys. Res. Commun.*, 293(5), 1370-1373 (2002).
63. Shi WF, Jiang JP, Xu N, Huang ZM, Wang YY. Inhibitory effects of reserpine and carbonyl cyanide *m*-chlorophenylhydrazone on fluoroquinolone resistance of *Acinetobacter baumannii*. *Chin. Med. J.*, 118(4), 340-343 (2005).

64. Saenz Y, Ruiz J, Zarazaga M, Teixido M, Torres C, Vila J. Effect of the efflux pump inhibitor Phe-Arg-beta-naphthylamide on the MIC values of the quinolones, tetracycline and chloramphenicol, in *Escherichia coli* isolates of different origin. *J. Antimicrob. Chemother.*, 53(3), 544-545 (2004).
65. Coban AY, Tanriverdi Cayci Y, Erturan Z, Durupinar B. Effects of efflux pump inhibitors phenyl-arginine-beta-naphthylamide and 1-(1-naphthylmethyl)-piperazine on the antimicrobial susceptibility of *Pseudomonas aeruginosa* isolates from cystic fibrosis patients. *J. Chemother.*, 21(5), 592-594 (2009).
66. Markham PN. Inhibition of the emergence of ciprofloxacin resistance in *Streptococcus pneumoniae* by the multidrug efflux inhibitor reserpine. *Antimicrob. Agents Chemother.*, 43(4), 988-989 (1999).
67. Schmitz FJ, Fluit AC, Luckefahr M *et al.* The effect of reserpine, an inhibitor of multidrug efflux pumps, on the in-vitro activities of ciprofloxacin, sparfloxacin and moxifloxacin against clinical isolates of *Staphylococcus aureus*. *J. Antimicrob. Chemother.*, 42(6), 807-810 (1998).
68. Mullin S, Mani N, Grossman TH. Inhibition of antibiotic efflux in bacteria by the novel multidrug resistance inhibitors biricodar (VX-710) and timcodar (VX-853). *Antimicrob. Agents Chemother.*, 48(11), 4171-4176 (2004).
69. Debono M, Abbott BJ, Molloy RM *et al.* Enzymatic and chemical modifications of lipopeptide antibiotic A21978C: the synthesis and evaluation of daptomycin (LY146032). *J. Antibiot.*, 41(8), 1093-1105 (1988).
70. Tally FP, DeBruin MF. Development of daptomycin for gram-positive infections. *J. Antimicrob. Chemother.*, 46(4), 523-526 (2000).
71. Brickner SJ, Hutchinson DK, Barbachyn MR *et al.* Synthesis and antibacterial activity of U-100592 and U-100766, two oxazolidinone antibacterial agents for the potential treatment of multidrug-resistant gram-positive bacterial infections. *J. Med. Chem.*, 39(3), 673-679 (1996).
72. Barbachyn MR, Ford CW. Oxazolidinone structure-activity relationships leading to linezolid. *Angew. Chem. Int. Ed.*, 42(18), 2010-2023 (2003).
73. Kloss P, Xiong L, Shinabarger DL, Mankin AS. Resistance mutations in 23 S rRNA identify the site of action of the protein synthesis inhibitor linezolid in the ribosomal peptidyl transferase center. *J. Mol. Biol.*, 294(1), 93-101 (1999).
74. Jones RN, Della-Latta P, Lee LV, Biedenbach DJ. Linezolid-resistant *Enterococcus faecium* isolated from a patient without prior exposure to an oxazolidinone: report from

- the SENTRY Antimicrobial Surveillance Program. *Diagn. Microbiol. Infect. Dis.*, 42(2), 137-139 (2002).
75. Jung D, Rozek A, Okon M, Hancock RE. Structural transitions as determinants of the action of the calcium-dependent antibiotic daptomycin. *Chem. Biol.*, 11(7), 949-957 (2004).
 76. Hayden MK, Rezai K, Hayes RA, Lolans K, Quinn JP, Weinstein RA. Development of Daptomycin resistance in vivo in methicillin-resistant *Staphylococcus aureus*. *J. Clin. Microbiol.*, 43(10), 5285-5287 (2005).
 77. Lee do K, Kim Y, Park KS, Yang JW, Kim K, Ha NJ. Antimicrobial activity of mupirocin, daptomycin, linezolid, quinupristin/dalfopristin and tigecycline against vancomycin-resistant enterococci (VRE) from clinical isolates in Korea (1998 and 2005). *J. Biochem. Mol. Biol.*, 40(6), 881-887 (2007).
 78. Wynn RL. FDA new drug approvals in 2004. *Gen. Dent.*, 53(4), 246-248 (2005).
 79. Wynn RL. FDA new drug approvals in 2005. *Gen. Dent.*, 54(4), 230-233 (2006).
 80. Wynn RL. FDA new drug approvals in 2006. *Gen. Dent.*, 55(4), 275-279 (2007).
 81. Wynn RL. FDA new drug approvals in 2007. *Gen. Dent.*, 56(6), 506-510 (2008).
 82. Wynn RL. FDA new drug approvals in 2008. *Gen. Dent.*, 57(4), 300-304 (2009).
 83. Kaitin KI, Dimasi JA. Pharmaceutical innovation in the 21st century: new drug approvals in the first decade, 2000-2009. *Clin. Pharmacol. Ther.*, (2010).
 84. Wynn RL. FDA new drug approvals in 2009. *Gen. Dent.*, 58(4), 280-284 (2010).
 85. Champney WS, Rodgers WK. Retapamulin inhibition of translation and 50S ribosomal subunit formation in *Staphylococcus aureus* cells. *Antimicrob. Agents Chemother.*, 51(9), 3385-3387 (2007).
 86. Yan K, Madden L, Choudhry AE, Voigt CS, Copeland RA, Gontarek RR. Biochemical characterization of the interactions of the novel pleuromutilin derivative retapamulin with bacterial ribosomes. *Antimicrob. Agents Chemother.*, 50(11), 3875-3881 (2006).
 87. Campbell JW, Cronan JE, Jr. Bacterial fatty acid biosynthesis: targets for antibacterial drug discovery. *Annu. Rev. Microbiol.*, 55, 305-332 (2001).
 88. Heath RJ, White SW, Rock CO. Lipid biosynthesis as a target for antibacterial agents. *Prog. Lipid Res.*, 40, 467 (2001).
 89. Rock CO, Heath RJ. Fatty acid biosynthesis as a target for novel antibacterials. *Curr. Opin. Investig. Drugs*, 5, 146 (2004).
 90. Wright HT, Reynold KA. Antibacterial targets in fatty acid biosynthesis. *Curr. Opin. Microbiol.*, 10, 447 (2007).

91. Zhang YM, White SW, Rock CO. Inhibiting bacterial fatty acid synthesis. *J. Biol. Chem.*, 281(26), 17541-17544 (2006).
92. Singer SJ, Nicolson GL. The fluid mosaic model of the structure of cell membranes. *Science*, 175(23), 720-731 (1972).
93. Raetz CR, Whitfield C. Lipopolysaccharide endotoxins. *Annu. Rev. Biochem.*, 71, 635-700 (2002).
94. The Global Plan to Stop TB, 2011-2015; World Health Organization (Geneva, Switzerland, 2010).
95. Mediterranean E. The Global Tuberculosis Epidemic; Nov. 2010 - Fact Sheet; No. 7883-02 (Kaiser Family Foundation, 2010).
96. Schaefer AL, Val DL, Hanzelka BL, John E. Cronan J, Greenberg EP. Generation of cell-to-cell signals in quorum sensing: Acyl homoserine lactone synthase activity of a purified *Vibrio fischeri* LuxI protein. *Proc. Natl. Acad. Sci. USA*, 93, 9505 (1996).
97. Raetz CRH, Garrett TA, Reynolds CM *et al.* Kdo₂-Lipid A of *Escherichia coli*, a defined endotoxin that activates macrophages via TLR-4 *J. Lipid Res.*, 47, 1097 (2006).
98. Pommerville JC. Alcamo's Fundamentals of Microbiology (Jones & Bartlett Learning, 2010).
99. Raetz CRH, Reynolds CM, Trent MS, Bishop RE. Lipid A modification systems in Gram-negative bacteria. *Annu. Rev. Biochem.*, 76, 295 (2005).
100. Daffé M, Reytrat JM. The mycobacterial cell envelope (ASM Press, 2008).
101. Schweizer E, Hofmann J. Microbial type I fatty acid synthases (FAS): major players in a network of cellular FAS systems. *Microbiol. Mol. Biol. Rev.*, 68(3), 501-517 (2004).
102. Witkowski A, Ghosal A, Joshi AK, Witkowska HE, Asturias FJ, Smith S. Head-to-head coiled arrangement of the subunits of the animal fatty acid synthase. *Chem. Biol.*, 11(12), 1667-1676 (2004).
103. Asturias FJ, Chadick JZ, Cheung IK *et al.* Structure and molecular organization of mammalian fatty acid synthase. *Nat. Struct. Mol. Biol.*, 12(3), 225-232 (2005).
104. Lomakin IB, Xiong Y, Steitz TA. The crystal structure of yeast fatty acid synthase, a cellular machine with eight active sites working together. *Cell*, 129, 319 (2007).
105. Smith S, Witkowski A, Joshi AK. Structural and functional organization of the animal fatty acid synthase. *Prog. Lipid Res.*, 42(4), 289-317 (2003).
106. Lu YJ, Zhang YM, Rock CO. Product diversity and regulation of type II fatty acid synthases. *Biochem. Cell Biol.*, 82(1), 145-155 (2004).

107. Kaneda T. Fatty acids of the genus *Bacillus*: an example of branched-chain preference. *Bacteriol. Rev.*, 41(2), 391-418 (1977).
108. Kuhajda FP, Jenner K, Wood FD *et al.* Fatty acid synthesis: a potential selective target for antineoplastic therapy. *Proc. Natl. Acad. Sci. USA*, 91(14), 6379-6383 (1994).
109. Byers DM, Meighen EA. Inhibition of *Vibrio harveyi* bioluminescence by cerulenin: in vivo evidence for covalent modification of the reductase enzyme involved in aldehyde synthesis. *J. Bacteriol.*, 171(7), 3866-3871 (1989).
110. Wall L, Meighen E. Covalent reaction of cerulenin at the active site of acyl-CoA reductase of *Photobacterium phosphoreum*. *Biochem. Cell. Biol.*, 67(2-3), 163-167 (1989).
111. Haapalainen AM, Merilainen G, Wierenga RK. The thiolase superfamily: condensing enzymes with diverse reaction specificities. *Trends Biochem. Sci.*, 31(1), 64-71 (2006).
112. Takayama K, Wang C, Besra GS. Pathway to synthesis and processing of mycolic acids in *Mycobacterium tuberculosis*. *Clin. Microbiol. Rev.*, 18(1), 81-101 (2005).
113. Cronan JE, Waldrop GL. Multi-subunit acetyl-CoA carboxylases. *Prog. Lipid Res.*, 41, 407 (2002).
114. Lin T-W, Melgar MM, Kurth D *et al.* Structure-based inhibitor design of AccD5, an essential acyl-CoA carboxylase carboxyltransferase domain of *Mycobacterium tuberculosis*. *Proc. Natl. Acad. Sci. USA*, 103, 3072 (2006).
115. Joseph-McCarthy D, Parris K, Huang A *et al.* Use of Structure-based drug design approaches to obtain novel anthranilic acid acyl carrier protein synthase inhibitors. *J. Med. Chem.*, 48, 7960 (2005).
116. White SW, Zheng J, Zhang Y-M, Rock CO. The structural biology of the type II fatty acid biosynthesis. *Annu. Rev. Biochem.*, 74, 791-831 (2005).
117. Qiu X, Janson CA, Konstantinidis AK *et al.* Crystal structure of beta-ketoacyl-acyl carrier protein synthase III. A key condensing enzyme in bacterial fatty acid biosynthesis. *J. Biol. Chem.*, 274(51), 36465-36471 (1999).
118. Price AC, Rock CO, White SW. The 1.3-Angstrom-resolution crystal structure of beta-ketoacyl-acyl carrier protein synthase II from *Streptococcus pneumoniae*. *J. Bacteriol.*, 185(14), 4136-4143 (2003).
119. Wang J, Kodali S, Lee SH *et al.* Discovery of platencin, a dual FabF and FabH inhibitor with *in vivo* antibiotic properties. *Proc. Natl. Acad. Sci. USA*, 104(18), 7612-7616 (2007).
120. Wang J, Soisson SM, Young K *et al.* Platensimycin is a selective FabF inhibitor with potent antibiotic properties. *Nature*, 441(7091), 358-361 (2006).

121. Machutta CA, Bommineni GR, Luckner SR *et al.* Slow onset inhibition of bacterial beta-ketoacyl-acyl carrier protein synthases by thiolactomycin. *J. Biol. Chem.*, 285(9), 6161-6169 (2009).
122. Patel MP, Liu WS, West J, Tew D, Meek TD, Thrall SH. Kinetic and chemical mechanisms of the fabG-encoded *Streptococcus pneumoniae* beta-ketoacyl-ACP reductase. *Biochemistry*, 44(50), 16753-16765 (2005).
123. Price AC, Zhang YM, Rock CO, White SW. Cofactor-induced conformational rearrangements establish a catalytically competent active site and a proton relay conduit in FabG. *Structure*, 12(3), 417-428 (2004).
124. Silva RG, de Carvalho LP, Blanchard JS, Santos DS, Basso LA. *Mycobacterium tuberculosis* beta-ketoacyl-acyl carrier protein (ACP) reductase: kinetic and chemical mechanisms. *Biochemistry*, 45(43), 13064-13073 (2006).
125. Wang H, Cronan JE. Functional replacement of the FabA and FabB proteins of *Escherichia coli* fatty acid synthesis by *Enterococcus faecalis* FabZ and FabF homologues. *J. Biol. Chem.*, 279(33), 34489 (2004).
126. Lu H, Tonge PJ. Mechanism and inhibition of the FabV enoyl-ACP reductase from *Burkholderia mallei*. *Biochemistry*, 49(6), 1281-1289 (2010).
127. Heath RJ, Rock CO. A triclosan-resistant bacterial enzyme. *Nature*, 406, 145 (2000).
128. Rozwarski DA, Vilcheze C, Sugantino M, Bittman R, Sacchettini JC. Crystal structure of the *Mycobacterium tuberculosis* enoyl-ACP reductase, InhA, in complex with NAD⁺ and a C16 fatty acyl substrate. *J. Biol. Chem.*, 274(22), 15582-15589 (1999).
129. Parikh S, Moynihan DP, Xiao G, Tonge PJ. Roles of tyrosine 158 and lysine 165 in the catalytic mechanism of InhA, the enoyl-ACP reductase from *Mycobacterium tuberculosis*. *Biochemistry*, 38(41), 13623-13634 (1999).
130. Rafi S, Novichenok P, Kolappan S *et al.* Structure of acyl carrier protein bound to FabI, the FASII enoyl reductase from *Escherichia coli*. *J. Biol. Chem.*, 281(51), 39285-39293 (2006).
131. Lu Y-J, Zhang Y-M, Grimes KD, Qi J, Lee RE, Rock CO. Acyl-phosphates initiate membrane phospholipid synthesis in Gram-positive pathogens. *Molecular Cell*, 23, 765 (2006).
132. Schujman GE, Mendoza Dd. Solving an old puzzle in phospholipid biosynthesis. *Nat. Chem. Biol.*, 2(11), 573 (2006).
133. Lambalot RH, Walsh CT. Cloning, overproduction, and characterization of the *Escherichia coli* holo-acyl carrier protein synthase. *J. Biol. Chem.*, 270(42), 24658 (1995).

134. Chu M, Mierzwa R, Xu L *et al.* Structure elucidation of Sch 538415, a novel acyl carrier protein synthase inhibitor from a microorganism. *Bioorg. Med. Chem. Lett.*, 13, 3827 (2003).
135. Gilbert AM, Kirisits M, Toy P *et al.* Anthranilate 4*H*-oxazol-5-ones: novel small molecule antibacterial acyl carrier protein synthase (AcpS) inhibitors. *Bioorg. Med. Chem. Lett.*, 14, 37 (2004).
136. Gronwald JW. *Biochem. Soc. Trans.*, 22, 616 (1994).
137. Zhang H, Tweel B, Tong L. Molecular basis for the inhibition of the carboxyltransferase domain of acetyl-coenzyme-A carboxylase by haloxyfop and diclofop. *Proc. Natl. Acad. Sci. USA*, 101(16), 5910 (2004).
138. Fredenhagen A, Tamura SY, Kenny PTM, Komura H, Naya Y, Nakanishi K. Andrimid, a new peptide antibiotic produced by an intracellular bacterial symbiont isolated from a brown planthopper. *J. Am. Chem. Soc.*, 109(14), 4409 (1987).
139. Davies SG, Dixon DJ. Asymmetric syntheses of moiramide B and andrimid. *J. Chem. Soc., Perkin Trans. I*, 2635 (1998).
140. Freiberg C, Brunner NA, Schiffer G *et al.* Identification and characterization of the first class of potent bacterial acetyl-CoA carboxylase inhibitors with antibacterial activity. *J. Biol. Chem.*, 279(25), 26066 (2004).
141. Brennan PJ, Nikaido H. The envelope of mycobacteria. *Annu. Rev. Biochem.*, 64, 29 (1995).
142. Minnikin DE, Kremer L, Dover LG, Besra GS. The methyl-branched fortifications of *Mycobacterium tuberculosis* *Chem. Biol.*, 9, 545 (2002).
143. Lin T-W, Melgar MM, Kurth D *et al.* Structure-based inhibitor design of AccD5, an essential acyl-CoA carboxylase carboxyltransferase domain of *Mycobacterium tuberculosis*. *Proc. Natl. Acad. Sci. USA*, 103, 3072 (2006).
144. Lin T-W, Nguyen T, Kurth D *et al.* Structure-based inhibitor design of AccD5/AccD6, essential carboxyltransferases of *Mycobacterium tuberculosis*. *FASEB J.*, 33, 839.834 (2008).
145. Kurth DG, Gago GM, Iglesia Adl *et al.* Accase 6 is the essential acetyl-CoA carboxylase involved in fatty acid and mycolic acid biosynthesis in mycobacteria. *Microbiology*, 155, 2664 (2009).
146. Liu W, Han C, Hua L, Chen K, Shen X, Jiang H. Characterization and inhibitor discovery of one novel malonyl-CoA: acyl carrier protein transacylase (MCAT) from *Helicobacter pylori*. *FEBS Lett.*, 580(2), 697 (2006).

147. He X, Reynolds KA. Purification, characterization, and identification of novel inhibitors of the b-ketoacyl-acyl carrier protein synthase III (FabH) from *Staphylococcus aureus*. *Antimicrob. Agents Chemother.*, 46(5), 1310 (2002).
148. He X, Reeve AM, Desai UR, Kellogg GE, Reynolds KA. 1,2-Dithiole-3-ones as potent inhibitors of the bacterial 3-ketoacyl acyl carrier protein synthase III (FabH). *Antimicrob. Agents Chemother.*, 48(8), 3093 (2004).
149. Lee JY, Jeong KW, Shin S, Lee JU, Kim Y. Antimicrobial natural products as beta-ketoacyl-acyl carrier protein synthase III inhibitors. *Bioorg. Med. Chem.*, 17(15), 5408-5413 (2009).
150. Lee JY, Jeong KW, Lee JU, Kang DI, Kim Y. Novel E. coli beta-ketoacyl-acyl carrier protein synthase III inhibitors as targeted antibiotics. *Bioorg. Med. Chem.*, 17(4), 1506-1513 (2009).
151. Khandekar SS, Gentry DR, Aller GSV *et al.* Identification, substrate specificity, and inhibition of the *Streptococcus pneumoniae* b-ketoacyl-acyl carrier protein synthase III (FabH). *J. Biol. Chem.*, 276(32), 30024 (2001).
152. Nie Z, Perretta C, Lu J *et al.* Structure-based design, synthesis, and study of potent inhibitors of b-ketoacyl-acyl carrier protein synthase III as potential antimicrobial agents. *J. Med. Chem.*, 48, 1596 (2005).
153. Young K, Jayasuriya H, Ondeyka JG *et al.* Discovery of FabH/FabF inhibitors from natural products. *Antimicrob. Agents Chemother.*, 50(2), 519 (2006).
154. Matsumae A, Nomura S, Hata T. Studies on cerulenin. IV. Biological characteristics of cerulenin. *J. Antibiot. (Tokyo)*, 17, 1 (1964).
155. Price AC, Choi K-H, Heath RJ, Li Z, White SW, Rock CO. Inhibition of b-ketoacyl-acyl carrier protein synthases by thiolactomycin and cerulenin. Structure and mechanism. *J. Biol. Chem.*, 276(9), 6551 (2001).
156. Kodali S, Galgoci A, Young K *et al.* Determination of Selectivity and Efficacy of Fatty Acid Synthesis Inhibitors. *J. Biol. Chem.*, 280, 1669 (2005).
157. Oishi H, Noto T, Sasaki H *et al.* Thiolactomycin, a new antibiotic. I. Taxonomy of the producing organism, fermentation and biological properties. *J. Antibiot. (Tokyo)*, 35, 391 (1982).
158. Noto T, Miyakawa S, Oishi H, Endo H, Okazaki H. Thiolactomycin, a new antibiotic. III. In vitro antibacterial activity. *J. Antibiot. (Tokyo)*, 35, 401 (1982).

159. Omura S, Iwai Y, Nakagawa A *et al.* Thiotetromycin, a new antibiotic. Taxonomy, production, isolation, and physicochemical and biological properties. *J. Antibiot. (Tokyo)*, 36, 109 (1983).
160. Zhang Y-M, Rock CO. Evaluation of epigallocatechin gallate and related plant polyphenols as inhibitors of the FabG and FabI reductases of bacterial type II fatty-acid synthase. *J. Biol. Chem.*, 279(30), 30994–31001 (2004).
161. Kass LR. The antibacterial activity of 3-decynoyl-*N*-acetylcysteamine: inhibition in vivo of β -hydroxydecanoyl thioester dehydrase. *J. Biol. Chem.*, 243(12), 3223-3228 (1968).
162. Morisaki M, Bloch K. Inhibition of β -hydroxydecanoyl thioester dehydrase by some allenic acids and their thioesters. *Bioorg. Chem.*, 1, 188-193 (1971).
163. Sharma SK, Kapoor M, Ramya TNC *et al.* Identification, characterization, and inhibition of *plasmodium falciparum* beta-hydroxyacyl-acyl carrier protein dehydratase (FabZ). *J. Biol. Chem.*, 278(46), 45661–45671 (2003).
164. Banerjee A, Dubnau E, Quemard A *et al.* *inhA*, a gene encoding a target for isoniazid and ethionamide in *Mycobacterium tuberculosis*. *Science*, 263, 227-230 (1994).
165. Rosner JL. Susceptibilities of *oxyR* regulon mutants of *Escherichia coli* and *Salmonella typhimurium* to isoniazid. *Antimicrob. Agents Chemother.*, 37, 2251-2253 (1993).
166. Rawat R, Whitty A, Tonge PJ. The isoniazid-NAD adduct is a slow, tight-binding inhibitor of *InhA*, the *Mycobacterium tuberculosis* enoyl reductase: Adduct affinity and drug resistance. *Proc. Natl. Acad. Sci. USA*, 100(24), 13881-13886 (2003).
167. Baulard AR, Betts JC, Engohang-Ndong J *et al.* Activation of the pro-drug ethionamide is regulated in *Mycobacteria*. *Proc. Natl. Acad. Sci. USA*, 275(36), 28326-28331 (2000).
168. Wang F, Langley R, Gulten G *et al.* Mechanism of thioamide drug action against *tuberculosis* and *leprosy*. *J. Exp. Med.*, 204(1), 73-78 (2007).
169. Heath RJ, Yu Y-T, Shapiro MA, Olson E, Rock CO. Broad-spectrum antimicrobial biocides target the FabI component of fatty acid synthesis. *J. Biol. Chem.*, 273, 30316 (1998).
170. Sullivan TJ, Truglio JJ, Boyne ME *et al.* High affinity *InhA* inhibitors with activity against drug-resistant strains of *Mycobacterium tuberculosis*. *ACS Chem. Biol.*, 1(1), 43-53 (2006).
171. Baldock C, Boer G-Jd, Rafferty JB, Stuitje AR, Rice DW. Mechanism of action of diazaborines. *Biochem. Pharm.*, 55, 1541-1549 (1998).

172. Davis MC, Franzblau SG, Martin AR. Synthesis and evaluation of benzodiazaborine compounds against *M. tuberculosis* H₃₇R_v *in vitro*. *Bioorg. Med. Chem. Lett.*, 8, 843-846 (1998).
173. Payne DJ, Miller WH, Berry V *et al.* Discovery of a novel and potent class of FabI-directed antibacterial agents. *Antimicrob. Agents Chemother.*, 46(10), 3118 (2002).
174. Seefeld MA, Miller WH, Newlander KA *et al.* Indole naphthyridinones as inhibitors of bacterial enoyl-ACP reductases FabI and FabK. *J. Med. Chem.*, 46, 1627 (2003).
175. Moche M, Schneider G, Edwards P, Dehesh K, Lindqvist Y. Structure of the complex between the antibiotic cerulenin and Its target, b-ketoacyl-acyl carrier protein synthase. *J. Biol. Chem.*, 274(10), 6031 (1999).
176. Morisaki N, Funabashi H, Shimazawa R *et al.* Effect of side-chain structure on inhibition of yeast fatty-acid synthase by cerulenin analogues. *Eur. J. Biochem.*, 211, 111 (1993).
177. Kuhajda FP, Pizer ES, Li JN, Mani NS, Frehywot GL, Townsend CA. Synthesis and antitumor activity of an inhibitor of fatty acid synthase. *Proc. Natl. Acad. Sci. USA*, 97(7), 3450 (2000).
178. Schujman GE, Choi K-H, Altabe S, Rock CO, Mendoza D. Response of *Bacillus subtilis* to cerulenin and acquisition of resistance. *J. Bacteriol.*, 183(10), 3032 (2001).
179. Miyakawa S, Suzuki K, Noto T, Harada Y, Okazaki H. Thiolactomycin, a new antibiotic. IV. Biological properties and chemotherapeutic activity in mice. *J. Antibiot. (Tokyo)*, 35, 411 (1982).
180. Vilcheze C, Williams R, Jacobs J. The mechanism of isoniazid killing: clarity through the scope of genetics. *Annu. Rev. Microbiol.*, 61, 35-50 (2007).
181. Mdluli K, Slayden RA, Zhu Y *et al.* Inhibition of a *Mycobacterium tuberculosis* -ketoacyl ACP synthase by isoniazid *Science*, 280, 1607-1610 (1998).
182. Ghosh AK, Xi K. Total synthesis of (-)-platensimycin, a novel antibacterial agent. *J. Org. Chem.*, 74(3), 1163-1170 (2009).
183. Argyrou A, Vetting MW, Aladegbami B, Blanchard JS. *Mycobacterium tuberculosis* dihydrofolate reductase is a target for isoniazid. *Nat. Struct. Mol. Biol.*, 13, 408-413 (2006).
184. Rouse DA, Li Z, Bai G-H, Morris SL. Characterization of the *katG* and *inhA* genes of isoniazid-resistant clinical isolates of *Mycobacterium tuberculosis*. *Antimicrob. Agents Chemother.*, 39(11), 2472-2477 (1995).
185. Rozwarski DA, Grant GA, Barton DH, W. R. Jacobs J, Sacchettini JC. Modification of the NADH of the isoniazid target (InhA) from *Mycobacterium tuberculosis*. *Science*, 279, 98-102 (1998).

186. Baldock C, Rafferty JB, Sedelnikova SE *et al.* A mechanism of drug action revealed by structural studies of enoyl reductase. *Science*, 274, 2107-2110 (1996).
187. Ward WHJ, Holdgate GA, Rowsell S *et al.* Kinetic and structural characteristics of the inhibition of enoyl (acyl carrier protein) reductase by triclosan. *Biochemistry*, 38, 12514-12525 (1999).
188. DeBarber AE, Mdluli K, Bosman M, Bekker L-G, Clifton E, Barry I. Ethionamide activation and sensitivity in multidrug-resistant *Mycobacterium tuberculosis*. *Proc. Natl. Acad. Sci. USA*, 97(17), 9677-9682 (2000).
189. Lu H, Tonge PJ. Inhibitors of FabI, an enzyme drug target in the bacterial fatty acid biosynthesis pathway. *Acc. Chem. Res.*, 41(1), 11-20 (2008).
190. Roujeinikova A, Sedelnikova S, Boer G-Jd *et al.* Inhibitor binding studies on enoyl reductase reveal conformational changes related to substrate recognition. *J. Biol. Chem.*, 274, 30811-30817).
191. Boer G-Jd, Pielage GJA, Nijkamp HJJ *et al.* Molecular genetic analysis of enoyl-acyl carrier protein reductase inhibition by diazaborine. *Mol. Microbiol.*, 31, 443-450 (1999).
192. McMurry LM, Oethinger M, Levy SB. Overexpression of *marA*, *soxS*, or *acrAB* produces resistance to triclosan in laboratory and clinical strains of *Escherichia coli*. *FEMS Microbiol. Lett.*, 166, 305-309 (1998).
193. Sivaraman S, Sullivan TJ, Johnson F *et al.* Inhibition of the bacterial enoyl reductase FabI by triclosan: a structure-reactivity analysis of FabI inhibition by triclosan analogues. *J. Med. Chem.*, 47(3), 509-518 (2004).
194. Altenbern RA. Cerulenin-inhibited cells of *Staphylococcus aureus* resume growth when supplemented with either a saturated or an unsaturated fatty acid. *Antimicrob. Agents Chemother.*, 11, 574-576 (1977).
195. Brinster S, Lamberet G, Staels B, Trieu-Cuot P, Gruss A, Poyart C. Type II fatty acid synthesis is not a suitable antibiotic target for Gram-positive pathogens. *Nature*, 458, 83-86 (2009).
196. Stone G, Wood P, Dixon L, Keyhan M, Matin A. Tetracycline rapidly reaches all the constituent cells of uropathogenic *Escherichia coli* biofilms. *Antimicrob. Agents Chemother.*, 46(8), 2458-2461 (2002).
197. Jenal U. Cyclic di-guanosine-monophosphate comes of age: a novel secondary messenger involved in modulating cell surface structures in bacteria? *Curr. Opin. Microbiol.*, 7(2), 185-191 (2004).

198. Kulasakara H, Lee V, Brencic A *et al.* Analysis of *Pseudomonas aeruginosa* diguanylate cyclases and phosphodiesterases reveals a role for bis-(3'-5')-cyclic-GMP in virulence. *Proc. Natl. Acad. Sci. USA*, 103(8), 2839-2844 (2006).
199. Ross P, Weinhouse H, Aloni Y *et al.* Regulation of cellulose synthesis in *Acetobacter xylinum* by cyclic diguanylic acid. *Nature*, 325(6101), 279-281 (1987).
200. Hickman JW, Tifrea DF, Harwood CS. A chemosensory system that regulates biofilm formation through modulation of cyclic diguanylate levels. *Proc. Natl. Acad. Sci. USA*, 102(40), 14422-14427 (2005).
201. Chan C, Paul R, Samoray D *et al.* Structural basis of activity and allosteric control of diguanylate cyclase. *Proc. Natl. Acad. Sci. USA*, 101(49), 17084-17089 (2004).
202. Galperin MY, Nikolskaya AN, Koonin EV. Novel domains of the prokaryotic two-component signal transduction systems. *FEMS Microbiol. Lett.*, 203(1), 11-21 (2001).
203. Romling U, Gomelsky M, Galperin MY. C-di-GMP: the dawning of a novel bacterial signalling system. *Mol. Microbiol.*, 57(3), 629-639 (2005).
204. Amikam D, Benziman M. Cyclic diguanylic acid and cellulose synthesis in *Agrobacterium tumefaciens*. *J. Bacteriol.*, 171(12), 6649-6655 (1989).
205. Mayer R, Ross P, Weinhouse H *et al.* Polypeptide composition of bacterial cyclic diguanylic acid-dependent cellulose synthase and the occurrence of immunologically crossreacting proteins in higher plants. *Proc. Natl. Acad. Sci. USA*, 88(12), 5472-5476 (1991).
206. Saxena IM, Brown RM, Jr. Identification of a second cellulose synthase gene (acsAII) in *Acetobacter xylinum*. *J. Bacteriol.*, 177(18), 5276-5283 (1995).
207. Weinhouse H, Sapir S, Amikam D *et al.* c-di-GMP-binding protein, a new factor regulating cellulose synthesis in *Acetobacter xylinum*. *FEBS Lett.*, 416(2), 207-211 (1997).
208. Amikam D, Galperin MY. PilZ domain is part of the bacterial c-di-GMP binding protein. *Bioinformatics*, 22(1), 3-6 (2006).
209. Alm RA, Boder AJ, Free PD, Mattick JS. Identification of a novel gene, pilZ, essential for type 4 fimbrial biogenesis in *Pseudomonas aeruginosa*. *J. Bacteriol.*, 178(1), 46-53 (1996).
210. Boehm A, Kaiser M, Li H *et al.* Second messenger-mediated adjustment of bacterial swimming velocity. *Cell*, 141(1), 107-116 (2010).

211. Pratt JT, Tamayo R, Tischler AD, Camilli A. PilZ domain proteins bind cyclic diguanylate and regulate diverse processes in *Vibrio cholerae*. *J. Biol. Chem.*, 282(17), 12860-12870 (2007).
212. Sudarsan N, Lee ER, Weinberg Z *et al.* Riboswitches in eubacteria sense the second messenger cyclic di-GMP. *Science*, 321(5887), 411-413 (2008).
213. Hengge R. Principles of c-di-GMP signaling in bacteria. *Nat. Rev. Microbiol.*, 7(4), 263-273 (2009).
214. Hecht GB, Newton A. Identification of a novel response regulator required for the swarmer-to-stalked-cell transition in *Caulobacter crescentus*. *J. Bacteriol.*, 177(21), 6223-6229 (1995).
215. Duerig A, Abel S, Folcher M *et al.* Second messenger-mediated spatiotemporal control of protein degradation regulates bacterial cell cycle progression. *Genes Dev.*, 23(1), 93-104 (2009).
216. Levi A, Folcher M, Jenal U, Shuman HA. Cyclic diguanylate signaling proteins control intracellular growth of *Legionella pneumophila*. *mBio*, 2(1), doi:10.1128/mBio.00316-00310 (2011).
217. Lee ER, Baker JL, Weinberg Z, Sudarsan N, Breaker RR. An allosteric self-splicing ribozyme triggered by a bacterial second messenger. *Science*, 329(5993), 845-848 (2010).
218. Pei JM, Grishin NV. GGDEF domain is homologous to adenylyl cyclase. *Proteins*, 42(2), 210-216 (2001).
219. Liu Y, Ruoho AE, Rao VD, Hurley JH. Catalytic mechanism of the adenylyl and guanylyl cyclases: modeling and mutational analysis. *Proc. Natl. Acad. Sci. USA*, 94(25), 13414-13419 (1997).
220. Rao F, Yang Y, Qi Y, Liang ZX. Catalytic mechanism of cyclic di-GMP-specific phosphodiesterase: a study of the EAL domain-containing RocR from *Pseudomonas aeruginosa*. *J. Bacteriol.*, 190(10), 3622-3631 (2008).
221. Merighi M, Lee VT, Hyodo M, Hayakawa Y, Lory S. The second messenger bis-(3'-5')-cyclic-GMP and its PilZ domain-containing receptor Alg44 are required for alginate biosynthesis in *Pseudomonas aeruginosa*. *Mol. Microbiol.*, 65(4), 876-895 (2007).
222. Christen M, Christen B, Allan MG *et al.* DgrA is a member of a new family of cyclic diguanosine monophosphate receptors and controls flagellar motor function in *Caulobacter crescentus*. *Proc. Natl. Acad. Sci. USA*, 104(10), 4112-4117 (2007).

223. Ryjenkov DA, Simm R, Romling U, Gomelsky M. The PilZ domain is a receptor for the second messenger c-di-GMP: the PilZ domain protein YcgR controls motility in enterobacteria. *J. Biol. Chem.*, 281(41), 30310-30314 (2006).
224. Hickman JW, Harwood CS. Identification of FleQ from *Pseudomonas aeruginosa* as a c-di-GMP-responsive transcription factor. *Mol. Microbiol.*, 69(2), 376-389 (2008).
225. Lee VT, Matewish JM, Kessler JL, Hyodo M, Hayakawa Y, Lory S. A cyclic-di-GMP receptor required for bacterial exopolysaccharide production. *Mol. Microbiol.*, 65(6), 1474-1484 (2007).
226. Zhang Z, Gaffney BL, Jones RA. c-di-GMP displays a monovalent metal ion-dependent polymorphism. *J. Am. Chem. Soc.*, 126(51), 16700-16701 (2004).
227. Zhang Z, Kim S, Gaffney BL, Jones RA. Polymorphism of the signaling molecule c-di-GMP. *J. Am. Chem. Soc.*, 128(21), 7015-7024 (2006).
228. Navarro MV, De N, Bae N, Wang Q, Sondermann H. Structural analysis of the GGDEF-EAL domain-containing c-di-GMP receptor FimX. *Structure*, 17(8), 1104-1116 (2009).
229. Ko J, Ryu KS, Kim H *et al.* Structure of PP4397 reveals the molecular basis for different c-di-GMP binding modes by Pilz domain proteins. *J. Mol. Biol.*, 398(1), 97-110 (2010).
230. Nakayama S, Kelsey I, Wang J, Sintim HO. *Chem. Commun.*, ASAP (2011).
231. Singh SB, Jayasuriya H, Herath KB *et al.* Isolation, enzyme-bound structure, and activity of platensimycin A1 from *Streptomyces platensis*. *Tetrahedron Lett.*, 50(37), 5182-5185 (2009).
232. Singh SB, Ondeyka JG, Herath KB *et al.* Isolation, enzyme-bound structure and antibacterial activity of platencin A1 from *Streptomyces platensis*. *Bioorg. Med. Chem. Lett.*, 19(16), 4756-4759 (2009).
233. Singh SB, Jayasuriya H, Ondeyka JG *et al.* Isolation, structure, and absolute stereochemistry of platensimycin, a broad spectrum antibiotic discovered using an antisense differential sensitivity strategy. *J. Am. Chem. Soc.*, 128(36), 11916-11920 (2006).
234. Nicolaou KC, Li A, Edmonds DJ. Total synthesis of platensimycin. *Angew. Chem. Int. Ed.*, 45(42), 7086-7090 (2006).
235. Ghosh AK, Xi K. Enantioselective synthesis of (–)-platensimycin oxatetracyclic core by using an intramolecular Diels-Alder reaction. *Org. Lett.*, 9(20), 4013-4016 (2007).
236. Lalic G, Corey EJ. An effective enantioselective route to the platensimycin core. *Org. Lett.*, 9(23), 4921-4923 (2007).

237. Li PF, Payette JN, Yamamoto H. Enantioselective route to platensimycin: An intramolecular robinson annulation approach. *J. Am. Chem. Soc.*, 129(31), 9534-9535 (2007).
238. Nicolaou KC, Edmonds DJ, Li A, Tria GS. Asymmetric total syntheses of platensimycin. *Angew. Chem. Int. Ed.*, 46(21), 3942-3945 (2007).
239. Nicolaou KC, Tang YF, Wang JH. Formal synthesis of (+/-)-platensimycin. *Chemical Communications*, (19), 1922-1923 (2007).
240. Tiefenbacher K, Mulzer J. Protecting-group-free formal synthesis of platensimycin. *Angew. Chem. Int. Ed.*, 46(42), 8074-8075 (2007).
241. Zou YF, Chen CH, Taylor CD, Foxman BM, Snider BB. Formal synthesis of (+/-)-platensimycin. *Org. Lett.*, 9(9), 1825-1828 (2007).
242. Kim CH, Jang KP, Choi SY, Chung YK, Lee E. A carbonyl ylide cycloaddition approach to platensimycin. *Angew. Chem. Int. Ed.*, 47(21), 4009-4011 (2008).
243. Nicolaou KC, Pappo D, Tsang KY, Gibe R, Chen DYK. A chiral pool based synthesis of platensimycin. *Angew. Chem. Int. Ed.*, 47(5), 944-946 (2008).
244. McGrath NA, Bartlett ES, Sittihan S, Njardarson JT. A concise ring-expansion route to the compact core of platensimycin. *Angew. Chem. Int. Ed.*, 48(45), 8543-8546 (2009).
245. Nicolaou KC, Li A, Ellery SP, Edmonds DJ. Rhodium-catalyzed asymmetric enyne cycloisomerization of terminal alkynes and formal total synthesis of (-)-platensimycin. *Angew. Chem. Int. Ed.*, 48(34), 6293-6295 (2009).
246. Yun SY, Zheng JC, Lee D. Stereoelectronic effect for the selectivity in C-H Insertion of alkylidene carbenes and its application to the synthesis of platensimycin. *J. Am. Chem. Soc.*, 131(24), 8413-8414 (2009).
247. Austin KAB, Banwell MG, Willis AC. A formal total synthesis of platencin. *Org. Lett.*, 10(20), 4465-4468 (2008).
248. Hayashida J, Rawal VH. Total synthesis of (+/-)-platencin. *Angew. Chem. Int. Ed.*, 47(23), 4373-4376 (2008).
249. Nicolaou KC, Toh QY, Chen DYK. An expedient asymmetric synthesis of platencin. *J. Am. Chem. Soc.*, 130(34), 11292-11293 (2008).
250. Nicolaou KC, Tria GS, Edmonds DJ. Total synthesis of platencin. *Angew. Chem. Int. Ed.*, 47(9), 1780-1783 (2008).
251. Tiefenbacher K, Mulzer J. Short formal synthesis of (-)-platencin. *Angew. Chem. Int. Ed.*, 47(33), 6199-6200 (2008).

252. Waalboer DCJ, Schaapman MC, van Delft FL, Rutjes FPJT. High-pressure entry into platencin. *Angew. Chem. Int. Ed.*, 47(35), 6576-6578 (2008).
253. Yun SY, Zheng JC, Lee D. Concise synthesis of the tricyclic core of platencin. *Angew. Chem. Int. Ed.*, 47(33), 6201-6203 (2008).
254. Ghosh AK, Xi K. A symmetry-based concise formal synthesis of platencin, a novel lead against "superbugs". *Angew. Chem. Int. Ed.*, 48(29), 5372-5375 (2009).
255. Nicolaou KC, Tria GS, Edmonds DJ, Kar M. Total syntheses of (+/-)-platencin and (-)-platencin. *J. Am. Chem. Soc.*, 131(43), 15909-15917 (2009).
256. Tiefenbacher K, Mulzer J. A Nine-Step Total Synthesis of (-)-Platencin. *J. Org. Chem.*, 74(8), 2937-2941 (2009).
257. Varseev GN, Maier ME. Formal Total Synthesis of Platencin. *Angew. Chem. Int. Ed.*, 48(20), 3685-3688 (2009).
258. Smanski MJ, Peterson RM, Rajski SR, Shen B. Engineered *Streptomyces platensis* Strains That Overproduce Antibiotics Platensimycin and Platencin. *Antimicrob. Agents Chemother.*, 53(4), 1299-1304 (2009).
259. Yu ZG, Smanski MJ, Peterson RM *et al.* Engineering of *Streptomyces platensis* MA7339 for Overproduction of Platencin and Congeners. *Org. Lett.*, 12(8), 1744-1747 (2010).
260. Heretsch P, Giannis A. An efficient entry to amino-substituted resorcylic acid derivatives for the synthesis of platensimycin and analogues. *Synthesis*, (17), 2614-2616 (2007).
261. Kaliappan KP, Ravikumar V. An expedient enantioselective strategy for the oxatetracyclic core of platensimycin. *Org. Lett.*, 9(12), 2417-2419 (2007).
262. Nicolaou KC, Lister T, Denton RM, Montero A, Edmonds DJ. Adamantaplatensimycin: a bioactive analogue of platensimycin. *Angew. Chem. Int. Ed.*, 46(25), 4712-4714 (2007).
263. Nicolaou KC, Tang Y, Wang J, Stepan AF, Li A, Montero A. Total synthesis and antibacterial properties of carbaplatensimycin. *J. Am. Chem. Soc.*, 129(48), 14850-14851 (2007).
264. Nicolaou KC, Stepan AF, Lister T *et al.* Design, synthesis, and biological evaluation of platensimycin analogues with varying degrees of molecular complexity. *J. Am. Chem. Soc.*, 130(39), 13110-13119 (2008).
265. Yeung YY, Corey EJ. A simple, efficient, and enantiocontrolled synthesis of a near-structural mimic of platensimycin. *Org. Lett.*, 10(17), 3877-3878 (2008).
266. Zhang CW, Ondeyka J, Zink DL, Burgess B, Wang J, Singh SB. Isolation, structure and fatty acid synthesis inhibitory activities of platensimycin B-1-B-3 from *Streptomyces platensis*. *Chem. Comm.*, (40), 5034-5036 (2008).

267. Jang KP, Kim CH, Na SW *et al.* 7-Phenylplatensimycin and 11-methyl-7-phenylplatensimycin: more potent analogs of platensimycin. *Bioorg. Med. Chem. Lett.*, 20(7), 2156-2158 (2009).
268. Jang KP, Kim CH, Na SW, Kim H, Kang H, Lee E. Isoplatensimycin: Synthesis and biological evaluation. *Bioorg. Med. Chem. Lett.*, 19(16), 4601-4602 (2009).
269. Maras N, Anderluh PS, Urleb U, Kocevar M. Simple synthesis of 3-acetamido-beta-resorcylic acids as potential FabF and FabH inhibitors without using protecting groups. *Synlett.*, (3), 437-440 (2009).
270. McNulty J, Nair JJ, Capretta A. A synthesis of sulfonamide analogs of platensimycin employing a palladium-mediated carbonylation strategy. *Tetrahedron Lett.*, 50(28), 4087-4091 (2009).
271. Patra M, Gasser G, Pinto A *et al.* Synthesis and biological evaluation of chromium bioorganometallics based on the antibiotic platensimycin lead structure. *Chem. Med. Chem.*, 4(11), 1930-1938 (2009).
272. Shen HC, Ding FX, Singh SB *et al.* Synthesis and biological evaluation of platensimycin analogs. *Bioorg. Med. Chem. Lett.*, 19(6), 1623-1627 (2009).
273. Wang J, Lee V, Sintim HO. Efforts towards the identification of simpler platensimycin analogues – The total synthesis of oxazinidinyll platensimycin. *Chem. Eur. J.*, 15, 2747 (2009).
274. Zhang C, Ondeyka J, Herath K *et al.* Platensimycin and platencin congeners from *Streptomyces platensis*. *J. Nat. Prod.*, ASAP (2011).
275. Barykina OV, Rossi KL, Rybak MJ, Snider BB. Synthesis and antibacterial properties of (–)-nor-platencin. *Org. Lett.*, 11(22), 5334-5337 (2009).
276. Tiefenbacher K, Gollner A, Mulzer J. Syntheses and Antibacterial Properties of iso-Platencin, Cl-iso-Platencin and Cl-Platencin: Identification of a New Lead Structure. *Chem. Eur. J.*, ASAP (2010).
277. Zhang CW, Ondeyka J, Guan ZQ *et al.* Isolation, structure and biological activities of platensimycin B-4 from *Streptomyces platensis*. *J. Antibiotics*, 62(12), 699-702 (2009).
278. Wright HT, Reynolds KA. Antibacterial targets in fatty acid biosynthesis. *Curr. Opin. Microbiol.*, 10(5), 447-453 (2007).
279. Tiefenbacher K, Mulzer J. Synthesis of platensimycin. *Angew. Chem. Int. Ed.*, 47(14), 2548-2555 (2008).
280. Nicolaou KC, Chen JS, Edmonds DJ, Estrada AA. Recent advances in the chemistry and biology of naturally occurring antibiotics. *Angew. Chem. Int. Ed.*, 48(4), 660-719 (2009).

281. Lu X, You Q. Recent advances on platensimycin: a potential antimicrobial agent. *Curr. Med. Chem.*, 17(12), 1139-1155 (2010).
282. Palanichamy K, Kaliappan KP. Discovery and syntheses of "superbug challengers"- platensimycin and platencin. *Chem. Asian J.*, 5(4), 668-703 (2010).
283. Hong SH, Sanders DP, Lee CW, Grubbs RH. Prevention of undesirable isomerization during olefin metathesis. *J. Am. Chem. Soc.*, 127, 17160 (2005).
284. Hong SH, Wenzel AG, Salguero TT, Day MW, Grubbs RH. Decomposition of Ruthenium Olefin Metathesis Catalysts. *J. Am. Chem. Soc.*, 129, 7961 (2007).
285. Cherest M, Felkin H, Prudent N. Torsional strain involving partial bonds. Stereochemistry of lithium aluminium hydride reduction of some simple open-chain ketones. *Tetrahedron Lett.*, 18, 2199-2200 (1968).
286. Cherest M, Felkin H. Torsional strain involving partial bonds. Steric course of reaction between allyl magnesium bromide and 4-*t*-butyl-cyclohexanone. *Tetrahedron Lett.*, 18, 2205-2206 (1968).
287. Mengel A, Reiser O. Around and beyond Cram's rule. *Chem. Rev.*, 99(5), 1191-1223 (1999).
288. Mehta G, Khan FA. Electronic control of Pi-facial selectivities in nucleophilic additions to 7-norbornanones. *J. Am. Chem. Soc.*, 112(16), 6140-6142 (1990).
289. Mehta G, Khan FA, Ganguly B, Chandrasekhar J. Importance of orbital and electrostatic interactions in determining Pi-facial selectivities in nucleophilic additions to endosubstituted bicyclo[2.2.2]octan-2-ones. *Chem. Comm.*, (23), 1711-1712 (1992).
290. Hahn JM, Lenoble WJ. Strongly enhanced stereoselectivity in the reduction of 5-substituted adamantanones by substitution of C5 by positive nitrogen. *J. Am. Chem. Soc.*, 114(5), 1916-1917 (1992).
291. Halterman RL, McEvoy MA. Diastereoselectivity in the reduction of sterically unbiased 2,2-diarylcyclopentanones. *J. Am. Chem. Soc.*, 112(18), 6690-6695 (1990).
292. Cieplak AS. Stereochemistry of nucleophilic-addition to cyclohexanone - the importance of 2-electron stabilizing interactions. *J. Am. Chem. Soc.*, 103(15), 4540-4552 (1981).
293. Cieplak AS, Tait BD, Johnson CR. Reversal of Pi-facial diastereoselection upon electronegative substitution of the substrate and the reagent. *J. Am. Chem. Soc.*, 111(22), 8447-8462 (1989).
294. The reductive amination was conducted in the polar protic solvent, MeOH; therefore dipole minimization might not play as great a role in product distribution.

295. Wang J, Sintim HO. Dialkylamino-2,4-dihydroxybenzoic Acids as Easily Synthesized Analogues of Platensimycin and Platencin with Comparable Antibacterial Properties. *Chem. Eur. J.*, 17(12), 3352-3357 (2011).
296. Alhamadsheh MM, Musayev F, Komissarov AA *et al.* Alkyl-CoA disulfides as inhibitors and mechanistic probes for FabH enzymes. *Chem. Biol.*, 14(5), 513-524 (2007).
297. Yu EW, Aires JR, Nikaido H. AcrB multidrug efflux pump of *Escherichia coli*: composite substrate-binding cavity of exceptional flexibility generates its extremely wide substrate specificity. *J. Bacteriol.*, 185(19), 5657-5664 (2003).
298. Gaussian 09, Revision A02. Frisch, M. J.; Trucks, G. W.; Schlegel, H. B.; Scuseria, G. E.; Robb, M. A.; Cheeseman, J. R.; Scalmani, G.; Barone, V.; Mennucci, B.; Petersson, G. A.; Nakatsuji, H.; Caricato, M.; Li, X.; Hratchian, H. P.; Izmaylov, A. F.; Bloino, J.; Zheng, G.; Sonnenberg, J. L.; Hada, M.; Ehara, M.; Toyota, K.; Fukuda, R.; Hasegawa, J.; Ishida, M.; Nakajima, T.; Honda, Y.; Kitao, O.; Nakai, H.; Vreven, T.; J. A. Montgomery, J.; Peralta, J. E.; Ogliaro, F.; Bearpark, M.; Heyd, J. J.; Brothers, E.; Kudin, K. N.; Staroverov, V. N.; Kobayashi, R.; Normand, J.; Raghavachari, K.; Rendell, A.; Burant, J. C.; Iyengar, S. S.; Tomasi, J.; Cossi, M.; Rega, N.; Millam, J. M.; Klene, M.; Knox, J. E.; Cross, J. B.; Bakken, V.; Adamo, C.; Jaramillo, J.; Gomperts, R.; Stratmann, R. E.; Yazyev, O.; Austin, A. J.; Cammi, R.; Pomelli, C.; Ochterski, J. W.; Martin, R. L.; Morokuma, K.; Zakrzewski, V. G.; Voth, G. A.; Salvador, P.; Dannenberg, J. J.; Dapprich, S.; Daniels, A. D.; Farkas, O.; Foresman, J. B.; Ortiz, J. V.; Cioslowski, J.; Fox, D. J.; Gaussian, Inc., Wallingford CT, 2009.
299. Kumagai Y, Matsuo J, Hayakawa Y, Rikihisa Y. Cyclic di-GMP signaling regulates invasion by *Ehrlichia chaffeensis* of human monocytes. *J. Bacteriol.*, 192(16), 4122-4133 (2010).
300. Egli M, Gessner RV, Williams LD *et al.* Atomic-resolution structure of the cellulose synthase regulator cyclic diguanylic acid. *Proc. Natl. Acad. Sci. USA*, 87(8), 3235-3239 (1990).
301. Xu Y, Kool ET. Chemical and enzymatic properties of bridging 5'-S-phosphorothioester linkages in DNA. *Nucleic Acids Res.*, 26(13), 3159-3164 (1998).
302. Smietana M, Kool ET. Efficient and simple solid-phase synthesis of short cyclic oligodeoxynucleotides bearing a phosphorothioate linkage. *Angew. Chem. Int. Ed. Engl.*, 41(19), 3704-3707; 3523 (2002).
303. Rybakov VN, Rivkin MI, Kumarev VP. *Nucleic Acids Res.*, 9, 189-201 (1981).
304. Chladek S, Nagyvary J. *J. Am. Soc. Chem.*, 94, 2079-2084 (1972).

305. Cosstick R, Vyle JS. *Nucleic Acids Res.*, 18, 829-835 (1990).
306. Mag M, Lüking S, Engels JW. *Nucleic Acids Res.*, 19, 1437-1441 (1991).
307. Vyle JS, Connolly B, Kemp D, Cosstick R. *Biochemistry*, 31, 3012-3018 (1992).
308. Kuimelis RG, McLaughlin LW. Cleavage properties of an oligonucleotide containing a bridged internucleotide 5'-phosphorothioate RNA linkage. *Nucleic Acids Res.*, 23(23), 4753-4760 (1995).
309. Kuimelis RG, McLaughlin LW. Ribozyme-mediated cleavage of a substrate analogue containing an internucleotide-bridging 5'-phosphorothioate: evidence for the single-metal model. *Biochemistry*, 35(16), 5308-5317 (1996).
310. Weinstein LB, Earnshaw DI, Cosstick R, Cech TR. *J. Am. Soc. Chem.*, 118, 10341–10350 (1996).
311. Liu X, Reese CB. *Tetrahedron Lett.*, 37, 925–928 (1996).
312. Krasteva PV, Fong JC, Shikuma NJ *et al.* *Vibrio cholerae* VpsT regulates matrix production and motility by directly sensing cyclic di-GMP. *Science*, 327(5967), 866-868 (2010).
313. De N, Navarro MV, Raghavan RV, Sondermann H. Determinants for the activation and autoinhibition of the diguanylate cyclase response regulator WspR. *J. Mol. Biol.*, 393(3), 619-633 (2009).
314. Ando I. Temperature effect of ¹H NMR chemical shifts of poly(vinyl chloride). *Die Makromolekulare Chemie*, 179, 2663-2665 (1978).
315. Zhao J, Veliath E, Kim S, Gaffney BL, Jones RA. Thiophosphate analogs of c-di-GMP: impact on polymorphism. *Nucleosides Nucleotides Nucleic Acids*, 28(5), 352-378 (2009).
316. Larsson A, Carlsson C, Jonsson M, Albinsson B. Characterization of the binding of the fluorescent dyes Yo and Yoyo to DNA by polarized-light spectroscopy. *J. Am. Chem. Soc.*, 116(19), 8459-8465 (1994).
317. Netzel TL, Nafisi K, Zhao M, Lenhard JR, Johnson I. Base-content dependence of emission enhancements, quantum yields, and lifetimes for cyanine dyes bound to double-strand DNA: Photophysical properties of monomeric and bichromophoric DNA stains. *J. Phys.Chem.*, 99(51), 17936-17947 (1995).
318. Beyhan S, Bilecen K, Salama SR, Casper-Lindley C, Yildiz FH. Regulation of rugosity and biofilm formation in *Vibrio cholerae*: comparison of VpsT and VpsR regulons and epistasis analysis of vpsT, vpsR, and hapR. *J. Bacteriol.*, 189(2), 388-402 (2007).
319. Chan C, Paul R, Samoray D *et al.* Structural basis of activity and allosteric control of diguanylate cyclase. *Proc. Natl. Acad. Sci. USA*, 101(49), 17084-17089 (2004).

320. Tchigvintsev A, Xu X, Singer A *et al.* Structural insight into the mechanism of c-di-GMP hydrolysis by EAL domain phosphodiesterases. *J. Mol. Biol.*, 402(3), 524-538).
321. Hickman JW, Tifrea DF, Harwood CS. A chemosensory system that regulates biofilm formation through modulation of cyclic diguanylate levels. *Proc. Natl. Acad. Sci. USA*, 102(40), 14422-14427 (2005).
322. Remminghorst U, Rehm BH. Alg44, a unique protein required for alginate biosynthesis in *Pseudomonas aeruginosa*. *FEBS Lett.*, 580(16), 3883-3888 (2006).
323. Kulasekara HD, Ventre I, Kulasekara BR, Lazdunski A, Filloux A, Lory S. A novel two-component system controls the expression of *Pseudomonas aeruginosa* fimbrial cup genes. *Mol. Microbiol.*, 55(2), 368-380 (2005).
324. Kotaka M, Dutta S, Lee HC *et al.* Expression, purification and preliminary crystallographic analysis of *Pseudomonas aeruginosa* RocR protein. *Acta Crystallogr. Sect. F Struct. Biol. Cryst. Commun.*, 65(Pt 10), 1035-1038 (2009).
325. Rao F, Qi Y, Chong HS *et al.* The functional role of a conserved loop in EAL domain-based cyclic di-GMP-specific phosphodiesterase. *J. Bacteriol.*, 191(15), 4722-4731 (2009).
326. Bloomfield V, Crothers D, Tinoco I. *Nucleic Acids*. (University Science Books, California, 1999).
327. Egli M, Gessner RV, Williams LD *et al.* Atomic-resolution structure of the cellulose synthase regulator cyclic diguanylic acid. *Proc. Natl. Acad. Sci. USA*, 87(8), 3235-3239 (1990).
328. Williams AA, Darwanto A, Theruvathu JA, Burdzy A, Neidigh JW, Sowers LC. Impact of sugar pucker on base pair and mispair stability. *Biochemistry*, 48(50), 11994-12004 (2009).
329. Gaffney BL, Veliath E, Zhao J, Jones RA. One-flask syntheses of c-di-GMP and the [Rp,Rp] and [Rp,Sp] thiophosphate analogues. *Org. Lett.*, 12(14), 3269-3271 (2010).
330. Hsu CYJ, Dennis D, Jones RA. Synthesis and physical characterization of bis-3'-5'-cyclic. *Nucleosides & Nucleotides*, 4(3), 377-389 (1985).
331. Ross P, Mayer R, Weinhouse H *et al.* The cyclic diguanylic acid regulatory system of cellulose synthesis in *Acetobacter xylinum*. Chemical synthesis and biological activity of cyclic nucleotide dimer, trimer, and phosphothioate derivatives. *J. Biol. Chem.*, 265(31), 18933-18943 (1990).
332. Hyodo M, Hayakawa Y. An improved method for synthesizing cyclic bis(3'-5')diguanylic acid (c-di-GMP). *Bull. Chem. Soc. Jpn.*, 77, 2089-2093 (2004).

333. Kiburu I, Shurer A, Yan L, Sintim HO. A simple solid-phase synthesis of the ubiquitous bacterial signaling molecule, c-di-GMP and analogues. *Mol. Biosyst.*, 4(6), 518-520 (2008).
334. Zahringer F, Massa C, Schirmer T. Efficient enzymatic production of the bacterial second messenger c-di-GMP by the diguanylate cyclase YdeH from *E. coli*. *Appl. Biochem. Biotechnol.*, 163(1), 71-79 (2010).
335. Ching SM, Tan WJ, Chua KL, Lam Y. Synthesis of cyclic di-nucleotidic acids as potential inhibitors targeting diguanylate cyclase. *Bioorg. Med. Chem.*, 18(18), 6657-6665 (2010).
336. Iyer RP, Egan W, Regan JB, Beaucage SL. 3H-1,2-Benzodithiole-3-one 1,1-dioxide as an improved sulfurizing reagent in the solid-phase synthesis of oligodeoxyribonucleide phosphorothioates *J. Am. Chem. Soc.*, 112(3), 1254-1255 (1990).
337. Wender PA, D'Angelo N, Elitzin VI *et al.* Function-oriented synthesis: studies aimed at the synthesis and mode of action of alpha-alkyldaphnane analogues. *Org. Lett.*, 9(9), 1829-1832 (2007).
338. Ii K, Ichikawa S, Al-Dabbagh B, Bouhss A, Matsuda A. Function-oriented synthesis of simplified caprazamycins: discovery of oxazolidine-containing uridine derivatives as antibacterial agents against drug-resistant bacteria. *J. Med. Chem.*, 53(9), 3793-3813 (2010).
339. Nakai Y, Tepp WH, Dickerson TJ, Johnson EA, Janda KD. Function-oriented synthesis applied to the anti-botulinum natural product toosendanin. *Bioorg. Med. Chem.*, 17(3), 1152-1157 (2009).
340. Wender PA, Verma VA. The design, synthesis, and evaluation of C7 diversified bryostatin analogs reveal a hot spot for PKC affinity. *Org. Lett.*, 10(15), 3331-3334 (2008).
341. Wender PA, Verma VA, Paxton TJ, Pillow TH. Function-oriented synthesis, step economy, and drug design. *Acc. Chem. Res.*, 41(1), 40-49 (2008).
342. Mooberry SL, Hilinski MK, Clark EA, Wender PA. Function-oriented synthesis: biological evaluation of laulimalide analogues derived from a last step cross metathesis diversification strategy. *Mol. Pharm.*, 5(5), 829-838 (2008).
343. Patnaik S, Kumar P, Garg BS, Gandhi RP, Gupta KC. Photomodulation of PS-modified oligonucleotides containing azobenzene substituent at pre-selected positions in phosphate backbone. *Bioorg. Med. Chem.*, 15(24), 7840-7849 (2007).

344. Di Bussolo V, Fiasella A, Romano MR, Favero L, Pineschi M, Crotti P. Stereoselective synthesis of 2,3-unsaturated-aza-O-glycosides via new diastereoisomeric N-Cbz-imino glycal-derived allyl epoxides. *Org. Lett.*, 9(22), 4479-4482 (2007).
345. Meyer DS, Schreiber SL. Acceleration of the Dess-Martin oxidation by water. *J. Org. Chem.*, 59, 7549-7552 (1994).
346. Sapountzis I, Dube H, Lewis R, Gommermann N, Knochel P. Synthesis of functionalized nitroarylmagnesium halides via an iodine-magnesium exchange. *J. Org. Chem.*, 70(7), 2445-2454 (2005).
347. Gani D, Young DW. *JCS Perkin Trans. I*, 1355-1362 (1985).
348. Corey EJ, Kim CU. *J. Am. Chem. Soc.*, 94, 7586-7587 (1972).
349. de Richter RK, Bonato M, Follet M, Kamenka JM. *J. Org. Chem.*, 55, 2855-2860 (1990).
350. Hayakawa Y, Kawai R, Hirata A *et al.* Acid/azole complexes as highly effective promoters in the synthesis of DNA and RNA oligomers via the phosphoramidite method. *J. Am. Chem. Soc.*, 123(34), 8165-8176 (2001).
351. Brear P, Freeman GR, Shankey MC, Trmcic M, Hodgson DR. Aqueous methods for the preparation of 5'-substituted guanosine derivatives. *Chem. Commun.*, (33), 4980-4981 (2009).
352. Zhang B, Cui Z, Sun L. Synthesis of 5'-deoxy-5'-thioguanosine-5'-monophosphorothioate and its incorporation into RNA 5'-termini. *Org. Lett.*, 3(2), 275-278 (2001).
353. Smietana M, Kool ET. Efficient and simple solid-phase synthesis of short cyclic oligodeoxynucleotides bearing a phosphorothioate linkage. *Angew. Chem. Int. Ed.*, 41(19), 3704-3707; 3523 (2002).
354. Becke AD. *J. Chem. Phys.*, 98, 5648-5652 (1993).
355. Lee C, Yang W, Parr RG. *Phys. Rev. B*, 37, 785-789 (1988).
356. Wang J, Zhou J, Nakayama S *et al.* Conservative change to the phosphate moiety of c-di-GMP remarkably affects its polymorphism and binding abilities to DGC, PDE and PilZ proteins. *Unpublished work*.
357. Keresztes I, Williard PG. Diffusion-ordered NMR spectroscopy (DOSY) of THF solvated *n*-butyllithium aggregates. *J. Am. Chem. Soc.* 122, 10228-10229 (2000).
358. Altieri AS, Hinton DP, Byrd RA. Association of biomolecular systems via pulsed-field gradient NMR self-diffusion measurements. *J. Am. Chem. Soc.* 117, 7566-7567 (1995).
359. Cohen Y, Avram L, Frish L. Diffusion NMR spectroscopy in supramolecular and combinatorial chemistry: An old parameter - New insights." *Angew. Chem. Int. Ed.* 44, 520-554 (2005).